BEILSTEIN JOURNAL OF ORGANIC CHEMISTRY

Synthetic probes for the study of biological function

Edited by Jeffrey Aubé

Generated on 03 November 2026, 09:01

Imprint

Beilstein Journal of Organic Chemistry
www.bjoc.org
ISSN 1860-5397
Email: journals-support@beilstein-institut.de

The *Beilstein Journal of Organic Chemistry* is published by the Beilstein-Institut zur Förderung der Chemischen Wissenschaften.

Beilstein-Institut zur Förderung der Chemischen Wissenschaften
Trakehner Straße 7–9
60487 Frankfurt am Main
Germany
www.beilstein-institut.de

The copyright to this document as a whole, which is published in the *Beilstein Journal of Organic Chemistry*, is held by the Beilstein-Institut zur Förderung der Chemischen Wissenschaften. The copyright to the individual articles in this document is held by the respective authors, subject to a Creative Commons Attribution license.

Beilstein Journal of Organic Chemistry

Synthetic probes for the study of biological function

Jeffrey Aubé

Editorial

Open Access

Address:
Department of Medicinal Chemistry, the University of Kansas, 2034 Becker Drive, Lawrence, Kansas, 66047, USA

Email:
Jeffrey Aubé - jaube@ku.edu

Beilstein J. Org. Chem. **2013,** *9,* 79–80.
doi:10.3762/bjoc.9.10

Received: 07 January 2013
Accepted: 09 January 2013
Published: 15 January 2013

This article is part of the Thematic Series "Synthetic probes for the study of biological function".

Guest Editor: J. Aubé

© 2013 Aubé; licensee Beilstein-Institut.
License and terms: see end of document.

From its beginnings, organic chemistry has been a partner to biology, often crossing the artificial boundary between the sciences to the benefit of both disciplines. This is even reflected in the use of the adjective “organic” to refer to the chemistry of carbon. As the field has matured, it has continued to address matters of *structure* and *synthesis* to increasingly encompass the grand challenge of designing and preparing molecules having a particular *function*. All three of these come together in the pursuit of new chemical probes for use in chemical biology.

This Thematic Series highlights some of the numerous ways that molecular tools inform biological research. The choice of the phrase “chemical probe” was deliberately vague and indeed its meaning often lies in the ears of the listener. The most common context is the case of a molecule used in chemical biology to help unravel the role of a particular cellular pathway. Biologists have numerous tools at their disposal, of course, and one important reason to select a small organic molecule as an inhibitor, say, is that it allows for temporal control of its effect. Of course, inhibitors (and other sorts of biologically active molecules) have a way of occasionally – very occasionally – turning into drugs, and this offers its own rationale for research in this direction. Regardless of the goal, the challenge of finding a small molecule that binds to a macromolecular target in a specific enough way to influence its function is considerable.

The combination of a binding event with a physical property such as fluorescence leads to another sort of probe, where the goal is to inform the researcher where a particular target may exist in a cell. In addition, the advent of phenotypic screening has created a strong demand for probes that can be used to help identify the target at which a screening hit is working. Each provides challenges to the chemist as it is necessary to retain the key binding event in such a way that also permits a useful read-out or physical capture of the intended target.

Meeting challenges such as those described above requires both biological insight and chemical know-how. It has often been said that a distinguishing characteristic of chemistry is its ability to introduce new forms of matter into the universe, and we now have over a hundred years of accumulated experience in doing just that. The structural diversity of molecules that function as probes is broad indeed, some of them complex enough that even the most discerning practitioner of organic synthesis may consider them as worthy of their efforts.

I would like to extend my most sincere thanks to the authors and reviewers who have made this Thematic Series possible and for their support of open access publication in organic chemistry. I hope that this Thematic Series will inspire many of its readers to lend their talents to this still-emerging branch of *chemistry*.

Jeff Aubé

Lawrence, January 2013

License and Terms

This is an Open Access article under the terms of the Creative Commons Attribution License (http://creativecommons.org/licenses/by/2.0), which permits unrestricted use, distribution, and reproduction in any medium, provided the original work is properly cited.

The license is subject to the *Beilstein Journal of Organic Chemistry* terms and conditions: (http://www.beilstein-journals.org/bjoc)

The definitive version of this article is the electronic one which can be found at: doi:10.3762/bjoc.9.10

Beilstein Journal of Organic Chemistry

Regioselective synthesis of 7,8-dihydroimidazo [5,1-*c*][1,2,4]triazine-3,6(2*H*,4*H*)-dione derivatives: A new drug-like heterocyclic scaffold

Nikolay T. Tzvetkov[1], Harald Euler[2] and Christa E. Müller[*1]

Full Research Paper

Open Access

Address:
[1]PharmaCenter Bonn, Pharmaceutical Sciences Bonn (PSB), University of Bonn, Pharmaceutical Institute, An der Immenburg 4, 53121 Bonn, Germany and [2]University of Bonn, Steinmann-Institute of Mineralogy, Poppelsdorfer Schloss, 53115 Bonn, Germany

Email:
Christa E. Müller[*] - christa.mueller@uni-bonn.de

* Corresponding author

Keywords:
hydantoins; hydrazides; imidazotriazines; N-alkylation; regio- and chemoselective reaction; thionation; X-ray structure

Beilstein J. Org. Chem. **2012,** *8,* 1584–1593.
doi:10.3762/bjoc.8.181

Received: 05 May 2012
Accepted: 16 August 2012
Published: 20 September 2012

This article is part of the Thematic Series "Synthetic probes for the study of biological function".

Guest Editor: J. Aube

© 2012 Tzvetkov et al; licensee Beilstein-Institut.
License and terms: see end of document.

Abstract

Dihydroimidazo[5,1-*c*][1,2,4]triazine-3,6(2*H*,4*H*)-dione derivatives were prepared by successive N3- and N1-alkylation of hydantoins, followed by regioselective thionation and subsequent cyclization under mild conditions. In a final alkylation step a further substituent may be introduced. The synthetic strategy allows broad structural variation of this new drug-like heterobicyclic scaffold. In addition to extensive NMR and MS analyses, the structure of one derivative was confirmed by X-ray crystallography.

Introduction

Imidazotriazines represent an important class of condensed heterobicycles that display a variety of significant biological activities, including anticancer [1], antimicrobial [2], anti-inflammatory [3] and neuroprotective [4] properties. The impressive array of biological effects of these compounds is associated with the 1,2,4-triazine ring as the core structural moiety, which also occurs in a number of natural products [5]. In addition, the 1,2,4-triazine scaffold has found application in pharmaceuticals and agrochemicals [6]. For example, some 7-phenylimidazo-[1,2-*b*][1,2,4]triazine derivatives of the general structure **1** (Figure 1) have been developed as selective ligands for γ-aminobutyric acid type A ($GABA_A$) receptors and are therefore of benefit in the treatment and prevention of adverse conditions of the central nervous system (CNS), including anxiety, convulsions and cognitive disorders [7]. Novel fused 1,2,4-triazine-4(6*H*)-ones **2** showed selective cytotoxicity at micromolar concentrations against a wide range of cancer cells [1,8], while other derivatives of **2** exhibited analgesic [9], antibacterial, and antiviral activities [2]. Compounds with the 1,2,3,4-tetrahydroimidazo[1,2-*b*][1,2,4]triazine frame-

work **3** were reported to be potentially useful as interleukin-1 (IL-1) and tumour necrosis factor (TNF) inhibitors for prophylactic and therapeutic treatment of chronic inflammatory diseases in which these cytokines are involved [3]. Recently, specifically substituted imidazo[1,5-*f*][1,2,4]triazines (**4**) have been developed as polo-like kinase (PLK) inhibitors with potential as anticancer therapeutics [10]. The 1,2,4-triazines **4** also exhibited inhibitory activities against glycogen synthase kinase 3 (GSK3β), and may therefore be developed for the treatment of haematological diseases, and inhibition of phosphodiesterase 10 (PDE10), which is potentially useful for the treatment of neurodegenerative diseases, especially Parkinson's disease [11].

The scaffolds **1**–**4** consist of a 1,2,4-triazine core, which arises from the ring fusion of C4a–N8 (**1**, **3** and **4**) or C8a–N5 atoms (**2**), and differ in the arrangement of the substitution pattern of the imidazotriazine framework (Figure 1).

The structural variation of imidazo[1,2,4]triazine derivatives poses a significant challenge, particularly if a broad variety of substituents is to be introduced. Several synthetic strategies involving combinatorial and sequential approaches, in particular intramolecular cyclocondensation reactions of functionalized 1,2,4-triazole and imidazole precursors, have been developed [5,6,12].

We have been interested in expanding the medicinal-chemical space of synthetic drug-like small molecules focusing on 6,5-heterobicyclic ring systems in order to increase the diversity of our proprietary compound library [13]. Criteria for selection of the target structures include the potential for biological activity and bioavailability (peroral, and possibly central nervous system), structural novelty, synthetic accessibility, and the possibility for broad structural variations. In particular, we planned to introduce sp^3-hybridized carbon atoms, to avoid completely flat aromatic structures that are prone to low solubility in water due to π-stacking effects.

We therefore identified the 1,2,4-triazine-containing scaffolds **IV** and **VIII** as promising novel target structures (Scheme 1). Depending on the starting material used, e.g., hydantoin **I**, or pyrazolidine-3,5-dione **V**, respectively, either 7,8-dihydroimidazo[5,1-*c*][1,2,4]triazine-3,6-diones **IV** (route A) or 6,8-dihydropyrazolo[5,1-*c*][1,2,4]triazine-3,7-dione derivatives **VIII** (route B) should be accessible. In either case two nitrogen atoms, N7/N6 and N2, may be substituted with a variety of residues; e.g., alkylation of N2 (R^5) in the very last step should allow an easy access to a library of compounds. Route B would proceed in four steps yielding product **VIII** starting from **V**, which may be obtained from the corresponding malonyl dichloride and hydrazine derivatives.

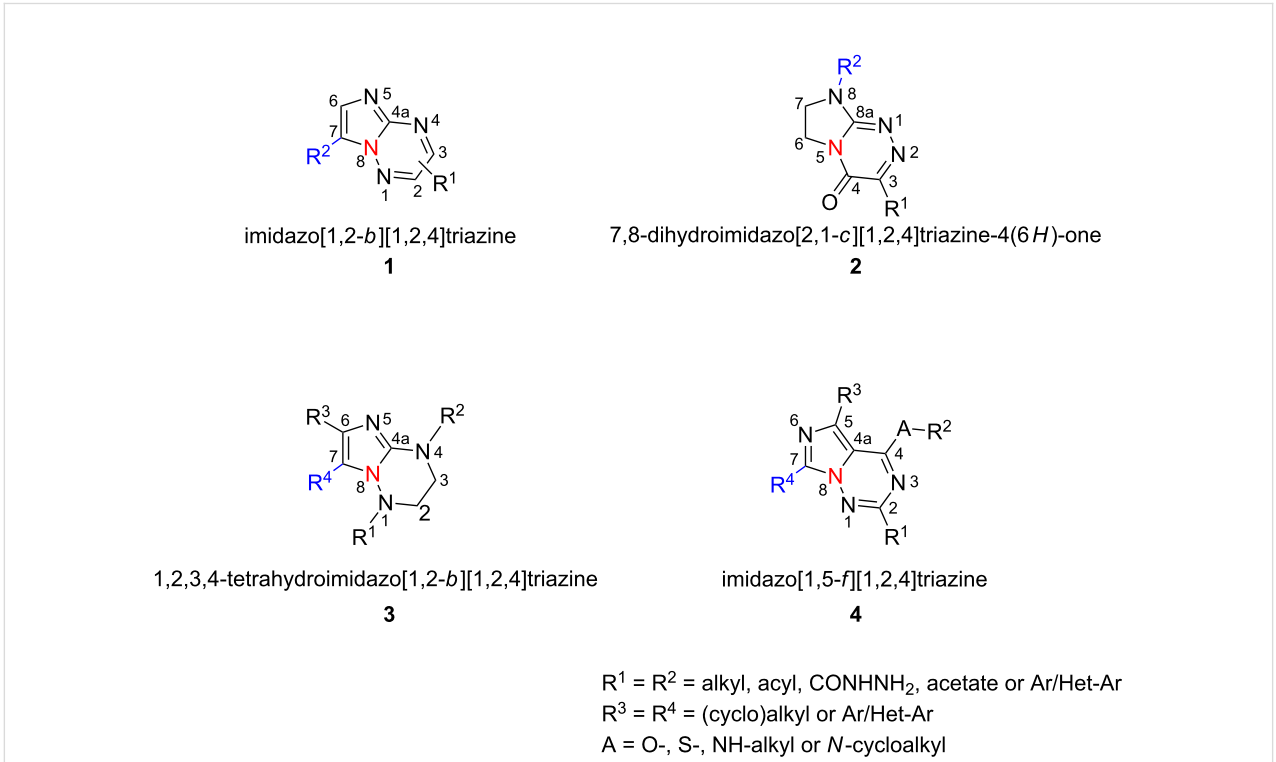
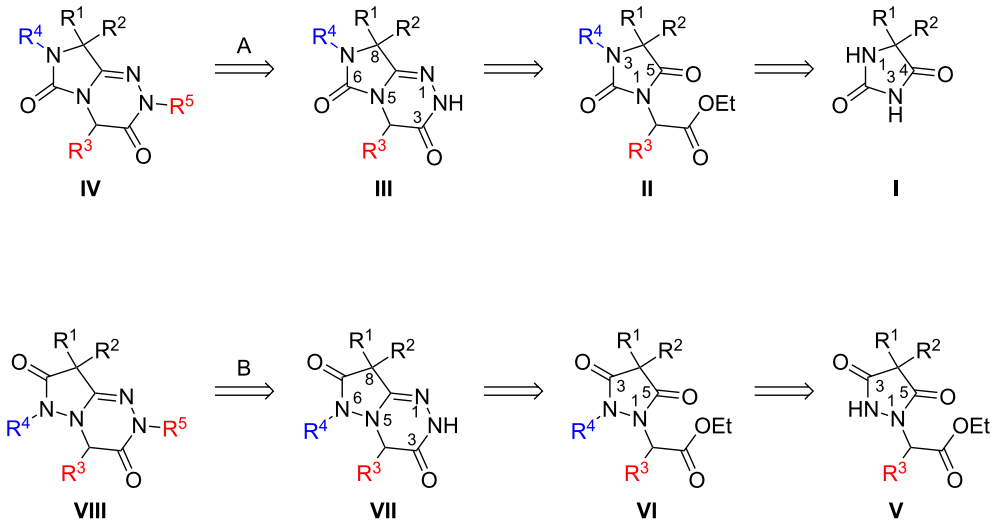


Figure 1: Biologically active imidazo[1,2,4]triazine scaffolds **1**–**4**.



Scheme 1: Retrosynthetic approaches towards novel 7,8-dihydroimidazo-[5,1-*c*][1,2,4]-triazine-3,6-diones **IV** and 6,8-dihydropyrazolo[5,1-*c*][1,2,4]triazine-3,7-diones **VIII**.

In the present study we focussed on synthetic route A starting from the commercially available hydantoins **I**, which would allow very broad structural diversity by introducing a variety of substituents and functionalities at different stages of the synthesis. As a first step ethyl (2,5-dioxoimidazolidin-1-yl)acetate derivative **II** is formed from hydantoins **I**. The condensation reaction of **II** with hydrazine, followed by a regioselective intramolecular heterocyclization, formally by dehydration, would afford the 7,8-dihydroimidazo[5,1-*c*][1,2,4]triazine-3,6-diones **III**. The success of this route, however, depends on two factors: (i) the preferred regioselectivity of the successive *N*-alkylation steps for the formation of **II**; and (ii) the regioselective cyclization of 2,5-dioxoimidazolidines **II** to the desired product **III**, which is expected to be favoured in the case of dimethylhydantoin derivatives ($R^1 = R^2 = Me$).

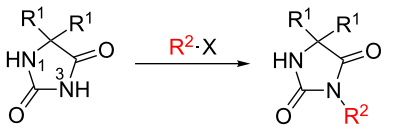
Results and Discussion

Chemistry

Following the proposed strategy for the formation of 7,8-dihydroimidazo[5,1-*c*][1,2,4]triazine-3,6-dione derivatives possessing aryl (R^4 = 3,4-dichlorobenzyl) and alkyl/alkynyl (R^5 = Me, propargyl) substituents at their nitrogen atoms 7 and 2, respectively, we started from the differently substituted hydantoins ($R^1 = R^2$ = H or Me) **5** and **6**. N3- and subsequent N1-alkylation led to the N1,N3-dialkylated hydantoin derivatives **12**–**18**. Alkylation reactions of hydantoins are well documented in the literature [14-18]. Depending on the alkylation reagents and reaction conditions, either N1- or N3-substituted hydantoins are accessible [14-17]. The details of the successfully conducted N3-alkylation of hydantoins **5** and **6** with various alkyl halides are shown in Table 1.

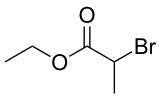
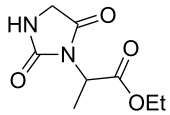
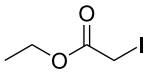
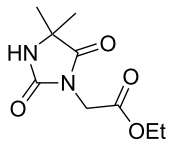
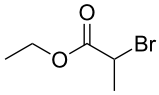
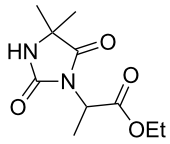
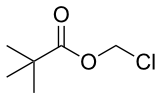
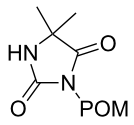
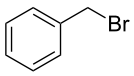
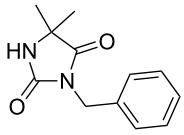
Alkylation of the thermodynamically preferred N3-position was achieved following a modified literature procedure, and the products could be obtained on a multigram scale [18]. In general, 1.1 equivalents of the corresponding alkylation reagent and potassium carbonate as a base in dry dimethylformamide (DMF) were used. The best yield (92%) was achieved with ethyl 2-bromopropionate and benzyl bromide as alkylating reagents. Although this procedure led to the direct formation of the desired N3-substituted products, the regioselectivity depended on the substitution pattern of **6**, due to the directing effect of the methyl groups. Thus, traces of a N1-substituted regioisomer were detected by LC/ESI-MS analysis in the conversion of **5** to product **7** (N3/N1-alkylation ratio 15:1). Direct N1,N3-dialkylation of **5**, however, was not observed. Alkylation with benzyl bromide was carried out in order to verify the N3-substitution yielding **11**, which had already been described in the literature [14]. 3-Benzyl-5,5-dimethylhydantoin (**11**) was obtained in 92% isolated yield (see Section Experimental in Supporting Information File 1), in comparison to 80% obtained by the literature procedure [14]. Compounds **7**–**11** were isolated after chromatographic purification in good to excellent yields and analyzed by NMR spectroscopy (^1H and ^{13}C) and LC/ESI-MS. In addition, we obtained an X-ray crystal structure of **11** [18], which confirmed the alkylation at the N3-position of 5,5-dimethylhydantoin (**6**). The subsequent N1-alkylation of 2,5-dioxoimidazolidines **7**–**10** to the corres-

Table 1: Yields and reaction conditions for the N3-alkylation of hydantoin derivatives **5** and **6**.



5: R^1 = H
6: R^1 = Me

7: R^1 = H
8–11: R^1 = Me

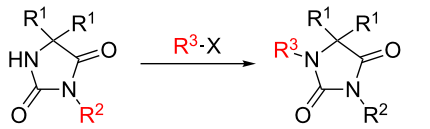
starting compound	R^2–X (1.1 equiv)	conditions	product	yield (%)
5		1.1 equiv K_2CO_3 DMF, 85 °C, 42 h	 **7**[a]	89
6		1.1 equiv K_2CO_3 DMF, 80 °C, 56 h	 **8**[a]	76
6		1.1 equiv K_2CO_3 DMF, 85 °C, 90 h	 **9**[a]	92
6	 = POM-Cl	1.1 equiv K_2CO_3 DMF, 85 °C, 28 h	 **10**	56
6		1.1 equiv K_2CO_3 DMF, 85 °C, 6 h	 **11**[b]	92

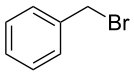
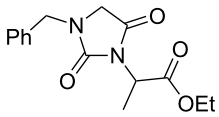
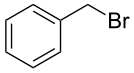
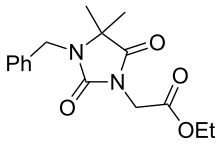
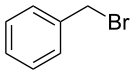
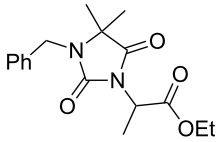
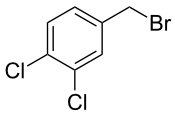
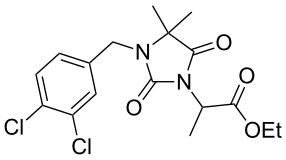
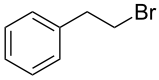
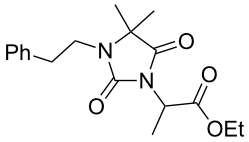
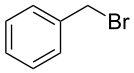
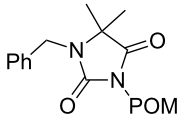
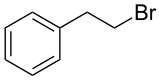
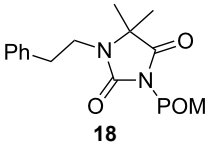
[a]Compounds **7** [19], **8** [19,20], **9** [19] have been described in the literature without detailed analytical data. [b]Analytical data for **11** [14] are in accordance with literature data.

ponding *N*,*N*-disubstituted hydantoins **12**–**18** was performed with 1.0–1.2 equiv of the appropriate alkylating reagent by using sodium hydride as a base in dry dimethylformamide (DMF) (Table 2). However, under these conditions the formation of compounds **12**–**18** strongly depended on the nature of the alkylating reagent, and therefore varying yields of dialkylated products were obtained. The reactions of **9** and **10** with 3,4-dichlorobenzyl bromide and phenethyl bromide, respectively, led to the formation of **15**, **16**, and **18** in poor to moderate yields. The alkylation with benzyl bromide worked well not only with sodium hydride (method 1) but also in the presence of potassium carbonate (method 2) as a base and gave rise to the disubstituted derivatives **12**–**14** and **17** in good yields. Products **12**–**18** were isolated after chromatographic purification (Table 2).

In order to demonstrate the tractability of the successive N1,N3-alkylation of hydantoin **6** we applied a three-step synthetic route to obtain compound **19** [17]. N3-Unsubstituted, N1-substituted hydantoins were obtained by a three-step synthetic procedure by reaction of **6** with pivaloyloxymethyl chloride (POM-Cl) to introduce a protecting group prior to N1-alkylation. Subsequently, the ester can easily be cleaved with lithium hydroxide in a methanol/tetrahydrofuran mixture at room temperature to afford 1-benzyl-5,5-dimethylimidazolidine-2,4-dione (**19**) (Scheme 2).

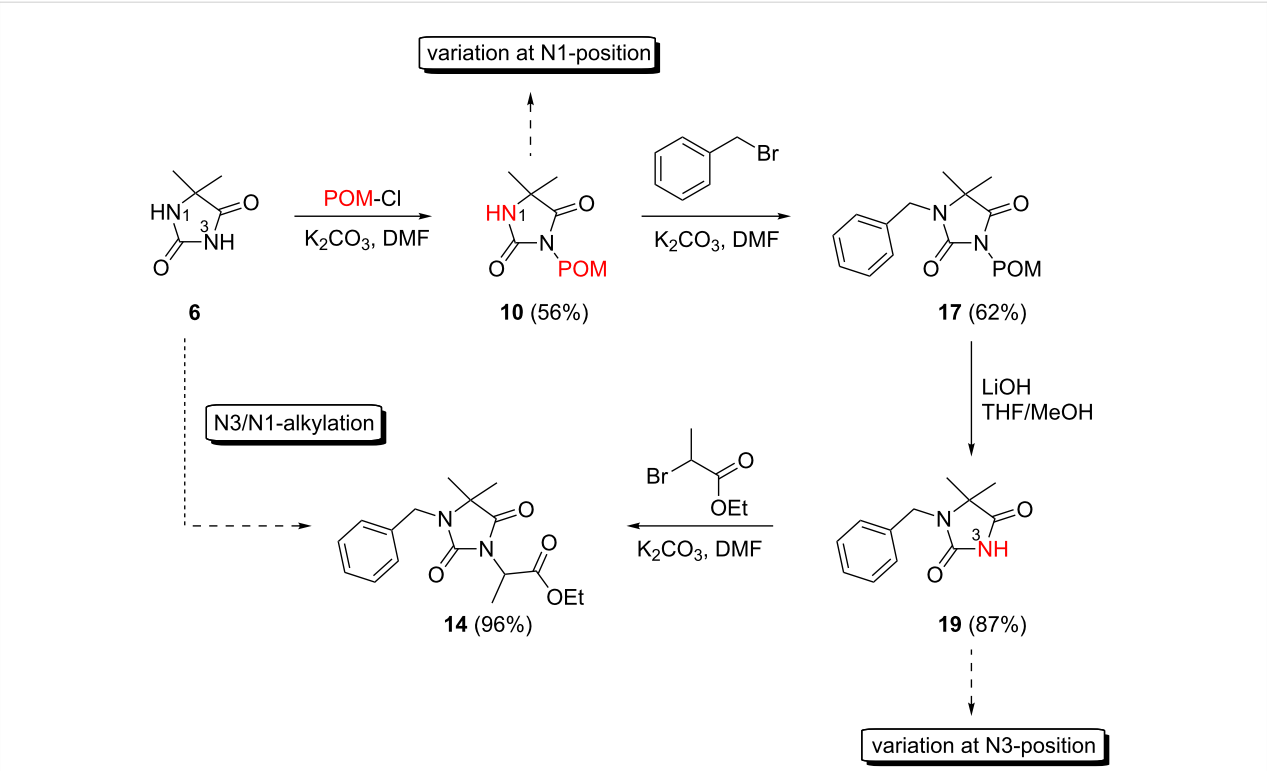
Table 2: Yields and reaction conditions of N1-alkylation of N3-substituted hydantoins **7**–**10**.



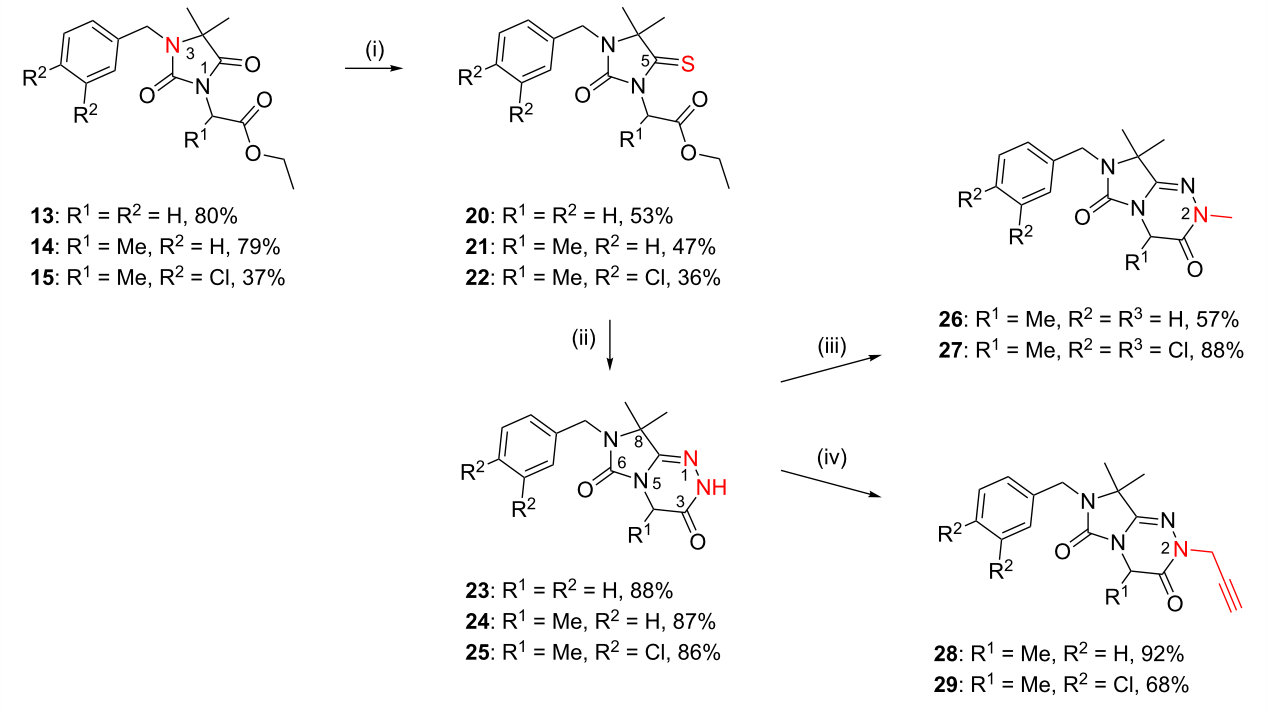
starting compound	R^3–X (1.0–1.2 equiv)	conditions	product	yield (%)
7		1.2 equiv NaH DMF, 85 °C, 66 h[a]	 **12**	70
8		1.0 equiv NaH DMF, 80 °C, 72 h[a]	 **13**	80
9		(1) 1.2 equiv NaH[a] DMF, 85 °C, 80 h (2) 1.1 equiv K_2CO_3 DMF, 80 °C, 72 h[b]	 **14**	79[a] 60[b]
9		1.2 equiv NaH DMF, 85 °C, 120 h[a]	 **15**	37
9		1.1 equiv NaH DMF, 85 °C, 68 h[a]	 **16**	18
10		1.2 equiv K_2CO_3 DMF, 85 °C, 72 h[b]	 **17**	62
10		1.2 equiv K_2CO_3 DMF, 85 °C, 69 h[b]	 **18**	28

[a]Method 1. [b]Method 2.

According to our retrosynthetic analysis (Scheme 1), and based on an efficient protocol for the regioselective *N*-alkylation of hydantoins, we applied a four-step procedure for the synthesis of differently substituted 7,8-dihydroimidazo[5,1-*c*][1,2,4]triazine-3,6-diones **23**–**29** (Scheme 3).



Scheme 2: Synthesis of N3-unsubstituted, N1-substituted hydantoin **19** by using a protection strategy.



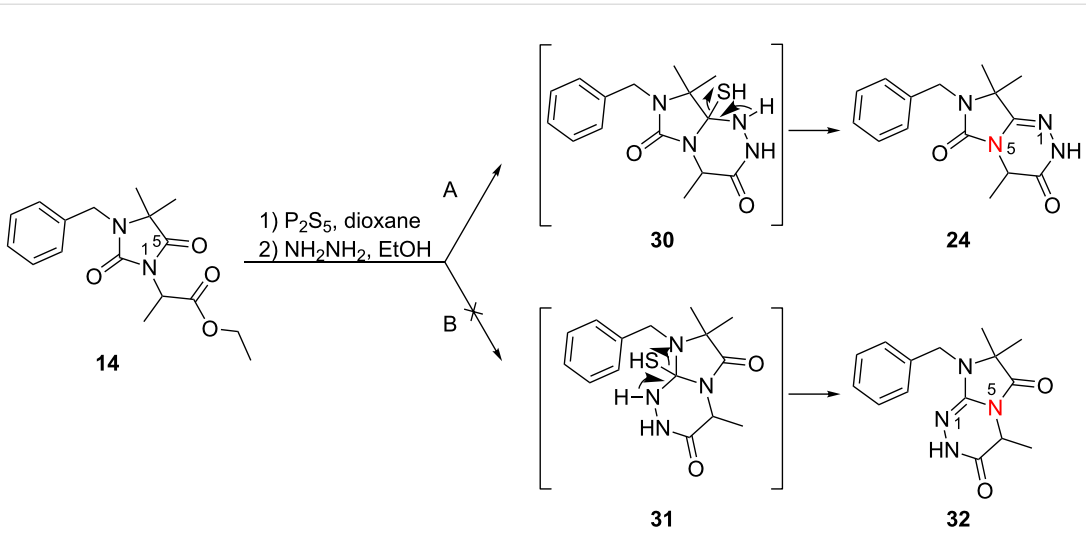
Scheme 3: Synthesis of 7,8-dihydroimidazo[5,1-*c*][1,2,4]triazine-3,6-diones **23**–**29**. Reagents and conditions: (i) P_2S_5, dioxane, reflux, 24 h; (ii) hydrazine monohydrate (20 equiv), EtOH, reflux 5–10 h; (iii) MeI (for **26**) or methyl methanesulfonate (for **27**), NaH, DMF, r.t.; (iv) propargyl bromide (80% in toluene), NaH, 85 °C, 48 h.

The main challenge in the synthesis of **23**–**25** was the construction of the 1,2,4-triazine ring. Direct reaction of **13**–**15** with hydrazine hydrate failed, and only the corresponding hydrazides were formed. Therefore, the C5 carbonyl group of **13**–**15** was regioselectively thionated with phosphorus pentasulfide in dioxane under reflux [21] (Scheme 4). The products were purified chromatographically and the preferred regioselectivity (C5 versus C2) was confirmed by NMR spectroscopy. The formation of C2-thiocarbonyl by-products was not observed under these reaction conditions. The highly regioselective formation of thioketones **20**–**22** may be due to electronic effects and prevention of the formation of certain tautomers by the C4-methyl groups in compounds **13**–**15** [22]. To investigate the influence of the C4-methyl groups on the regioselective thionation reaction, we treated unsubstituted 5,5-dimethylhydantoin **6** with phosphorus pentasulfide in dioxane for four hours. As reported in the literature, we observed only the preferred C4 thiocarbonyl product while the thionation of 5-unsubstituted hydantoin yields a mixture of 2- and 4-thionated products, indicating that the 5-dimethyl substitution was responsible for regioselective thionation [21].

The proposed intramolecular N1–C5 heterocondensation as a key step to form the desired imidazo[5,1-*c*][1,2,4]triazine-3,6-diones **23**–**25** was accomplished by reaction of the thioxoimidazolidines **20**–**22** with hydrazine hydrate [23-26]. Different reaction conditions were applied, e.g., variation of the solvent or the amount of hydrazine monohydrate that was used. The highest yields of compounds **23**–**25** (almost 90% on average) were obtained when the condensation was performed in ethanol with a large excess of hydrazine hydrate (20 equiv) under reflux for the appropriate reaction time. We observed that the adding of molecular sieves (4 Å) to the reaction medium greatly improved the yields of condensed products **23**–**25**. The regioselective two-step cyclization of **14** yielding imidazo[5,1-*c*][1,2,4]triazine-3,6-dione (**24**, pathway A) via an N5–C5 ring fusion is outlined in Scheme 4. Precursors **13** and **15** follow the same pathway A. A dehydrothionated intermediate (e.g., **30** in the preparation of **24**) is formed. Obviously, N1–C2 cyclization (pathway B) via **31** is not favoured, and **32** is not formed starting from **21**. The products **23**–**25** were purified by column chromatography and obtained on a multigram scale. Finally, the imidazotriazines were further functionalized by an N-alkylation reaction using different alkylating reagents under basic conditions (Scheme 3). Alkylation of **24** with methyl iodide led to **26**, whereas methyl methanesufonate was used as an alkylating reagent for the methylation of **25** yielding **27**. Reaction of **24** and **25** with propargyl bromide (80% in toluene) under basic conditions at 85 °C yielded the *N*-propargyl derivatives **28** and **29** (Scheme 3). The final products **26**–**29** were purified by column chromatography followed by preparative RP-HPLC, or by recrystallization; the pure products were obtained in good yields.

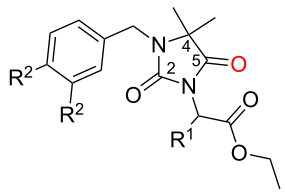
Structural analyses

Regioselectivity of the thionation reaction of the C5-carbonyl group was an essential precondition for a successful heterocondensation step yielding the desired imidazo[5,1-*c*][1,2,4]triazine-3,6-dione derivatives **23**–**25**. The structural assignment of the precursors (2,5-dioxoimidazolidines **13**–**15** and their thiocarbonyl analogues **20**–**22**) reported herein is based on their spectral data and, if necessary, supported by MMFF94 force field conformational analytical data [27]. The most important ^{13}C NMR chemical shifts δ (ppm) are reported in Table 3.

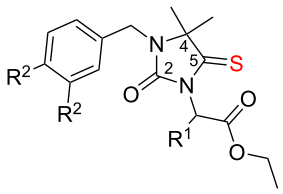


Scheme 4: Proposed regioselective two-step cyclization pathway to form **24** from **14**.

Table 3: ^{13}C NMR chemical shifts (determined at 125 MHz in DMSO-d_6) before and after thionation: comparison of **13**–**15** and **20**–**22**.



13: $R^1 = R^2 = H$
14: R^1 = Me, $R^2 = H$
15: R^1 = Me, R^2 = Cl



20: $R^1 = R^2 = H$
21: R^1 = Me, R^2 = H
22: R^1 = Me, R^2 = Cl

^{13}C assignment	**13**	**14**	**15**	**20**	**21**	**22**
C2	154.6	154.5	154.6	154.1	153.9	154.0
C4	62.2	61.8	61.9	70.9	70.8	70.8
C5	175.9	175.7	175.6	209.2	208.5	208.4

In the case of C5-thionation, the ^{13}C NMR signal for this carbon atom is shifted from about 176 to 208–209 ppm. In addition, the C4 signal is shifted from ca. 62 to 71 ppm upon thionation.

The structure determination of the condensed key products **24** and **25** was carried out by heteronuclear correlation NMR (HSQC and HMBC) in combination with ^{1}H and ^{13}C NMR, and additionally by LC/ESI-MS (*m*/*z* 287 $[M + H]^+$/285 $[M - H]^-$ for **24**, 355 $[M + H]^+$/353 $[M - H]^-$ for **25**). Molecular modelling was performed to calculate the respective geometries by using the MMFF95 force field [27] assuming an N1–C5 ring fusion during the intramolecular condensation reaction yielding **24** and **25** (Figure 2).

The structural assignments of **24** and **25** were confirmed by HSQC and, most importantly, by HMBC (see Supporting Information File 1). The analysis of two HMBC spectra of **24** and **25** showed key correlations between C8 and H^C/H^D as well as between C6 and H^C/H^D methylene protons. In the case of an alternative N1–C2 ring fusion (structure **32** in Scheme 4) such a correlation between the carbonyl C5-function and the methylene protons H^C/H^D would be not possible. The structure was additionally confirmed by X-ray analysis of **24** (Figure 3) [28]. The molecules in the crystal are held together by one type of intermolecular hydrogen bond, located between O2 and the hydrogen H1 of the N2, with a distance of d(O···H1–N2) = 1.9437(2) Å, d(H1–N2) = 0.93(2) Å and an angle of ∠(O2–H1–N2) = 155(2)°.

Physicochemical properties

In order to assess the physicochemical properties of imidazo[5,1-*c*][1,2,4]triazine-3,6-dione derivatives we determined water-solubility, log *P*, and pK_a values for compound **25**

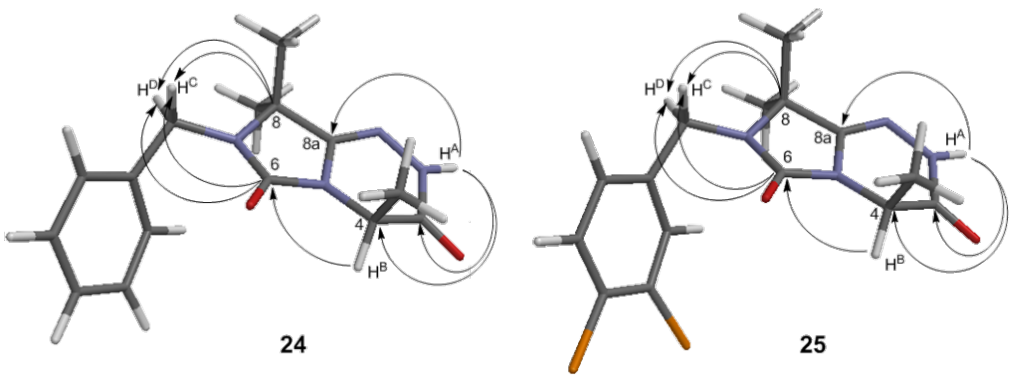


Figure 2: Optimized structure (MMFF95) and key HMBC correlations of imidazo[5,1-*c*][1,2,4]triazine-3,6(2*H*,4*H*)-diones **24** and **25**.

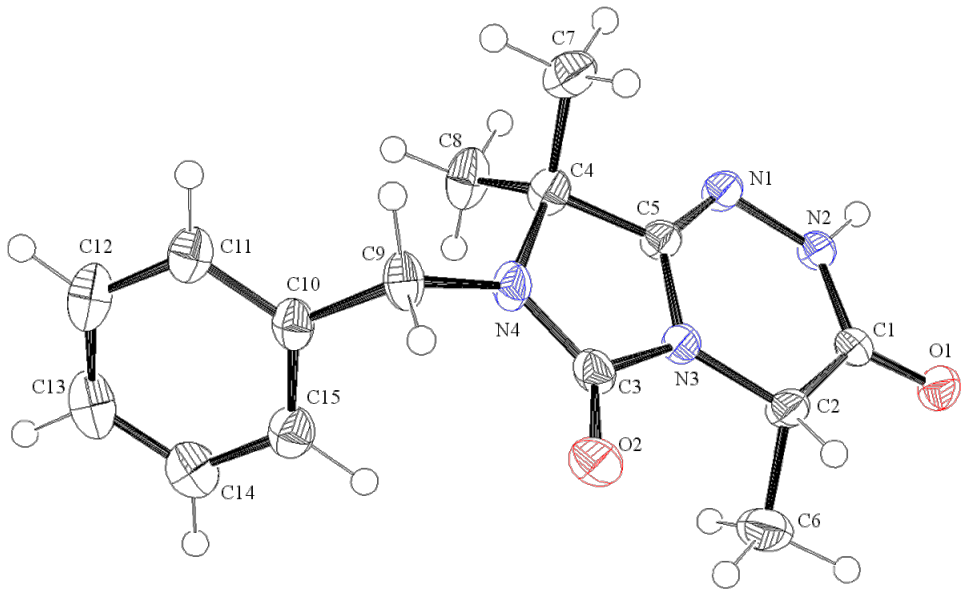


Figure 3: ORTEP diagram of **24** showing the atomic numbering. The thermal ellipsoids are drawn at the 50% probability level.

as a representative of this new class of heterocyclic compounds. Water solubility at physiological pH of 7.4 was found to be 47 µg/mL, which is a suitable range for perorally active drugs. A pK_a value of 10.0, and a log*P* value of 3 was determined. Thus, the molecule will be uncharged under physiological conditions and the log*P* value is in a range which allows us to predict oral bioavailability [29].

Conclusion

In conclusion, we have designed and synthesized novel fused 7,8-dihydroimidazo-[5,1-*c*][1,2,4]triazine-3,6(2*H*,4*H*)-dione derivatives, i.e., a novel class of small heterocyclic molecules with drug-like properties, thereby expanding the druggable chemical space. For this purpose, we have developed a four-step convergent synthetic concept to access the imidazo[5,1-*c*][1,2,4]triazine frameworks starting from the commercially available 5,5-dimethylhydantoin **6**. The reaction sequence involves successive *N*-alkylations of the corresponding hydantoin, followed by C5-thionation and an intramolecular heterocondensation reaction with hydrazine hydrate as a key step affording the imidazo[5,1-*c*][1,2,4]triazine-3,6-dione derivatives **23**–**25** in a regioselective manner. The synthetic procedure was optimized for all steps and can easily be carried out on a multigram scale. The experimentally determined physicochemical properties of prototypic compound **25** are indicative of drug-like properties suitable for peroral application. Alkylation in the final step allows the introduction of additional diversity and the preparation of compound libraries. The new synthetic strategy should also allow for the preparation of other, related heterobicyclic systems possessing different ring-members, ring sizes, and a variety of substituents.

Supporting Information

Supporting Information File 1

Assays for determination of physicochemical properties of **25**, experimental details and copies of NMR (1D and 2D) and LC/ESI-MS spectra of compounds **24** and **25**.
[http://www.beilstein-journals.org/bjoc/content/supplementary/1860-5397-8-181-S1.pdf]

Acknowledgements

A. Reiner, S. Terhart-Krabbe, M. Schneider and H. Passgang are gratefully acknowledged for skillful technical assistance. Dr. G. Schnakenburg and C. Rödde, Department for X-ray Single Crystal Structure Solution, Institute for Inorganic Chemistry, are acknowledged for collecting the dataset of compound **24**. Dr. F. Pineda and Dr. M. Wiese are acknowledged for the determination of physicochemical data of compound **25**. We are grateful to the German Federal Ministry of Education and Research (BMBF) and UCB Pharma for financial support (BIOPHARMA Neuroallianz project).

Dedication

Dedicated to the late Dr. Frédéric Denonne, who inspired this work: to a great medicinal chemist, a fantastic colleague, and a wonderful person who died much too young.

References

1. Sztanke, K.; Pasternak, K.; Rzymowska, J.; Sztanke, M.; Kandefer-Szerszeń, M. *Eur. J. Med. Chem.* **2008,** *43,* 1085–1094. doi:10.1016/j.ejmech.2007.07.009
2. Sztanke, K.; Pasternak, K.; Rajtar, B.; Sztanke, M.; Majek, M.; Polz-Dacewicz, M. *Bioorg. Med. Chem.* **2007,** *15,* 5480–5486. doi:10.1016/j.bmc.2007.05.048
3. Oku, T.; Kawai, Y.; Marusawa, H.; Tanaka, H. Imidazotriazine derivatives. WO001992012154A1, July 23, 1992.
4. Siegel, S.; Wilmen, A.; Röhrig, S.; Svenstrup, N.; Gnoth, M. J.; Heitmeier, S.; Rester, U. Imidazo-, Pyrazolopyrazine and Imidazotriazine und ihre Verwendung. DE102007032349A1, Jan 15, 2009.
5. Maechling, S.; Good, J.; Lindell, S. D. *J. Comb. Chem.* **2010,** *12,* 818–821. doi:10.1021/cc1001617
6. Kirkman, J. K.; Lindell, S. D.; Maechling, S.; Slawin, A. M. Z.; Moody, C. J. *Org. Biomol. Chem.* **2008,** *6,* 4452–4459. doi:10.1039/b810850a
7. Bettati, M.; Blurton, P.; Carling, W. R.; Chambers, M. S.; Halett, D. J.; Jennings, A.; Lewis, R. T.; Russell, M. G. N.; Street, L. J.; Szekeres, H. J.; Van Neil, M. B. Imidazo-triazine derivatives as ligands for GABA recaptors. US000006936608B2, Aug 30, 2005.
8. Sztanke, K.; Tuzimski, T.; Sztanke, M.; Rzymowska, J.; Pasternak, K. *Bioorg. Med. Chem.* **2011,** *19,* 5103–5116. doi:10.1016/j.bmc.2011.07.027
9. Sztanke, K.; Markowski, W.; Świeboda, R.; Polak, B. *Eur. J. Med. Chem.* **2010,** *45,* 2644–2649. doi:10.1016/j.ejmech.2010.01.068
10. Cheung, M.; King, N. P.; Kuntz, K. W.; Mook, R. A., Jr.; Pobanz, M. A.; Salovich, J. M.; Wilson, B. J. Imidazotriazine compounds. US000007462614B2, Dec 9, 2008.
11. Bauser, M.; Brückner, D.; Burkhardt, N.; Ergüden, J. K.; Flubacher, D.; Friedl, A.; Gerlach, I.; Hendrix, M.; Hinz, V.; Jork, R.; Naab, P.; Niewöhner, U.; Repp, T. O.; Schauss, D.; Schlemmer, K.-H.; Stoltefuss, J.; Tersteegen, A. Imidazotriazines for use as phosphodiesterase inhibitors. WO002003000693A1, Jan 30, 2003.
12. Molina, P.; Lorenzo, A.; Aller, E. *Synthesis* **1989,** 843–847. doi:10.1055/s-1989-27406
13. Substanzbibliothek — Fachgruppe Pharmazie. http://mueller-group.pharma.uni-bonn.de/bibliothek (accessed May 4, 2012).
14. Jordan, T. E.; Ginsburg, S. *J. Am. Chem. Soc.* **1949,** *71,* 2258. doi:10.1021/ja01174a518
15. Orazi, O. O.; Corral, R. A. *Tetrahedron* **1961,** *15,* 93–99. doi:10.1016/0040-4020(61)80012-4
16. Katritzky, A. R.; Grzeskowiak, N. E.; Siddiqui, T.; Jayaram, C.; Vassilatos, S. N. *J. Chem. Res., Synop.* **1982,** 528.
17. Schläpfer-Dähler, M.; Mukherjee-Müller, G.; Heimgartner, H. *Helv. Chim. Acta* **1992,** *75,* 1251–1261. doi:10.1002/hlca.19920750425
18. Euler, H.; Barbier, B.; Tzvetkov, N. T.; Müller, C. E. *Z. Kristallogr. - New Cryst. Struct.* **2009,** *224,* 601–602. doi:10.1524/ncrs.2009.0264
19. Haga, T.; Toki, T.; Koyanagi, T.; Asai, N.; Yoshida, K.; Imai, O.; Yamamoto, K. Organophosphorus based compound, productio thereof and insecticide, acaricide, nematicide and agent for killing insect pest in soil containing the same compound. JP000002000793A, Jan 5, 1990.
20. Curtin, L. M.; Dai, Y.; Davidsen, S. K.; Dellaria, J. F., Jr.; Florjancic, A. S.; Gong, J.; Guo, Y.; Heyman, H. R.; Holms, J. H.; Michaelides, M. R.; Stacey, J. R.; Steinman, D. H.; Wada, C. K.; Xu, L. Reverse hydroxamate inhibitors of matrix metalloproteinases. US000006294573B1, Sept 25, 2001.
21. Cristiani, F.; Devillanova, F. A.; Diaz, A.; Isaia, F.; Verani, G. *Phosphorus Sulfur Relat. Elem.* **1985,** *22,* 23–31. doi:10.1080/03086648508073350
22. Cherkasov, R. A.; Kutyrev, G. A.; Pudovik, A. N. *Tetrahedron* **1985,** *41,* 2567–2624. doi:10.1016/S0040-4020(01)96363-X
23. Jakubkiene, V.; Paulauskaite, R.; Vainilavicius, P. *Chem. Heterocycl. Compd.* **2007,** *43,* 485–489. doi:10.1007/s10593-007-0070-5
24. Eberle, M. K.; Schirm, P. *J. Heterocycl. Chem.* **1977,** *14,* 59–63. doi:10.1002/jhet.5570140111
25. Brugger, M.; Wamhoff, H.; Korte, F. *Justus Liebigs Ann. Chem.* **1972,** *755,* 101–105. doi:10.1002/jlac.19727550112
26. Deodhar, K. D.; D'Sa, A. D.; Pednekar, S. R.; Kanekar, D. S. *Synthesis* **1982,** 853–854. doi:10.1055/s-1982-29972
27. All calculations were carried out at a semiempirical level (AM1) with Titan V1.05, Schrödinger Inc., Wavefunction Inc. (18. August 2000).
28. CCDC–**878004** (**24**) contains the supplementary crystallographic data for this paper. Copies of the data can be obtained free of charge from the Cambridge Crystallographic Data Centre via http://www.ccdc.cam.ac.uk/data_request/cif (fax: +44-(0)1223-336033 or email: deposit@ccdc.cam.ac.uk).
29. Keserü, G. M.; Makara, G. M. *Nat. Rev. Drug Discovery* **2009,** *8,* 203–212. doi:10.1038/nrd2796

License and Terms

This is an Open Access article under the terms of the Creative Commons Attribution License (http://creativecommons.org/licenses/by/2.0), which permits unrestricted use, distribution, and reproduction in any medium, provided the original work is properly cited.

The license is subject to the *Beilstein Journal of Organic Chemistry* terms and conditions: (http://www.beilstein-journals.org/bjoc)

The definitive version of this article is the electronic one which can be found at: doi:10.3762/bjoc.8.181

Beilstein Journal of Organic Chemistry

trans-2-(2,5-Dimethoxy-4-iodophenyl)cyclopropylamine and *trans*-2-(2,5-dimethoxy-4-bromophenyl)cyclopropylamine as potent agonists for the 5-HT$_2$ receptor family

Adam Pigott[1], Stewart Frescas[1], John D. McCorvy[1], Xi-Ping Huang[2], Bryan L. Roth[2] and David E. Nichols[*1,§]

Full Research Paper

Open Access

Address:
[1]Department of Medicinal Chemistry and Molecular Pharmacology, College of Pharmacy, Purdue University, West Lafayette, IN 47907, USA and [2]National Institute of Mental Health, Psychoactive Drug Screening Program, Department of Pharmacology, School of Medicine, University of North Carolina, Chapel Hill, NC 27599, USA

Email:
David E. Nichols[*] - drdave@purdue.edu

* Corresponding author
§ Tel 765-494-1461; fax 765 494-1414

Keywords:
cyclopropanation; diazomethane; hallucinogen; 5-HT$_{2A}$ agonist; receptor probe; *trans*-2-phenylcyclopropylamines

Beilstein J. Org. Chem. **2012,** *8,* 1705–1709.
doi:10.3762/bjoc.8.194

Received: 14 June 2012
Accepted: 06 September 2012
Published: 08 October 2012

This article is part of the Thematic Series "Synthetic probes for the study of biological function".

Guest Editor: J. Aube

© 2012 Pigott et al; licensee Beilstein-Institut.
License and terms: see end of document.

Abstract

A strategy to replace the ethylamine side chain of 2,5-dimethoxy-4-iodoamphetamine (DOI, **1a**), and 2,5-dimethoxy-4-bromoamphetamine (DOB, **1b**) with a cyclopropylamine moiety was successful in leading to compounds with high affinity at the 5-HT$_2$ family of receptors; and the more potent stereoisomer of the cyclopropane analogues had the expected (−)-(1*R*,2*S*)-configuration. Screening for affinity at various serotonin receptor subtypes, however, revealed that the cyclopropane congeners also had increased affinity at several sites in addition to the 5-HT$_{2A}$ and 5-HT$_{2B}$ receptors. Therefore, at appropriate doses – although (−)-**4** and (−)-**5** may be useful as tools to probe 5-HT$_2$ receptor function – one would need to be mindful that their selectivity for 5-HT$_{2A}$ receptors is somewhat less than for DOI itself.

Introduction

Among the molecules that have proven very valuable to neuroscientists studying brain serotonin systems is the substituted phenethylamine derivative 2,5-dimethoxy-4-iodoamphetamine (DOI, **1a**, Figure 1), a potent but nonspecific agonist ligand for serotonin 5-HT$_{2A}$ and 5-HT$_{2C}$ receptors. It is relatively inexpensive and has been widely used throughout the neuroscience community to study behaviors mediated by 5-HT$_2$ family receptors. Indeed, as of June 12, 2012, a PubMed search of the terms DOI + 5-HT$_2$ yielded 577 hits, spanning from 1984 to the present. Despite the fact that no significant abuse of DOI has

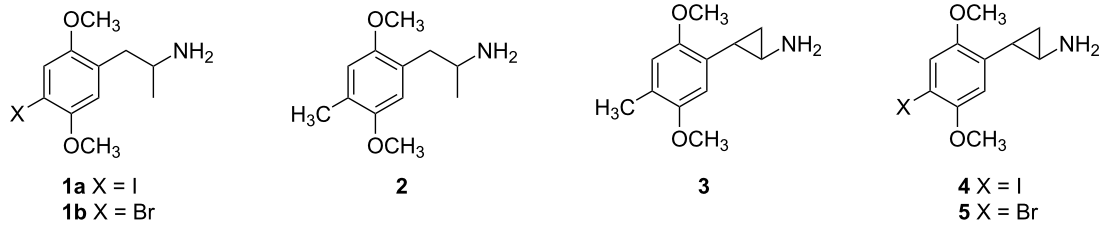


Figure 1: Structures of well-known serotonin 5-HT_{2A} agonists **1a,b**, **2**, and **3**, and compounds **4** and **5** reported in this paper.

been reported, this substance has been scheduled in a number of countries and has been considered for scheduling by the U.S. Drug Enforcement Administration (DEA). Classification as a controlled substance will be a setback to the neuroscience community because it effectively prevents experiments in any laboratory that does not have a proper license for the use of DOI. To illustrate this point, a related compound – bromo congener **1b** (DOB) – presently is a controlled substance and only 52 hits for DOB + 5-HT_2 were obtained from PubMed, compared with 577 for DOI over the same period of time.

Anticipating the potential need for a substance to replace DOI as a research tool, we sought to identify a molecule that might have pharmacological properties which are identical, or at least very similar to those of **1a**. We had previously characterized the cyclopropane analogue of a hallucinogenic amphetamine known as DOM (**2**) and had shown that **3** (DMCPA) had high potency both in vitro and in vivo [1-3]. We thus considered whether the cyclopropane analogues **4** and **5** might be useful research tools. Accordingly, this report details the synthesis of racemic *trans*-1-(2,5-dimethoxy-4-iodophenyl)-2-aminocyclopropane (**4**) and its bromo homolog **5**, the resolution of **4** into its (−)-(1*R*,2*S*)-enantiomer, as well as the resolution of the cyclopropane carboxylic acid precursor and subsequent bromination to provide both enantiomers of **5**.

Table 1: Affinity values (K_i in nM) at human 5-HT_{2A} and 5-HT_{2C} receptors. All values represent mean and SEM from at least three independent experiments.

	^{3}H-ketanserin	^{3}H-mesulergine
Compound	5-HT_{2A} K_i in (nM)	5-HT_{2C} K_i in (nM)
(±)-**1a**	7.6 ± 0.9	35 ± 6
(±)-**1b**	8.9 ± 0.5	31 ± 5
(±)-**4**	1.5 ± 0.1	17 ± 3
(±)-**5**	1.4 ± 0.3	7.5 ± 1.1

Table 2: Potency and percent max values for calcium release at 5-HT_{2A} and 5-HT_{2C} receptors. All values represent mean and SEM from at least three independent experiments.

	5-HT_{2A}		5-HT_{2C}	
Compound	EC_{50} (nM)	%max	EC_{50} (nM)	%max
(−)-**1a**	3.3 ± 0.7	87 ± 1	8.7 ± 0.2	50 ± 5
(−)-**1b**	5.8 ± 1.3	75 ± 7	28 ± 4	59 ± 7
(−)-**4**	2.0 ± 0.3	89 ± 4	21 ± 4	63 ± 6
(−)-**5**	6.3 ± 1.6	76 ± 10	32 ± 8	77 ± 6

Results and Discussion

Racemic **4** and **5** were compared in radioligand competition assays against radiolabeled antagonists defined at the human 5-HT_{2A} and 5-HT_{2C} receptors and compared with racemic **1a** and **1b**. The results are shown in Table 1. As can be seen, the cyclopropane analogues **4** and **5** showed affinities for the 5-HT_{2A} receptor 5–6-fold greater than **1a** and **1b**. Affinities at the 5-HT_{2C} receptor were about two-fold higher than for **1a** and **1b**.

The more potent (−)-enantiomers were then tested for functional potency using a calcium release assay. The EC_{50} values and maximal effect at the 5-HT_{2A} receptor were virtually identical for **1a** and **4**, and for **1b** and **5** (Table 2).

At the 5-HT_{2C} receptor **1a** was the most potent, with an EC_{50} that was about three times lower than for **1b**, **4**, or **5**. In functional assays, therefore, the cyclopropane analogues **4** and **5** compared to **1a** or **1b** appeared as potent and had a similar degree of maximal stimulation at each of the respective 5-HT_2 receptors.

We then carried out a broader screen of **4** and **5** for affinities at a range of other 5-HT receptor isoforms (Table 3). Their affinities at other 5-HT receptors, however, were higher than for **1a**. In particular, the introduction of the cyclopropane appears to increase significantly affinities at the 5-HT_{1A}, 5HT_{1B}, and 5-HT_{1D} receptors. In that regard, although (−)-**4** and (−)-**5** have affinities at the 5-HT_{2A} receptor somewhat higher than **1a**, their

Table 3: Affinity values (K_i in nM) at selected serotonin receptor isoforms.

Cmpd	5-HT_{1A}	5-HT_{1B}	5-HT_{1D}	5-HT_{1E}	5-HT_{2A}	5-HT_{2B}	5-HT_{2C}	5-HT_6	5-HT_7
(±)-**1a**	<50%[a]	<50%[a]	<50%[a]	1090	9	3	19	1380	850
(±)-**4**	410	290	535	1660	9	10	17	100	580
(−)-**4**	150	230	90	1380	2.4	6	7.4	70	260
(+)-5	210	<50%[a]	<50%[a]	<50%[a]	540	20	130	NA	170
(−)-5	220	375	390	890	3	4	9	45	120

[a]<50% displacement at 10^{-6} M.

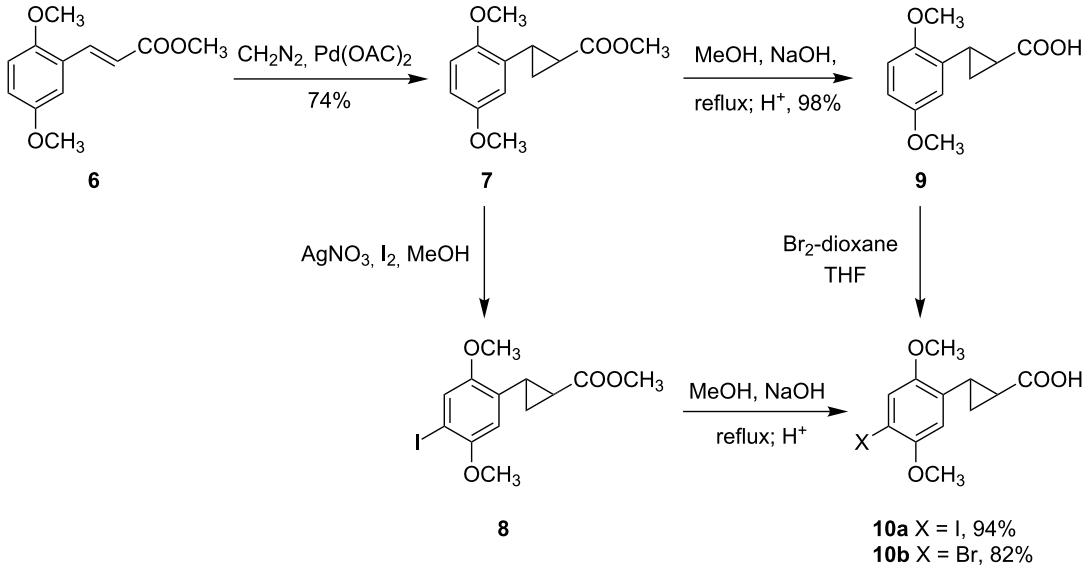
selectivity over the 5-HT_{1A} receptor is less than 100-fold. As shown in Table 1, both **4** and **5** are extremely potent ligands in vitro. Furthermore, as anticipated, it was the (−)-enantiomers that proved to have highest affinity. We included (+)-**5** in Table 3 simply to illustrate the difference in affinity between the two enantiomers. We assume that the final compounds have the (−)-(1*R*,2*S*) and (+)-(1*S*,2*R*) absolute configurations based on our earlier work establishing the absolute configuration of **3** [2], and the fact that substitutions at the 4-position of the aromatic ring in chiral substituted amphetamines do not change the sign of optical rotation [4]. The biological data are consistent with those configuration assignments.

Chemistry

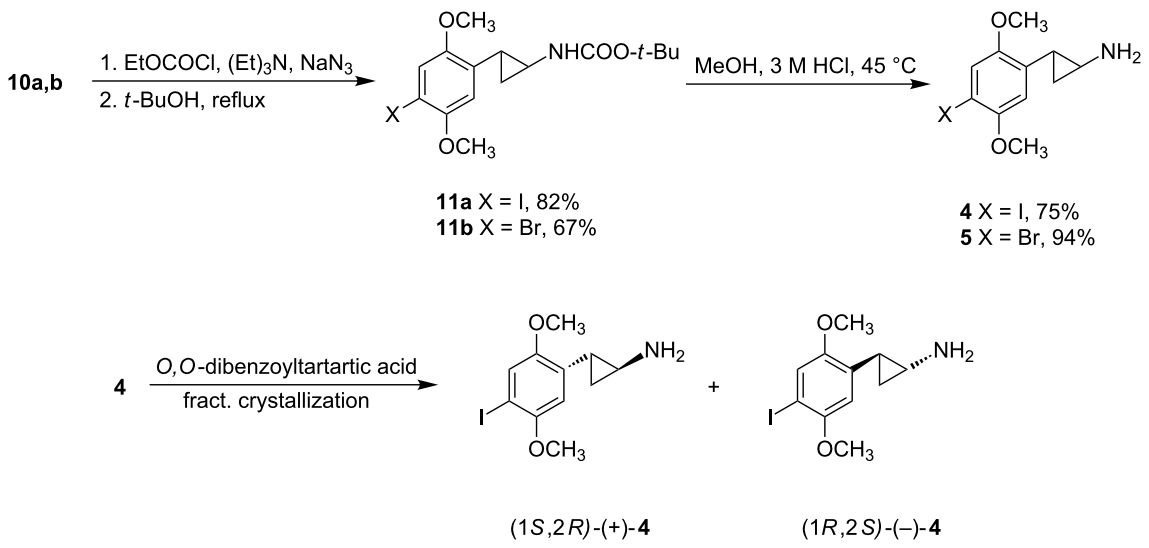
We reasoned that a palladium-mediated cyclopropanation of the corresponding cinnamic acids would provide the required cyclopropanecarboxylic acid (Scheme 1); which could be readily converted to the amine by a Curtius type rearrangement (Scheme 2). In our previous synthesis [2] we had employed an *N*-carbobenzoxy intermediate, followed by catalytic debenzylation over Pd(C); but those conditions would lead to dehalogenation in the present series, so we instead employed acid-catalyzed removal of a BOC protecting group (Scheme 2).

Thus, we first prepared 2-(2,5-dimethoxyphenyl)cyclopropanecarboxylic acid methyl ester (**7**) from the corresponding cinnamic ester **6** [5], followed by $I_2/AgNO_3$ iodination (Scheme 1), and base hydrolysis of the resulting ester to provide iodo acid **10a**. Hydrolysis of ester **7** followed by bromination of acid **9** using Br_2-dioxane complex gave a good yield of bromo acid **10b**.

These acids were readily converted to their isocyanates using the Weinstock modification of the Curtius rearrangement [6]. Those isocyanates were heated with *tert*-butanol to afford the corresponding carbamates **11a** and **11b** (Scheme 2). A brief treatment of these with 3 M HCl at 45 °C cleanly affected N-deprotection and afforded the desired final amines **4** and **5**.



Scheme 1: Synthesis of arylcyclopropane carboxylic acids from the corresponding cinnamic acids, followed by halogenation.



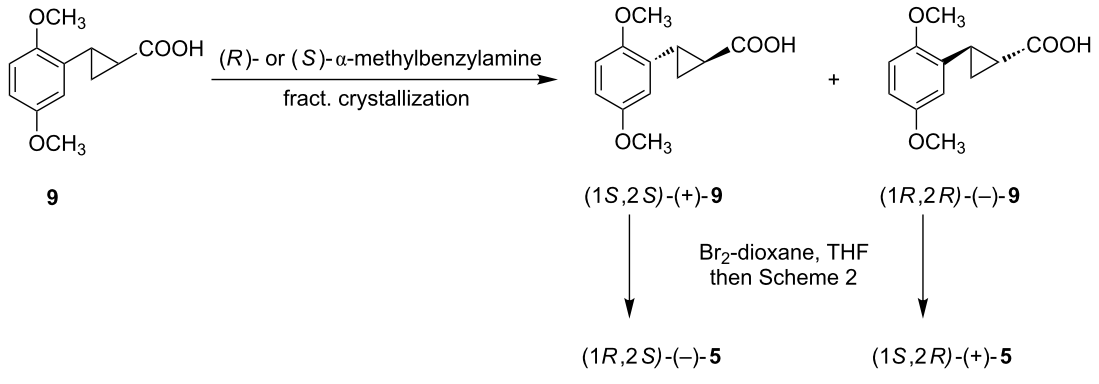
Scheme 2: Conversion of arylcyclopropane carboxylic acids **10a,b** to the amines **4** and **5**, and chemical resolution of **4** into its enantiomers.

The stereochemistry of the more potent enantiomer of DOI is (−)-(*R*) [7], and of **3** is (−)-(1*R*,2*S*) [2]. We therefore undertook the resolution of the enantiomers of DOI by fractional crystallization of the diastereomeric salts prepared with di-*O,O*-benzoyltartaric acid. Unfortunately, we discovered that heating solutions of the dibenzoyltartrate salt of **4** in EtOH or iPrOH led to nearly complete decomposition, presumably through a cyclopropane ring-opening pathway. The apparent need to recrystallize the *O,O*-dibenzoyltartrate salts from a nonprotic solvent led us to employ warm acetone, which proved satisfactory. The resolution went well, achieving constant optical rotation after only three crystallizations. The salt was converted to the free base, which was dissolved in dry Et_2O, followed by addition of the stoichiometric amount of ethereal HCl. The salt precipitated out of solution and could be used directly for pharmacological experiments. Attempts to recrystallize the HCl salt from protic solvents also led to nearly complete decomposition, although salts of bromo compound **5** appeared somewhat more stable.

We then followed a more efficient divergent approach to obtain the enantiomers of **5** that employed resolution of the cyclopropane carboxylic acid, followed by bromination, and then conversion to the cyclopropylamine (Scheme 3). We are aware that the use of chiral auxiliaries in the cyclopropanation step could directly afford the chiral cyclopropane acids [8], but time and resources did not allow us to pursue that approach.

Conclusion

In conclusion, our strategy to replace the ethylamine side chain of **1a** (or **1b**) with a cyclopropylamine moiety was successful in leading to compounds with high affinity at the 5-HT_2 family of receptors; and the more potent stereoisomer of the cyclo-



Scheme 3: Chemical resolution of arylcyclopropane carboxylic acid **9** followed by bromination.

propane analogues had the expected (−)-1*R*,2*S*-configuration. However, at appropriate doses, although (−)-**4** and (−)-**5** may be useful as tools to probe 5-HT_2 receptor function, one would also need to be mindful that their selectivity for 5-HT_{2A} over 5-HT_{1A} is only about 70-fold.

The most efficient approach appears to be the synthesis of the chiral cyclopropane carboxylic acids, followed by derivatization at the 4-position. This approach would be most appealing if a chiral auxiliary was used in the cyclopropanation step [8]. We also note that compound **4** was less stable than **5** under recrystallization conditions, an instability we did not observe during our earlier work with **3**. We have observed even greater instability in 2-(indol-3-yl)cyclopropylamines [8,9], suggesting that electron "excessive" π-systems, or the ability to "donate" electrons through resonance (i.e. Br and I), leads to cyclopropane ring instability in 2-arylcyclopropylamines.

Supporting Information

Supporting Information File 1

Experimental details for all new compounds as well as the pharmacological methods used to measure receptor affinity and functional activity.
[http://www.beilstein-journals.org/bjoc/content/supplementary/1860-5397-8-194-S1.pdf]

Acknowledgments

This research was supported by the Robert C. and Charlotte P. Anderson endowment.

References

1. Nichols, D. E.; Pfister, W. R.; Yim, G. K. W. *Life Sci.* **1978,** *22,* 2165–2170. doi:10.1016/0024-3205(78)90567-2
2. Nichols, D. E.; Woodard, R.; Hathaway, B. A.; Lowy, M. T.; Yim, G. K. W. *J. Med. Chem.* **1979,** *22,* 458–460. doi:10.1021/jm00190a021
3. Johnson, M. P.; Mathis, C. A.; Shulgin, A. T.; Hoffman, A. J.; Nichols, D. E. *Pharmacol. Biochem. Behav.* **1990,** *35,* 211–217. doi:10.1016/0091-3057(90)90228-A
4. Nichols, D. E.; Barfknecht, C. F.; Rusterholz, D. B.; Benington, F.; Morin, R. D. *J. Med. Chem.* **1973,** *16,* 480–483. doi:10.1021/jm00263a013
5. Peterson, J. R.; Russell, M. E.; Surjasasmita, I. B. *J. Chem. Eng. Data* **1988,** *33,* 534–537. doi:10.1021/je00054a042
6. Weinstock, J. *J. Org. Chem.* **1961,** *26,* 3511. doi:10.1021/jo01067a604
7. Johnson, M. P.; Hoffman, A. J.; Nichols, D. E.; Mathis, C. A. *Neuropharmacology* **1987,** *26,* 1803–1806. doi:10.1016/0028-3908(87)90138-9
8. Vangveravong, S.; Nichols, D. E. *J. Org. Chem.* **1995,** *60,* 3409–3413. doi:10.1021/jo00116a028
9. Vangveravong, S.; Kanthasamy, A.; Lucaites, V. L.; Nelson, D. L.; Nichols, D. E. *J. Med. Chem.* **1998,** *41,* 4995–5001. doi:10.1021/jm980318q

License and Terms

This is an Open Access article under the terms of the Creative Commons Attribution License (http://creativecommons.org/licenses/by/2.0), which permits unrestricted use, distribution, and reproduction in any medium, provided the original work is properly cited.

The license is subject to the *Beilstein Journal of Organic Chemistry* terms and conditions: (http://www.beilstein-journals.org/bjoc)

The definitive version of this article is the electronic one which can be found at:
doi:10.3762/bjoc.8.194

Beilstein Journal of Organic Chemistry

Hydrophobic analogues of rhodamine B and rhodamine 101: potent fluorescent probes of mitochondria in living *C. elegans*

Laurie F. Mottram[1], Safiyyah Forbes[1], Brian D. Ackley[2] and Blake R. Peterson[*1]

Full Research Paper

Open Access

Address:
[1]Department of Medicinal Chemistry, The University of Kansas, Lawrence, KS 66045, United States and [2]Department of Molecular Biosciences, The University of Kansas, Lawrence, KS 66045, United States

Email:
Blake R. Peterson[*] - brpeters@ku.edu

* Corresponding author

Keywords:
Caenorhabditis elegans; chemical biology; fission; fluorophores; fluorescence; fusion; imaging; in vivo; microscopy; mitochondria; model organisms; organelle; rhodamine; spectroscopy

Beilstein J. Org. Chem. **2012,** *8,* 2156–2165.
doi:10.3762/bjoc.8.243

Received: 29 September 2012
Accepted: 09 November 2012
Published: 11 December 2012

This article is part of the Thematic Series "Synthetic probes for the study of biological function".

Guest Editor: J. Aube

© 2012 Mottram et al; licensee Beilstein-Institut.
License and terms: see end of document.

Abstract

Mitochondria undergo dynamic fusion and fission events that affect the structure and function of these critical energy-producing cellular organelles. Defects in these dynamic processes have been implicated in a wide range of human diseases including ischemia, neurodegeneration, metabolic disease, and cancer. To provide new tools for imaging of mitochondria in vivo, we synthesized novel hydrophobic analogues of the red fluorescent dyes rhodamine B and rhodamine 101 that replace the carboxylate with a methyl group. Compared to the parent compounds, methyl analogues termed HRB and HR101 exhibit slightly red-shifted absorbance and emission spectra (5–9 nm), modest reductions in molar extinction coefficent and quantum yield, and enhanced partitioning into octanol compared with aqueous buffer of 10-fold or more. Comparison of living *C. elegans* (nematode roundworm) animals treated with the classic fluorescent mitochondrial stains rhodamine 123, rhodamine 6G, and rhodamine B, as well as the structurally related fluorophores rhodamine 101, and basic violet 11, revealed that HRB and HR101 are the most potent mitochondrial probes, enabling imaging of mitochondrial motility, fusion, and fission in the germline and other tissues by confocal laser scanning microscopy after treatment for 2 h at concentrations as low as 100 picomolar. Because transgenes are poorly expressed in the germline of these animals, these small molecules represent superior tools for labeling dynamic mitochondria in this tissue compared with the expression of mitochondria-targeted fluorescent proteins. The high bioavailabilty of these novel fluorescent probes may facilitate the identification of agents and factors that affect diverse aspects of mitochondrial biology in vivo.

Introduction

Fluorescent molecular probes represent critical tools for studies of chemical biology [1]. These compounds allow the creation of sensitive enzyme substrates, sensors of a wide variety of analytes, and specific markers of cellular organelles and other components. Although many structurally diverse fluorophores have been reported, many common fluorophores such as dianionic fluorescein (**1**, Figure 1) are defined by highly polar conjugated π systems. This high polarity confers substantial aqueous solubility, which is beneficial for some applications, such as protein labeling, but also results in low cellular permeability in assays involving living cells. Hydrophobic analogues of fluorescein such as Tokyo Green (**2**) [2], Pennsylvania Green (**3**) [3,4], and others [5] have been synthesized that replace a carboxylate with a methyl group or other less polar functionality. These hydrophobic analogues are generally more effective at penetrating cellular membranes [2,4].

Rhodamines such as rhodamine 123 (**4**), rhodamine B (**5**), basic violet 11 (**6**), rhodamine 6G (**7**), and rhodamine 101 (**8**) are renowned for their red-shifted fluorescence, photostability, and high quantum yields over a wide range of pH values (i.e., pH 4–10). These fluorophores penetrate cells more readily than analogous fluorescein derivatives, because the negative plasma membrane potential within the cytoplasm of cells (typically −30 to −60 mV) represents less of a barrier to entry to cations and zwitterions, compared with anionic compounds. Moreover, the delocalized cationic π-system of rhodamines further promotes their accumulation in energy-producing mitochondria, due to the even stronger negative potential across mitochondrial inner membranes (typically −120 to −180 mV, depending on cell type) [6-9]. This membrane potential is critical for ATP synthesis, and is generated by pumping of protons across the mitochondrial inner membrane by the respiratory chain. Many delocalized lipophilic cations preferentially accumulate in these organelles, and some rosamines, i.e., compounds that lack the carboxylate of rhodamines [10], have been shown to potently depolarize mitochondria. Elevated mitochondrial membrane potential is a hallmark of cancer cell lines [11,12], and depolarization of mitochondria by rhodamines and rosamines can confer selective anticancer activity both in vitro and in vivo in animal models [13].

Under nontoxic conditions, rhodamines and mitochondria-targeted fluorescent proteins have been extensively used for imaging and analysis of these organelles in cell culture, enabling studies of dynamic fusion and fission events that are critical for mitochondrial structure and function [8,14-17]. Agents and factors that affect fusion and fission of mitochondria are of substantial interest [18] because disregulation of these dynamic processes has been implicated in a wide range of human diseases, including ischemia, neurodegeneration, metabolic disease, and cancer [19,20].

In vivo, the pharmacokinetics of some rhodamines have been evaluated [21-23], and some have been used for imaging of mitochondria in the optically transparent model organism *C. elegans* (nematode worm) [24,25]. However, rhodamine 123 (**4**) [25], rhodamine B (**5**) [26], rhodamine 6G (**7**) [24], rhodamine

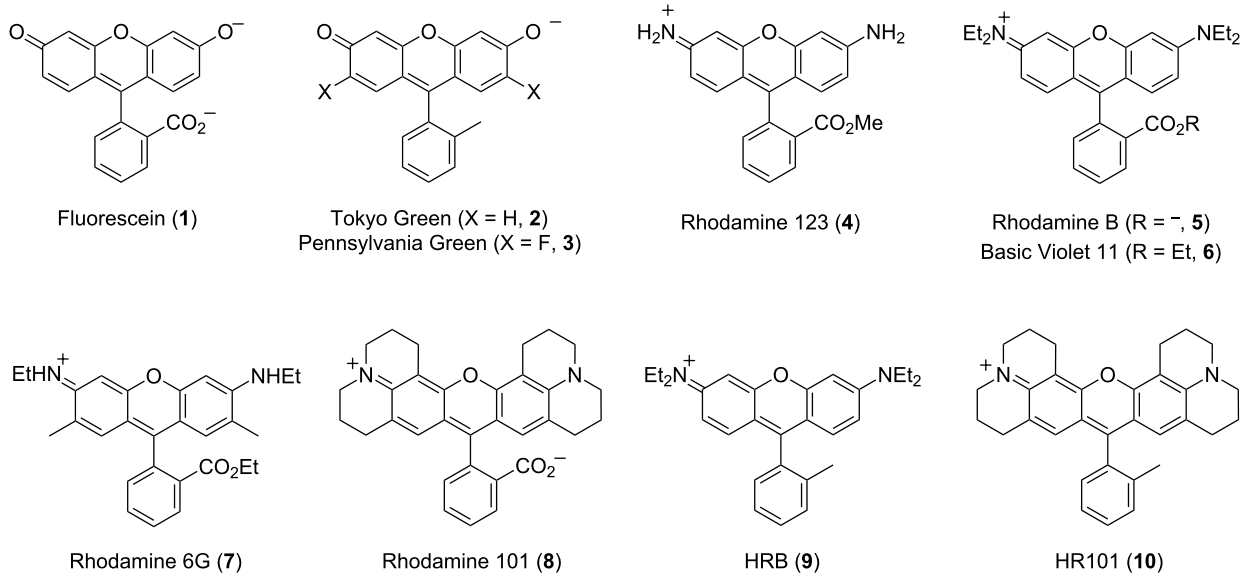


Figure 1: Structures of known fluorophores (**1**–**8**) and novel hydrophobic analogues of rhodamine (HRB, **9**, and HR101, **10**).

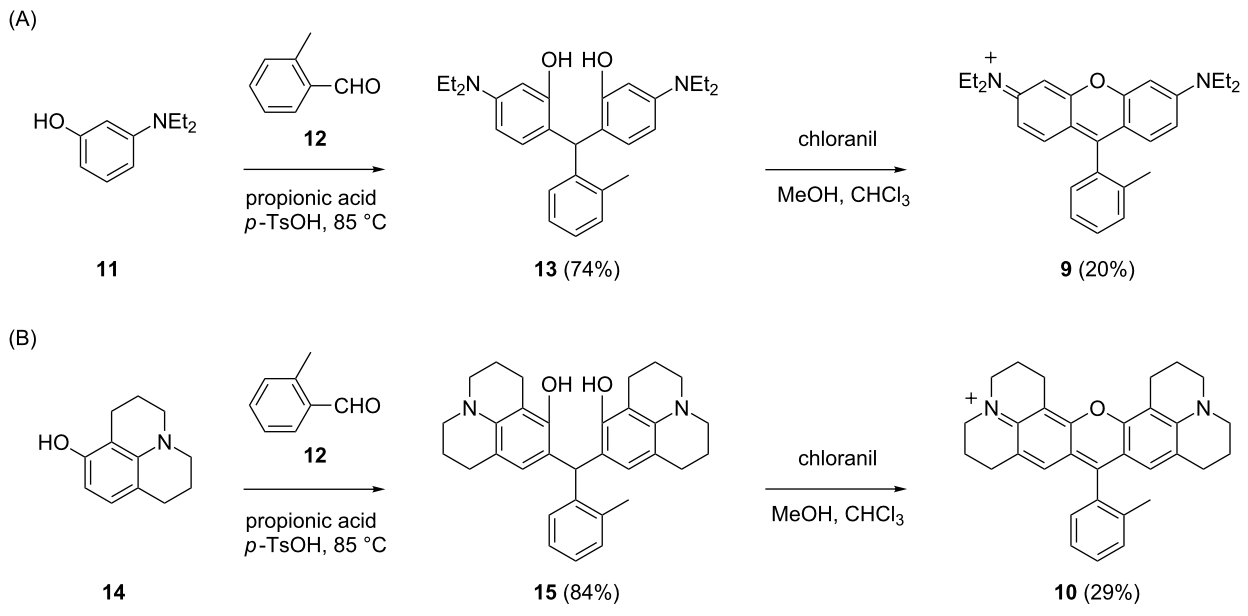
B hexyl ester [27], and tetramethylrhodamine ethyl ester [27] are of low potency in living *C. elegans*, typically requiring treatment times of up to 48 h [24], often at concentrations as high as 30 μM [27]. This low potency may have led some investigators interested in imaging fusion and fission of mitochondria in *C. elegans* [28] to forego the use of small-molecule fluorescent probes and instead to use time-consuming molecular biology methods to generate transgenic animals that express fluorescent proteins, such as mitoGFP, that are targeted to this organelle. In general, the choice to use small-molecule probes or molecular-biology-based approaches for these types of imaging applications can be challenging because of our limited understanding of the bioavailability and bioaccumulation of small molecules in this model organism [29-34]. In general, these soil-dwelling nematodes are considered to be substantially less pemeant to small molecules than other animals, and most drug-like compounds do not efficiently accumulate in worms [30]. Consequently, to observe biological effects, many pharmacological agents must be added to *C. elegans* at concentrations orders of magnitude higher than are used with mammalian cells in culture [35,36]. For some hydrophobic compounds, delivery systems [31,32] can improve their uptake.

We hypothesized that poor bioavailability of rhodamines in *C. elegans* may be responsible for their low potency as probes of mitochondria in this organism. We reasoned that the relatively high polarity of these charged compounds (e.g., LogD rhodamine 123 (**4**) = 0.53 [37], −0.62 [9]), offering functional groups for possible xenobiotic metabolism in the intestine or other tissues [29,30], may limit absorption. Rhodamine esters such as **4**, **6**, and **7** may also be substrates of esterases [38] in vivo, resulting in the production of more polar fluorophores that may be inefficiently absorbed. To test this hypothesis, we synthesized novel hydrophobic analogues of rhodamine B (**5**) and rhodamine 101 (**8**) that replace the carboxylate with a methyl group (Figure 1). The resulting analogues, termed HRB **9** and HR101 **10**, allowed evaluation of how subtle changes in chemical structure impact photophysical and physicochemical properties and the utility of rhodamines and analogues for imaging mitochondria in *C. elegans*. These studies revealed that the hydrophobic rosamines HRB **9** and HR101 **10** represent highly potent and selective fluorescent probes of these organelles. Treatment of *C. elegans* with these compounds for as little as two hours at concentrations as low as 100 pM enables selective imaging of mitochondria in vivo, including visualization of the dynamics of fusion and fission of these organelles in the germline of living animals.

Results and Discussion

Synthesis of fluorophores

As shown in Scheme 1, the triarylmethane scaffolds of HRB **9** and HR101 **10** were synthesized by condensation of the corresponding dialkyaminophenol with *o*-tolualdehyde (**12**) [39]. Oxidative cyclization of triarylmethanes with the quinone oxidant chloranil provided **9** and **10** in modest yield. 8-Hydroxyjulolidine (**14**) for synthesis of HR101 **10** was either purchased commercially or prepared as previously described [40].



Scheme 1: Synthesis of the HRB **9** and HR101 **10** fluorophores.

Photophysical and physicochemical properties

The absorbance (panel A) and fluorescence emission (panel B) spectra of fluorophores **4**, **5**, and **8**–**10** are shown in Figure 2.

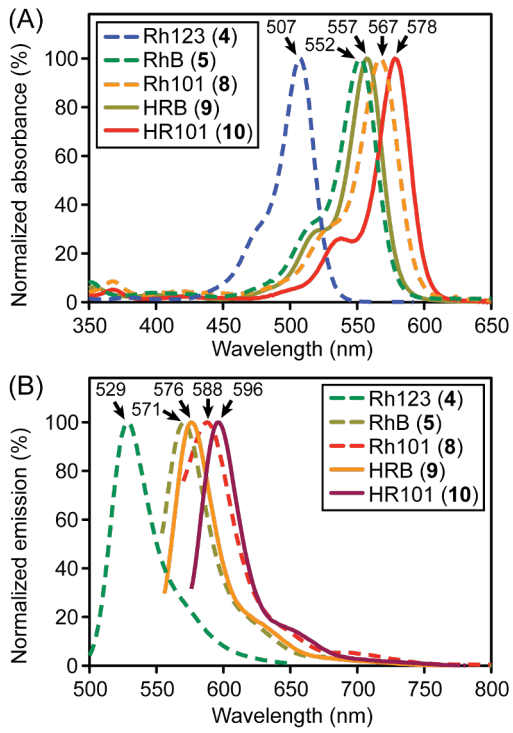


Figure 2: Normalized absorbance (Panel A) and fluorescence emission (Panel B) spectra. Fluorophores were analyzed at 10 μM (absorbance) or 5 nM (fluorescence) in MeOH. The spectra for rhodamine 123 (**4**) in MeOH were downloaded from a publically accessible database [41]. Maximum absorbance and emission wavelengths are indicated with arrows.

The red-shifted spectra of HR101 **10** compared with HRB **9** can be explained by greater delocalization of the lone pairs on nitrogen due to restricted rotation about C–N bonds conferred by the fused rings of **10**. By using the method of Williams [42], the quantum yields of **9** and **10** were determined relative to rhodamine B (**5**) and rhodamine 6G (**7**, Figure 3, panels A and B), and the extinction coefficients of these compounds were quantified (Figure 3, panel C). The replacement of the carboxylate of rhodamine B (**5**) and rhodamine 101 (**8**) with a methyl group slightly red shifted the absorbance and emission spectra in methanol (5 nm and 8 to 9 nm, respectively). This change also decreased the molar extinction coefficient, as compared with the reported [43] molar extinction coefficient of rhodamine B (**5**) of 106,000 M^{-1} cm^{-1} (at 545 nm in ethanol) with HRB (**9**, 83,000 M^{-1} cm^{-1} at 555 nm in methanol). Additionally, a modest reduction in quantum yield of ~0.3 for both fluorophores was observed.

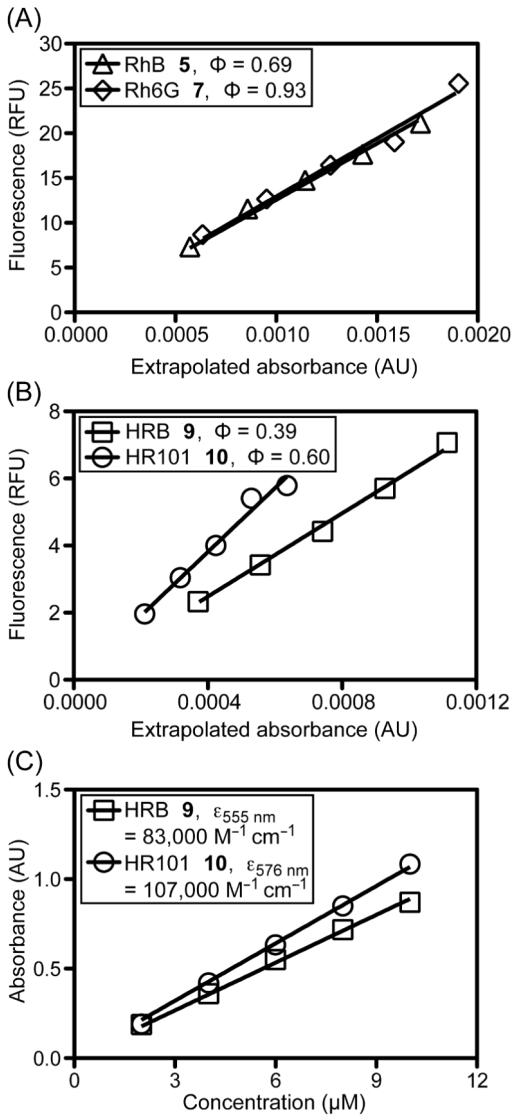


Figure 3: Linear regression used to determine spectroscopic parameters of HRB **9** and HR101 **10** in MeOH. Panels A and B: Determination of quantum yields relative to rhodamine B (**5**) [44] and rhodamine 6G (**7**) [45]. Panel C: Quantification of molar extinction coefficients.

Spectroscopic studies revealed that HRB **9** and HR101 **10** are not as bright as the carboxylate-containing parent dyes. However, because the fluorescence intensity is directly proportional to the product of the extinction coefficient and the quantum yield at excitation levels below saturation, these analogues represent very bright fluorophores for imaging applications. Potentially more important for activity in vivo, replacement of the carboxylate of rhodamine B (**5**) and rhodamine 101 (**8**) with a methyl group was predicted to substantially enhance hydrophobicity. Previously reported measurements of log *D* in octanol/neutral buffer solutions of rhodamine 123 (**4**), rhodamine B (**5**), and rhodamine 6G (**7**), measurements of the log *D* of rhodamine 101 (**8**), HRB **9**, and HR101 **10** by using a

fluorescence-based shake-flask method, and *c*·log *P* values for compounds **4**–**10** calculated by using a recent version of CambridgeSoft ChemBioDraw software, are shown in Table 1. Although some differences exist between the calculated and measured values, the relative trends illustrate how structural modifications of these compounds are likely to affect fluorophore solubility and cellular permeability.

Table 1: Partition constants of fluorophores.

Fluorophore	c·log P^a	log $D_{octanol/buffer}$
Rhodamine 123 (**4**)	1.5	0.5 [37], −0.6 [9]
Rhodamine B (**5**)	−1.1	2.3 [46]
Basic Violet 11 (**6**)	3.7	N.D.[b]
Rhodamine 6G (**7**)	6.5	2.1 [37]
Rhodamine 101 (**8**)	3.8	5.2[c]
HRB **9**	3.4	5.9[c]
HR101 **10**	8.6	6.2[c]

[a]Calculated with ChemBioDraw Ultra, version 12.0.3, from structures bearing functional groups at ionization states predicted to dominate at pH 7 (as shown in Figure 1). [b]N.D. Not determined. [c]Determined in octanol/buffer$_{pH\ 7.4}$ by using a fluorescence-based shake-flask method.

Imaging of fluorophores in vivo by confocal microscopy

To visualize the absorption and distribution of synthetic rhodamines and analogues in vivo, living adult *C. elegans* were initially subjected to an acute treatment followed by confocal laser scanning microscopy of mechanically immobilized whole animals (20× objective). In contrast to previous reports where treatment with rhodamines for 36–48 h was required [24,26], treatment with HRB **9** and HR101 **10** yielded observable fluorescence in some animals within 30 min, with most animals becoming fluorescent within 2 h. In the assay shown in Figure 4, adult animals were treated with rhodamine 123 (**4**), rhodamine B (**5**), basic violet 11 (**6**), rhodamine 6G (**7**), rhodamine 101 (**8**), HRB (**9**), and HR101 (**10**) at identical fixed concentrations of 100 pM or 1 nM for 2 h. Among the fluorophores examined, HRB **9**, HR101 **10**, and basic violet 11 (**6**) showed the highest bioaccumulation, and the fluorescence of these three compounds could be detected at much lower concentrations than the more polar rhodamine 123 (**4**), rhodamine B (**5**), rhodamine 6G (**7**), and rhodamine 101 (**8**) fluorophores. Although basic violet 11 (**6**) was relatively potent, this compound appeared to be of low selectivity, staining multiple intracellular structures including membranes, mitochondria and nuclei, and occasionally was observed in the cytosol of cells of living animals. Unlike all of the other fluorophores tested, HRB **9** and HR101 **10** engendered strong fluorescence in vivo after 2 h at concentrations as low as 100 pM.

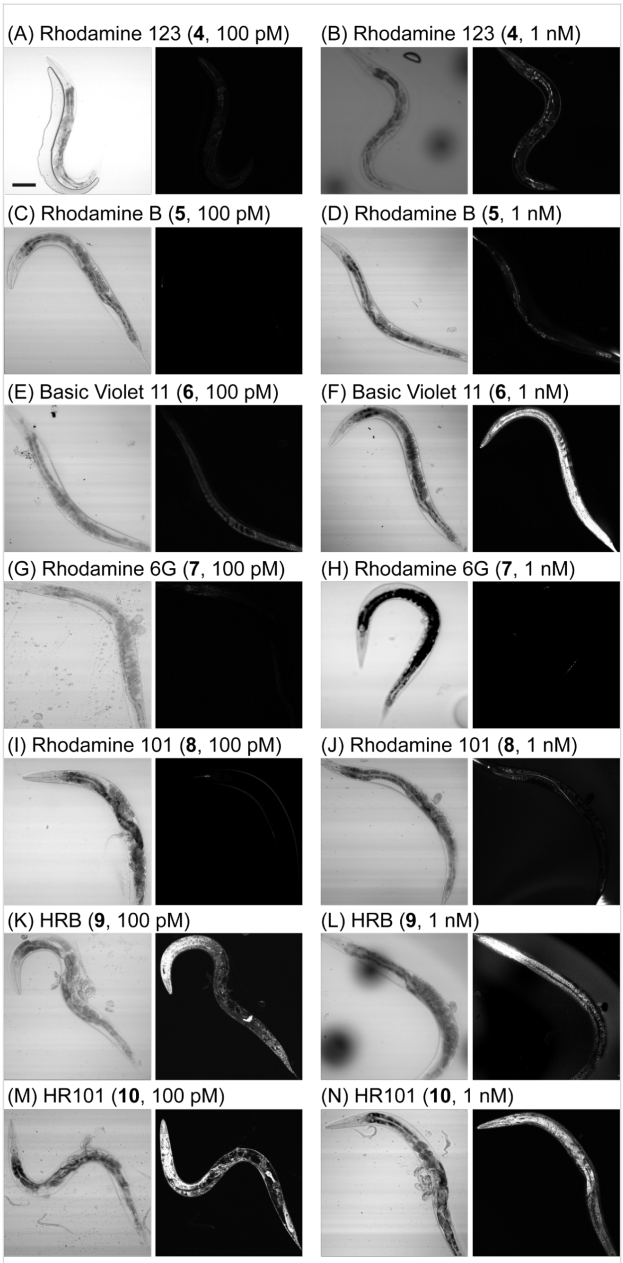


Figure 4: Differential interference contrast (DIC, left panels) and confocal laser scanning (right panels) micrographs of living *C. elegans* (20× objective) treated with synthetic compounds for 2 h followed by transfer to an imaging pad containing polystyrene beads for immobilization. The weak signal observed with rhodamine 123 at 1 nM (panel B) was independently identified as autofluorescence of the intestine. Animals are oriented with the anterior end (head) to the left and the ventral side (base) down and/or toward the left. Scale bar = 100 microns.

Higher magnification confocal microscopy (60× objective) using a variety of fluorophore concentrations revealed that most cells of living *C. elegans* accumulate the fluorophores rhodamine 6G (**7**), HRB **9**, and HR101 **10** after treatment for 2 h (Figure 5). Under these conditions, the more polar rhodamine 101 (**8**) was observed to be excluded from some

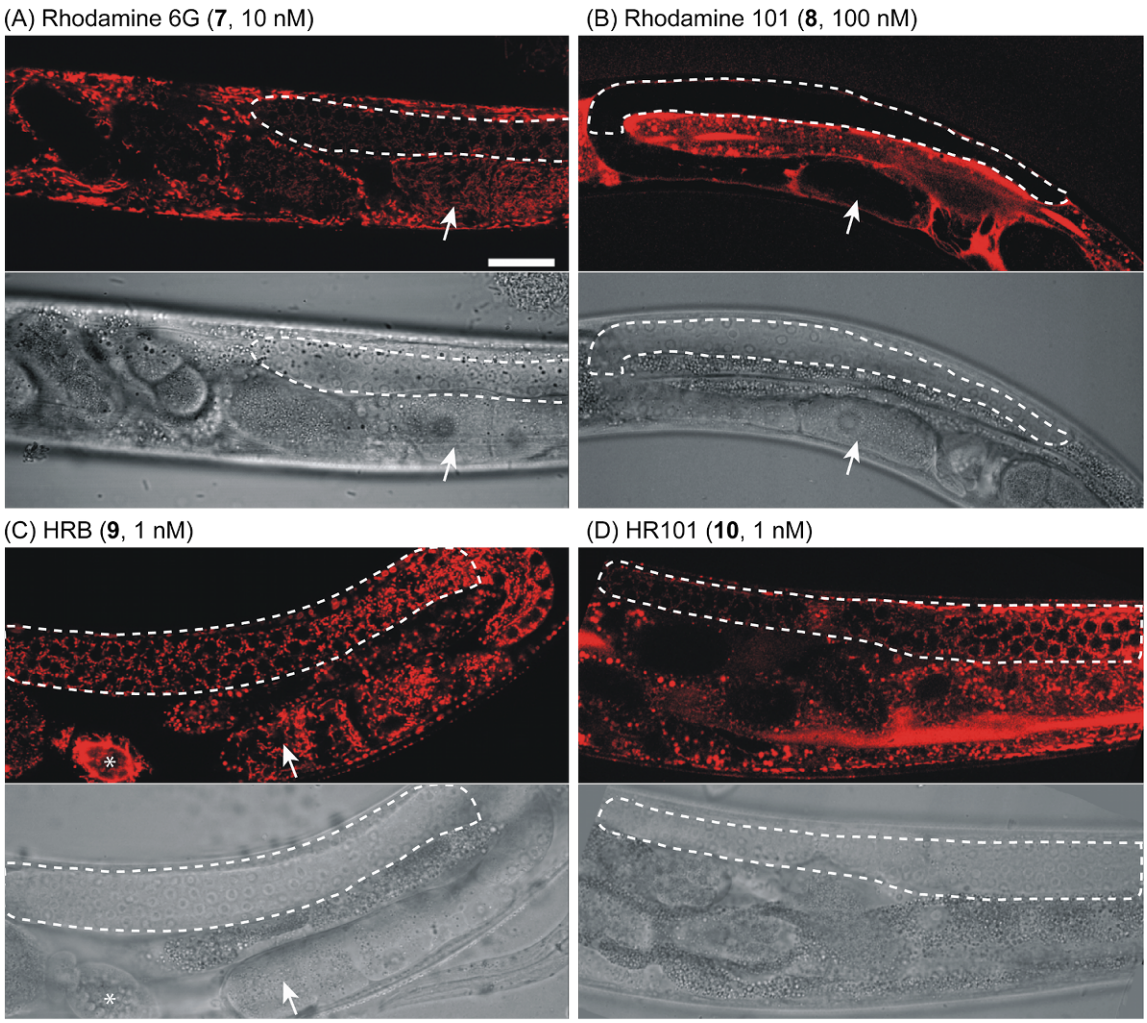


Figure 5: Panels A–D: High magnification confocal (top panels) and DIC micrographs (bottom panels, 60× objective) of young adult *C. elegans* after treatment with fluorophores for 2 h. The distal gonad containing the germline is shown marked by white dashed lines, the anterior of the animal is to the left, and ventral is down. In Panels C, and D, strong labeling of tubular mitochondria surrounding the mitotic nuclei of the gonad can be observed as well as strong staining of mitochondria within oocytes (white arrows indicate the most proximal oocyte, where visible) and the fibrous organelle (marked with an asterisk in panel C) of spermatheca. Scale bar = 25 microns.

cells and tissues. Labeling of specific organelles by rhodamine 6G (**7**), HRB **9**, and HR101 **10** was observed in hypodermis, muscle, neurons (data not shown), and the germline of these animals (Figure 5). Examination of the pattern of staining in the germline, part of the distal gonad containing a population of germ cells that lack complete borders, demonstrated that the more specific rhodamine derivatives illuminate tubular or punctate organelles (Figure 5 and Figure 6) that are highly motile (Figure 6 and movie, Supporting Information File 1), consistent with predominant accumulation in mitochondria. These structures elongated and contracted (see movie, Supporting Information File 1) and underwent fusion and fission (Figure 6) consistent with other studies of mitochondria in *C. elegans* [24]. Comparative imaging indicated that rhodamine 6G (**7**), HRB **9**, and HR101 **10** represent the most specific mitochondrial stains, with similar profiles of mitochondrial labeling within the germline, but the more hydrophobic fluorophores exhibited 10-fold higher potency. In contrast, the more polar rhodamine 101 (**8**), even at a 100-fold higher concentration compared with HRB **9** and HR101 **10**, did not penetrate into the germline under these conditions (Figure 5).

Conclusion

Genetically encoded fluorophores such as green fluorescent protein (GFP) have revolutionized cell biology and studies of physiological processes. However, fluorescent small-molecule probes continue to offer advantages for some imaging applications. One advantage illustrated here is the ability to examine

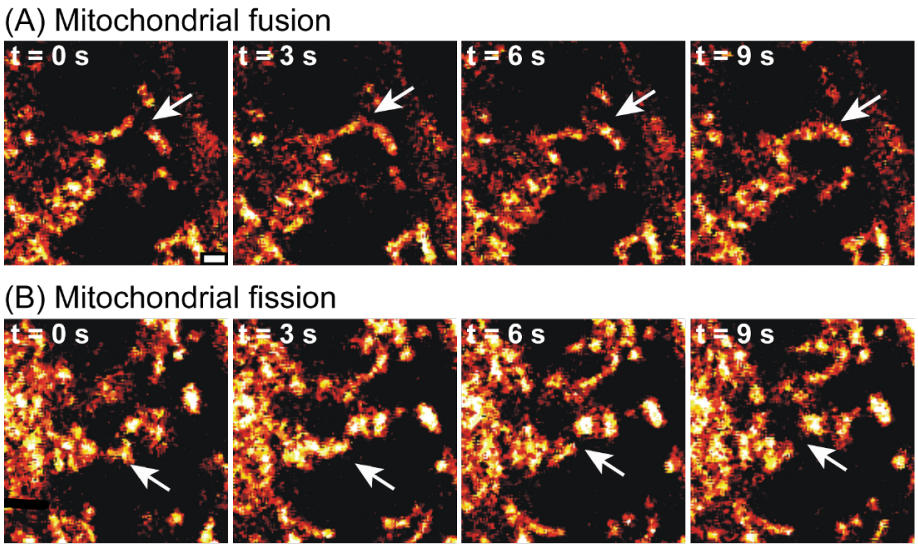


Figure 6: Images of mitochondrial motility, fusion, and fission in the germline of *C. elegans* extracted from confocal video microscopy. White arrows indicate fusion and fission of specific mitochondria. Prior to imaging, animals were treated with HRB (**9**, 1 nM, 2 h). Scale bar = 1 micron.

mitochondrial fusion and fission dynamics in the germline of living *C. elegans* after acute treatment with the hydrophobic rhodamine analogues HRB **9** and HR101 **10**. In this tissue, genetically encoded proteins are unsuitable for imaging of mitochondria, because transgenes are poorly expressed in the germline of *C. elegans*. However, genetically encoded fluorescent markers are advantageous in other contexts in that they can be more easily spatially confined to specific tissues of *C. elegans* by using cell-type specific promoters to drive gene expression. The rapid accumulation (within 2 h) and high potency (effective at ≥ 100 pM) of HRB **9** and HR101 **10** can be contrasted with previous studies [26] of rhodamine B (**5**) that employed treatment with 2 μM for 36 h to image mitochondria in the germline of *C. elegans*. These new probes rapidly accumulate in mitochondria at low concentrations because of their more favorable pharmacokinetic properties.

Animals treated with HRB **9** and HR101 **10** at 10 nM for 2 h were viable and exhibited grossly wild-type movement, suggesting that mitochondrial function remains largely if not completely intact during labeling with low concentrations of these probes. In contrast, treatment with much higher concentrations of these probes (e.g., ≥1 mM) under these conditions conferred some toxicity (data not shown). By comparison, treatment of *C. elegans* with the mitochondrial poison sodium azide at 25–50 mM rapidly causes paralysis and eventually causes death. Consequently, the high potency, low apparent toxicity, and rapid uptake of HRB **9** and HR101 **10** by *C. elegans* has the potential to be useful in a variety of applications. For screening purposes, these compounds may be used to rapidly examine multiple genotypes of interest without the need to introduce the genetically encoded sensor to each genetic background under investigation. Alternatively, a genetically encoded fluorescent protein may be complemented with these molecular probes to perform experiments such as fluorescence recovery after photobleaching (FRAP), where one of the markers remains unbleached. Chemical probes also have a variety of half-lives in vivo, a property that may be beneficial in some assays compared to long-lived fluorescent markers, such as mitoGFP and related proteins. High-content screening of chemical libraries against *C. elegans* treated with HRB **9** and HR101 **10** may facilitate the identification of inhibitors of mitochondrial fusion or fission effective in vivo, potentially enabling the discovery of new leads for the treatment of diseases associated with dysfunctional mitochondria.

A challenge associated with chemical biology studies in *C. elegans* is the low permeability of this animal to small molecules. For example, many bioactive compounds require at least a 10-fold higher dose to exhibit activity in *C. elegans* compared to other organisms [30], due to a number of physical and enzymatic barriers to entry of small molecules. On the exterior surface of *C. elegans*, the cuticular exoskeleton of these animals is a highly cross-linked carbohydrate-rich outer layer that limits access of molecules to the epidermis for potential uptake. For oral administration, molecules that are ingested by these animals must pass through an intestine replete with a wide range of xenobiotic detoxification enzymes, including

cytochrome P450s, phase-II transferases, and efflux pumps such as P-glycoprotein [35], to reach target tissues [29]. Thus, compounds such as HRB **9** and HR101 **10** that show high potency in this animal have passed through a stringent biological filter, providing a basis to justify studies in more complex and costly animal models. Fluorescence-imaging studies of small molecules in *C. elegans* have the potential to provide a deeper understanding of molecular modifications that facilitate the access of compounds to targets in vivo and may improve our ability to design more effective therapeutics and probes.

Experimental

Synthesis

Chemical reagents were obtained from Acros, Aldrich, Alfa Aesar, or TCI America. Solvents were from EM Science. Commercial grade reagents were used without further purification unless otherwise noted. Anhydrous solvents were obtained after passage through a drying column of a solvent-purification system from GlassContour (Laguna Beach, CA). All reactions were performed under an atmosphere of dry argon or nitrogen. Reactions were monitored by analytical thin-layer chromatography on plates coated with 0.25 mm silica gel 60 F_{254} (EM Science). TLC plates were visualized by UV irradiation (254 nm) or stained with a solution of phosphomolybdic acid and sulfuric acid in ethanol (1:1:20). Flash column chromatography employed ICN SiliTech Silica Gel (32–63 μm). Melting points were measured with a Thomas Hoover capillary melting point apparatus and are uncorrected. Infrared spectra were obtained with a Perkin Elmer 1600 Series FTIR. NMR spectra were obtained with Bruker CDPX-300, DPX-300, or DRX-400 instruments with chemical shifts reported in parts per million (ppm, δ) referenced to either $CDCl_3$ (^{1}H, 7.27 ppm; ^{13}C, 77.23 ppm), or DMSO-d_6 (^{1}H, 2.50 ppm; ^{13}C, 39.51 ppm). High-resolution mass spectra were obtained from mass spectrometry facilities at the University of Kansas or The Pennsylvania State University (ESI and TOF). Peaks are reported as *m*/*z*. Absorbance spectra were obtained with an Agilient 8453 UV–vis spectrophotometer. Fluorescence measurements employed either a PTi MD-5020 or a Perkin-Elmer LS55 fluorescence spectrometer with a 10 nm excitation slit width.

5-(Diethylamino)-2-{[4-(diethylamino)-2-hydroxyphenyl](2-methylphenyl)methyl}phenol (13): 3-Diethylaminophenol (**11**, 500 mg, 3.0 mmol) and *o*-tolualdehyde (**12**, 175 μL, 1.5 mmol) were dissolved in propionic acid (15 mL) and catalytic *p*-TsOH acid was added. The reaction was purged with argon and heated to 80–85 °C. The reaction was monitored by TLC by quenching aliquots (100 μL) in aqueous saturated sodium bicarbonate (200 μL), followed by extraction of the organic material with EtOAc (200 μL). When all starting materials had been consumed (5 h), the solution was cooled to 0 °C and poured into excess aqueous sodium acetate (3 M, 100 mL) to neutralize the propionic acid and precipitate the triarylmethane. The filtrate was collected by vacuum filtration, washed with copious amounts of water, and dried under reduced pressure to provide **13** (480 mg, 74%) as a tan solid. Mp 68–70 °CM; ^{1}H NMR (400 MHz, $CDCl_3$) δ 7.02 (m, 3H), 6.90 (d, J = 6.8 Hz, 1H), 6.51 (d, J = 8.3 Hz, 1H), 6.05 (m, 4H), 5.55 (s, 1H), 3.10 (q, J = 6.9 Hz, 8H), 2.10 (s, 3H), 0.98 (t, J = 6.9 Hz, 12H); ^{13}C NMR (75 MHz, $CDCl_3$) δ 154.8, 148.1, 140.8, 136.8, 130.4, 130.4, 130.2, 115.2, 105.0, 104.8, 100.2, 100.0, 44.2, 40.8, 19.4, 12.4; IR (film) ν_{max}: 3457, 2971, 1620, 1521 cm^{-1}; HRMS (ESI$^+$, TOF, *m*/*z*): $[M + H]^+$ calcd for $C_{28}H_{36}O_2N_2$, 433.2850; found, 433.2848.

6-(Diethylamino)-*N*,*N*-diethyl-9-(2-methylphenyl)-3*H*-xanthen-3-imine (HRB, 9): 5-(Diethylamino)-2-{[4-(diethylamino)-2-hydroxyphenyl](2-methylphenyl)methyl}phenol (**13**, 100 mg, 0.23 mmol) and chloranil (85 mg, 0.34 mmol) were dissolved in MeOH/$CHCl_3$ (1:1, 10 mL). The solution was stirred at 23 °C for 1 h. When the reaction was complete as evidenced by TLC, the solvent was removed under reduced pressure and the residue was applied directly to a column of silica gel. Flash chromatography (MeOH/$CHCl_3$ 1:9) afforded **9** (21 mg, 20%) as a purple film of the chloride salt. ^{1}H NMR (300 MHz, $CDCl_3$) δ 7.54–7.38 (m, 3H), 7.16–7.13 (m, 3H), 6.86–6.79 (m, 4H), 3.62 (q, J = 7.2 Hz, 8H), 2.06 (s, 3H), 1.33 (t, J = 7.1 Hz, 12H); ^{13}C NMR (75 MHz, $CDCl_3$) δ 157.9, 157.8, 155.6, 135.8, 131.6, 131.4, 130.7, 130.1, 128.7, 126.1, 114.0, 113.4, 96.5, 46.0, 19.5, 12.4; IR (film) ν_{max}: 2981, 1590, 1179 cm^{-1}; HRMS (ESI$^+$, TOF, *m*/*z*): $[M]^+$ calcd for $C_{28}H_{33}ON_2$, 413.2587; found, 413.2583.

9,9'-[(2-Methylphenyl)methylene]bis(2,3,6,7-tetrahydro-1*H*,5*H*-pyrido[3,2,1-*ij*]quinolin-8-ol) (15): 8-Hydroxyjulolidine (**14**, 500 mg, 2.6 mmol) and *o*-tolualdehyde (**12**, 154 μL, 1.3 mmol) were dissolved in propionic acid (15 mL) and catalytic *p*-TsOH acid was added. The reaction was performed as described for the preparation of **13** to afford **15** (525 mg, 84%) as a gray solid. Mp 170–174 °C; ^{1}H NMR (400 MHz, $CDCl_3$) δ 7.12–7.04 (m, 3H), 6.73 (d, J_1 = 7.5 Hz, 1H), 6.34 (3, 2H), 6.02 (s, 1H), 3.35 (m, 4H), 3.24 (m, 4H), 2.69 (m, 8H), 2.12 (s, 3H), 2.10 (m, 8H); ^{13}C NMR (75 MHz, $CDCl_3$) δ 150.3, 139.8, 136.1, 132.5, 129.8, 127.9, 127.7, 125.8, 125.0, 119.6, 116.6, 52.1, 51.5, 39.9, 24.8, 20.1, 19.7, 19.1, 18.5 (× 2); IR (film) ν_{max}: 3270, 2953, 1673, 1471 cm^{-1}; HRMS (ESI$^+$, TOF, *m*/*z*): $[M + H]^+$ calcd for $C_{32}H_{36}O_2N_2$, 481.2850; found, 481.2875.

16-(2-Methylphenyl)-3-oxa-9,23-diazaheptacyclo-[17.7.1.1$^{\{5,9\}}$.0$^{\{2,17\}}$.0$^{\{4,15\}}$.0$^{\{23,27\}}$.0$^{\{13,28\}}$]octacosa-1(27),2(17),4,9(28),13,15,18-heptaen-9-ium (HR101, 10): 9,9'-[(2-Methylphenyl)methylene]bis(2,3,6,7-tetrahydro-1*H*,5*H*-

pyrido[3,2,1-*ij*]quinolin-8-ol) (**15**, 91 mg, 0.19 mmol) and chloranil (69 mg, 0.28 mmol) in MeOH/$CHCl_3$ (1:1, 10 mL) were stirred at 23 °C for 1 h. When the reaction had been complete as evidenced by TLC, the solvent was removed under reduced pressure, and the residue was applied directly to a column of silica gel. Flash chromatography (MeOH/$CHCl_3$, 1:9) afforded **10** (27 mg, 29%) as a purple film of the chloride salt. ^{1}H NMR (400 MHz, $CDCl_3$) δ 7.44–7.25 (m, 3H), 7.07 (d, J = 6.9 Hz, 1H), 6.56 (s, 2H), 3.41 (m, 8H), 2.97 (t, J = 6.2 Hz, 4H), 2.58 (t, J = 5.9 Hz, 4H), 2.01 (p, J = 6.3 Hz, 4H), 1.90 (s, 3H), 1.84 (p, J = 5.3 Hz, 4H); ^{13}C NMR (75 MHz, $CDCl_3$) δ 156.0, 153.6, 152.6, 137.2, 133.9, 131.6, 130.2, 127.1 (× 2), 125.5, 113.9, 106.7, 51.8, 51.4, 28.5, 21.7, 20.9, 20.8, 19.6; IR (film) ν_{max}: 2923, 1682, 1596, 1298 cm^{-1}; HRMS (ESI$^+$, TOF, *m*/*z*): $[M]^+$ calcd for $C_{32}H_{33}ON_2$, 461.2587; found, 461.2580.

Determination of log *D* values

Values of log *D* were measured by dissolution of solids in 1:1 octanol/phosphate buffer (4 mL total volume, 5 mM phosphate, pH 7.4) to provide 5 mM solutions of the fluorophore. Samples were shaken for 24 h at 25 °C to equilibrate. The top and bottom 1 mL fractions were isolated and centrifuged at 15,000 rpm (no precipitate was observed for any of the samples). Aliquots of these fractions were diluted in octanol (derived from the top fraction) or buffer (derived bottom fraction) to generate stock solutions (10×) appropriate for analysis. These stock solutions were further diluted 10-fold and analyzed in a solvent mixture comprising ethanol (80%), octanol (10%), and phosphate buffer (10%, pH 7.4). The ratio of fluorescence emission at λ_{max} was used to calculate log *D*.

Biological evaluation

The N2 strain of *C. elegans* was cultured as described [47] and maintained at 20–22.5 °C. Fluorophores were added to normal growth media (NMG) liquid (at 45–55 °C), poured into Petri dishes (60 mm), and allowed to cool until solidified. Fluorophores, were prepared fresh as DMSO stocks (1000×) from dry powders and used immediately. The final amount of DMSO exposed to animals did not exceed 0.1%. Storage of fluorophores as frozen solutions in DMSO is not recommended and can result in loss of potency. Prepared media were seeded with the normal food source of OP50 *E. coli* and incubated overnight at room temperature to dry. Adult *C. elegans* animals (10–20) were added to the media and allowed to feed freely for 2 h prior to imaging. Animals were transferred and imaged on 10% agarose pads in the presence of 2.5% (w/v) polystyrene beads (50 nm, Bangs Laboratory) to prevent movement. Imaging employed an Olympus FV1000 laser scanning confocal microscope and Fluoview software. Images were acquired with Planapochromat objectives.

Supporting Information

Supporting Information File 1

Supplementary time-lapse confocal microscopy video showing dynamics of mitochondrial fusion and fission in a living adult *C. elegans* animal imaged after treatment with HRB (**9**, 1 nM) for 2 h followed by immobilization on an agarose pad containing polystyrene beads. Frames were acquired every 3.3 seconds, and are animated at 3 frames per second. The animal in the video is oriented such that the ventral side is left and the anterior is toward the top of the frame. The distal (mitotic) gonad arm is on the right half of the animal, whereas the proximal oocytes are on the left. Dynamic motility of mitochondria in the gonad including elongation, collapse, fusion, and fission can be observed.
[http://www.beilstein-journals.org/bjoc/content/supplementary/1860-5397-8-243-S1.mov]

Acknowledgements

We thank the NIH (R01-CA83831, RC1-GM091086, and P20-GM103638) for financial support. S.F. thanks the NIH for an IRACDA postdoctoral fellowship.

References

1. Lavis, L. D.; Raines, R. T. *ACS Chem. Biol.* **2008,** *3,* 142–155. doi:10.1021/cb700248m
2. Urano, Y.; Kamiya, M.; Kanda, K.; Ueno, T.; Hirose, K.; Nagano, T. *J. Am. Chem. Soc.* **2005,** *127,* 4888–4894. doi:10.1021/ja043919h
3. Mottram, L. F.; Boonyarattanakalin, S.; Kovel, R. E.; Peterson, B. R. *Org. Lett.* **2006,** *8,* 581–584. doi:10.1021/ol052655g
4. Mottram, L. F.; Maddox, E.; Schwab, M.; Beaufils, F.; Peterson, B. R. *Org. Lett.* **2007,** *9,* 3741–3744. doi:10.1021/ol7015093
5. Koide, K.; Song, F.; de Groh, E. D.; Garner, A. L.; Mitchell, V. D.; Davidson, L. A.; Hukriede, N. A. *ChemBioChem* **2008,** *9,* 214–218. doi:10.1002/cbic.200700565
6. Nicholls, D. G. *Eur. J. Biochem.* **1974,** *50,* 305–315. doi:10.1111/j.1432-1033.1974.tb03899.x
7. Chen, L. B. *Annu. Rev. Cell Biol.* **1988,** *4,* 155–181. doi:10.1146/annurev.cb.04.110188.001103
8. Perry, S. W.; Norman, J. P.; Barbieri, J.; Brown, E. B.; Gelbard, H. A. *BioTechniques* **2011,** *50,* 98–115. doi:10.2144/000113610
9. Belostotsky, I.; da Silva, S. M.; Paez, M. G.; Indig, G. L. *Biotech. Histochem.* **2011,** *86,* 302–314. doi:10.3109/10520295.2010.483656
10. Wu, L.; Burgess, K. *J. Org. Chem.* **2008,** *73,* 8711–8718. doi:10.1021/jo800902j
11. Modica-Napolitano, J. S.; Aprille, J. R. *Adv. Drug Delivery Rev.* **2001,** *49,* 63–70. doi:10.1016/S0169-409X(01)00125-9
12. Lim, S. H.; Wu, L.; Burgess, K.; Lee, H. B. *Anti-Cancer Drugs* **2009,** *20,* 461–468. doi:10.1097/CAD.0b013e32832b7bee
13. Smith, R. A. J.; Hartley, R. C.; Murphy, M. P. *Antioxid. Redox Signaling* **2011,** *15,* 3021–3038. doi:10.1089/ars.2011.3969

14. Lemasters, J. J.; Ramshesh, V. K. *Methods Cell Biol.* **2007,** *80,* 283–295. doi:10.1016/S0091-679X(06)80014-2
15. Huang, H.; Frohman, M. A. *Methods Cell Biol.* **2012,** *108,* 131–145. doi:10.1016/B978-0-12-386487-1.00007-9
16. Liu, X. G.; Weaver, D.; Shirihai, O.; Hajnoczky, G. *EMBO J.* **2009,** *28,* 3074–3089. doi:10.1038/emboj.2009.255
17. Chan, D. C. *Annu. Rev. Cell Dev. Biol.* **2006,** *22,* 79–99. doi:10.1146/annurev.cellbio.22.010305.104638
18. Wang, D.; Wang, J.; Bonamy, G. M. C.; Meeusen, S.; Brusch, R. G.; Turk, C.; Yang, P.; Schultz, P. G. *Angew. Chem., Int. Ed.* **2012,** *51,* 9302–9305. doi:10.1002/anie.201204589
19. Chan, D. C. *Cell* **2006,** *125,* 1241–1252. doi:10.1016/j.cell.2006.06.010
20. Corrado, M.; Scorrano, L.; Campello, S. *Int. J. Cell Biol.* **2012,** *2012,* 729290. doi:10.1155/2012/729290
21. Sweatman, T. W.; Seshadri, R.; Israel, M. *Cancer Chemother. Pharmacol.* **1990,** *27,* 205–210. doi:10.1007/BF00685714
22. Elliott, G. S.; Mason, R. W.; Edwards, I. R. J. *J. Toxicol., Clin. Toxicol.* **1990,** *28,* 45–59. doi:10.3109/15563659008993475
23. Cygalova, L. H.; Hofman, J.; Ceckova, M.; Staud, F. *J. Pharmacol. Exp. Ther.* **2009,** *331,* 1118–1125. doi:10.1124/jpet.109.160564
24. Labrousse, A. M.; Zappaterra, M. D.; Rube, D. A.; van der Bliek, A. M. *Mol. Cell* **1999,** *4,* 815–826. doi:10.1016/S1097-2765(00)80391-3
25. Kanazawa, T.; Zappaterra, M. D.; Hasegawa, A.; Wright, A. P.; Newman-Smith, E. D.; Buttle, K. F.; McDonald, K.; Mannella, C. A.; van der Bliek, A. M. *PLoS Genet.* **2008,** *4,* e1000022. doi:10.1371/journal.pgen.1000022
26. Deng, X.; Yin, X.; Allan, R.; Lu, D. D.; Maurer, C. W.; Haimovitz-Friedman, A.; Fuks, Z.; Shaham, S.; Kolesnick, R. *Science* **2008,** *322,* 110–115. doi:10.1126/science.1158111
27. Jagasia, R.; Grote, P.; Westermann, B.; Conradt, B. *Nature* **2005,** *433,* 754–760. doi:10.1038/nature03316
28. Lu, Y.; Rolland, S. G.; Conradt, B. *Proc. Natl. Acad. Sci. U. S. A.* **2011,** *108,* E813–E822. doi:10.1073/pnas.1103218108
29. Lindblom, T. H.; Dodd, A. K. *J. Exp. Zool., Part A* **2006,** *305,* 720–730. doi:10.1002/jez.a.324
30. Burns, A. R.; Wallace, I. M.; Wildenhain, J.; Tyers, M.; Giaever, G.; Bader, G. D.; Nislow, C.; Cutler, S. R.; Roy, P. J. *Nat. Chem. Biol.* **2010,** *6,* 549–557. doi:10.1038/nchembio.380
31. Kashima, N.; Fujikura, Y.; Komura, T.; Fujiwara, S.; Sakamoto, M.; Terao, K.; Nishikawa, Y. *Biogerontology* **2012,** *13,* 337–344. doi:10.1007/s10522-012-9378-3
32. Kokel, D.; Li, Y.; Qin, J.; Xue, D. *Nat. Chem. Biol.* **2006,** *2,* 338–345. doi:10.1038/nchembio791
33. Grünz, G.; Haas, K.; Soukup, S.; Klingenspor, M.; Kulling, S. E.; Daniel, H.; Spanier, B. *Mech. Ageing Dev.* **2012,** *133,* 1–10. doi:10.1016/j.mad.2011.11.005
34. Surco-Laos, F.; Cabello, J.; Gómez-Orte, E.; González-Manzano, S.; González-Paramás, A. M.; Santos-Buelga, C.; Dueñas, M. *Food Funct.* **2011,** *2,* 445–456. doi:10.1039/c1fo10049a
35. Broeks, A.; Janssen, H. W.; Calafat, J.; Plasterk, R. H. *EMBO J.* **1995,** *14,* 1858–1866.
36. Kwok, T. C. Y.; Ricker, N.; Fraser, R.; Chan, A. W.; Burns, A.; Stanley, E. F.; McCourt, P.; Cutler, S. R.; Roy, P. J. *Nature* **2006,** *441,* 91–95. doi:10.1038/nature04657
37. Lampidis, T. J.; Castello, C.; del Giglio, A.; Pressman, B. C.; Viallet, P.; Trevorrow, K. W.; Valet, G. K.; Tapiero, H.; Savaraj, N. *Biochem. Pharmacol.* **1989,** *38,* 4267–4271. doi:10.1016/0006-2952(89)90525-X
38. Satoh, T.; Hosokawa, M. *Annu. Rev. Pharmacol. Toxicol.* **1998,** *38,* 257–288. doi:10.1146/annurev.pharmtox.38.1.257
39. Martin, V. V.; Rothe, A.; Gee, K. R. *Bioorg. Med. Chem. Lett.* **2005,** *15,* 1851–1855. doi:10.1016/j.bmcl.2005.02.017
40. Kauffman, J. M.; Imbesi, S. J.; Aziz, M. A. *Org. Prep. Proced. Int.* **2001,** *33,* 603–613. doi:10.1080/00304940109356622
41. Fluorophores.org, Database of Fluorescent Dyes and Applications. http://www.fluorophores.tugraz.at (accessed Nov 19, 2012).
42. Williams, A. T. R.; Winfield, S. A.; Miller, J. N. *Analyst* **1983,** *108,* 1067–1071. doi:10.1039/an9830801067
43. Dixon, J. M.; Taniguchi, M.; Lindsey, J. S. *Photochem. Photobiol.* **2005,** *81,* 212–213. doi:10.1562/2004-11-06-TSN-361.1
44. Velapoldi, R. A.; Tonnesen, H. H. *J. Fluoresc.* **2004,** *14,* 465–472. doi:10.1023/B:JOFL.0000031828.96368.c1
45. Magde, D.; Wong, R.; Seybold, P. G. *Photochem. Photobiol.* **2002,** *75,* 327–334. doi:10.1562/0031-8655(2002)075<0327:FQYATR>2.0.CO;2
46. Toropainen, E.; Ranta, V. P.; Talvitie, A.; Suhonen, P.; Urtti, A. *Invest. Ophthalmol. Visual Sci.* **2001,** *42,* 2942–2948.
47. Brenner, S. *Genetics* **1974,** *77,* 71–94.

License and Terms

This is an Open Access article under the terms of the Creative Commons Attribution License (http://creativecommons.org/licenses/by/2.0), which permits unrestricted use, distribution, and reproduction in any medium, provided the original work is properly cited.

The license is subject to the *Beilstein Journal of Organic Chemistry* terms and conditions: (http://www.beilstein-journals.org/bjoc)

The definitive version of this article is the electronic one which can be found at: doi:10.3762/bjoc.8.243

Beilstein Journal of Organic Chemistry

Chemical–biological characterization of a cruzain inhibitor reveals a second target and a mammalian off-target

Jonathan W. Choy[1,2,3], Clifford Bryant[1,2], Claudia M. Calvet[4,5,6], Patricia S. Doyle[4,5], Shamila S. Gunatilleke[4,5], Siegfried S. F. Leung[2], Kenny K. H. Ang[1,2], Steven Chen[1,2], Jiri Gut[4,5], Juan A. Oses-Prieto[2], Jonathan B. Johnston[2], Michelle R. Arkin[1,2,4], Alma L. Burlingame[2], Jack Taunton[3], Matthew P. Jacobson[2], James M. McKerrow[4,5], Larissa M. Podust[4,5] and Adam R. Renslo[*1,2,4]

Full Research Paper

Open Access

Address:
[1]Small Molecule Discovery Center, University of California San Francisco, 1700 4th Street, San Francisco, CA, 94158, USA, [2]Department of Pharmaceutical Chemistry, University of California San Francisco, 1700 4th Street, San Francisco, CA, 94158, USA, [3]Department of Cellular and Molecular Pharmacology, University of California San Francisco, 1700 4th Street, San Francisco, CA, 94158, USA, [4]Center for Discovery and Innovation in Parasitic Diseases, University of California San Francisco, 1700 4th Street, San Francisco, CA, 94158, USA, [5]Department of Pathology, University of California San Francisco, 1700 4th Street, San Francisco, CA, 94158, USA and [6]Cellular Ultra-Structure Laboratory, Oswaldo Cruz Institute (IOC), FIOCRUZ, Rio de Janeiro, RJ, Brazil 21040-362

Email:
Adam R. Renslo[*] - adam.renslo@ucsf.edu

* Corresponding author

Keywords:
activity-based probes; Chagas' disease; cruzain; CYP51; 14-α-demethylase; hybrid drugs; *Trypanosoma cruzi*

Beilstein J. Org. Chem. **2013,** *9,* 15–25.
doi:10.3762/bjoc.9.3

Received: 01 October 2012
Accepted: 27 November 2012
Published: 04 January 2013

This article is part of the Thematic Series "Synthetic probes for the study of biological function".

Guest Editor: J. Aube

© 2013 Choy et al; licensee Beilstein-Institut.
License and terms: see end of document.

Abstract

Inhibition of the *Trypanosoma cruzi* cysteine protease cruzain has been proposed as a therapeutic approach for the treatment of Chagas' disease. Among the best-studied cruzain inhibitors to date is the vinylsulfone K777 (**1**), which has proven effective in animal models of Chagas' disease. Recent structure–activity studies aimed at addressing potential liabilities of **1** have now produced analogues such as *N*-[(2*S*)-1-[[(*E*,3*S*)-1-(benzenesulfonyl)-5-phenylpent-1-en-3-yl]amino]-3-(4-methylphenyl)-1-oxopropan-2-yl]pyridine-4-carboxamide (**4**), which is trypanocidal at ten-fold lower concentrations than for **1**. We now find that the trypanocidal activity of **4** derives primarily from the inhibition of *T. cruzi* 14-α-demethylase (*Tc*CYP51), a cytochrome P450

enzyme involved in the biosynthesis of ergosterol in the parasite. Compound **4** also inhibits mammalian CYP isoforms but is trypanocidal at concentrations below those required to significantly inhibit mammalian CYPs in vitro. A chemical-proteomics approach employing an activity-based probe derived from **1** was used to identify mammalian cathepsin B as a potentially important off-target of **1** and **4**. Computational docking studies and the evaluation of truncated analogues of **4** reveal structural determinants for *Tc*CYP51 binding, information that will be useful in further optimization of this new class of inhibitors.

Introduction

The kinetoplastid protozoan *Trypanosoma cruzi* is the causative agent of Chagas' disease, a leading cause of heart failure in endemic regions of Latin America [1]. The parasite is transmitted by the reduviid bug and the disease manifests in an initial acute phase, followed by a chronic phase that can last decades and typically culminates in heart failure. The existing treatment for Chagas' disease involves extended therapy with nifurtimox or benznidazole, both of which are associated with undesirable side-effects and have limited efficacy against the chronic stage of the disease [2,3]. This situation has spurred the search for more effective and better tolerated therapeutics [4-6]. Among a number of drug targets being investigated are cruzain [7-10], the major cysteine protease active in the parasite, and *T. cruzi* CYP51 (*Tc*CYP51), a 14-α-demethylase enzyme of the cytochrome P450 family required for ergosterol biosynthesis [11-14]. *Tc*CYP51 is analogous to the fungal enzyme targeted by the azole class of antifungals, and the observation that some of these drugs (e.g., posaconazole) also inhibit *Tc*CYP51 has led to their preclinical and clinical investigation as potential new treatments for Chagas' disease [2,15,16].

Cruzain is a cathepsin-L-like protease of the papain family thought to be important for intracellular replication and differentiation of the *T. cruzi* parasite [17]. A variety of small-molecule cruzain inhibitors have been described, the majority of which act irreversibly by reaction with the catalytic cysteine in the enzyme active site [18-27]. One of the earliest cruzain inhibitors identified and perhaps the best studied to date is the vinysulfone K777 (**1**, Figure 1). This irreversible inhibitor has demonstrated efficacy in animal models of Chagas' disease [28,29] and continues to undergo preclinical evaluation leading towards a possible human clinical trial.

Despite many favorable properties, some aspects of **1** are suboptimal from a drug-development perspective. For example, compound **1** is known to be a mechanism-based (irreversible)

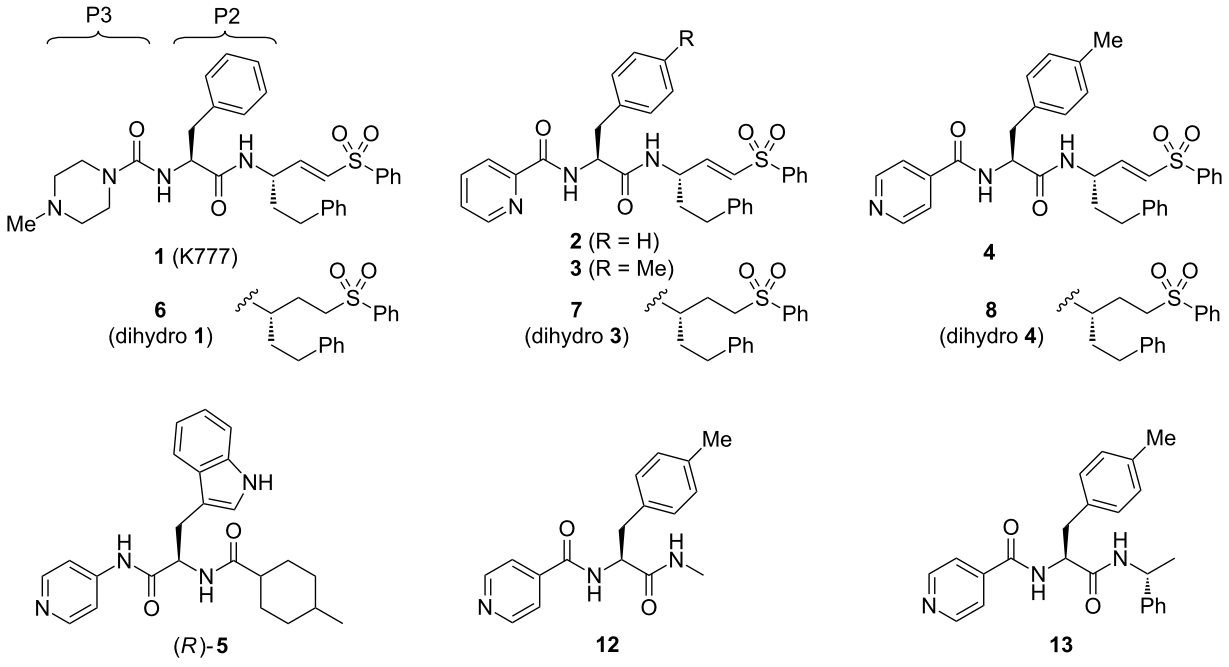


Figure 1: Chemical structures of vinylsulfone-based cruzain inhibitors **1**–**4**, known *Tc*CYP51 inhibitor **5**, dihydro controls **6**–**8**, and truncated analogues **12** and **13**. The "P2" and "P3" side chains of **1** are labeled and bind, respectively, in the S2 and S3 sub-sites of the cruzain active site.

inhibitor of CYP3A4, an enzyme responsible for the metabolism of many drugs, including **1** itself [30]. In pharmacokinetic studies, compound **1** exhibits nonlinear exposure with escalating dose and is known to be a substrate of the drug transporter P-glycoprotein (P-gp). Finally, as a basic (protonatable) drug species, **1** could potentially accumulate in acidic lysosomes, where mammalian cathepsins (potential off-targets of **1**) are located. The issue of lysosomotropism figured prominently in the discovery and clinical development of cathepsin K inhibitors for osteoporosis. The first such inhibitor to successfully navigate human clinical trials is odanacatib, which was intentionally designed as a nonbasic drug species to minimize the potential for lysosomotropic behavior [31,32].

We sought to address the question of lysosomotropism by preparing analogues of **1** in which the basic piperazine substituent at "P3" (which binds the S3 subsite of cruzain) was replaced with nonbasic or weakly basic heterocycles. In our initial structure–activity study [21], we found that analogue **2** (Figure 1), bearing a 2-pyridylamide at the P3 position, possessed trypanocidal activity that was on par with **1** (Table 1). However, none of the nonbasic analogues examined proved superior to **1** and only 2-pyridyl analogues such as **2** and **3** appeared even comparable. We therefore turned to more dramatic structural alteration and successfully identified and structurally characterized a new nonpeptidic cruzain inhibitor chemotype [24]. Most recently, we returned to reinvestigate nonbasic analogues of **1** and now report that 4-pyridyl analogues such as **4** (Figure 1) are significantly more trypanocidal than **1** or **2**, and unexpectedly exert their trypanocidal effects primarily by inhibition of *Tc*CYP51 rather than cruzain.

Results and Discussion

Structure–activity studies

Our exploration of the P3 position in **1** included the evaluation of regioisomeric 2-, 3-, and 4-pyridyl congeners in the context of various P2 side chains. In many such analogue series, we found that regioisomeric analogues possessed similar cruzain activities in vitro, while the 4-pyridyl examples consistently demonstrated superior trypanocidal activity against cultured *T. cruzi* parasites. For example, 4-pyridyl analogues (e.g., **4**) exhibited sub-micromolar minimal trypanocidal concentration values (MTC = 0.6 μM) while the MTC values for 2-pyridyl (e.g., **3**) and 3-pyridyl analogues were typically ≈10 μM, which was similar to the MTC of **1** (Table 1). The MTC represents the minimum concentration of test compound required to completely clear *T. cruzi* parasites from J774 macrophage host cells over a 40-day experiment, with the test compound being administered during the initial 28 days.

The enhanced potency of 4-pyridyl analogues as compared to **1** or their regioisomeric analogues was not predictable on the basis of in vitro cruzain activity (Table 1). Nor could the trends be explained as an effect of lysosomotropism, since enhanced potency was observed only for the 4-pyridyl analogues and not for 2- or 3-pyridyl analogues, which have similar pK_a values.

Table 1: In vitro biochemical and cellular activities of test compounds and controls. (n.a. = not active (cruzain IC_{50} > 50 μM); BNZ = benzindazole; POSA = posaconazole).

compound	cruzain activity	*Tc*CYP51 activity		*T. cruzi* growth inhibition	
	k_{inact}/K_i ($s^{-1}\cdot M^{-1}$)	in vitro K_D (nM)	cellular activity (Y/N, conc.)[a]	MTC[b] (μM)	HCS[c] EC_{90} (μM)
1	118,000	>2,000	N (1.6 μM)	8	0.10
2	120,000	—	—	10	—
3	16,000	>2,000	N (2.0 μM)	8	1.85
4	67,300	≤5	Y (0.2 μM)	0.6	0.10
5	—	≤5	Y (5.0 μM)	≤10[d]	—
6	n.a.	>2,000	N (2.0 μM)	>10	>10
7	n.a.	>2,000	N (0.1 μM)	>10	>10
8	n.a.	≤5	Y (0.1 μM)	0.25	0.11
9	81,500	—	—	5[e]	0.017
12	n.a.	620 ± 260	—	>10	>10
13	n.a.	75 ± 26	—	1[f]	3.9
BNZ	—	—	—	10	7.2
POSA	—	≤5	Y (0.1 μM)	0.003	2.7

[a]Compound affects ergosterol biosynthesis at indicated concentration as determined by GC/MS analysis. [b]Minimum effective concentration that clears J774 host cells of parasites at day 40 of the experiment, following 28 days of treatment. [c]Concentration that reduces parasite load in C2C12 cells by 90% relative to untreated controls. [d]Concentrations lower than 10 μM were not examined. [e]Experiment performed in BESM host cell rather than J774 cells. [f]Read at day 12 following 7 days treatment.

Instead, we considered that additional target(s) may be responsible for the surprising potency of the 4-pyridyl analogues. Specifically, we were aware that a 4-pyridyl ring comprises the putative heme-binding moiety in a new class of *Tc*CYP51 inhibitors represented by compound **5** (Figure 1). Other structural similarities of **4** and **5** suggested that compound **4** could conceivably bind *Tc*CYP51.

To test the hypothesis that **4** may also target *Tc*CYP51, we examined the binding of this compound to *Tc*CYP51 using a UV–vis spectroscopic binding assay described previously [33]. Indeed, compound **4** bound *Tc*CYP51 with an estimated $K_D \leq 5$ nM, a value comparable to the binding affinity of the known *Tc*CYP51 inhibitor **5** [16]. 2-Pyridyl analogue **3** did not measurably bind *Tc*CYP51 ($K_D > 2{,}000$ nM, Table 1), whereas the corresponding 3-pyridyl congener (not shown) binds about 100-fold more weakly ($K_D \approx 500$ nM) than **4**. These findings were thus consistent with our hypothesis that the 4-pyridyl ring in **4** is involved in binding *Tc*CYP51. The 2-pyridyl ring system in **3** is presumably unable to chelate heme in *Tc*CYP51 due to steric hindrance from the immediately adjacent amide linkage.

Computational docking studies

We next employed computational docking and a model derived from the crystal structure of *Tc*CYP51 to compare predicted binding modes of **4** and (*R*)-**5**. The two ligands were docked by using the induced-fit docking protocol with Glide XP [34], and the models were further refined by minimizing the energies of the ligand and surrounding residues (within 5 Å of ligand) using PRIME [35]. Finally, binding scores were computed by using both Glide XP and the MM/GMSA method. Compound **4** was predicted to bind in a similar fashion as (*R*)-**5**, with the 4-pyridyl ring chelating the heme-iron atom and the tolyl ring at P2 contacting many of the same residues (e.g., Try103, Phe110) predicted to interact with the tryptophan ring of (*R*)-**5** (Figure 2A). This same hydrophobic site in *Tc*CYP51 binds the fluoroaryl rings of fluconazole and posaconazole in co-crystal structures [14]. The predicted binding mode of the enantiomer (*S*)-**5** was described previously [16] and is distinct from that proposed for **4** and (*R*)-**5**.

Thus, computational docking provides a conceptual picture of how compound **4** – notionally a cruzain inhibitor – might also bind *Tc*CYP51. Interestingly, this is not the first time that potent *Tc*CYP51 binding has been discovered in a molecule originally intended for a different target. Buckner and Gelb unexpectedly found that the human protein farnesyltransferase (PFT) inhibitor tipifarnib exerts its antitrypanosomal effects through inhibition of *Tc*CYP51 [36]. Subsequently, these researchers succeeded in divorcing PFT activity from *Tc*CYP51 inhibition in the tipifarnib scaffold, producing new lead compounds with compelling properties [37-39].

Inhibition of mammalian CYPs

A concern with any inhibitor of *Tc*CYP51 is the potential for cross reactivity with mammalian cytochrome P450 (CYP)

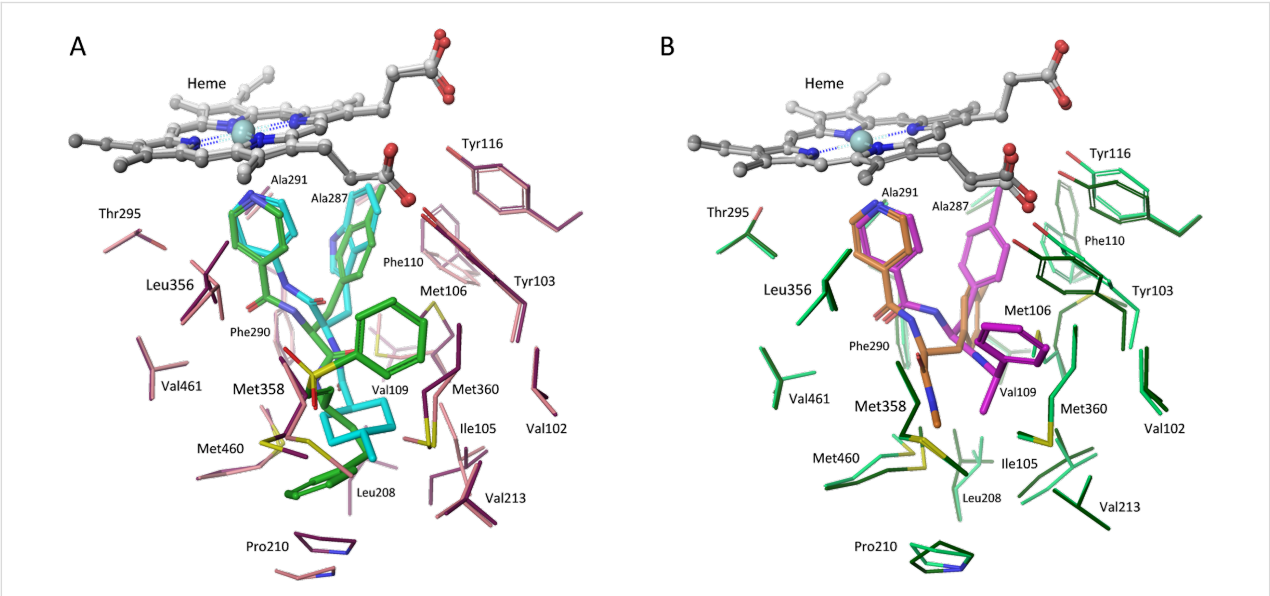


Figure 2: Computational docking models. (A) Predicted binding modes of **4** and (*R*)-**5** bound to *Tc*CYP51. For **4**, the ligand, the protein, and the heme group are shown in green, pink, and grey, respectively. For (*R*)-**5**, the ligand, the protein, and the heme group are shown in cyan, purple, and white, respectively. Heme-iron chelation and hydrophobic binding interactions dominate in the models. (B) Predicted binding models of truncated analogues **12** and **13** to *Tc*CYP51. For **12**, the ligand, the protein, and the heme group are shown in orange, light green, and light grey, respectively. For **13**, the ligand, the protein, and the heme group are shown in magenta, dark green, and dark grey, respectively.

enzymes, especially those CYPs involved in drug metabolism, like CYP3A4. To assess this risk, we evaluated the inhibitory activities of **4** and **1** across a panel of relevant mammalian CYP enzymes (Table 2). Both **4** and **1** inhibited all CYPs in the panel, with IC_{50} values generally in the low micromolar range. Although compound **4** did inhibit CYP3A4, the potency of inhibition (IC_{50} = 0.8 μM) was less than that exhibited by the antifungal drug ketoconazole (IC_{50} = 0.086 μM). It should be noted that the substrate-derived IC_{50} values from the CYP panel are not directly comparable to the K_D values for binding to *Tc*CYP51. What can be said is that the antitrypanosomal effects of **4** are realized at concentrations (EC_{90} = 0.1 μM, MTC = 0.5 μM) well below the in vitro potency of the compound across the CYP panel (average $IC_{50} \approx 7$ μM). Compound **4** thus possesses reasonable selectivity with regard to off-target CYP inhibition, and represents a reasonable starting point from which further improvements in selectivity may be undertaken.

Table 2: In vitro inhibition of important mammalian CYP enzymes.

compound	IC_{50} (μM)				
	1A2	2C9	2C19	2D6	3A4
1	24	32	7.6	26	1.7
4	22	5.5	3.4	2.7	0.8
ketoconazole	—	—	—	—	0.086

Given the similar IC_{50} values for **1** and **4** against CYP3A4, we were curious to determine whether **4** is an irreversible inhibitor of this enzyme, as is the case for **1** [30]. Irreversible inhibition is typically assessed by measuring the activity of microsomal CYPs following pre-incubation with or without NADPH. Consistent with earlier studies [30], compound **1** exhibited irreversible inhibition of CYP3A4 as reflected in a significantly lower IC_{50} value with NADPH pre-incubation (Table 3). In contrast, compound **4** showed behavior typical of reversible inhibition, with no NADPH-dependent shift in the IC_{50} value. In the case of CYP2C19, both compounds were found to be reversible inhibitors. These results suggest that CYP inhibition by **4** involves reversible binding of the parent molecule, while the inhibition of CYP3A4 conferred by **1** is dependent on initial conversion to a reactive metabolite. Whatever the explanation, reversible inhibition of CYP enzymes (as with **4**) is clearly preferable to irreversible inhibition from a drug-safety perspective.

Table 3: Mechanism of inhibition studies for compounds **1** and **4**. These data suggest that inhibition of CYP3A4 by **1** is irreversible in nature.

compound	2C19 IC_{50} (μM)		3A4 IC_{50} (μM)	
	+NADPH	−NADPH	+NADPH	−NADPH
1	5.54	8.22	**0.0059**	1.08
4	0.300	0.170	0.117	0.046

Inhibition of *Tc*CYP51 in live parasites

We next sought to better define the relative importance of *Tc*CYP51 and cruzain inhibition in the antitrypanosomal effects of compound **4**. Since the 2-pyridyl analogue **3** was found to not bind *Tc*CYP51, this compound could serve as a control for the cruzain-derived (and/or other cysteine-protease-derived) effects of **4**. To provide controls lacking activity against cysteine proteases, we reduced the vinylsulfone function in analogues **1**, **3**, and **4** to afford the dihydro analogues **6**–**8** (Figure 3). As expected, these analogues were devoid of any detectable cruzain inhibitory activity (IC_{50} > 50 μM, Table 1). Compounds **3**, **4**, **7** and **8** thus comprised a set of analogues with complementary activity profiles against the two putative targets: **4** (cruzain and *Tc*CYP51 inhibition), **8** (*Tc*CYP51 inhibition only), **3** (cruzain inhibition only), and **7** (neither activity).

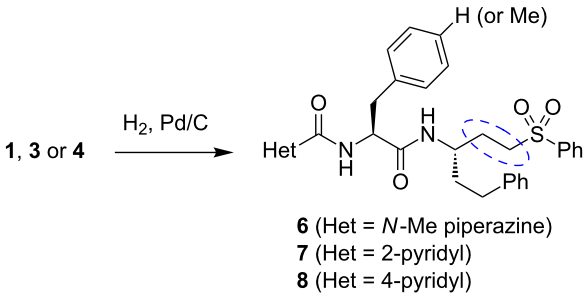


Figure 3: Synthesis of the additional control compound **6**–**8**, the reduced forms of analogues **1**, **3**, and **4** respectively.

Compounds **3**, **4**, **7**, and **8** were evaluated for potency against intracellular *T. cruzi* parasites by using two different assays. The reported EC_{90} values (Table 1) represent compound concentrations required to reduce parasite numbers in C2C12 host cells by 90% as compared to untreated controls, as determined by using a high-content imaging-based screening (HCS) approach [33,40]. This high-throughput assay provides a rapid measure of the initial acute effects of test compound on parasite viability. The more laborious MTC assay identifies compound concentrations that clear parasites from the host cell, as determined ca. two weeks after the conclusion of a four-week course of treatment. This MTC assay therefore provides a measure of trypanocidal action that cannot be drawn from the more rapid HCS assay. We judge that MTC values are more representative of the therapeutic drug levels that would likely be

required to produce efficacy in an animal model of Chagas' disease.

The antitrypanosomal effects of compounds **3**, **4**, **7**, and **8** were in general agreement with their in vitro activities against the two putative targets (Table 1). Analogue **7**, devoid of either activity in vitro, showed no effects on *T. cruzi* parasites in either the HCS or MTC assay. Analogue **3**, possessing primarily cysteine-protease-derived effects, was effective in both assays and equipotent to **1** in the MTC assay. Putatively dual-targeted analogue **4** was about 10-fold more potent than **1** in the MTC assay and equipotent by HCS. Most unexpectedly, we found that compound **8**, which lacks any cruzain-derived effects of **4**, was equipotent to **4** by HCS and 2–4 times more potent than **4** in the MTC assay.

The in vitro and cell-based activities of **4** and **8** suggest *Tc*CYP51 as a relevant target of these compounds. To assess inhibition of *Tc*CYP51 in live parasites we analyzed the sterol composition of intracellular *T. cruzi* parasites treated with test compounds **3**–**8**, **1**, or posaconazole as a positive control. The analysis was performed by employing GC/MS as reported previously for compound **5** [33]. The GC/MS trace for uninfected host cells establishes that the additional peaks observed in infected cells are of *T. cruzi* origin (peaks labeled **a**-**i**, Figure 4). Treatment with the known *Tc*CYP51 inhibitor posaconazole produces an increase in the relative abundance of *Tc*CYP51 substrates lanosterol (**f**) and eburicol (**h**) and accordingly, a reduction in the abundance of downstream sterols such as fecosterol (**e**) and cholesta-7,24-dien-3β-ol (**a**), among others. Treatment with **1** had little effect on sterol composition as expected, whereas treatment with compound **4** or **8** produced effects very similar to those observed in posaconazole treated parasites (Figure 4 and Supporting Information File 1). The other test compounds evaluated (**3**, **6**, **7**) produced no significant change in lipid composition, as expected since these compounds do not inhibit *Tc*CYP51 in vitro (Supporting Information File 1). Test compounds were necessarily studied at concentrations below their MTC, so as to retain a population of viable parasites for analysis.

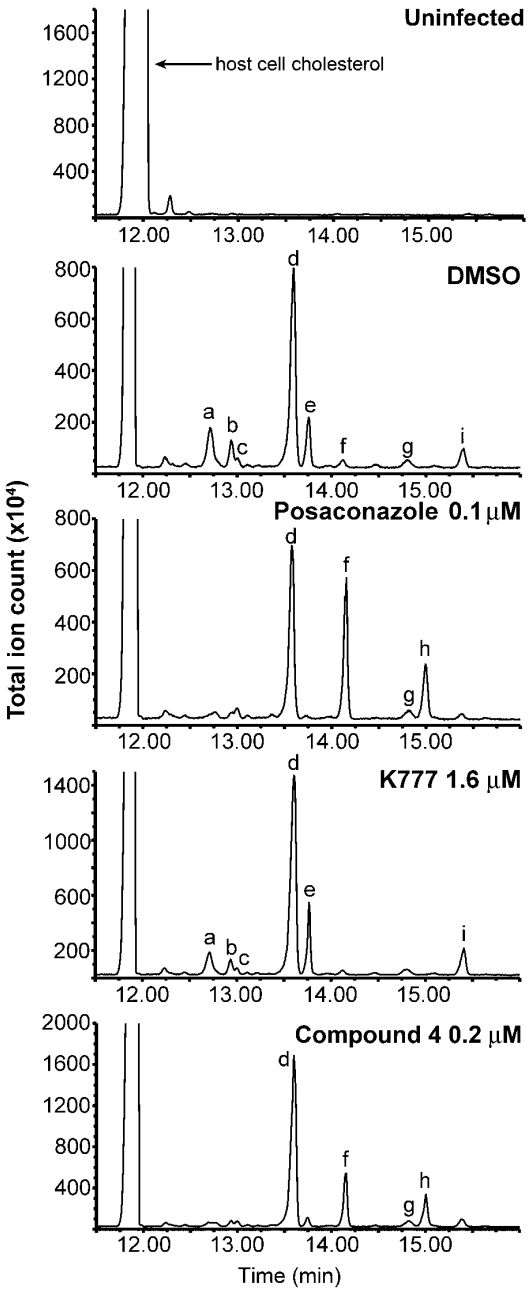


Figure 4: GC/MS analysis of lipid extracts from *T. cruzi* parasites treated with test compounds. DMSO and K777 (**1**) were used as negative controls; posaconazole served as a positive control. The analysis of **4** was performed concurrently with other CYP51 inhibitors described recently [33] and, thus, the spectra for the controls shown above are reproduced from the earlier report. Spectra of lipid extracts from parasites treated with **3**, **6**, **7**, and **8** are provided in Supporting Information File 1. Uninfected host cell panel (top) demonstrates that chromatographic peaks labeled **a** to **i** in subsequent panels are of *T. cruzi* origin. These peaks are assigned as **a** - cholesta-7,24-dien-3β-ol, $[M]^{\bullet+}$ = *m*/*z* 454; **b** - cholesta-8,24-dien-3β-ol (zymosterol), $[M]^{\bullet+}$ = *m*/*z* 470; **c** - 24-methyl-7-en-cholesta-en-3β-ol, $[M]^{\bullet+}$ = *m*/*z* 472; **d** - ergosta-7,24-diene-3β-ol (episterol), $[M]^{\bullet+}$ = *m*/*z* 470; **e** - ergosta-8,24-diene-3β-ol (fecosterol), $[M]^{\bullet+}$ = *m*/*z* 470; **f** - lanosterol, $[M]^{\bullet+}$ = *m*/*z* 498; **g** - 4-methylepisterol, $[M]^{\bullet+}$ = *m*/*z* 484; **h** - eburicol, $[M]^{\bullet+}$ = *m*/*z* 512; **i** - 24-ethyl-7,24(24')-encholestadien-3β-ol, $[M]^{\bullet+}$ = *m*/*z* 484.

An activity-based probe reveals an off-target of 1 and 4

We next sought to evaluate the cysteine-protease-related effects of the various test compounds in *T. cruzi* parasites. To do this, we designed and synthesized the "clickable" activity-based probe **9** in which a propargyl group (replacing methyl in **1**) serves as a chemical handle for conjugation to TAMRA- or biotin-containing reagents (**10** and **11**, respectively, Figure 5). Probe **9** was found to be equipotent to **1** against cruzain in vitro and retained similar effects against *T. cruzi* parasites in both the

HCS and MTC assays. Thus, the cysteine protease target(s) of **9** in parasite and host cell can reasonably be assumed to be the same as for **1** and close analogues such as **4**.

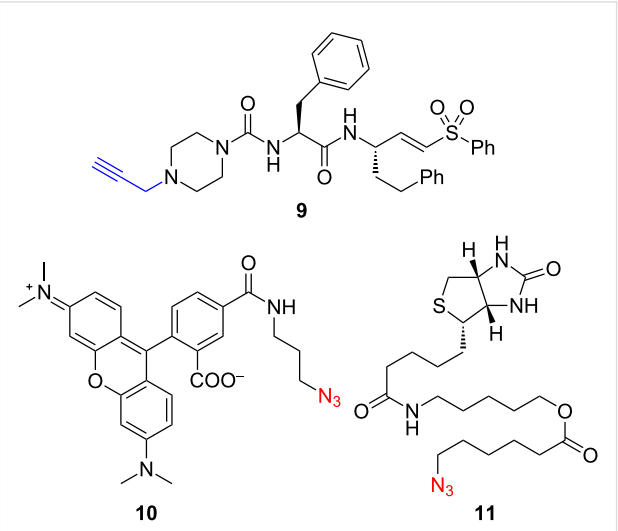


Figure 5: Chemical structures of compound **9**, a "clickable" activity-based probe based on **1** and complementary azide-containing reagents **10** and **11**.

Independently, another group recently reported the synthesis of **9** and its use to identify putative targets of **1** in the related parasite *Trypanosoma brucei* [41]. Our efforts to similarly identify targets of **1** in *T. cruzi* were complicated by the presence of a host-cell protein that was apparently a major target of **9**. In a typical experiment, intracellular *T. cruzi* amastigotes were treated with **9** for 1 hour, followed by cell lysis, "click" reaction with TAMRA azide **10**, and separation/visualization by SDS-PAGE. Regardless of the host cell employed (J774 macrophage, or C2C12), only one prominently labeled band at ≈35 kDa was observed in these experiments. This band was attributed to a host-cell protein as it appeared also in analogous experiments employing uninfected cells. In fact, we could not conclusively identify any unique bands of parasitic origin in our experiments, although such bands might well have escaped detection due to lower abundance and labeling below the limit of fluorescence detection.

The discovery of a potential mammalian off-target of probe **9** (and presumably also of **1**) was of considerable interest, so we explored this finding further. To determine if this protein was also a target of **1** and **4**, we conducted competition experiments in C2C12 cells. Hence, pre-incubation of cells with competitor compound at either 1 μM or 10 μM for one hour was followed by treatment for one hour with **9**, followed by cell lysis, conjugation to **10**, separation (SDS-PAGE), and detection by rhodamine fluorescence as before. In these experiments, pretreatment with 10 μM of compound **1**, **3**, or **4** successfully blocked labeling of the ≈35 kDa band by probe **9**, thus indicating that these compounds also react with this target (Figure 6). As expected, the nonelectrophilic dihydro forms of **1** and **4** (i.e., compounds **6** and **8**) did not compete for labeling by **9**. Taken together, these results strongly suggest that compounds **1**, **3** and **4** react irreversibly with the ≈35 kDa protein in a process involving the electrophilic vinylsulfone moiety.

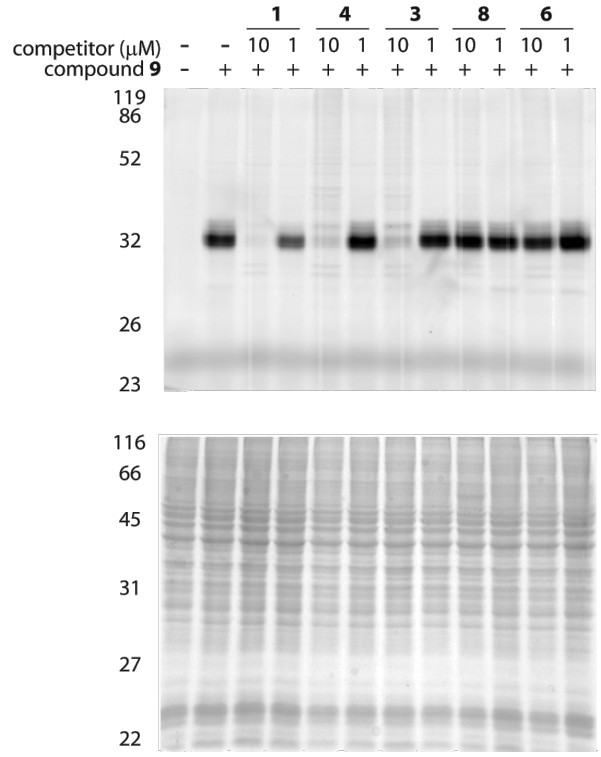


Figure 6: Competitive labeling of host cell (C2C12) proteins. Intact cells were labeled with probe **9** following a competitive pre-incubation step with compounds **1**, **4**, **3**, **8**, or **6**. After cell lysis, protein adducts of **9** were conjugated to rhodamide-based dye **10**. The gel image at the top shows rhodamine fluorescence. The gel image at the bottom is of the coomassie stained gel. A successfully competed band is observed at ≈35 kDa, and this was subsequently identified as cathepsin B.

Chemical proteomics

We next applied mass spectrometric analysis to identify the ≈35 kDa band, which was an apparent target of the electrophilic inhibitors described above. To enrich for this protein, C2C12 cells were labeled with **9** as before and then reacted with the biotin azide reagent **11**, followed by biotin capture onto streptavidin beads. A base-cleavable ester function was introduced in the linker of **11**, and this allowed enriched proteins to be released from beads by treatment with sodium hydroxide. The liberated proteins were separated by SDS-PAGE, and the relevant band at ≈35 kDa extracted from the gel. An in-gel trypsin digest [42] was followed by UPLC separation of the

tryptic peptides and MS/MS analysis using a hybrid linear ion-trap-Orbitrap mass spectrometer. Tandem mass spectra acquired were searched against the UniProtKb database employing ProteinProspector; four MS/MS spectra corresponding to the same peptide sequence were identified (Figure 7). This sequence was found to correspond to the tryptic peptide spanning resides S264-R281 from mouse cathepsin B (uniprot P10605). Significantly, this peptide was not found in analogous experiments where pre-incubation with **1** or **4** (at 10 μM) preceded labeling with **9**, nor in an experiment in which **9** was not added. Thus, cathepsin B is very likely the host-cell protein target of compounds **1** and **4** identified in the competition experiments with compound **9**.

The identification of cathepsin B as a relevant cellular off-target of **1** and **4** is potentially significant. On the one hand, the HCS EC_{90} values of **1** and **4** are at least 10-fold lower than the concentrations of these compounds used in the competition experiments. Thus, one might expect to achieve effects on parasite viability before significant inhibition of cathepsin B is conferred. On the other hand, the MTC for **1** (8 μM) lies squarely in the range at which the compound effectively competes for cathepsin B labeling by **9**. Thus, if micromolar concentrations of **1** are indeed required to achieve a therapeutic effect in animals, one might well be concerned about the effects on host cathepsin B. Thus, the experiments with **9** identified a potential off-target while also providing an experimental means for testing the effects of new analogues on this off-target in a relevant, cellular context.

Defining a new lead scaffold for *Tc*CYP51 inhibition

The similar cellular potencies of **4** and its reduced form **8** suggest that cruzain inhibition plays a relatively minor role in the trypanocidal action of **4.** To a first approximation, the cruzain- and *Tc*CYP51-derived effects of **4** should be similar to those of its close analogues **3** (MTC ≈ 10 μM) and **8** (MTC ≈ 0.25 μM), respectively. Unless the effects of inhibiting both targets are synergistic, which is not supported by the data, there would appear to be little benefit gained by combining a relatively weak cruzain-derived effect with a much more potent insult conferred by *Tc*CYP51 inhibition. Moreover, it now seems likely that electrophilic compounds such as **1** and **4** may be partially consumed in nonproductive reactions with host-cell proteases (e.g., cathepsin B) and/or other cytosolic nucleophiles (e.g., glutathione). This possibility is supported by our competitive labeling experiments (Figure 6) and by in vitro studies employing physiological concentrations of glutathione (Supporting Information File 1). With regard to the inhibitor chemotypes covered here, there appears to be little rationale for targeting both cruzain and *Tc*CYP51. On the other hand, the surprising potency of analogue **8** does suggest this as a new lead scaffold for the development of novel *Tc*CYP51 inhibitors.

We next sought to define the minimal pharmacophore within **8** required for inhibition of *Tc*CYP51 in vitro and anti-trypanosomal effects in whole cells. We therefore synthesized truncated analogues of **8**, such as **12** and **13** (Figure 1). These compounds retain the 4-pyridyl ring and neighboring tolyl side

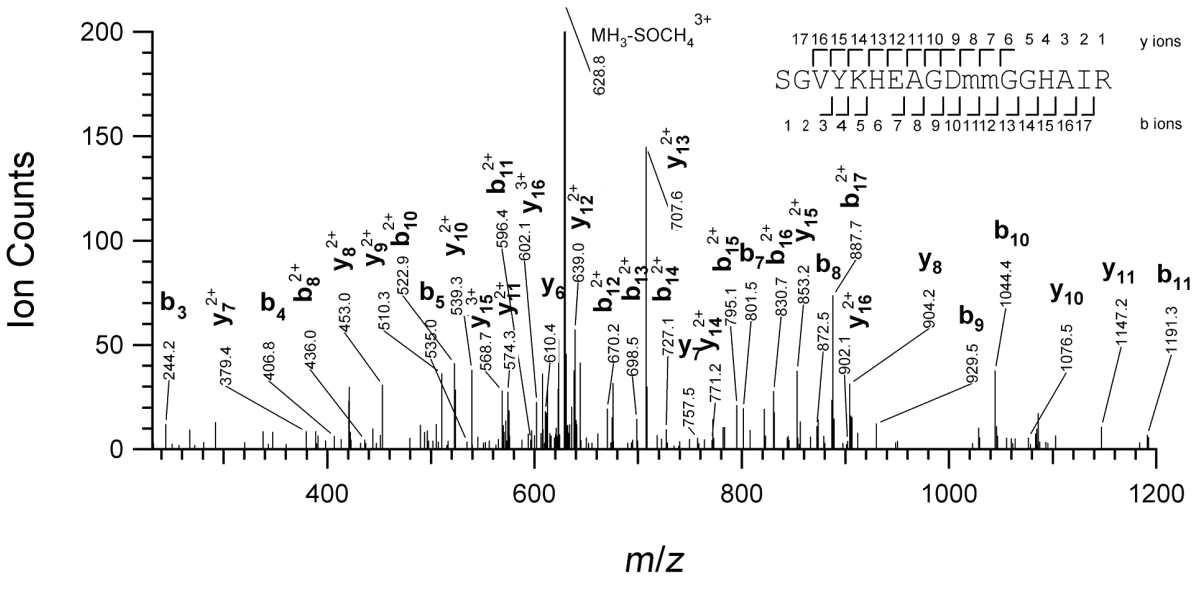


Figure 7: MS/MS spectrum of the tryptic peptide S264-R281 from mouse cathepsin B, identified in pull-down experiments employing compound **9** in C2C12 cells. Observed sequence ions are labeled (m = oxidized methionine).

chain of **8** while dispensing with those substituents further removed from the putative heme-binding moiety. Interestingly, the truncated analogues **12** and **13** bound *Tc*CYP51 significantly more weakly than **4** or **8** (Table 1), suggesting that side chains relatively far removed from the 4-pyridyl ring nonetheless play an important role in binding.

Computational docking of **12** and **13** provided some insight into the observed binding trends. Analogue **13** adopts a docking pose very similar to **4** with respect to the 4-pyridyl and tolyl ring systems. When compared to the poses for **4** or **13**, the tolyl ring in **12** projects much less deeply into the aromatic pocket formed by Phe110 and Tyr103 (Figure 2). Neither **12** nor **13** form interactions with more distal residues (e.g., Leu208, Pro210) that are predicted to form productive contacts with **4**. Thus, a larger number of hydrophobic contacts and better orientation of some side chains may explain the binding trends for **4**, **12**, and **13**. Interestingly, the rank-order binding affinities of **4**, **12**, and **13** were correctly predicted by the MM-GBSA method applied to the binding models of these compounds (Supporting Information File 1). This suggests that such models could serve to aid in the design of new *Tc*CYP51 inhibitors derived from this scaffold.

The antitrypanosomal activities of analogues **12** and **13** could be correlated with their in vitro binding affinities for *Tc*CYP51 (Table 1). Hence, analogue **13** (K_D = 75 nM) shows reduced antitrypanosomal activity when compared to **8** ($K_D \approx 5$ nM). Still weaker-binding analogue **12** (K_D = 620 nM) exhibited no antitrypanosomal effect at the highest concentration examined (10 μM). Thus, compound **13** can be considered to represent a "minimal pharmacophore" that retains reasonable affinity for *Tc*CYP51 in vitro while also conferring an effect on *T. cruzi* parasites in culture. Future work will focus on further refining the in vitro and cellular potency of this scaffold, with compound **13** serving as a chemical departure point.

Conclusion

Structure–activity studies are often conducted with the underlying assumption that molecular mechanisms are the same within congeneric analogue series. This assumption is reinforced when activity in biochemical assays can be correlated with cell-based activity. Of course perfect correlation is rarely observed, even when a series is in fact "on-target". Especially perilous is the construction of mechanistic hypotheses based solely on the correlation of in vitro biochemical assay data with gross phenotypic endpoints such as parasite growth inhibition or cell death. As demonstrated here, even seemingly trivial structural changes within a congeneric SAR series can produce analogues with disparate molecular mechanisms of action. Advisable approaches to deal with these uncertainties include the use of cell-based counter assays that can detect action at specific targets or signaling pathways of interest. Activity-based probes can serve as useful tools to verify on-target action during the course of chemical optimization campaigns.

Supporting Information

The Supporting Information features a table with experimentally determined and computationally predicted binding affinities, additional GC/MS spectra from lipid-analysis studies, time courses for reaction of compounds **1** and **6** with glutathione in vitro, and synthetic schemes for analogues **4**, **9**, **11**, **12**, and **13**, as well as experimental procedures.

Supporting Information File 1

Figures, schemes, and experimental procedures.
[http://www.beilstein-journals.org/bjoc/content/supplementary/1860-5397-9-3-S1.pdf]

Acknowledgements

The authors acknowledge research support from the Sandler Foundation (to ARR), NIH RO1 AI095437 (to LMP), Conselho Nacional de Desenvolvimento Cientifico e Tecnologico and FIOCRUZ (to CMC). JBJ was supported by NIH RO1 AI74824 (to Prof. Ortiz de Montellano, UCSF). Mass spectrometry was provided by the Bio-Organic Biomedical Mass Spectrometry Resource at UCSF (A.L. Burlingame, Director) and supported by the Biomedical Technology Research Centers program of the NIH National Institute of General Medical Sciences, NIH NIGMS 8P41GM103481. MPJ is a consultant to Schrodinger, LLC.

References

1. de Souza, W. *Microbes Infect.* **2007,** *9,* 544–545. doi:10.1016/j.micinf.2006.12.014
2. Urbina, J. A. *Mem. Inst. Oswaldo Cruz* **2009,** *104* (Suppl. 1), 311–318. doi:10.1590/S0074-02762009000900041
3. Castro, J. A.; de Mecca, M. M.; Bartel, L. C. *Hum. Exp. Toxicol.* **2006,** *25,* 471–479. doi:10.1191/0960327106het653oa
4. Renslo, A. R.; McKerrow, J. H. *Nat. Chem. Biol.* **2006,** *2,* 701–710. doi:10.1038/nchembio837
5. McKerrow, J. H.; Doyle, P. S.; Engel, J. C.; Podust, L. M.; Robertson, S. A.; Ferreira, R.; Saxton, T.; Arkin, M.; Kerr, I. D.; Brinen, L. S.; Craik, C. S. *Mem. Inst. Oswaldo Cruz* **2009,** *104* (Suppl. 1), 263–269. doi:10.1590/S0074-02762009000900034
6. Urbina, J. A. *J. Mol. Med. (Heidelberg, Ger.)* **1999,** *77,* 332–338. doi:10.1007/s001090050359
7. McKerrow, J. H.; Engel, J. C.; Caffrey, C. R. *Bioorg. Med. Chem.* **1999,** *7,* 639–644. doi:10.1016/S0968-0896(99)00008-5
8. Eakin, A. E.; McGrath, M. E.; McKerrow, J. H.; Fletterick, R. J.; Craik, C. S. *J. Biol. Chem.* **1993,** *268,* 6115–6118.

9. McKerrow, J. H.; McGrath, M. E.; Engel, J. C. *Parasitol. Today* **1995,** *11,* 279–282. doi:10.1016/0169-4758(95)80039-5
10. McGrath, M. E.; Eakin, A. E.; Engel, J. C.; McKerrow, J. H.; Craik, C. S.; Fletterick, R. J. *J. Mol. Biol.* **1995,** *247,* 251–259. doi:10.1006/jmbi.1994.0137
11. Buckner, F. S.; Joubert, B. M.; Boyle, S. M.; Eastman, R. T.; Verlinde, C. L. M. J.; Matsuda, S. P. T. *Mol. Biochem. Parasitol.* **2003,** *132,* 75–81. doi:10.1016/j.molbiopara.2003.07.004
12. Hankins, E. G.; Gillespie, J. R.; Aikenhead, K.; Buckner, F. S. *Mol. Biochem. Parasitol.* **2005,** *144,* 68–75. doi:10.1016/j.molbiopara.2005.08.002
13. Podust, L. M.; von Kries, J. P.; Eddine, A. N.; Kim, Y.; Yermalitskaya, L. V.; Kuehne, R.; Ouellet, H.; Warrier, T.; Alteköster, M.; Lee, J.-S.; Rademann, J.; Oschkinat, H.; Kaufmann, S. H. E.; Waterman, M. R. *Antimicrob. Agents Chemother.* **2007,** *51,* 3915–3923. doi:10.1128/AAC.00311-07
14. Chen, C.-K.; Leung, S. S. F.; Guilbert, C.; Jacobson, M. P.; McKerrow, J. H.; Podust, L. M. *PLoS Negl. Trop. Dis.* **2010,** *4,* e651. doi:10.1371/journal.pntd.0000651
15. Urbina, J. A. *Acta Trop.* **2010,** *115,* 55–68. doi:10.1016/j.actatropica.2009.10.023
16. Doyle, P. S.; Chen, C.-K.; Johnston, J. B.; Hopkins, S. D.; Leung, S. S. F.; Jacobson, M. P.; Engel, J. C.; McKerrow, J. H.; Podust, L. M. *Antimicrob. Agents Chemother.* **2010,** *54,* 2480–2488. doi:10.1128/AAC.00281-10
17. Harth, G.; Andrews, N.; Mills, A. A.; Engel, J. C.; Smith, R.; McKerrow, J. H. *Mol. Biochem. Parasitol.* **1993,** *58,* 17–24. doi:10.1016/0166-6851(93)90086-D
18. Roush, W. R.; Cheng, J.; Knapp-Reed, B.; Alvarez-Hernandez, A.; McKerrow, J. H.; Hansell, E.; Engel, J. C. *Bioorg. Med. Chem. Lett.* **2001,** *11,* 2759–2762. doi:10.1016/S0960-894X(01)00566-2
19. Huang, L.; Lee, A.; Ellman, J. A. *J. Med. Chem.* **2002,** *45,* 676–684. doi:10.1021/jm010333m
20. Greenbaum, D. C.; Mackey, Z.; Hansell, E.; Doyle, P.; Gut, J.; Caffrey, C. R.; Lehrman, J.; Rosenthal, P. J.; McKerrow, J. H.; Chibale, K. *J. Med. Chem.* **2004,** *47,* 3212–3219. doi:10.1021/jm030549j
21. Jaishankar, P.; Hansell, E.; Zhao, D.-M.; Doyle, P. S.; McKerrow, J. H.; Renslo, A. R. *Bioorg. Med. Chem. Lett.* **2008,** *18,* 624–628. doi:10.1016/j.bmcl.2007.11.070
22. Brak, K.; Doyle, P. S.; McKerrow, J. H.; Ellman, J. A. *J. Am. Chem. Soc.* **2008,** *130,* 6404–6410. doi:10.1021/ja710254m
23. Chen, Y. T.; Lira, R.; Hansell, E.; McKerrow, J. H.; Roush, W. R. *Bioorg. Med. Chem. Lett.* **2008,** *18,* 5860–5863. doi:10.1016/j.bmcl.2008.06.012
24. Bryant, C.; Kerr, I. D.; Debnath, M.; Ang, K. K. H.; Ratnam, J.; Ferreira, R. S.; Jaishankar, P.; Zhao, D.; Arkin, M. R.; McKerrow, J. H.; Brinen, L. S.; Renslo, A. R. *Bioorg. Med. Chem. Lett.* **2009,** *19,* 6218–6221. doi:10.1016/j.bmcl.2009.08.098
25. Brak, K.; Kerr, I. D.; Barrett, K. T.; Fuchi, N.; Debnath, M.; Ang, K.; Engel, J. C.; McKerrow, J. H.; Doyle, P. S.; Brinen, L. S.; Ellman, J. A. *J. Med. Chem.* **2010,** *53,* 1763–1773. doi:10.1021/jm901633v
26. Mott, B. T.; Ferreira, R. S.; Simeonov, A.; Jadhav, A.; Ang, K. K.-H.; Leister, W.; Shen, M.; Silveira, J. T.; Doyle, P. S.; Arkin, M. R.; McKerrow, J. H.; Inglese, J.; Austin, C. P.; Thomas, C. J.; Shoichet, B. K.; Maloney, D. J. *J. Med. Chem.* **2010,** *53,* 52–60. doi:10.1021/jm901069a
27. Beaulieu, C.; Isabel, E.; Fortier, A.; Massé, F.; Mellon, C.; Méthot, N.; Ndao, M.; Nicoll-Griffith, D.; Lee, D.; Park, H.; Black, W. C. *Bioorg. Med. Chem. Lett.* **2010,** *20,* 7444–7449. doi:10.1016/j.bmcl.2010.10.015
28. Engel, J. C.; Doyle, P. S.; Hsieh, I.; McKerrow, J. H. *J. Exp. Med.* **1998,** *188,* 725–734. doi:10.1084/jem.188.4.725
29. Barr, S. C.; Warner, K. L.; Kornreic, B. G.; Piscitelli, J.; Wolfe, A.; Benet, L.; McKerrow, J. H. *Antimicrob. Agents Chemother.* **2005,** *49,* 5160–5161. doi:10.1128/AAC.49.12.5160-5161.2005
30. Jacobsen, W.; Christians, U.; Benet, L. Z. *Drug Metab. Dispos.* **2000,** *28,* 1343–1351.
31. Falgueyret, J.-P.; Desmarais, S.; Oballa, R.; Black, W. C.; Cromlish, W.; Khougaz, K.; Lamontagne, S.; Massé, F.; Riendeau, D.; Toulmond, S.; Percival, M. D. *J. Med. Chem.* **2005,** *48,* 7535–7543. doi:10.1021/jm0504961
32. Robichaud, J.; Black, W. C.; Thérien, M.; Paquet, J.; Oballa, R. M.; Bayly, C. I.; McKay, D. J.; Wang, Q.; Isabel, E.; Léger, S.; Mellon, C.; Kimmel, D. B.; Wesolowski, G.; Percival, M. D.; Massé, F.; Desmarais, S.; Falgueyret, J.-P.; Crane, S. N. *J. Med. Chem.* **2008,** *51,* 6410–6420. doi:10.1021/jm800610j
33. Gunatilleke, S. S.; Calvet, C. M.; Johnston, J. B.; Chen, C. K.; Erenburg, G.; Gut, J.; Engel, J. C.; Ang, K. K.; Mulvaney, J.; Chen, S.; Arkin, M. R.; McKerrow, J. H.; Podust, L. M. *PLoS Negl. Trop. Dis.* **2012,** *6,* e1736.
34. Sherman, W.; Day, T.; Jacobson, M. P.; Friesner, R. A.; Farid, R. *J. Med. Chem.* **2006,** *49,* 534–553. doi:10.1021/jm050540c
35. Zhu, K.; Shirts, M. R.; Friesner, R. A.; Jacobson, M. P. *J. Chem. Theory Comput.* **2007,** *3,* 640–648. doi:10.1021/ct600129f
36. Hucke, O.; Gelb, M. H.; Verlinde, C. L. M. J.; Buckner, F. S. *J. Med. Chem.* **2005,** *48,* 5415–5418. doi:10.1021/jm050441z
37. Kraus, J. M.; Verlinde, C. L. M. J.; Karimi, M.; Lepesheva, G. I.; Gelb, M. H.; Buckner, F. S. *J. Med. Chem.* **2009,** *52,* 1639–1647. doi:10.1021/jm801313t
38. Chennamaneni, N. K.; Arif, J.; Buckner, F. S.; Gelb, M. H. *Bioorg. Med. Chem. Lett.* **2009,** *19,* 6582–6584. doi:10.1016/j.bmcl.2009.10.029
39. Kraus, J. M.; Tatipaka, H. B.; McGuffin, S. A.; Chennamaneni, N. K.; Karimi, M.; Arif, J.; Verlinde, C. L. M. J.; Buckner, F. S.; Gelb, M. H. *J. Med. Chem.* **2010,** *53,* 3887–3898. doi:10.1021/jm9013136
40. Engel, J. C.; Ang, K. K. H.; Chen, S.; Arkin, M. R.; McKerrow, J. H.; Doyle, P. S. *Antimicrob. Agents Chemother.* **2010,** *54,* 3326–3334. doi:10.1128/AAC.01777-09
41. Yang, P.-Y.; Wang, M.; He, C. Y.; Yao, S. Q. *Chem. Commun.* **2012,** *48,* 835–837. doi:10.1039/c1cc16178d
42. Rosenfeld, J.; Capdevielle, J.; Guillemot, J. C.; Ferrara, P. *Anal. Biochem.* **1992,** *203,* 173–179. doi:10.1016/0003-2697(92)90061-B

License and Terms

This is an Open Access article under the terms of the Creative Commons Attribution License (http://creativecommons.org/licenses/by/2.0), which permits unrestricted use, distribution, and reproduction in any medium, provided the original work is properly cited.

The license is subject to the *Beilstein Journal of Organic Chemistry* terms and conditions: (http://www.beilstein-journals.org/bjoc)

The definitive version of this article is the electronic one which can be found at: doi:10.3762/bjoc.9.3

Beilstein Journal of Organic Chemistry

Thioester derivatives of the natural product psammaplin A as potent histone deacetylase inhibitors

Matthias G. J. Baud[1], Thomas Leiser[2], Vanessa Petrucci[3], Mekala Gunaratnam[3], Stephen Neidle[3], Franz-Josef Meyer-Almes[2] and Matthew J. Fuchter[*1]

Letter

Open Access

Address:
[1]Department of Chemistry, Imperial College London, London SW7 2AZ, United Kingdom, [2]Department of Chemical Engineering and Biotechnology, University of Applied Sciences, Schnittspahnstraße 12, 64287 Darmstadt, Germany and [3]Cancer Research UK Biomolecular Structure Group, UCL School of Pharmacy, 29-39 Brunswick Square, London WC1N 1AX, United Kingdom

Email:
Matthew J. Fuchter[*] - m.fuchter@imperial.ac.uk

* Corresponding author

Keywords:
epigenetics; histone deacetylase; natural product; prodrug; psammaplin A; thioester

Beilstein J. Org. Chem. **2013,** *9,* 81–88.
doi:10.3762/bjoc.9.11

Received: 29 September 2012
Accepted: 11 December 2012
Published: 15 January 2013

This article is part of the Thematic Series "Synthetic probes for the study of biological function".

Guest Editor: J. Aubé

© 2013 Baud et al; licensee Beilstein-Institut.
License and terms: see end of document.

Abstract

There has been significant interest in the bioactivity of the natural product psammaplin A, most recently as a potent and isoform selective HDAC inhibitor. Here we report our preliminary studies on thioester HDAC inhibitors derived from the active monomeric (thiol) form of psammaplin A, as a means to improve compound delivery into cells. We have discovered that such compounds exhibit both potent cytotoxicity and enzymatic inhibitory activity against recombinant HDAC1. The latter effect is surprising since previous SAR suggested that modification of the thiol functionality should detrimentally affect HDAC potency. We therefore also report our preliminary studies on the mechanism of action of this observed effect.

Introduction

Chromatin is a macromolecular complex consisting of DNA, histone and nonhistone proteins. The epigenetic control of chromatin organization plays a major role in the regulation of gene expression, and consequently cell differentiation, proliferation and survival. Such control is mediated by a myriad of remodelling proteins, able to bind to, and covalently modify, chromatin [1,2]. In recent years, it has become increasingly apparent that misregulation of epigenetic pathways contributes to oncogenesis [3,4] and small molecule inhibitors of these pathways have emerged as highly attractive targets for anticancer therapies [5,6]. Inhibitors of epigenetic pathways should not only be useful as anticancer drugs, but also as molecular probes to study

the causative relationships between specific epigenetic modifications, their biological outcomes, and how their misregulation is involved in diseases such as cancer [1,2].

The dynamic post-translational acetylation/deacetylation of histone proteins is one of the most commonly studied epigenetic events, and occurs at specific lysine residues on the N-terminal histone tails, which project out from the nucleosome (the fundamental repeating unit of chromatin). Acetylation/deacetylation of such lysine residues is achieved by the action of histone acetyltransferases (HATs) and histone deacetylases (HDACs), respectively. Histone deacetylation by HDACs causes transcriptional repression through both chromatin condensation and chromatin signalling. To date, 18 human genes encoding proven or putative HDACs have been identified [7]. HDACs fall into two categories: the zinc-dependent enzymes (class I, II and IV) and the NAD^+-dependent enzymes (class III, also called sirtuins) [5]. Class I HDACs (HDAC1, 2, 3, 8) are mostly present in the nucleus, whereas class II HDACs are tissue specific and shuttle between the cytoplasm and the nucleus [8,9]. Class II can be further subdivided into class IIa (HDAC4, 5, 7, 9) and class IIb (HDAC6, 10). HDAC11 constitutes its own class IV. Despite their name, several HDACs are able to deacetylate a number of nonhistone protein substrates [10,11]. Sirtuins are structurally and mechanistically distinct enzymes.

To date, only two compounds that inhibit HDACs have been FDA approved: suberoylanilide hydroxamic acid (SAHA, **1,** trade name Zolinza by Merck & Co.) and romidepsin **2** (trade name Istodax by Celgene) for the treatment of cutaneous T-cell lymphoma (CTCL, Figure 1) [12-14]. The success of these compounds in the clinic has led to a significant interest in the further discovery of structurally novel HDAC inhibitors that, in particular, exhibit improved isoform selectivity.

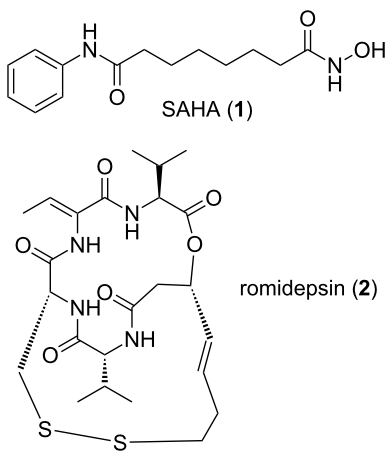
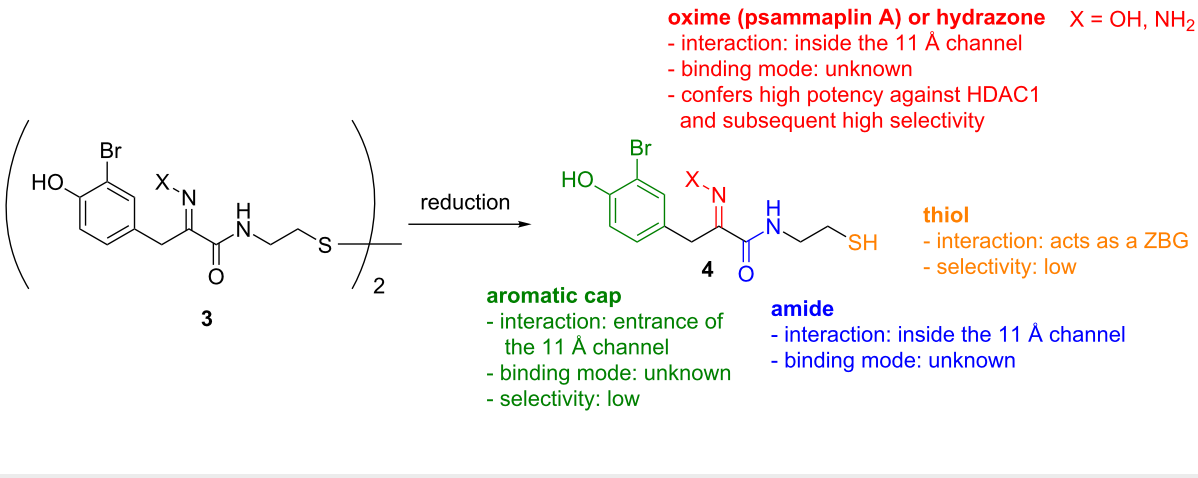


Figure 1: FDA approved HDAC inhibitors for the treatment of CTCL.

Among the myriad of previously reported HDAC inhibitors, psammaplin A [15-18] (**3**, X = OH, Scheme 1, left) displays an intriguing structure. It is a symmetric, dimeric hydroxyiminotyrosine-based natural product, characterised in 1987, and represents the first example of a disulfide and oxime containing metabolite isolated from a marine sponge. Since its initial report by Crews and co-workers as a potent HDAC inhibitor [16], psammaplin A has provided inspiration for the development of new HDAC inhibitors with novel structures [19]. Recently, we [20] and others [21] reported an in-depth structure–activity relationship of this natural product against its HDAC targets. Dissection of its activity against a panel of HDACs allowed us to highlight structural features responsible for its high inhibitory



Scheme 1: SAR of psammaplin A against zinc-dependant HDACs. Adapted from Baud et al. [20].

potency and selectivity. In particular, we unambiguously demonstrated that, similarly to the natural product and clinically approved romidepsin, psammaplin A is a prodrug, requiring reduction of its disulfide functionality to the corresponding thiol monomer **4** (X = OH), in order to potently inhibit HDACs (Scheme 1, right). The resulting thiol moiety acts as a zinc binding group within the active site of the HDAC protein. Furthermore, we demonstrated the importance of the oxime unit of psammaplin A and related analogues for high potency and selectivity against recombinant HDAC1 (rHDAC1) in vitro (Scheme 1). More recently, we disclosed highly potent heterocyclic *N*-thioethylamide-based HDAC inhibitors based on the psammaplin A pharmacophore and rationalised the results using computational modelling [22].

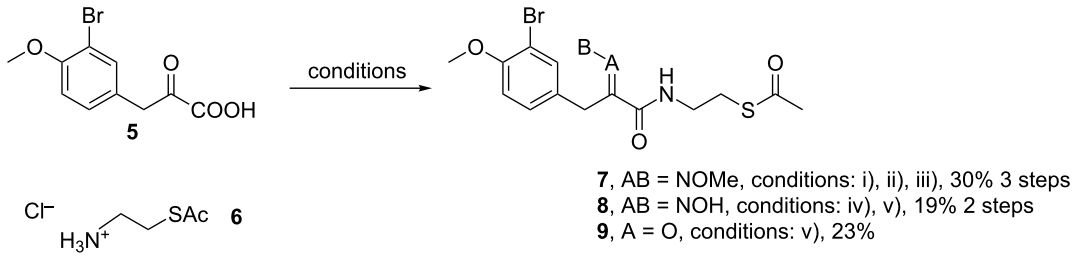
While prereduced psammaplin A and thiol-containing analogues displayed nanomolar to subnanomolar potencies in vitro, they only displayed modest potencies in cell-based assays against A549 (human lung carcinoma), MCF7 (human breast carcinoma) and WI38 (normal human lung fibroblast) cell lines. We attributed this to the low permeability and/or stability of the free thiol in cells. While the use of nonreduced disulfide functionality (e.g., present in the parental psammaplin A (**3**), X = OH) is one strategy to "protect" the free thiol and allow for its effective dosing into cells, this prodrug strategy is reliant on intracellular reduction of the disulfide to the active thiol form. As such, cellular potency would be expected to correlate significantly with the cellular levels of reductants such as glutathione [23]. An alternative prodrug approach to "protect" the thiol active form of psammaplin A analogues would be to form the corresponding thioester; the active thiol being generated in cells after cleavage of the acyl group by nonselective esterases. In support of this approach, Miyata and co-workers synthesised a number of SAHA-derived thioesters during their research of nonhydroxamate inhibitors of HDACs, which exhibited moderate to high potency in enzymatic and cell-based assays [24,25]. Interestingly, the potencies of their compounds were higher than the potencies of their corresponding dimeric disulfide analogues, and this was thought to reflect the rate of thioester hydrolysis versus the rate of disulfide reduction. We therefore commenced a study to prepare thioester derivatives of our psammaplin A analogues to investigate whether this would be an effective strategy to optimise these potent and selective HDAC inhibitors.

Results and Discussion

Synthesis of acetate-protected thiol analogues of psammaplin A

We designed and synthesised several acetate-protected psammaplin A analogues. The structures of our thioester-based probes are shown in Scheme 2. We recently demonstrated [20] that variation of the aromatic substitution pattern had only a marginal influence on the HDAC inhibitory potency of psammaplin A analogues in vitro. Therefore, the native phenol was replaced by its methylated homologue for ease of synthesis, notably to avoid side reactions during the carbodiimide-mediated coupling step, whereby we had previously found the phenol to act as a competitive nucleophile. Since we had previously demonstrated the importance of the oxime (Scheme 1) for HDAC potency and selectivity, we prepared probes with these different functionalities in order to allow comparison of our data to our previously generated in vitro and in cell SAR data [20].

Condensation between acid **5** and *O*-methylhydroxylamine, followed by EDC coupling with *S*-2-aminoethyl ethanethioate **6** [26] afforded thioacetate analogue **7** (Scheme 2). Condensation of acid **5** with hydroxylamine, followed by coupling with **6** using DCC and *N*-hydroxyphthalimide [27] as coupling reagents afforded thioacetate **8**. The latter conditions were also applied to **5** and afforded thioacetate analogue **9**. The isolated yields for products **8** and **9** were unoptimised, and our previous work suggests that these could be improved with further refinement of the reaction conditions [28].



Scheme 2: Synthesis of **7–9**. Conditions: (i) HCl·H_2NOMe, pyridine, rt, 12 h; (ii) EDC, NHS, dioxane, rt, 3 h; (iii) **6**, Et_3N, dioxane/MeOH, rt; (iv) HCl·H_2NOH, pyridine, rt, 12 h; (v) DCC, NOHP, **6**, Et_3N, dioxane, rt, 24 h.

Thioesters **7**–**9** were assayed against A549, MCF7 and WI38 cell lines, in addition to recombinant human rHDAC1 (class I) and recombinant human HDAC6 (rHDAC6, class II) as previously reported [20]. Psammaplin A (**3**), prereduced psammaplin A thiol (**4**), and SAHA (**1**) were included as control compounds. The results are shown in Table 1. $IC_{50}^{6/1}$ is defined by the ratio $IC_{50}^{HDAC6}/IC_{50}^{HDAC1}$ and was used as an indicator of isoform selectivity in vitro.

The synthesised thioesters displayed modest but significant cytotoxic activity in our cell-based assays (Table 1, columns 1–3). Compound **8**, which contains an oxime moiety, was the most potent compound in each case, followed by methyloxime **7**, and finally ketone **9**. These findings parallel our previous SAR data for the corresponding thiols [20], and reflect the previously established potency ranking for the AB system: NOH > NOMe > O. The most sensitive cell line to treatment was the MCF7 breast cancer cell line, with the most potent thioester **8** displaying an IC_{50} of 3.2 μM. Such sensitivity correlates with previous SAR data [20]. While being moderately potent against MCF7 cells (21 μM), **9** was inactive against A549 and WI38 cells at the highest concentration tested (50 μM). Similar to our previously reported SAR and mechanistic studies, a correlation between HDAC inhibition and cytotoxicity is clearly observable for these psammaplin A prodrugs.

Notably, in enzyme assays, the potencies of our acetate-protected analogues approached those of their corresponding thiols (Table 1, see note[a]), while being approximately 10-fold more potent than the parental disulfide series (Table 1, see note[a]). For example, **8** was found to be highly potent against rHDAC1, displaying an IC_{50} of 5 nM. With the exception of **9**, acetyl-protected compounds were found to be 2.5 (**8**) to 8 times (**7**) less potent than the corresponding free thiol analogues against rHDAC1. Curiously, acetyl-protected compounds **7**–**9** were found to be moderately active to completely inactive against rHDAC6 in each case, highlighting the important isoform selectivity of these compounds.

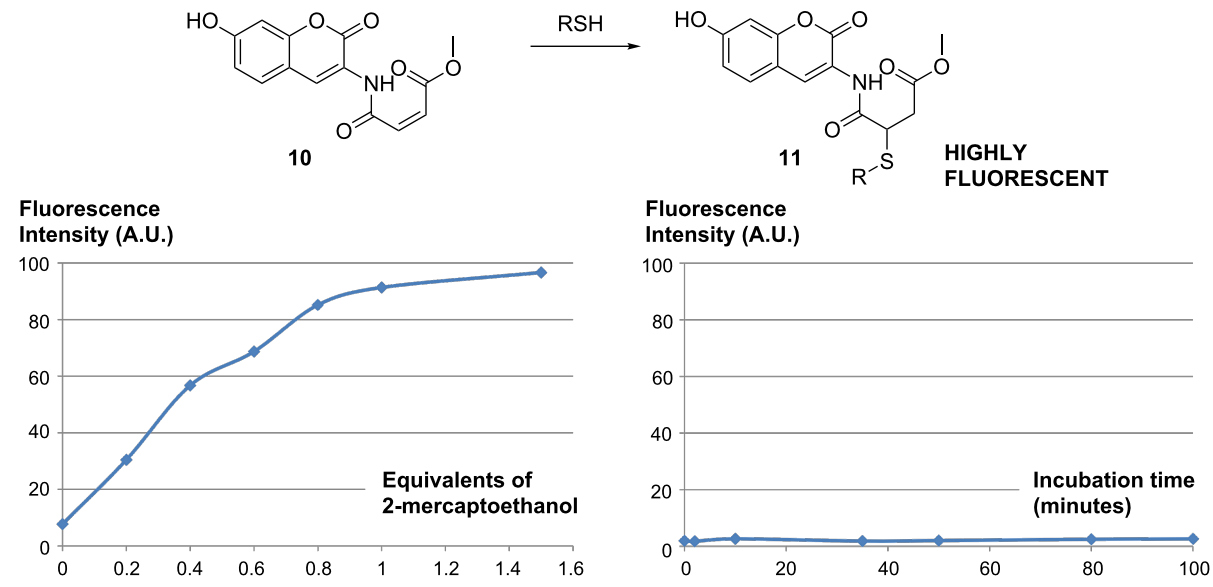
The mechanistic origin for the high potency of the supposed prodrug thioesters in cell-free assays was unclear: Such compounds were designed to be cleaved to give the active (thiol) inhibitor in cells, and presumably exhibit a decreased potency against the target HDAC, prior to cleavage of the acetyl group. As previously mentioned, Miyata and co-workers synthesised a number of SAHA-based thioesters, which exhibited moderate to high potency in both enzymatic and cell based assays. The enzymatic assays they employed, however, used cell extracts as the source of HDACs, potentially containing esterases, which may have cleaved the thioester during the assay. On the contrary, we observed the same pattern with purified rHDAC1 and purified rHDAC6, which obviously contains no such potential for esterase-driven hydrolysis. Recently, Williams reported the high potency of the natural product largazole, bearing an octanoyl-protected thiol, against HDACs [29]. While the deprotected analogue displayed nanomolar to subnanomolar potency in vitro against purified HDACs, the native thioester was still highly potent. They hypothesized that the octanoyl group was cleaved in situ to liberate the active thiol; however, no rigorous studies were reported to confirm this.

We therefore undertook preliminary studies to attempt to shed light on the reasons for the high potency of our thioesters in the enzymatic assays. We first envisaged that our assay buffer could potentially be responsible for thioester hydrolysis. We prepared and used synthetic probe **10** [30] (Scheme 3) in order to test this hypothesis. Coumarin-based probe **10** is known to react extremely fast with thiols through a Michael addition reaction. While the fluorescence of **10** is efficiently quenched by the intramolecular double bond, upon reaction with thiols, a highly

Table 1: Biological data.

Compound	A549 IC_{50} (μM)	MCF7 IC_{50} (μM)	WI38 IC_{50} (μM)	rHDAC1 IC_{50} (μM)	rHDAC6 IC_{50} (μM)	$IC_{50}^{6/1}$
SAHA (**1**)	n.d.	n.d.	n.d.	0.030	0.21	7
PSA (**3**)	7.5	1.3	3.4	0.045	2.8	62
PSA-SH (**4**)	2.5	2.4	3.4	0.001	0.36	360
8[a]	8.3 (4.1/0.16)	3.2 (0.63/0.61)	5.2 (2.2/1.1)	0.005 (0.043/0.002)	23 (2.0/3.2)	4560 (46/1772)
7[a]	44 (46/5.1)	12 (13/12)	17 (n.d./10)	0.12 (0.22/0.015)	>50 (>50/2.7)	>417 (>230/180)
9[a]	>50 (10/11)	21 (3.9/3.4)	>50 (4.1/14)	0.48 (9.0/1.1)	9.5 (8/0.25)	>20 (0.9/0.22)

[a]In brackets are data for the corresponding disulfides and thiols respectively, obtained from Baud et al [20].



Scheme 3: Top: Generation of the fluorescent adduct **11** after reaction of probe **10** with thiols. Bottom left: Fluorescence intensity at 465 nm (Y-axis, A.U.) as a function of the number of equivalents of 2-mercaptoethanol added (X-axis). Bottom right: Fluorescence intensity at 465 nm (Y-axis, A.U.) as a function of the incubation time (X-axis, minutes) of probe **10** with thioester **8**.

fluorescent conjugate **11** is produced. This system has been found to be particularly efficient to quantify thiol concentration in biological systems [30].

Control experiments were performed using 2-mercaptoethanol as the thiol source [30]. Fluorescence spectra of **10** (10^{-6} M **10** in buffer FB-188 [31]) were recorded after incubation with 0, 0.2, 0.4, 0.6, 0.8, 1.0 and 1.5 equiv 2-mercaptoethanol (Scheme 3, bottom left). As expected, a linear relationship between fluorescence intensity and the concentration of thiol could be observed between 0 and 1.0 equiv, confirming the sensitivity and reliability of this system at low concentration. When our HDACi thioester **8** was incubated with probe **10** (Scheme 3, bottom right) under the buffer conditions, however, no significant variation of the fluorescence intensity was observed. The standard incubation time of thioesters in our HDAC inhibitor assay is 20–30 minutes; however, no evidence of thiol formation was observed after up to 100 minutes of incubation in the assay buffer. This data therefore does not support the hydrolysis of our thioester inhibitors in the assay buffer. Two explanations could be envisaged to explain this result: (1) The thioester is stable to the assay buffer and therefore does not contribute to the in situ generation of the free thiol. (2) The quantity of free thiol generated in situ in this experiment was too low to be quantified.

An alternative hypothesis for the high potency of the thioester inhibitors is that the HDAC enzyme cleaves the acetyl group directly, utilizing its intrinsic deacetylase activity. Inhibition of rHDAC1 was measured (at the IC_{50} concentration of thioester) as a function of the initial incubation time (1–60 minutes) of rHDAC1 with thioesters **7** and **9** (Figure 2). No variation of enzymatic inhibition could be observed in each case, excluding rHDAC1 as the source of hydrolysis. Finally, we assessed whether the use of thioester inhibitors could influence the assay readout, when using our coupled HDAC assay. Trypsin-dependant generation of the fluorescence intensity (2^{nd} step of our coupled assay) was discounted as a source of false-positive activity, since trypsin was used in a large excess (430 μM) compared to the thioesters (low micromolar to nanomolar). Direct compound inhibition of trypsin would therefore not be significant in the overall readout on stoichiometry grounds.

Conclusion

In conclusion, we have demonstrated that highly potent and selective HDAC inhibitors can be discovered by preparing thioester derivatives of the natural product psammaplin A and close analogues. Such thioesters display significant cytotoxicity against several cancer cell lines. While initially envisaged as a prodrug approach, we found these thioesters to retain highly potent enzymatic activity using purified HDAC enzymes. Our preliminary results in the investigation of the origin of this effect have discounted hydrolysis of the thioester under the buffered conditions of the assay and direct cleavage of the acetyl group by the deacetylase enzyme. It therefore remains highly plausible that the thioacetate group can function as a potent zinc-binding group in its own right. While this hypothesis requires further validation, it opens up exciting new possi-

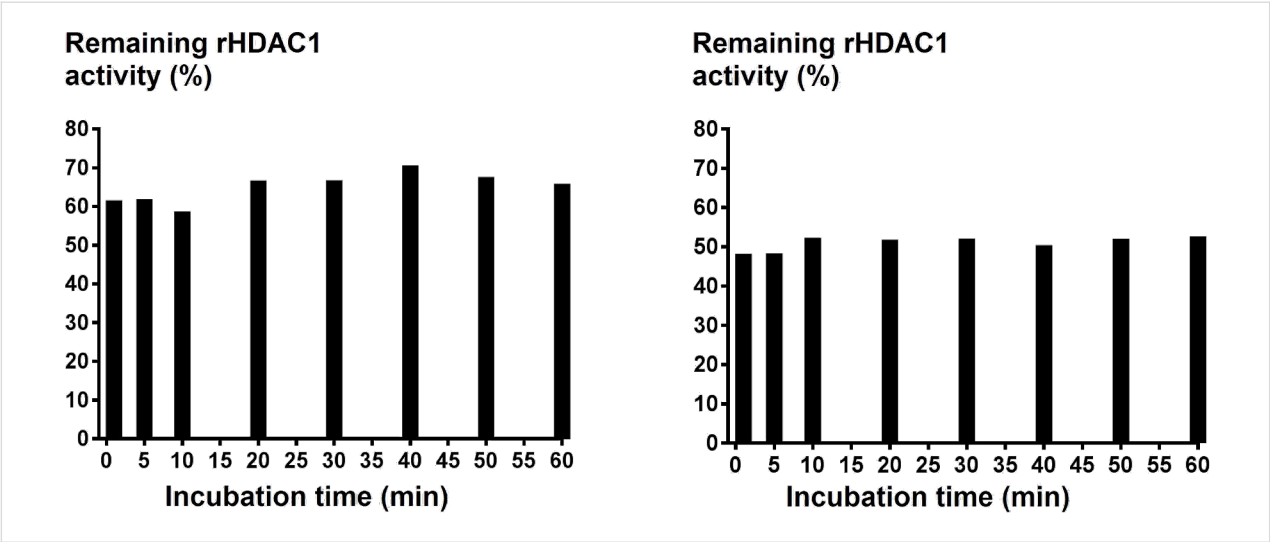
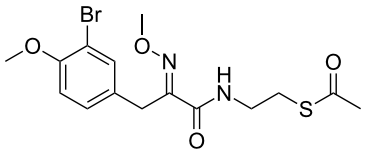


Figure 2: rHDAC1 was incubated with a predetermined IC_{50} concentration of **7** (left) and **9** (right) for 1–60 minutes, and the remaining rHDAC1 activity (Y-axis, %) was recorded and plotted as a function of the incubation time (X-axis, minutes).

bilities to prepare HDAC inhibitors bearing diverse thioester zinc-binding groups. Variation of the thioester functionality to protect its lability in cells and potentially orient suitable functionality into the internal cavity of HDACs [32] remain exciting avenues for future research.

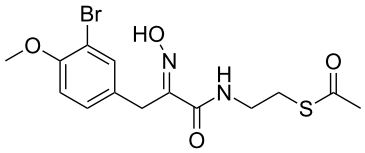
Experimental

(*E*)-(*S*)-2-(3-(3-Bromo-4-methoxyphenyl)-2-(methoxyimino)propanamido)ethyl ethanethioate (**7**)



Compound **7** (216 mg, 30% from acid **5**) was prepared according to previously reported procedures [28] and obtained as a yellowish oil after purification by flash column chromatography (AcOEt/CH_2Cl_2, 2:98). R_f 0.35 (AcOEt/CH_2Cl_2 2:98); IR: 1674, 1520, 1495, 1044 cm^{-1}; ^1H NMR (400 MHz, $CDCl_3$) δ 2.33 (s, 3H, CH_3C), 3.04 (t, J = 6.6 Hz, 2H, CH_2S), 3.48 (m, 2H, CH_2N), 3.81 (s, 2H, 4-CH_2), 3.84 (s, 3H, CH_3O-1), 4.01 (s, 3H, CH_3O-N), 6.78 (d, J = 8.4 Hz, 1H, 2-H), 6.97 (br t, 1H, NH), 7.21 (dd, J = 8.4, 2.1 Hz, 1H, 3-H), 7.46 (d, J = 2.1 Hz, 1H, 5-H); ^{13}C NMR (100 MHz, $CDCl_3$) δ 28.4, 28.6, 30.6, 39.1, 56.2, 63.1, 111.4, 111.8, 129.4, 129.8, 133.9, 151.4, 154.4, 162.6, 195.6; HRMS (ESI^+) m/z: $[M + H]^+$ calcd for $C_{15}H_{20}BrN_2O_4S$, 403.0322; found, 403.0336; Anal. calcd for $C_{15}H_{19}BrN_2O_4S$: C, 44.67; H, 4.75; N, 6.95; found: C, 44.74; H, 4.78; N, 6.89.

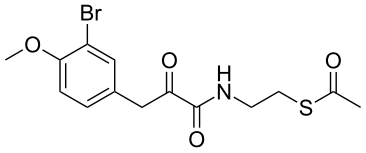
(*E*)-(*S*)-2-(3-(3-Bromo-4-methoxyphenyl)-2-(hydroxyimino)propanamido)ethyl ethanethioate (**8**)



To a solution of crude acid **5** (1 equiv) in freshly distilled pyridine (2 mL/mmol), under argon, was added hydroxylamine hydrochloride (1.5 equiv). The resulting mixture was stirred overnight at rt. Pyridine was then removed in vacuo, and the residue was dissolved in 1 N HCl (5.5 mL/mmol) and extracted three times with ethyl acetate (5.5 mL/mmol). The combined organic layers were dried (Na_2SO_4), filtered and concentrated to afford the relatively pure oxime intermediate, used for the next step without further purification. To a solution of this crude oxime derivative in dioxane (10 mL/mmol) under argon was added DCC (1 equiv) and *N*-hydroxyphthalimide (1 equiv). After 2 hours of stirring at rt, 2-acetylsulfanylethylammonium chloride (**6**, 1 equiv) and triethylamine (2.1 equiv) were added, and the resulting mixture was stirred overnight at rt. On the following day, the solvent was evaporated, and the product (50 mg, 19% from acid **5**) was obtained as a white powder after purification by flash column chromatography (AcOEt/CH_2Cl_2 2:8) and trituration in warm AcOEt. Mp 167–169 °C; R_f 0.6 (AcOEt/CH_2Cl_2, 2:8); ^1H NMR (400 MHz, CD_3OD) δ 2.29 (s, 3H, CH_3C), 3.01 (t, J = 6.6 Hz, 2H, CH_2S), 3.41 (m, 2H, CH_2N), 3.82 (s, 2H, 4-CH_2), 3.83 (s, 3H, CH_3O), 6.91 (d, J = 8.5 Hz, 1H, 2-H), 7.22 (dd, J = 8.5, 2.1 Hz, 1H, 3-H), 7.44 (d, J = 2.1 Hz, 1H, 5-H); ^{13}C NMR (100 MHz, $CDCl_3$) δ 28.7, 29.4,

30.4, 39.9, 56.7, 112.1, 113.1, 130.5, 131.8, 134.7, 152.9, 155.9, 165.9, 197.1; HRMS (ESI$^+$) *m*/*z*: [M + H]$^+$ calcd for $C_{14}H_{18}BrN_2O_4S$, 389.0165; found, 389.0164; Anal calcd for $C_{14}H_{17}BrN_2O_4S$: C, 43.20; H, 4.40; N, 7.20; found: C, 43.29; H, 4.32; N, 7.32.

(*S*)-2-(3-(3-Bromo-4-methoxyphenyl)-2-oxopropanamido)ethyl ethanethioate (**9**)



To a solution of acid **5** under argon in dioxane (5.5 mL/mmol) was added DCC (1 equiv), *N*-hydroxyphthalimide (1 equiv). After 2 hours of stirring at rt, 2-acetylsulfanylethylammonium chloride (**6**, 1 equiv) and triethylamine (2.1 equiv) were added and the resulting mixture was stirred overnight at rt. The day after the solvent was evaporated and the product (64 mg, 23%) was purified by flash column chromatography (AcOEt/CH_2Cl_2 1:9) and trituration in Bu_2O. Mp 93–95 °C; R_f 0.65 (AcOEt/CH_2Cl_2, 1:9); IR: 1685, 1523, 1498, 1106 cm^{-1}; ^{1}H NMR (400 MHz, $CDCl_3$) δ 2.35 (s, 3H, CH_3C), 3.05 (t, *J* = 6.4 Hz, 2H, CH_2S), 3.50 (m, 2H, CH_2N), 3.88 (s, 3H, CH_3O), 4.13 (s, 2H, $CH_2C(O)$), 6.86 (d, *J* = 8.5 Hz, 1H, 2-H), 7.16 (dd, J = 8.5, 2.1 Hz, 1H, 3-H), 7.21 (br t, 1H, NH), 7.42 (d, *J* = 2.1 Hz, 1H, 5-H); ^{13}C NMR (100 MHz, $CDCl_3$) δ 28.3, 30.6, 39.3, 41.7, 56.2, 111.7, 112.0, 125.9, 130.0, 134.5, 155.1, 159.9, 195.2, 195.5; HRMS (ESI$^+$) *m*/*z*: [M + H]$^+$ calcd for $C_{14}H_{17}BrNO_4S$, 374.0056; found, 374.0061; Anal calcd for $C_{14}H_{16}BrNO_4S$: C, 44.93; H, 4.31; N, 3.74; found: C, 45.04; H, 4.27; N, 3.81.

HDAC assays

HDAC assays were performed as previously reported [20]. The recombinant human histone deacetylases rHDAC1 and rHDAC6 were obtained from BPS Bioscience (US).

All reactions were performed in black half area 96-well microplates (Greiner bio-one, Germany) according to the general procedure described by Wegener et al. with some minor modifications. The reaction buffer contained 50 mM KH_2PO_4/K_2HPO_4, 15 mM Tris/HCl, pH 8, 250 mM NaCl, 0.001% (v/v) Pluronic, and 250 µM EDTA. The buffer components were purchased from Merck (Germany), Roth (Germany) and Sigma-Aldrich.

A serial dilution of test compounds was pre-incubated with 7.4 nM rHDAC1 or 2.8 nM rHDAC6, at 21 ± 1 °C in the dark for different periods of time as indicated. The enzyme reaction was initiated by the addition of Boc-Lys(Ac)-AMC substrate. The reaction mixture was incubated at 30 °C in the dark and stopped after 60 min by the addition of a mixture of 70 µM trypsin and 200 nM SAHA. The fluorescence of AMC served as an indirect measure of HDAC enzyme activity. The kinetics of AMC release was measured on a PolarStar fluorescence plate reader (BMG) with an excitation wavelength of 340 nm and an emission wavelength of 460 nm. Complete cleavage of deacetylated Boc-Lys-AMC by trypsin was achieved after about 10–15 min. The fluorescence intensity of the plateau was averaged over at least 5 min and normalized with respect to the percentage of enzyme activity. Finally, the normalized fluorescence intensities were plotted versus the concentration of test compounds and fitted to a four-parameter logistic model to calculate the IC_{50} values.

Acknowledgements

This work was supported by the Association for International Cancer Research (AICR) (08-0407).

References

1. Strahl, B. D.; Allis, C. D. *Nature* **2000,** *403,* 41–45. doi:10.1038/47412
2. Kouzarides, T. *Cell* **2007,** *128,* 693–705. doi:10.1016/j.cell.2007.02.005
3. Jones, P. A.; Baylin, S. B. *Cell* **2007,** *128,* 683–692. doi:10.1016/j.cell.2007.01.029
4. Feinberg, A. P.; Ohlsson, R.; Henikoff, S. *Nat. Rev. Genet.* **2006,** *7,* 21–33. doi:10.1038/nrg1748
5. Yoo, C. B.; Jones, P. A. *Nat. Rev. Drug Discovery* **2006,** *5,* 37–50. doi:10.1038/nrd1930
6. Cherblanc, F.; Chapman-Rothe, N.; Brown, R.; Fuchter, M. J. *Future Med. Chem.* **2012,** *4,* 425–446. doi:10.4155/fmc.12.7
7. Biel, M.; Wascholowski, V.; Giannis, A. *Angew. Chem., Int. Ed.* **2005,** *44,* 3186–3216. doi:10.1002/anie.200461346
8. Johnstone, R. W. *Nat. Rev. Drug Discovery* **2002,** *1,* 287–299. doi:10.1038/nrd772
9. Xu, W. S.; Parmigiani, R. B.; Marks, P. A. *Oncogene* **2007,** *26,* 5541–5552. doi:10.1038/sj.onc.1210620
10. Crabb, S. J.; Howell, M.; Rogers, H.; Ishfaq, M.; Yurek-George, A.; Carey, K.; Pickering, B. M.; East, P.; Mitter, R.; Maeda, S.; Johnson, P. W. M.; Townsend, P.; Shin-ya, K.; Yoshida, M.; Ganesan, A.; Packham, G. *Biochem. Pharmacol.* **2008,** *76,* 463–475. doi:10.1016/j.bcp.2008.06.004
11. Miller, T. A.; Witter, D. J.; Belvedere, S. *J. Med. Chem.* **2003,** *46,* 5097–5116. doi:10.1021/jm0303094
12. Marks, P. A.; Breslow, R. *Nat. Biotechnol.* **2007,** *25,* 84–90. doi:10.1038/nbt1272
13. Mann, B. S.; Johnson, J. R.; Cohen, M. H.; Justice, R.; Pazdur, R. *Oncologist* **2007,** *12,* 1247–1252. doi:10.1634/theoncologist.12-10-1247
14. Whittaker, S. J.; Demierre, M.-F.; Kim, E. J.; Rook, A. H.; Lerner, A.; Duvic, M.; Scarisbrick, J.; Reddy, S.; Robak, T.; Becker, J. C.; Samtsov, A.; MacCulloch, W.; Kim, Y. H. *J. Clin. Oncol.* **2010,** *28,* 4485–4491. doi:10.1200/JCO.2010.28.9066
15. Arabshahi, L.; Schmitz, F. J. *J. Org. Chem.* **1987,** *52,* 3584–3586. doi:10.1021/jo00392a016

16. Piña, I. C.; Gautschi, J. T.; Wang, G.-Y.-S.; Sanders, M. L.; Schmitz, F. J.; France, D.; Cornell-Kennon, S.; Sambucetti, L. C.; Remiszewski, S. W.; Perez, L. B.; Bair, K. W.; Crews, P. *J. Org. Chem.* **2003,** *68,* 3866–3873. doi:10.1021/jo034248t
17. Quiñoà, E.; Crews, P. *Tetrahedron Lett.* **1987,** *28,* 3229–3232. doi:10.1016/S0040-4039(00)95478-9
18. Rodriguez, A. D.; Akee, R. K.; Scheuer, P. J. *Tetrahedron Lett.* **1987,** *28,* 4989–4992. doi:10.1016/S0040-4039(00)96677-2
19. Nebbioso, A.; Pereira, R.; Khanwalkar, H.; Matarese, F.; García-Rodriguez, J.; Miceli, M.; Logie, C.; Kedinger, V.; Ferrara, F.; Stunnenberg, H. G.; de Lera, A. R.; Gronemeyer, H.; Altucci, L. *Mol. Cancer Ther.* **2011,** *10,* 2394–2404. doi:10.1158/1535-7163.MCT-11-0525
20. Baud, M. G. J.; Leiser, T.; Haus, P.; Samlal, S.; Wong, A. C.; Wood, R. J.; Petrucci, V.; Gunaratnam, M.; Hughes, S.; Buluwela, L.; Turlais, F.; Neidle, S.; Meyer-Almes, F.-J.; White, A. J. P.; Fuchter, M. J. *J. Med. Chem.* **2012,** *55,* 1731–1750. doi:10.1021/jm2016182
21. García, J.; Franci, G.; Pereira, R.; Benedetti, R.; Nebbioso, A.; Rodríguez-Barrios, F.; Gronemeyer, H.; Altucci, L.; de Lera, A. R. *Bioorg. Med. Chem.* **2011,** *19,* 3637–3649. doi:10.1016/j.bmc.2010.12.026
22. Baud, M. G. J.; Haus, P.; Leiser, T.; Meyer-Almes, F.-J.; Fuchter, M. J. *ChemMedChem* **2013,** *8,* 149–156. doi:10.1002/cmdc.201200450
23. Kim, D. H.; Shin, J.; Kwon, H. J. *Exp. Mol. Med.* **2007,** *39,* 47–55.
24. Suzuki, T.; Matsuura, A.; Kouketsu, A.; Nakagawa, H.; Miyata, N. *Bioorg. Med. Chem. Lett.* **2005,** *15,* 331–335. doi:10.1016/j.bmcl.2004.10.074
25. Suzuki, T.; Nagano, Y.; Kouketsu, A.; Matsuura, A.; Maruyama, S.; Kurotaki, M.; Nakagawa, H.; Miyata, N. *J. Med. Chem.* **2005,** *48,* 1019–1032. doi:10.1021/jm049207j
26. Baddiley, J.; Thain, E. M. *J. Chem. Soc.* **1951,** 3425–3426. doi:10.1039/jr9510003425
27. Hoshino, O.; Murakata, M.; Yamada, K. *Bioorg. Med. Chem. Lett.* **1992,** *2,* 1561–1562. doi:10.1016/S0960-894X(00)80429-1
28. Baud, M. G. J.; Leiser, T.; Meyer-Almes, F.-J.; Fuchter, M. J. *Org. Biomol. Chem.* **2011,** *9,* 659–662. doi:10.1039/c0ob00824a
29. Bowers, A.; West, N.; Taunton, J.; Schreiber, S. L.; Bradner, J. E.; Williams, R. M. *J. Am. Chem. Soc.* **2008,** *130,* 11219–11222. doi:10.1021/ja8033763
30. Yi, L.; Li, H.; Sun, L.; Liu, L.; Zhang, C.; Xi, Z. *Angew. Chem., Int. Ed.* **2009,** *121,* 4094–4097. doi:10.1002/ange.200805693
31. Hildmann, C.; Ninkovic, M.; Dietrich, R.; Wegener, D.; Riester, D.; Zimmermann, T.; Birch, O. M.; Bernegger, C.; Loidl, P.; Schwienhorst, A. *J. Bacteriol.* **2004,** *186,* 2328–2339. doi:10.1128/JB.186.8.2328-2339.2004
32. Haider, S.; Joseph, C. G.; Neidle, S.; Fierke, C. A.; Fuchter, M. J. *Bioorg. Med. Chem. Lett.* **2011,** *21,* 2129–2132. doi:10.1016/j.bmcl.2011.01.128

License and Terms

This is an Open Access article under the terms of the Creative Commons Attribution License (http://creativecommons.org/licenses/by/2.0), which permits unrestricted use, distribution, and reproduction in any medium, provided the original work is properly cited.

The license is subject to the *Beilstein Journal of Organic Chemistry* terms and conditions: (http://www.beilstein-journals.org/bjoc)

The definitive version of this article is the electronic one which can be found at: doi:10.3762/bjoc.9.11

Beilstein Journal of Organic Chemistry

An improved synthesis of a fluorophosphonate–polyethylene glycol–biotin probe and its use against competitive substrates

Hao Xu[‡1,2], Hairat Sabit[‡2], Gordon L. Amidon[2] and H. D. Hollis Showalter[*1,3]

Full Research Paper

Open Access

Address:
[1]Department of Medicinal Chemistry, University of Michigan, Ann Arbor, MI 48109-1065, USA, [2]Department of Pharmaceutical Sciences, University of Michigan, Ann Arbor, MI 48109-1065, USA and [3]Vahlteich Medicinal Chemistry Core, University of Michigan, Ann Arbor, MI 48109-1065, USA

Email:
H. D. Hollis Showalter[*] - showalh@umich.edu

* Corresponding author ‡ Equal contributors

Keywords:
biotin; fluorophosphonate; high turnover rate; reversible substrate

Beilstein J. Org. Chem. **2013,** *9,* 89–96.
doi:10.3762/bjoc.9.12

Received: 11 September 2012
Accepted: 24 December 2012
Published: 15 January 2013

This article is part of the Thematic Series "Synthetic probes for the study of biological function".

Guest Editor: J. Aubé

© 2013 Xu et al; licensee Beilstein-Institut.
License and terms: see end of document.

Abstract

The fluorophosphonate (FP) moiety attached to a biotin tag is a prototype chemical probe used to quantitatively analyze and enrich active serine hydrolases in complex proteomes in an approach called activity-based protein profiling (ABPP). In this study we have designed a novel synthetic route to a known FP probe linked by polyethylene glycol to a biotin tag (FP–PEG–biotin). Our route markedly increases the efficiency of the probe synthesis and overcomes several problems of a prior synthesis. As a proof of principle, FP–PEG–biotin was evaluated against isolated protein mixtures and different rat-tissue homogenates, showing its ability to specifically target serine hydrolases. We also assessed the ability of FP–PEG–biotin to compete with substrates that have high enzyme turnover rates. The reduced protein-band intensities resulting in these competition studies demonstrate a new application of FP-based probes seldom explored before.

Introduction

One of the goals of chemical biology is to develop small–molecule- and biomolecule-based probes to interrogate biological processes. In this regard, fluorophosphonate (FP) probes have been extensively used in activity-based protein profiling (ABPP) in proteomic studies [1,2]. FP probes, specifically designed to target serine hydrolases, originate from diisopropyl fluorophosphonate (DFP) [3,4]. DFP is a serine hydrolase covalent inhibitor and from it have evolved analytical tools in which "handles", such as biotin, rhodamine, and alkyne have been appended via a variety of linking chains [5-8]. These FP analogues have proven to be powerful tools in the profiling of complex proteome samples [9] and in the identification of

selective inhibitors [10,11]. However, very few cases have been published in which these probes have been utilized in the study of enzymes with reversible substrates. These substrates are usually endogenous or exogenous organic molecules with small molecular weights. Their functional groups are enzymatically modified with high specificity and efficiency, behaving quite differently from inhibitors due to their high turnover rates. Thus, competition assays between substrates and FP probes are more difficult to perform due to the rapid kinetics and covalent binding properties of the probes.

The FP–PEG–biotin compound **1**, shown in Figure 1, was first synthesized by the Cravatt group and utilized for affinity isolation of enzymes by pull-down with avidin beads followed by mass-spectrometry analysis [6]. Our interest in generating **1** on a larger scale to use in our research led us to consider an alternative and more expeditious synthesis. This was driven by several concerns of the original route including (a) a poor overall yield, (b) challenges in the chromatographic purification of some intermediates due to their hydrophilicity and lack of a UV chromophore, and (c) generating and then carrying the fluorophosphonate moiety through two steps with an attendant concern of its high reactivity and potential for toxicity to the laboratory chemist [12,13]. In our efforts to address those shortcomings, we report a novel synthetic route to FP–PEG–biotin **1**, and provide some preliminary results of studies in which this probe was utilized in competition experiments with reversible enzyme substrates.

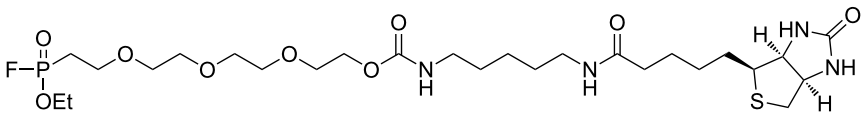
Results

Synthesis

The route to target probe **1** is delineated in Scheme 1. Monobenzylation of tetraethylene glycol (**2**) was carried out by the procedure of Jiang et al. [14] to give ether **3** in 78% yield. This was then subjected to a two-step procedure to provide the novel iodo ether **4b**. Thus, tosylation of **3** utilizing a slight modification of literature conditions [15] gave **4a**, which was subjected to Finkelstein conditions by utilizing a procedure reported for a related compound [16] to afford **4b** in a combined 90% yield. The phosphonate moiety was installed under standard Arbuzov conditions by heating **4b** under reflux in neat triethyl phosphite for 1 h to provide novel intermediate **5** in 92% yield following purification by column chromatography. Clean removal of the benzyl protecting group under standard conditions of catalytic hydrogenolysis provided, in 96% yield, the known phosphonate polyether alcohol **6**, the synthesis of which had been accomplished previously by a different route [17]. Activation of the alcohol moiety of **6** to the succinimidyl carbonate **7** was carried out under standard conditions in 87% yield following chromatographic purification. Coupling of **7** to the in situ generated 5-(biotinamido)pentaneamine fragment **12**, made from Boc-protected diamine **10** in a known two-step process [18], was carried out under mild conditions to provide novel precursor **8** in 76% yield following purification. The stage was now set for a two-step modification of the phosphonate moiety. Reaction of **8** with lithium azide in hot DMF, under conditions developed for the monodealkylation of phosphonic acid dialkyl esters of nucleosides [19], provided the novel monoethyl ester **9** in 87% yield following purification by a two-stage chromatographic procedure. Penultimate intermediate **9** was then cleanly converted to the fluorophosphonate utilizing the standard fluoridating reagent (DAST in dichloromethane) at −42 °C. Workup provided the FP probe **1** [20] in 80% yield, which was pure enough to use directly in biological studies. Due to the absence of a UV chromophore, the purity of FP–PEG–biotin **1** could not be determined by HPLC. TLC analysis was also problematic due to its reactivity with the highly polar solvent mixture required to move it up a plate. Nevertheless, we deem **1** to be of high purity due to the cleanliness of its NMR spectra (^{1}H, ^{13}C, ^{19}F, ^{31}P). The structural assignments of all compounds were supported by diagnostic peaks in the ^{1}H and ^{13}C NMR spectra and by mass spectrometry. Digital copies of all NMR spectra are given in Supporting Information File 1.

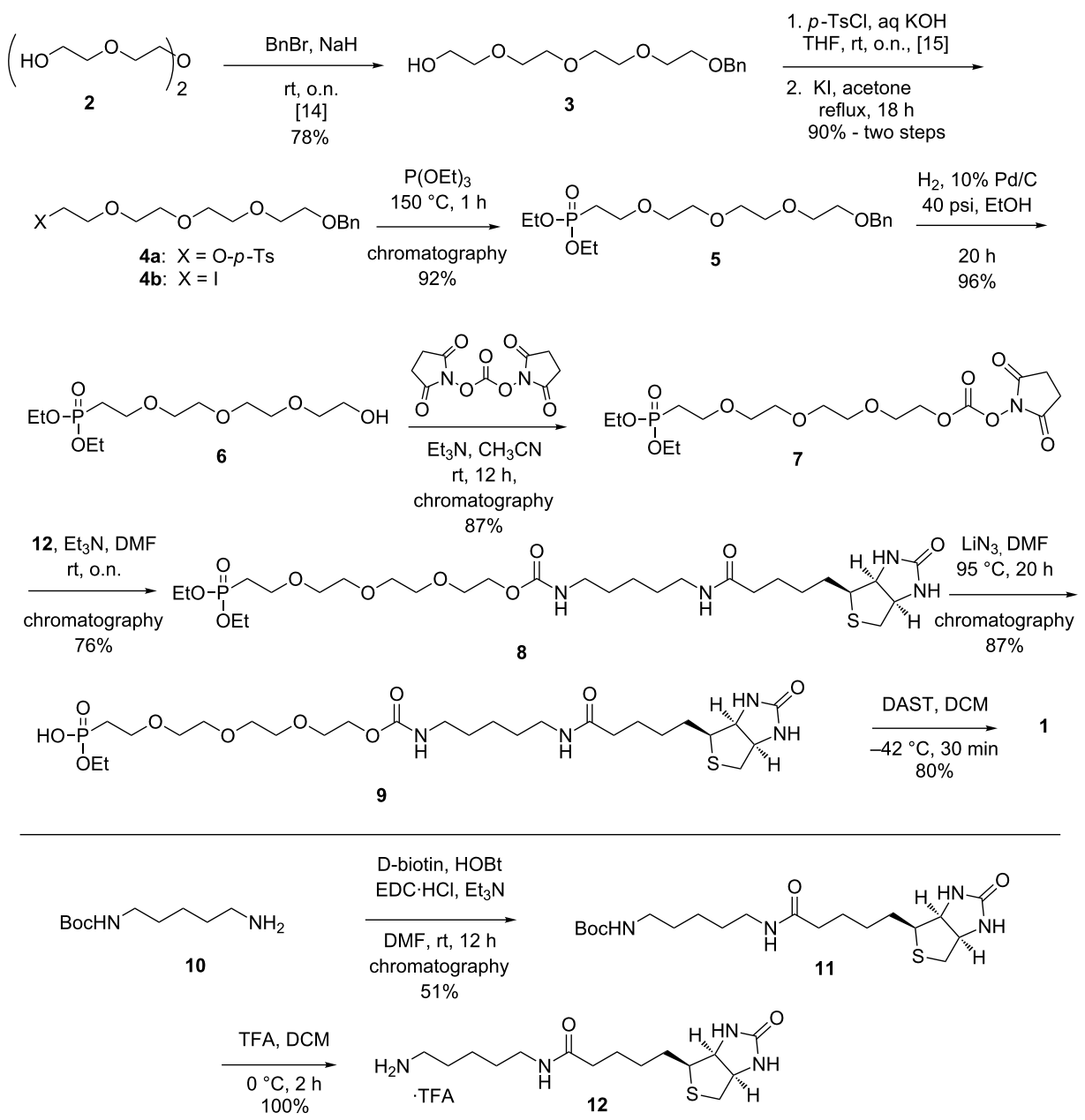
Evaluation of FP–PEG–biotin probe

To validate the labelling efficiency of the FP–PEG–biotin probe **1** synthesized by our new route, we utilized it in the purification of four arbitrarily mixed proteins including bovine serum albumin (BSA), porcine carboxylesterase (pCES), nucleoside phosphorylase (NP), and trypsin (Figure 2A). Thus, the protein mixture was incubated with probe **1** for one hour followed by the addition of avidin agarose and further incubation. Trypsin and pCES, which are serine hydrolases, bound to the probe and were removed from the mixture, as shown in lane 3. We also assayed FP probe **1** against different rat-tissue samples as



1

Figure 1: Structure of FP–PEG–biotin **1**.



Scheme 1: Synthetic scheme to FP–PEG–biotin probe **1**.

described in Supporting Information File 1. Rat stomach, small intestine, colon, liver, lung, heart, kidney, brain, testis proteome homogenates (1 mg/ml) in 50 mM Tris buffer (pH 8.0) were each treated with the FP probe for one hour at room temperature. Each run was separated on a gel and electrophoretically transferred onto a Hybond PVDF membrane and blotted with streptavidin. The results are shown in Figure 2B. The different patterns indicate that the FP probe can effectively select out serine hydrolase enzymes amongst the various tissue samples examined, as had been observed previously in studies by the Cravatt group [21].

Kinetic study of FP probe labelling activity

An incubation-time control study is the key toward successfully monitoring the competition between FP probe **1** and a reversible substrate with a high turnover rate. Hence, over a long incubation time, the substrate will be competed out with the active enzyme covalently linked to the probe, even though the concentration of added substrate is high compared to the probe. Enzymes have different kinetic properties in the same proteome sample, and a single enzyme can have different preferences for FP probes with different linkers [6]. Thus it is important to perform kinetic studies on a specific tissue or cell line before

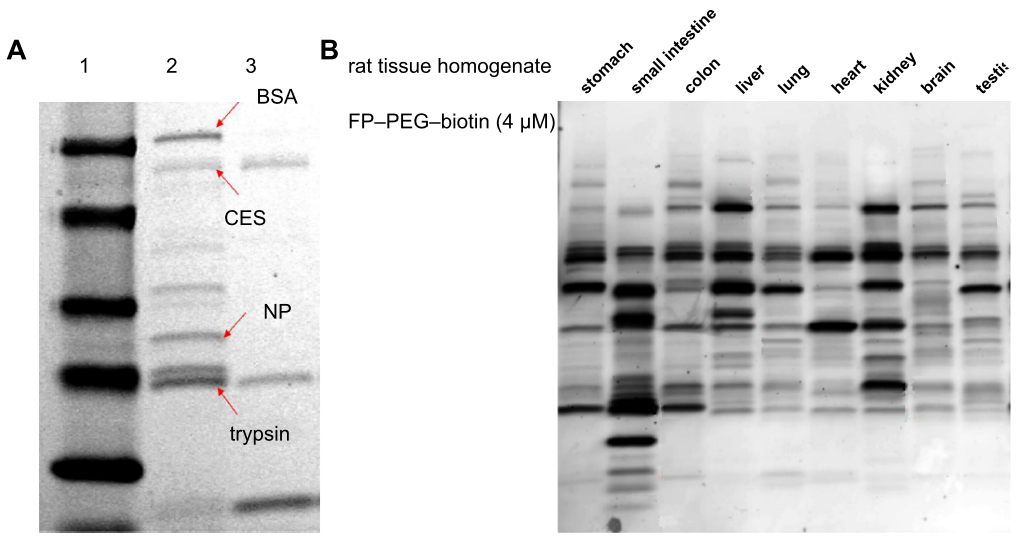


Figure 2: Labeling and affinity isolation of serine hydrolases by FP–PEG–biotin **1**. (A) Lane 1: Protein standard. Lane 2: Mixture of BSA, pCES, NP, trypsin before purification. Lane 3: Purification results. (B) Rat tissue homogenates were prepared in 50 mM Tris buffer (pH 8.0) as 1 mg/mL samples from each tissue and incubated with FP–PEG–biotin **1** (4 μM) at room temperature for 1 h. Samples were quenched with 5× sample loading buffer, heated at 85 °C for 5 min, and separated by SDS-PAGE. Protein samples were transferred to a PVDF membrane, blotted by streptavidin alkaline phosphatase, and visualized by incubation with ECF substrate.

the start of competition experiments. Toward this end, Caco-2 samples were prepared and incubated with FP–PEG–biotin **1** over different time courses ranging from 1 to 30 min (Figure 3). The sample from each trial was then separated by SDS-PAGE and blotted by streptavidin. A proteome sample was also incubated with DMSO for 10 min as a control. As all competitive exchanges between the FP probe and substrates occur within less than 15 min, data collection was limited to 30 min.

The band intensities from endogenous streptavidin-binding proteins, indicated in the control lane, did not change with incubation time. Neither did the intensity of the band around 64 kD (thin arrow), suggesting that this protein bound to the FP probe very quickly (≈50% within 1 min). In contrast, the 49 kD enzyme band (hollow arrow) showed a clear time-dependent reaction. Due to their lower expression levels, reaction of **1** with other enzymes (dark arrows) could not be detected below three minutes incubation time. Therefore, depending on the type and expression levels of serine hydrolase being investigated, different incubation times are required in order to observe a clear signal.

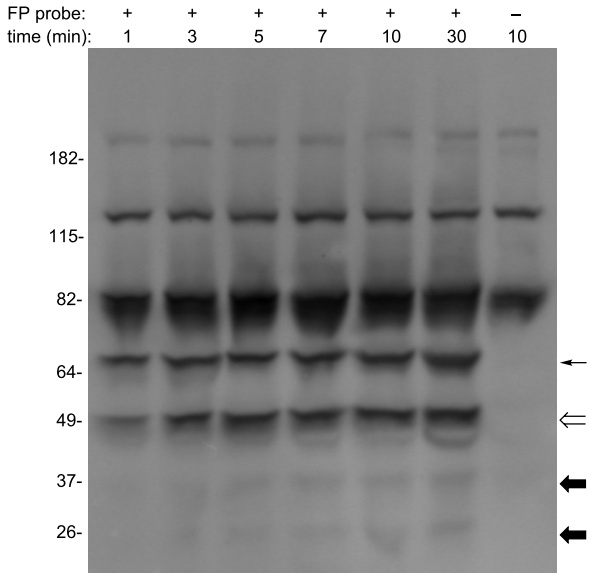


Figure 3: Kinetic study on FP labelling reactions. Caco-2 cell homogenates (1 mg/mL) were treated at room temperature with FP–PEG–biotin **1** (4 μM) for the indicated times, followed by the termination of reaction with 5× SDS-PAGE loading buffer. The results were analysed by 4–20% SDS-PAGE gel and streptavidin blotting. Serine hydrolases that reacted with the FP probe in a time-dependent manner are highlighted (thin, hollow and dark arrows, respectively).

Competition study

The identification of novel serine hydrolases and the screening of their covalent inhibitors against FP-biotin type probes have been extensively studied [9-11]. The general approach for serine hydrolase small molecule inhibitor development is based on the competition between an FP probe and inhibitor. To demonstrate this, a candidate inhibitor (or DMSO control) is incubated against a prepared proteome sample over a period of time. Then the sample is treated with an FP probe followed by additional incubation time. One then monitors the differential in

fluorescence signal between the inhibitor and control samples. From this, selectivity and potency can be determined.

To assess the possibility of utilizing FP probe **1** in the study of hydrolases that have substrates with high turnover rates, we chose to compete **1** against the enzyme that hydrolyzes the ester group of enalapril and oseltamivir. Enalapril and oseltamivir are commercially available prodrugs, which are converted to enalaprilat and oseltamivir carboxylate, respectively, after being absorbed in the intestine. Carboxylesterase [22], a common esterase existing in multiple human tissues, is shown to be active in the hydrolysis of both enalapril and oseltamivir [23,24]. Each is hydrolyzed at a high turnover rate. In a control run, pCES (± preheated) was treated with 4 μM FP–PEG–biotin **1** (Figure 4A, lanes 1 and 2). Then in subsequent runs, non-preheated samples of enzyme were treated with enalapril (1 mM, 3 mM) for 15 min, followed by the addition of FP–PEG–biotin (4 μM) and further incubation for 15 min at room temperature (lanes 3–5). Western blot analysis showed a clear reduction in band intensity. At 6 mM enalapril (lane 5), the band was not detectable, indicating that the competition is concentration dependent. In a similar manner, reaction of oseltamivir (10 mM) with pCES followed by the addition of FP–PEG–biotin (4 μM) showed that the pCES band intensity was reduced (Figure 4B). Thus, the reduced band intensities suggest that it is feasible to apply FP–PEG–biotin **1**, a covalent serine hydrolases probe, to the study of enzyme substrates with high turnover.

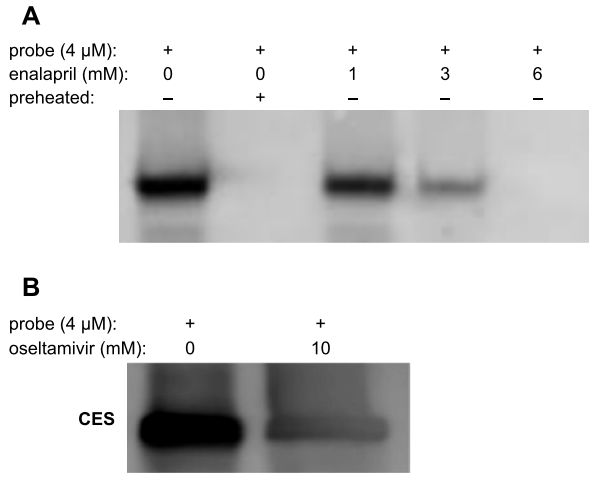


Figure 4: Competition assay between FP–PEG–biotin and enzyme hydrolysis reactions. (A) Enalapril at the indicated concentration was incubated in pCES (100 ng/mL) for 15 min, followed by the addition of FP probe **1** and further incubation for 15 min. Reactions were terminated by the addition of 5× SDS-PAGE loading buffer and then heated at 85 °C for 5 min. Samples were separated by SDS-PAGE and blotted by streptavidin. (B) Enzyme samples with oseltamivir were treated in the same way as enalapril.

Discussion

Fluorophosphonate probes with different analytical handles, such as rhodamine and alkyne, are being used to identify and characterize the in vivo proteome. Biotin-based probes that bind to streptavidin play an essential role in isolating and analyzing serine hydrolases. In our studies with FP–PEG–biotin probe **1**, we required large enough quantities that we decided to re-engineer the original synthesis of Kidd et al. [6]. Our major modifications involved (a) the introduction of a benzyl protecting group (in place of the TBS of the original synthesis) onto the PEG moiety to facilitate the early stages of the synthesis by providing a UV-active chromophore for easy detection; (b) introduction of a high yielding two-step iodination process, which avoids chromatography; and (c) reversing the sequence of fluoridation and amidation reactions such that the reactive FP moiety can be introduced in the last step. Overall, these modifications make for a more scalable, higher yielding sequence and importantly isolate the handling of reactive and potentially toxic FP compounds to a single step, namely the last one.

FP probes have been used mostly in the development of covalent inhibitors for pharmacologically interesting serine hydrolases due to their strong binding and rapid labeling properties. We have shown that for serine hydrolases with reversible substrates, FP probes can also be useful tools if their concentration and incubation times are properly controlled. We have demonstrated this in our studies with enalapril (6 mM) and oseltamivir (10 mM), which can each compete with FP–PEG–biotin probe **1** at a low concentration (4 μM) wherein the substrates bind reversibly to carboxylesterase and the probe binds covalently.

Conclusion

Several steps of the original synthesis of FP–PEG–biotin probe **1** have been modified, leading to a higher overall yield and easier manipulation. Starting from common precursor **2**, our synthesis requires only four chromatographic purifications over nine steps and provides a 28.5% overall yield of **1**. In contrast, the Cravatt sequence requires six chromatographic purifications over eight steps with an overall yield of 1%. The subsequent evaluation of **1** in biological studies demonstrates its ability to interact with serine hydrolases from several proteome samples. Additionally, preliminary kinetic and competition studies of probe **1** with reversible substrates have been conducted, showing that FP probes can be utilized for the investigation of reversible substrate activities as long as sufficient care is taken to identify the time course of reaction.

Experimental

All reagents were commercially available and used without further purification. ^{1}H and ^{13}C NMR spectra were obtained on

Bruker 300 or Bruker 500 MHz spectrometers with $CDCl_3$, d_6-DMSO, or d_4-methanol as solvent, and chemical shifts are reported relative to the residual solvent peak in δ (ppm). Mass spectrometry analysis was performed by using a Waters LCT time-of-flight mass spectrometry instrument. Flash column chromatography was performed with silica gel (220–240 mesh). Thin-layer chromatography (TLC) was performed on silica gel GHLF plates (250 microns) purchased from Analtech. Developed TLC plates were visualized with a UV lamp at 254 nm or by iodine staining. Extraction solutions were dried over $MgSO_4$ prior to concentration.

1-Phenyl-2,5,8,11-tetraoxatridecan-13-yl 4-methylbenzenesulfonate (4a): This compound was made by a slight modification of the literature procedure [15]. An ice-cold solution of tetraethylene glycol monobenzyl ether (**3**; 13.9 g, 48.9 mmol; made by the procedure of Jiang et al. [14]) in 70 mL of THF was treated with KOH (9.85 g, 171.1 mmol) dissolved in 50 mL of water. A solution of *p*-toluenesulfonyl chloride (11.18 g, 58.7 mmol) in 36 mL of THF was added dropwise to the reaction mixture, which was then gradually warmed to room temperature and stirred overnight. The reaction mixture was poured into sat. aq ammonium chloride and extracted with dichloromethane (3×). The combined extracts were dried and concentrated to leave 21.11 g (98%) of **4a** as a light yellow oil: R_f 0.26 (hexanes/ethyl acetate, 1:1); ^{1}H NMR (300 MHz, $CDCl_3$) δ 7.80–7.77 (d, J = 8 Hz, 2H), 7.34–7.26 (m, 7H), 4.56 (s, 2H), 4.14 (t, J = 4.5 Hz, 2H), 3.69–3.58 (m, 14 H), 2.44 (s, 3H); ^{13}C NMR (75 MHz, $CDCl_3$) δ 144.8, 138.2, 132.9, 129.8, 128.4, 128.0, 127.7, 127.6, 73.2, 70.7, 70.6, 70.5, 69.4, 69.2, 68.6, 21.7; MS *m*/*z*: 461.0 $[M + Na]^+$.

13-Iodo-1-phenyl-2,5,8,11-tetraoxatridecane (4b): The synthesis of **4b** utilized a procedure reported for a related compound [16]. A mixture of KI (23.97 g, 144.4 mmol) and sulfonate ester **4a** (21.11 g, 48.14 mmol) in 250 mL of acetone was heated under reflux for 18 h. After cooling to room temperature, the reaction mixture was filtered and the collected salts were rinsed with acetone. The filtrate was concentrated to an oil, which was diluted with dichloromethane. The solution was washed sequentially with sat. aq $Na_2S_2O_3$ and brine, dried, and concentrated to give 17.44 g (92%) of **4b** as a clear oil: R_f 0.37 (hexanes/ethyl acetate, 2:1) ; ^{1}H NMR ($CDCl_3$, 300 MHz) δ 7.35–7.26 (m, 5H), 4.57 (s, 2H), 3.77–3.63 (m, 14H), 3.24 (t, J = 6.5 Hz, 2H); ^{13}C NMR (75 MHz, $CDCl_3$) δ 138.3, 128.4, 127.7, 127.6, 73.2, 72.0, 70.7, 70.68, 70.63, 70.2, 69.4, 3.0; MS *m*/*z*: 416.9 $[M + Na]^+$.

Diethyl (1-phenyl-2,5,8,11-tetraoxatridecan-13-yl)phosphonate (5): Iodobenzyl polyether **4b** (17.44 g, 44.23 mmol) and triethyl phosphite (32 mL, 183.9 mmol) were mixed in an oven-dried round-bottom flask and heated under reflux for 1 h. Excess triethyl phosphite was removed under vacuum and the reaction mixture was directly loaded onto a silica-gel column, which was eluted with ethyl acetate and then methanol/ethyl acetate (5:95). Product fractions were combined and concentrated to give 16.5 g (92%) of **5** as a light yellow oil: R_f 0.11 (ethyl acetate); ^{1}H NMR (500 MHz, $CDCl_3$) δ 7.33–7.27 (m, 5H), 4.55 (s, 2H), 4.06 (q, J = 7 Hz, 4H), 3.6 (m, 14H), 2.16–2.05 (m, 2H), 1.30 (t, J = 7 Hz, 6H); ^{13}C NMR (125 MHz, $CDCl_3$) δ 138.2, 128.4, 127.7, 127.6, 73.2, 70.66, 70.63, 70.4, 70.2, 69.4, 65.1, 61.65, 61.60, 27.5, 26.5, 16.46, 16.42; MS *m*/*z*: 405.1 $[M + Na]^+$.

Diethyl (2-(2-(2-(2-hydroxyethoxy)ethoxy)ethoxy)ethyl)-phosphonate (6): A mixture of diethylphosphonate polyether **5** (3 g, 7.4 mmol), 10% Pd/C (0.3 g) and 100 mL ethanol in a 250 mL hydrogenation vessel was hydrogenated at 40 psi H_2 for about 20 h. The reaction mixture was rapidly filtered over Celite, and concentrated under reduced pressure to give 2.23 g (96%) of **6** as a clear oil: the ^{1}H and ^{13}C NMR are the same as previously reported for **6** made by a different procedure [17]; MS *m*/*z*: 315.1 $[M + H]^+$.

2-(2-(2-(2-(Diethoxyphosphoryl)ethoxy)ethoxy)ethoxy)ethyl (2,5-dioxopyrrolidin-1-yl)carbonate (7): A mixture of diethylphosphonate polyether alcohol **6** (0.5 g, 1.6 mmol), *N*,*N*-disuccinimidyl carbonate (2.04 g, 8 mmol), triethylamine (1.1 mL, 8 mmol), and anhydrous acetonitrile (4.5 mL) was stirred at room temperature for 12 h. The mixture was concentrated to an oil, which was distributed between dichloromethane and water. The organic phase was dried and concentrated to a yellow oil, which was then purified by silica-gel chromatography. Elution with dichloromethane/methanol (98:2 to 95:5) followed by pooling and concentration of product fractions provided 0.64 g (87%) of **7** as a light brown oil: the ^{1}H and ^{13}C NMR are the same as previously reported for **7** made by a different procedure [17]; MS *m*/*z*: 456.1 $[M + H]^+$.

2-(2-(2-(2-(Diethoxyphosphoryl)ethoxy)ethoxy)ethoxy)ethyl (5-(5-((3a*S*,4*S*,6a*R*)-2-oxohexahydro-1*H*-thieno[3,4-*d*]imidazol-4-yl)pentanamido)pentyl)carbamate (8): A solution of in situ synthesized 5-(biotinamido)pentaneamine, trifluoroacetic acid salt, **12** (see below) in 2 mL of DMF was treated with triethylamine (0.4 mL) at 0 °C and stirred at room temperature for 10 min. Diethyl phosphonate polyether succinimidyl carbonate **7** (145 mg, 0.31 mmol) was then added and the solution was stirred at room temperature overnight. The reaction mixture was distributed between ethyl acetate and brine, and the organic phase was dried. Concentration left a brown oil, which was purified by silica-gel chromatography eluting with dichloromethane/methanol/NH_4OH (92:8:0.5 to

90:10:1). Product fractions were pooled and concentrated to leave 324 mg (76%) of **8** as a pale white solid: ^{1}H NMR (500 MHz, $CDCl_3$) δ 6.66 (br s, 1H), 6.61 (br s, 1H), 6.03 (br s, 1H), 5.42 (br s, 1H), 4.46 (t, *J* = 6 Hz, 1H), 4.26 (t, *J* = 6 Hz, 1H), 4.14–4.12 (m, 2H), 4.06–4.02 (m, 4H), 3.64–3.58 (m, 12H), 3.15–3.06 (m, 7H), 2.84 (dd, *J* = 5 Hz, 13 Hz, 1H), 2.69 (d, *J* = 13 Hz, 1H), 2.13 (t, *J* = 7.3 Hz, 2H), 2.10–2.05 (m, 2H), 1.63–1.59 (m, 4H), 1.45–1.37 (m, 6H), 1.29–1.25 (m, 6H); ^{13}C NMR (125 MHz, $CDCl_3$) δ 173.4, 164.2, 156.6, 70.5, 70.4, 70.1, 69.6, 65.0, 63.7, 61.8, 61.7, 61.6, 60.2, 55.7, 40.6, 40.5, 39.2, 35.8, 29.5, 28.9, 28.2, 28.0, 27.4, 26.3, 25.7, 23.9, 16.4, 16.3; MS *m*/*z*: 669.2 $[M + H]^+$.

2-(2-(2-(2-(Ethoxy(hydroxy)phosphoryl)ethoxy)ethoxy)ethoxy)ethyl (5-(5-((3a*S*,4*S*,6a*R*)-2-oxohexahydro-1*H*-thieno[3,4-*d*]imidazol-4-yl)pentanamido)pentyl)carbamate (9): A mixture of lithium azide (200 mg, 4.1 mmol), diethyl phosphonate polyether carbamate **8** (150 mg, 0.22 mmol), and 2 mL of DMF was stirred at 95 °C for 18 h. DMF was removed under vacuum to leave a yellow oil, which was diluted with water and loaded onto a column of Amberlite–IR120 (H^+) resin. The column was eluted with DI water and the collected eluate was evacuated at 30 mm/Hg with stirring for 30 min at rt (to draw off hydrazoic acid) and then lyophilized to leave a crude yellow residue, which was purified by flash chromatography. Gradient elution with dichloromethane/methanol/NH_4OH (70:30:2 and then 80:20:1) followed by pooling and concentration of product fractions left 0.125 g (87%) of **9** as a colorless solid: ^{1}H NMR (500 MHz, CD_3OD) δ 4.53–4.50 (m, 1H), 4.34–4.31 (m, 1H), 4.18 (t, *J* = 4.6 Hz, 2H), 3.95–3.89 (m, 2H), 3.76–3.62 (m, 12H), 3.28–3.18 (m, 3H), 3.12 (t, *J* = 7 Hz, 2H), 2.95 (dd, *J* = 4.9 Hz, 12.9 Hz, 1H), 2.73 (d, *J* = 12.9 Hz, 1H), 2.22 (t, *J* = 7.3 Hz, 2H), 1.97–1.91 (m, 2H), 1.80–1.37 (m, 12H), 1.26 (t, *J* = 7 Hz, 3H); ^{13}C NMR (125 MHz, CD_3OD) δ 174.5, 164.7, 157.3, 69.8, 69.7, 69.5, 69.2, 66.7, 63.4, 62.0, 60.2, 59.6, 55.6, 40.3, 39.7, 38.9, 35.5, 29.2, 28.7, 28.4, 28.1, 28.0, 25.6, 23.8, 15.9, 15.8; MS *m*/*z*: 641.2 $[M + H]^+$.

2-(2-(2-(2-(Ethoxy(fluoro)phosphoryl)ethoxy)ethoxy)ethoxy)ethyl (5-(5-((3a*S*,4*S*,6a*R*)-2-oxohexahydro-1*H*-thieno[3,4-*d*]imidazol-4-yl)pentanamido)pentyl)carbamate (FP–PEG–biotin; 1): To a solution of monoethyl phosphonate polyether carbamate **9** (46 mg, 0.072 mmol) in 1 mL of anhydrous dichloromethane at −42 °C was added (diethylamino)sulfur trifluoride (DAST; 26.4 μL, 0.022 mmol). The mixture was stirred for 30 min and quenched with water at −42 °C. After stirring at room temperature for 10 min, the mixture was extracted with dichloromethane (3×). The organic phase was dried and concentrated to a yellow oil that was evacuated under high vacuum to leave 37 mg (80%) of **1**, which was used directly in biological studies: ^{1}H NMR (500 MHz, $CDCl_3$) δ 6.38 (br s, 1H), 5.60 (br s, 1H), 5.36 (br s, 1H), 5.29 (br s, 1H), 4.51 (m, 1H), 4.40–4.21 (m, 5H), 3.90–3.55 (m,12H), 3.30–3.11 (m, 5H), 2.92 (dd, *J* = 4.9, 12.9 Hz, 1H), 2.74 (d, *J* = 12.9 Hz, 1H), 2.35–2.18 (m, 4H), 1.85–1.40 (m, 12H); 1.31 (t, *J* = 6.0 Hz, 3H); ^{13}C NMR (125 MHz, $CDCl_3$) δ 173.3, 163.9, 156.6, 70.5, 70.4, 69.6, 64.2, 63.7, 63.6, 63.5, 61.8, 60.2 55.7, 40.6, 39.2, 35.8, 29.5, 28.9, 28.1, 28.0, 26.8, 25.7, 24.9, 23.8, 16.4, 16.3; ^{19}F NMR (282 MHz, $CDCl_3$) δ −59.4, −63.2; ^{31}P NMR (121 MHz, $CDCl_3$) δ 32.8, 24.0; MS *m*/*z*: 643.2 $[M + H]^+$.

***tert*-Butyl (5-(5-((3a*S*,4*S*,6a*R*)-2-oxohexahydro-1*H*-thieno[3,4-*d*]imidazol-4-yl)pentanamido)pentyl)carbamate (11):** This compound was made by the procedure of Konoki et al. [18] from *tert*-butyl (5-aminopentyl)carbamate (**10**; made by the procedure of Kaur et al. [25]) and D-biotin. The ^{1}H NMR spectrum is the same as previously reported [18]; ^{13}C NMR (125 MHz, $CDCl_3$) δ 173.3, 164.2, 156.2, 79.1, 61.8, 60.2, 55.8, 40.5, 40.3, 39.2, 36.0, 29.7, 29.1, 28.4, 28.2, 28.0, 25.8, 23.9; MS *m*/*z*: 451.1 $[M + Na]^+$.

***N*-(5-Aminopentyl)-5-((3a*S*,4*S*,6a*R*)-2-oxohexahydro-1*H*-thieno[3,4-*d*]imidazol-4-yl)pentanamide (12):** This compound was made similar to the procedure of Konoki et al. [18]. To an ice-cold solution of *tert*-butyl 5-(biotinamidopentyl)carbamate (**11**; 136 mg, 0.32 mmol) in dichloromethane (2.0 mL) was added dropwise trifluoroacetic acid (1.0 mL). The cooling bath was removed and the mixture was stirred for 2 h. The solution was concentrated in vacuo to a yellow oil, which was used in the next step without further purification: ^{1}H NMR (300 MHz, CD_3OD) δ 4.45 (dd, *J* = 8.0, 5.5 Hz, 1H), 4.26 (dd, *J* = 7.5, 4.5 Hz, 1H), 3.15–3.11 (m, 3H), 2.90–2.85 (m, 1H), 2.67–2.61 (m, 3H), 2.16 (t, *J* = 7.5 Hz, 2H), 1.71–1.48 (m, 4H), 1.42–1.33 (m, 8H); MS *m*/*z*: 329.1 $[M + H]^+$.

Supporting Information

Supporting Information File 1

Biology experimental details and digital NMR spectra for synthesized compounds.
[http://www.beilstein-journals.org/bjoc/content/supplementary/1860-5397-9-12-S1.pdf]

Acknowledgements

The authors thank members of the Vahlteich Medicinal Chemistry Core for helpful synthetic suggestions, Dr. Chester Provoda for his biology suggestions, and Kefeng Sun and Yasuhiro Tsume for their help with biology experiments. Financial support to HX from the National Institutes of Health (GM 037188) is gratefully acknowledged.

References

1. Saghatelian, A.; Cravatt, B. F. *Nat. Chem. Biol.* **2005,** *1,* 130. doi:10.1038/nchembio0805-130
2. Berger, A. B.; Vitorino, P. M.; Bogyo, M. *Am. J. PharmacoGenomics* **2004,** *4,* 371. doi:10.2165/00129785-200404060-00004
3. Walsh, C. *Enzymatic Reaction Mechanisms;* W. H. Freeman & Co: San Francisco, 1979.
4. Creighton, T. E. *Proteins: Structures and Molecular Properties,* 2nd ed.; W. H. Freeman & Co: New York, 1993.
5. Liu, Y.; Patricelli, M. P.; Cravatt, B. F. *Proc. Natl. Acad. Sci. U. S. A.* **1999,** *96,* 14694. doi:10.1073/pnas.96.26.14694
6. Kidd, D.; Liu, Y.; Cravatt, B. F. *Biochemistry* **2001,** *40,* 4005. doi:10.1021/bi002579j
7. Patricelli, M. P.; Giang, D. K.; Stamp, L. M.; Burbaum, J. J. *Proteomics* **2001,** *1,* 1067. doi:10.1002/1615-9861(200109)1:9<1067::AID-PROT1067>3.0.CO;2-4
8. Gillet, L. C. J.; Namoto, K.; Ruchti, A.; Hoving, S.; Boesch, D.; Inverardi, B.; Mueller, D.; Coulot, M.; Schindler, P.; Schweigler, P.; Bernardi, A.; Gil-Parrado, S. *Mol. Cell. Proteomics* **2008,** *7,* 1241. doi:10.1074/mcp.M700505-MCP200
9. Jessani, N.; Liu, Y.; Humphrey, M.; Cravatt, B. F. *Proc. Natl. Acad. Sci. U. S. A.* **2002,** *99,* 10335. doi:10.1073/pnas.162187599
10. Leung, D.; Hardouin, C.; Boger, D. L.; Cravatt, B. F. *Nat. Biotechnol.* **2003,** *21,* 687. doi:10.1038/nbt826
11. Bachovchin, D. A.; Brown, S. J.; Rosen, H.; Cravatt, B. F. *Nat. Biotechnol.* **2009,** *27,* 387. doi:10.1038/nbt.1531
12. Sivalingam, N.; Basivireddy, J.; Pulimood, A. B.; Balasubramanian, K. A.; Jacob, M. *Toxicol. in Vitro* **2009,** *23,* 887. doi:10.1016/j.tiv.2009.05.008
13. Quistad, G. B.; Klintenberg, R.; Casida, J. E. *Toxicol. Sci.* **2005,** *86,* 291. doi:10.1093/toxsci/kfi195
14. Jiang, Z.-X.; Yu, Y. B. *Synthesis* **2008,** 215. doi:10.1055/s-2007-1000857
15. Shan, M.; Bujotzek, A.; Abendroth, F.; Wellner, A.; Gust, R.; Seitz, O.; Weber, M.; Haag, R. *ChemBioChem* **2011,** *12,* 2587. doi:10.1002/cbic.201100529
16. Bar-Nir, B. B.-A.; Kadla, J. F. *Carbohydr. Polym.* **2009,** *76,* 60. doi:10.1016/j.carbpol.2008.09.026
17. Nickel, S.; Kaschani, F.; Colby, T.; van der Hoorn, R. A. L.; Kaiser, M. *Bioorg. Med. Chem.* **2012,** *20,* 601. doi:10.1016/j.bmc.2011.06.041
18. Konoki, K.; Sugiyama, N.; Murata, M.; Tachibana, K.; Hatanaka, Y. *Tetrahedron* **2000,** *56,* 9003. doi:10.1016/S0040-4020(00)00752-3
19. Holý, A. *Synthesis* **1998,** 381. doi:10.1055/s-1998-2047
20. Cravatt, B. F.; Sorensen, E.; Patricelli, M.; Lovato, M.; Adam, G. Proteomic Analysis. WO Patent WO2001077684A2, Oct 18, 2001.
21. Bachovchin, D. A.; Ji, T.; Li, W.; Simon, G. M.; Blankman, J. L.; Adibekian, A.; Hoover, H.; Niessen, S.; Cravatt, B. F. *Proc. Natl. Acad. Sci. U. S. A.* **2010,** *107,* 20941. doi:10.1073/pnas.1011663107
22. Ross, M. K.; Borazjani, A.; Wang, R.; Crow, J. A.; Xie, S. *Arch. Biochem. Biophys.* **2012,** *522,* 44. doi:10.1016/j.abb.2012.04.010
23. Larmour, I.; Jackson, B.; Cubela, R.; Johnston, C. *J. Clin. Pharmacol.* **1985,** *19,* 701. doi:10.1111/j.1365-2125.1985.tb02699.x
24. Shi, D.; Yang, J.; Yang, D.; LeCluyse, E. L.; Black, C.; You, L.; Akhlaghi, F.; Yan, B. *J. Pharmacol. Exp. Ther.* **2006,** *319,* 1477. doi:10.1124/jpet.106.111807
25. Kaur, N.; Zhou, B.; Breitbeil, F.; Hardy, K.; Kraft, K. S.; Trantcheva, I.; Phanstiel, O., IV. *Mol. Pharmaceutics* **2008,** *5,* 294. doi:10.1021/mp700096e

License and Terms

This is an Open Access article under the terms of the Creative Commons Attribution License (http://creativecommons.org/licenses/by/2.0), which permits unrestricted use, distribution, and reproduction in any medium, provided the original work is properly cited.

The license is subject to the *Beilstein Journal of Organic Chemistry* terms and conditions: (http://www.beilstein-journals.org/bjoc)

The definitive version of this article is the electronic one which can be found at: doi:10.3762/bjoc.9.12

Beilstein Journal of Organic Chemistry

Asymmetric synthesis of host-directed inhibitors of myxoviruses

Terry W. Moore[1], Kasinath Sana[1], Dan Yan[2,3], Pahk Thepchatri[1], John M. Ndungu[1], Manohar T. Saindane[1], Mark A. Lockwood[1], Michael G. Natchus[1], Dennis C. Liotta[1,4], Richard K. Plemper[2,3,5], James P. Snyder[1,4] and Aiming Sun[*1,§]

Full Research Paper

Open Access

Address:
[1]Emory Institute for Drug Development, Emory University, 1515 Dickey Drive, Atlanta, GA 30322, USA, [2]Department of Pediatrics, Emory University School of Medicine, 2015 Uppergate Drive, Atlanta, GA 30322, USA, [3]Children's Healthcare of Atlanta, 2015 Uppergate Drive, Atlanta, GA 30322, USA, [4]Department of Chemistry, Emory University, 1515 Dickey Drive, Atlanta, GA 30322, USA and [5]Department of Microbiology & Immunology, Emory University School of Medicine, 1510 Clifton Road, Atlanta, GA 30322, USA

Email:
Aiming Sun[*] - asun2@emory.edu

* Corresponding author
§ Phone: 404-712-8680; Fax: 404-727-6689

Keywords:
asymmetric synthesis; benzimidazole; host-directed; myxovirus; small molecule inhibitor

Beilstein J. Org. Chem. **2013,** *9,* 197–203.
doi:10.3762/bjoc.9.23

Received: 26 September 2012
Accepted: 07 January 2013
Published: 30 January 2013

This article is part of the Thematic Series "Synthetic probes for the study of biological function".

Guest Editor: J. Aubé

© 2013 Moore et al; licensee Beilstein-Institut.
License and terms: see end of document.

Abstract

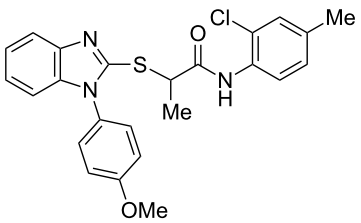
High-throughput screening (HTS) previously identified benzimidazole **1** (JMN3-003) as a compound with broad antiviral activity against different influenza viruses and paramyxovirus strains. In pursuit of a lead compound from this series for development, we sought to increase both the potency and the aqueous solubility of **1**. Lead optimization has achieved compounds with potent antiviral activity against a panel of myxovirus family members (EC_{50} values in the low nanomolar range) and much improved aqueous solubilities relative to that of **1**. Additionally, we have devised a robust synthetic strategy for preparing **1** and congeners in an enantio-enriched fashion, which has allowed us to demonstrate that the (*S*)-enantiomers are generally 7- to 110-fold more potent than the corresponding (*R*)-isomers.

Introduction

Myxoviruses are divided into two evolutionarily distinct yet related families: the orthomyxoviridae, which is composed largely of the influenza viruses, and the paramyxoviridae, which includes respiratory syncytial virus (RSV), measles virus (MeV), human parainfluenza virus (HPIV) and others [1]. Because myxoviruses are responsible for the majority of human

morbidity and mortality cases due to viral respiratory illness globally, a therapeutic strategy that targets these viruses could have a substantial impact on human health [2-5]. Although antivirals typically seek to disable viral proteins, cellular host proteins can also be targeted, as is the case with selzentry, which inactivates the coreceptor (CCR5) for human immunodeficiency virus (HIV) entry [6]. The former approach is likely to yield compounds with a narrow spectrum of antiviral activities, and such inhibitors will certainly face the inevitable challenge of resistance [7,8]. Our research group has been actively engaged in the identification of small molecule inhibitors against myxoviruses in recent years [8-12], with a particular focus on the development of agents that target host-cell proteins enabling viral reproduction. Advantages of this strategy include a vastly expanded list of potential targets; a broader spectrum of activity, because many of the relevant host proteins are shared among related viruses; and, in principle, less susceptibility to the development of resistance.

Using high-throughput screening, in combination with counter-screening for detecting a broadened viral target spectrum that extends to other pathogens of the myxovirus families, our research group has been successful in identifying small-molecule antiviral hits resident in host cells [13]. One such molecule recently described is benzimidazole **1** [14] (Figure 1). Although the compound is active in vitro against a number of different para- and orthomyxoviruses, **1** has poor water solubility (<15 μg/mL), which may contribute to its low oral bioavailability [15]. Additionally, it was shown that the methyl group at the stereogenic center alpha to the carbonyl is important for biological activity [8,12,14]. Compound **1** was previously prepared as the racemate, but subsequently separated into enantiomers by chiral HPLC. To enable large-scale preparation of the pure isomers for further pharmacokinetic and animal studies, we present here an asymmetric synthesis of **1** and its congeners with improved aqueous solubility and antiviral potency.



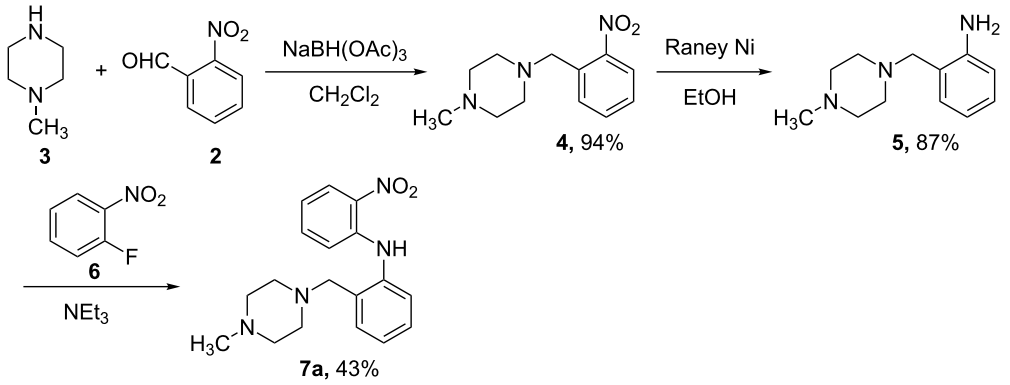
1 (JMN3-003)

Figure 1: Structure of first-generation lead compound **1**.

Results and Discussion

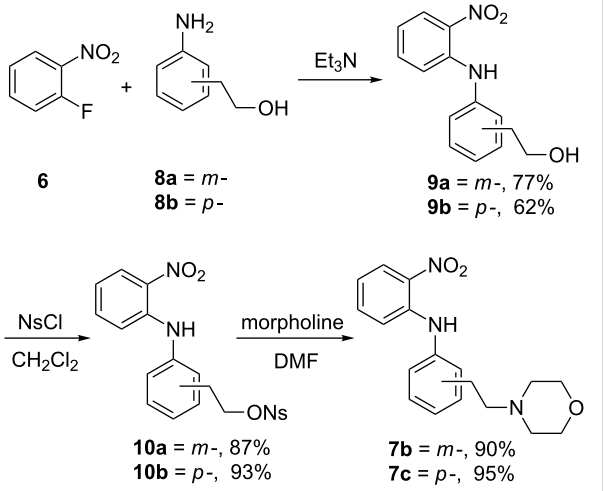
Design. We previously reported a series of compounds with antiviral activity against a number of myxoviruses [8,12,14]. Structure–activity relationship (SAR) studies suggested both the 2-chloro-4-methylanilide and the central α-thiopropionamide to be moieties that confer good activity. Relatively unexplored in our previous work was the importance of the *p*-methoxyphenyl ring as well as the influence of the stereochemistry at the chiral center. In the current work, we examine the replacement of the *p*-methoxyphenyl ring with basic moieties that may increase aqueous solubility while maintaining activity, and we also developed synthetic routes to produce each enantiomer of these compounds.

Synthesis. The compounds were prepared by modifications of our previously reported routes. Briefly, nitroanilines **7** were obtained by one of two routes: *ortho*-nitrobenzaldehyde (**2**) was treated with *N*-methylpiperazine (**3**) in the presence of sodium triacetoxyborohydride to give nitrobenzene **4**, which was reduced under hydrogenation conditions to provide aniline **5**. *o*-Fluoronitrobenzene (**6**) was coupled with the previously formed aniline under S_NAr conditions to furnish anilino nitrobenzene **7a** (Scheme 1). Alternatively, *meta*- and *para*-nitrophenylethanols **8** were combined with *o*-fluoronitrobenzene (**6**) to deliver *o*-nitroanilines **9**. The hydroxy groups of **9**



Scheme 1: Synthesis of anilino nitrobenzene **7a**.

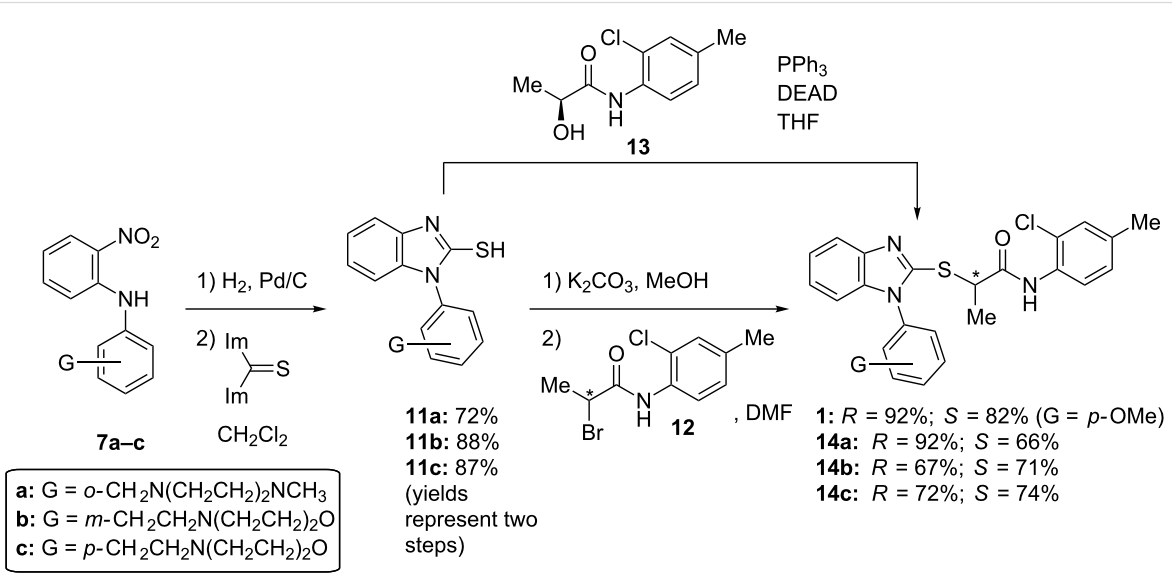
were activated as the *p*-nitrobenzenesulfonates **10** and displaced with morpholine to give *o*-nitroanilines **7b** and **7c** (Scheme 2). Hydrogenation was used to reduce *o*-nitroanilines **7** followed by cyclization using thiocarbonyldiimidazole to yield benzothiazoles **11**. In the case of the racemates, these were combined with α-bromopropionamide **12** to afford racemic **14** (Scheme 3).



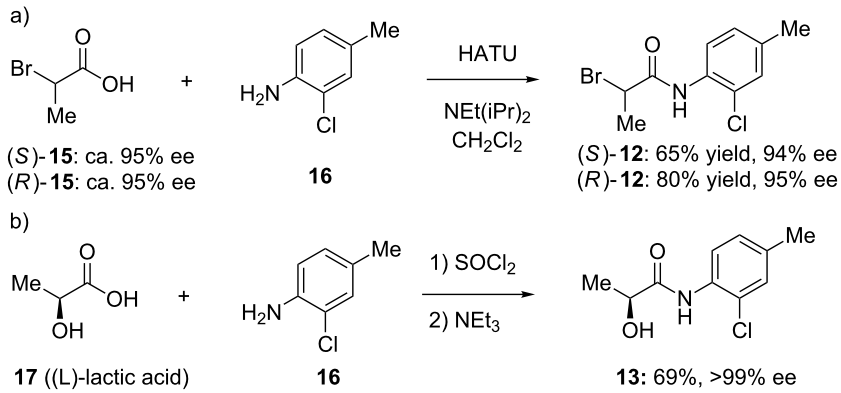
Scheme 2: Preparation of morpholinyl-*o*-nitroanilines.

To address the issue of stereochemical control, we developed two strategies for preparing the compounds enantioselectively. The first approach utilized commercially available (*R*)- or (*S*)-2-bromopropionic acid (**15**) from the chiral pool in a two-step sequence (Scheme 4a). The first step involved amide bond formation of 2-bromopropionic acid (**15**) with 2-chloro-4-methylaniline (**16**) by using HATU (*O*-(7-azabenzotriazol-1-yl)-*N,N,N′,N′*-tetramethyluronium hexafluorophosphate), a reagent known to limit racemization in peptide coupling reactions [16]. The enantiomeric excesses of the starting materials were ca. 95%. No erosion of stereochemistry in the products **12** was observed as determined by chiral HPLC. Recrystallization of **12** from ethanol did not increase the enantiomeric excess of the α-bromoamide. Interestingly, the final product can be achieved in both high yield and ee by adding the preformed potassium salt of the 2-mercaptobenzimidazole **11** to (*S*)- or (*R*)-α-bromopropionamides **12**. Using a substoichiometric amount of potassium carbonate (0.9 equiv) in warm methanol, followed by removal of solvents under vacuum, provided a convenient route to the potassium salt of **11**. The salt was suspended in anhydrous DMF and added dropwise to a cold (0 °C) solution of the previously formed bromides, to give the desired products **1** and **14** in high yield (80–90%) with little to no loss in enantiomeric excess. Isolating the potassium salt proved necessary, as attempts at preforming the potassium salt in dry DMF, followed by addition to the chiral α-bromoamide, led to ee's of ca. 60%. Although both chiral acids are readily available from commercial sources, their enantiomeric excesses seem to be limited to ca. 95%. For these studies, ee's >90% were sufficient; if material with higher enantiopurity is needed, we note that one recrystallization of (*S*)-**1** from ethyl ether increases the enantiomeric excess from 94% to 97.4%.

In an alternative approach that provides material with high enantiomeric excess (>98% ee), we utilized the Mitsunobu reaction of 2-mercaptobenzimidazoles with an amide obtained from (L)-lactic acid (**17**). Using one equivalent each of 2-mercapto-



Scheme 3: Asymmetric synthesis of (*R*)- and (*S*)-isomers by using two different approaches.



Scheme 4: Preparation of chiral propionamides by HATU-mediated coupling (a) or thionyl chloride-mediated coupling (b).

benzimidazole and α-hydroxyamide **13** (prepared from thionyl chloride-mediated coupling of (L)-lactic acid (**17**) and 2-chloro-4-methylaniline (**16**) [17] (Scheme 4b)) in the presence of a slight excess of triphenylphosphine and diethyl azodicarboxylate, we acquired the desired products **14** in good yield and ee. This methodology is attractive because of the high ee that can be obtained from the inexpensive and readily available (L)-lactic acid (**17**). However, the enantiomeric (D)-lactic acid is substantially more expensive, and as seen below, the products arising from (L)-lactic acid are less active, making this route less attractive than the route utilizing chiral α-bromopropionamides **12**.

Crystal structures of (*R*)- and (*S*)-**1** obtained by crystallization from ethyl ether allowed us to unambiguously assign the absolute configuration of each enantiomer. Shown in Figure 2 are the (*S*)-enantiomer (left, magenta) and (*R*)-enantiomer (right, cyan) of **1**. It is interesting to note that the hydrogen-bond formed between the amide N–H and the unsubstituted benzimidazole nitrogen in these crystal structures results in pseudo seven-membered rings. Whether this conformation is biologically relevant is unknown.

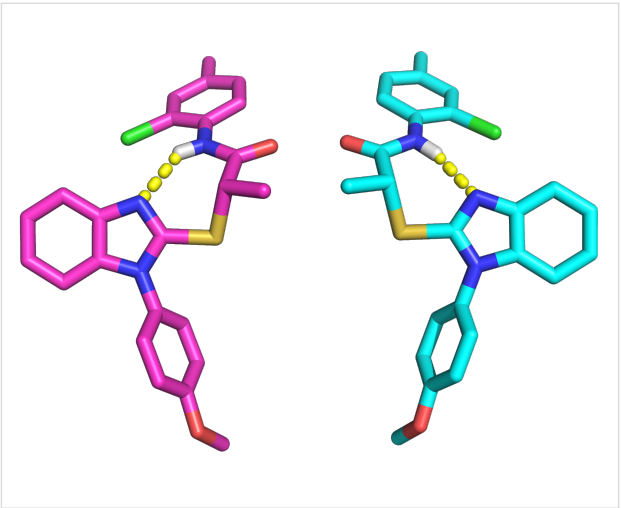


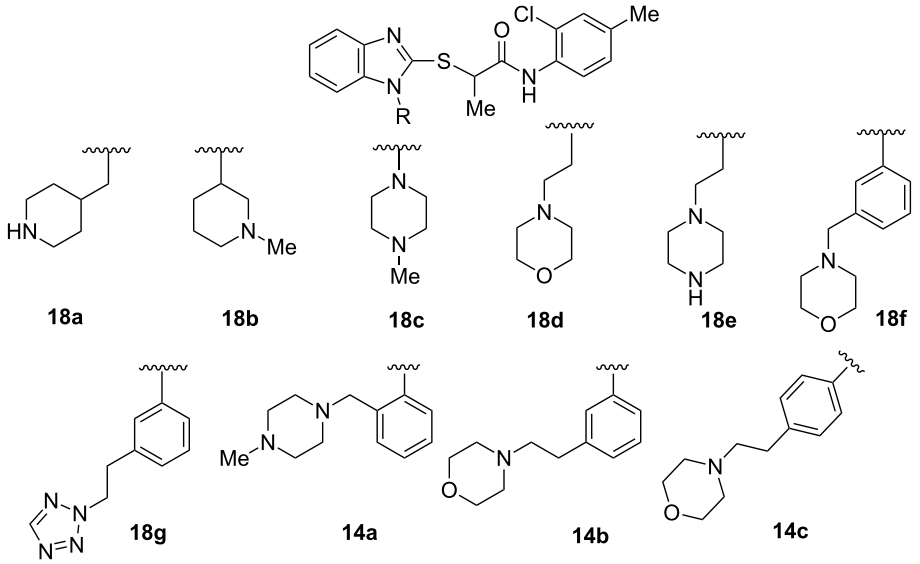
Figure 2: Renderings of crystal structures of (*S*)- (left, magenta) and (*R*)- (right, cyan) enantiomers of **1**.

Structure–activity relationships

A small set of compounds was synthesized based on variations of **1** by replacing the *p*-methoxyphenyl group with other substituted phenyl rings or heterocyclic rings. The compounds were initially assayed in two screening assays: (1) a measles virus cytopathic effect (CPE) reduction assay [12] and (2) a solubility assay based on laser nephelometry [18]. Unfortunately, compounds with the highest aqueous solubilities (>100 μg/mL) had the poorest antiviral activity (i.e., **18a** and **18e**, Table 1). To explore the possibility of increasing solubility by salt formation, the L-tartaric acid salt and benzenesulfonic acid salts of the most active compound **18f** were synthesized (Figure 3) and subjected to solubility testing. However, these salts failed to improve solubility compared with the parent. Several compounds exhibited moderate antiviral activities but poor to moderate aqueous solubilities (i.e., **1**, **18b**, **18d**, and **18f**, Table 1). Since **14a**, **14b**, and **14c** showed good antiviral activities, as well as moderate aqueous solubilities, we decided to examine the broader antiviral activities of these compounds and to determine what, if any, effect the stereocenter present in each of these compounds may cause.

We were motivated by the results of these two assays to more completely characterize the antiviral activities and solubility parameters of the most promising compounds. We assayed the compounds in three additional biological assays: (1) a firefly luciferase minireplicon assay whose output is driven by infection with influenza A/sw/Texas/2009 (WSN); (2) an assay using a renilla luciferase reporter embedded as an additional transcription unit in the genome of a measles virus (MeV) recombinant; and (3) a colorimetric assay that measures reduction of MTT

Table 1: In vitro screening of analogues of **1**.



Compd.	MeV[a] (CPE, μM)	Aqueous solubility[b] (μg/mL at pH 7.4)	Compd.	MeV[a] (CPE, μM)	Aqueous solubility[b] (μg/mL at pH 7.4)
1	3.1	<15	**18f**-tartrate	ND[c]	<15
18a	>75	140	**18f**-benzene sulfonate	ND	<15
18b	>0.29	19	**18g**	0.05[d]	<15
18c	>75	<15	**14a**	0.179	20
18d	4.9	22	**14b**	0.20	15
18e	>75	120	**14c**	0.6	25
18f	0.27	<15			

[a]50% inhibitory concentrations were calculated by using the variable-slope (four parameters) nonlinear regression-fitting algorithm embedded in the Prism 5 software package (GraphPad Software). Values represent averages of four experiments; highest concentration assessed, 75 μM. [b]Determined through laser nephelometry; [c]ND. Not determined. [d]Virus yield reduction assay was used.

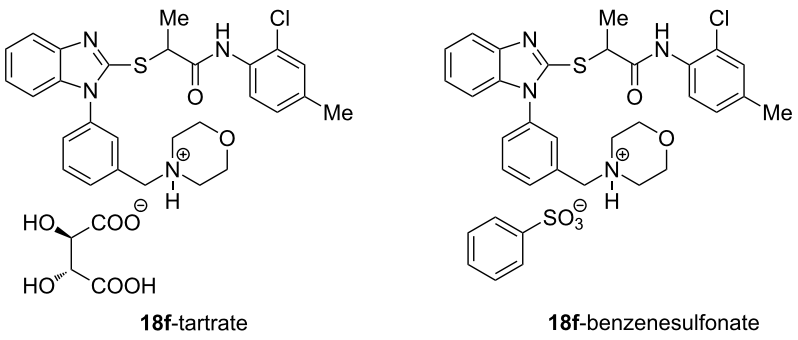
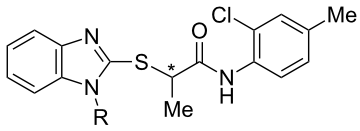


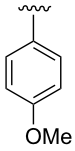
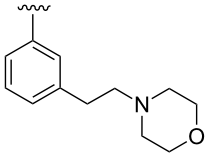
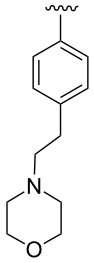
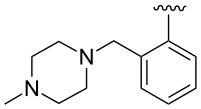
Figure 3: L-Tartaric acid salt (**18f**-tartrate) and benzenesulfonic acid salt (**18f**-benzenesulfonate) of **18f**.

(3-(4,5-dimethylthiazol-2-yl)-2,5-diphenyltetrazolium bromide) as a surrogate for general cytotoxicity, reported here as CC_{50}. Additionally, the aqueous solubilities of the compounds were measured by using laser nephelometry at pH 3.0, 5.0, and 7.4 (Table 2).

Analysis of the data reveals several trends. First, with the exception of a single case in which enantiomer potencies are similar (**14c**, $\Delta EC_{50} \leq$ 3-fold), six other comparisons reveal the (*S*)-enantiomer to be more active than the (*R*)-form by 7 to 110-fold. Although we do not know the identity of the specific bio-

Table 2: Antiviral potencies and solubilities for **1** and analogues.



Compd.	R	EC_{50} (nM)[a]		Solubility (μg/mL)[b]			CC_{50} (nM)[c]
		MeV	WSN	pH 3.0	pH 5.0	pH 7.4	
1		31	13				>50000
(*S*)-**1**		37	5	<15	<15	<15	>50000
(*R*)-**1**		880	160				>50000
14b		13	0.3				>50000
(*S*)-**14b**		11	1	158	33	15	>50000
(*R*)-**14b**		210	110				>50000
14c		110	43				ND[d]
(*S*)-**14c**		180	36	212	51	25	ND
(*R*)-**14c**		530	120				ND
14a		41	8				ND
(*S*)-**14a**[e]		68	4	>300	92	20	25000
(*R*)-**14a**[e]		470	120				ND

[a]50% effective concentrations were calculated by using the variable-slope (four parameters) nonlinear regression-fitting algorithm embedded in the Prism 5 software package (GraphPad Software). Values represent averages of four experiments; highest concentration assessed 75 μM. [b]Determined through laser nephelometry. [c]Determined through MTT assay, highest concentration assessed 50 μM. [d]ND: Not determined. [e]Assayed as a 1:1 mixture of atropisomers. Details of the separation of the atropisomers will be discussed elsewhere.

logical target(s), the enantio-discrimination implies to us that the molecules bind in a well-defined binding pocket that is able to accommodate the *S*-enantiomer more readily than the (*R*)-enantiomer.

We note that the activity trends for the (*S*)- and (*R*)-enantiomers against the measles and WSN influenza strain are qualitatively similar. However, for antiviral potency differences between the racemate and the (*S*)-enantiomer, the attenuation is indistinguishable under the testing conditions. Accordingly, we attribute the assay discrepancy to the inherent variability in the assay system.

While the compounds appear to be active against both influenza and measles virus, they are somewhat more active against the influenza virus strain (WSN) than against the measles virus. Among the compounds surveyed, (*S*)-**14b** is the most potent compound, with EC_{50} values of 1–11 nM against the two viruses. Because the CC_{50} values of the compounds are greater than 50 μM, the upper limit of the assay, we assume that the compounds are not generally cytotoxic, giving selectivity indices (CC_{50}/EC_{50}) for the active enantiomers of at least 10^3–10^4.

We have also assayed the most active compounds in a human parainfluenza viral (HPIV) titer assay based on plaque assay titration. The values for (*S*)-**1**, (*S*)-**14a**, (*S*)-**14b**, and (*S*)-**14c** are 80, 13, 80, and 11 nM, respectively. These data further corroborate the broad-spectrum activity of these compounds.

Lastly, the solubilities of the compounds have been improved relative to that of **1**. At all pH values examined, the aqueous

solubility of **1** was below the limits of detection of the nephelometry assay (i.e., <15 μg/mL). However, compounds bearing basic amine functionalities have improved solubilities relative to **1**, particularly at acidic pH values, but also at pH 7.4.

Conclusion

We have extended our previously published work on host-directed inhibitors of myxovirus replication by preparing analogues that positively address the poor aqueous solubility of **1** (JMN3-003) while simultaneously improving its potency. The compounds presented here furnish EC_{50} values as low as 1 nM with aqueous solubilities ranging from 15–25 μg/mL at pH 7.4 to >300 μg/mL at pH 3.0. Additionally, we have developed two complementary methods for the synthesis of each of the enantiomers of the compounds discussed and have unequivocally demonstrated that the (*S*)-enantiomer is more active in this series than the (*R*)-enantiomer. Further work from our laboratories regarding the in vivo efficacy of these compounds is underway.

Supporting Information

Contains detailed synthetic procedures and characterization data for molecules described herein, a more detailed description of the laser nephelometry assay, and data tables for the crystal structures of (*S*)-**1** and (*R*)-**1**.

Supporting Information File 1

Detailed synthetic procedures and characterization data.
[http://www.beilstein-journals.org/bjoc/content/supplementary/1860-5397-9-23-S1.pdf]

Acknowledgments

This work was supported, in part, by Public Health Service Grants AI071002 and AI085328 (to R. K. P.) from the NIH/NIAID and by Public Health Service Grant HG003918-02 (to J.P.S.) from the NIH. We also thank Deborah Culver for solubility testing and Dr. John Bacsa for helpful discussions of crystal structures.

References

1. König, R.; Stertz, S.; Zhou, Y.; Inoue, A.; Hoffmann, H.-H.; Bhattacharyya, S.; Alamares, J. G.; Tscherne, D. M.; Ortigoza, M. B.; Liang, Y.; Gao, Q.; Andrews, S. E.; Bandyopadhyay, S.; Jesus, P. D.; Tu, B. P.; Pache, L.; Shih, C.; Orth, A.; Bonamy, G.; Miraglia, L.; Ideker, T.; García-Sastre, A.; Young, J. A. T.; Palese, P.; Shaw, M. L.; Chanda, S. K. *Nature* **2010,** *463,* 813–817. doi:10.1038/nature08699
2. Martin, P.; Jensen, D. M. J. *Gastroenterol. Hepatol.* **2008,** *23,* 844–855. doi:10.1111/j.1440-1746.2008.05398.x
3. Dixit, N. M.; Perelson, A. S. *Cell. Mol. Life Sci.* **2006,** *63,* 832–842. doi:10.1007/s00018-005-5455-y
4. Buckwold, V. E.; Wei, J.; Wenzel-Mathers, M.; Russell, J. *Antimicrob. Agents Chemother.* **2003,** *47,* 2293–2298. doi:10.1128/AAC.47.7.2293-2298.2003
5. Willis, R. C.; Carson, D. A.; Seegmiller, J. E. *Proc. Natl. Acad. Sci. U. S. A.* **1978,** *75,* 3042–3044. doi:10.1073/pnas.75.7.3042
6. De Clercq, E. *Nat. Rev. Drug Discovery* **2002,** *1,* 13–25. doi:10.1038/nrd703
7. Whitley, R. J.; Roizman, B. *Lancet* **2001,** *357,* 1513–1518. doi:10.1016/S0140-6736(00)04638-9
8. Yoon, J.-J.; Krumm, S. A.; Ndungu, J. M.; Hoffman, V.; Bankamp, B.; Rota, P. A.; Sun, A.; Snyder, J. P.; Plemper, R. K. *Antimicrob. Agents Chemother.* **2009,** *53,* 3860–3870. doi:10.1128/AAC.00503-09
9. Sun, A.; Yoon, J. J.; Yin, Y.; Prussia, A.; Yang, Y.; Min, J.; Plemper, R. K.; Snyder, J. P. *J. Med. Chem.* **2008,** *51,* 3731–3741. doi:10.1021/jm701239a
10. White, L. K.; Yoon, J.-J.; Lee, J. K.; Sun, A.; Du, Y.; Fu, H.; Snyder, J. P.; Plemper, R. K. *Antimicrob. Agents Chemother.* **2007,** *51,* 2293–2303. doi:10.1128/AAC.00289-07
11. Sun, A.; Chandrakumar, N.; Yoon, J.-J.; Plemper, R. K.; Snyder, J. P. *Bioorg. Med. Chem. Lett.* **2007,** *17,* 5199–5203. doi:10.1016/j.bmcl.2007.06.084
12. Krumm, S. A.; Ndungu, J. M.; Yoon, J.-J.; Dochow, M.; Sun, A.; Natchus, M.; Snyder, J. P.; Plemper, R. K. *PLoS One* **2011,** *6,* e20069. doi:10.1371/journal.pone.0020069
13. Yoon, J.-J.; Chawla, D.; Paal, T.; Ndungu, M.; Du, Y.; Kurtkaya, S.; Sun, A.; Snyder, J. P.; Plemper, R. K. *J. Biomol. Screening* **2008,** *13,* 591–608. doi:10.1177/1087057108321089
14. Sun, A.; Ndungu, J. M.; Krumm, S. A.; Yoon, J.-J.; Thepatchri, P.; Natchus, M.; Plemper, R. K.; Snyder, J. P. *ACS Med. Chem. Lett.* **2011,** *2,* 798–803. doi:10.1021/ml200125r
15. Pharmacokinetics Study of JMN3-003. Unpublished results.
16. Carpino, L. A. *J. Am. Chem. Soc.* **1993,** *115,* 4397–4398. doi:10.1021/ja00063a082
17. Nair, V. P.; Mustafa, S. M.; Mohler, M. L.; Yang, J.; Kirkovsky, L. I.; Dalton, J. T.; Miller, D. D. *Tetrahedron Lett.* **2005,** *46,* 4821–4823. doi:10.1016/j.tetlet.2005.04.143
18. Hoelke, B.; Gieringer, S.; Arlt, M.; Saal, C. *Anal. Chem.* **2009,** *81,* 3165–3172. doi:10.1021/ac9000089

License and Terms

This is an Open Access article under the terms of the Creative Commons Attribution License (http://creativecommons.org/licenses/by/2.0), which permits unrestricted use, distribution, and reproduction in any medium, provided the original work is properly cited.

The license is subject to the *Beilstein Journal of Organic Chemistry* terms and conditions: (http://www.beilstein-journals.org/bjoc)

The definitive version of this article is the electronic one which can be found at:
doi:10.3762/bjoc.9.23

Beilstein Journal of Organic Chemistry

Development of peptidomimetic ligands of Pro-Leu-Gly-NH_2 as allosteric modulators of the dopamine D_2 receptor

Swapna Bhagwanth[1], Ram K. Mishra[2] and Rodney L. Johnson[*1]

Review

Open Access

Address:
[1]Department of Medicinal Chemistry, University of Minnesota, 308 Harvard Street SE, Minneapolis, MN 55455, USA and [2]Department of Psychiatry and Behavioral Neurosciences, McMaster University, 1200 Main Street W, Hamilton, Ontario L8N 3Z5, Canada

Email:
Rodney L. Johnson[*] - johns022@umn.edu

* Corresponding author

Keywords:
allosteric modulation; dopamine D_2 receptor; peptidomimetic; Pro-Leu-Gly-NH_2; spiro-bicyclic scaffold

Beilstein J. Org. Chem. **2013,** *9,* 204–214.
doi:10.3762/bjoc.9.24

Received: 01 October 2012
Accepted: 24 December 2012
Published: 30 January 2013

This article is part of the Thematic Series "Synthetic probes for the study of biological function".

Guest Editor: J. Aubé

© 2013 Bhagwanth et al; licensee Beilstein-Institut.
License and terms: see end of document.

Abstract

A variety of stable, small-molecule peptidomimetic ligands have been developed to elucidate the mechanism by which the neuropeptide Pro-Leu-Gly-NH_2 (PLG) modulates dopaminergic neurotransmission. Photoaffinity labeling ligands based upon PLG peptidomimetics have been used to establish that PLG binds to the D_2 dopamine receptor at a site that is different from the orthosteric site, thus making PLG and its peptidomimetics allosteric modulators of the dopamine receptor. Through the design, synthesis and pharmacological evaluation of conformationally constrained peptidomimetics containing lactam, bicyclic, and spiro-bicyclic scaffolds, support was provided for the hypothesis that the bioactive conformation of PLG is a type II β-turn. In addition, studies with peptidomimetics designed to mimic either a type VI β-turn or polyproline II helix conformation yielded molecules that were able to modulate dopamine receptors because of their ability to place the carboxamide NH_2 pharmacophore in the same topological space as that seen in the type II β-turn. Extensive studies with the spiro-bicyclic PLG peptidomimetics also established that both positive and negative modes of modulation were possible for the same series of peptidomimetics simply as a result of minor differences in the stereochemistry about the bridgehead carbon within the scaffold. This information was used to transform existing positive modulators into negative modulators, which demonstrated that small structural changes in the spiro-bicyclic dopamine receptor modulators are capable of causing major changes in the modulatory activity of PLG peptidomimetics.

Review

There has been an increasing effort to identify molecules that are able to act as allosteric regulators of specific G protein-coupled receptors (GPCRs), since such ligands have the potential to serve as novel therapeutic agents that are able to provide a means of fine-tuning receptor responses to orthosteric agonists or antagonists. In recent years, the identification of allosteric

modulators for GCPRs has increased significantly. The adenosine, muscarinic, chemokine, dopamine, serotonin, calcium-sensing, and metabotropic glutamate receptors are just some examples of GPCRs for which allosteric modulators have been reported [1,2].

The neuropeptide Pro-Leu-Gly-NH_2 (PLG) has been shown to be a positive allosteric modulator of the dopamine D_2 receptor [3]. PLG was initially isolated from brain tissue in the search for hypothalamic releasing factors, wherein it was found to inhibit the release of melanocyte stimulating hormone from the pituitary gland [4]. Early on, however, it was found that PLG also possessed significant neuropharmacological activity as a modulator of dopaminergic neurotransmission within the CNS [5], as illustrated by its ability to potentiate the behavioral effects of L-DOPA [6], to enhance the affinity of dopamine receptor agonists to dopamine receptors [7], and to prevent neuroleptic drug-induced supersensitivity of post-synaptic dopamine receptors [8]. The molecular basis behind this enhancement of dopaminergic neurotransmission did not become known until several decades later when photoaffinity-labeling peptidomimetics of PLG were used to show that PLG and its peptidomimetics act as allosteric modulators of the dopamine D_2 receptor [3,9]. This represents one of the few examples where a known endogenous molecule has demonstrated allosteric receptor-modulating activity, since most allosteric modulators discovered to date are exogenous synthetic molecules that have been identified through screening protocols and then subsequently optimized through structural modification [2].

Although PLG's pharmacological profile suggested that this compound would have potential in treating neurological diseases such as Parkinson's disease and tardive dyskinesia, the peptide nature of PLG limits its potential as a drug [10,11]. Thus, efforts were initiated to design peptidomimetic analogues of PLG in the hope of developing agents that would possess the same activity as PLG, but have better pharmacokinetic properties. As described below, these efforts have led to peptidomimetics that have helped elucidate the bioactive conformation of PLG, as well as the mechanism by which these compounds positively modulate dopamine receptors. In addition, these efforts have led to the discovery of peptidomimetics that negatively modulate dopamine receptors.

PLG peptidomimetic design

Although several studies of structure–activity relationships on PLG had been carried out early on [12-14], these studies did not provide information about the conformation PLG adopts to produce its pharmacological actions. NMR spectroscopic studies [15] and computational studies [16] indicated that PLG, although a flexible molecule, assumes turn conformations. The X-ray crystal structure of PLG showed that it existed in a type II β-turn [17]. We began our PLG peptidomimetic development studies by trying to understand what is the bioactive conformation of PLG. Our working hypothesis was that PLG exists in a type II β-turn conformation when it produces its effects. To test this hypothesis, a series of conformationally constrained analogues of PLG were designed that would restrict PLG in such a conformation. The overall approach employed is summarized in Figure 1 and it involved the incorporation of one or more bridging units between the atoms of the peptide backbone, thereby constricting one or more of the four torsion angles (Φ_2, ψ_2, Φ_3, and ψ_3) that define the postulated turn structure of PLG.

Lactam PLG peptidomimetics

The first confomationally constrained analogues of PLG synthesized incorporated the lactam approach developed by Freidinger et al. [18] to provide PLG peptidomimetics of type **A** (Figure 1). The lactam scaffold constrains the ψ_2 torsion angle, the value of which varies depending upon the nature of X. In addition, the type of β-turn that is mimicked is dictated by the chirality of C-3. Lactams **1**, **2**, **4**–**6**, and **9** (Figure 2) were active in enhancing the binding of the dopamine receptor agonist 2-amino-6,7-dihydroxy-1,2,3,4-tetrahydronaphthalene (ADTN) to dopamine receptors, while **3**, **7**, and **8** were inactive [19,20]. The activity seen with **2** and the inactivity of **3** supported the hypothesis that the bioactive conformation of PLG was a type II β-turn, since the (*R*)-isomer of the γ-lactam mimics a type II β-turn, while the (*S*)-isomer supports a type II' β-turn structure. Although an X-ray structure of **2** showed that the γ-lactam constraint restricted the ψ_2 torsion angle to 141.9°, i.e., a value close to the 120° seen in an ideal type II β-turn [21], **2** did not exist in a type II β-turn conformation in the crystal state. The same dependence on chirality was seen with δ-lactam analogues **6** and **7**. In contrast, in the case of the ε-lactam analogues **8** and **9**, it is the lactam with the (*S*)-chirality that possesses the activity. This was expected, as previous studies had shown that the (*R*)-ε-lactam restricts the ψ_2 torsion angle to around −168°, while the (*S*)-ε-lactam restricts the ψ_2 torsion angle to around +168°. This positive ψ_2 value is consistent with the positive ψ_2 value required of an ideal type II β-turn [22].

In the series of lactam PLG peptidomimetics shown in Figure 2, peptidomimetic **2** was found to be the most potent in enhancing the binding of the dopamine receptor agonist ADTN to isolated dopamine receptors. It was over a 1000-fold more potent than PLG [19]. Like PLG, this enhanced binding of agonists to the dopamine receptor produced by **2** was brought about by increasing the affinity of agonists to the receptor and by shifting the ratio of low- and high-affinity states of the dopamine receptor to the high-affinity state, which couples to the

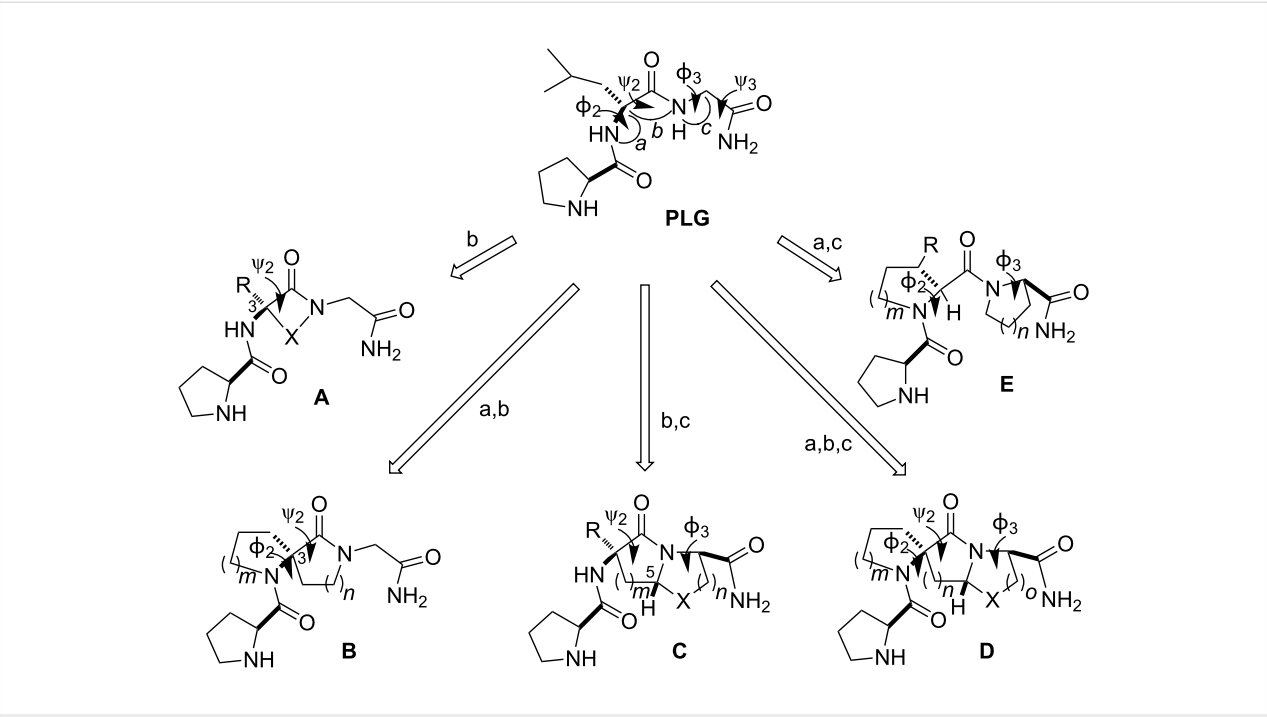


Figure 1: PLG peptidomimetic design approach. The Φ_2, ψ_2, Φ_3, and ψ_3 torsion angles define the postulated β-turn structure of PLG and a–c represent bridging connections made between the designated atoms of the peptide backbone to generate the peptidomimetic analogues **A**–**E** of PLG.

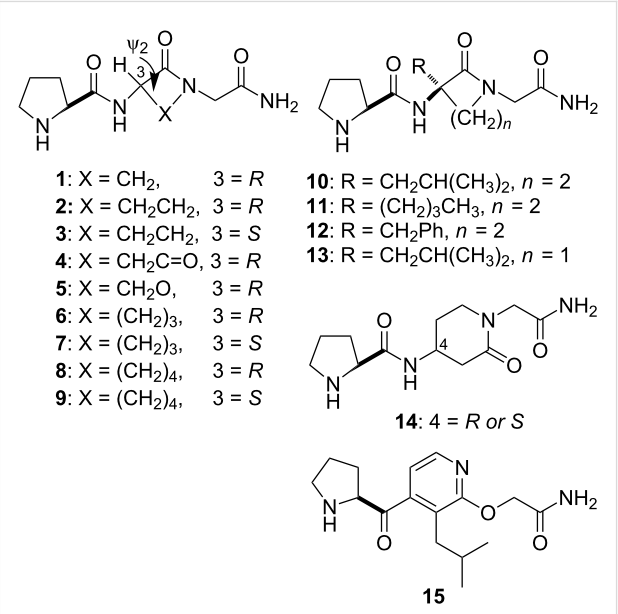


Figure 2: Lactam-based PLG peptidomimetics.

G-proteins [23]. Studies carried out in cell lines transfected with human dopamine receptor subtypes have shown that PLG and **2** enhance agonist binding to the D_{2S}, D_{2L} and D_4 dopamine receptor subtypes, whereas the D_1 and D_3 receptor subtypes are unaffected [24]. Peptidomimetic **2** was also more potent than PLG in in vivo assay systems, including (1) potentiation of apomorphine-dependent rotational behavior in 6-hydroxydopamine lesioned rats [25]; (2) protection against 1-methyl-4-phenyl-1,2,3,6-tetrahydropyridine (MPTP)-induced degeneration of the nigrostriatal dopaminergic pathway [26]; (3) antagonism of antipsychotic drug-induced vacuous chewing movements in the rat model of human tardive dyskinesia [27]; and (4) prevention of NMDA receptor antagonist (MK-801)-induced deficits in social interaction in rats [28].

In the initial design of the γ-lactam PLG peptidomimetic **2**, the isobutyl side chain of the leucyl residue was not incorporated into the structure, in order to simplify the synthesis. The potent activity of γ-lactam peptidomimetic **2** indicated that the isobutyl side chain was not an absolute requirement for modulating dopamine receptors. The synthesis of analogues of **2** in which lipophilic moieties were incorporated into the structure to mimic the isobutyl side chain of the leucyl residue of PLG yielded analogues **10**–**12** (Figure 2) with increased activity, suggesting that the lipophilic side chain was enhancing the binding of the compounds to the PLG binding site presumably by accessing a hydrophobic binding pocket [29,30]. A similar effect was seen with the substituted β-lactam analogue of PLG, compound **13**, developed by Palomo et al. [31].

Other scaffolds have been employed successfully to generate PLG peptidomimetics. A β-amino acid approach to the Freidinger lactams that employs the piperidin-2-one scaffold

yielded the active PLG peptidomimetic **14** [32]. Another example is the pyridine-based PLG peptidomimetics developed by Saitton et al. [33,34] and illustrated by **15**. Peptidomimetic **15** cannot adopt a type II β-turn, but rather exists in an extended conformation. Thus, the activity seen with **15** is not consistent with the postulated type II β-turn bioactive conformation hypothesis that is supported by the lactam and other highly conformationally constrained PLG peptidomimetics that have been developed. It was suggested that **15** is interacting with the PLG modulatory binding site in a different manner than **2** and its analogues [33]. Possible support for such a hypothesis can be seen in the different activity profiles of α,α-disubstituted glycine analogues of PLG and the corresponding α,α-disubstituted derivatives of lactam PLG peptidomimetic **2** [35]. In addition, subsequent studies, as detailed below, have shown that conformationally restricted molecules constrained in different conformations, but capable of projecting the key pharmacophores in the same relative area of space, produce active PLG peptidomimetics.

Design of photoaffinity labels to identify the PLG modulatory site

γ-Lactam peptidomimetic **2** served as a useful platform on which to build ligands that proved useful in delineating the target at which PLG and its peptidomimetics act. A series of potential photoaffinity ligands was developed by placing a photoreactive moiety at different points about **2** (**16**–**21**, Figure 3) [3,36]. These photoaffinity ligands were found to retain the ability to modulate dopamine receptors to varying degrees, thus indicating that the incorporation of the photoreactive moieties did not have a significantly adverse effect on ligand binding to the modulatory site. Cross-linking of photoaffinity ligands **21b** and **21c** with the modulatory site gave a receptor preparation in which the dopamine receptor was modulated by the covalently linked photoaffinity ligand [3]. A radiolabeled form of photoaffinity ligand **16c** was used to demonstrate that the site at which PLG and its peptidomimetics act to produce their dopamine receptor modulatory effects is located on the dopamine receptor [9]. This represented the first direct evidence that PLG and its peptidomimetics were acting as allosteric modulators of the dopamine receptor.

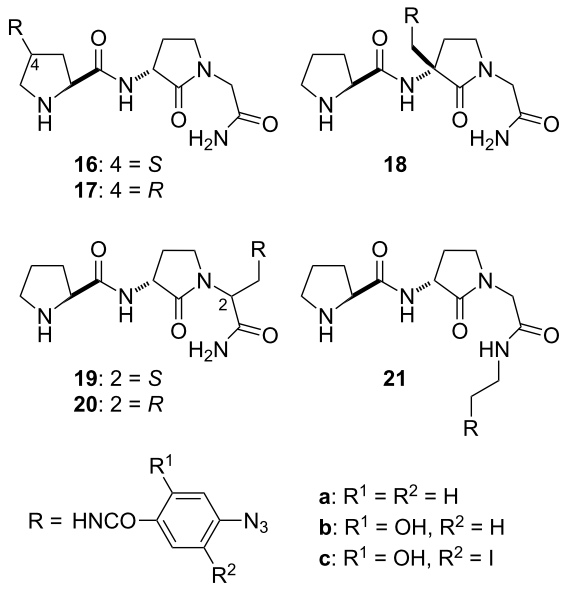


Figure 3: Lactam-based photoaffinity ligands of the PLG modulatory site.

Spiro and bicyclic PLG peptidomimetics

The incorporation of a bridging unit into lactam **2** from C-3 to the adjacent amide bond nitrogen yields the spiro-based PLG peptidomimetics of type **B** (Figure 1). The spiro lactam scaffolds restrict the Φ_2 and ψ_2 torsional angles of a β-turn and depending upon the chirality of the central carbon atom these constraints can either mimic a type II or type II' β-turn [37-40].

The insertion of a thiomethylene bridging unit from lactam C-5 to the acetamide α-carbon provides the bicyclic PLG peptidomimetics of type **C** (Figure 1). The result is a thiazolidine ring fused with the lactam ring. Although other types of bridging units have been employed in developing bicycle-based peptidomimetics, the thiomethylene unit is quite attractive as the synthesis into such systems is simplified, because the amino acid cysteine can be used. This bicyclic constraint was initially developed by Nagai and Sato [41]. In this constrained system, it is the ψ_2 and Φ_3 torsion angles that are constrained to values near those of an ideal type II β-turn as determined through computational calculations [42].

Of these two constrained systems, the bicyclic PLG peptidomimetics **22** and **23** (Figure 4) provided derivatives with significant dopamine-receptor-modulating activity [42]. As in the lactam series, the biological activity of the bicylic derivatives was enhanced by incorporating hydrophobic moieties of the bicyclic ring system that would be in a position to access the hydrophobic pocket believed to be interacting with the leucyl side chain of PLG, peptidomimetics **24**–**26** (Figure 4) [43].

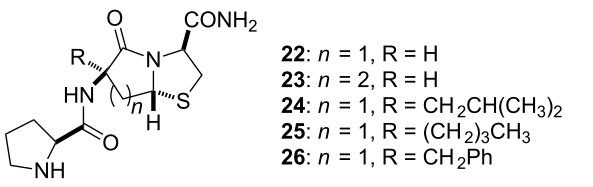


Figure 4: Bicyclic PLG peptidomimetics.

Spiro-bicyclic PLG peptidomimetics

By combining the spiro and bicyclic constraints into a single structure, spiro-bicyclic PLG peptidomimetics of type **D** (Figure 1) were obtained. These highly restricted scaffolds constrain three of the four torsion angles that define a turn structure, Φ_2, ψ_2, and Φ_3, making them among the best scaffolds at locking a peptide into a turn structure. The 5.5.5 spiro-bicyclic scaffold of peptidomimetic **27** (Figure 5) was found to mimic a type II β-turn as demonstrated through computational studies [44]. Peptidomimetic **27** was shown to enhance the binding of dopamine receptor agonists to the dopamine receptor in a manner similar to that of PLG [45]. Subsequently, it was shown that the 5.5.6 (**28**) and 5.6.5 (**29**) spiro-bicyclic scaffolds also served as excellent mimics of a type II β-turn [46]. In fact, peptidomimetics **28** and **29a** were more active than **27** in shifting the ratio of low and high affinity states of the dopamine receptor to the high affinity state and in enhancing apomorphine-induced rotations in the 6-hydroxydopamine-lesion rat model of Parkinson's disease [46]. The results showed that modifying the ring sizes of the spiro-bicyclic scaffolds had a significant effect on the activity of the spiro-bicyclic peptidomimetic and because of the highly restricted nature of the spiro-bicyclic systems the results provided strong evidence in support of the hypothesis that the bioactive conformation of PLG was that of a type II β-turn.

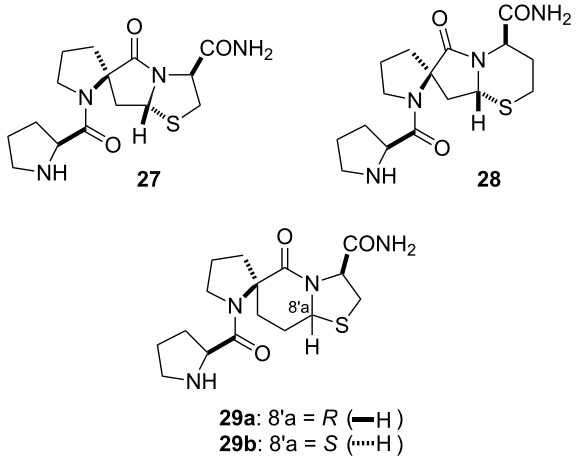
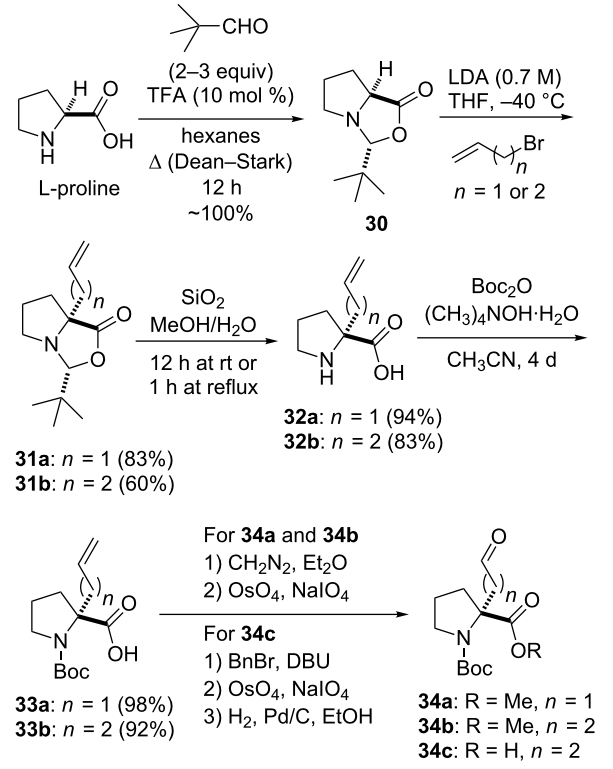


Figure 5: Spiro-bicyclic PLG peptidomimetics.

The synthetic approach to the novel highly constrained spiro-bicyclic turn mimics found in PLG peptidomimetics **27**–**29** relied on α-alkylaldehyde proline derivatives (**34**, Scheme 1) as key starting materials [44,46]. These aldehyde intermediates were obtained from L-proline via the highly moisture-labile oxazolidinone **30** of Seebach's "self-regeneration of chirality" methodology [47]. Stereoselective alkylation of **30** provided alkylated oxazolidinone **31** and cleavage of this *N*,*O*-acetal provided α-alkylated proline **32**, which when Boc-protected gave **33**. The formation of **34a** and **34b** was accomplished by initial esterification of **33a** and **33b**, respectively, followed by oxidative cleavage of the double bond in each case with OsO_4/$NaIO_4$ [46]. An efficient and reproducible conversion of **33b** into **34c** was developed that consisted of the following three-step route: (1) benzyl ester formation, (2) oxidative cleavage of the double bond with OsO_4/$NaIO_4$, and (3) hydrogenolysis of the benzyl ester [36,48].

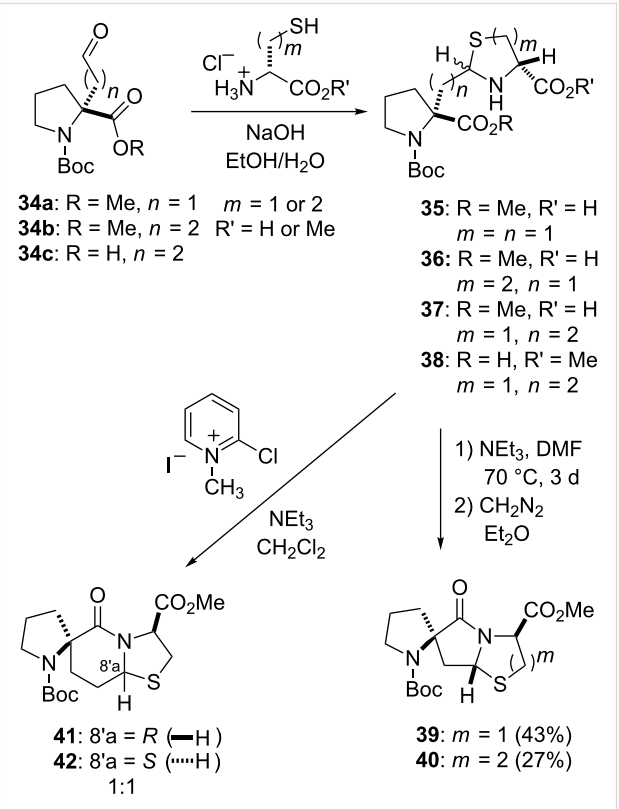


Scheme 1: Synthesis of α-alkylaldehyde proline derivatives by Seebach's "self-regeneration of chirality" methodology.

Although the Seebach methodology provides a highly stereoselective way to α-alkylated prolines, there are several shortcomings to the originally developed protocols [47]. In the oxazolidinone formation reaction, these shortcomings include the need for a large excess of the costly pivalaldehyde, long condensation reaction times of 3–4 days, and issues surrounding the isolation and handling of the moisture-sensitive oxazolidinone. By replacing pentane (capable of forming a 2% azeotrope with water) with hexanes (capable of forming a 6% azeotrope with water) it was found that the reaction time could be significantly reduced from several days to 12–18 hours and that the amount of pivalaldehyde could be reduced from six to two equivalents [49]. With respect to the *N*,*O*-acetal cleavage reaction, wherein **31** is converted to **32**, the hydrolysis of **31** was originally carried out under rigorous acidic conditions (aqueous HCl under

reflux) and purification of the resulting α-alkylated proline **32** required tedious ion-exchange chromatography [47]. It was subsequently found that simply stirring a solution of the alkylated oxazolidinone **31** in a methanol/water solution with silica gel (200–400 mesh, 60 Å) either at room temperature for 12 hours [50] or under reflux for 1 hour [49], followed by simple filtration procedures, provided α-alkylated proline **32** in analytically pure form and in excellent yield. Protection of the amino group of **32** by using typical procedures gives lower yields than what is normally observed for this type of amine protection, probably due to steric factors resulting from the presence of the new fully substituted carbon center that has been introduced alpha to the amino group. However, Boc-protected α-alkylated proline derivatives could be obtained in yields greater than 90% through conversion of the α-alkylated proline to its salt form with tetramethylammonium hydroxide in CH_3CN during the amine protection reaction [51].

The construction of the spiro-bicyclic scaffolds was accomplished through the condensation of α-alkylaldehyde proline derivatives **34a**–**c** with either D-cysteine or D-homocysteine derivatives to give diastereoisomeric mixtures of thiazolidines **35**, **37** and **38** and thiazines **36**, respectively (Scheme 2). Formation of the lactam ring from the thiazine and thiazolidines to generate the spiro-bicyclic systems was accomplished by two



Scheme 2: Synthetic approaches to the spiro-bicyclic scaffolds.

different methods. In one approach, thermal cyclization of **35** and **36** followed by esterification gave the cyclized 5.5.5- and 5.5.6-spiro bicyclic products, **39** and **40**, respectively [44,46]. In this approach, only one of two possible diastereoisomeric products was obtained in each case. Thiazolidine **37** could not be cyclized under these conditions to generate the corresponding 5.6.5 spiro-bicyclic system. Instead, the 5.6.5 spiro-bicyclic system was obtained by activation of the free carboxylic acid of **38** with Mukaiyama's reagent (2-chloro-1-methylpyridinium iodide (CMPI) [52]) followed by in situ lactam formation [46]. Under these advantageous kinetic conditions, two diastereoisomers of the 5.6.5 spiro-bicyclic system, **41** and **42**, were obtained in a 1:1 ratio. The two diastereoisomers vary only in the stereochemistry at C-8'a.

PLG peptidomimetics mimicking type VI β-turn and polyproline II helix conformations

Early SAR studies on PLG showed that when the glycinamide residue was substituted with both L-and D-prolinamide residues, active dopamine receptor modulating peptides **43** and **44** (Figure 6) were obtained [13]. Likewise, triproline analogues of PLG, peptides **45** and **46**, in which the C-terminal residue was either L-or D-prolinamide gave active compounds [53]. These results presented a paradox. It was expected that only those PLG analogues possessing a D-prolyl residue at the C-terminal end would show activity, as only those analogues would be capable of assuming the postulated type II β-turn bioactive conformation of PLG. Since the prolyl analogues possessing a C-terminal L-prolyl residue would not be able to assume a type II β-turn, the fact that they were active was not consistent with the hypothesis that the bioactive conformation of PLG is a type II β-turn. It was speculated that the prolyl derivatives with the C-terminal L-prolyl residue are capable of adopting a conformation that places key pharmacophore moieties in the same relative topological space that these moieties occupy in the peptidomimetics constrained to a type II β-turn [36,48,49].

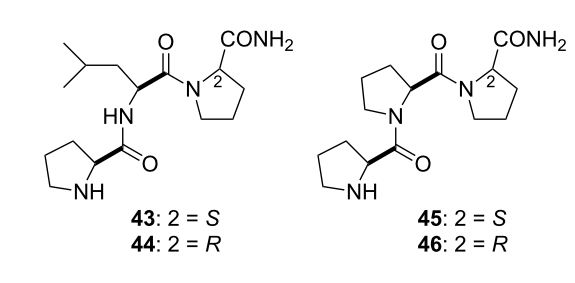


Figure 6: Prolyl PLG analogues.

Analysis of possible conformations that the homochiral prolyl peptides could assume indicated two possibilities, as depicted in

Figure 7. In one case, the presence of a prolyl residue introduces the possibility of a *cis*-amide bond at the C-terminus with the result being a type VI β-turn conformation. To test this hypothesis, Germanas' indolizidinone scaffold [54] was employed as the type VI β-turn conformation mimic to design **47** and **48** (Figure 7A) [49,55]. A second possibility was that triproline **45** could assume a polyproline II helix conformation, wherein all the Pro–Pro amide bonds are in a *trans*-configuration. For testing this hypothesis, the spiro-bicyclic peptidomimetics **49a** and **49b** were designed to mimic the polyproline II helix conformation (Figure 7B) [48,56]. These two spiro-bicyclic peptidomimetics are C-3' epimers of the spiro-bicyclic type II β-turn mimics **29a** and **29b**.

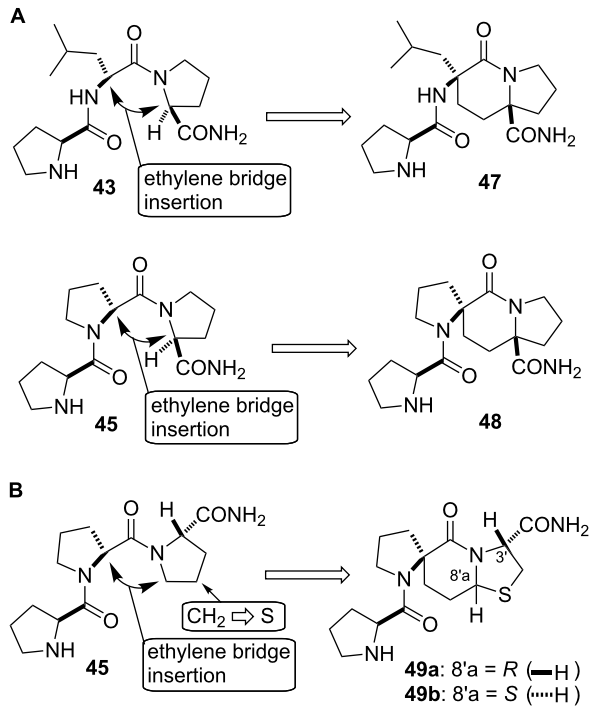
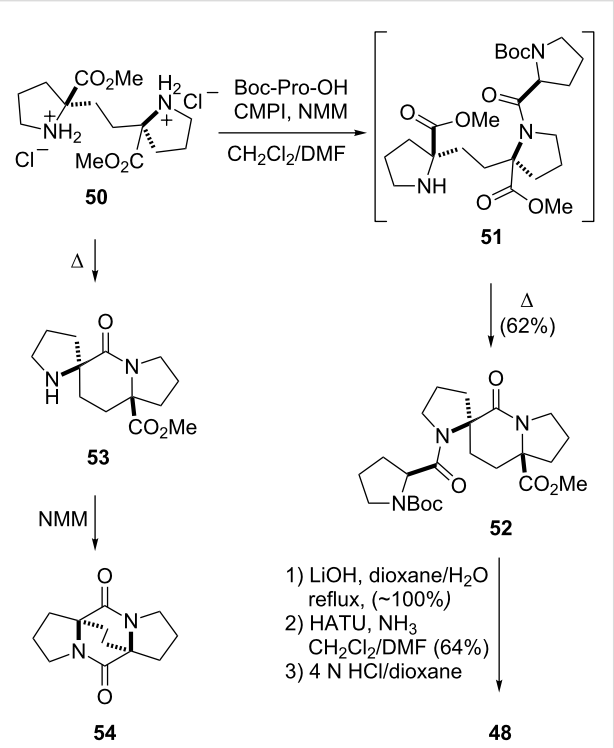


Figure 7: (**A**) Type VI β-turn mimics. An ethylene bridge connection in **43** and **45** between the α-carbon of the second residue and the α-carbon of the C-terminal prolyl residue that is in a *cis*-amide bond configuration yields spiro-bycyclic PLG peptidomimetics **47** and **48** constrained in a type VI β-turn conformation. (**B**) Polyproline II helix mimics. An ethylene bridge connection in **45** between the α-carbon of the second prolyl residue and the δ-carbon of the C-terminal prolyl residue that is in a *trans*-amide bond configuration, and the replacement of the γ-CH_2 with S yields spiro-bicyclic PLG peptidomimetics **49a** and **49b** in a polyproline II helix conformation.

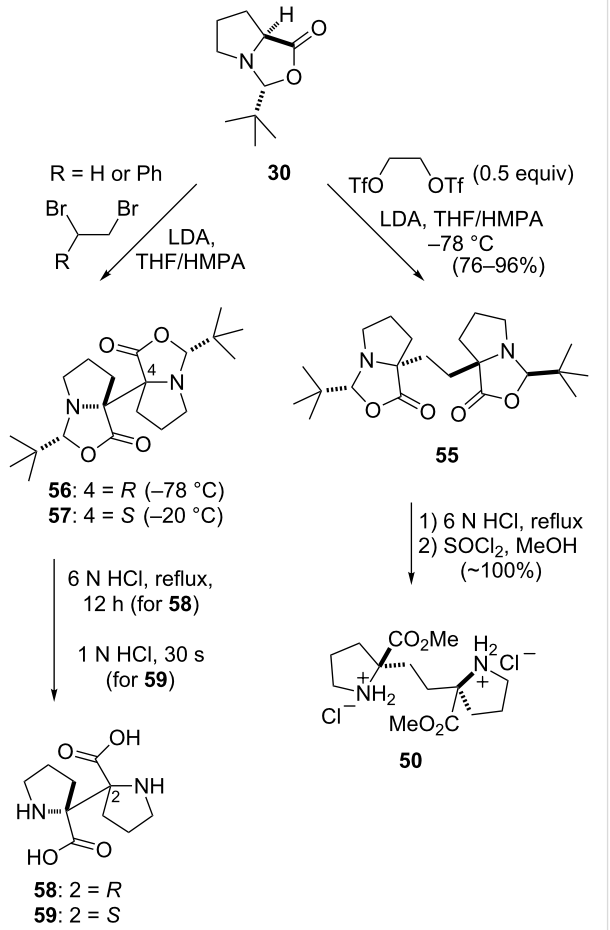
In the retrosynthetic analysis of spiro-bicyclic type VI β-turn mimic **48**, a disconnection at the lactam bond in the indolizidinone core was envisioned, which would give rise to a symmetric unit of two prolines linked enantioselectively via a two-carbon linkage at their α-carbons [55]. Such an approach proved successful, as shown in Scheme 3. The ethylene-linked biproline derivative **50** was readily converted to spiro-bicyclic **52** under conditions wherein the CMPI-activated ester of Boc-Pro-OH was coupled to **50** to give the acylated biproline intermediate **51**, which when heated cyclized to **52** [55]. The sterically congested nature of the spiro indolizidinone scaffold, due in part to its boat-shaped conformation, was illustrated by the observation that when **50** was converted to spiro indolizidinone **53**, this material could not be efficiently acylated with Boc-Pro-OH under a variety of coupling conditions. Instead, **53** had a propensity to convert to the diketopiperazine **54**. Also, the methyl ester of **52** resisted direct amidation under a variety of standard conditions. Rather, **52** had to be hydrolyzed to the acid and then coupled to NH_3 with 2-(1*H*-7-azabenzotriazol-1-yl)-1,1,3,3-tetramethyluronium hexafluorophosphate (HATU) as the coupling reagent in order to provide the primary carboxamide intermediate, which could be deprotected to give **48**.



Scheme 3: Synthesis of spiro-bicyclic type VI β-turn mimic **48**.

The lithium enolate of Seebach's oxazolidinone **30** served as the starting material for the stereoselective synthesis of ethylene-linked biproline derivative **50**. The nature of the bis-electrophile proved to be crucial to the outcome of the alkylation reaction (Scheme 4). The alkylation of **30** with either symmetric (1,2-dibromoethane) or asymmetric (1,2-dibromo-1-phenylethane) vicinal dihalides resulted in the efficient dimerization of **30** to afford the biprolyl oxazolidinones **56** and **57**, which served as precursors to the corresponding novel (*R*,*R*)-

α,α'-biproline **58** and *meso*-α,α'-biproline **59** [57]. In contrast, the reaction of the more electrophilic alkylating agent glycol bistriflate with the enolate of **30** provided the desired dimer **55**, which after acid hydrolysis of the dimer followed by Fischer esterification yielded **50** [55].



Scheme 4: Biproline formation from Seebach's oxazolidinone.

The type VI β-turn PLG peptidomimetics **47** and **48** and the spiro-bicyclic polyproline II helix PLG peptidomimetic **49a** were shown to possess positive dopamine-receptor modulatory activity as demonstrated by their ability to enhance the binding of the dopamine receptor agonist *N*-propylnorapomorphine (NPA) to dopamine D_2 receptors [48,49]. These results provide evidence for the hypothesis that the homochiral prolyl peptides **43** and **45** are able to adopt either a type VI β-turn or a polyproline II helix as their bioactive conformation. It is postulated that these highly constrained molecules are able to produce a modulatory response because each can present the necessary topological arrangement of key pharmacophore moieties in a manner similar to that of PLG peptidomimetics that are restricted to a type II β-turn conformation. A comparison of the Φ, ψ, and ω torsion angles of the type II β-turn, the type VI β-turn, and the polyproline II helix conformational types indicates that they each possess similar torsion angles at their N-termini, but they differ at their C-termini. However, they all place the carboxamide NH_2 pharmacophore in the same relative position in space [48,49].

Peptidomimetic negative modulators of the D_2 dopamine receptor

Biological evaluation of the C-8'a epimer of the type II β-turn PLG peptidomimetic **29a**, spiro-bicyclic **29b**, and of the C-8'a epimer of the polyproline II helix PLG peptidomimetic **49a**, spiro-bicyclic **49b**, revealed that the **29b** and **49b** diastereoisomers were not positive modulators of the D_2 dopamine receptors, but rather were negative modulators of the receptor as they decreased the binding of the dopamine receptor agonist *N*-propylnorapomorphine to the receptor [48]. The fact that all four peptidomimetics were capable of displacing a PLG peptidomimetic radioligand in a competitive binding assay indicated that the positive and negative modulators are interacting with the same allosteric site on the D_2 dopamine receptor. The structural difference between **29a** and **29b** and between **49a** and **49b** is the chirality at the C-8'a bridgehead carbon atom. This difference, it was postulated, has an effect on the conformation adopted by the thiazolidine ring within the spiro-bicyclic scaffold. In particular, modelling studies suggested that the pucker of the thiazolidine ring in negative modulators **29b** and **49b** caused the C-2' carbon to occupy a different area of topological space than this carbon occupies in the positive modulators **29a** and **49a** [48].

It was speculated that the different conformational effects between the negative and positive allosteric modulators translated into different conformational changes when these ligands bound to the allosteric binding site. This in turn produced different conformational effects at the orthosteric site where the dopamine receptor agonists bind. To test this hypothesis, the syntheses of β-dimethyl derivatives of **29a**, **29b**, **49a**, and **49b**, i.e., spiro-bicyclic peptidomimetics **60**–**63** (Figure 8), respectively, were carried out [58].

In the case of the positive allosteric modulators, **29a** and **49a**, we postulated that by placing the dimethyl groups on the C-2' carbon of the thiazolidine ring to give the corresponding analogues **60** and **61**, we would be placing steric bulk in the same region of topological space occupied by the C-2' carbon in the different pucker conformation of the negative modulators **29b** and **49b**. It was predicted that the dimethyl substitution on a positive allosteric modulator would convert it into a negative allosteric modulator. The dimethyl analogues, **60** and **61**

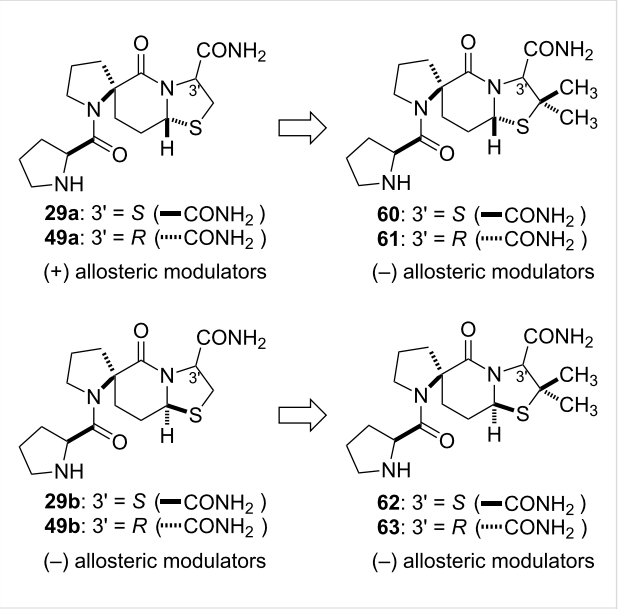


Figure 8: Positive and negative allosteric modulators of the D_2 dopamine receptor based on the 5.6.5 spiro-bicyclic scaffold.

showed significant negative modulatory activity, as demonstrated by their ability to negatively affect the binding of the dopamine receptor agonist NPA to the D_2 receptor and to shift the EC_{50} value for [^{3}H]NPA binding to dopamine D_2 receptors by 2.7- and 2.8-fold, respectively, compared to the control [58]. Thus, both compounds decreased the affinity of the agonist NPA to the D_2 dopamine receptor. The results supported the proposition that the introduction of dimethyl groups into the structure of the positive modulators resulted in molecules that resembled the conformational characteristics of the unsubstituted negative allosteric modulators.

The introduction of dimethyl groups into the structure of the negative modulators **29b** and **49b** gave analogues **62** and **63**, respectively. These analogues also exhibited negative allosteric modulatory activity, albeit at a lower level than the unsubstituted peptidomimetics. Molecular models of **49b** and **63**, for example, show that the thiazolidine C-2' carbons of these two molecules overlay quite well, but that the methyl groups of **63** now occupy topographical space outside that occupied by the thiazolidine C-2' carbon of **49b**. It was speculated that this may produce adverse steric effects and that this may be responsible for the observed weaker activity seen with **62** and **63**.

Conclusion

The development of PLG peptidomimetic probes has proved valuable in helping to elucidate the structural and molecular mechanism by which an endogenous neuropeptide, PLG, modulates dopaminergic neurotransmission. This knowledge will be useful in developing novel central nervous system (CNS) drugs to treat conditions in which the dopamine receptors are directly implicated (i.e., Parkinson's disease, schizophrenia, Gilles de la Tourette syndrome, etc.) [59-61]. Within the context of G-protein coupled receptors, this work illustrates the potential value of receptor modulation as a means of perturbing traditional ligand–receptor interaction [62,63] and it demonstrates that this can be a successful platform for understanding biological function with peptidomimetic probes.

Acknowledgements

The author's work that is described in this review was supported by NIH Grant NS20036 to R. L. J.

References

1. De Amici, M.; Dallanoce, C.; Holzgrabe, U.; Tränkle, C.; Mohr, K. *Med. Res. Rev.* **2010,** *30,* 463–549. doi:10.1002/med.20166
2. Melancon, B. J.; Hopkins, C. R.; Wood, M. R.; Emmitte, K. A.; Niswender, C. M.; Christopoulos, A.; Conn, P. J.; Lindsley, C. W. *J. Med. Chem.* **2012,** *55,* 1445–1464. doi:10.1021/jm201139r
3. Fisher, A.; Mann, A.; Verma, V.; Thomas, N.; Mishra, R. K.; Johnson, R. L. *J. Med. Chem.* **2006,** *49,* 307–317. doi:10.1021/jm050644n
4. Nair, R. M. G.; Kastin, A. J.; Schally, A. V. *Biochem. Biophys. Res. Commun.* **1971,** *43,* 1376–1381. doi:10.1016/S0006-291X(71)80026-8
5. Mishra, R. K.; Chiu, S.; Chiu, P.; Mishra, C. P. *Methods Find. Exp. Clin. Pharmacol.* **1983,** *5,* 203–233.
6. Plotnikoff, N. P.; Kastin, A. J.; Anderson, M. S.; Schally, A. V. *Life Sci.* **1971,** *10,* 1279–1283. doi:10.1016/0024-3205(71)90326-2
7. Srivastava, L. K.; Bajwa, S. B.; Johnson, R. L.; Mishra, R. K. *J. Neurochem.* **1988,** *50,* 960–968. doi:10.1111/j.1471-4159.1988.tb03005.x
8. Chiu, S.; Paulose, C. S.; Mishra, R. K. *Science* **1981,** *214,* 1261–1262. doi:10.1126/science.6117947
9. Mann, A.; Verma, V.; Basu, D.; Skoblenick, K. J.; Beyaert, M. G. R.; Fisher, A.; Thomas, N.; Johnson, R. L.; Mishra, R. K. *Eur. J. Pharmacol.* **2010,** *641,* 96–101. doi:10.1016/j.ejphar.2010.05.018
10. Ehrensing, R. H.; Kastin, A. J.; Larsons, P. F.; Bishop, G. A. *Dis. Nerv. Syst.* **1977,** *38,* 303–307.
11. Mishra, R. K.; Chiu, S.; Singh, A. N.; Kazmi, S. M. I.; Rajakumar, A.; Johnson, R. L. *Drugs Future* **1986,** *11,* 203–207.
12. Bjoerkman, S.; Castensson, S.; Sievertsson, H. *J. Med. Chem.* **1979,** *22,* 931–935. doi:10.1021/jm00194a009
13. Johnson, R. L.; Rajakumar, G.; Mishra, R. K. *J. Med. Chem.* **1986,** *29,* 2100–2104. doi:10.1021/jm00160a051
14. Johnson, R. L.; Rajakumar, G.; Yu, K. L.; Mishra, R. K. *J. Med. Chem.* **1986,** *29,* 2104–2107. doi:10.1021/jm00160a052
15. Walter, R.; Bernal, I.; Johnson, L. F. In *Chemistry and Biology of Peptides;* Meinhofer, J., Ed.; Ann Arbor Science: Ann Arbor, MI, 1972; pp 131–135.
16. Zimmerman, S. S.; Baum, R.; Scheraga, H. A. *Int. J. Pept. Protein Res.* **1982,** *19,* 143–152. doi:10.1111/j.1399-3011.1982.tb02602.x
17. Reed, L. L.; Johnson, P. L. *J. Am. Chem. Soc.* **1973,** *95,* 7523–7524. doi:10.1021/ja00803a062
18. Freidinger, R. M.; Perlow, D. S.; Veber, D. F. *J. Org. Chem.* **1982,** *47,* 104–109. doi:10.1021/jo00340a023

19. Yu, K. L.; Rajakumar, G.; Srivastava, L. K.; Mishra, R. K.; Johnson, R. L. *J. Med. Chem.* **1988,** *31,* 1430–1436. doi:10.1021/jm00402a031
20. Sreenivasan, U.; Mishra, R. K.; Johnson, R. L. *J. Med. Chem.* **1993,** *36,* 256–263. doi:10.1021/jm00054a010
21. Valle, G.; Crisma, M.; Toniolo, C.; Yu, K.-L.; Johnson, R. L. *Int. J. Pept. Protein Res.* **1989,** *33,* 181–190. doi:10.1111/j.1399-3011.1989.tb00207.x
22. Freidinger, R. M.; Veber, D. F.; Hirschmann, R.; Paege, L. M. *Int. J. Pept. Protein Res.* **1980,** *16,* 464–470. doi:10.1111/j.1399-3011.1980.tb02970.x
23. Mishra, R. K.; Srivastava, L. K.; Johnson, R. L. *Prog. Neuro-Psychopharmacol. Biol. Psychiatry* **1990,** *14,* 821–827. doi:10.1016/0278-5846(90)90054-K
24. Verma, V.; Mann, A.; Costain, W.; Pontoriero, G.; Castellano, J. M.; Skoblenick, K.; Gupta, S. K.; Pristupa, Z.; Niznik, H. B.; Johnson, R. L.; Nair, V. D.; Mishra, R. K. *J. Pharmacol. Exp. Ther.* **2005,** *315,* 1228–1236. doi:10.1124/jpet.105.091256
25. Mishra, R. K.; Marcotte, E. R.; Chugh, A.; Barlas, C.; Whan, D.; Johnson, R. L. *Peptides* **1997,** *18,* 1209–1215. doi:10.1016/S0196-9781(97)00147-2
26. Marcotte, E. R.; Chugh, A.; Mishra, R. K.; Johnson, R. L. *Peptides* **1998,** *19,* 403–406. doi:10.1016/S0196-9781(97)00321-5
27. Sharma, S.; Paladino, P.; Gabriele, J.; Saeedi, H.; Henry, P.; Chang, M.; Mishra, R. K.; Johnson, R. L. *Peptides* **2003,** *24,* 313–319. doi:10.1016/S0196-9781(03)00045-7
28. Dyck, B.; Guest, K.; Sookram, C.; Basu, D.; Johnson, R. L.; Mishra, R. K. *Schizophr. Res.* **2011,** *125,* 88–92. doi:10.1016/j.schres.2010.09.025
29. Dolbeare, K.; Pontoriero, G. F.; Gupta, S. K.; Mishra, R. K.; Johnson, R. L. *J. Med. Chem.* **2003,** *46,* 727–733. doi:10.1021/jm020441o
30. Castellano, J. M.; Batrynchuk, J.; Dolbeare, K.; Verma, V.; Mann, A.; Skoblenick, K. J.; Johnson, R. L.; Mishra, R. K. *Peptides* **2007,** *28,* 2009–2015. doi:10.1016/j.peptides.2007.07.026
31. Palomo, C.; Aizpurua, J. M.; Benito, A.; Miranda, J. I.; Fratila, R. M.; Matute, C.; Domercq, M.; Gago, F.; Martin-Santamaria, S.; Linden, A. *J. Am. Chem. Soc.* **2003,** *125,* 16243–16260. doi:10.1021/ja038180a
32. Weber, K.; Ohnmacht, U.; Gmeiner, P. *J. Org. Chem.* **2000,** *65,* 7406–7416. doi:10.1021/jo000555c
33. Saitton, S.; Del Tredici, A. L.; Mohell, N.; Vollinga, R. C.; Boström, D.; Kihlberg, J.; Luthman, K. *J. Med. Chem.* **2004,** *47,* 6595–6602. doi:10.1021/jm049484q
34. Saitton, S.; Del Tredici, A. L.; Saxin, M.; Stenström, T.; Kihlberg, J.; Luthman, K. *Org. Biomol. Chem.* **2008,** *6,* 1647–1654. doi:10.1039/b718058f
35. Evans, M. C.; Pradhan, A.; Venkatraman, S.; Ojala, W. H.; Gleason, W. B.; Mishra, R. K.; Johnson, R. L. *J. Med. Chem.* **1999,** *42,* 1441–1447. doi:10.1021/jm980656r
36. Raghavan, B. Synthesis of 5.6.6 Spiro Bicyclic Lactams and Photoaffinity Labeling Ligands as PLG Analogues and Stereoselective Synthesis of Alpha-substituted Gamma Lactams. Ph.D. Thesis, University of Minnesota, MN, USA, 2006.
37. Hinds, M. G.; Welsh, J. H.; Brennend, D. M.; Fisher, J.; Glennie, M. J.; Richards, N. G. J.; Turner, D. L.; Robinson, J. A. *J. Med. Chem.* **1991,** *34,* 1777–1789. doi:10.1021/jm00110a005
38. Ward, P.; Ewan, G. B.; Jordan, C. C.; Ireland, S. J.; Hagan, R. M.; Brown, J. R. *J. Med. Chem.* **1990,** *33,* 1848–1851. doi:10.1021/jm00169a003
39. Genin, M. J.; Gleason, W. B.; Johnson, R. L. *J. Org. Chem.* **1993,** *58,* 860–866. doi:10.1021/jo00056a018
40. Genin, M. J.; Ojala, W. H.; Gleason, W. B.; Johnson, R. L. *J. Org. Chem.* **1993,** *58,* 2334–2337. doi:10.1021/jo00060a062
41. Nagai, U.; Sato, K. *Tetrahedron Lett.* **1985,** *26,* 647–650. doi:10.1016/S0040-4039(00)89169-8
42. Subasinghe, N. L.; Bontems, R. J.; McIntee, E.; Mishra, R. K.; Johnson, R. L. *J. Med. Chem.* **1993,** *36,* 2356–2361. doi:10.1021/jm00068a013
43. Khalil, E. M.; Pradhan, A.; Ojala, W. H.; Gleason, W. B.; Mishra, R. K.; Johnson, R. L. *J. Med. Chem.* **1999,** *42,* 2977–2987. doi:10.1021/jm990140n
44. Genin, M. J.; Johnson, R. L. *J. Am. Chem. Soc.* **1992,** *114,* 8778–8783. doi:10.1021/ja00049a005
45. Genin, M. J.; Mishra, R. K.; Johnson, R. L. *J. Med. Chem.* **1993,** *36,* 3481–3483. doi:10.1021/jm00074a032
46. Khalil, E. M.; Ojala, W. H.; Pradhan, A.; Nair, V. D.; Gleason, W. B.; Mishra, R. K.; Johnson, R. J. *J. Med. Chem.* **1999,** *42,* 628–637. doi:10.1021/jm980525q
47. Seebach, D.; Boes, M.; Naef, R.; Schweizer, W. *J. Am. Chem. Soc.* **1983,** *105,* 5390–5398. doi:10.1021/ja00354a034
48. Raghavan, B.; Skoblenick, K. J.; Bhagwanth, S.; Argintaru, N.; Mishra, R. K.; Johnson, R. L. *J. Med. Chem.* **2009,** *52,* 2043–2051. doi:10.1021/jm801575w
49. Vartak, A. P.; Skoblenick, K.; Thomas, N.; Mishra, R. K.; Johnson, R. L. *J. Med. Chem.* **2007,** *50,* 6725–6729. doi:10.1021/jm070895r
50. Genin, M. J.; Baures, P. W.; Johnson, R. L. *Tetrahedron Lett.* **1994,** *35,* 4967–4968. doi:10.1016/S0040-4039(00)73294-1
51. Khalil, E. M.; Subasinghe, N. L.; Johnson, R. L. *Tetrahedron Lett.* **1996,** *37,* 3441–3444. doi:10.1016/0040-4039(96)00589-8
52. Mukaiyama, T.; Usui, M.; Saigo, K. *Chem. Lett.* **1976,** *5,* 49–50. doi:10.1246/cl.1976.49
53. Baures, P. W.; Pradhan, A.; Ojala, W. H.; Gleason, W. B.; Mishra, R. K.; Johnson, R. L. *Bioorg. Med. Chem. Lett.* **1999,** *9,* 2349–2352. doi:10.1016/S0960-894X(99)00386-8
54. Kim, K.; Dumas, J.-P.; Germanas, J. P. *J. Org. Chem.* **1996,** *61,* 3138–3144. doi:10.1021/jo960012w
55. Vartak, A. P.; Johnson, R. L. *Org. Lett.* **2006,** *8,* 983–986. doi:10.1021/ol0600335
56. Witter, D. J.; Famiglietti, S. J.; Cambier, J. C.; Castelhano, A. L. *Bioorg. Med. Chem. Lett.* **1998,** *8,* 3137–3142. doi:10.1016/S0960-894X(98)00577-0
57. Vartak, A. P.; Young, V. G., Jr.; Johnson, R. L. *Org. Lett.* **2005,** *7,* 35–38. doi:10.1021/ol047958+
58. Bhagwanth, S.; Mishra, S.; Daya, R.; Mah, J.; Mishra, R. K.; Johnson, R. L. *ACS Chem. Neurosci.* **2012,** *3,* 274–284. doi:10.1021/cn200096u
59. Seeman, P. In *Dopamine Receptors;* Creese, I.; Faser, C. M., Eds.; 1988; pp 230–245.
60. Civelli, O.; Bunzow, J. R.; Grandy, D. K. *Annu. Rev. Pharmacol. Toxicol.* **1993,** *33,* 281–307. doi:10.1146/annurev.pa.33.040193.001433
61. Bonci, A.; Bernardi, G.; Grillner, P.; Mercuri, N. B. *Trends Pharmacol. Sci.* **2003,** *24,* 172–177. doi:10.1016/S0165-6147(03)00068-3
62. Kourounakis, A. P.; van der Klein, P.; Ijzerman, A. P. In *Drug Discovery Strategies and Methods;* Makriyannis, A.; Beigel, D., Eds.; Marcel Dekker, Inc.: New York, NY, 2004; pp 221–244.
63. Rees, S.; Morrow, D.; Kenakin, T. *Recept. Channels* **2002,** *8,* 261–268.

License and Terms

This is an Open Access article under the terms of the Creative Commons Attribution License (http://creativecommons.org/licenses/by/2.0), which permits unrestricted use, distribution, and reproduction in any medium, provided the original work is properly cited.

The license is subject to the *Beilstein Journal of Organic Chemistry* terms and conditions: (http://www.beilstein-journals.org/bjoc)

The definitive version of this article is the electronic one which can be found at: doi:10.3762/bjoc.9.24

Beilstein Journal of Organic Chemistry

A new synthetic protocol for coumarin amino acid

Xinyi Xu[1,2], Xiaosong Hu[*1,3] and Jiangyun Wang[*1]

Full Research Paper

Open Access

Address:
[1]Laboratory of Noncoding RNA, Institute of Biophysics, Chinese Academy of Sciences, Beijing 100101, China, [2]Graduate University of the Chinese Academy of Sciences, Beijing 100864, China and [3]Department of Chemistry, School of Science, Wuhan University of Technology, Wuhan 430070, China

Email:
Xiaosong Hu[*] - xhu@moon.ibp.ac.cn; Jiangyun Wang[*] - jwang@ibp.ac.cn

* Corresponding author

Keywords:
coumarin; fluorescent probe; halogen derivatives; non-natural amino acid; Pechmann condensation

Beilstein J. Org. Chem. **2013,** *9,* 254–259.
doi:10.3762/bjoc.9.30

Received: 03 October 2012
Accepted: 08 January 2013
Published: 06 February 2013

This article is part of the Thematic Series "Synthetic probes for the study of biological function".

Guest Editor: J. Aubé

© 2013 Xu et al; licensee Beilstein-Institut.
License and terms: see end of document.

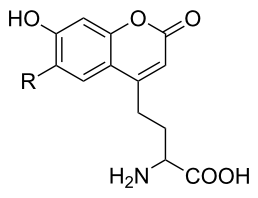
Abstract

The hydrochloride of the racemic amino acid (2-(7-hydroxycoumarin-4-yl)ethyl)glycine, which can serve as a fluorescent probe in proteins, and two halogen derivatives of it, were synthesized by using a new synthetic protocol in five steps. It is less costly and relatively easy to prepare this kind of fluorescent amino acid with the new synthetic method. Furthermore, it can be applied to synthesize other derivatives of the coumarin amino acid with some specific properties.

Introduction

Since α-L-(2-(7-hydroxycoumarin-4-yl)ethyl)glycine (**1a**, Figure 1), a fluorescent non-natural amino acid, was genetically incorporated at a defined site in proteins in living organisms for the first time by Schultz and co-workers [1] there have been more and more applications related to it [2-8]. Compound **1a** is of great interest to scientists because the 7-hydroxycoumarin moiety has a high fluorescence quantum yield and a large Stokes shift. Its excellent fluorescence properties make it a great candidate to substitute green fluorescent protein (GFP) in the application of fluorescent labeling of living cells. Compared with GFP, compound **1a** is small, and can be incorporated at any defined site in proteins; whereas GFP is large, which will cause significant perturbation, and can only be fused to the C- or N-terminus of the target protein [9]. The coumarin amino acid **1a** (Figure 1) is sensitive to both pH and solvent polarity, which makes it a good probe to investigate protein functionalities and biological processes related to them. The following examples are several applications of it. Shan and co-workers used compound **1a** to form a FRET pair with the dye BODIPY-Fl to study the dynamics of protein–protein interactions [2]. Wang and co-workers genetically incorporated **1a** to a position near to amino acids, which can be phosphorylated to investigate how phosphorylation affects the fluorescence properties of **1a**, and the variation in the fluorescence intensity can be used to probe the phosphorylation status of certain amino acids [3]. Chapman and co-workers studied the FtsZ protein with genetically incorporated **1a** [4]. The fluorescence of **1a** was utilized to study the assembling of FtsZ in vivo, especially how the Z-ring

is formed by FtsZ. This cannot be achieved by using GFP labeling technique since GFP is relatively insensitive to the pH and the solvent polarity of the solution. Many more examples of the usage of **1a** have also been reported [5-8]. Due to the high importance of **1a**, there has been a great need for a highly efficient and practical protocol for its synthesis.



1

1a: R = H
1b: R = F
1c: R = Cl

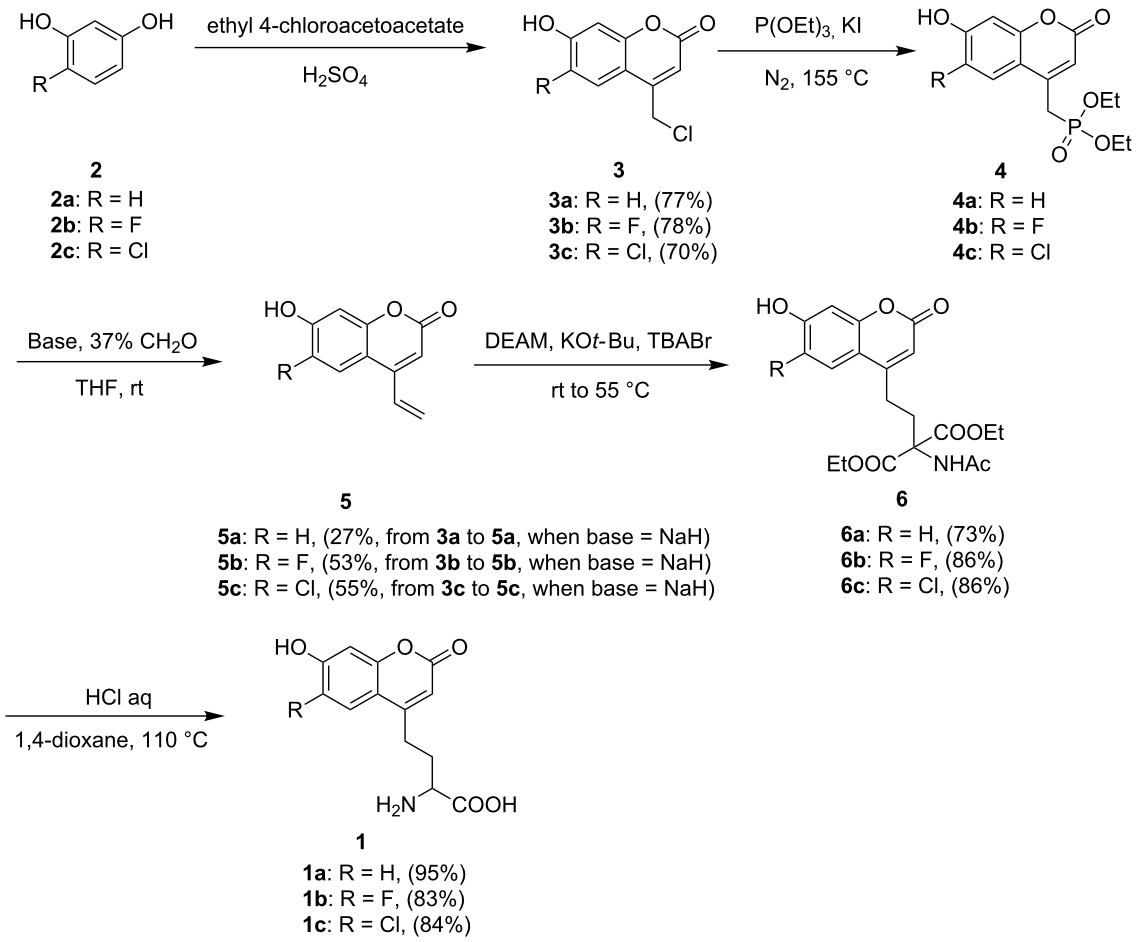
Figure 1: The chemical structure of a series of fluorescent amino acids. (**1a**) α-(2-(7-hydroxycoumarin-4-yl)ethyl)glycine; (**1b**) α-(2-(6-fluoro-7-hydroxycoumarin-4-yl)ethyl)glycine; (**1c**) α-(2-(6-chloro-7-hydroxycoumarin-4-yl)ethyl)glycine.

There are two major different approaches available in the literature to synthesize compound **1a**. Approach 1 was reported by Schultz and co-workers, and it was the first synthetic protocol to provide **1a** as an enantiomerically pure amino acid in L-configuration [1]. In this approach, *N*-α-Cbz-L-glutamic acid α-benzyl ester was first converted into the side-chain β-keto ester and then it was reacted with resorcinol in methanesulfonic acid to afford **1a**. The biggest shortcoming of this approach is that the purification of the final product requires a costly preparative reversed-phase HPLC system. Other drawbacks of this approach include that the reactant Z-Glu-OBzl is expensive, and it is difficult to characterize some of the intermediates formed. Approach 2 was designed by Braun and Dittrich to provide an alternative path for the synthesis of **1a** [10]. It started from a coumarinylacetic acid, which was then reduced to an alcohol by borane-dimethyl sulfide. After the phenolic hydroxy group was protected with a *tert*-butyl(dimethyl)silyl group, the alcohol was converted into a bromide and was used to alkylate a glycine enolate synthon to afford an imine. All the protecting groups were then removed and racemic amino acid **1a** was afforded. This approach prevents the tedious and costly HPLC purification step used in approach 1. However, it can only provide compound **1a** as a racemic mixture, and some reagents used are not readily available. Due to the great importance of coumarin amino acid, we designed a new synthetic protocol for compound **1a** and two further halogen derivatives (**1b** and **1c**). This new approach avoids some of the problems discussed above. It has a good overall yield and only requires reagents that are relatively cheap or easy to prepare. Compounds **1b** and **1c** have different sensitivities to pH and solvent polarity, and can serve as new fluorescent probes in a variety of applications.

Results and Discussion

Scheme 1 gives an outline of the new protocol used to synthesize compound **1**. First, the coumarin ring with a 4-chloromethyl group (compound **3**) was formed through Pechmann condensation [11] from ethyl 4-chloroacetoacetate and resorcinol or its 6-halogenated derivatives (**3a**, 77.4% yield; **3b**, 78.0%; **3c**, 70.0%). By suspending compound **3** in triethyl phosphate with a catalytic amount of sodium iodide and heating the mixture under reflux, phosphonate **4** was prepared and used directly in the next step without purification. Compound **4** was first treated with sodium hydride or other bases and then reacted with formaldehyde to form terminal alkene **5** through a Horner–Wadsworth–Emmons reaction [12] (two-step overall yields are 27%, 53% and 55% for **3a** to **5a**, **3b** to **5b** and **3c** to **5c**, respectively, if sodium hydride was used). In the presence of potassium *tert*-butoxide and a catalytic amount of tetrabutylammonium bromide, alkene **5** reacted with diethyl acetamidomalonate (DEAM) [13] to form malonate **6** in high yield (**6a**, 73.1% yield; **6b**, 86.0%; **6c**, 86.0%). It was then heated under reflux in aqueous HCl solution (12 M) to completely remove the protecting groups to afford the racemic coumarin amino acid **1** (**1a**, 95% yield; **1b**, 83%; **1c**, 84.3%).

This is a short and practical approach for the synthesis of coumarin amino acid **1**. The Pechmann condensation was chosen to assemble the coumarin ring, since the yield is high and derivatives with substituents at the 5-, 6- or 8-position can be prepared [14-16]. In this paper, we report the synthesis of 6-fluoro and 6-chloro derivatives of compound **1a** through Pechmann condensation. The functional group introduced at these positions will further improve the fluorescent property of the coumarin amino acids, or add new chemical handles to the coumarin ring for some specific investigations. The Horner–Wadsworth–Emmons reaction was applied to install the terminal alkene at the 4-position. Compared with the Wittig reaction, the Horner–Wadsworth–Emmons reaction has a significant advantage: The resulting phosphate byproduct can be readily separated, whereas the byproduct triphenylphosphine oxide generated in the Wittig reaction is difficult to remove [17]. The effect of the base used in the Horner–Wadsworth–Emmons reaction on the reaction yield was investigated (Table 1). Three different bases including sodium hydride, 1,8-diazabicycloundec-7-ene (DBU) and potassium *tert*-butoxide (KO*t*-Bu) were used, and the reactions were carried out at 25 °C for 5 h. DBU gave the best yield in the synthesis of **5a**, **5b** or **5c**, whereas there was no reaction at all when KO*t*-Bu was used. This indicates that KO*t*-Bu is not basic enough to deprotonate



Scheme 1: Synthetic route to fluorescent amino acids **1a**, **1b** and **1c**.

the α-hydrogen of phosphonate **4** at 25 °C. However, when the reaction temperature was raised to 55 °C, the deprotonation happened and compound **5** was afforded with good yield (Table 2). This indicates that the reaction temperature has a significant effect on the Horner–Wadsworth–Emmons reaction. Since the coumarin ring could be opened under basic conditions, especially at high temperature [18], we need to choose proper base and reaction temperature to get the optimized yield of terminal alkene **5**. Based on the experimental results, DBU is the best base among the three, and the reaction can be carried out at room temperature to obtain a relatively good yield. Alkylation of DEAM is widely used to synthesize α-amino acids [13], which was also applied here to prepare the coumarin amino acids. Through Michael addition reaction of DEAM to terminal alkene **5**, malonate **6** was formed in high yield, and it was followed by the total hydrolysis of compound **6** with concentrated aqueous HCl solution to afford the coumarin amino acid **1**. We found that the hydrolysis needed a high concentration of

Table 1: Effect of different bases on the yield of compounds **5a**, **5b** and **5c**[a].

Compound	NaH	DBU	KO*t*-Bu
5a	27%	45%	No reaction
5b	51%	59%	No reaction
5c	45%	55%	No reaction

[a]Reaction temperature: 25 °C; reaction time: 5 h; solvent: THF; equiv of compound **4**/equiv of base = 1/5.

Table 2: Effect of temperature on the yield of compounds **5a**, **5b** and **5c**[a].

Compound	25 °C	55 °C
5a	No reaction	52%
5b	No reaction	47%
5c	No reaction	48%

[a]Base: KO*t*-Bu; reaction time: 5 h; solvent: THF; equiv of compound **4**/equiv of base = 1/5.

aqueous HCl solution (12 M) and a relatively long reaction time (10 h) to reach completion.

Though this new protocol also affords the coumarin non-natural amino acids in racemic form, similar to approach 2, it has some advantages that make it practical for the preparation of these fluorescent amino acids. First, the overall yields of the products are good compared with the two approaches reported**,** and all the reagents are commercially available and relatively cheap. Second, a tedious HPLC purification step is not necessary and only flash chromatography is required. Last, but most important, derivatives with a substituent at the 6-position can be prepared, which greatly expands the usage of this synthetic protocol. Coumarin non-natural amino acids with a substituent at the 5- or 8-position can also be prepared and a respective study is ongoing in our laboratory.

The L-enantiomer was proved to be able to be incorporated into a protein exclusively from the racemic mixture. In the presence of the synthetase CouRS and *Mj*tRNA$^{Tyr}_{CUA}$, in *E. coli* [1], an amber codon was substituted for Ile-38 in thioredoxin-1 (TRX-TAG38), and protein expression was carried out in the LB medium with the addition of 1 mM of racemic coumarin amino acid **1a**. The protein expression was also carried out without **1a** as a negative control. The synthetase/tRNA pair could uniquely specify **1a** in response to the TAG codon, which made the expression of TRX-TAG38 possible. The protein was then purified and analyzed by the SDS-PAGE gel (Figure 2). It showed that the full length protein (12.9 kDa) was only expressed in the presence of **1a**; even the final product was racemic. Since thioredoxin has no intrinsic fluorescence, the fluorescent band corresponding to mutant thioredoxin in the right panel of Figure 2 must come from incorporated **1a**. The L-enantiomer is assumed to be accepted exclusively from the racemic mixture since there is not any report indicating that D-amino acids exist in proteins. A related report proved that in the incorporation of a non-natural amino acid into a protein, the L-enantiomer is accepted exclusively from the racemic mixture [19]. Nevertheless, crystallization of the TAG38 mutant thioredoxin is under way to obtain the X-ray crystal structure of it, which will give direct proof of the exclusive incorporation of the L-enantiomer of **1a**.

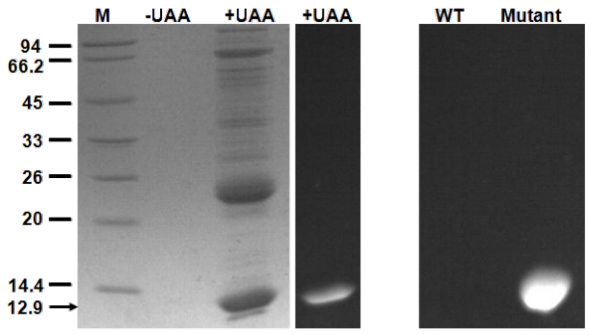


Figure 2: Coomassie-stained SDS-PAGE (left) of TAG38 mutant thioredoxin (indicated by the black arrow) expression in the presence and absence of 1 mM **1a**. The right panel shows the fluorescence image of wild-type and TAG38 mutant thioredoxin.

6-Halogenated derivatives were also synthesized with this new protocol; these derivatives should have similar extinction coefficients and quantum yields as compound **1a**, according to the literature [20,21]. However, their p*K*a values are significantly different from those of **1a**, as shown in Table 3. The p*K*a values are calculated from the absorbance at 360 nm at different pH values illustrated in Figure 3, by using the Henderson–Hasselbalch equation. The halogenation of **1a** at the 6-position decreases the p*K*a value, which makes compounds **1b** and **1c**

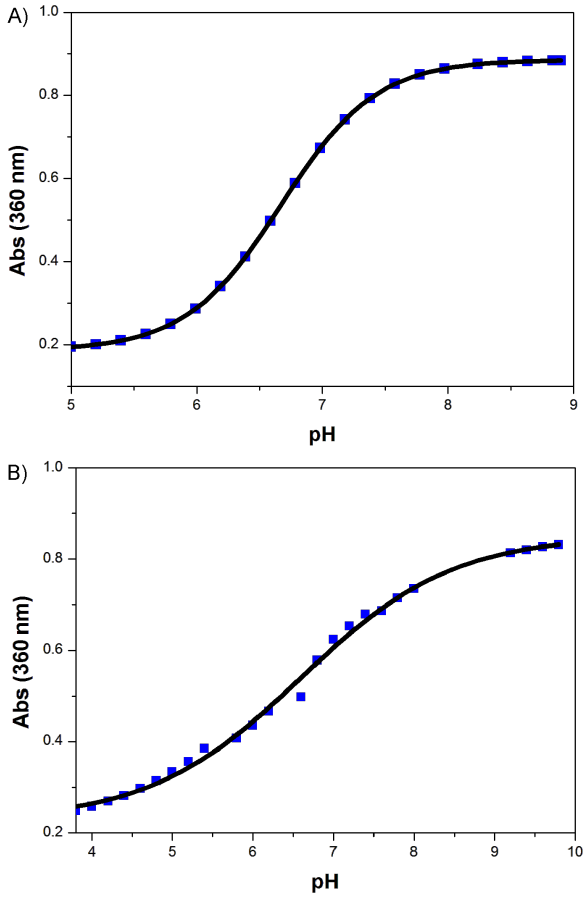


Figure 3: Absorbance of compounds **1b** and **1c** at 360 nm as a function of pH value. (A) Absorption spectrum of 50 μM compound **1b** in 200 mM sodium phosphate buffer (pH 5.8–8.0), 200 mM sodium acetate buffer (pH 3.7–5.6) or 50 mM Tris-HCl buffer (pH 8.2–8.9). (B) Absorption spectrum of 25 μM compound **1c** in 200 mM sodium phosphate buffer (pH 5.8–8.0) or sodium acetate buffer (pH 3.7–5.6).

Table 3: p*K*a values of compounds **1a**, **1b** and **1c** and their corresponding wavelengths of maximum emission.

Compound	p*K*a	Wavelength of maximum emission
1a	7.8	456 nm
1b	6.6	448 nm
1c	6.3	452 nm

good substitutes for **1a** in fluorescent labeling and other investigations in biological systems. Screening for the synthetase/tRNA pair for **1b** and **1c** is under way. Fluorescent emission spectra of **1b** and **1c** at different pH values were both acquired (Figure 4). The fluorescence intensities of these two compounds are greatly enhanced upon increasing pH value of the solutions. This fluorescence property can be used to monitor the pH value of some acidic organelles, which may be difficult or even impossible for other investigating technologies. For the 6-fluorinated compound **1b**, its ^{19}F NMR is another important property suitable for probing the biological system. Coupling the fluorescent emission spectrum with its ^{19}F NMR spectrum, it will provide a very powerful means in biological investigations and analysis with small molecules.

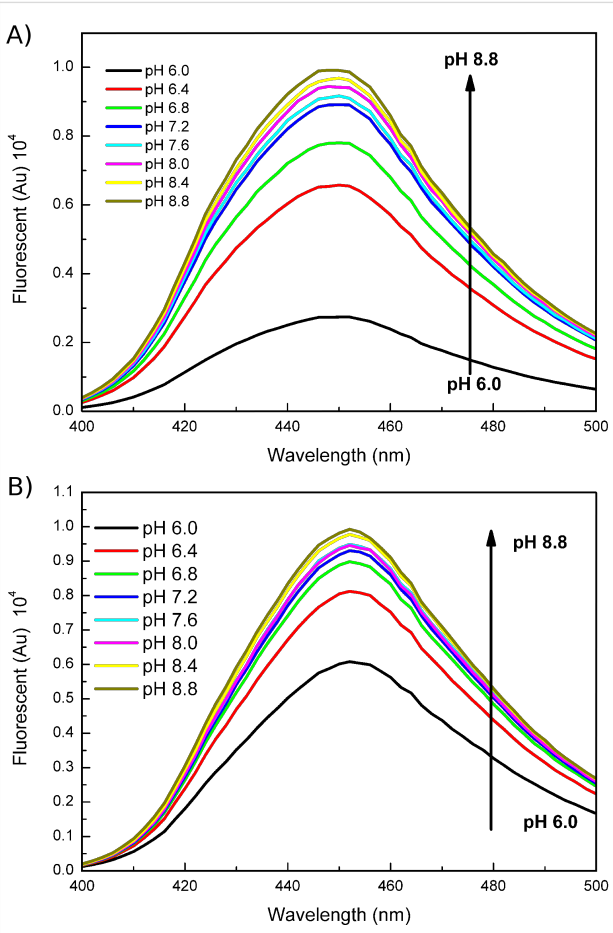


Figure 4: Effect of the pH value of the solution on the fluorescence emission spectra of compounds **1b** and **1c**. (A) Fluorescence emission spectrum of compound **1b**. (B) Fluorescence emission spectrum of compound **1c**.

Conclusion

In summary, a new protocol for the synthesis of several fluorescent coumarin non-natural amino acids in good yields was designed. This protocol only requires relatively cheap reagents and five reaction steps in total. The separation and purification processes are much easier and an HPLC purification step is unnecessary. Thus, it is more economical and less tedious compared with previously reported protocols. 6-Halogenated coumarin non-natural amino acids have different fluorescence properties and other functionalities, which makes them good probes for various biological studies. That a series of related coumarin non-natural amino acids can be prepared with this synthetic protocol is its most important advantages. Other derivatives with a 5- and 8-substituent are being synthesized and their fluorescence properties will be studied. The drawback of this protocol is that we cannot obtain the pure L-enantiomer, and only a racemic mixture was synthesized. However we proved that the L-enantiomer can be incorporated into protein exclusively, which indicated that the racemic product is good enough for biological studies. Nevertheless, pursuit of a synthetic protocol affording the pure L-enantiomer is still our next goal.

By the chemical synthesis and genetic encoding of the fluorescent non-natural amino acids, fluorescent groups can easily be incorporated at defined sites of proteins directly in living organisms. The fluorescent group wouldn't cause significant perturbations on proteins due to its small size, thus, it greatly extends the scope of fluorescence imaging techniques. Compound **1a** has a p*K*a of 7.8 and only its conjugate base is fluorescent. This limits its usage in the fluorescence imaging in vivo, such as in the study of receptor-mediated endocytosis. The protein involved in the endocytosis needs to be translocated from cytoplasm, which has a pH around 7, to the endosomes and lysosomes, which have pH values around 5 [22]. Since the fluorescence of compound **1a** is relatively weak at acidic conditions, compound **1b** and **1c** with lower p*K*a are important and thus synthesized. They will be more fluorescent in an acidic environment, which makes them better probes for endocytosis than compound **1a**. With the new synthetic protocol, compound **1b** and **1c** now can be prepared in a straightforward manner. The remaining unsolved problem in our work is on the molecular biology side, the focus of which is the screening of the specific aminoacyl-tRNA synthetases capable of recognizing **1b** or **1c**. Once we get the synthetases, compound **1b** and **1c** will be very useful probes of organellar pH and pH-dependent cellular

processes. More coumarin amino acids with specific properties can also be prepared by using our new synthetic protocol, which makes it an important one in this research area.

Supporting Information

Supporting Information File 1

Experimental and analytical data.
[http://www.beilstein-journals.org/bjoc/content/supplementary/1860-5397-9-30-S1.pdf]

Acknowledgements

We gratefully acknowledge the National Science Foundation of China (21102172 to X.H. and 90913022 to J.W.) and the Major State Basic Research Program of China (2010CB912301 and 2009CB825505 to J.W.) for financial support. X.H. also gratefully thank the Scientific Research Foundation for the Returned Overseas Chinese Scholars, State Education Ministry, the Fundamental Research Funds for the Central Universities (Wuhan University of Technology: 133114001)", and "the Self-determined and Innovative Research Funds of Wuhan University of Technology" for financial support.

References

1. Wang, J.; Xie, J.; Schultz, P. G. *J. Am. Chem. Soc.* **2006,** *128,* 8738–8739. doi:10.1021/ja062666k
2. Saraogi, I.; Zhang, D.; Chandrasekaran, S.; Shan, S.-o. *J. Am. Chem. Soc.* **2011,** *133,* 14936–14939. doi:10.1021/ja206626g
3. Lacey, V. K.; Parrish, A. R.; Han, S.; Shen, Z.; Briggs, S. P.; Ma, Y.; Wang, L. *Angew. Chem., Int. Ed.* **2011,** *50,* 8692–8696. doi:10.1002/anie.201102923
4. Charbon, G.; Brustad, E.; Scott, K. A.; Wang, J.; Løbner-Olesen, A.; Schultz, P. G.; Jacobs-Wagner, C.; Chapman, E. *ChemBioChem* **2011,** *12,* 1818–1821. doi:10.1002/cbic.201100282
5. Ugwumba, I. N.; Ozawa, K.; Xu, Z.-Q.; Ely, F.; Foo, J.-L.; Herlt, A. J.; Coppin, C.; Brown, S.; Taylor, M. C.; Ollis, D. L.; Mander, L. N.; Schenk, G.; Dixon, N. E.; Otting, G.; Oakeshott, J. G.; Jackson, C. J. *J. Am. Chem. Soc.* **2011,** *133,* 326–333. doi:10.1021/ja106416g
6. Li, S. *ChemBioChem* **2011,** *12,* 2729–2731. doi:10.1002/cbic.201100554
7. Charbon, G.; Wang, J.; Brustad, E.; Schultz, P. G.; Horwich, A. L.; Jacobs-Wagner, C.; Chapman, E. *Bioorg. Med. Chem. Lett.* **2011,** *21,* 6067–6070. doi:10.1016/j.bmcl.2011.08.057
8. Ho, D.; Lugo, M. R.; Lomize, A. L.; Pogozheva, I. D.; Singh, S. P.; Schwan, A. L.; Merrill, A. R. *Biochemistry* **2011,** *50,* 4830–4842. doi:10.1021/bi101934e
9. Tsien, R. Y. *Annu. Rev. Biochem.* **1998,** *67,* 509–544. doi:10.1146/annurev.biochem.67.1.509
10. Braun, M.; Dittrich, T. *Beilstein J. Org. Chem.* **2010,** *6,* No. 69. doi:10.3762/bjoc.6.69
11. von Pechmann, H.; Duisberg, C. *Ber. Dtsch. Chem. Ges.* **1883,** *16,* 2119–2128.
12. Wadsworth, W. S., Jr.; Emmons, W. D. *J. Am. Chem. Soc.* **1961,** *83,* 1733–1738. doi:10.1021/ja01468a042
13. Haudegond, J. P.; Chauvin, Y.; Commereuc, D. *J. Org. Chem.* **1979,** *44,* 3063–3065. doi:10.1021/jo01331a020
14. Trost, B. M.; Toste, F. D.; Greenman, K. *J. Am. Chem. Soc.* **2003,** *125,* 4518–4526. doi:10.1021/ja0286573
15. Herath, H. M. T. B.; Müller, K.; Diyabalanage, H. V. K. *J. Heterocycl. Chem.* **2004,** *41,* 23–28. doi:10.1002/jhet.5570410104
16. Gündüz, C.; Salan, Ü.; Bulut, M. *J. Heterocycl. Chem.* **2009,** *46,* 567–570. doi:10.1002/jhet.90
17. Boutagy, J.; Thomas, R. *Chem. Rev.* **1974,** *74,* 87–99. doi:10.1021/cr60287a005
18. Ramesh, D.; Srinivasan, M. *Curr. Sci.* **1984,** *53,* 369–371.
19. Cellitti, S. E.; Jones, D. H.; Lagpacan, L.; Hao, X.; Zhang, Q.; Hu, H.; Brittain, S. M.; Brinker, A.; Caldwell, J.; Bursulaya, B.; Spraggon, G.; Brock, A.; Ryu, Y.; Uno, T.; Schultz, P. G.; Geierstanger, B. H. *J. Am. Chem. Soc.* **2008,** *130,* 9268–9281. doi:10.1021/ja801602q
20. Sun, W.-C.; Gee, K. R.; Haugland, R. P. *Bioorg. Med. Chem. Lett.* **1998,** *8,* 3107–3110. doi:10.1016/S0960-894X(98)00578-2
21. Brun, M.-P.; Bischoff, L.; Garbay, C. *Angew. Chem., Int. Ed.* **2004,** *43,* 3432–3436. doi:10.1002/anie.200454116
22. Conner, S. D.; Schmid, S. L. *Nature* **2003,** *422,* 37–44. doi:10.1038/nature01451

License and Terms

This is an Open Access article under the terms of the Creative Commons Attribution License (http://creativecommons.org/licenses/by/2.0), which permits unrestricted use, distribution, and reproduction in any medium, provided the original work is properly cited.

The license is subject to the *Beilstein Journal of Organic Chemistry* terms and conditions: (http://www.beilstein-journals.org/bjoc)

The definitive version of this article is the electronic one which can be found at:
doi:10.3762/bjoc.9.30

Beilstein Journal of Organic Chemistry

From bead to flask: Synthesis of a complex β-amido-amide for probe-development studies

Kevin S. Martin[1,2], Cristian Soldi[1], Kellan N. Candee[1], Hiromi I. Wettersten[2,3], Robert H. Weiss[2,3,4] and Jared T. Shaw[*1,2,4]

Full Research Paper

Open Access

Address:
[1]Department of Chemistry, University of California, Davis, CA 95616, USA, [2]Comparative Pathology Graduate Group, University of California, Davis, CA 95616, USA, [3]Division of Nephrology, Dept. of Internal Medicine, University of California, Davis, Medical Center, Sacramento, CA 95817, USA and [4]UC Davis Comprehensive Cancer Center, 2279 45th Street Sacramento, CA 95817, USA

Email:
Jared T. Shaw[*] - jtshaw@ucdavis.edu

* Corresponding author

Keywords:
β-amino acid; benzimidazole; multicomponent reaction

Beilstein J. Org. Chem. **2013,** *9,* 260–264.
doi:10.3762/bjoc.9.31

Received: 09 October 2012
Accepted: 07 January 2013
Published: 06 February 2013

This article is part of the Thematic Series "Synthetic probes for the study of biological function".

Guest Editor: J. Aubé

© 2013 Martin et al; licensee Beilstein-Institut.
License and terms: see end of document.

Abstract

A concise synthesis of benzimidazole-substituted β-amido-amide LLW62 is presented. The original synthesis of compounds related to LLW62 was developed on Rink resin as part of a "one-bead, one-compound" combinatorial approach for on-bead screening purposes. The current synthesis is carried out in solution and is amenable to scale-up for follow-up studies on LLW62 and investigations of related structures. The key step involves the use of a β-amino acid-forming three-component reaction (3CR), the scope of which defines its role in the synthetic strategy.

Introduction

Library syntheses and high-throughput screening can often be combined to enable the discovery of new small-molecule probes that modulate biological phenomena [1]. Although the use of solid-phase, split-pool combinatorial synthesis for the preparation of solutions of small-molecule libraries has declined, the use of these compounds for on-bead screening has resulted in recent screening innovations [1,2]. The Lam and Kurth groups have published several "one-bead, one-compound" (OBOC) library syntheses of heterocyclic structures for a variety of screening endeavors [3-12]. Some of these compounds were identified as inhibitors of p21, which is a protein that modulates the activity of cyclin kinases [13-15]. One function of p21 is that it acts downstream of p53 to repair DNA-damaged cells and may function to convey anti-apoptotic activity to cancer cells (Figure 1) [13]. As such, an inhibitor of p21 could sensitize malignant cells to DNA-damaging chemical and radiation therapy by subverting this p21-mediated DNA repair process [14-17]. In this study, we developed a synthesis of LLW62 (**1**, Figure 2), which is a complex benzimidazole-substituted β-amido-amide similar in structure to inhibitors of p21 that were reported previously to support studies of this compound as a biological probe [14,15].

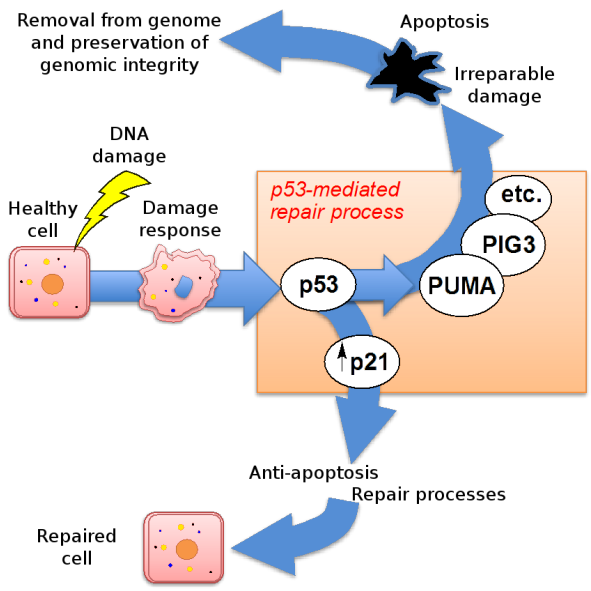


Figure 1: p21 determines the fate of DNA-damaged [13] cells.

The synthesis of **1** emanates from a one-pot, three-component reaction (3CR) of an arylaldehyde, malonic acid (**5**), and ammonium acetate, which assembles the β-amino acid core (Figure 2) [14,15,18]. In the reported synthesis of **1**, a protected β-amino acid core was attached to Rink-amide resin and carried through to **1** by a series of elaboration and tagging steps [14,15]. Synthetic intermediates in this route were not characterized, and **1** was ultimately purified by high-performance liquid chromatography and partially characterized by matrix-assisted laser desorption/ionization mass spectrometry [14]. In the current synthesis, we set out to develop a concise and scalable solution-phase route to **1** and provide characterization data for **1** and all intermediate compounds.

In our retrosynthetic analysis, we envisioned **1** coming from acylation of benzimidazole **3** with isocyanate **2** (Figure 2). We initially sought to avoid nitration, protection and deprotection steps and access this intermediate by performing a late-stage 3CR with benzimidazole **4**, which would be available from nitrile **6** or acid **7** (Figure 2, A). Although synthesis of **4** proceeded without difficulty from acid **7**, this route was unsuccessful at a late stage for a reason that we describe below. We next envisioned benzimidazole **3** emanating from β-amino ester **10,** which could be accessed in a few steps starting with an early stage 3CR of aldehyde **11**, malonic acid (**5**), and ammonium acetate (Figure 2, B). Gratifyingly, **10** was converted to the requisite benzimidizole **3** in three steps and carried through to **1**.

Results and Discussion

Our initial target was benzimidazole **4**, which we envisioned originating from nitrile **6** or acid **7**, each of which is commercially available (Figure 2). We first attempted to synthesize **4** from **6**, which would lead to the shortest possible synthesis of **1**. Nitrile **6** was treated with *N*-(3-aminopropyl)pyrrolidine (**8**) to produce aniline **12** in 81% yield (Scheme 1) [19]. This compound was reduced to aniline **13** in 79% yield and converted to the benzimidizole **14** in 63% yield with aldehyde **9** under oxidative conditions. The resultant nitrile proved to be extremely

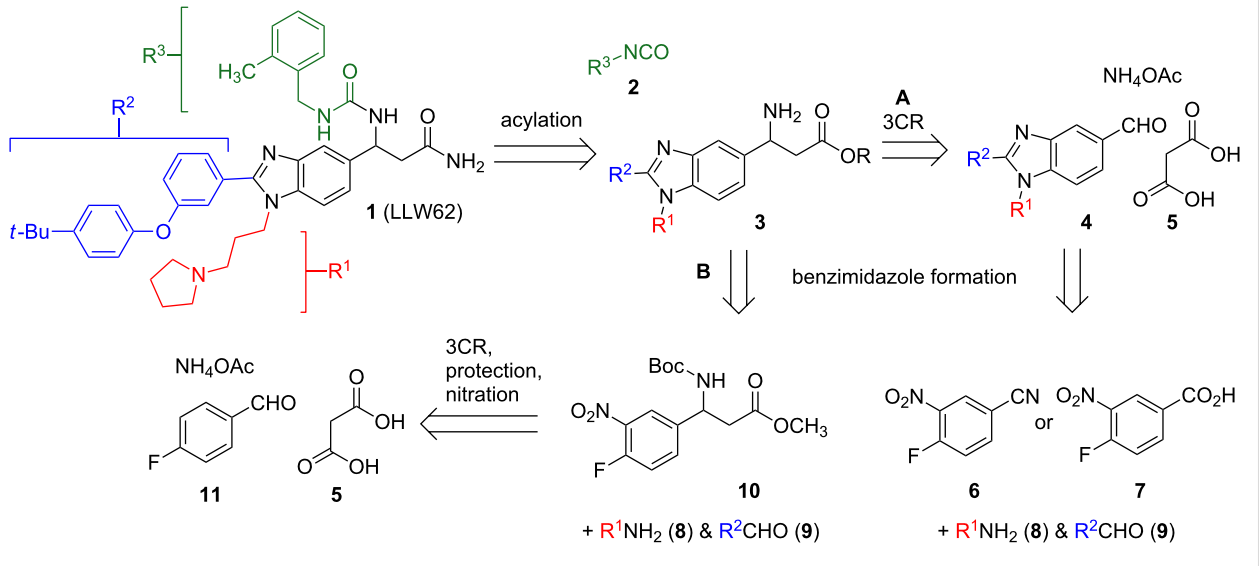
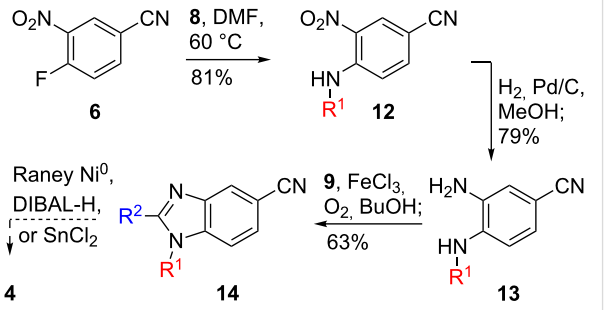


Figure 2: Retrosynthetic analysis of LLW62 (**1**) from acid **7** (A) or aldehyde **11** (B).

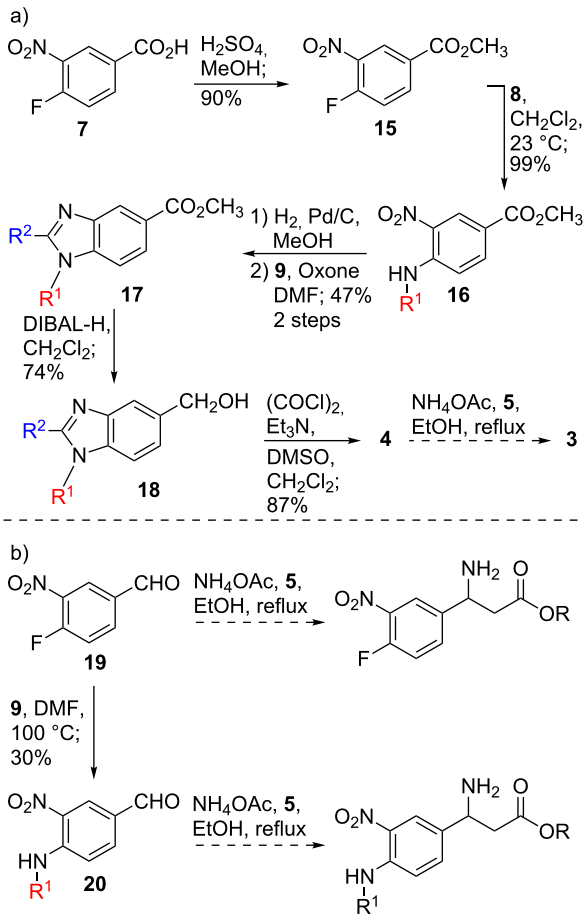
insoluble and difficult to handle. Several reduction conditions were attempted to produce benzimidazole **4** with no success. In addition, attempts to use the nitrile in a Blaise-type reaction or similar nucleophilic addition were also unsuccessful (not shown). Although nitrile **6** would have provided the shortest, most direct entry into the requisite β-amino core structure, we turned our attention to another route to **4**.



Scheme 1: Attempted synthesis of aldehyde **4** from nitrile **6**.

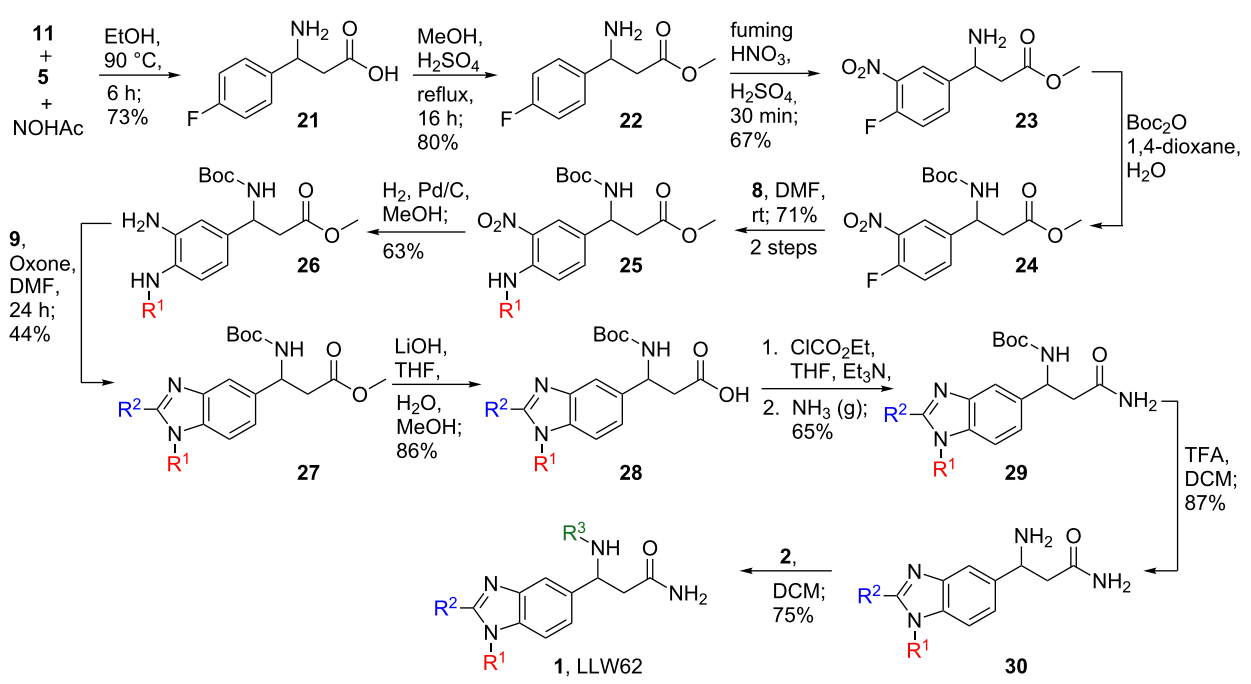
Acid **7** was immediately more promising as a starting material for benzimidazole **4**. Commercially available **7** was converted to methyl ester **15** in 90% yield, due to its ease of handling (Scheme 2) [20]. Next, S_NAr displacement of the fluoride of **15** by *N*-(3-aminopropyl)pyrrolidine (**8**) proceeded in high yield, 99%, to give aniline **16** [20]. Reduction of the nitro group was nearly quantitative and subsequent benzimidazole formation with Oxone furnished benzimidazole **17** in 47% yield over two steps [20,21]. The ester of **17** was smoothly reduced to the alcohol **18**, in 74% yield, and immediately oxidized to the aldehyde **4**, in 87% yield. Unfortunately, **4** produced none of the desired β-amino acid **3** under several different variants of the 3CR with malonic acid (**5**) and ammonium acetate. Tan and Weaver demonstrated previously that the β-amino acid forming 3CR works best for electron-rich aldehydes and poorly for electron-deficient aldehydes [18]. Thus, we suspected that aldehyde **4** may be too electron poor for the 3CR to work efficiently. Our suspicions were supported by attempting 3CRs on aldehydes **19** and **20**, each of which has a single nitro group, and neither was successful in this transformation.

An early-stage 3CR enabled the use of the least electron-poor aldehyde in this key step (Scheme 3). Heating of 4-fluorobenzaldehyde (**11**), malonic acid and ammonium acetate under reflux proceeded smoothly, as previously described, to furnish β-amino acid **21** in 73% yield [18]. Methylation of **21** (80%) followed by nitration of **22** (67%), boc protection of **23** and S_NAr displacement of the fluoride in **24** with amine **8** (71% over two steps), and finally reduction of the nitro group of **25**



Scheme 2: (A) Synthesis of **4** from acid **7** and (B) attempted β-amino acid-forming 3CRs.

(63%) provided aniline **26** as our key intermediate for forming the benzimidazole core of **1**. We next attempted to produce **27** under the higher yielding oxidative conditions described for the formation of nitrile containing benzimidazole **14**. The yield for this reaction was significantly lower, less than 50%, compared to the reaction to produce **14**, and we observed some transesterification of the methyl ester with butanol to produce a mixture of **27** and the butyl ester of **27** as the major products (not shown). We thus turned to using Oxone, and benzimidazole formation proceeded in acceptable yield (44%) from aniline **26** to furnish **27.** Benzimidazole **27** was then saponified under basic conditions to give acid **28** (86%) [21]. Installation of the primary amide of **1** was then achieved in a single pot by treatment of **28** with ethyl chloroformate to make the mixed anhydride followed by displacement with ammonia gas to produce **29** in 65% yield [22]. Final Boc deprotection of **29** with TFA (87%) and subsequent acylation of the free amine of **30** with isocyanate **2** (75%) provided the desired compound **1** in 11 total steps and 3% overall yield.



Scheme 3: Synthesis of LLW62 by using an early stage 3CR.

Conclusion

We have completed a solution-phase synthesis of **1** and thus provided a common route to related compounds that may emerge from future on-bead screening experiments. The key step was the 3CR to form the β-amino acid core structure. Although the electronic requirements of this reaction limit it to electron-rich, or at least not excessively electron poor, aromatic aldehydes, application of this transformation early in the synthesis ultimately proved successful. Although this route is not suitable for large-scale production of **1**, multigram quantities of this compound and benzimidazoles of comparable complexity are easily accessible for early stage studies of these compounds in vitro and in vivo using model organisms.

Supporting Information

Supporting Information File 1

Experimental procedures and compound characterization.
[http://www.beilstein-journals.org/bjoc/content/supplementary/1860-5397-9-31-S1.pdf]

Acknowledgements

This work was supported by the National Science Foundation (CAREER award to JTS) and the National Institutes of Health (NIGMS/P41GM089153). CS thanks CAPES (Coordenação de Aperfeiçoamento de Pessoal de Nível Superior) and the Brazilian Ministry of Education for a postdoctoral fellowship. RHW acknowledges research support from the NIH (NCI/1R01CA135401; NIDDK/1R01DK082690) and the Medical Service of the US Department of Veterans' Affairs. The authors thank Dr. Ruiwu Liu and Professor Kit S. Lam (Division of Hematology and Oncology, Department of Internal Medicine, University of California Davis Comprehensive Cancer Center) for helpful discussions.

References

1. Dolle, R. E.; Le Bourdonnec, B.; Worm, K.; Morales, G. A.; Thomas, C. J.; Zhang, W. *J. Comb. Chem.* **2010,** *12,* 765–806. doi:10.1021/cc100128w
2. Kodadek, T. *Chem. Commun.* **2011,** *47,* 9757–9763. doi:10.1039/c1cc12102b
3. Aina, O. H.; Marik, J.; Liu, R.; Lau, D. H.; Lam, K. S. *Mol. Cancer Ther.* **2005,** *4,* 806–813. doi:10.1158/1535-7163.MCT-05-0029
4. Dixon, S.; Ziebart, K. T.; He, Z.; Jeddeloh, M.; Yoo, C. L.; Wang, X.; Lehman, A.; Lam, K. S.; Toney, M. D.; Kurth, M. J. *J. Med. Chem.* **2006,** *49,* 7413–7426. doi:10.1021/jm0609869
5. Zhang, H.; Aina, O. H.; Lam, K. S.; de Vere White, R.; Evans, C.; Henderson, P.; Lara, P. N.; Wang, X.; Bassuk, J. A.; Pan, C.-x. *Urol. Oncol.: Semin. Orig. Invest.* **2012,** *30,* 635–645. doi:10.1016/j.urolonc.2010.06.011
6. Lam, K. S.; Lehman, A. L.; Song, A.; Doan, N.; Enstrom, A. M.; Maxwell, J.; Liu, R. *Methods Enzymol.* **2003,** *369,* 298–322. doi:10.1016/S0076-6879(03)69017-8
7. Lam, K. S.; Salmon, S. E.; Hersh, E. M.; Hruby, V. J.; Kazmierski, W. M.; Knapp, R. J. *Nature* **1991,** *354,* 82–84. doi:10.1038/354082a0
8. Liu, G.; Fan, Y.; Zhao, Z.; Lam, K. S. *Zhongguo Yaowu Huaxue Zazhi* **2002,** *12,* 311–318.

9. Miyamoto, S.; Liu, R.; Hung, S.; Wang, X.; Lam, K. S. *Anal. Biochem.* **2008,** *374,* 112–120. doi:10.1016/j.ab.2007.10.028
10. Park, S. I.; Renil, M.; Vikstrom, B.; Amro, N.; Song, L.-w.; Xu, B.-l.; Lam, K. S. *Lett. Pept. Sci.* **2001,** *8,* 171–178. doi:10.1023/A:1016297601361
11. Xiao, W.; Wang, Y.; Lau, E. Y.; Luo, J.; Yao, N.; Shi, C.; Meza, L.; Tseng, H.; Maeda, Y.; Kumaresan, P.; Liu, R.; Lightstone, F. C.; Takada, Y.; Lam, K. S. *Mol. Cancer Ther.* **2010,** *9,* 2714–2723. doi:10.1158/1535-7163.MCT-10-0308
12. Dixon, S. M.; Milinkevich, K. A.; Fujii, J.; Liu, R.; Yao, N.; Lam, K. S.; Kurth, M. J. *J. Comb. Chem.* **2007,** *9,* 143–157. doi:10.1021/cc060090p
13. Weiss, R. H. *Cancer Cell* **2003,** *4,* 425–429. doi:10.1016/S1535-6108(03)00308-8
14. Weiss, R.; Park, S.-H.; Lam, K. S.; Liu, R. Inhibitors of Cyclin Kinase Inhibitor p21. WO Patent WO2010039668A2, April 8, 2010.
15. Park, S. H.; Wang, X.; Liu, R.; Lam, K. S.; Weiss, R. H. *Cancer Biol. Ther.* **2008,** *7,* 2015–2022. doi:10.4161/cbt.7.12.7069
16. Park, S.-H.; Park, J.-Y.; Weiss, R. H. *J. Urol.* **2008,** *180,* 352–360. doi:10.1016/j.juro.2008.02.038
17. Weiss, R. H.; Borowsky, A. D.; Seligson, D.; Lin, P.-Y.; Dillard-Telm, L.; Belldegrun, A. S.; Figlin, R. A.; Pantuck, A. D. *J. Urol.* **2007,** *177,* 63–69. doi:10.1016/j.juro.2006.08.073
18. Tan, C. Y. K.; Weaver, D. F. *Tetrahedron* **2002,** *58,* 7449–7461. doi:10.1016/S0040-4020(02)00824-4
19. Göker, H.; Kuş, C.; Boykin, D. W.; Yildiz, S.; Altanlar, N. *Bioorg. Med. Chem.* **2002,** *10,* 2589–2596. doi:10.1016/S0968-0896(02)00103-7
20. Dietrich, S. A.; Lindauer, R.; Stierlin, C.; Gertsch, J.; Matesanz, R.; Notararigo, S.; Diaz, J. F.; Altmann, K.-H. *Chem.–Eur. J.* **2009,** *15,* 10144–10157. doi:10.1002/chem.200901376
21. Cellier, M.; Fabrega, O. J.; Fazackerley, E.; James, A. L.; Orenga, S.; Perry, J. D.; Salwatura, V. L.; Stanforth, S. P. *Bioorg. Med. Chem.* **2011,** *19,* 2903–2910. doi:10.1016/j.bmc.2011.03.043
22. Yan, S.; Larson, G.; Wu, J. Z.; Appleby, T.; Ding, Y.; Hamatake, R.; Hong, Z.; Yao, N. *Bioorg. Med. Chem. Lett.* **2007,** *17,* 63–67. doi:10.1016/j.bmcl.2006.09.095

License and Terms

This is an Open Access article under the terms of the Creative Commons Attribution License (http://creativecommons.org/licenses/by/2.0), which permits unrestricted use, distribution, and reproduction in any medium, provided the original work is properly cited.

The license is subject to the *Beilstein Journal of Organic Chemistry* terms and conditions: (http://www.beilstein-journals.org/bjoc)

The definitive version of this article is the electronic one which can be found at: doi:10.3762/bjoc.9.31

Beilstein Journal of Organic Chemistry

Synthesis and evaluation of cell-permeable biotinylated PU-H71 derivatives as tumor Hsp90 probes

Tony Taldone[*,‡1], Anna Rodina[‡1], Erica M. DaGama Gomes[1], Matthew Riolo[1], Hardik J. Patel[1], Raul Alonso-Sabadell[1], Danuta Zatorska[1], Maulik R. Patel[1], Sarah Kishinevsky[1] and Gabriela Chiosis[*1,2,3]

Full Research Paper

Open Access

Address:
[1]Molecular Pharmacology and Chemistry Program, Sloan-Kettering Institute, 1275 York Avenue, New York, NY 10065, USA, [2]Department of Medicine, Memorial Sloan-Kettering Cancer Center, 1275 York Avenue, New York, NY 10065, USA and [3]Department of Pharmacology, Weill Graduate School of Medical Sciences, 1300 York Avenue, New York, NY 10065, USA

Email:
Tony Taldone[*] - taldonet@mskcc.org; Gabriela Chiosis[*] - chiosisg@mskcc.org

* Corresponding author ‡ Equal contributors

Keywords:
affinity capture; biotin; flow cytometry; fluorescence microscopy; PU-H71; tumor Hsp90

Beilstein J. Org. Chem. **2013,** *9,* 544–556.
doi:10.3762/bjoc.9.60

Received: 10 October 2012
Accepted: 20 February 2013
Published: 15 March 2013

This article is part of the Thematic Series "Synthetic probes for the study of biological function".

Guest Editor: J. Aubé

© 2013 Taldone et al; licensee Beilstein-Institut.
License and terms: see end of document.

Abstract

The attachment of biotin to a small molecule provides a powerful tool in biology. Here, we present a systematic approach to identify biotinylated analogues of the Hsp90 inhibitor PU-H71 that are capable of permeating cell membranes so as to enable the investigation of Hsp90 complexes in live cells. The identified derivative **2g** can isolate Hsp90 through affinity purification and, as we show, represents a unique and useful tool to probe tumor Hsp90 biology in live cells by affinity capture, flow cytometry and confocal microscopy. To our knowledge, **2g** is the only reported biotinylated Hsp90 probe to have such combined characteristics.

Introduction

Heat shock protein 90 (Hsp90) is a molecular chaperone that functions to properly fold proteins to their active conformation through its ATPase activity [1]. These client proteins include many that are involved in malignant cell transformations (i.e., HER2, EGFR, mutant ER, HIF1α, Raf-1, AKT, mutant p53). As a result of this, as well as the ability to block multiple signaling pathways through inhibition of a single target, Hsp90 has become one of the most pursued molecular targets for anticancer therapy [2,3]. As a testament to this, there are numerous ongoing clinical trials evaluating Hsp90 inhibitors from a

variety of chemotypes [4]. Although there are potentially numerous ways to block the activity of Hsp90, the most successful to date, as exemplified by its exclusivity in mode of action by those advanced to clinical trials, has been the ATP-competitive inhibitors that bind to the N-terminal nucleotide binding pocket [4,5].

Hsp90 belongs to the family of GHKL (G = DNA gyrase subunit B; H = Hsp90; K = histidine kinases; L = MutL) ATPases, which is distinguished by a unique bent shape of its nucleotide binding pocket [6]. This distinctive shape has enabled for the design of highly selective ATP-competitive inhibitors of Hsp90. Through the efforts of multiple drug-discovery groups, many classes of inhibitors have been identified [3,5,7,8]. While much is known about the general types of structures that inhibit Hsp90 and their structure–activity relationship, less is understood about Hsp90 tumor biology. As a result we and others have been actively engaged in the synthesis of chemical tools designed to probe the function of Hsp90 in transformed systems [9-11]. One class of Hsp90 inhibitors of interest is the purine scaffold, including its representative PU-H71 (**1a**). This agent, currently in clinical investigation for cancer, binds to the N-terminal nucleotide binding pocket of Hsp90 [12].

We have shown that PU-H71 selects for tumor Hsp90 species, and therefore labeled derivatives of PU-H71 may be used to specifically dissect, in a tumor-by-tumor manner, the abundance and the functions of the oncogenic Hsp90 [13,14]. Specifically, these tools, which may selectively retrieve only those Hsp90 complexes that are "available" for inhibition, will allow for a better characterization of the "oncogenic Hsp90", both with regards to its onco-client protein content and the nature of its distinct post-translational modifications. This is in contrast to immunoprecipitation of Hsp90, which we have shown to identify and isolate both "oncogenic Hsp90" (i.e., PU-H71-binding) and "housekeeping Hsp90" (i.e., PU-H71 nonbinding) complexes.

The attachment of biotin to a small molecule provides a powerful tool in biology. As research tools, biotin-labeled chemical tools have the potential to extend the study of single targets to a particular class of molecules or even to an entire proteome. In addition, the development of biotinylated chemical tools that penetrate live cells and, thus, are designed both to probe and to modulate the activity of biomolecules in live biological systems, allows for a type of "live biochemistry and biology" that can complement traditional biochemical and biological approaches by promoting molecular characterization of biomolecules both in vitro and within their natural biological contexts.

In one application, biotinylated probes may be subjected to streptavidin-containing beads to identify potential direct and indirect interactors of the small molecule through affinity capture. Streptavidin binds to biotin in the strongest noncovalent interaction known, with $K_d \sim 1 \times 10^{-14}$ M. As we have already shown with PU-H71 attached directly onto beads, its ability to bind to Hsp90 in client-protein-bound complexes may be used to identify and analyze the drivers of oncogenic transformations on a tumor-by-tumor basis [13]. Therefore, we believe that there is considerable value in preparing biotinylated analogues of PU-H71 (**1a**) with the ability to permeate cell membranes so as to enable the investigation of oncogenic Hsp90 complexes in live cells. In contrast to PU-H71 beads, which are limited to cell homogenates, these compounds may be further used to investigate Hsp90 complexes in live cells, which represents a more physiologically relevant state. These tools also have use in flow cytometry and microscopy, whereby fluorescently labeled antibodies to biotin are used, as we describe below.

Results and Discussion

Design and synthesis of biotinylated purine scaffold Hsp90 probes

Geldanamycin (GM) is a benzoquinone ansamycin first isolated from a fermentation broth of *Streptomyces hygroscopicus* [15] and was the first reported Hsp90 inhibitor [16]. It has played a paramount role as a probe molecule to investigate Hsp90 biology, and in fact the attachment of GM to solid support enabled the identification of Hsp90 as the target of its anticancer activity through affinity purification [16]. Biotinylated GM has also been synthesized and has been proposed as a tool to identify proteins other than Hsp90 that GM may directly bind to [17]. Since the available evidence suggests GM cannot efficiently trap Hsp90 in client-bound complexes [13,18], it appears that GM–biotin is of limited use beyond identifying potential direct interactors. In contrast, PU-H71 (**1a**) is highly selective for Hsp90 and furthermore can efficiently bind to and trap Hsp90 in client-bound complexes allowing for the identification of global tumor Hsp90 proteomes by mass spectrometry [13].

We therefore set out here to design a series of biotinylated analogues derived from the purine scaffold Hsp90 inhibitor PU-H71 (**1a**) with the purpose of identifying compounds capable of permeating cancer-cell membranes, binding selectively to intracellular oncogenic Hsp90 in live cancer cells, and able to trap and isolate Hsp90 bound to tumor-specific onco-client proteins. Because the biotin tag enables pull-down experiments through subsequent binding to streptavidin or avidin, a further requirement for our probe is that the linker be of sufficient length to enable the concomitant binding to Hsp90 and

streptavidin. Thus, in the design of these probes, the type of linker, as well as its length, was systematically altered so as to identify compounds that demonstrate such combined properties (Figure 1).

As such we have prepared a number of biotinylated analogues, derived from **1a** and **1b**, containing linkers of various lengths (1 to 17 atoms) and hydrophobicities (polyethylene-, amide- and/or alkyl-containing). In addition, an amine-linked biotin analogue **2a**, which we have reported previously [9], was also prepared for comparison purposes. This differs from the others by the presence of an ionizable amine in the linker region. Although **2a** is a potent Hsp90 binder, it is less effective at capturing Hsp90 complexes and has poor cancer-cell permeability (Figure 2) and was therefore of limited use and served as a further impetus for the synthesis of the novel probes described here.

A critical factor in the design of biotinylated purine-scaffold Hsp90 probes is the site of attachment of biotin. From previous work including X-ray crystal structure [19], extensive SAR [20,21], and docking experiments [9], the N9-position of the purine scaffold was shown to be an ideal site for attachment since it is directed towards the solvent. Furthermore, the amino group of **1a** or the desisopropyl analogue **1b** provided a convenient handle with which to attach biotin directly or via a linker through an amide bond. We chose to make analogues of both **1a** and **1b** because the isopropyl group in **1a** may result in considerable effects on cell-permeability properties due to its increased lipophilicity, while having little effect on the affinity for Hsp90. While it is essential that the linker be of sufficient length to enable the concomitant binding to Hsp90 and streptavidin, it is also important that it is not exceedingly long for two reasons. First, the possibility and extent of nonspecific binding increases with longer linkers. Second, longer linkers result in a

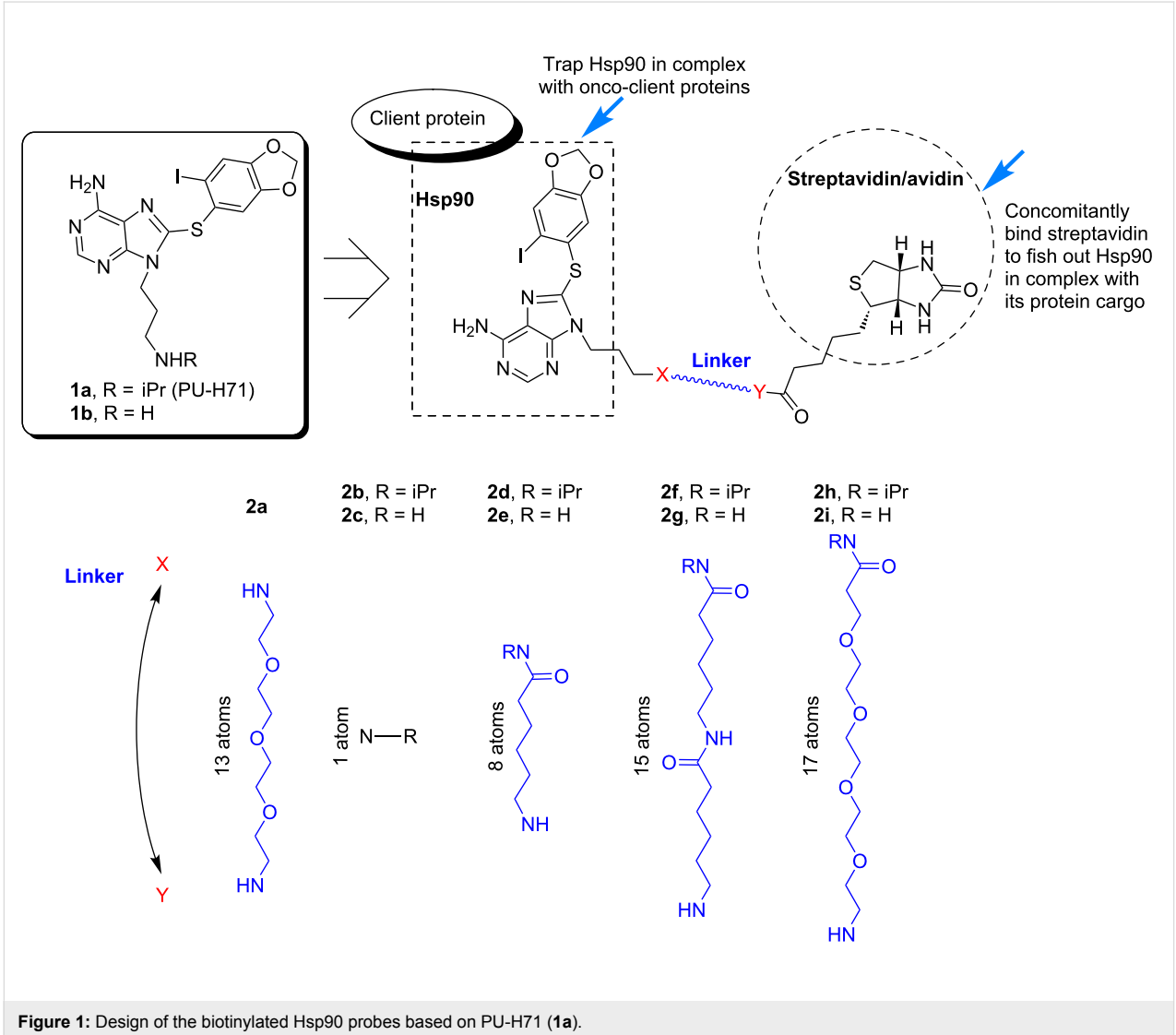


Figure 1: Design of the biotinylated Hsp90 probes based on PU-H71 (**1a**).

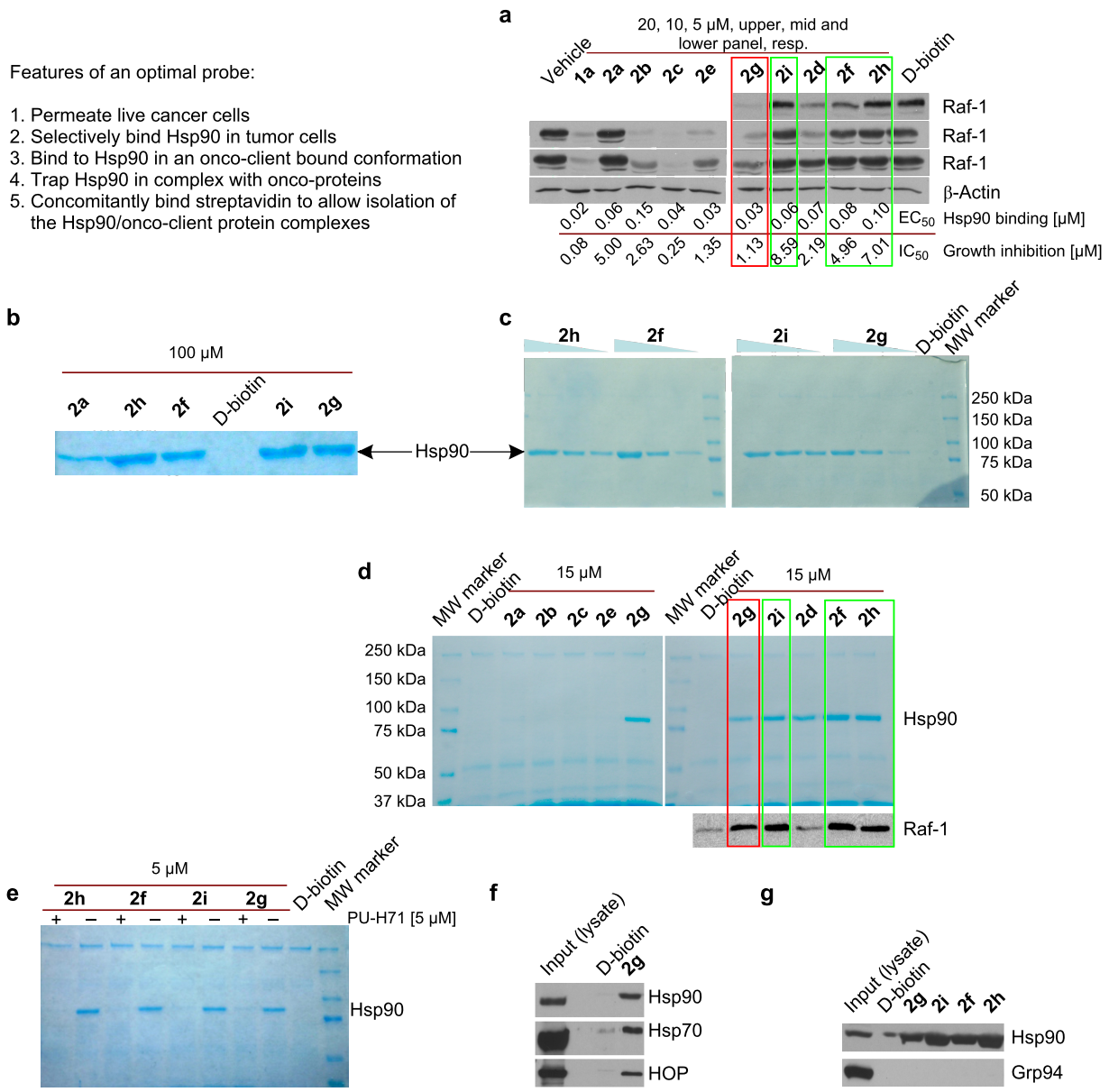
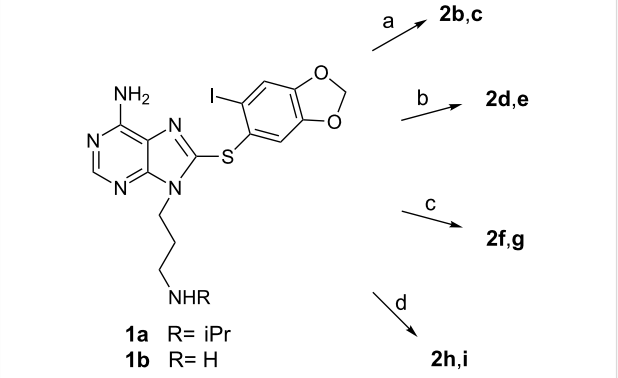


Figure 2: Analysis of the affinity and selectivity of the biotinylated probes for Hsp90. (a) K562 cancer cells were treated for 24 h with DMSO (vehicle), PU-H71 (1 µM) or indicated biotinylated probes (5, 10 and 20 µM) and the effect of these agents on Raf-1 steady-state levels was analyzed by Western blot. β-Actin was used as a protein loading control, because its levels remain unchanged following Hsp90 inhibition. The affinity of these agents for Hsp90 as present in a cancer-cell homogenate and their effect on K562 cell growth are presented under the immunoblot figure. Values were determined as indicated in the Experimental section. (b) and (c) K562 lysates or (d) K562 cells were incubated for 4 h with the indicated concentrations of the indicated probes. Live cells were permeabilized prior to the affinity purification step. After washing with high-salt lysis buffer (b,c) or lysis buffer (d), protein complexes purified on streptavidin agarose beads were visualized by Coomassie blue staining. (d) For the indicated experimental conditions, protein complexes were also identified by immunobloting (see Raf-1). MW marker = molecular weight marker. D-Biotin was used to test for background binding of the streptavidin agarose beads. (e) Binding of probes (5 µM) to Hsp90 is competitively blocked by cell pre-treatment with PU-H71 (**1a**, 5 µM). (f) Experiment set-up as in (d). Affinity purified Hsp90 in complex with its regulatory co-chaperones Hsp70 and HOP was analyzed by Western blot. (g) K562 lysates were incubated overnight with the indicated probes (50 µM). Affinity purified proteins were identified by Western blot.

higher molecular weight of the compound, which can adversely affect their permeability across cell membranes.

The synthesis of the biotinylated molecules is shown in Scheme 1 and in each case occurs in a single step from **1a** or **1b**. **2b** and **2c** were prepared from **1a** or **1b**, respectively, in 99% and 56% yield by DCC coupling with D-biotin under sonication (Scheme 1, step a). **2d**–**2i** were prepared by reaction of **1a** or **1b** with three different commercially available *N*-hydroxysuccinimide (NHS) active ester containing biotin

molecules (Scheme 1, steps b–d). Whereas reactions with **1b** occurred at rt and were complete after 1 h giving the desired products in good yield (72–88%), reactions with **1a** required heating at 35 °C and were incomplete after 6 h as evidenced by recovery of a significant amount of unreacted starting material. The yields of isolated products ranged from 29–41%. **2d** and **2e** were prepared from EZ-Link® NHS-LC-Biotin (Scheme 1, step b). **2f** and **2g** were prepared from EZ-Link® NHS-LC-LC-Biotin (Scheme 1, step c). **2h** and **2i** were prepared from EZ-Link® NHS-PEG_4-Biotin (Scheme 1, step d). **2a** was prepared as reported previously [9], by amination of the corresponding bromide with EZ-Link® Amine-PEO_3-Biotin.

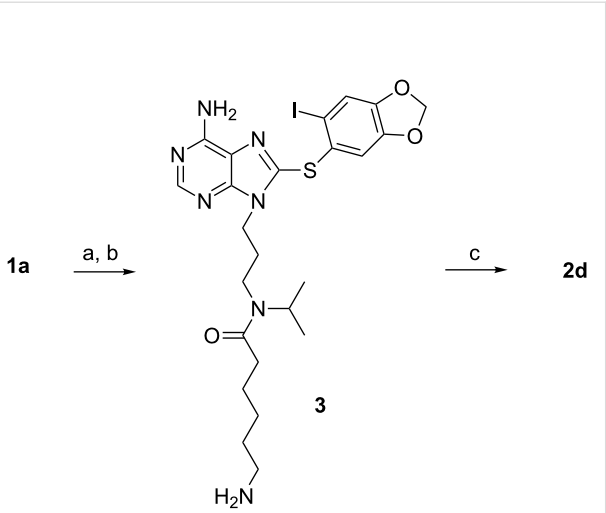


Scheme 1: Reagents and conditions: (a) D-biotin, DCC, DMAP, CH_2Cl_2, sonicate; (b) EZ-Link® NHS-LC-Biotin, DIEA, DMF, 35 °C or rt; (c) EZ-Link® NHS-LC-LC-Biotin, DIEA, DMF, 35 °C or rt; (d) EZ-Link® NHS-PEG_4-Biotin, DIEA, DMF, 35 °C or rt.

It should be noted that in each of the products (**2b**, **2d**, **2f**, **2h**) derived from **1a** it was not immediately clear whether these were a mixture of two compounds or rotamers, despite the seeming unambiguity in the synthesis. While HPLC showed a single homogeneous peak, the NMR spectrum was very complicated. To settle this, **2d** was prepared by an alternate synthesis (Scheme 2). DCC coupling of **1a** with 6-Boc-aminocaproic acid yielded **3** following removal of the Boc group, which was further reacted with D-biotin to give a product with identical NMR and HPLC profile to **2d**, confirming that a mixture of two rotamers was present and not a mixture of two compounds. Additionally, intermediate **3** also demonstrates a complex NMR spectrum indicative of the presence of two rotamers. All of this shows that, unlike the proton, the isopropyl group is bulky enough to hinder rotation of the tertiary amides and to enable identification of two rotamers by NMR [22].

Biological evaluation of the biotinylated Hsp90 probes

As indicated above, there are several requirements for a biotinylated probe to be useful in dissecting Hsp90 tumor biology in live cells. First, the probe should retain selective and tight binding to tumor Hsp90. Second, it should permeate live cells and while inside the cell, should bind to the oncogenic Hsp90. Upon cell permeabilization, the probe should retain Hsp90 binding and concomitantly bind to streptavidin allowing for subsequent isolation of Hsp90. Third, if isolation of oncogenic Hsp90 in complex with its tumor-specific client proteins is the desired outcome, the probe should also trap and lock the Hsp90/protein complex, so that it is maintained throughout the subsequent permeabilization and purification steps.



Scheme 2: Reagents and conditions: (a) 6-Boc-aminocaproic acid, DCC, DMAP, CH_2Cl_2, rt; (b) TFA, CH_2Cl_2, rt; (c) D-biotin, DCC, DMAP, CH_2Cl_2, sonicate.

Requirement 1: Retain tight binding to tumor Hsp90

To ensure the biotinylated compounds still retained affinity for tumor Hsp90, they were each evaluated in a fluorescence polarization (FP) assay by using a cancer-cell homogenate (i.e., SKBr3 human breast cancer lysate). This assay measures competitive binding to tumor cell Hsp90 complexes [23]. Each compound retained a good affinity for Hsp90, with values ranging from 30 to 150 nM (Figure 2a, Hsp90 binding). Two general trends were observed. First, compared to the PU-H71 analogues, the desisopropyl analogues bound on average with approximately 2-fold greater affinity (i.e., **2c** versus **2b**, **2e** versus **2d**, **2g** versus **2f**, **2i** versus **2h**), despite the fact that both **1a** and **1b** bound Hsp90 with similar affinity (24.5 versus 26 nM for **1a** and **1b**, respectively). This is likely a result of increased steric crowding of the bulky isopropyl group in analogues of **1a**. Second, in terms of the linkers, the carbon series appeared to have a somewhat higher Hsp90 affinity than the ethylene glycol series (i.e., **2d** and **2f** versus **2h**; **2e** and **2g** versus **2i**). In sum however, all of the compounds retained good

affinity for Hsp90, supporting our notion for the ideal site of biotinylation, and were thus suitable for further analysis.

Requirement 2: Permeate live cancer cells and bind to oncogenic Hsp90

Having shown that each of the prepared biotinylated molecules retained good affinity for Hsp90, we next evaluated these compounds in two functional read-outs that together measure that the probe has entered a live cancer cell and once inside the cell, has bound to a substantial fraction of oncogenic Hsp90 molecules. Specifically, K562 is a human leukemia cell line dependent on Hsp90 for survival [13]. Thus, in such cells, occupancy of Hsp90's regulatory pocket by small molecules results in inhibition of its cancer-sheltering properties, leading to cell-growth inhibition associated with degradation of Hsp90-chaperoned onco-proteins. These, such as is the case for Raf-1 in K562 cells, become ubiquitinated and targeted for proteasomal degradation leading to a decrease in their steady-state levels (Figure 2a, Raf-1) [24].

While the biotinylated analogues displayed decreased potency compared to **1a**, it was clear from these results that some were capable of entering live cells in such concentrations as to substantially occupy the oncogenic Hsp90 sites (Figure 2a, for derivatives **2b**, **2c**, **2e**, **2g** and **2d** almost complete Raf-1 degradation associated with cell-growth inhibition in a similar concentration range). Other derivatives, such as **2i**, **2f** and **2h** failed to exhibit such properties (Figure 2a).

From the results, several conclusions concerning linker length and type can be drawn. In general, as the chain length increased, the ability to enter into the cancer cell decreased. With regards to linker nature, the polyethylene glycol linker containing derivatives (i.e., **2a**, **2h** and **2i**) performed poorest by this measure. Unexpectedly, derivatives **2g** and **2f** both containing the same 15-atom linker and differing only by the presence of H (on derivative **2g**) or iPr (on derivative **2f**) exhibited distinct behaviors, with only **2g** appearing to be substantially taken up by the cancer cell.

Requirement 3: Bind concomitantly to Hsp90 and streptavidin

Having identified which compounds were capable or not of permeating live cancer cells, we next wanted to determine whether the chain length was optimal to maintain concomitant binding to Hsp90 and streptavidin, so as to allow for isolation and identification of Hsp90/onco-client complexes from cancer cells. For this purpose, K562 lysates (Figure 2b and c) were incubated with the biotinylated ligands and the complexes captured on streptavidin beads. To test for the probe's selectivity, pull-downs were performed with increasing concentrations of biotinylated derivatives (10, 25 and 50 μM; Figure 2c). Additionally, affinity-purified complexes were washed with high-salt buffer to remove Hsp90-bound co-chaperones and client proteins (Figure 2b and c).

Of the new biotin derivatives, only **2h**, **2f**, **2g** and **2i** performed better than **2a** and isolated substantial amounts of Hsp90 (Figure 2b and c). We were unable to affinity purify Hsp90 with derivatives **2b**, **2c** and **2e**, indicating that while these compounds entered the cancer cell and bound to intracellular Hsp90 (Figure 2a), the linker was of unfavorable length and did not allow for concomitant binding to streptavidin through the biotin end of the probe. Consequently, isolation of Hsp90 from the cell homogenate failed with these biotinylated probes. As reported, **2a** containing a 13-atom linker was a modest probe for affinity purifications (Figure 2b and [9]), suggesting that for Hsp90, a linker longer than 13-atoms, and more exactly of 15-atoms or longer, was needed to maintain concomitant Hsp90 and streptavidin binding.

Requirement 4: Trap Hsp90 in an onco-client-bound conformation and isolate the endogenous Hsp90/onco-client complexes from live cells

To test for the probes' ability to isolate Hsp90 in secondary and tertiary complexes, such as those containing onco-client proteins, affinity purifications were also performed from live K562 cancer cells (Figure 2d). In such a case, the biotinylated tool is added to live cells where the compound binds to Hsp90 in an onco-client-bound conformation, locking and preserving the endogenous Hsp90/protein complexes throughout the subsequent experimental steps (i.e., permeabilization). In contrast, when adding a biotinylated tool to cell homogenates, one may encounter two potential limitations. First, due to the dynamic nature of the Hsp90/client protein interactions, the endogenous complexes may be lost during the homogenization process and thus, pull-downs from homogenates may miss important interactors. Second, during homogenization, certain proteins may lose their well-regulated conformation and potentially aggregate. Such misfolded proteins are prone to be captured by chaperones resulting in "false positives" (i.e., nonendogenous Hsp90 client proteins). False positives increase the "background" on the affinity resin, and the higher the background, the poorer the identification of relevant endogenous Hsp90 complexes will be. Therefore, while it is true that following the addition of the biotinylated tool to cells, these are permeabilized or fixed/permeabilized and thus no longer alive, the capture of the oncogenic Hsp90 complexes takes place in the live cell.

Consequently, in live-cell experiments, cells were first incubated with the biotinylated PU-H71 derivatives to trap and maintain the onco-client complexed to Hsp90. Next, cells were

ruptured into a physiological buffer containing molybdate. The purpose of this step is to release the proteins from the cell yet maintain the Hsp90/onco-client protein complexes intact. Following capture of these complexes on the streptavidin beads, complexes were applied to a denaturing gel, then probed by both Coomassie stain (Figure 2d, top panel) and immunoblot (Figure 2d, bottom panel Raf-1 blot). The Coomassie blue stained gels of these pull-downs showed a single band at approximately 90 kDa for derivatives **2g**, **2i**, **2d**, **2f** and **2h** (Figure 2d), which was competitively blocked by pretreatment of cells with a soluble ligand (Figure 2e) indicating concomitant binding to Hsp90 and streptavidin, and moreover confirming selective and strong binding between these probes and Hsp90.

Analogues of 1-atom linker (**2b** and **2c**) and 8-atom linker (**2d** and **2e**) showed a faint band or no band at 90 kDa, a finding similar to experiments performed in cell homogenates, indicating that the linker was of inadequate length for the purpose of affinity purification. Derivative **2d** behaved erratically over several experiments, showing either faint or no isolation of Hsp90 (Figure 2d and not shown). We potentially attribute such behavior to interbatch variability in the loading capacity and nature of the streptavidin beads. **2d** being of borderline characteristics with regards to chain (i.e., eight atoms in length and containing the sterically constraining iPr) and cancer-cell permeability (Figure 2a) would fail to isolate Hsp90 in amounts visible by Coomassie staining when low-capacity streptavidin beads are used. As such, we advise against the use of this derivative as a chemical tool. Most efficient at isolating Hsp90 in complex with an onco-client protein such as Raf-1 were derivatives with 15-atom (**2f** and **2g**) and 17-atom linkers (**2h** and **2i**) (Figure 2d, Hsp90 and Raf-1). From cells, **2g** affinity purifies Hsp90 in complex with its regulatory cochaperones, Hsp70 and HSP-organizing protein (HOP) [1,2,13] (Figure 2f).

It is important to note that the affinity purification strength of the biotinylated probes is weaker than that of directly solid-support-linked PU-H71. This is likely a consequence of the solid-support loading capacity. While direct attachment of a ligand to the bead can result in high local concentrations of ligand, the attachment of ligand indirectly by means of biotin-streptavidin is limited by the concentration of streptavidin available on the solid support. It is obvious that much lower numbers of bulky streptavidin molecules can be attached on any solid support when compared to a low-molecular-weight ligand, such as PU-H71. Therefore, for isolation and identification of entire Hsp90 proteome isolations by mass spectrometry, as we recently reported [13], the beads containing PU-H71 directly attached by a covalent link remain the most efficient probe, and we continue to recommend their use for such purposes.

Interestingly, when tested for Hsp90 paralogue-selectivity, we noted for the **2g**, **2i**, **2f** and **2h** derivatives a substantial preference for the affinity purification of the cytosolic Hsp90 over the endoplastic reticulum (ER) paralogue, Grp94 (Figure 2g). This is a surprising finding, because PU-H71 is a pan-Hsp90 inhibitor that binds equally well to the cytosolic and the ER paralogues (Chiosis G, personal communication). We tested the affinity of **2g**, **2i**, **2f** and **2h** for the two paralogues, and identically to the parent ligand PU-H71, we determined little preference for Hsp90 over Grp94 (45 versus 451 nM for **2g**; 83 versus 226 nM for **2i**; 98 versus 210 nM for **2f**; 137 versus 313 nM for **2h**). These findings indicate that the selectivity profile was unlikely imparted by the ligand. More likely, the ligand binds to both Hsp90 and Grp94 in the cell extract; however, isolation of the Grp94 complex on the streptavidin beads fails because of the inappropriate nature of the linker. Such was the case for probes **2b** and **2c** (see above), which, although they both bound effectively to Hsp90, could not concomitantly bind Hsp90 and streptavidin, and thus isolation of Hsp90 from extracts failed with such probes.

Potential uses of the biotinylated Hsp90 probes

Having shown that the probes bind to tumor Hsp90, we went on to demonstrate several potential uses for probe **2g**. In addition to affinity-purification of oncogenic Hsp90 from distinct tumors, the biotinylated probes are useful to measure the drug-accessible tumor Hsp90 by both flow cytometry and microscopy techniques. We exemplify here such use in the K562 leukemia cells in the determination of cell-surface (Figure 3a) and intracellular (Figure 3b and c) Hsp90 by flow cytometry and by fluorescent microscopy (Figure 3c). For the measurement of intracellular Hsp90, the use of digitonin was effective in allowing the entry of the antibiotin antibody for probe detection (Figure 3b). Both digitonin and saponin can be used to reversibly open cellular pores and allow antibody entry, thus allowing for retention of cell viability, if this is desired [25]. Staining with CD45, a plasma membrane protein, was used as a positive control for detection of cell-surface Hsp90 (Figure 3a and b). The contribution to the signal of endogenous levels of biotin in the cell was accounted for by the use of cells stained with a fluorescently labeled antibiotin antibody (control, Figure 3).

Conclusion

In our continuing efforts to develop tools that may be used to better understand tumor Hsp90 biology, we have prepared a series of biotinylated analogues of the purine scaffold Hsp90 inhibitor PU-H71 (**1a**) and its desisopropyl analogue **1b**. The goal of this study was to optimize probe **2a** [9] and develop analogues capable of efficiently permeating the cancer cell membrane so that they may be used as tools to investigate onco-

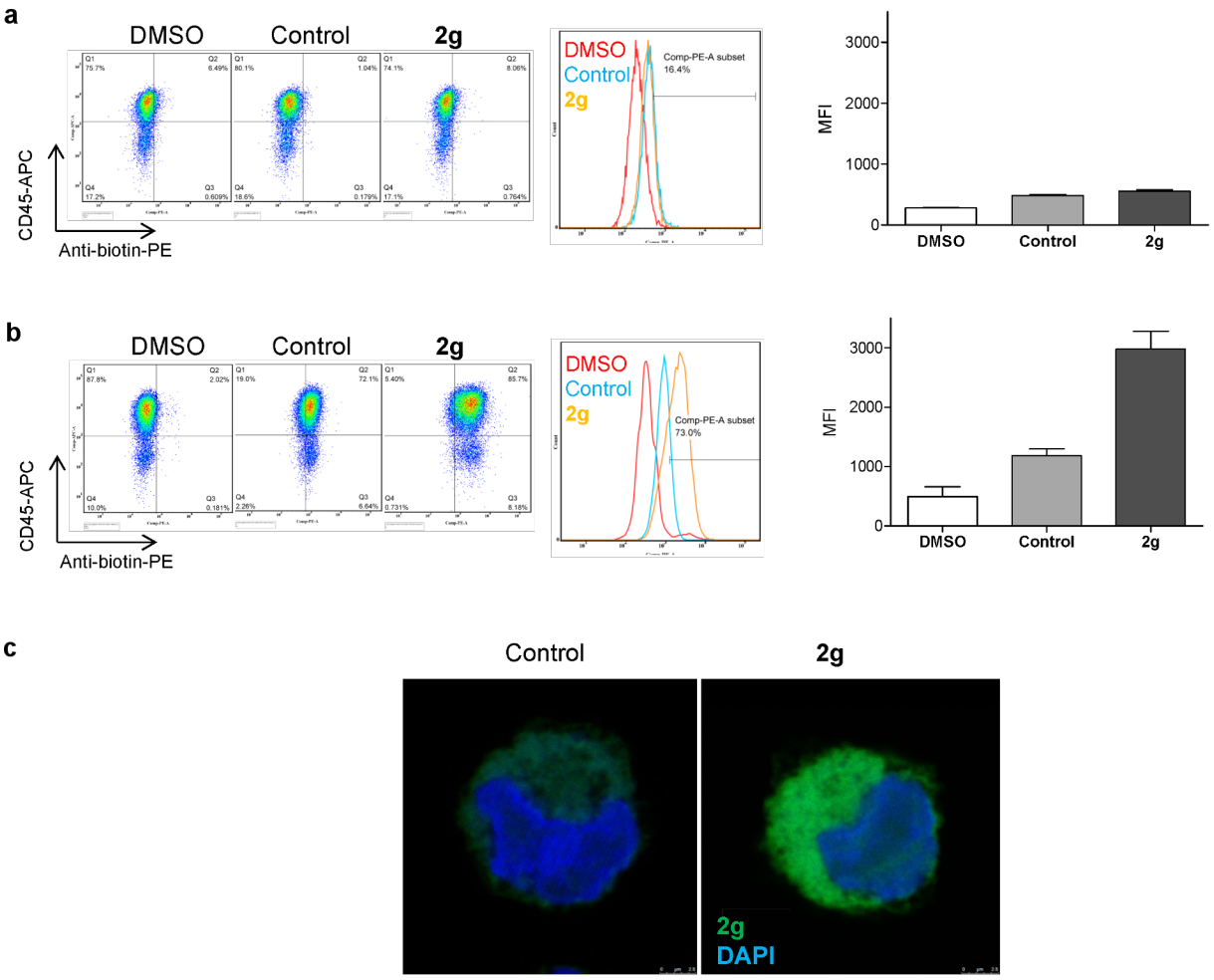


Figure 3: Use of probe **2g** to detect oncogenic Hsp90 by flow cytometry (a) and (b) and by microscopy (c). For (b) and (c) cells were permeabilized with digitonin. DMSO, cells treated with vehicle only; control, cells treated with vehicle and stained with antibiotin-PE for flow cytometry and antibiotin-FITC for fluorescent microscopy; **2g**, cells treated with probe **2g** and stained with antibiotin-PE for flow cytometry and antibiotin-FITC for fluorescent microscopy. MFI, mean fluorescence intensity. CD45 is a plasma-membrane protein. For microscopy, nuclei were stained with DAPI. (a) and (b) right panels; quantification of repeat experiments (n = 2).

genic Hsp90 and its complexes from live cells by affinity capture, flow cytometry and microscopy.

Of all probes, we found only **2g** to be very effective at both permeating cancer cell membranes and binding to and isolating Hsp90 onco-protein complexes from live cells (Figure 2a and d; red boxes), and its use is thus indicated for such applications. Probes **2i**, **2f** and **2h** remain of a yet uncharacterized category (Figure 2a and d; green boxes). Unlike probe **2g**, probes **2i** and **2h**, and to some degree **2f**, failed to substantially degrade Raf-1 at concentrations as high as 20 μM (Figure 2a). When incubated at such concentrations with live cells, a step followed by permeabilization of cells and complex capture on streptavidin beads, Hsp90 bound to Raf-1 was however isolated with these probes (Figure 2d). While apparently a paradoxical finding, one must note that **2h** and **2i** have in common the long 17-atom linker. It is possible that such compounds are prone to being trapped in the lipid bilayers of the plasma membrane, and thus, significant amounts become available for binding to intracellular Hsp90 only after the cell-permeabilization step (such as is performed in Figure 2d). Alternatively, it is plausible that these compounds get into the cell and become available for binding to the oncogenic Hsp90 complex in the live cell. The long chain however, characteristic of these probes, may interfere with

recruitment of an E3 ligase to the Hsp90/onco-client complex, and proteasomal degradation of the client protein may be impeded as a result. We are conducting follow-up experiments to investigate such hypotheses; however, these studies are outside the scope of this manuscript.

In conclusion, our work identifies **2g** as a probe for endogenous oncogenic Hsp90 and its protein clientele in live cells. The probe shows good affinity for tumor Hsp90 as demonstrated by FP, and good permeability as demonstrated by the two phenotypic read-outs of oncogenic Hsp90 inhibition (i.e., cytotoxicity and the ability to down regulate an Hsp90 onco-client protein in the relevant cancer cell background). **2g** can isolate Hsp90 through affinity purification from both cancer cell homogenates and live cells and is capable of trapping Hsp90 in an onco-client-bound conformation facilitating the isolation of such complexes and their analysis and identification through classical biochemical techniques (i.e., Western blot). The probe, as we demonstrate here, is also of use in detecting and analyzing tumor Hsp90 by flow cytometry and microscopy. To our knowledge, **2g** is the only reported biotinylated Hsp90 probe to have such combined characteristics, and thus represents a unique useful tool to investigate Hsp90 tumor biology.

Experimental

General

^{1}H NMR spectra were recorded on a Bruker 500 or 600 MHz instrument. Chemical shifts were reported in δ values in parts per million (ppm) downfield from TMS as the internal standard. ^{1}H data were reported as follows: chemical shift, multiplicity (s = singlet, d = doublet, t = triplet, q = quartet, br = broad, m = multiplet), coupling constant (Hz), integration. High-resolution mass spectra were recorded on a Waters LCT Premier system. Low-resolution mass spectra were obtained on a Waters Acquity Ultra Performance LC with electrospray ionization and SQ detector. High-performance liquid chromatography analyses were performed on a Waters Autopurification system with PDA, MicroMass ZQ, and ELSD detector, and a reversed-phase column (Waters X-Bridge C18, 4.6 × 150 mm, 5 µm) using a gradient of (a) H_2O + 0.1% TFA and (b) CH_3CN + 0.1% TFA, 5 to 95% b over 13 minutes at 1.2 mL/min. All reactions were performed under argon protection. EZ-Link® NHS-LC-Biotin, EZ-Link® NHS-LC-LC-Biotin, EZ-Link® NHS-PEG_4-Biotin, and EZ-Link® Amine-PEO_3-Biotin were purchased from Pierce (Rockford, Il). **1a** [20], **1b** [10] and biotinylated analogue **2a** [9] were prepared as previously described.

Synthesis of probes

(2b). 1a (30 mg, 0.059 mmol), D-biotin (19 mg, 0.078 mmol), DCC (24 mg, 0.117 mmol) and a catalytic amount of DMAP in CH_2Cl_2 (1 mL) were sonicated for 9 h. The reaction mixture was concentrated under reduced pressure and the resulting residue was purified by preparative TLC (CH_2Cl_2/MeOH-NH_3 (7 N), 10:1) to give 43.2 mg (99%) of **2b**. ^{1}H NMR (600 MHz, $CDCl_3$, 2 rotamers) δ 8.22 (s, 1H), 7.22 (s, 0.6H), 7.21 (s, 0.4H), 6.87 (s, 0.6H), 6.76 (s, 0.4H), 6.25 (br s, 0.6H), 6.16 (br s, 0.4H), 5.96–5.88 (m, 2H), 5.85 (br s, 0.6H), 5.78 (br s, 0.4H), 4.63–4.54 (m, 0.6H), 4.45–4.32 (m, 1.6H), 4.25–4.21 (m, 0.4H), 4.19–4.11 (m, 1.4H), 4.07–4.00 (m, 0.6H), 3.95–3.88 (m, 0.4H), 3.22–2.97 (m, 2.4H), 2.84–2.78 (m, 1H), 2.77–2.69 (m, 0.6H), 2.68–2.62 (m, 1H), 2.27–2.22 (m, 0.6H), 2.05–1.94 (m, 1.4H), 1.89–1.74 (m, 1.4H), 1.72–1.43 (m, 3H), 1.40–1.16 (m, 3.6H), 1.06–1.00 (m, 4H), 0.97 (d, J = 6.7 Hz, 2H); MS (ESI) m/z: 739.2 $[M + H]^+$; HRMS–ESI (m/z): $[M + H]^+$ calcd for $C_{28}H_{36}IN_8O_4S_2$, 739.1346; found, 739.1353; HPLC: t_R = 9.83.

(2c). 1b (9.1 mg, 0.0193 mmol), D-biotin (7.1 mg, 0.0290 mmol), DCC (8 mg, 0.0386 mmol) and a catalytic amount of DMAP in CH_2Cl_2 (1 mL) was sonicated for 5 h. The reaction mixture was concentrated under reduced pressure and the resulting residue was purified by preparative TLC (CH_2Cl_2/MeOH-NH_3 (7 N), 10:1) to give 7.5 mg (56%) of **2c**. ^{1}H NMR (600 MHz, $CDCl_3$/MeOH-d_4) δ 7.97 (s, 1H), 7.17 (s, 1H), 6.86 (s, 1H), 5.84 (s, 2H), 4.27–4.23 (m, 1H), 4.09–4.05 (m, 1H), 4.03 (t, J = 7.2 Hz, 2H), 3.02 (t, J = 6.4 Hz, 2H), 2.97–2.90 (m, 1H), 2.67 (dd, J = 4.9, 12.8 Hz, 1H), 2.49 (d, J = 12.8 Hz, 1H), 2.01 (t, J = 7.5 Hz, 2H), 1.83–1.75 (m, 2H), 1.54–1.34 (m, 4H), 1.27–1.18 (m, 2H); MS (ESI) m/z: 697.1 $[M + H]^+$; HRMS–ESI (m/z): $[M + H]^+$ calcd for $C_{25}H_{30}IN_8O_4S_2$, 697.0876; found, 697.0904; HPLC: t_R = 9.00.

(2d). 1a (15 mg, 0.0292 mmol), EZ-Link® NHS-LC-Biotin (14.6 mg, 0.0321 mmol) and DIEA (7.5 mg, 10.2 µL, 0.0584 mmol) in DMF (0.5 mL) was heated at 35 °C for 6 h. The reaction mixture was concentrated under reduced pressure and the resulting residue was purified by preparative TLC (CH_2Cl_2/MeOH-NH_3 (7 N), 10:1) to give 10.3 mg (41%) of **2d**. In addition, 6.9 mg of unreacted **1a** was recovered to give an actual yield of 77%. ^{1}H NMR (500 MHz, $CDCl_3$, 2 rotamers) δ 8.29–8.26 (m, 1H), 7.29 (s, 0.4H), 7.28 (s, 0.6H), 6.87 (s, 0.4H), 6.85 (s, 0.6H), 6.76 (br s, 0.4H), 6.74 (br s, 0.6H), 6.63–6.51 (br s, 2H), 6.00–5.96 (m, 2H), 5.68 (br s, 0.4H), 5.58 (br s, 0.6H), 4.64–4.56 (m, 0.4H), 4.52–4.45 (m, 1H), 4.36–4.28 (m, 1H), 4.27–4.20 (m, 2H), 4.09–4.01 (m, 0.6H), 3.32–3.08 (m, 5H), 2.94–2.86 (m, 1H), 2.76–2.69 (m, 1H), 2.37–2.31 (m, 1H), 2.22–1.96 (m, 4H), 1.96–1.89 (m, 1H), 1.80–1.30 (m, 12H), 1.16–1.10 (m, 4H), 1.09–1.04 (m, 2H); MS (ESI) m/z: 852.3 $[M + H]^+$; HRMS–ESI (m/z): $[M + H]^+$ calcd for $C_{34}H_{47}IN_9O_5S_2$, 852.2186; found, 852.2206; HPLC: t_R = 8.82.

(2e). 1b (16.9 mg, 0.0359 mmol), EZ-Link® NHS-LC-Biotin (17.9 mg, 0.0394 mmol) and DIEA (9.3 mg, 12.5 µL,

0.0718 mmol) in DMF (0.5 mL) was stirred at rt for 1 h. The reaction mixture was concentrated under reduced pressure and the resulting residue was purified by preparative TLC (CH_2Cl_2/MeOH-NH_3 (7 N), 10:1) to give 20.8 mg (72%) of **2e**. ^{1}H NMR (500 MHz, $CDCl_3$) δ 8.22 (s, 1H), 7.52 (t, *J* = 5.6 Hz, 1H), 7.36 (s, 1H), 7.03 (s, 1H), 6.66 (t, *J* = 5.5 Hz, 1H), 6.25 (br s, 2H), 6.03 (s, 2H), 4.52–4.47 (m, 1H), 4.33–4.28 (m, 1H), 4.25 (t, *J* = 6.8 Hz, 2H), 3.25–3.17 (m, 4H), 3.17–3.11 (m, 1H), 2.90 (dd, *J* = 5.0, 12.9 Hz, 1H), 2.79–2.63 (m, 1H), 2.24 (t, *J* = 7.4 Hz, 2H), 2.19–2.13 (m, 2H), 2.02–1.94 (m, 2H), 1.74–1.58 (m, 6H), 1.56–1.48 (m, 2H), 1.46–1.31 (m, 4H); MS (ESI) *m*/*z*: 810.3 [M + H]$^+$; HRMS–ESI (*m*/*z*): [M + H]$^+$ calcd for $C_{31}H_{41}IN_9O_5S_2$, 810.1717; found, 810.1703; HPLC: t_R = 8.00.

(2f). 1a (15 mg, 0.0292 mmol), EZ-Link® NHS-LC-LC-Biotin (18.2 mg, 0.0321 mmol) and DIEA (7.5 mg, 10.2 µL, 0.0584 mmol) in DMF (0.5 mL) was heated at 35 °C for 6 h. The reaction mixture was concentrated under reduced pressure and the resulting residue was purified by preparatory TLC (CH_2Cl_2/MeOH-NH_3 (7 N), 10:1) to give 8.2 mg (29%) of **2f**. In addition, 9.6 mg of unreacted **1a** was recovered to give an actual yield of 81%. ^{1}H NMR (500 MHz, $CDCl_3$/MeOH-d_4, 2 rotamers) δ 8.18 (s, 0.4H), 8.16 (s, 0.6H), 7.31 (s, 1H), 6.98 (s, 0.6H), 6.95 (s, 0.4H), 6.90–6.80 (m, 2H), 5.98 (s, 2H), 4.55–4.47 (m, 0.4H), 4.47–4.41 (m, 1H), 4.27–4.23 (m, 1H), 4.22–4.16 (m, 2H), 4.03–3.95 (m, 0.6H), 3.34–3.31 (m, 0.6H), 3.24–3.19 (m, 1.4H), 3.17–3.07 (m, 5H), 2.89–2.82 (m, 1H), 2.70–2.64 (m, 1H), 2.32–2.25 (m, 1H), 2.16–1.94 (m, 7H), 1.70–1.18 (m, 18H), 1.09 (d, *J* = 6.7 Hz, 4H), 1.03 (d, *J* = 6.8 Hz, 2H); MS (ESI) *m*/*z*: 965.5 [M + H]$^+$; HRMS–ESI (*m*/*z*): [M + H]$^+$ calcd. for $C_{40}H_{58}IN_{10}O_6S_2$, 965.3027; found, 965.3010; HPLC: t_R = 8.73.

(2g). 1b (16.6 mg, 0.0352 mmol), EZ-Link® NHS-LC-LC-Biotin (22.0 mg, 0.0387 mmol) and DIEA (9.1 mg, 12.3 µL, 0.0704 mmol) in DMF (0.5 mL) was stirred at rt for 1 h. The reaction mixture was concentrated under reduced pressure and the resulting residue was purified by preparative TLC (CH_2Cl_2/MeOH-NH_3 (7 N), 10:1) to give 27.8 mg (86%) of **2g**. ^{1}H NMR (500 MHz, $CDCl_3$/MeOH-d_4) δ 8.12 (s, 1H), 7.60 (m, 1H), 7.30 (s, 1H), 7.09 (m, 1H), 6.98 (s, 1H), 5.97 (s, 2H), 4.44–4.38 (m, 1H), 4.24–4.20 (m, 1H), 4.17 (t, *J* = 7.1 Hz, 2H), 3.18–3.04 (m, 7H), 2.83 (dd, *J* = 5.0, 12.9 Hz, 1H), 2.64 (d, *J* = 12.8 Hz, 1H), 2.16 (t, *J* = 7.5 Hz, 2H), 2.12–2.03 (m, 4H), 1.96–1.88 (m, 2H), 1.66–1.18 (m, 18H); MS (ESI) *m*/*z*: 923.4 [M + H]$^+$; HRMS–ESI (*m*/*z*): [M + H]$^+$ calcd for $C_{37}H_{52}IN_{10}O_6S_2$, 923.2558; found, 923.2595; HPLC: t_R = 7.95.

(2h). 1a (15 mg, 0.0292 mmol), EZ-Link® NHS-PEG_4-Biotin (18.9 mg, 0.0321 mmol) and DIEA (7.5 mg, 10.2 µL, 0.0584 mmol) in DMF (0.5 mL) was heated at 35 °C for 6 h. The reaction mixture was concentrated under reduced pressure, and the resulting residue was purified by preparatory TLC (CH_2Cl_2/MeOH-NH_3 (7 N), 10:1) to give 9.3 mg (32%) of **2h**. In addition, 9.0 mg of unreacted **1a** was recovered to give an actual yield of 81%. ^{1}H NMR (500 MHz, $CDCl_3$/MeOH-d_4, 2 rotamers) δ 8.18 (s, 0.4H), 8.16 (s, 0.6H), 7.32–7.30 (m, 1H), 6.98 (s, 0.6H), 6.96 (s, 0.4H), 5.98 (s, 2H), 4.56–4.49 (m, 0.4H), 4.46–4.39 (m, 1H), 4.27–4.22 (m, 1H), 4.21–4.15 (m, 2H), 4.07–3.99 (m, 0.6H), 3.71–3.66 (m, 2H), 3.61–3.51 (m, 12H), 3.50–3.45 (m, 2H), 3.38–3.29 (m, 2H), 3.25–3.16 (m, 2H), 3.12–3.07 (m, 1H), 2.88–2.81 (m, 1H), 2.68–2.63 (m, 1H), 2.63–2.57 (m, 1.2H), 2.47–2.41 (m, 0.8H), 2.18–1.98 (m, 4H), 1.70–1.52 (m, 4H), 1.41–1.32 (m, 2H), 1.08 (d, *J* = 6.7 Hz, 4H), 1.02 (d, *J* = 6.8 Hz, 2H); MS (ESI) *m*/*z*: 986.5 [M + H]$^+$; HRMS–ESI (*m*/*z*): [M + H]$^+$ calcd for $C_{39}H_{57}IN_9O_9S_2$, 986.2765; found, 986.2757; HPLC: t_R = 8.53.

(2i). 1b (17.6 mg, 0.0374 mmol), EZ-Link® NHS-PEG_4-Biotin (24.2 mg, 0.0411 mmol) and DIEA (9.7 mg, 13 µL, 0.0704 mmol) in DMF (0.5 mL) was stirred at rt for 1 h. The reaction mixture was concentrated under reduced pressure and the resulting residue was purified by preparative TLC (CH_2Cl_2/MeOH-NH_3 (7 N), 10:1) to give 31.0 mg (88%) of **2i**. ^{1}H NMR (500 MHz, $CDCl_3$) δ 8.29 (s, 1H), 7.51 (t, *J* = 5.8 Hz, 1H), 7.32 (s, 1H), 7.03 (t, *J* = 5.3 Hz, 1H), 6.90 (s, 1H), 6.79 (s, 1H), 6.57 (br s, 2H), 6.01 (s, 2H), 5.97 (s, 1H), 4.53–4.48 (m, 1H), 4.35–4.25 (m, 3H), 3.79 (t, *J* = 6.1 Hz, 2H), 3.68–3.59 (m, 12H), 3.57 (t, *J* = 5.1 Hz, 2H), 3.46–3.40 (m, 2H), 3.24–3.18 (m, 2H), 3.18–3.12 (m, 1H), 2.90 (dd, *J* = 5.0, 12.8 Hz, 1H), 2.75 (d, *J* = 12.7 Hz, 1H), 2.54 (t, *J* = 6.0 Hz, 2H), 2.20 (t, *J* = 7.4 Hz, 2H), 2.01–1.40 (m, 2H), 1.79–1.59 (m, 4H), 1.48–1.38 (m, 2H); MS (ESI) *m*/*z*: 944.4 [M + H]$^+$; HRMS–ESI (*m*/*z)*: [M + H]$^+$ calcd for $C_{36}H_{51}IN_9O_9S_2$, 944.2296; found, 944.2307; HPLC: t_R = 7.82.

6-Amino-*N*-(3-(6-amino-8-(6-iodobenzo[*d*][1,3]dioxol-5-ylthio)-9*H*-purin-9-yl)propyl)-*N*-isopropylhexanamide (3). **1a** (50 mg, 0.0975 mmol), 6-Boc-aminocaproic acid (29 mg, 0.127 mmol), DCC (40.2 mg, 0.195 mmol) and a catalytic amount of DMAP in CH_2Cl_2 (1.5 mL) was stirred at rt overnight. The reaction mixture was concentrated under reduced pressure, and the resulting residue was partially purified by preparative TLC (CH_2Cl_2/MeOH-NH_3 (7 N), 12:1) to give a residue, which was dissolved in TFA/CH_2Cl_2 (0.4:1.6 mL) and stirred for 20 min at rt. The reaction mixture was concentrated under reduced pressure and the resulting residue was purified by preparative TLC (CH_2Cl_2/MeOH-NH_3 (7 N), 10:1) to give 55 mg (90%) of **3**. ^{1}H NMR (500 MHz, $CDCl_3$, 2 rotamers) δ 8.38–8.34 (m, 1H), 7.35 (s, 0.4H), 7.33 (s, 0.6H), 6.98 (s, 0.4H), 6.93 (s, 0.6H), 6.05–6.01 (m, 2H), 5.72 (br s, 2H), 4.69–4.63 (m, 0.4H), 4.29 (t, *J* = 7.2 Hz, 2H),

4.10–4.02 (m, 0.6H), 3.31–3.25 (m, 1.2H), 3.20–3.14 (m, 0.8H), 2.80–2.70 (m, 2H), 2.37 (t, J = 7.5 Hz, 1.2H), 2.15–2.06 (m, 2H), 2.01–1.89 (m, 0.8H), 1.70–1.62 (m, 1.2H), 1.58–1.48 (m, 2H), 1.45–1.36 (m, 2H), 1.24–1.16 (m, 0.8H), 1.14 (d, J = 6.7 Hz, 3.6H), 1.09 (d, J = 6.9 Hz, 2.4H); MS (ESI) m/z: 626.2 $[M + H]^+$; HRMS–ESI (m/z): $[M + H]^+$ calcd for $C_{24}H_{33}IN_7O_3S$, 626.1410; found, 626.1411; HPLC: t_R = 7.92.

(2d). 3 (50 mg, 0.0798 mmol), D-biotin (25.3 mg, 0.1037 mmol), DCC (32.9 mg, 0.1596 mmol) and a catalytic amount of DMAP in CH_2Cl_2 (2 mL) was sonicated for 6 h. The reaction mixture was concentrated under reduced pressure and the resulting residue was purified by preparative TLC (CH_2Cl_2/MeOH-NH_3 (7 N), 10:1) to give 31.9 mg (47%) of **2d**. MS (ESI) m/z: 852.3 $[M + H]^+$; HPLC: t_R = 8.82.

Biological evaluation of probes

Hsp90 competition assay. For the competition studies, fluorescence polarization (FP) assays were performed as previously reported [9,23]. Briefly, FP measurements were performed on an Analyst GT instrument (Molecular Devices, Sunnyvale, CA). Measurements were taken in black 96-well microtiter plates (Corning # 3650) where both the excitation and the emission occurred from the top of the wells. A stock of 10 μM GM-cy3B was prepared in DMSO and diluted with Felts buffer (20 mM Hepes (K), pH 7.3, 50 mM KCl, 2 mM DTT, 5 mM $MgCl_2$, 20 mM Na_2MoO_4, and 0.01% NP40 with 0.1 mg/mL BGG). To each 96-well were added 6 nM fluorescent GM (GM-cy3B), 3 μg SKBr3 lysate (total protein), and test compound (initial stock in DMSO) in a final volume of 100 μL Felts buffer. Compounds were added in triplicate wells. For each assay, background wells (buffer only), tracer controls (free, fluorescent GM only) and bound GM controls (fluorescent GM in the presence of SKBr3 lysate) were included on each assay plate. GM was used as positive control. The assay plate was incubated on a shaker at 4 °C for 24 h and the FP values in mP were measured. The fraction of tracer bound to Hsp90 was correlated to the mP value and plotted against values of competitor concentrations. The inhibitor concentration at which 50% of bound GM was displaced was obtained by fitting the data. All experimental data were analyzed using SOFTmax Pro 4.3.1 and plotted using Prism 4.0 (Graphpad Software Inc., San Diego, CA).

Western blotting. The K562 cell line was purchased from the American Type Culture Collection (Manassas, VA) and cultured in Roswell Park Memorial Institute (RPMI) supplemented with 10% fetal bovine serum, 1% L-glutamine, 1% penicillin and streptomycin. Cells were plated for 24 h prior to treatment for the indicated times with DMSO (vehicle) or with the indicated compounds. Protein extracts were prepared in 50 mM Tris pH 7.4, 150 mM NaCl and 1% NP-40 lysis buffer. Protein concentrations were measured by using the BCA kit (Pierce) according to the manufacturer's instructions. Protein lysates (50 μg) were resolved by SDS-PAGE, transferred onto nitrocellulose membrane and incubated with an anti-Raf-1 antibody from rabbit (1:500, sc-133, Santa Cruz) or anti-β-actin from mouse (1:2,500, A1978, Sigma-Aldrich). Membranes were then incubated with the corresponding peroxidase-conjugated secondary antibody (1:3,000 dilution) and visualized by the ECL detection reagent (Amersham).

Chemical precipitation from cells. K562 cells were treated with the indicated compounds for 4 h, after which cells were collected and washed three times with PBS. Protein extracts were prepared by sonicating cells in 20 mM HEPES, pH 7.3, 50 mM KCl, 5 mM $MgCl_2$, 20 mM Na_2MoO_4, 0.01% NP40 lysis buffer. Streptavidin agarose beads (40 μL) (Thermo Scientific) were washed three times with the lysis buffer and added to 500 μg of the total cellular protein extract diluted in lysis buffer to a final volume of 120 μL. Samples were incubated at 4 °C for 1 h, washed five times with the lysis buffer (or high salt buffer containing 1 M NaCl added to the lysis buffer) and applied to SDS-PAGE. Gels were stained with Coomassie blue (BioRad) according to the manufacturer's instructions.

Competitive binding. K562 cells were pretreated with PU-H71 (5 μM) for 30 min, followed by treatment for 4 h with the indicated biotinylated probe (5 μM). Cells were washed three times with PBS and sonicated in Felts buffer. Protein (500 μg) was added to streptavidin beads, and samples were incubated for 1 h at 4 °C. Affinity-purified protein was washed and then applied to SDS-PAGE.

Chemical precipitation from cell lysates. K562 cells were sonicated in 20 mM HEPES, pH 7.3, 50 mM KCl, 5 mM $MgCl_2$, 20 mM Na_2MoO_4, and 0.01% NP40 lysis buffer containing added protease inhibitors. Affinity beads were prepared by addition of the biotinylated probes to the streptavidin agarose resin (40 μL) (Thermo Scientific), which was first washed three times with the lysis buffer. Following incubation at 4 °C for 1 h, the obtained Hsp90 affinity beads were washed three times with lysis buffer to remove any unbound materials. The protein extract (500 μg) was then added to the probe-bound beads, and samples were incubated at 4 °C overnight. Following five washes with lysis buffer, the protein isolates were subjected to SDS-PAGE.

Growth inhibition assay. The effect of compounds on cell growth was evaluated with the Alamar Blue assay [26]. In summary, K562 cells were plated at 20,000 cells/well on Costar 96-well plates. Treatment with the probes added at the indi-

cated concentrations in triplicate wells was performed on the subsequent day and lasted for 72 h. The Alamar Blue reagent resazurin (440 μM stock) was added at the end of the treatment to result in a final concentration of 50 μM. Plates were read 6 h later by using the Analyst GT instrument (Fluorescence intensity mode, excitation 530 nm, emission 580 nm, with 560 nm dichroic mirror). Results were analyzed in SoftMax Pro. The percentage of cell growth inhibition was calculated by comparing fluorescence readings obtained from treated versus control cells, accounting for the initial cell population (time zero). The IC_{50} was calculated as the drug concentration that inhibits cell growth by 50%.

Flow cytometry analysis. **Live cells**. K562 cells were pretreated for 4 h with the indicated biotinylated probe, washed and stained on ice with CD45-Allophycocyanin (APC) (eBioscience) in PBS/5% FBS for 30 min. Cells were then washed and stained on ice with 0.125 μg of Anti-Biotin-PE in PBS/5% FBS for 45 min, followed by 4',6-diamidino-2-phenylindole (DAPI) (1 μg/mL) staining. Mean fluorescence intensity (MFI) of phycoerythrin (PE) was determined in DAPI negative viable cells. **Digitonin permeabilized cells**. K562 cells were pretreated for 4 h with the indicated biotinylated probes, washed and stained on ice with CD45-APC in PBS/5% FBS for 30 min. CD45 is expressed on the cell surface of all hematopoietic cells excluding mature erythrocytes and platelets. Cells were then fixed for 30 min with Cytofix buffer (BD Biosciences), washed and permeabilized with digitonin (10 μg/mL), followed by washing and staining with 0.125 μg of anti-Biotin-PE in the presence of digitonin for 30 min. Cells were then stained with DAPI (1 μg/mL). Cells were washed and then analyzed by flow cytometry (LSR-II, BD Biosciences).

Fluorescence microscopy. K562 cells were treated with 10 μM **2g** or DMSO (control) at 37 °C for 4 h. Cells were then collected, washed twice with PBS and attached to a chamber slide by centrifugation at 1,000 rpm at 4 °C for 5 min. Cells were then fixed with 4% paraformaldehyde in PBS at room temperature for 15 min and then washed twice with PBS. Cells were permeabilized with 50 μg/μL digitonin (Gold Biotechnology special grade Cat# D-180-250) in PBS at room temperature for 15 min. Cells were washed twice with PBS and incubated in 10% BSA in PBS at room temperature for 1.5 h. Cells were then washed twice with PBS and incubated with Anti-Biotin-FITC antibody (Sigma cat# F6762), diluted 1:50 in PBS, at room temperature for 1 h. Cells were then washed twice with PBS and stained with DAPI in ProLong Gold anti-fade reagent (Life Technologies cat# P36935) at which point a cover slip was attached to the chamber slide. Slides were visualized using a Leica SP5 Upright point-scanning confocal microscope at an objective of 40× oil (x = 2048, y = 2048, z = 1).

Acknowledgements

G.C. is funded by Leukemia and Lymphoma Society, Breast Cancer Research Fund, W.H. Goodwin and A. Goodwin and the Commonwealth Cancer Foundation for Research, The Experimental Therapeutics Center of Memorial Sloan-Kettering Cancer Center (MSKCC), 1U01 AG032969-01A1, 1R21 CA158609-01A1, 1R21 AI090501 and 1R01 CA155226-01. T.T. is funded by Susan G. Komen for the Cure (KG091313) and the Department of Defense, Breast Cancer Research Program (PDF-BC093421). We also thank Dr. George Sukenick and Dr. Hui Liu of the NMR Analytical Core Facility at MSKCC for expert mass spectral analysis.

References

1. Taipale, M.; Jarosz, D. F.; Lindquist, S. *Nat. Rev. Mol. Cell Biol.* **2010,** *11,* 515–528. doi:10.1038/nrm2918
2. Workman, P.; Burrows, F.; Neckers, L.; Rosen, N. *Ann. N. Y. Acad. Sci.* **2007,** *1113,* 202–216. doi:10.1196/annals.1391.012
3. Janin, Y. L. *Drug Discovery Today* **2010,** *15,* 342–353. doi:10.1016/j.drudis.2010.03.002
4. Jhaveri, K.; Taldone, T.; Modi, S.; Chiosis, G. *Biochim. Biophys. Acta* **2012,** *1823,* 742–755. doi:10.1016/j.bbamcr.2011.10.008
5. Patel, H. J.; Modi, S.; Chiosis, G.; Taldone, T. *Expert Opin. Drug Discovery* **2011,** *6,* 559–587. doi:10.1517/17460441.2011.563296
6. Chène, P. *Nat. Rev. Drug Discovery* **2002,** *1,* 665–673. doi:10.1038/nrd894
7. Porter, J. R.; Fritz, C. C.; Depew, K. M. *Curr. Opin. Chem. Biol.* **2010,** *14,* 412–420. doi:10.1016/j.cbpa.2010.03.019
8. Donnelly, A.; Blagg, B. S. J. *Curr. Med. Chem.* **2008,** *15,* 2702–2717. doi:10.2174/092986708786242895
9. Taldone, T.; Zatorska, D.; Patel, P. D.; Zong, H.; Rodina, A.; Ahn, J. H.; Moulick, K.; Guzman, M. L.; Chiosis, G. *Bioorg. Med. Chem.* **2011,** *19,* 2603–2614. doi:10.1016/j.bmc.2011.03.013
10. Taldone, T.; Gomes-DaGama, E. M.; Zong, H.; Sen, S.; Alpaugh, M. L.; Zatorska, D.; Alonso-Sabadell, R.; Guzman, M. L.; Chiosis, G. *Bioorg. Med. Chem. Lett.* **2011,** *21,* 5347–5352. doi:10.1016/j.bmcl.2011.07.026
11. Hughes, P. F.; Barrott, J. J.; Carlson, D. A.; Loiselle, D. R.; Speer, B. L.; Bodoor, K.; Rund, L. A.; Haystead, T. A. J. *Bioorg. Med. Chem.* **2012,** *20,* 3298–3305. doi:10.1016/j.bmc.2012.03.043
12. Taldone, T.; Chiosis, G. *Curr. Top. Med. Chem.* **2009,** *9,* 1436–1446. doi:10.2174/156802609789895737
13. Moulick, K.; Ahn, J. H.; Zong, H.; Rodina, A.; Cerchietti, L.; Gomes-DaGama, E. M.; Caldas-Lopes, E.; Beebe, K.; Perna, F.; Hatzi, K.; Vu, L. P.; Zhao, X.; Zatorska, D.; Taldone, T.; Smith-Jones, P.; Alpaugh, M.; Gross, S. S.; Pillarsetty, N.; Ku, T.; Lewis, J. S.; Larson, S. M.; Levine, R.; Erdjument-Bromage, H.; Guzman, M. L.; Nimer, S. D.; Melnick, A.; Neckers, L.; Chiosis, G. *Nat. Chem. Biol.* **2011,** *7,* 818–826. doi:10.1038/nchembio.670
14. Darby, J. F.; Workman, P. *Nature* **2011,** *478,* 334–335. doi:10.1038/478334b
15. DeBoer, C.; Meulman, P. A.; Wnuk, R. J.; Peterson, D. H. *J. Antibiot.* **1970,** *23,* 442–447. doi:10.7164/antibiotics.23.442

16. Whitesell, L.; Mimnaugh, E. G.; De Costa, B.; Myers, C. E.; Neckers, L. M. *Proc. Natl. Acad. Sci. U. S. A.* **1994,** *91,* 8324–8328. doi:10.1073/pnas.91.18.8324
17. Clevenger, R. C.; Raibel, J. M.; Peck, A. M.; Blagg, B. S. J. *J. Org. Chem.* **2004,** *69,* 4375–4380. doi:10.1021/jo049848m
18. Tsaytler, P. A.; Krijgsveld, J.; Goerdayal, S. S.; Rüdiger, S.; Egmond, M. R. *Cell Stress Chaperones* **2009,** *14,* 629–638. doi:10.1007/s12192-009-0115-z
19. Immormino, R. M.; Kang, Y.; Chiosis, G.; Gewirth, D. T. *J. Med. Chem.* **2006,** *49,* 4953–4960. doi:10.1021/jm060297x
20. He, H.; Zatorska, D.; Kim, J.; Aguirre, J.; Llauger, L.; She, Y.; Wu, N.; Immormino, R. M.; Gewirth, D. T.; Chiosis, G. *J. Med. Chem.* **2006,** *49,* 381–390. doi:10.1021/jm0508078
21. Biamonte, M. A.; Shi, J.; Hong, K.; Hurst, D. C.; Zhang, L.; Fan, J.; Busch, D. J.; Karjian, P. L.; Maldonado, A. A.; Sensintaffar, J. L.; Yang, Y.-C.; Kamal, A.; Lough, R. E.; Lundgren, K.; Burrows, F. J.; Timony, G. A.; Boehm, M. F.; Kasibhatla, S. R. *J. Med. Chem.* **2006,** *49,* 817–828. doi:10.1021/jm0503087
22. Andrés, J. M.; Manzano, R.; Pedrosa, R. *Chem.–Eur. J.* **2008,** *14,* 5116–5119. doi:10.1002/chem.200800633
23. Du, Y.; Moulick, K.; Rodina, A.; Aguirre, J.; Felts, S.; Dingledine, R.; Fu, H.; Chiosis, G. *J. Biomol. Screening* **2007,** *12,* 915–924. doi:10.1177/1087057107306067
24. Schulte, T. W.; An, W. G.; Neckers, L. M. *Biochem. Biophys. Res. Commun.* **1997,** *239,* 655–659. doi:10.1006/bbrc.1997.7527
25. Hawley, T. S.; Hawley, R. G., Eds. *Methods in Molecular Biology: Flow Cytometry Protocols,* 2nd ed.; Humana Press Inc.: Totowa, NJ, 2004. doi:10.1385/1592597734
26. O'Brien, J.; Wilson, I.; Orton, T.; Pognan, F. *Eur. J. Biochem.* **2000,** *267,* 5421–5426. doi:10.1046/j.1432-1327.2000.01606.x

License and Terms

This is an Open Access article under the terms of the Creative Commons Attribution License (http://creativecommons.org/licenses/by/2.0), which permits unrestricted use, distribution, and reproduction in any medium, provided the original work is properly cited.

The license is subject to the *Beilstein Journal of Organic Chemistry* terms and conditions: (http://www.beilstein-journals.org/bjoc)

The definitive version of this article is the electronic one which can be found at: doi:10.3762/bjoc.9.60

Beilstein Journal of Organic Chemistry

Recent progress in the discovery of small molecules for the treatment of amyotrophic lateral sclerosis (ALS)

Allison S. Limpert, Margrith E. Mattmann and Nicholas D. P. Cosford*

Review

Open Access

Address:
Apoptosis and Cell Death Research Program, Sanford-Burnham Medical Research Institute, 10901 N. Torrey Pines Road, La Jolla, California 92037, United States

Email:
Nicholas D. P. Cosford* - ncosford@sanfordburnham.org

* Corresponding author

Keywords:
amyotrophic lateral sclerosis (ALS); copper/zinc (Cu-Zn) superoxide dismutase 1 (SOD1); glutamate toxicity; neurodegeneration; oxidative stress

Beilstein J. Org. Chem. **2013,** *9,* 717–732.
doi:10.3762/bjoc.9.82

Received: 20 December 2012
Accepted: 07 March 2013
Published: 15 April 2013

This article is part of the Thematic Series "Synthetic probes for the study of biological function".

Guest Editor: J. Aubé

© 2013 Limpert et al; licensee Beilstein-Institut.
License and terms: see end of document.

Abstract

Amyotrophic lateral sclerosis (ALS) is a fatal neurodegenerative disorder with few therapeutic options. While several gene mutations have been implicated in ALS, the exact cause of neuronal dysfunction is unknown and motor neurons of affected individuals display numerous cellular abnormalities. Ongoing efforts to develop novel ALS treatments involve the identification of small molecules targeting specific mechanisms of neuronal pathology, including glutamate excitotoxicity, mutant protein aggregation, endoplasmic reticulum (ER) stress, loss of trophic factors, oxidative stress, or neuroinflammation. Herein, we review recent advances in the discovery and preclinical characterization of lead compounds that may ultimately provide novel drugs to treat patients suffering from ALS.

Introduction

Amyotrophic lateral sclerosis (ALS), also known as Lou Gehrig's disease, is a progressive neurodegenerative disease that leads to the dysfunction and death of motor neurons in both the motor cortex and spinal cord. This adult-onset disorder leads to paralysis and eventual death, most commonly by asphyxiation. Symptoms typically include muscle weakness and wasting, cramps, poor reflexes, twitching, and speech problems [1]. Few treatment options exist for this fatal disease, which typically results in death within 2–5 years of diagnosis [2]. Currently, riluzole (**1**), a compound which reduces glutamate excitotoxicity, is the only FDA approved drug for the treatment of ALS. However, its benefits are meager, as it has no effects on disease symptoms and only extends lifespan for an average of 2–3 months [3].

World-wide, the incidence of ALS is 1–2 in 100,000 individuals with about 90% of cases being sporadic (sALS) and 10% of all cases characterized as familial (fALS) [4]. Several gene

mutations have been identified that contribute to this disorder with 20% of fALS cases being linked to mutations in the copper/zinc (Cu-Zn) superoxide dismutase 1 (SOD1) gene [4]. Many cellular pathologies have been characterized in ALS, including, but not limited to glutamate toxicity, protein misfolding and aggregation, endoplasmic reticulum (ER) stress, loss of trophic factors, oxidative stress, inflammation, disrupted protein trafficking, and mitochondrial dysfunction [5]. Therapeutic development has been based around the targeting of these mechanisms of cellular dysfunction.

Currently, several drugs are in phase III clinical trials for the treatment of ALS (comprehensively reviewed in Glicksman, 2012 [3] and Dunkel et al., 2012 [5]). These drugs include dexpramipexole (**2**), a mitochondrial stabilizer; arimoclomol (**3**), a heat-shock protein (hsp) coinducer; olesoxime (**4**), a mitochondrial pore modulator; ceftriaxone (**5**), an inducer of the glial glutamate transporter (GLT1, EAAT2); and edaravone (**6**), a free-radical scavenging agent (Figure 1). Our focus in this review is to primarily highlight novel small molecules in the discovery and preclinical development stages for the treatment of ALS and to discuss their relevance in the context of current advances in the field.

Review

Animal models of ALS

The discovery of genetic mutations in fALS has led to the development of transgenic mouse models and cell-culture systems to study this disorder. The most common of these mouse models carries the SOD1 G93A mutation where glycine is substituted for alanine at position 93 in the superoxide dismutase 1 protein [6,7]. Other related mutations in SOD1 include H46R, A4V, and G85R. These mutations are not believed to reduce the function of the SOD1 protein; however, they have been hypothesized to cause selective motor-neuron death through a toxic gain of function [8]. Mutant isoforms of the SOD1 protein form intercellular aggregates leading to disruption of the proteasome, ER stress, mitochondrial dysfunction, and other cellular deficits and damage [8]. SOD1 mutant mice display prominent motor-neuron degeneration and have many of the hallmarks of human ALS, including progressive hindlimb weakness, increasing weight loss, and eventual paralysis and death [8]. Recently, additional genes have been implicated in ALS, such as TARDBP, which encodes for the trans-activating response (TAR) DNA-binding protein 43 (TDP-43), FUS/TLS, which encodes the RNA-binding protein fused in sarcoma, and VAPB, a gene encoding the vesicle-associated membrane-protein-associated protein B/C, and animal models based on mutations in these genes have been developed [8].

Despite obvious parallels with human ALS, to date these transgenic mouse models have proven ineffective in producing potential drug therapies [6]. Many drugs that show efficacy in mouse models have been unproductive in patient trials. Furthermore, riluzole [6-(trifluoromethoxy)-2-aminobenzothiazole], the only FDA approved compound for ALS, produced only very modest effects on disease progression in SOD1 G93A transgenic mice when administered prior to symptom onset [4]. These results highlight the limitations of these animal models in drug development and question how effective these models are in therapeutic discovery.

Reduction in glutamate toxicity

Riluzole (**1**), the only currently approved treatment for attenuating disease progression in ALS patients, both inhibits the release of glutamate and noncompetitively inhibits postsynaptic NMDA and AMPA receptors [6]. However, riluzole demonstrates variable drug exposure in addition to highly differential serum concentrations among ALS patients following oral administration [9]. This variability correlates with the heteroge-

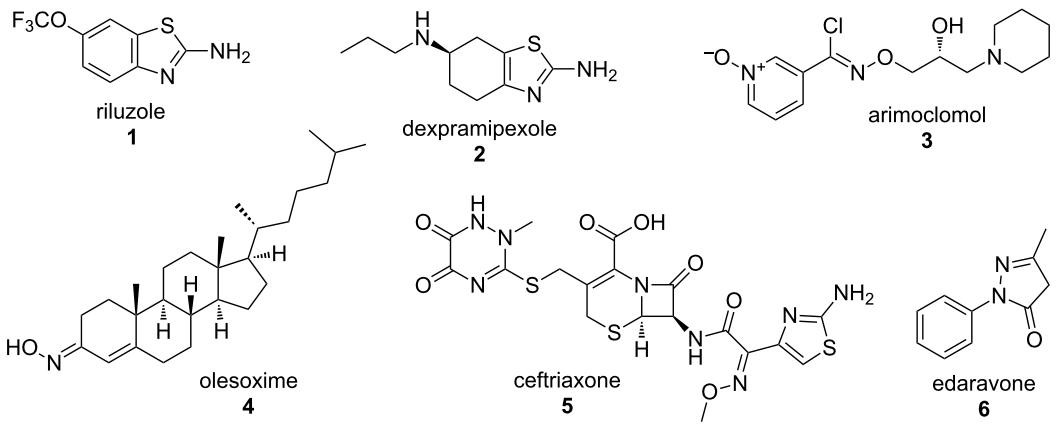


Figure 1: FDA-approved riluzole (**1**) and other ALS drugs currently in phase III clinical trials (**2**–**6**).

neous patient expression of the cytochrome P450 (CYP) isoform CYP1A2, which provides the primary mechanism of riluzole metabolism [10,11]. Given this variability in metabolism within the patient population, recent studies have focused around creating riluzole prodrugs that would exhibit higher stability in vivo [11]. For example, McDonnell et al. [11], identified and evaluated a group of 23 riluzole prodrugs for their potential use in the treatment of glutamate toxicity in ALS and other disorders. Potential drug candidates were prepared through the conversion of the exocyclic amine to single alpha amides, carbamates, succinamides, or amide linkages from γ-aminobutyric acids (Figure 2). It is expected that these compounds would be cleaved by amidases or esterases found in plasma to generate riluzole. The stability of these analogues was tested in simulated gastric fluid, simulated intestinal fluid, and in liver microsomes to determine whether the drugs would enter the plasma intact. Further, the liberation of riluzole from the prodrugs was evaluated in plasma. One compound, an *O*-benzylserine derivative of riluzole (Figure 2, **1b**), was identified as a candidate prodrug appropriate for in vivo testing, due to its stability in in vitro intestinal and microsomal assays and its ability to withstand metabolism by CYP1A2 [11]. Further development of this prodrug may allow for consistent riluzole plasma levels and thus more efficacious treatment among ALS patients.

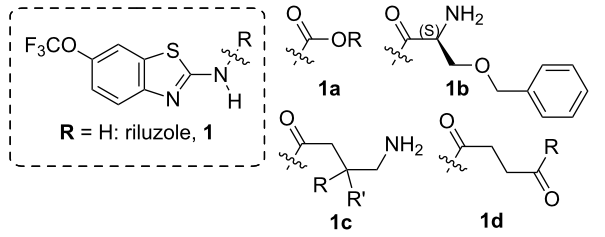


Figure 2: Riluzole (left) and prodrugs developed by McDonnell et al. [11].

The modest success of riluzole in ALS treatment and the role of glutamate excitotoxicity in numerous disease states have motivated further drug development focused on the modulation of glutamate signaling. In particular, evidence for an essential role of glutamate toxicity in ALS has come from the analysis of cerebrospinal fluid (CSF) from ALS patients, which shows a three-fold increase in glutamate and *N*-acetyl-aspartyl glutamate (NAAG, Figure 3) levels relative to controls [12,13]. Furthermore, exposure of CSF extracted from ALS patients kills healthy motor neurons in culture [14]. Together, these data point to an excess of glutamatergic signaling in ALS and suggest that decreasing glutamate levels may have therapeutic benefits in ALS patients. The actions of glutamate, the primary excitatory neurotransmitter in the nervous system, are terminated by the uptake of glutamate away from the synapse by numerous glutamate transporters [15]. In particular, the Na^+-dependent excitatory amino acid transporter 2 (EAAT2), which is present on glial cells surrounding the neuronal synapse [12], is predominantly involved in the clearance of glutamate from the synapse. Thus, activators of EAAT2 have the potential to reduce glutamate toxicity in vivo and attenuate the disease progression of ALS.

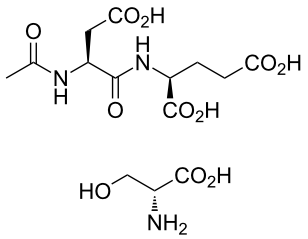


Figure 3: Neurotransmitters *N*-acetyl-aspartyl glutamate (NAAG, top) and D-serine (bottom).

As EAAT2 expression is highly regulated at the translational level, one strategy for increasing EAAT2 activity is to use small molecules to increase the translation of EAAT2 mRNA [6]. This strategy, employed by Colton et al. [6], prompted the screening of a library of 140,000 compounds by using an ELISA-based assay for EAAT2 protein expression. This screen resulted in 293 hits for compounds increasing EAAT2 expression. Of these, three were selected as lead compounds for further optimization based on their potency and lack of cellular toxicity, although it should be noted that the structures of the hits were not disclosed [6]. Additionally, the EAAT2 protein induced by these lead compounds was found to be functional and exhibit appropriate cellular localization [6].

Using these identified lead compounds, Xing et al. [16] performed chemical optimization to develop additional analogues for potential use as therapeutic agents. Structure–activity relationship (SAR) studies revealed that the thioether and pyridazine moieties were essential molecular components for increasing EAAT2 protein levels [16]. Of the analogues developed, several thiopyridazine derivatives (Figure 4) were found to increase EAAT2 levels greater than six-fold over endogenous levels in primary astrocyte (PA)-EAAT2 cells (an astrocyte cell line stably expressing mRNA for EAAT2) at concentrations of less than 5 μM. Additionally, one derivative was found to increase EAAT2 levels 3–4-fold at only 0.5 μM [16]. These compounds will prove useful for evaluating the potential of EAAT2 activators in animal models of ALS and in the study of other diseases where glutamate toxicity plays an essential role.

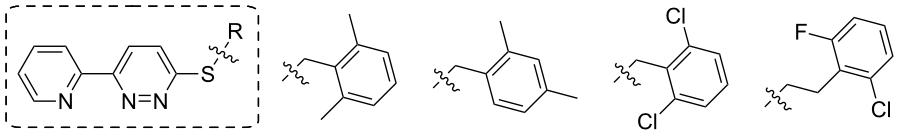


Figure 4: Thiopyridazines developed to increase EAAT2 protein levels.

In addition to dysregulation of glutamate levels in ALS patients, recent studies have also detected elevated levels of D-serine (Figure 3), an activator/co-agonist of the *N*-methyl-D-aspartate (NMDA) ionotropic glutamate receptor, in the spinal cord of both ALS patients and transgenic mice carrying the SOD1 G93A mutation [17,18]. This increase in D-serine corresponded with a reduction of D-amino acid oxidase (DAO) in SOD1 mutant mice, the enzyme responsible for the metabolism of D-amino acids including D-serine. Interestingly, a new mutation in the D-amino acid oxidase (DAO) gene has been recently characterized to contribute to fALS [19]. This R199W DAO mutation inhibits the function of DAO, increases ubiquitin-containing aggregates, and reduces cell viability when expressed in neuroblastoma-spinal cord (NSC)-34 cells, a motor neuron cell line [19]. Since D-serine serves as a co-agonist at the glycine site of the NMDA glutamate receptor, increases in D-serine are likely to contribute to glutamate excitotoxicity in ALS patients. These data suggest that reducing D-serine levels through activation of DAO or reduction of serine racemase (SR), the enzyme responsible for D-serine synthesis, may be therapeutically beneficial [20]. Furthermore, drugs modulating NMDA receptor signaling may also prove beneficial to ALS treatment.

The contribution of improper glutamate regulation to ALS pathology is further highlighted by studies demonstrating abnormal metabotrophic glutamate (mGlu) receptor expression in ALS patients. Elevated levels of Group I, II, and III mGlu receptors have been reported in astrocytes of ALS patients, while a decrease in the levels of Group II mGlu receptors has been detected in neurons of the spinal cord in these patients [21]. Furthermore, T-lymphocytes in ALS patients display reduced $mGlu_2$ receptor levels as compared to controls [22]. These data substantiate the role of glutamatergic dysfunction in ALS and indicate that non-neuronal cells may be affected [22].

Targeting SOD1 mutations

Due to the role of SOD1 mutations in fALS and the reproduction of human ALS pathology in mouse models carrying mutant SOD1 genes, one strategy to attenuate ALS pathology is to develop small molecules that reduce SOD1 protein levels. Support for targeting SOD1 protein expression has come from animal studies demonstrating that the reduction of SOD1 protein levels in motor neurons causes these cells to become resistant to ALS-induced cellular death [23]. In order to identify small molecules that downregulate the transcription of SOD1, Murakami et al. [24] developed a high-throughput screening assay using an H4 human astrocytoma cell line expressing a SOD1 luciferase reporter construct. Following a screen of a library of 9600 small molecules, 325 compounds were identified as hits, with 2 compounds demonstrating selectivity in downregulating SOD1 protein levels without discernible cellular toxicity following secondary assays [24]. One of these compounds was chosen for further analysis due to its considerably lower 50% effective concentration (EC_{50}). Interestingly, this selected hit compound, 3-(1*H*-benzo[*d*]imidazol-2-yl)-6-chloro-4*H*-chromen-4-one (052C9, **7**; Figure 5), was found to reduce phosphorylation of the transcription factor Nrf2, a known activator of cellular stress genes as well as an upregulator of SOD1 transcription [24].

A similar high-throughput screen was performed by Wright et al. [25], who assayed 30,000 small molecules for SOD1 transcriptional repression by employing a PC12 (phenochromacytoma) cell line stably expressing the human SOD1 promoter flanked by green fluorescent protein (GFP) [25]. This screening

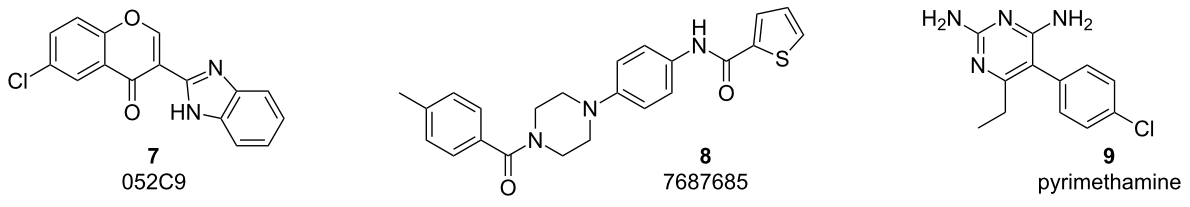


Figure 5: Compounds shown to reduce SOD1 expression.

strategy identified 20 compound hits, for which the activity was confirmed through secondary assays and analyzed for cytotoxicity. Compound 7687685 (**8**; Figure 5) was demonstrated to both reduce endogenous SOD1 protein levels in human cells and also repress several other genes implicated in ALS including FUS and TARDBP [25]. However, in in vivo studies performed in SOD1 G93A transgenic mice, compound **8** exhibited only a small (5%) reduction of SOD1 protein levels in spinal-cord extracts. Due to the toxicity of the compound when administered in higher doses, compound **8** is unlikely to be useful for the treatment of ALS patients, although this screening strategy may prove relevant for the development of further small molecule inhibitors [25].

Conflicting data have arisen surrounding the ability of the antimalarial compound pyrimethamine (**9**; Figure 5) to reduce SOD1 protein levels. Lange et al. [26] identified a dose-dependent reduction in SOD1 expression in cultured human cells and performed a phase I pilot study in 16 ALS patients. This study analyzed blood and CSF samples of patients treated with the drug for 18 weeks and determined that SOD1 levels were significantly reduced in CSF and in leukocytes of these individuals [26]. However, Wright et al. [27] were unable to confirm these results in either cultured cells or in mice treated with pyrimethamine. In contrast, these studies found that the concentrations of pyrimethamine required to reduce transcriptional activity from the SOD1 promoter by 42% caused a 68% reduction in cellular viability, thus leading to the conclusion that the reduction in SOD1 levels was due to nonspecific cytotoxicity. In other cell types, as well as in animal studies, pyrimethamine was unable to reduce SOD1 protein levels as compared to controls [27]. These conflicting results are likely due to differences in how SOD1 protein levels were assessed as well as due to differences between human and mouse fluid samples. Further studies will be required to determine the effects of pyrimethamine treatment on SOD1 protein expression and more importantly assess whether or not it is able to attenuate ALS pathology.

Mutations in SOD1 lead to cellular toxicity not through loss of function of the SOD1 protein, but rather through a toxic gain of function, whereby SOD1 mutants aggregate in intercellular inclusions leading to cellular dysfunction. Due to this mechanism of SOD1-induced cellular death, compounds that reduce the aggregation of SOD1 protein may be able to protect cells from damage. Benmohamed et al. [28] developed a screening strategy to analyze the ability of small molecules to reduce mutant SOD1 aggregates in a cell-culture model [28]. Using PC12 cells transfected with an inducible SOD1 G93A construct [29], a library of over 50,000 small-molecule compounds was initially screened for the ability to enhance cellular viability in the presence of the mutant SOD1 protein [28]. Hits from this screen were then subjected to several counter screens including a mutant SOD1 aggregation assay that utilized a cell line expressing a SOD1 G85R mutant protein [29] coupled to yellow fluorescent protein (YFP). Following incubation with the selected compounds, the SOD1 G85R YFP cells were imaged using a high throughput fluorescent microscopy system and analyzed for the number of SOD1 aggregates per cell [28]. This screening strategy, combined with chemoinformatic methodologies used to cluster structurally similar compounds, allowed the researchers to identify three distinct chemical series that were selected for optimization based on their ability to reduce both cellular toxicity and mutant SOD1 protein aggregation: arylsulfanyl pyrazolones (ASP, **10**), cyclohexane-1,3-diones (CHD, **11**), and pyrimidine 2,4,6-triones (PYT, **12**; Figure 6).

The ASP derivatives were subjected to structural optimization and the resulting compounds were then evaluated in pharmacokinetic (PK) assays. Two ASP compounds, which demonstrated activity in cell viability and SOD1 aggregation assays,

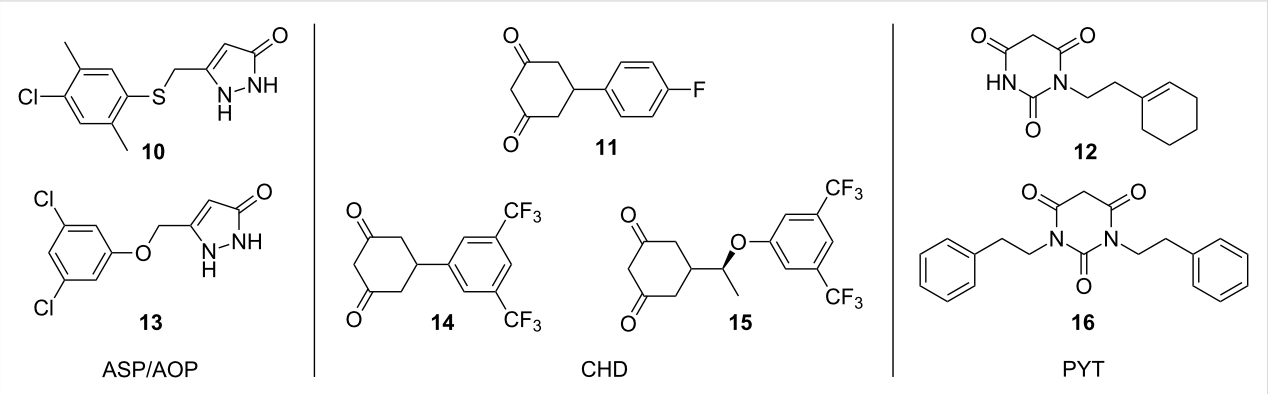


Figure 6: Families of compounds (named in italics) capable of reducing SOD1-induced cellular toxicity and mutant SOD1 protein aggregation. Top: selected compounds identified in high-throughput screening. Bottom: advanced compounds.

were found to have low microsomal stability and poor brain accumulation, respectively [30]. Metabolic profiling and further chemical modification were performed to increase the stability and potency of ASP derivatives, and this ultimately led to replacement of the thioether with an ether linkage and the identification of a new aryloxanyl pyrazolone (AOP) scaffold exemplified by compound **13** [31]. The new AOP analogues were optimized and tested in cell-viability assays in primary neurons, as well as aggregation assays in SOD1 mutant-expressing cells. Compound **13** displayed high activity in these assays as well as a promising pharmacokinetic profile including good penetration of the blood–brain barrier (BBB) and was further tested in a SOD1 G93A transgenic mouse model. Mutant mice treated with compound **13** by intraperitoneal (i.p.) injection at 20 mg/kg daily, starting at 6 weeks of age, displayed a 13.3% increase in lifespan as compared to controls [31], suggesting that the AOP scaffold is potentially suitable for therapeutic development for the treatment of ALS. Several important findings in the development of pyrazolone compounds included the identification of an *N*1-benzyl substituted pyrazolone, which displayed enhanced potency along with the discovery that the *N*2-H group participates in hydrogen-bond-donating interactions with the biological target [32].

SAR around the CHD scaffold **11** determined that 3,5-ditrifluoromethyl analogue **14** had the highest potency of these derivatives. Additionally, **14** possessed favorable PK, demonstrating high plasma stability and oral bioavailability, as well as high brain accumulation [33]. Due to its advantageous pharmacological properties, **14** was tested in SOD1 G93A transgenic mice to determine whether it was able to extend lifespan and alleviate symptoms in a mouse model of ALS. However, this compound demonstrated no therapeutic benefit. Additional studies demonstrated that **14** exhibited poor activity in primary cortical neurons due to low penetration of neuronal cells [33]. Further SAR around this series led to new chiral CHD analogues, such as compound **15** (Figure 6), with higher neuronal permeability and potency. Additionally, these compounds were found to be active in the cytotoxicity screen performed in SOD1 G93A-PC12 cells and displayed favorable PK profiles. Importantly, compound **15** exhibited a 90% increase in activity in primary cortical neurons [34]. Because of these favorable properties, this analogue was tested in SOD1 G93A transgenic mice that were treated daily by i.p. administration with 30 mg/kg of CHD derivative compound **15** starting at 6 weeks (prior to symptom presentation). A 13% increase in lifespan was observed in treated animals as compared to controls [34].

SAR studies with PYT scaffold **12** were also successful in identifying an analogue with properties suitable for use as a novel therapeutic for ALS. Modifications to the PYT backbone were made and subsequent compounds were tested in both the previously described cytotoxicity assay as well as the SOD1 aggregation assay. Compound **16** was found to be highly active in both of these assays and additionally demonstrated high potency and low toxicity, as well as excellent solubility and plasma stability [35]. Further studies indicated that compound **16** was able to cross the BBB and exhibited good oral bioavailability [35].

An alternative strategy to prevent the aggregation of SOD1 was employed by Ray et al. [36], who designed small molecules to stabilize the SOD1 native dimer, theorizing that SOD1 monomerization was required for aggregate formation [36]. Examination of the mutant SOD1 A4V dimer interface detected hydrophobic cavities that could be filled to enhance protein stability. When these cavities were filled by genetic mutagenesis of the SOD1 protein, enhanced dimer stability was detected [36]. An in silico screen was performed to identify compounds with the potential to bind at the dimer interface and the top 100 hits were screened in an SOD1 A4V aggregation assay. Fifteen compounds inhibited the aggregation of SOD1 A4V proteins and were successfully found to prevent the aggregation of other SOD1 mutants, G85R and G93A [36].

However, when tested for SOD1 protein binding in the presence of human blood plasma, these compounds performed poorly, binding with higher affinity to blood proteins than to SOD1, suggesting that these compounds may have significant off-target activity [37]. Docking calculations were performed to model the inhibitors at the dimer interface and a database of small molecules was screened to identify molecules that satisfied the docking constraints [37]. Twenty new compounds were identified and analyzed for inhibition of SOD1 A4V aggregation as well as binding to SOD1 in the presence of human plasma. Six of these compounds (Figure 7) tested positively in these assays [37], indicating that they may be excellent starting points for therapeutic development for ALS.

Targeting TDP-43

While SOD1 mutations are frequently studied, these mutations account for about 20% of familial ALS and only 2–3% of all ALS cases [2]. Recent studies have focused on creating small molecules that target other mutant proteins associated with ALS. Trans-activating response (TAR) DNA-binding protein 43 (TDP-43) is a nucleotide-binding protein important for gene transcription and mRNA splicing, transport, and stabilization [38]. Mutations in the TARDBP gene, which encodes TDP-43, are responsible for up to 6.5% of fALS [1]. In the neurons of ALS patients, TDP-43 protein is decreased in the nucleus and accumulates in cytoplasmic inclusions where it can sequester

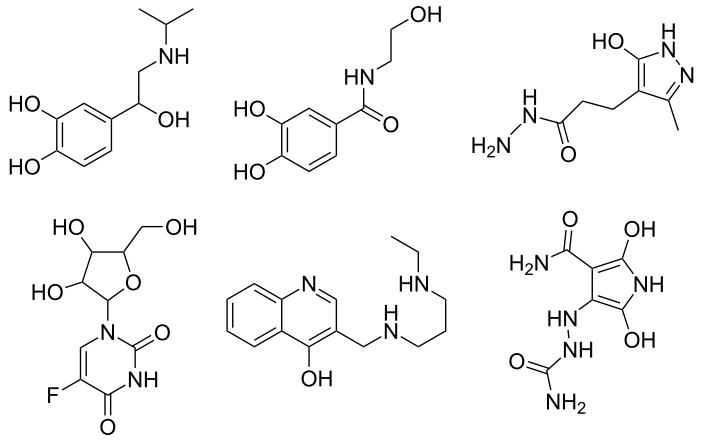


Figure 7: Compounds identified by Nowak and co-workers [37] in silico that selectively bind SOD1 over human plasma and inhibit A4V-SOD1 aggregation.

cytoplasmic RNAs in stress granules [39-41]. One approach to alleviate the pathology caused by mutant TDP-43 is to identify small molecules that inhibit the binding of TDP-43 to nucleotides. Cassel et al. [42] developed a high-throughput screening assay whereby TDP-43 nucleotide binding could be assessed. A screen of 7360 compounds yielded a series of small molecules that disrupt oligonucleotide binding to TDP-43 protein [42]. Later, this series of 4-aminoquinoline derivatives (Figure 8) was tested for its ability to regulate TDP-43 [43].

TDP-43 expression levels must be appropriately regulated by the cell as either overexpression or deletion of TDP-43 causes cellular death. Caspases 3 and 7 can mediate the reduction of TDP-43 protein levels through cleavage of TDP-43 and subsequent clearance of the cleaved products by the proteasome [44]. Cleavage-resistant mutations in TDP-43 are highly toxic to the cell [44]. Cassel et al. [43] hypothesized that the 4-aminoquinoline series identified in their HTS screen may increase the rate of caspase cleavage of TDP-43 and thus affect its cellular accumulation. In this study, several 4-aminoquinoline derivatives (Figure 8) were found to bind to TDP-43, decrease its association with oligonucleotides, and increase caspase-mediated cleavage of the protein [43]. Furthermore, treatment of H4 cells with these compounds modestly reduced intercellular levels of TDP-43 [43] as well as histone deacetylase 6 (HDAC-6) and autophagy-related protein 7 (ATG-7), proteins known to be regulated by TDP-43 [45,46]. Since reduction of TDP-43 levels in motor neurons may prove to be beneficial to ALS treatment, further development and validation of this series of small molecules may prove valuable for future therapeutic development.

Another mechanism to attenuate the toxicity of TDP-43 is to prevent its aggregation into intercellular inclusions. In a study by Parker et al. [38], treatment of SH-SY5Y cells with paraquat to induce cellular stress through mitochondrial inhibition led to the formation of TDP-43 aggregates in the cytoplasm. The formation of TDP-43-containing cellular inclusions was dependent on the activation of stress-induced kinases such as c-Jun N-terminal kinase (JNK). Treatment of cells with bis(thiosemicarbazonato)copper complexes (Cu(II)(btsc)s; Figure 9), reduced stress-induced kinase activity and prevented TDP-43 aggregation [38]. Cu(II)(btsc)s have previously been demonstrated to have neuroprotective effects in mouse models of neurodegeneration [47] and elicited similar results in cells overexpressing TDP-43. These data suggest that Cu(II)(btsc)s, such as compound **17**, may be beneficial in the treatment

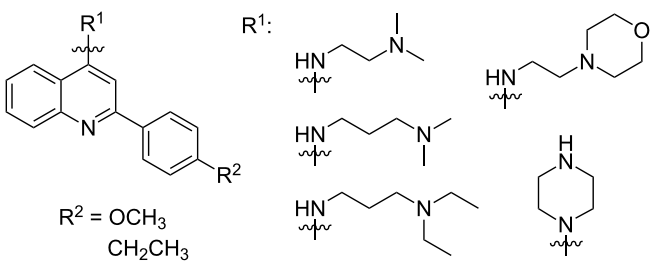
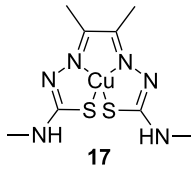


Figure 8: 4-Aminoquinolines developed by Cassel and co-workers [43] for disruption of oligonucleotide/TDP-43 binding.



17

Figure 9: Cu(II)(atsm), an example of a Cu(II)(btsc) copper complex.

of ALS by modulating kinase activity and reducing protein aggregation.

The removal of dysfunctional proteins and organelles from the cell can occur by the process of autophagy, whereby autophagosomes engulf cellular material, which is then degraded by the lysosome [48]. One strategy to reduce TDP-43-containing cytoplasmic inclusions is to induce autophagy by using known pharmacological activators (Figure 10), such as tamoxifen (**18**), carbamazepine (**19**), spermidine (**20**), or rapamycin (**21**). Studies using these compounds to enhance autophagy in disease models with TDP-43 proteinopathies have discovered a clearance of cytoplasmic TDP-43, as well as a reduction in caspase activation and cellular death corresponding with an upregulation of autophagic markers [48]. Transgenic mice overexpressing TDP-43 in the forebrain display deficiencies in cognition as early as 2 months of age and impairment of motor function at 6 months of age. Treatment of these mice with 10 mg/kg rapamycin by i.p. three times weekly increased their performance in the Morris water maze test at 3 months of age and enhanced rotarod performance at 6 months of age [48]. Together, these data indicate that enhancement of autophagy may reduce cellular death and behavioral dysfunction associated with TDP-43 mutations.

Modulation of trophic factors

One pathological characteristic of ALS is the loss of trophic factors that promote the health and stability of motor neurons. Compounds that increase growth factor-induced neuronal support have been tested in both cellular and mouse models of ALS with moderate success. For example, in a study performed by Shimazawa et al. [49] a small molecule (SUN N8075, **22**, Figure 11), which is currently in clinical trials for the treatment of stroke, protected SH-SY5Y cells against pharmacologically induced ER stress-mediated cell death. Further investigation into the mechanism of action of this compound revealed that **22** potentiated the upregulation of VGF nerve growth factor inducible protein (VGF) in response to cell stress [49]. This potentiation enhanced the activation of cellular survival signals and reduced caspase cleavage. However, siRNA targeting VGF abolished the protective response to **22**, indicating that VGF upregulation was central to the activity of this compound [49].

The importance of VGF in ALS disease progression has been supported by studies of ALS patients, which report a reduction in VGF levels in the CSF of individuals with ALS as compared to control samples from healthy individuals [50]. To determine if **22** could successfully treat ALS symptoms in animal models, transgenic mice carrying the human SOD1 G93A mutation were treated subcutaneously (s.c.) with 30 mg/kg **22** starting at 10 weeks of age and continuing for the lifespan of the animal. Treated animals displayed delayed disease onset and progression as established by rotarod performance. Additionally, animals treated with **22** exhibited a mean increase in lifespan by 10.9%. The effects of **22** were replicated in a transgenic rat model of ALS, where this compound again displayed modest effects on delaying motor function decline and increasing survival [49].

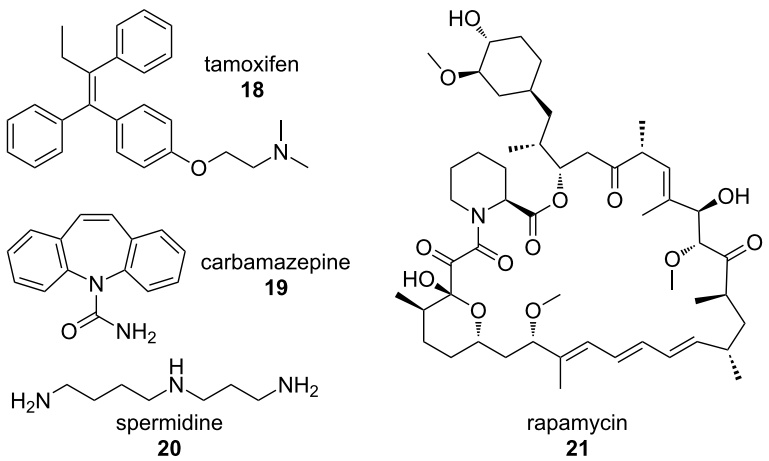


Figure 10: Pharmacological inducers of autophagy.

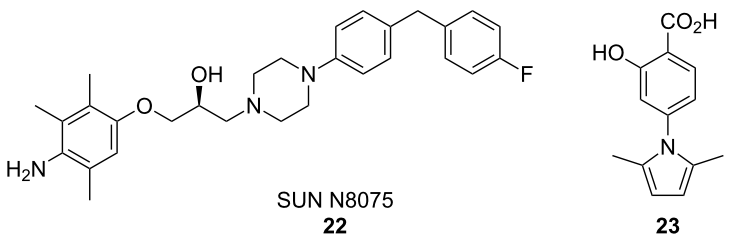


Figure 11: Compounds used to evaluate the effects of trophic factors on ALS disease progression.

A novel study by Van Hoecke et al. [51] has implicated the Ephrin/Eph system in determining motor neuron susceptibility to degeneration in ALS. Ephrins and their cognate receptors (Eph) are important in nervous-system development where they assist with axonal pathfinding and repulsion. In adults these signaling molecules have been demonstrated to play essential roles in synapse formation and plasticity [52]. In this study, Hoecke et al. [51] used a zebrafish model of ALS to determine modifying factors that could influence disease progression and identified the mammalian EPHA4 gene as a potential disease modifier. To confirm these genetic data, 4-(2,5-dimethyl-1*H*-pyrrol-1-yl)-2-hydroxybenzoic acid (**23**) was used to inhibit EphA4 in mutant zebrafish. This treatment resulted in the rescue of SOD1-induced axonopathy in zebrafish overexpressing a mutant SOD1 isoform. Further studies were performed by genetically reducing EPHA4 gene dosage in mice carrying the hSOD1 G93A mutation. Mice with reduced EphA4 displayed prolonged survival of motor neurons coupled with increased motor performance and lifespan. Rat models of ALS were also employed in this comprehensive study. Rats expressing SOD1 G93A were treated with Epha4 blocking peptide through intracerebroventricular (i.c.v.) injection. Rats injected with blocking peptide exhibited delayed disease onset and prolonged survival. In studies of ALS patients, patients with lower levels of EphA4 protein correlated with later disease onset and individuals carrying mutations in the EPHA4 gene displayed increased survival rates [51]. Finally, studies were performed in zebrafish expressing mutant TDP-43 protein. Inhibition of Epha4 through pharmacologic or genetic methods also rescued axonal deficiencies in this ALS model.

Together these studies suggest that pathways induced by trophic factors that affect growth, development and survival of neuronal cells, are essential components of ALS disease progression. Therapeutics that increase the expression of a prosurvival factor, such as VGF, or inhibit the action of a repressive signaling molecule, such as Epha4, may have a profound effect on patient outcome. Further studies are needed to determine the effects of enhancing VGF or antagonizing Epha4 on other cellular pathways before these treatments have the potential for human testing.

Neuroprotective compounds

An alternative approach for the treatment of ALS is the use of known neuroprotective or neurogenic compounds (Figure 12). In a screen of a chemically diverse compound

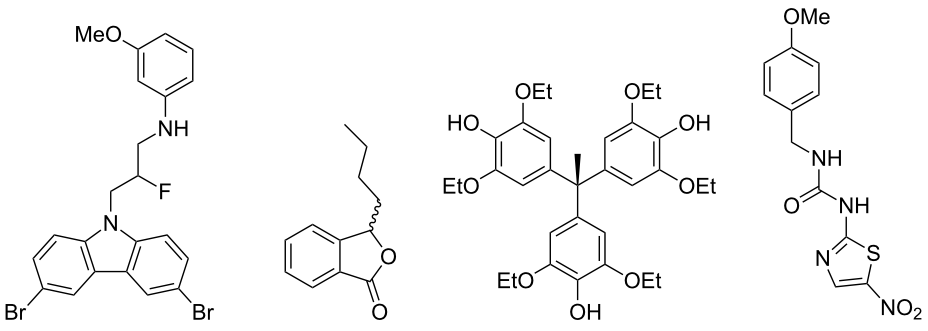


Figure 12: Compounds identified as neuroprotective.

library, Pieper et al. identified an aminopropyl carbazole, P7C3, which was found to increase adult hippocampal neurogenesis in an in vivo assay [53]. Further optimization of this compound through structure–activity relationship (SAR) analysis led to the development of an analogue, P7C3A20 (**24**), which has a replacement of the hydroxy group at the chiral center of the linker with a fluorine atom and an addition of a 3-methoxy group to the aniline ring [53]. This compound demonstrated higher potency and was found to protect spinal cord neurons from death in mice expressing the SOD1 G93A mutation. When delivered at the disease onset, **24** demonstrated a reduction in symptom progression as characterized by rotarod tests, and examination of walking gait and stride length [54]. While these data suggest that the use of this compound and its derivatives in treating neurodegenerative disease may be promising, further optimization is required to improve efficacy and solubility as well as reduce toxicity.

Studies using DL-3-*n*-butylphthalide (**25**), a compound approved for use in stroke patients in China, have reported that the treatment of transgenic SOD1 G93A mice can improve motor symptoms and increase lifespan. Oral administration of this compound at 60 mg/kg daily prior to symptom presentation, resulted in no delay in onset of hindlimb weakness, but decreased the progression of motor dysfunction as tested by rotarod [55]. When DL-3-*n*-butylphthalide treatment was initiated following disease onset, SOD1 G93A mice displayed increased survival of motor neurons in the spinal cord and a reduction in astrocyte and microglial activation. Furthermore, transgenic animals treated with this compound increase the expression of the Nrf2 transcription factor, which promotes the expression of anti-inflammatory and prosurvival genes [55].

In a novel approach to inducing neuroprotection, Eitan et al. [56] used triaryl compound 4,4',4''-(ethane-1,1,1-triyl)tris(2,6-diethoxyphenol), designated AGS-499 (**26**), to increase telomerase expression in neuronal cells. Telomerase is a protein complex that maintains the length and integrity of telomeres in developing and dividing cells. In differentiated neurons, telomerase activity is typically absent [57]; however, some studies have indicated that some brain regions maintain active telomerase into adulthood [58,59]. Brain injury results in an increase in telomerase activity and transgenic mice overexpressing telomerase reverse transcriptase (TERT), an essential component of the active telomerase enzyme, displayed a marked resistance to neurotoxicity [60].

Treatment of mice with **26** resulted in an increase in telomerase activity in the forebrain, spinal cord, and brainstem and protected neurons from NMDA-induced toxicity [56]. SOD1 G93A mutant mice injected with **26** displayed a 14.6% reduction in the progression of neurological symptoms as analyzed by limb assessment as well as a 16.4% increase in lifespan [56]. These benefits were mediated by a marked increase in motor neuron survival in the spinal cord. Furthermore, treatment of both rodent motor neuron cultures and human cells with **26** increased TERT levels and protected cells from oxidative stress [56].

An alternative strategy to inducing neuroprotection is to inhibit the signaling molecules that antagonize cellular survival and promote neuron death in disease models. Glycogen synthase kinase-3 (GSK-3) is an essential signaling molecule involved in many cellular processes including glycogen metabolism, cell-cycle regulation, cellular proliferation, and apoptosis. However, studies using tissue samples from ALS patients report that they display elevated GSK-3 levels in the spinal cord [61]. Increased GSK-3 activity has also been reported in the motor neurons of SOD1 G93A mutant mice [62]. Using a GSK-3 inhibitor that crosses the BBB (**27**), Koh et al. [63] examined the effects of reducing GSK-3 activity in mouse models of ALS. SOD1 G93A mice were injected with **27** intraperitoneally at 60 days old. Treated mice displayed delayed symptom onset, reduction in motor deficits as measured by rotarod test, and increased motor neuron survival in the spinal cord. Further investigation determined that the inhibition of GSK-3 in SOD1 G93A mice led to a decrease in cleaved caspase-3 and cytosolic cytochrome c in the spinal cord [63], indicating that the inhibition of GSK3 may be neuroprotective in this disease model. Furthermore, treatment of SOD1 G93A with GSK-3 inhibitors reduced markers of inflammation in the spinal cord [63], suggesting a reduction in glial reactivity.

Reduction in oxidative stress and inflammation

Another hallmark of ALS is chronic neuronal exposure to oxidative stress and inflammation and thus several treatment strategies are focused on the reduction of these cellular pathologies. One mechanism to reduce oxidative stress in neurons is to upregulate signaling through the NF-E2-related factor 2/antioxidant response element (Nrf2/ARE) pathway, which is responsible for the upregulation of antioxidant and prosurvival genes. Neymotin et al. [64] tested two related compounds, 2-cyano-3,12-dioxoolean-1,9-dien-28-oic acid-ethylamide (CDDO-EA, **28**, Figure 13) and CDDO-trifluoroethylamide (CDDO-TFEA, **29**), synthetic triterpenoid analogues derived from oleanolic acid [64] for their ability to activate Nrf2/ARE signaling in cell culture and mouse models of ALS. NSC-34 cells expressing SOD1 G93A were treated with **29** and activation of Nrf2 was tested. In response to treatment, the expression of Nrf2 and the Nrf2 regulated genes, NQO-1 (NAD(P)H quinine oxidoreductase), HO-1 (heme oxygenase-1), and glutathione reductase

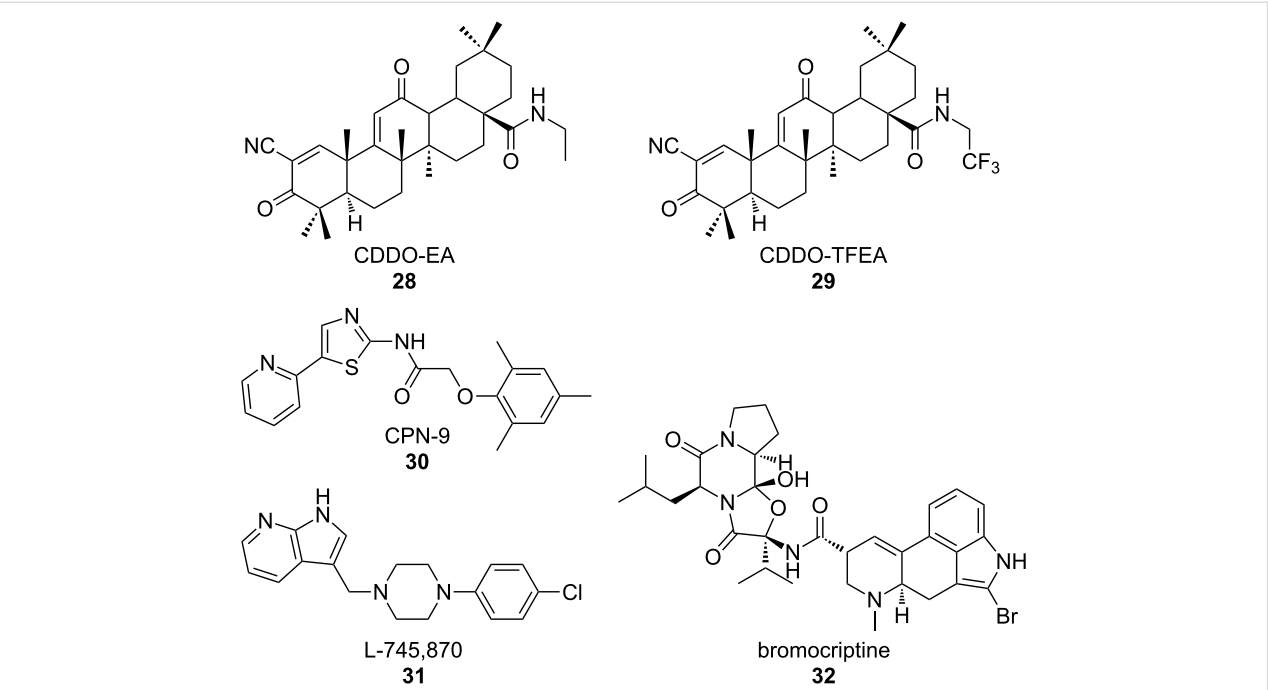


Figure 13: Compounds developed to reduce oxidative stress and inflammation.

were significantly increased. Furthermore, primary rat neurons treated with **29** displayed an increased nuclear translocation of Nrf2 [64]. Oral treatment of transgenic SOD1 G93A mice with either **28** or **29** resulted in an increase in Nrf2 expression and nuclear localization. The levels of Nrf2-regulated antioxidant genes were also elevated in the spinal cords of treated mice as analyzed by RT-PCR. Importantly, treatment of SOD1 G93A mice with **28** or **29** resulted in reduced weight loss, decreased motor decline and increased lifespan [64].

Using a virtual screening system to discover oxidative-stress-reducing agents, Kanno et al. [65] identified a small molecule, *N*-(5-(2-pyridyl)(1,3-thiazol-2-yl))-2-(2,4,6-trimethylphenoxy)acetamide, termed CPN-9 (**30**). Compound **30** was initially tested for protection against pharmacologically induced oxidative stress and was determined to be highly cytoprotective in HeLa cells. When tested against a variety of cell-stress inducers, **30** only protected against cellular death induced by oxidative-stress pathways [65]. To determine the mechanism by which **30** selectively protects against oxidative damage, the expression of stress-activated proteins HO-1 and p21/CDKN1A was tested. Both stress-induced proteins showed increased expression, and activation of the Nrf2 transcription factor also increased. Compound **30** was demonstrated to induce ARE promoter activity in SH-SY5Y cells by using a luciferase reporter assay [65]. These data demonstrate that **30** confers resistance to oxidative stress by upregulation of the Nrf2/ARE transcriptional pathway.

Due to its success at inhibiting cellular death in cultured cells, **30** was then tested in transgenic mice expressing the hSOD1 H46R mutant gene. Following chronic administration of **30** following symptom onset, disease progression was attenuated as determined by feet clasping and rearing behavior. Mice treated with **30** performed better in functional assays, including rotarod testing and footprint analysis where treated animals showed reduced gait abnormalities. Furthermore, treatment with CPN-9 diminished motor neuron loss in the spinal cord and extended survival following disease onset [65].

Further studies aimed at reducing oxidative stress in ALS models were performed by Tanaka et al. [66], who utilized a dopamine D4 receptor antagonist, L-745,870 (**31**), to selectively inhibit oxidative-stress-induced cell death. Compound **31** was previously determined to upregulate neuronal apoptosis inhibitory protein (NAIP/BIRC1), a cytoprotective protein that ameliorates oxidative-stress-induced cellular death [67]. Intragastric administration of **31** to SOD1 H46R mice, prior to symptom onset, was discovered to delay symptom onset as determined by limb movement, rearing activity, and foot clasping behaviors. Additionally, treatment with **31** delayed weight loss and motor dysfunction as examined by a balance-beam test. Spinal-cord tissue from treated and untreated SOD1 H46R mice was examined for motor-neuron loss and markers of microglial activation. Treated animals displayed reduction in both loss of neurons as well as decreased activation of microglial cells [66]. Additionally, SOD1 H46R mice were

treated with **31** following the presentation of disease symptoms. Mice treated with **30** exhibited prolonged survival rates as compared to untreated animals [66].

Additional work from this group identified the dopamine D2 receptor agonist, bromocriptine (**32**), as an NAIP upregulating compound that reduced oxidative stress through the upregulation of antioxidant proteins, such as activating transcription factor 3 (ATF3) and HO-1 [68]. In vivo studies where **32** was administered to SOD1 H46R mice following symptom presentation revealed that **32** delayed disease progression as determined by feet clasping and rearing behaviors as well as improved motor function as analyzed by the balance-beam test, vertical pole test, and footprint analysis. Furthermore, treatment with **32** prolonged the post-onset survival of SOD1 H46R animals [68]. These studies indicate that the attenuation of oxidative-stress pathways through the upregulation of antioxidant genes can reduce disease progression in ALS models.

Novel mechanisms

Histone deacetylase (HDAC) inhibitors: Several gene analysis studies have discovered distinct gene expression profiles in ALS patients [69,70], indicating that transcriptional dysfunction may contribute to ALS pathology [71]. One mechanism of eliciting changes in gene expression is through the acetylation of histone proteins, which allows access of gene sequences to transcriptional complexes. SOD1 G93A mice have markedly reduced histone acetylation following disease onset as compared to control animals [71,72], supporting a role for aberrant transcriptional activity in disease progression. Consequently, histone deacetylase (HDAC) inhibitors were tested in ALS mouse models [71,72]. Ryu et al. [71] treated SOD1 G93A mice with 400 mg/kg sodium 4-phenylbutyrate (PBA, **33**, Figure 14) by i.p. injection both prior to, and following, disease onset. Treated animals displayed increased performance on rotarod tests, improved stride length, and extended lifespan as compared to untreated animals [71]. Furthermore, astrogliosis and neuron loss in the lumbar spinal cord were attenuated with drug treatment [71], indicating that inhibition of HDACs was neuroprotective in ALS models.

Yoo et al. [72] obtained similar results using the HDAC inhibitor trichostatin A (**34**). Compound **34** was injected intraperitoneally at 1 mg/kg, 5 days a week following symptom onset in SOD1 G93A mice that had been crossed with a mouse line expressing yellow fluorescent protein (YFP) under the Thy1 promoter. These mice express YFP in motor neurons, allowing for innervation at neuromuscular junctions (NMJ) to be analyzed. Treatment with **34** increased histone acetylation in the spinal cord and skeletal muscle of SOD1 G93A mice, which corresponded with reduced motor neuron death and gliosis in the spinal cord of these animals [72]. Additionally, NMJ innervation was improved in mice treated with **34**. Behavioral testing demonstrated that rotarod performance and grip strength were improved in treated animals. Compound **34** also modestly prolonged lifespan [72].

Glial mitochondrial function: Although ALS is characterized by motor neuron degeneration and death, glial cells have been demonstrated to play essential roles in disease pathogenesis [73]. Inhibition of SOD1 G93A expression specifically in astrocytes increased survival in mice carrying the SOD1 G93A mutation [74], indicating the importance of glial cells to ALS progression. SOD1 mutations in astrocytes promote decreased mitochondrial function [75], an aberrant phenotype, and neurotoxicity [76]. Dichloroacetate (DCA, **35**), a compound which inhibits the pyruvate dehydrogenase enzyme, modulates mitochondrial activity [75]. Miquel et al. [75], treated SOD1 G93A mice with **35** added at 500 mg/L to their drinking water. This

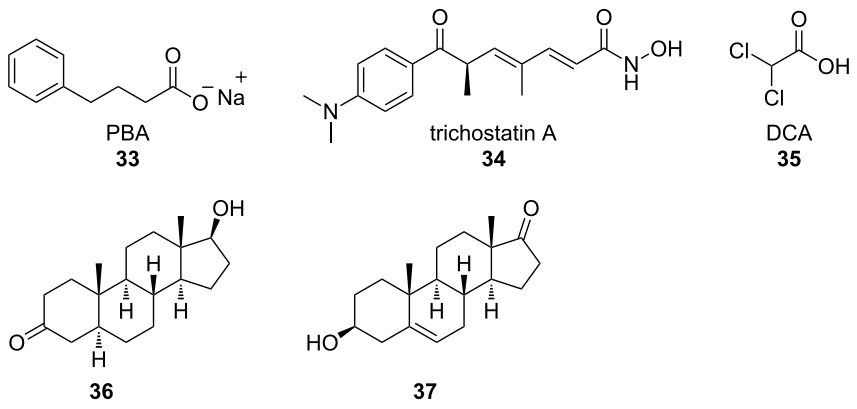


Figure 14: Probes used to elucidate the roles of distinct gene-expression profiles in ALS patients.

treatment reduced astrocyte reactivity and motor neuron death, as well as prolonged the lifespan of the treated animals by two weeks.

Steroid treatment: Dihydrotestosterone (DHT, **36**) treatment increases muscle mass and has been demonstrated to be neuroprotective [77]. Chronic diseases, such as ALS, which display muscle wasting may benefit from androgen treatment. To determine whether DHT treatment can ameliorate symptoms in an ALS mouse model, Yoo et al. [77] subcutaneously inserted a silastic tube containing **36** into SOD1 G93A mutant male mice at postnatal day 75. Weight and area of the gastrocnemius (GN) and tibialis anterior (TA) muscles were taken at postnatal day 120. SOD1 G93A mice treated with DHT exhibited a 32% increase in weight of the GN muscle and a 43% increase in TA muscle as compared to untreated controls [77]. Additionally, orchidectomized SOD1 G93A mice were evaluated and it was discovered that the reduced androgen concentrations in these animals exacerbated the loss in muscle weight. Cross-sectional area measurement of the GN and TA muscle displayed similar results. Compound **36**-treated SOD1 G93A mice also displayed increased muscle strength compared with untreated or orchidectomized SOD1 G93A mice, as analyzed by a grip-strength meter [77]. Interestingly, treatment with **36** increases the levels of insulin-like growth factor (IGF) 1 and 2, which induces myoblast growth and differentiation, while concomitantly decreasing the expression of muscle RING finger 1 (MuRF-1), a protein that can induce muscle atrophy [77]. The upregulation of IGF-1 and -2 and downregulation of MuRF-1 corresponded with modest increases in performance in functional tests, including the rotarod test and gait analyses. Furthermore, axonal loss and motor neuron death were slightly decreased in DHT-treated SOD1 G93A animals compared with controls [77].

However, a conflicting study has found that androgens have little effect on ALS mouse models [78]. SOD1 G93A transgenic rats were gonadectomized or treated with a neurosteroid, dehydroepiandrosterone (DHEA, **37**) prior to symptom onset. Disease progression, symptom onset, and lifespan were not affected by either **37** treatment or gonadectomy, suggesting that steroids have little effect on ALS disease pathology [78]. These conflicting results may be explained by the specific compounds that were used or the analyses that were performed. Interestingly, these studies employed different rodent models, with females being present in the DHEA study, while the DHT study was done exclusively with males. Sexual dimorphism has been previously reported in animal models of ALS, with males and females displaying differences in symptom onset and progression [78]. In ALS patients, women have fewer reported cases than men [78] suggesting that this sexual dimorphism may be replicated in humans.

Conclusion

ALS is a complex disorder that is characterized by multiple cellular pathologies including glutamate excitotoxicity, protein aggregation, ER stress, trophic factor deregulation, oxidative stress, inflammation, and mitochondrial dysfunction. Although some cases of ALS can be attributed to known gene mutations, the cause of ALS remains largely undefined. Therefore, current treatment strategies for ALS involve the targeting of specific cellular dysfunctions.

As mutations in the SOD1 gene have been identified in 20% of fALS patients, the creation of small molecules that specifically target SOD1 has become a popular strategy for drug development. Unfortunately, due to the relatively small patient population with these specific mutations, this strategy alone may not have a large impact on ALS disease treatment. However, several new studies have focused on the prevention or reduction of SOD1 or TDP-43 aggregation. These studies may have broad applications, as mutations that lead to improper protein aggregation are a common feature in many neurological disorders including ALS [79], Charcot Marie Tooth disease [80], Alzheimer's disease [81], and Huntington's disease [82]. The discovery of small molecules that prevent or clear protein aggregates may prove to be valuable for the treatment of multiple disorders.

Another common strategy for the treatment of ALS is the use of compounds that elicit neuroprotection, either by upregulating molecules that promote neuronal survival or by antagonizing cellular pathways that result in neuronal death. While several of these compounds have shown promising results in SOD1 mutant animal models, it remains to be seen whether these strategies will prove effective in long-term human treatment where neurons may be exposed to multiple cellular insults.

Although progress has been made towards the development of improved ALS treatments, including several compounds in phase III clinical trials, it remains to be seen whether these treatments will prove to be efficacious in ALS patients. Various screening approaches and targeted drug design, as outlined in this review, have identified a number of small molecules that will prove useful in the discovery and validation of novel cellular targets for the treatment of ALS (Figure 15). Figure 15 illustrates the specific cellular target of each compound discussed in this review. Additionally, Table 1 in the supporting information lists each chemical structure, name, reference, and mechanism of action. Future studies toward these targets will begin to provide the necessary proof-of-concept for these alternative therapeutic approaches, lead to a greater understanding of the pathogenesis of ALS, and may lead to novel therapeutics with improved efficacy in ALS.

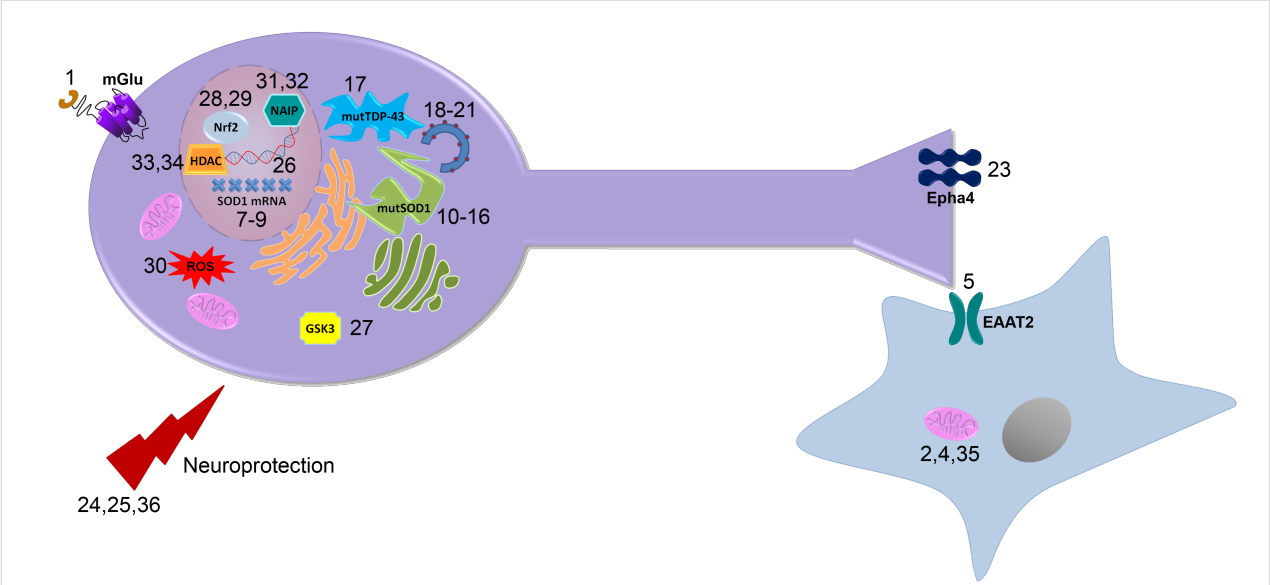


Figure 15: Targets of potential therapeutics: This diagram illustrates the physiological targets of each compound discussed in the review and how these compounds are believed to function in vivo.

Supporting Information

Supporting information features a table of each compound discussed in the review. This table contains the chemical structure, name, references and mechanism of action.

Supporting Information File 1

Table of compounds.
[http://www.beilstein-journals.org/bjoc/content/supplementary/1860-5397-9-82-S1.xls]

Acknowledgements

The authors would like to acknowledge financial support from the Department of Defense through grant number W81XWH-12-1-0373 awarded to NDPC. The authors also acknowledge Douglas Sheffler for assistance with the design of the graphical abstract and Figure 15.

References

1. Pratt, A. J.; Getzoff, E. D.; Perry, J. J. *Degener. Neurol. Neuromuscul. Dis.* **2012,** *2012,* 1–14. doi:10.2147/DNND.S19803
2. Rosen, D. R.; Siddique, T.; Patterson, D.; Figlewicz, D. A.; Sapp, P.; Hentati, A.; Donaldson, D.; Goto, J.; O'Regan, J. P.; Deng, H.-X.; Rahmani, Z.; Krizus, A.; McKenna-Yasek, D.; Cayabyab, A.; Gaston, S. M.; Berger, R.; Tanzi, R. E.; Halperin, J. J.; Herzfeldt, B.; Van den Bergh, R.; Hung, W.-Y.; Bird, T.; Deng, G.; Mulder, D. W.; Smyth, C.; Laing, N. G.; Soriano, E.; Pericak–Vance, M. A.; Haines, J.; Rouleau, G. A.; Gusella, J. S.; Horvitz, H. R.; Brown, R. H., Jr. *Nature* **1993,** *362,* 59–62. doi:10.1038/362059a0
3. Glicksman, M. A. *Expert Opin. Drug Discov.* **2011,** *6,* 1127–1138. doi:10.1517/17460441.2011.628654
4. Contestabile, A. *Curr. Med. Chem.* **2011,** *18,* 5655–5665. doi:10.2174/092986711798347289
5. Dunkel, P.; Chai, C. L. L.; Sperlágh, B.; Huleatt, P. B.; Mátyus, P. *Expert Opin. Invest. Drugs* **2012,** *21,* 1267–1308. doi:10.1517/13543784.2012.703178
6. Colton, C. K.; Kong, Q.; Lai, L.; Zhu, M. X.; Seyb, K. I.; Cuny, G. D.; Xian, J.; Glicksman, M. A.; Glenn Lin, C.-L. *J. Biomol. Screen* **2010,** *15,* 653–662. doi:10.1177/1087057110370998
7. Gurney, M. E.; Pu, H.; Chiu, A. Y.; Dal Canto, M. C.; Polchow, C. Y.; Alexander, D. D.; Caliendo, J.; Hentati, A.; Kwon, Y. W.; Deng, H.-X.; Chen, W.; Zhai, P.; Sufit, R. L.; Siddique, T. *Science* **1994,** *264,* 1772–1775. doi:10.1126/science.8209258
8. Van Den Bosch, L. *J. Biomed. Biotechnol.* **2011,** *2011,* 348765. doi:10.1155/2011/348765
9. Groeneveld, G. J.; van Kan, H. J. M.; Sastre Toraño, J.; Veldink, J. H.; Guchelaar, H.-J.; Wokke, J. H. J.; van den Berg, L. H. *J. Neurol. Sci.* **2001,** *191,* 121–125. doi:10.1016/S0022-510X(01)00613-X
10. van Kan, H. J. M.; Groeneveld, G. J.; Kalmijn, S.; Spieksma, M.; van den Berg, L. H.; Guchelaar, H. J. *Br. J. Clin. Pharmacol.* **2005,** *59,* 310–313. doi:10.1111/j.1365-2125.2004.02233.x
11. McDonnell, M. E.; Vera, M. D.; Blass, B. E.; Pelletier, J. C.; King, R. C.; Fernandez-Metzler, C.; Smith, G. R.; Wrobel, J.; Chen, S.; Wall, B. A.; Reitz, A. B. *Bioorg. Med. Chem.* **2012,** *20,* 5642–5648. doi:10.1016/j.bmc.2012.07.004
12. Cheah, B. C.; Vucic, S.; Krishnan, A. V.; Kiernan, M. C. *Curr. Med. Chem.* **2010,** *17,* 1942–1959. doi:10.2174/092986710791163939
13. Rothstein, J. D.; Tsai, G.; Kuncl, R. W.; Clawson, L.; Cornblath, D. R.; Drachman, D. B.; Pestronk, A.; Stauch, B. L.; Coyle, J. T. *Ann. Neurol.* **1990,** *28,* 18–25. doi:10.1002/ana.410280106
14. Rothstein, J. D.; Van Kammen, M.; Levey, A. I.; Martin, L. J.; Kuncl, R. W. *Ann. Neurol.* **1995,** *38,* 73–84. doi:10.1002/ana.410380114

15. Danbolt, N. C. *Prog. Neurobiol.* **2001,** *65,* 1–105. doi:10.1016/S0301-0082(00)00067-8
16. Xing, X.; Chang, L.-C.; Kong, Q.; Colton, C. K.; Lai, L.; Glicksman, M. A.; Lin, C.-L. G.; Cuny, G. D. *Bioorg. Med. Chem. Lett.* **2011,** *21,* 5774–5777. doi:10.1016/j.bmcl.2011.08.009
17. Sasabe, J.; Chiba, T.; Yamada, M.; Okamoto, K.; Nishimoto, I.; Matsuoka, M.; Aiso, S. *EMBO J.* **2007,** *26,* 4149–4159. doi:10.1038/sj.emboj.7601840
18. Sasabe, J.; Miyoshi, Y.; Suzuki, M.; Mita, M.; Konno, R.; Matsuoka, M.; Hamase, K.; Aiso, S. *Proc. Natl. Acad. Sci. U. S. A.* **2012,** *109,* 627–632. doi:10.1073/pnas.1114639109
19. Mitchell, J.; Paul, P.; Chen, H.-J.; Morris, A.; Payling, M.; Falchi, M.; Habgood, J.; Panoutsou, S.; Winkler, S.; Tisato, V.; Hajitou, A.; Smith, B.; Vance, C.; Shaw, C.; Mazarakis, N. D.; de Belleroche, J. *Proc. Natl. Acad. Sci. U. S. A.* **2010,** *107,* 7556–7561. doi:10.1073/pnas.0914128107
20. Paul, P.; de Belleroche, J. *Amino Acids* **2012,** *43,* 1823–1831. doi:10.1007/s00726-012-1385-9
21. Aronica, E.; Catania, M. V.; Geurts, J.; Yankaya, B.; Troost, D. *Neuroscience* **2001,** *105,* 509–520. doi:10.1016/S0306-4522(01)00181-6
22. Poulopoulou, C.; Davaki, P.; Koliaraki, V.; Kolovou, D.; Markakis, I.; Vassilopoulos, D. *Ann. Neurol.* **2005,** *58,* 946–949. doi:10.1002/ana.20675
23. Reaume, A. G.; Elliott, J. L.; Hoffman, E. K.; Kowall, N. W.; Ferrante, R. J.; Siwek, D. F.; Wilcox, H. M.; Flood, D. G.; Beal, M. F.; Brown, R. H., Jr.; Scott, R. W.; Snider, W. D. *Nat. Genet.* **1996,** *13,* 43–47. doi:10.1038/ng0596-43
24. Murakami, G.; Inoue, H.; Tsukita, K.; Asai, Y.; Amagai, Y.; Aiba, K.; Shimogawa, H.; Uesugi, M.; Nakatsuji, N.; Takahashi, R. J. *Biomol. Screen.* **2011,** *16,* 405–414. doi:10.1177/1087057110397888
25. Wright, P. D.; Wightman, N.; Huang, M.; Weiss, A.; Sapp, P. C.; Cuny, G. D.; Ivinson, A. J.; Glicksman, M. A.; Ferrante, R. J.; Matson, W.; Matson, S.; Brown, R. H., Jr. *Front. Biosci., Elite Ed.* **2012,** *4,* 2801–2808. doi:10.2741/E584
26. Lange, D. J.; Andersen, P. M.; Remanan, R.; Marklund, S.; Benjamin, D. *Amyotroph. Lateral Scler.* **2013,** *14,* 199–204. doi:10.3109/17482968.2012.724074
27. Wright, P. D.; Huang, M.; Weiss, A.; Matthews, J.; Wightman, N.; Glicksman, M.; Brown, R. H., Jr. *Neurosci. Lett.* **2010,** *482,* 188–192. doi:10.1016/j.neulet.2010.07.020
28. Benmohamed, R.; Arvanites, A. C.; Kim, J.; Ferrante, R. J.; Silverman, R. B.; Morimoto, R. I.; Kirsch, D. R. *Amyotroph. Lateral Scler.* **2011,** *12,* 87–96. doi:10.3109/17482968.2010.522586
29. Matsumoto, G.; Stojanovic, A.; Holmberg, C. I.; Kim, S.; Morimoto, R. I. *J. Cell Biol.* **2005,** *171,* 75–85. doi:10.1083/jcb.200504050
30. Chen, T.; Benmohamed, R.; Arvanites, A. C.; Ralay Ranaivo, H.; Morimoto, R. I.; Ferrante, R. J.; Watterson, D. M.; Kirsch, D. R.; Silverman, R. B. *Bioorg. Med. Chem.* **2011,** *19,* 613–622. doi:10.1016/j.bmc.2010.10.052
31. Chen, T.; Benmohamed, R.; Kim, J.; Smith, K.; Amante, D.; Morimoto, R. I.; Kirsch, D. R.; Ferrante, R. J.; Silverman, R. B. *J. Med. Chem.* **2012,** *55,* 515–527. doi:10.1021/jm2014277
32. Trippier, P. C.; Benmohammed, R.; Kirsch, D. R.; Silverman, R. B. *Bioorg. Med. Chem. Lett.* **2012,** *22,* 6647–6650. doi:10.1016/j.bmcl.2012.08.114
33. Zhang, W.; Benmohamed, R.; Arvanites, A. C.; Morimoto, R. I.; Ferrante, R. J.; Kirsch, D. R.; Silverman, R. B. *Bioorg. Med. Chem.* **2012,** *20,* 1029–1045. doi:10.1016/j.bmc.2011.11.039
34. Zhang, Y.; Benmohamed, R.; Zhang, W.; Kim, J.; Edgerly, C. K.; Zhu, Y.; Morimoto, R. I.; Ferrante, R. J.; Kirsch, D. R.; Silverman, R. B. *Med. Chem. Lett.* **2012,** *3,* 584–587. doi:10.1021/ml3000963
35. Xia, G.; Benmohamed, R.; Kim, J.; Arvanites, A. C.; Morimoto, R. I.; Ferrante, R. J.; Kirsch, D. R.; Silverman, R. B. *J. Med. Chem.* **2011,** *54,* 2409–2421. doi:10.1021/jm101549k
36. Ray, S. S.; Nowak, R. J.; Brown, R. H., Jr.; Lansbury, P. T., Jr. *Proc. Natl. Acad. Sci. U. S. A.* **2005,** *102,* 3639–3644. doi:10.1073/pnas.0408277102
37. Nowak, R. J.; Cuny, G. D.; Choi, S.; Lansbury, P. T.; Ray, S. S. *J. Med. Chem.* **2010,** *53,* 2709–2718. doi:10.1021/jm901062p
38. Parker, S. J.; Meyerowitz, J.; James, J. L.; Liddell, J. R.; Nonaka, T.; Hasegawa, M.; Kanninen, K. M.; Lim, S.; Paterson, B. M.; Donnelly, P. S.; Crouch, P. J.; White, A. R. *PLoS One* **2012,** *7,* e42277. doi:10.1371/journal.pone.0042277
39. Kwong, L. K.; Neumann, M.; Sampathu, D. M.; Lee, V. M.-Y.; Trojanowski, J. Q. *Acta Neuropathol.* **2007,** *114,* 63–70. doi:10.1007/s00401-007-0226-5
40. Liu-Yesucevitz, L.; Bilgutay, A.; Zhang, Y.-J.; Vanderweyde, T.; Citro, A.; Mehta, T.; Zaarur, N.; McKee, A.; Bowser, R.; Sherman, M.; Petrucelli, L.; Wolozin, B. *PLoS One* **2010,** *5,* e13250. doi:10.1371/journal.pone.0013250
41. Neumann, M.; Sampathu, D. M.; Kwong, L. K.; Truax, A. C.; Micsenyi, M. C.; Chou, T. T.; Bruce, J.; Schuck, T.; Grossman, M.; Clark, C. M.; McCluskey, L. F.; Miller, B. L.; Masliah, E.; Mackenzie, I. R.; Feldman, H.; Feiden, W.; Kretzschmar, H. A.; Trojanowski, J. Q.; Lee, V. M.-Y. *Science* **2006,** *314,* 130–133. doi:10.1126/science.1134108
42. Cassel, J. A.; Blass, B. E.; Reitz, A. B.; Pawlyk, A. C. *J. Biomol. Screen.* **2010,** *15,* 1099–1106. doi:10.1177/1087057110382778
43. Cassel, J. A.; McDonnell, M. E.; Velvadapu, V.; Andrianov, V.; Reitz, A. B. *Biochimie* **2012,** *94,* 1974–1981. doi:10.1016/j.biochi.2012.05.020
44. Suzuki, H.; Lee, K.; Matsuoka, M. *J. Biol. Chem.* **2011,** *286,* 13171–13183. doi:10.1074/jbc.M110.197483
45. Kim, S. H.; Shanware, N. P.; Bowler, M. J.; Tibbetts, R. S. *J. Biol. Chem.* **2010,** *285,* 34097–34105. doi:10.1074/jbc.M110.154831
46. Bose, J. K.; Huang, C.-C.; Shen, C.-K. *J. Biol. Chem.* **2011,** *286,* 44441–44448. doi:10.1074/jbc.M111.237115
47. Bica, L.; Crouch, P. J.; Cappai, R.; White, A. R. *Mol. BioSyst.* **2009,** *5,* 134–142. doi:10.1039/b816577g
48. Wang, I.-F.; Guo, B.-S.; Liu, Y.-C.; Wu, C.-C.; Yang, C.-H.; Tsai, K.-J.; Shen, C.-K. J. *Proc. Natl. Acad. Sci. U. S. A.* **2012,** *109,* 15024–15029. doi:10.1073/pnas.1206362109
49. Shimazawa, M.; Tanaka, H.; Ito, Y.; Morimoto, N.; Tsuruma, K.; Kadokura, M.; Tamura, S.; Inoue, T.; Yamada, M.; Takahashi, H.; Warita, H.; Aoki, M.; Hara, H. *PLoS One* **2010,** *5,* e15307. doi:10.1371/journal.pone.0015307
50. Zhao, Z.; Lange, D. J.; Ho, L.; Bonini, S.; Shao, B.; Salton, S. R.; Thomas, S.; Pasinetti, G. M. *Int. J. Med. Sci.* **2008,** *5,* 92–99. doi:10.7150/ijms.5.92
51. Van Hoecke, A.; Schoonaert, L.; Lemmens, R.; Timmers, M.; Staats, K. A.; Laird, A. S.; Peeters, E.; Philips, T.; Goris, A.; Dubois, B.; Andersen, P. M.; Al-Chalabi, A.; Thijs, V.; Turnley, A. M.; van Vught, P. W.; Veldink, J. H.; Hardiman, O.; Van Den Bosch, L.; Gonzalez-Perez, P.; Van Damme, P.; Brown, R. H., Jr.; van den Berg, L. H.; Robberecht, W. *Nat. Med.* **2012,** *18,* 1418–1422. doi:10.1038/nm.2901
52. Klein, R. *Nat. Neurosci.* **2009,** *12,* 15–20. doi:10.1038/nn.2231

53. Pieper, A. A.; Xie, S.; Capota, E.; Estill, S. J.; Zhong, J.; Long, J. M.; Becker, G. L.; Huntington, P.; Goldman, S. E.; Shen, C.-H.; Capota, M.; Britt, J. K.; Kotti, T.; Ure, K.; Brat, D. J.; Williams, N. S.; MacMillan, K. S.; Naidoo, J.; Melito, L.; Hsieh, J.; De Brabander, J.; Ready, J. M.; McKnight, S. L. *Cell* **2010,** *142,* 39–51. doi:10.1016/j.cell.2010.06.018
54. Tesla, R.; Wolf, H. P.; Xu, P.; Drawbridge, J.; Estill, S. J.; Huntington, P.; McDaniel, L.; Knobbe, W.; Burket, A.; Tran, S.; Starwalt, R.; Morlock, L.; Naidoo, J.; Williams, N. S.; Ready, J. M.; McKnight, S. L.; Pieper, A. A. *Proc. Natl. Acad. Sci. U. S. A.* **2012,** *109,* 17016–17021. doi:10.1073/pnas.1213960109
55. Feng, X.; Peng, Y.; Liu, M.; Cui, L. *Neuropharmacology* **2012,** *62,* 1004–1010. doi:10.1016/j.neuropharm.2011.10.009
56. Eitan, E.; Tichon, A.; Gazit, A.; Gitler, D.; Slavin, S.; Priel, E. *EMBO Mol. Med.* **2012,** *4,* 313–329. doi:10.1002/emmm.201200212
57. Klapper, W.; Parwaresch, R.; Krupp, G. *Mech. Ageing Dev.* **2001,** *122,* 695–712. doi:10.1016/S0047-6374(01)00223-8
58. Caporaso, G. L.; Lim, D. A.; Alvarez-Buylla, A.; Chao, M. V. *Mol. Cell. Neurosci.* **2003,** *23,* 693–702. doi:10.1016/S1044-7431(03)00103-9
59. Lee, J.; Jo, Y. S.; Sung, Y. H.; Hwang, I. K.; Kim, H.; Kim, S.-Y.; Yi, S. S.; Choi, J.-S.; Sun, W.; Seong, J. K.; Lee, H.-W. *Neurochem. Res.* **2010,** *35,* 211–218. doi:10.1007/s11064-009-0044-3
60. Lee, J.; Sung, Y. H.; Cheong, C.; Choi, Y. S.; Jeon, H. K.; Sun, W.; Hahn, W. C.; Ishikawa, F.; Lee, H.-W. *Oncogene* **2008,** *27,* 3754–3760. doi:10.1038/sj.onc.1211037
61. Hu, J.-H.; Zhang, H.; Wagey, R.; Krieger, C.; Pelech, S. L. *J. Neurochem.* **2003,** *85,* 432–442. doi:10.1046/j.1471-4159.2003.01670.x
62. Koh, S.-H.; Lee, Y.-B.; Kim, K. S.; Kim, H.-J.; Kim, M.; Lee, Y. J.; Kim, J.; Lee, K. W.; Kim, S. H. *Eur. J. Neurosci.* **2005,** *22,* 301–309. doi:10.1111/j.1460-9568.2005.04191.x
63. Koh, S.-H.; Kim, Y.; Kim, H. Y.; Hwang, S.; Lee, C. H.; Kim, S. H. *Exp. Neurol.* **2007,** *205,* 336–346. doi:10.1016/j.expneurol.2007.03.004
64. Neymotin, A.; Calingasan, N. Y.; Wille, E.; Naseri, N.; Petri, S.; Damiano, M.; Liby, K. T.; Risingsong, R.; Sporn, M.; Beal, M. F.; Kiaei, M. *Free Radical Biol. Med.* **2011,** *51,* 88–96. doi:10.1016/j.freeradbiomed.2011.03.027
65. Kanno, T.; Tanaka, K.; Yanagisawa, Y.; Yasutake, K.; Hadano, S.; Yoshii, F.; Hirayama, N.; Ikeda, J.-E. *Free Radical Biol. Med.* **2012,** *53,* 2028–2042. doi:10.1016/j.freeradbiomed.2012.09.010
66. Tanaka, K.; Okada, Y.; Kanno, T.; Otomo, A.; Yanagisawa, Y.; Shouguchi-Miyata, J.; Suga, E.; Kohiki, E.; Onoe, K.; Osuga, H.; Aoki, M.; Hadano, S.; Itoyama, Y.; Ikeda, J.-E. *Exp. Neurol.* **2008,** *211,* 378–386. doi:10.1016/j.expneurol.2008.02.004
67. Okada, Y.; Sakai, H.; Kohiki, E.; Suga, E.; Yanagisawa, Y.; Tanaka, K.; Hadano, S.; Osuga, H.; Ikeda, J.-E. *J. Cereb. Blood Flow. Metab.* **2005,** *25,* 794–806. doi:10.1038/sj.jcbfm.9600078
68. Tanaka, K.; Kanno, T.; Yanagisawa, Y.; Yasutake, K.; Hadano, S.; Yoshii, F.; Ikeda, J.-E. *Exp. Neurol.* **2011,** *232,* 41–52. doi:10.1016/j.expneurol.2011.08.001
69. Malaspina, A.; Kaushik, N.; de Belleroche, J. *J. Neurochem.* **2001,** *77,* 132–145. doi:10.1046/j.1471-4159.2001.00231.x
70. Ishigaki, S.; Niwa, J.-i.; Ando, Y.; Yoshihara, T.; Sawada, K.-i.; Doyu, M.; Yamamoto, M.; Kato, K.; Yotsumoto, Y.; Sobue, G. *FEBS Lett.* **2002,** *531,* 354–358. doi:10.1016/S0014-5793(02)03546-9
71. Ryu, H.; Smith, K.; Camelo, S. I.; Carreras, I.; Lee, J.; Iglesias, A. H.; Dangond, F.; Cormier, K. A.; Cudkowicz, M. E.; Brown, R. H., Jr.; Ferrante, R. J. *J. Neurochem.* **2005,** *93,* 1087–1098. doi:10.1111/j.1471-4159.2005.03077.x
72. Yoo, Y.-E.; Ko, C.-P. *Exp. Neurol.* **2011,** *231,* 147–159. doi:10.1016/j.expneurol.2011.06.003
73. Boillée, S.; Vande Velde, C.; Cleveland, D. W. *Neuron* **2006,** *52,* 39–59. doi:10.1016/j.neuron.2006.09.018
74. Yamanaka, K.; Chun, S. J.; Boillee, S.; Fujimori-Tonou, N.; Yamashita, H.; Gutmann, D. H.; Takahashi, R.; Misawa, H.; Cleveland, D. W. *Nat. Neurosci.* **2008,** *11,* 251–253. doi:10.1038/nn2047
75. Miquel, E.; Cassina, A.; Martínez-Palma, L.; Bolatto, C.; Trías, E.; Gandelman, M.; Radi, R.; Barbeito, L.; Cassina, P. *PLoS One* **2012,** *7,* e34776. doi:10.1371/journal.pone.0034776
76. Díaz-Amarilla, P.; Olivera-Bravo, S.; Trias, E.; Cragnolini, A.; Martínez-Palma, L.; Cassina, P.; Beckman, J.; Barbeito, L. *Proc. Natl. Acad. Sci. U. S. A.* **2011,** *108,* 18126–18131. doi:10.1073/pnas.1110689108
77. Yoo, Y.-E.; Ko, C.-P. *PLoS One* **2012,** *7,* e37258. doi:10.1371/journal.pone.0037258
78. Hayes-Punzo, A.; Mulcrone, P.; Meyer, M.; McHugh, J.; Svendsen, C. N.; Suzuki, M. *Amyotroph. Lateral Scler.* **2012,** *13,* 311–314. doi:10.3109/17482968.2012.654393
79. Bendotti, C.; Marino, M.; Cheroni, C.; Fontana, E.; Crippa, V.; Poletti, A.; De Biasi, S. *Prog. Neurobiol.* **2012,** *97,* 101–126. doi:10.1016/j.pneurobio.2011.10.001
80. Niemann, A.; Berger, P.; Suter, U. *NeuroMol. Med.* **2006,** *8,* 217–241. doi:10.1385/NMM:8:1:217
81. Cavallucci, V.; D'Amelio, M.; Cecconi, F. *Mol. Neurobiol.* **2012,** *45,* 366–378. doi:10.1007/s12035-012-8251-3
82. Zheng, Z.; Diamond, M. I. *Prog. Mol. Biol. Transl. Sci.* **2012,** *107,* 189–214. doi:10.1016/B978-0-12-385883-2.00010-2

License and Terms

This is an Open Access article under the terms of the Creative Commons Attribution License (http://creativecommons.org/licenses/by/2.0), which permits unrestricted use, distribution, and reproduction in any medium, provided the original work is properly cited.

The license is subject to the *Beilstein Journal of Organic Chemistry* terms and conditions: (http://www.beilstein-journals.org/bjoc)

The definitive version of this article is the electronic one which can be found at: doi:10.3762/bjoc.9.82

Beilstein Journal of Organic Chemistry

Synthesis and physicochemical characterization of novel phenotypic probes targeting the nuclear factor-kappa B signaling pathway

Paul M. Hershberger[1], Satyamaheshwar Peddibhotla[1], E. Hampton Sessions[1], Daniela B. Divlianska[1], Ricardo G. Correa[2], Anthony B. Pinkerton[2], John C. Reed[2] and Gregory P. Roth[*1]

Full Research Paper

Open Access

Address:
[1]Conrad Prebys Center for Chemical Genomics, Sanford-Burnham Medical Research Institute at Lake Nona, 6400 Sanger Road Orlando, FL 32827, USA and [2]Sanford-Burnham Medical Research Institute, 10901 North Torrey Pines Road, La Jolla, CA 92037, USA

Email:
Gregory P. Roth[*] - groth@sanfordburnham.org

* Corresponding author

Keywords:
ML029; ML130; ML146; ML236; ML237

Beilstein J. Org. Chem. **2013,** *9,* 900–907.
doi:10.3762/bjoc.9.103

Received: 16 January 2013
Accepted: 22 April 2013
Published: 08 May 2013

This article is part of the Thematic Series "Synthetic probes for the study of biological function".

Guest Editor: J. Aubé

© 2013 Hershberger et al; licensee Beilstein-Institut.
License and terms: see end of document.

Abstract

Activation of nuclear factor-kappa B (NF-κB) and related upstream signal transduction pathways have long been associated with the pathogenesis of a variety of inflammatory diseases and has recently been implicated in the onset of cancer. This report provides a synthetic and compound-based property summary of five pathway-related small-molecule chemical probes identified and optimized within the National Institutes of Health-Molecular Libraries Probe Center Network (NIH-MLPCN) initiative. The chemical probes discussed herein represent first-in-class, non-kinase-based modulators of the NF-κB signaling pathway, which were identified and optimized through either cellular phenotypic or specific protein-target-based screening strategies. Accordingly, the resulting new chemical probes may allow for better fundamental understanding of this highly complex biochemical signaling network and could advance future therapeutic translation toward the clinical setting.

Introduction

The Molecular Libraries Network was established in 2005 as an academic pilot-scale (MLSCN) screening effort for exploring potential new therapeutic targets stemming from the human genome project. After initial successes in high-throughput chemical screening (HTS), efforts in medicinal chemistry and exploratory pharmacology were added in order to leverage and advance the small-molecule compounds discovered within the HTS process. The program then advanced a broader probe-

production initiative (MLPCN) in 2008. This consortium resulted in the harnessing of chemical biology resources from four comprehensive centers and five specialty centers, which focused on either medicinal chemistry or a specific technical screening capability as an overall academic, collaborative scientific network [1]. In general terms, the overall vision and NIH mission encompasses the discovery of unique chemical tools that will be useful to interested scientific investigators to assist them with advancing basic in vitro and in vivo studies for testing new hypotheses in disease modulation.

Within this report, the outcomes of two Sanford-Burnham projects for chemical probe discovery are discussed, highlighting five examples of thematic small-molecule chemical probes discovered through our center's efforts. Within the realm of immunology and inflammation research, many cellular pathways leading to the activation of NF-κB family of transcription factors have been identified and several excellent reviews are available [2-5]. In general, these pathways have been shown to participate in host defense, immunity, and inflammation and even have implications in cancer. Thus, dysregulation of NF-κB activity contributes to numerous autoimmune and inflammatory disease states. With this, the availability of new chemical pathway probes will further enhance understanding of this complex network.

The first project encompassed the synthesis and characterization of three phenotypic probes designed to be selective modulators of the NF-κB signaling pathway in either human embryonic kidney (HEK) 293, HEK 293T or pre-B leukemia 697 cells. The second project focused on two probes that are target-oriented within the NF-κB pathway and are specific modulators of the intracellular signaling protein, nucleotide-binding oligomerization domain-1 (NOD1).

Within each project area first-in-class chemical probes were identified and characterized as new research-tool compounds. The synthetic routes for each probe, including their general physicochemical and pharmacological properties, are summarized in this report.

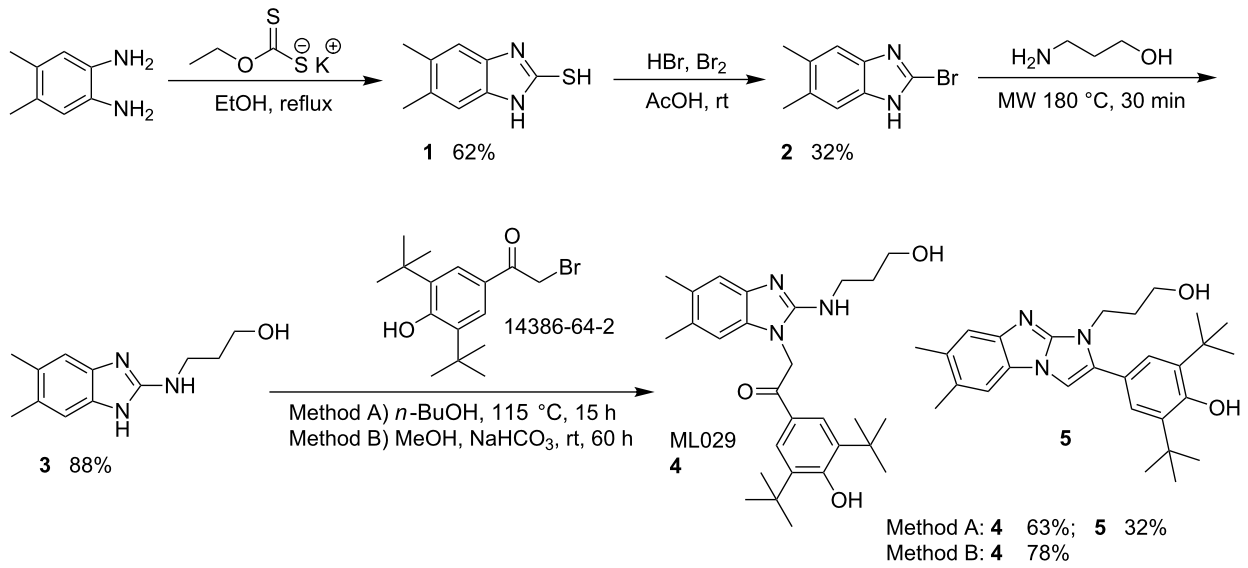
Results and Discussion

Phenotypic screening for noncanonical NF-κB pathway selective inhibitors of IL-8 production in HEK 293, HEK 293T (ML029) and 697 pre-B cells (ML236 and ML237): Most pathways for NF-κB activation converge on the IκB kinases (IKKs), and more than nine signaling routes have been identified [6]. While IKKs therefore represent attractive targets for drug discovery programs, the selectivity envisioned for an acceptable therapeutic index has remained elusive as inhibitors of IKKs indiscriminately suppress all known NF-κB activation pathways. Within this project, new probes were sought that were not active via the currently known receptor-driven pathways and IκB kinases, but attenuated NF-κB transcriptional activity as measured by a luciferase-based reporter gene assay with validation using a panel of known receptor and kinase-based counter screens [7].

Because activation of NF-κB is known to be initiated through protein kinase C (PKC), we hypothesized that selectivity could be possible by the fact that PKC activation occurs downstream from cell membrane antigen and growth-factor receptors yet is still upstream of IKKγ, potentially by inhibition of a new target protein or novel protein–protein interaction. Using cell-based HTS reporter gene assays, a series of chemical probes were identified that selectively inhibit this unique PKC-induced NF-κB pathway without modulating other NF-κB activation pathways such as those including the cytosolic proteins CARMA1, Bcl-10, MALT1, TRAF6 and Ubc13 [8].

The first probe identified within this series was the benzimidazole ML029 (**4**), which exhibited an IC_{50} of 0.07 μM in the HEK 293 cell assay with corresponding well-defined structure–activity relationships (SAR) through analogue synthesis [9]. This probe was discovered after two separate screening campaigns totaling ~110,000 compounds. At concentrations up to 8 μM, **4** failed to suppress PKCβ and PKCθ (the PKC family members implicated in TCR/BCR signaling) and IKKβ, while known PKC and IKK inhibitors and the broad-spectrum kinase inhibitor staurosporine afforded potent inhibition [9-11]. Further selectivity profiling revealed that **4** inhibited (>50% at 10 uM) only 3 out of the 353 kinases surveyed by using a KINOMEscan™ (DiscoveRx) platform. None of these 3 (TLK1 (70% inhibition), Raf (57%), and JAK2 (53%)) are relevant to NF-κB pathway regulation.

To prepare **4**, a synthetic route (Scheme 1) was optimized in a manner that allowed for the preparation of related analogues [9]. The intermediate **1** was prepared through condensation of 4,5-dimethylbenzene-1,2-diamine with potassium ethyl xanthate in ethanol under reflux. Bromination of **1** led to the key intermediate 2-bromo-5,6-dimethylbenzimidazole (**2**), which reacted smoothly with 3-aminopropanol to give the amine **3** in high yield and purity after extraction. The solvent-free microwave process employed was superior to traditional oil-bath thermal heating, which tended to generate crude material requiring extensive purification. Ultimately, probe **4** was prepared (Scheme 1, Method A) in moderate yield by reaction of **3** with α-bromo-3,5-di-*tert*-butyl-4-hydroxyacetophenone in *n*-butanol under reflux. Importantly, formation of the tricyclic condensation side product **5** was completely eliminated by performing the reaction with sodium bicarbonate at 23 °C in methanol

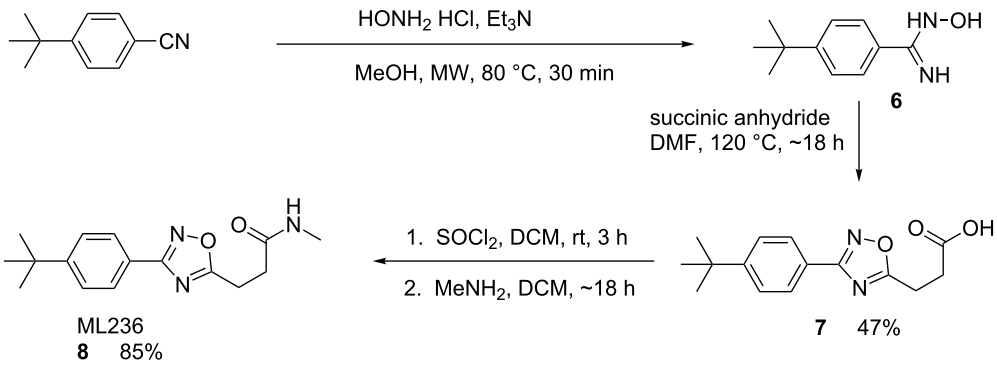


Scheme 1: Synthesis of ML029 (**4**).

(Scheme 1, Method B). Thus, compound **4** was isolated as a lyophilized white powder in 78% yield and >98% purity.

Deeper in vitro biological investigation using **4** as a chemical probe showed that it was not active (>30 μM) in more physiologically relevant HEK 293T and 697 pre-B cell lines. Therefore, an HTS campaign was initiated to identify compounds active in these specific cell subtypes by using the established HTS NF-κB reporter gene assay format. This included screening of a larger (~330,600 compound) MLSMR collection to ensure identification of additional chemical scaffolds not previously available. From this campaign two new cell-active NF-κB inhibitors were derived that were both selective against the NF-κB pathway induced by known PKC activators (phorbol myristic acetate (PMA)/ionomycin) and were selective toward the 697 pre-B cell line. It is interesting to note that no compounds meeting probe selectivity criteria were identified within the T cell (HEK 293T) specific assay. The first oxadiazole-based probe ML236 (**8**) was potent (0.035 μM) in the 697 pre-B cell line and >400-fold selective over both the NF-κB activation in HEK 293T cells and against TNFα-mediated NF-κB activation. In comparison, the second oxazole-based probe **12** is also potent (0.2 μM) in the 697 pre-B cell line and >400-fold selective over both the NF-κB activation in HEK 293T cells and against TNFα mediated NF-κB activation as measured in our reporter gene assay format.

Probe **8** was synthesized as shown in Scheme 2 [12]. Reaction of 4-*tert*-butyl-cyanobenzene with hydroxylamine hydrochloride under microwave heating conditions resulted in the hydroxyamidine **6**. This intermediate was condensed with succinic anhydride to provide the oxadiazole acid **7**. Conversion of **7** to the corresponding acid chloride and subsequent amidation with excess methylamine afforded **8** in excellent



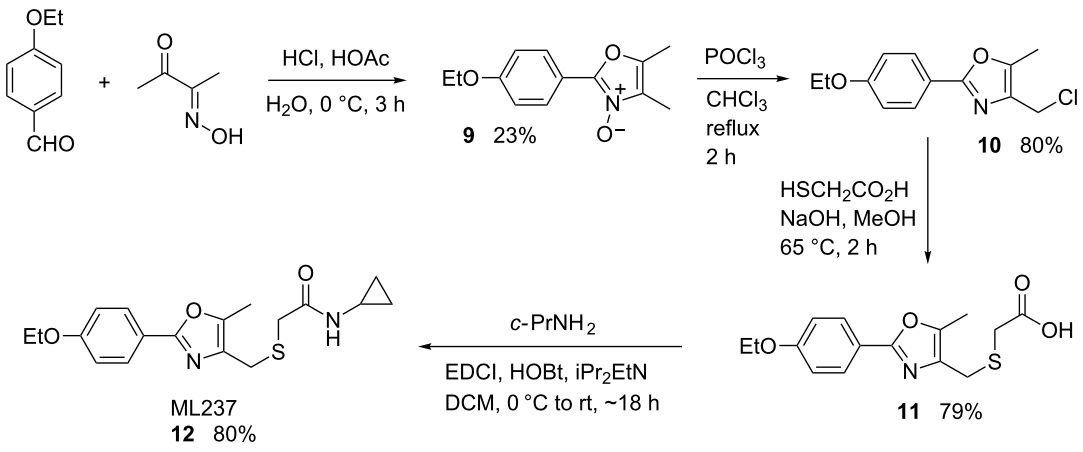
Scheme 2: Synthesis of ML236 (**8**).

yield after normal phase chromatography. This route was employed to make a variety of analogues and was generally conducted efficiently without purification of any intermediates. This enabled several analogues to be prepared in parallel, using mass-directed reverse-phase preparative HPLC to recover the pure isolates.

The second related probe, ML237, (**12**) was synthesized as shown in Scheme 3 [12]. Commercially available 4-ethoxybenzaldehyde was condensed with diacetyl monoxime under acidic conditions. The resulting oxazole *N*-oxide **9** was converted to the chloromethyloxazole **10** via selective chlorination with phosphorous oxychloride in good yield. Addition of thioglycolic acid led to the carboxylic acid **11**, which was coupled to cyclopropylamine to give **12** using a standard amidation protocol. The compound was purified by normal phase chromatography and was recovered as a white solid with a sharply defined melting point. The route was also amenable toward the preparation of related analogues. Generally, **9** was used without purification and the entire route was conducted efficiently without chromatographic purification of intermediates.

As a summary of project one, three novel chemical probes were discovered and optimized within this initiative. Tractable and efficient synthetic routes have been developed and are reported. One HEK 293T and two 697 pre-B cell specific probes are now available as research tools either through the Sanford-Burnham Center or through commercial sources. These probes were identified from a phenotypic screen and thus the precise cellular protein target is yet to be identified. Each probe performs in a noncanonical manner and inhibits NF-κB activity outside of the known, well-characterized pathways [7]. Determination of the precise signaling mechanism is the subject of ongoing research in our laboratories.

Discovering modulators of NF-κB signaling via selective nucleotide-binding oligomerization domain-1 (NOD1) inhibition (ML130 and ML146): The second program targeted proteins in the mammalian innate immune system that confer defense by detection of specific microbial ligands, or pathogen-associated molecular pattern microbial sensors known to house NOD1 (nucleotide-binding oligomerization domain-1 protein). Dysregulation of the NOD signaling pathway is also strongly associated with exacerbation of postinfection systemic disease states; however, its upregulation at the gene level can enhance systemic innate immunity [13]. The NOD1 cytosolic bacterial sensor falls within this class of NF-κB transcription pathway activators [14]. The NOD-like receptor (NLR) family reportedly comprises a large number of proteins from both vertebrate and invertebrate animal species, with >20 human proteins recognized [15-21]. Some NLR proteins have been shown to detect bacterial cell-wall components including lipopolysaccharides and/or peptidoglycan (NOD1 or 2) along with those of bacterial flagellin [22-25]. Importantly, the NOD1 protein primarily recognizes Gram-negative bacteria, in contrast to the more widely studied sensor NOD2, which participates in immunity against Gram-positive bacteria. Additionally, NOD1 has been associated with the induction of NF-κB activation, caspase-1 activation and apoptosis [26-28]. Genetic mutations in NOD are associated with numerous inflammatory conditions, including Crohn's disease and pancreatitis [29-34]. The identification of probes relevant to the NOD family of NLR proteins will improve understanding of the NOD1-mediated signaling pathway and also may translate to the discovery of new therapeutics for inflammatory diseases.

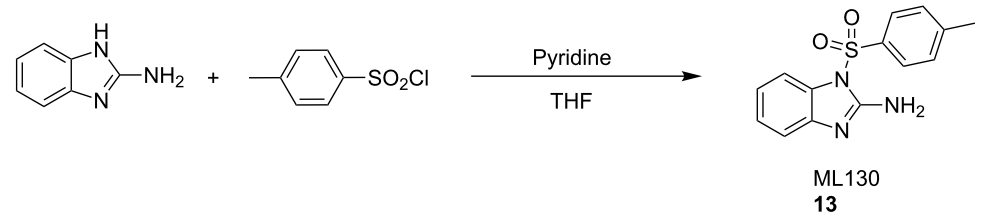


Scheme 3: Synthesis of ML237 (**12**).

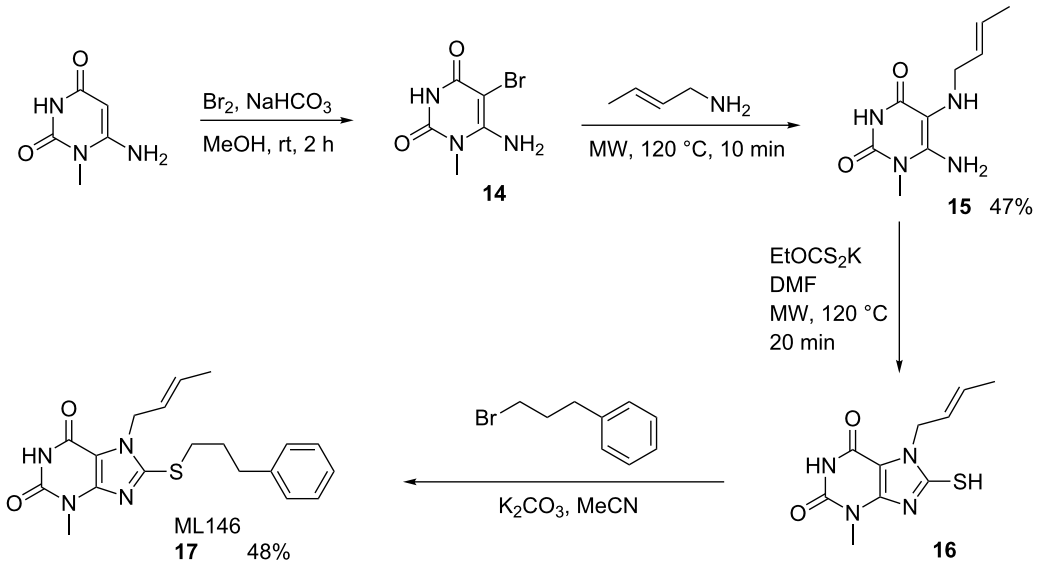
Probes **ML130** (**13**) and **ML146** (**17**) were identified as NOD1-selective molecules from an HTS campaign involving ~290,000 compounds. Compound **13** (IC_{50} = 0.52 μM) and compound **17** (IC_{50} = 1.54 μM) each inhibited γ-tri-DAP-stimulated (a gamma-tri-diaminopimelic acid derivative and NOD1-dependent signaling ligand) luciferase production in HEK 293T cells, which has endogenous NOD1 levels at submicromolar concentration as determined in a NF-κB-linked reporter assay. Both probes selectively (>40-fold for **13**, >8-fold for **17**) inhibited NOD1-dependent activation of the NF-κB pathway without inhibiting MDP-stimulated (muramyl dipeptide and a NOD2-dependent signaling ligand) signal transduction in reporter cell lines containing either low or overexpressed NOD2 proteins. Probes **13** and **17** were also selective over the non-NOD-stimulated NF-κB pathways (TNF-α, doxorubicin and PMA/ionomycin) in these reporter assays. Both of the probes, and their close analogues as discovered through SAR studies, selectively inhibited IL-8 secretion and the biologically relevant terminal effect of NOD1 (γ-tri-DAP) dependent NF-κB activation. Additionally, they neither inhibited NOD2-dependent nor TNF-α-dependent IL-8 secretion in biologically relevant MCF-7 cells. While **13** is the more potent and selective of these probes, **17** also met probe criteria and represents a second *bonafide* scaffold for a NOD1-selective probe.

ML130 (**13**) was synthesized as shown in Scheme 4 [35]. Commercially available 2-aminobenzimidazole was treated with *p*-toluenesulfonyl chloride in the presence of pyridine to obtain **13**. By performing the reaction at high concentration, it was generally simple to purify the reaction mixture directly without work up using normal-phase chromatography.

ML146 (**17**) was synthesized as shown in Scheme 5. Commercially available 6-amino-1-methyluracil was brominated to give **14**, which was reacted without purification with crotylamine under microwave heating conditions to provide **15**. Reaction of **15** with potassium ethyl xanthogenate, again under microwave heating conditions, led to the bicyclic thiol **16**. Without purification, **16** was added to 1-bromo-3-phenylpropane in the presence of potassium carbonate to provide **17**. Several analogues were efficiently prepared without chromatographic purification



Scheme 4: Synthesis of ML130 (**13**).



Scheme 5: Synthesis of ML146 (**17**).

Table 1: Calculated properties of probes.

Property	4	8	12	13	17
Molecular weight [g/mol]	465.6	287.3	346.4	287.3	370.4
Molecular formula	$C_{28}H_{39}N_3O_3$	$C_{16}H_{21}N_3O_2$	$C_{18}H_{22}N_2O_3S$	$C_{14}H_{13}N_3O_2S$	$C_{19}H_{22}N_4O_2S$
XLogP3-AA	7.2	3.0	3.1	3.2	3.5
H-Bond donors	3	1	1	1	1
H-Bond acceptors	5	4	4	4	3
Polar surface area [Å^2]	85.2	68.0	89.7	86.4	67.2
Heavy atom count	34	21	24	20	26

of intermediates, and the final compounds were purified by normal-phase chromatography if necessary [12].

As a summary of the second project, two novel chemical probes that are selective for NOD1 but not NOD2 signaling, were discovered and optimized within the scope of the program. Tractable and efficient synthetic methods have been employed and are reported. Both NOD1 selective probes are now available as research tools either through the Sanford-Burnham Center or through commercial sources.

Chemical probe physicochemical and pharmacological properties

Overall, the project probes presented physicochemical properties consistent with those of well-recognized drug-like molecules (Table 1). Molecular weights ranged from 287 to 465 g/mol. Calculated log *P* values were between 3.1 and 3.5 with the exception of **4**, which had an exceptionally high lipophilic value of 7.2 due to the presence of two *tert*-butyl moieties on the phenyl ring. The probes all contain from one to five H-bond donors and acceptors, and polar surface areas ranging from 67 to 90 Å^2. Based on current hit-to-lead trends within the pharmaceutical industry, all probes discussed provide qualified starting points for advanced lead-optimization programs.

The probes were evaluated using known in vitro ADME/T assays to understand their overall pharmacological properties (Table 2). Probe **4** exhibited good solubility especially as the pH decreased from 6.2 to 5, thereby mitigating the high calculated log *P* to some degree. Probes **8** and **12** also showed good solubility. Probe **13** had moderate solubility, and **17** showed the lowest solubility across the pH range but still approximately equal to its IC_{50} value. The PAMPA (parallel artificial membrane permeability assay) assay is used as an in vitro model of passive, transcellular permeability. An artificial membrane immobilized on a filter is placed between a donor and acceptor compartment. In this test, the probes exhibited good cell permeability overall. Although metabolic stability was poor in the presence of murine microsomes, all five probes were more stable in the presence of human hepatic microsomes. Most notably, **8** showed no apparent instability when subjected to

Table 2: Summary of in vitro ADME/T properties of probes.

Property	4	8	12	13	17
Aqueous solubility (μM) pH 5.0/6.2/7.4	90/1.1/1.5	92/101/103	112/133/160	7.0/5.9/7.0	1.5/1.8/1.7
PAMPA P_e (10^{-6} cm/s)[a] Donor pH: 5.0/6.2/7.4 Acceptor pH: 7.4	299/710/441	751/755/746	513/541/59	491/562/382	1269/1516/1344
Hepatic microsome stability[b] Human/mouse (% remaining)	26/0.5	100/4.9	22.7/0	41.8/0.8	8.8/0.86
Hepatic toxicity LC_{50} (μM)	>50	>50	>50	>50	>50

[a]Compound at 50 μM (typical PAMPA P_e permeability classification: low 5 × 10^{-6}, moderate 250 × 10^{-6}, high 1000 × 10^{-6}); [b]Compound at 1 μM, 60 min.

human hepatic microsomes after one hour of exposure. It is not yet known whether it represents a species specific CPY450 inhibitor. Importantly, none of the probes showed evidence of cytotoxicity in immortalized human hepatocytes (Fa2N-4 cells) and in the NCI-60 cell line cytotoxicity panel with 10 and 50 μM test concentrations [36].

Conclusion

The high-throughput screening of cell-based phenotypic and specific NOD1 protein-based assay targets within the NF-κB pathway has generated a series of unique chemical probes that are now available and useful for investigators to access and utilize in future studies. The compounds are well characterized using in vitro assay panels and are not pathway-associated kinase-family inhibitors. Research efforts are ongoing to improve molecular potency and properties to make each chemical scaffold family suitable for advanced in vivo studies. Each probe represents a low-molecular-weight, "rule of 5" compliant starting point for target identification or lead optimization efforts. In screening the MLSMR, and with subsequent analogue synthesis, we have demonstrated that unique and tractable hits can be identified by using the available NIH-MLSMR compound collection.

Supporting Information

Supporting Information File 1

Experimental procedures for synthesizing compounds **1**–**4** and **6**–**17**.
[http://www.beilstein-journals.org/bjoc/content/supplementary/1860-5397-9-103-S1.pdf]

Supporting Information File 2

NMR Spectra for ML029 (**4**), ML236 (**8**), ML237 (**12**), ML130 (**13**) and ML146 (**17**).
[http://www.beilstein-journals.org/bjoc/content/supplementary/1860-5397-9-103-S2.pdf]

Acknowledgements

The authors thank Michael Vicchiarelli and Arianna Mangravita-Novo in the SBMRI pharmacology Core for providing the ADME/T pharmacological profile data, and Paul Diaz for contributions to the NF-κB research program in the John Reed lab. We also gratefully recognize SBMRI compound management, assay development, HTS and Medicinal Chemistry Core team efforts in enabling these projects that resulted in the reported chemical probes and related analogues. We thank Dr.'s Pasha Khan and Jun Pu for synthetic efforts within these projects. This work was supported under federal grants U54 HG005033, R03 MH084844 and U01 AI078048 to JCR.

References

1. Molecular Libraries Program. http://mli.nih.gov/mli/mlpcn/.
2. Tracey, K. J.; Cerami, A. *Annu. Rev. Cell Biol.* **1993,** *9,* 317–343. doi:10.1146/annurev.cb.09.110193.001533
3. Baud, V.; Karin, M. *Nat. Rev. Drug Discovery* **2009,** *8,* 33–40. doi:10.1038/nrd2781
4. Bonizzi, G.; Karin, M. *Trends Immunol.* **2004,** *25,* 280–288. doi:10.1016/j.it.2004.03.008
5. Gilmore, T. D. *Oncogene* **2006,** *25,* 6680–6684. doi:10.1038/sj.onc.1209954
6. Karin, M.; Delhase, M. *Semin. Immunol.* **2000,** *12,* 85–98. doi:10.1006/smim.2000.0210
7. Shi, R.; Re, D.; Dudl, E.; Cuddy, M.; Okolotowicz, K. J.; Dahl, R.; Su, Y.; Hurder, A.; Kitada, S.; Peddibhotla, S.; Roth, G. P.; Smith, L. H.; Kipps, T. J.; Cosford, N.; Cashman, J.; Reed, J. C. *ACS Chem. Biol.* **2010,** *5,* 287–299. doi:10.1021/cb9003089
8. Thome, M. *Nat. Rev. Immunol.* **2004,** *4,* 348–359. doi:10.1038/nri1352
9. Peddibhotla, S.; Shi, R.; Khan, P.; Smith, L. H.; Mangravita-Novo, A.; Vicchiarelli, M. I.; Su, Y.; Okolotowicz, K. J.; Cashman, J. R.; Reed, J. C.; Roth, G. P. *J. Med. Chem.* **2010,** *53,* 4793–4797. doi:10.1021/jm1000248
10. For assay details see Supporting Information File 1 and PubChem link to AIDs 465 and 1384; http://pubchem.ncbi.nlm.nih.gov/assay/assay.cgi?aid=465; http://pubchem.ncbi.nlm.nih.gov/assay/assay.cgi?aid= 1384).
11. Okolotowicz, K. J.; Shi, R.; Zheng, X.; MacDonald, M.; Reed, J. C.; Cashman, J. R. *Bioorg. Med. Chem.* **2010,** *18,* 1918–1924. doi:10.1016/j.bmc.2010.01.039
12. All published MLPCN probe reports can be found within the public resource known as the NCBI Bookshelf: http://mli.nih.gov/mli/mlp-probes/ This page has a link called "Probe Report Web Table", which accesses an Excel file that allows released probe reports to be viewed. Reports for ML029, ML130, and ML146 are viewable as of 11 Jan 2013; the report for ML236 and ML237 should be released to this site in 2013.
13. Clarke, T. B.; Davis, K. M.; Lysenko, E. S.; Zhou, A. Y.; Yimin, Y.; Weiser, J. N. *Nat. Med.* **2010,** *16,* 228–231. doi:10.1038/nm.2087
14. Strober, W.; Murray, P. J.; Kitani, A.; Watanabe, T. *Nat. Rev. Immunol.* **2006,** *6,* 9–20. doi:10.1038/nri1747
15. Chamaillard, M.; Girardin, S. E.; Viala, J.; Philpott, D. J. *Cell. Microbiol.* **2003,** *5,* 581–592. doi:10.1046/j.1462-5822.2003.00304.x
16. Inohara, N.; Nuñez, G. *Nat. Rev. Immunol.* **2003,** *3,* 371–382. doi:10.1038/nri1086
17. Inohara, N.; Nuñez, G. *Oncogene* **2001,** *20,* 6473–6481. doi:10.1038/sj.onc.1204787
18. Inohara, N.; Ogura, Y.; Nuñez, G. *Curr. Opin. Immunol.* **2002,** *5,* 76–80.
19. Kawai, T.; Akira, S. *Int. Immunol.* **2009,** *21,* 317–337. doi:10.1093/intimm/dxp017
20. Rietdijk, S. T.; Burwell, T.; Bertin, J.; Coyle, A. J. *Curr. Opin. Pharmacol.* **2008,** *8,* 261–266. doi:10.1016/j.coph.2008.04.003
21. Murray, P. J. *Curr. Opin. Immunol.* **2005,** *17,* 352–358. doi:10.1016/j.coi.2005.05.006
22. Girardin, S. E.; Boneca, I. G.; Viala, J.; Chamaillard, M.; Labigne, A.; Thomas, G.; Philpott, D. J.; Sansonetti, P. J. *J. Biol. Chem.* **2003,** *278,* 8869–8872. doi:10.1074/jbc.C200651200

23. Chamaillard, M.; Hashimoto, M.; Horie, Y.; Masumoto, J.; Qiu, S.; Saab, L.; Ogura, Y.; Kawasaki, A.; Fukase, K.; Kusumoto, S.; Valvano, M. A.; Foster, S. J.; Mak, T. W.; Nuñez, G.; Inohara, N. *Nat. Immunol.* **2003,** *4,* 702–707. doi:10.1038/ni945
24. Uehara, A.; Fujimoto, Y.; Kawasaki, A.; Kusumoto, S.; Fukase, K.; Takada, H. *J. Immunol.* **2006,** *177,* 1796–1804.
25. Girardin, S. E.; Travassos, L. H.; Hervé, M.; Blanot, D.; Boneca, I. G.; Philpott, D. J.; Sansonetti, P. J.; Mengin-Lecreulx, D. *J. Biol. Chem.* **2003,** *278,* 41702–41708. doi:10.1074/jbc.M307198200
26. Franchi, L.; Amer, A.; Body-Malapel, M.; Kanneganti, T. D.; Özören, N.; Jagirdar, R.; Inohara, N.; Vandenabeele, P.; Bertin, J.; Coyle, A.; Grant, E. P.; Nuñez, G. *Nat. Immunol.* **2006,** *7,* 576–582. doi:10.1038/ni1346
27. Miao, E. A.; Alpuche-Aranda, C. M.; Dors, M.; Clark, A. E.; Bader, M. W. *Nat. Immunol.* **2006,** *7,* 569–575. doi:10.1038/ni1344
28. Kanazawa, N.; Okafuji, I.; Kambe, N.; Nishikomori, R.; Nakata-Hizume, M.; Nagai, S.; Fuji, A.; Yuasa, T.; Manki, A.; Sakurai, Y.; Nakajima, M.; Kobayashi, H.; Fujiwara, I.; Tsutsumi, H.; Utani, A.; Nishigori, C.; Heike, T.; Nakahata, T.; Miyachi, Y. *Blood* **2005,** *105,* 1195–1197. doi:10.1182/blood-2004-07-2972
29. Carneiro, L. A.; Travassos, L. H.; Girardin, S. E. *Ann. Med.* **2007,** *39,* 581–593. doi:10.1080/07853890701576172
30. Inohara, N.; Ogura, Y.; Fontalba, A.; Gutierrez, O.; Pons, F.; Crespo, J.; Fukase, K.; Inamura, S.; Kusumoto, S.; Hashimoto, M.; Foster, S. J.; Moran, A. P.; Fernandez-Luna, J. L.; Nuñez, G. *J. Biol. Chem.* **2003,** *278,* 5509–5512. doi:10.1074/jbc.C200673200
31. Hugot, J. P.; Chamaillard, M.; Zouali, H.; Lesage, S.; Cézard, J. P.; Belaiche, J.; Almer, S.; Tysk, C.; O'Morain, C. A.; Gassull, M.; Binder, V.; Finkel, Y.; Cortot, A.; Modigliani, R.; Laurent-Puig, P.; Gower-Rousseau, C.; Macry, J.; Colombel, J. F.; Sahbatou, M.; Thomas, G. *Nature* **2001,** *411,* 599–603. doi:10.1038/35079107
32. Ogura, Y.; Bonen, D. K.; Inohara, N.; Nicolae, D. L.; Chen, F. F.; Ramos, R.; Britton, H.; Moran, T.; Karaliuskas, R.; Duerr, R. H.; Achkar, J.-P.; Brant, S. R.; Bayless, T. M.; Kirschner, B. S.; Hanauer, S. B.; Nuñez, G.; Cho, J. H. *Nature* **2001,** *411,* 603–606. doi:10.1038/35079114
33. Miceli-Richard, C.; Lesage, S.; Rybojad, M.; Prieur, A.-M.; Manouvrier-Hanu, S.; Hafner, R.; Chamaillard, M.; Zouali, H.; Thomas, G.; Hugot, J.-P. *Nat. Genet.* **2001,** *29,* 19–20. doi:10.1038/ng720
34. Maeda, S.; Hsu, L.-C.; Liu, H.; Bankston, L. A.; Iimura, M.; Kagnoff, M. F.; Eckmann, L.; Karin, M. *Science* **2005,** *307,* 734–738. doi:10.1126/science.1103685
35. Khan, P. M.; Correa, R. G.; Divlianska, D. B.; Peddibhotla, S.; Sessions, E. H.; Magnuson, G.; Brown, B.; Suyama, E.; Yuan, H.; Mangravita-Novo, A.; Vicchiarelli, M.; Su, Y.; Vasile, S.; Smith, L. H.; Diaz, P. W.; Reed, J. C.; Roth, G. P. *ACS Med. Chem. Lett.* **2011,** *2,* 780–785. doi:10.1021/ml200158b
36. NCI60 screening. http://dtp.nci.nih.gov/branches/btb/ivclsp.html.

License and Terms

This is an Open Access article under the terms of the Creative Commons Attribution License (http://creativecommons.org/licenses/by/2.0), which permits unrestricted use, distribution, and reproduction in any medium, provided the original work is properly cited.

The license is subject to the *Beilstein Journal of Organic Chemistry* terms and conditions: (http://www.beilstein-journals.org/bjoc)

The definitive version of this article is the electronic one which can be found at: doi:10.3762/bjoc.9.103

Beilstein Journal of Organic Chemistry

Isotopically labeled sulfur compounds and synthetic selenium and tellurium analogues to study sulfur metabolism in marine bacteria

Nelson L. Brock[1], Christian A. Citron[1], Claudia Zell[1,2], Martine Berger[2], Irene Wagner-Döbler[3], Jörn Petersen[4], Thorsten Brinkhoff[2], Meinhard Simon[2] and Jeroen S. Dickschat[*1]

Full Research Paper

Open Access

Address:
[1]Institute of Organic Chemistry, TU Braunschweig, Hagenring 30, 38106 Braunschweig, Germany, [2]Institute for Chemistry and Biology of the Marine Environment (ICBM), University of Oldenburg, Carl-von-Ossietzky-Str. 9–11, 26129 Oldenburg, Germany, [3]Helmholtz Center for Infection Research, Inhoffenstraße 7, 38124 Braunschweig, Germany and [4]Leibniz-Institut DSMZ - Deutsche Sammlung von Mikroorganismen und Zellkulturen GmbH, Inhoffenstraße 7b, 38124 Braunschweig, Germany

Email:
Jeroen S. Dickschat[*] - j.dickschat@tu-bs.de

* Corresponding author

Keywords:
dimethylsulfoniopropionate; *Roseobacter* clade; selenium metabolism; sulfur metabolism; volatiles

Beilstein J. Org. Chem. **2013,** *9,* 942–950.
doi:10.3762/bjoc.9.108

Received: 30 January 2013
Accepted: 26 April 2013
Published: 15 May 2013

This article is part of the Thematic Series "Synthetic probes for the study of biological function".

Guest Editor: J. Aubé

© 2013 Brock et al; licensee Beilstein-Institut.
License and terms: see end of document.

Abstract

Members of the marine *Roseobacter* clade can degrade dimethylsulfoniopropionate (DMSP) via competing pathways releasing either methanethiol (MeSH) or dimethyl sulfide (DMS). Deuterium-labeled [$^2H_6$]DMSP and the synthetic DMSP analogue dimethyltelluriopropionate (DMTeP) were used in feeding experiments with the *Roseobacter* clade members *Phaeobacter gallaeciensis* DSM 17395 and *Ruegeria pomeroyi* DSS-3, and their volatile metabolites were analyzed by closed-loop stripping and solid-phase microextraction coupled to GC–MS. Feeding experiments with [$^2H_6$]DMSP resulted in the incorporation of a deuterium label into MeSH and DMS. Knockout of relevant genes from the known DMSP demethylation pathway to MeSH showed in both species a residual production of [$^2H_3$]MeSH, suggesting that a second demethylation pathway is active. The role of DMSP degradation pathways for MeSH and DMS formation was further investigated by using the synthetic analogue DMTeP as a probe in feeding experiments with the wild-type strain and knockout mutants. Feeding of DMTeP to the *R. pomeroyi* knockout mutant resulted in a diminished, but not abolished production of demethylation pathway products. These results further corroborated the proposed second demethylation activity in *R. pomeroyi*. Isotopically labeled [$^2H_3$]methionine and $^{34}SO_4^{2-}$, synthesized from elemental $^{34}S_8$, were tested to identify alternative sulfur sources besides DMSP for the MeSH production in *P. gallaeciensis*. Methionine proved to be a viable sulfur source for the MeSH volatiles, whereas incorporation of labeling from sulfate was not

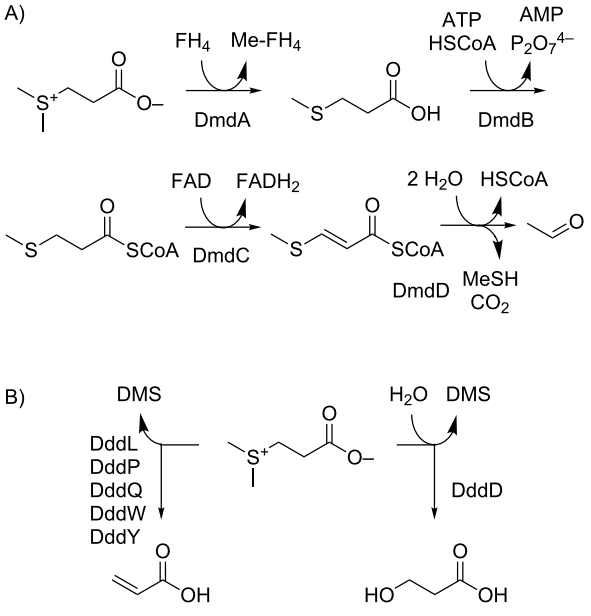
observed. Moreover, the utilization of selenite and selenate salts by marine alphaproteobacteria for the production of methylated selenium volatiles was explored and resulted in the production of numerous methaneselenol-derived volatiles via reduction and methylation. The pathway of selenate/selenite reduction, however, proved to be strictly separated from sulfate reduction.

Introduction

The *Roseobacter* clade within the class of alphaproteobacteria is found both in seawater and marine sediments and occurs often in association with marine algae [1]. Genome data from sequenced clade members revealed that pathways for the degradation of aromatic compounds and sulfur metabolic pathways are widespread [2]. This is reflected by their volatile bouquets that are dominated by sulfur compounds such as polysulfides **1** and **2** (Figure 1), thiosulfonates **3**, thioesters **4**, or sulfones **5**, and phenylacetate-derived volatiles such as the moderately antibacterial compounds tropone (**6**) and tropone hydrate **7** [3-6]. The cooperation of phenylacetate degradation and sulfur metabolism is manifested in the production of the antibiotic tropodithietic acid (TDA, **8**) [7,8] and the roseobacticides, a class of algicides, represented by, e.g., roseobacticide A (**9**) [9,10].

The high abundance of sulfur volatiles throughout the *Roseobacter* clade raises the question about the nature of their sulfur sources. The most important organic sulfur metabolite in marine environments is dimethylsulfoniopropionate (DMSP), which is produced by a wide range of marine organisms and in especially large amounts by dinoflagellates [11]. DMSP is degraded by marine bacteria either under the formation of methanethiol (MeSH) or of dimethyl sulfide (DMS) with a large impact on both the global sulfur cycle and climate [12,13].

DMSP degradation to MeSH starts with the DmdA mediated demethylation to 3-(methylthio)propionate (Scheme 1A) [14,15] followed by its conversion into its CoA-thioester by DmdB and oxidation by the FAD-dependent dehydrogenase DmdC. The addition of water to 3-(methylthio)acryloyl-CoA by the enoyl-CoA hydratase DmdD results in a hemithioacetal, which collapses under release of acetaldehyde, carbon dioxide and MeSH [16]. Several enzymes for the cleavage of DMS from DMSP (Scheme 1B) have been described [11]. DddD catalyzes the hydrolysis of DMSP to 3-hydroxypropionate and DMS, while five different classes of enzymes (DddP, DddL, DddQ, DddW, DddY) have been identified for the lysis of DMSP to acrylate and DMS.



Scheme 1: Degradation of DMSP via (A) demethylation pathway and (B) cleavage pathways. FH_4: tetrahydrofolate.

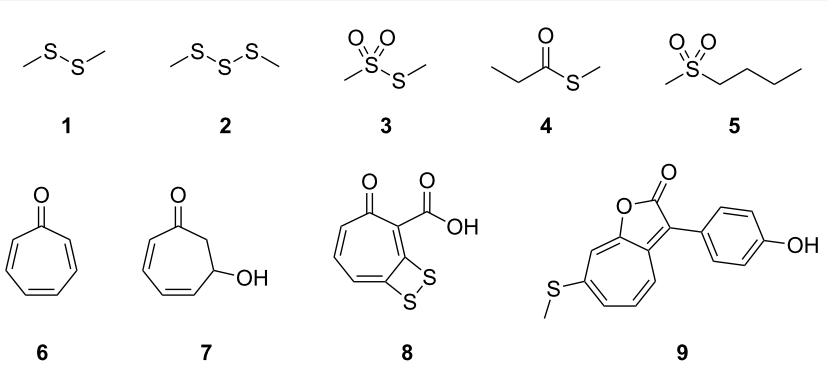
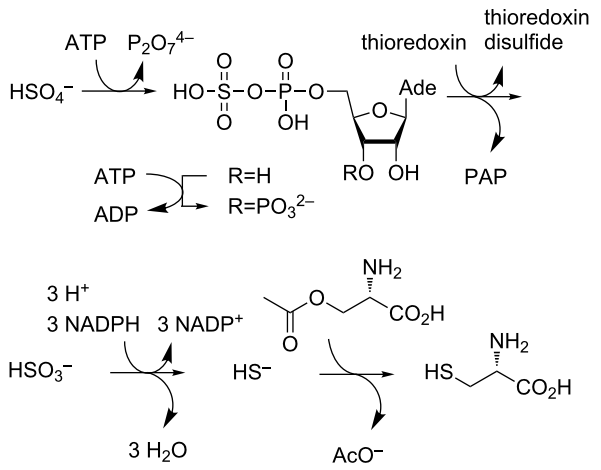


Figure 1: *Roseobacter* clade metabolites.

A second obvious candidate as a source for sulfur volatiles is inorganic sulfate, which can be reduced by *Roseobacter* clade members to hydrogen sulfide via adenylyl sulfate, 3'-phosphoadenylyl sulfate, and sulfite (Scheme 2) [17]. Hydrogen sulfide enters the amino acid pool by reaction with *O*-acetyl-L-serine to L-cysteine. Elemental sulfur, hydrogen sulfide, or thiosulfate can be funneled via the lithotrophic sulfur oxidation (Sox) pathway to sulfate [18-22].



Scheme 2: Sulfate reduction pathway and incorporation of sulfur into the amino acid pool. PAP: adenosine 3',5'-bisphosphate.

Analogous degradation steps for the selenium and tellurium derivatives of DMSP (dimethylseleniopropionate, DMSeP, and dimethyltelluriopropionate, DMTeP) and the reduction of selenate, selenite, tellurate, and tellurite may be possible via the described pathways. However, in *Desulfovibrio desulfuricans* subsp. *aestuarii* only minor amounts of selenate are reduced via the sulfate reduction pathway [23]. Instead, a special selenate reductase SerABC for selenate reduction to selenite was characterized from *Thauera selenatis* [24].

The effective degradation of DMSP by members of the *Roseobacter* clade via the demethylation pathway to MeSH was demonstrated in a previous study using a closed-loop stripping apparatus (CLSA) for the trapping of volatiles on charcoal [25]. The substrate scope of the involved enzymatic machinery was tested in feeding experiments with DMSeP, which is produced by the salt marsh cordgrass *Spartina alternifolia* amended with selenate [26], and the non-natural analogue DMTeP. DMSeP was effectively metabolized to give methaneselenol-derived volatiles, whereas the verification of tellurium-containing volatiles from DMTeP remained elusive [25].

Here we report the results of an in-depth investigation of sulfur metabolic pathways to volatile sulfur compounds in marine alphaproteobacteria by feeding of isotopically labeled sulfur compounds and synthetic selenium and tellurium analogues to wildtype and relevant mutant strains. A reinvestigation of DMTeP conversion by marine bacteria from the *Roseobacter* clade into methylated tellurium volatiles using a modified analytical technique is also presented.

Results and Discussion

Usage of [$^2H_6$]DMSP and DMTeP as synthetic probes to study DMSP degradation pathways in marine bacteria

The volatiles released by agar-plate cultures of *Phaeobacter gallaeciensis* DSM 17395 and *Ruegeria pomeroyi* DSS-3 strains grown on half-strength MB2216 medium supplemented with [$^2H_6$]DMSP or DMTeP were collected by solid-phase microextraction (SPME) and by CLSA. The obtained headspace extracts were subsequently analyzed by GC–MS, leading to the identification of the volatiles dimethyl disulfide (**1**), dimethyl trisulfide (**2**), *S*-methyl methanethiosulfonate (**3**), dimethyl telluride (**4**), dimethyl telluryl sulfide (**5**), and dimethyl ditelluride (**6**), which are shown in Figure 2. Representative chromatograms are depicted in Figures 3–5.

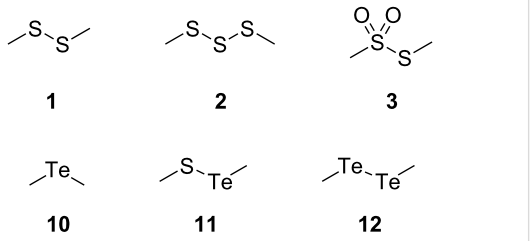


Figure 2: Volatiles from *P. gallaeciensis* DSM 17395 and *R. pomeroyi* DSS-3. Feeding of [$^2H_6$]DMSP results in deuterium incorporation into compounds **1**–**3**, feeding of DMTeP results in the formation of compounds **10**–**12**.

Investigating DMSP degradation pathways in *Phaeobacter gallaeciensis* DSM 17395

Based on the genetic information, *P. gallaeciensis* should be able to perform both DMSP degradation pathways, as a *dmd*-gene cluster for the demethylation pathway is located on a 262 kb plasmid and a gene for the lyase DddP is encoded on its chromosome. Isotopically labeled [$^2H_6$]DMSP was efficiently incorporated into methanethiol-derived sulfur volatiles like dimethyl disulfide (**1**), dimethyl trisulfide (**2**), and *S*-methyl methanethiosulfonate (**3**) by *P. gallaeciensis* (incorporation rate 91%). Knockout of the *dmdA*-gene significantly diminished this incorporation rate (27%). The ratio of DMS production was increased from below 0.05% of the total sulfur-containing volatile material in the wild type strain to about 2% in the *dmdA*

knockout mutant. The decreased incorporation rate and the relatively higher amounts of the DMSP lysis product DMS can be explained with the blockage of the *dmd* demethylation pathway. To rule out a spontaneous decomposition of DMSP to 3-(methylthio)propionate that would serve as a substrate for *dmd*-gene-mediated liberation of MeSH even in the absence of an active *dmdA* gene, [$^2H_6$]DMSP was fed to a knockout mutant with a loss of the 262 kb plasmid [26]. This plasmid-cured strain exhibited the same reduced incorporation rates (32%) of deuterium label into the MeSH-derived volatiles. The residual demethylation activity may be due to other as yet unidentified enzymes involved in the liberation of MeSH from DMSP that can, however, not be located on the 262 kb plasmid. Consistent with previous results [25], after feeding of DMTeP to *P. gallaeciensis* no tellurium compounds were detected in the CLSA headspace extracts (Figure 3A), although a strong metallic to garlic-like smell as typical for organotellurium compounds evolved from the agar-plate cultures. However, SPME extracts of *P. gallaeciensis* cultures amended with the same amount of DMTeP and grown under identical conditions as in the CLSA-based experiment were dominated by dimethyl ditelluride (**12**), accompanied by dimethyl telluryl sulfide (**11**) and dimethyl telluride (**10**, Figure 3B). This demonstrated that the SPME method is more sensitive for the analysis of organotellurium compounds than is CLSA. Compound **12** can arise by oxidative dimerization of the unnatural demethylation pathway product methanetellurol, whereas **11** is the cross-coupling product of methanetellurol and methanethiol that is also formed during growth on MB2216 medium alone [25]. In contrast to DMSP and DMSeP, which are degraded by *P. gallaeciensis* mainly via the demethylation pathway (>99%) [25], a significant contribution of the cleavage pathway (21% by peak integration) was observed for the degradation of DMTeP.

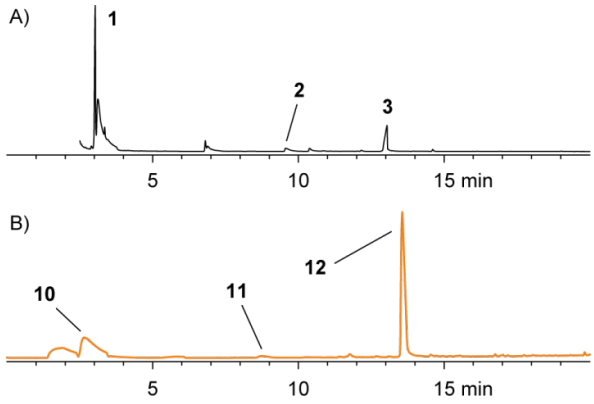


Figure 3: Chromatograms of headspace extracts from *P. gallaeciensis* DSM 17395 after feeding of DMTeP by the use of (A) CLSA (black) and (B) SPME (orange).

Investigating DMSP degradation pathways in *Ruegeria pomeroyi* DSS-3 (DSM 15171^T)

Genes for three DMSP lyases (*dddP*, *dddQ*, and *dddW*) and for the demethylation pathway (*dmdA–D*) are encoded in the genome of *R. pomeroyi* DSS-3. Feeding of [$^2H_6$]DMSP to this strain led to its degradation via the demethylation pathway (90%) and the cleavage pathway (10%). This ratio of the two pathways was determined by comparison of the peak areas in the gas chromatogram of SPME extracts (Figure 4A, the peak area of the MeSH dimer **1** has to be considered twice; compounds **2** and **3** also originating from MeSH were not considered, because they were only produced in trace amounts). A reduced demethylation activity was observed by feeding of [$^2H_6$]DMSP to a *dmdA*$^-$ knockout mutant strain of DSS-3. The incorporation rates of the deuterium labeling into the MeSH-derived volatiles were reduced (64% for **1**) in comparison to the wild type strain (95%) and the ratio of the cleavage pathway increased to 35% (Figure 4B). The incorporation of isotopic labeling from [$^2H_6$]DMSP by the *dmdA*$^-$ mutant strongly suggests that also in *R. pomeroyi* a second pathway for DMSP demethylation is present, which is in contrast to previous reports [14]. Knockout of *dddQ* gave the opposite result and decreased the ratio of the cleavage pathway to 1%, demonstrating its premier responsibility for DMSP lysis in the concert of the three lyases in *R. pomeroyi* (Figure 4C).

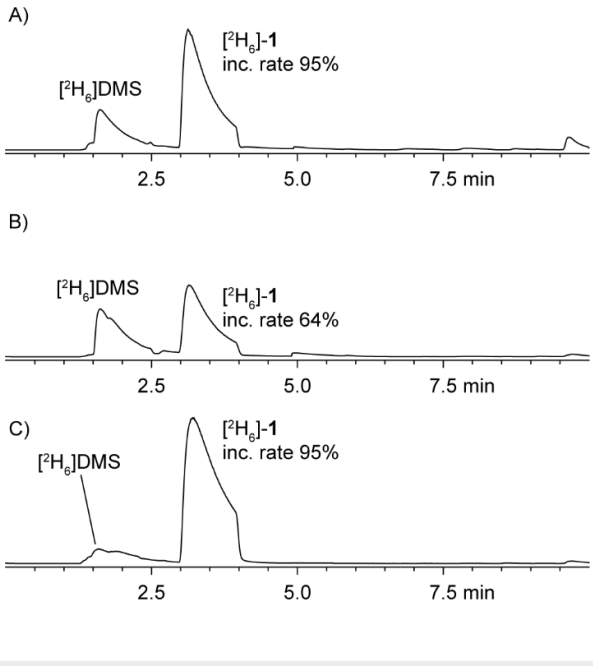


Figure 4: Chromatograms of headspace extracts obtained after feeding of [$^2H_6$]DMSP by the use of SPME from (A) *R. pomeroyi* DSS-3 wild type, (B) *R. pomeroyi* DSS-3 *dmdA*$^-$, and (C) *R. pomeroyi* DSS-3 *dddQ*$^-$. Trace amounts of [$^2H_6$]-**2** and [$^2H_6$]-**3** were also found (not shown).

Feeding of DMTeP to the *R. pomeroyi* wild type strain resulted in the production of large amounts of the demethylation pathway product **12** besides minor amounts of **11** and the lysis product dimethyl telluride (**10**; Figure 5). The total amounts of organotellurium volatiles were much higher than those observed for *P. gallaeciensis*, and therefore, even the CLSA technique that proved to be not suitable to collect tellurium volatiles from *P. gallaeciensis* cultures grown on DMTeP was in this case successfully applied. The *R. pomeroyi dmdA*$^-$ knockout mutant showed significantly reduced production of **11** and **12**, but small residual amounts likely evolving via the second unidentified demethylation pathway could still be detected. Knockout of the gene encoding for the DMSP lyase *dddQ* had no effect on the production of **10**. This is in sharp contrast to the observations made with [$^2H_6$]DMSP, implicating a rather narrow substrate specificity for DMSP of DddQ. One or both of the remaining two lyases DddP and DddW may be responsible for the strain's capability to lyse DMTeP. The potential of DddP for DMTeP lysis has already been evaluated in *P. gallaeciensis* whose genome only encodes DddP as a single DMSP lyase, while no conclusions can be drawn on the participation of DddW.

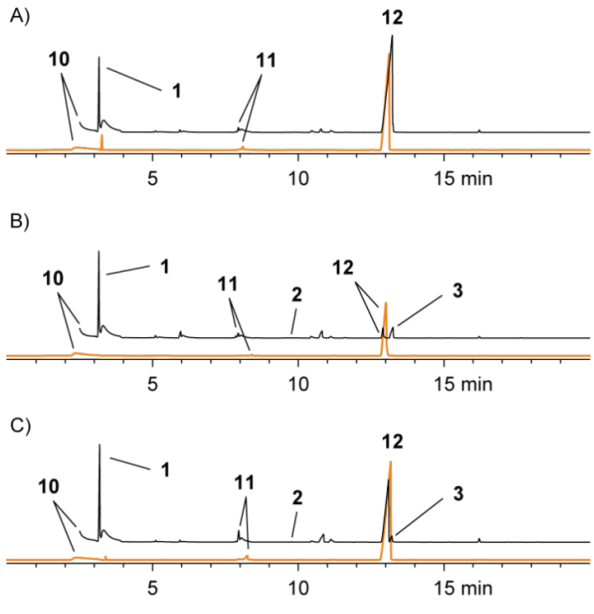


Figure 5: Chromatograms of headspace extracts from (A) *R. pomeroyi* DSS-3 wild type, (B) *R. pomeroyi* DSS-3 *dmdA*$^-$, and (C) *R. pomeroyi* DSS-3 *dddQ*$^-$ after feeding of DMTeP by use of CLSA (black) and SPME (orange).

Exploring the source of methanethiol

Two possible sources for MeSH production from MB2216 medium are sulfate via reduction to sulfide and methylation, or methionine via γ-lysis. The participation of both mechanisms was explored by feeding of isotopically labeled sulfate, thiosulfate and methionine. The volatiles released by agar-plate cultures of *P. gallaeciensis* fed with $NaH^{34}SO_4$ or $Na^{34}SSO_3$, both synthesized from elemental $^{34}S_8$ (Scheme 3), were collected by using a CLSA and analyzed by GC–MS. No incorporation of the ^{34}S-labeling from sulfate or thiosulfate into the MeSH-derived volatiles was observed, pointing strongly away from a significant involvement of sulfate reduction in the biosynthesis of MeSH. Instead, feeding of [*methyl*-$^2H_3$]methionine led to an effective incorporation of the deuterium labeling into **1** (85% incorporation rate, Figure S1 of Supporting Information File 1) and other MeSH-derived volatiles.

Selenium volatiles from marine alphaproteobacteria

Agar-plate cultures of *P. gallaeciensis* grown on half-strength MB2216 medium, plain or amended with different selenium salts, were analyzed with the CLSA technique. A variety of sulfur and selenium-containing volatiles was identified, as summarized in Figure 6. The respective gas chromatograms are shown in Figure 7.

Feeding of Na_2SeO_4 to *P. gallaeciensis* resulted in the formation of a number of selenium volatiles including dimethyl diselenide (**20**) and dimethyl triselenide (**21**). In addition, the mixed sulfur/selenium compounds dimethylselenyl sulfide (**15**), bis(methylthio) selenide (**16**), methylseleno disulfide (**17**), methyl methylthio diselenide (**18**), and bis(methylseleno) sulfide (**19**) were found. A similar headspace composition was observed in the feeding experiment with Na_2SeO_3. All selenium compounds are derived from methaneselenol, and their formation by *P. gallaeciensis* has previously been observed in feeding experiments with dimethylseleniopropionate [25]. The participation of the sulfate reduction pathway in the reduction of selenate and selenite to methaneselenol was tested by knockout of the genes for the bifunctional sulfate adenylyltransferase/adenylylsulfate kinase (*cysC*, strain WP73, locus tag PGA1_c24800) and the sulfite reductase (*cysI*, strain WP45, locus tag PGA1_c20760). No significant differences of the volatile profiles were observed in feeding experiments with the

$$^{34}S_8 + 8\ Na_2SO_3 \longrightarrow 8\ Na_2{}^{34}SSO_3$$

$$Na_2{}^{34}SSO_3 + 4\ Cl_2 + 5\ H_2O \longrightarrow NaH^{34}SO_4 + NaHSO_4 + 8\ HCl$$

Scheme 3: Synthesis of ^{34}S-labeled thiosulfate and sulfate.

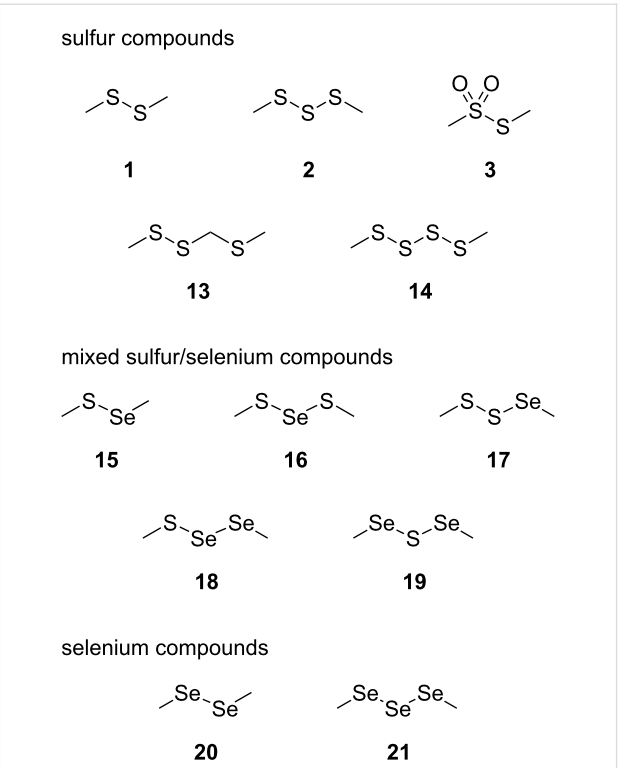


Figure 6: Volatiles from *P. gallaeciensis* after feeding of selenate and selenite.

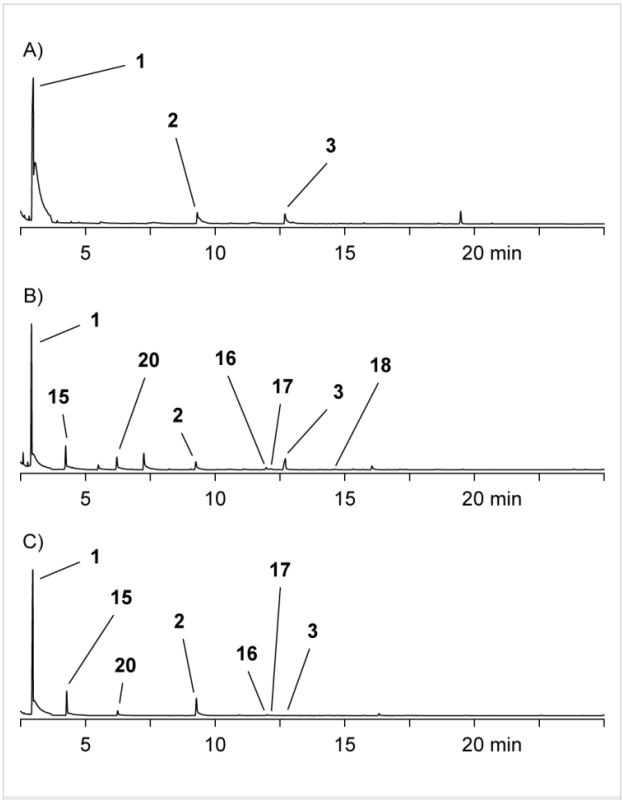


Figure 7: Chromatograms of headspace extracts from *P. gallaeciensis* grown on (A) 50% MB2216, (B) 50% MB2216 + 1 mmol/l Na_2SeO_4, (C) 50% MB2216 + 1 mmol/l Na_2SeO_3.

mutant strains compared to the wild type, indicating that as yet unidentified enzymes are responsible for the selenate/selenite reduction in *P. gallaeciensis*. These respective genes are not located on the 262 kb plasmid pPGA1_262, as the plasmid-cured mutant strain [27] was still able to produce methylated selenium volatiles from selenate and selenite.

The same sulfur and selenium volatiles were also found in the CLSA headspace analyses with agar plate cultures of *Roseobacter denitrificans* DSM 7001^T, *Oceanibulbus indolifex* DSM 14862^T, *Dinoroseobacter shibae* DSM 16493^T, *Labrenzia alexandrii* DFL-11^T, *Roseovarius mucosus* DFL-24^T, and *Hoeflea phototrophica* DFL-43^T (Supporting Information File 1, Figure S2). The production of methylated selenium volatiles from the selenate and selenite salts was especially pronounced for *H. phototrophica* from the order rhizobiales, a close relative of *Roseobacter* clade bacteria. In addition, the sulfur volatiles bis(methylthio)methane (**22**), *S*-methyl propanethioate (**23**), 4-(methylthio)butan-2-one (**24**), *S*-methyl 3-(methylthio)propanethioate (**25**), and benzothiazole (**26**) were found in strain-specific patterns (Figure 8). Cyclic sulfur volatiles, such as 1,2,4-trithiolane (**27**), 1,2,4,5-tetrathiane (**28**), and lenthionine (**29**), compounds that are known from Shiitake mushrooms (*Lentinus edodes*) [28-30], were solely produced by *R. denitrificans*.

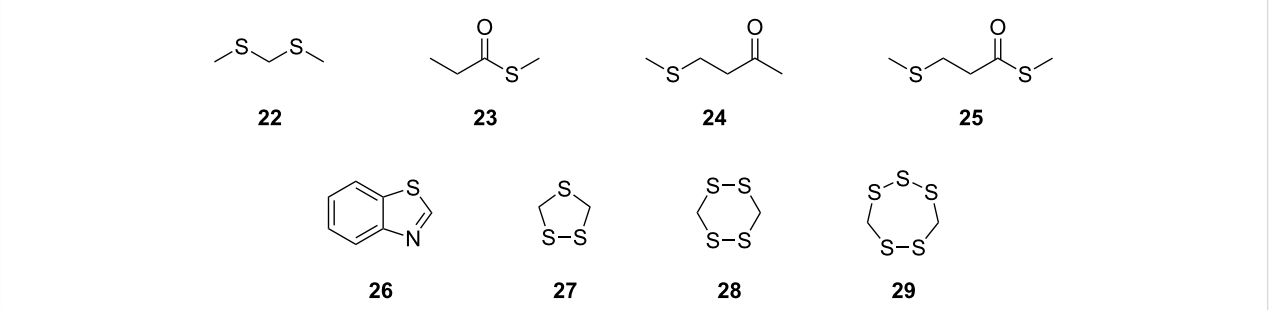


Figure 8: Additional sulfur volatiles.

Conclusion

In summary, we have shown that isotopically labeled natural sulfur compounds and their (synthetic) selenium and tellurium analogues can be applied in feeding experiments that give valuable insights into the sulfur metabolic pathways of marine bacteria. Deuterated [$^2H_6$]DMSP and its artificial analogue DMTeP can be transformed by lysis into [$^2H_6$]dimethyl sulfide and dimethyl telluride, or via the demethylation pathway to [$^2H_3$]MeSH and methanetellurol, respectively. Knockout of *dmdA* in *P. gallaeciensis* and *R. pomeroyi* demonstrated its major involvement in the demethylation pathway, but residual demethylation activity was observed suggesting the presence of a second DMSP demethylation pathway. Further experiments, preferably in vitro with the different classes of purified DMSP lyases, will be required to investigate their participation in DMTeP lysis. On full medium, containing both methionine and sulfate, feeding experiments with [*methyl*-$^2H_3$]methionine demonstrated that methionine γ-lysis is an important pathway for MeSH production in *P. gallaeciensis*. Sulfate reduction and methylation was not observed in feeding experiments with ^{34}S-labeled sulfate or thiosulfate, likely because sulfate reduction was not active under the experimental growth conditions. This is in sharp contrast to the observations that large amounts of methaneselenol-derived volatiles are released during growth of *P. gallaeciensis* and several other marine bacteria on sodium selenate, also requiring reduction and methylation. These observations suggest that the formation of volatiles from selenate is a detoxification mechanism that is strictly separated from sulfate reduction, as was confirmed by investigation of a *P. gallaeciensis* knockout mutant impaired in sulfate reduction. This strict pathway separation may help to avoid incorporation of toxic selenium into other sulfur metabolic pathways such as sulfur amino acid metabolism. Future experiments in our laboratory will be performed to identify the genes involved in selenate reduction in marine bacteria.

Experimental

Strains and culture conditions: A complete list of all wild type and mutant strains used in this study is given in Supporting Information File 1, Table S1. *Phaeobacter gallaeciensis* DSM 17395 [17], *Ruegeria pomeroyi* DSS-3 (DSM 15171^T) [31], *Roseobacter denitrificans* OCh 114 (DSM 7001^T) [32], *Oceanibulbus indolifex* HEL-45 (DSM 14862^T) [33], *Dinoroseobacter shibae* DFL-12 (DSM 16493^T) [34], *Labrenzia alexandrii* DFL-11 (DSM 17067^T) [35], *Hoeflea phototrophica* DFL-43 (DSM 17068^T) [36], and *Roseovarius mucosus* DFL-24 (DSM 17069^T) [37] were precultured in half-strength marine broth (peptone (2.5 g/L), yeast extract (0.5 g/L), Fe(III) citrate (0.05 g/L), NaCl (9.725 g/L), $MgCl_2$ (2.95 g/L), Na_2SO_4 (1.62 g/L), $CaCl_2$ (0.9 g/L), KCl (0.275 g/L), $NaHCO_3$ (0.08 g/L), KBr (0.04 g/L), $SrCl_2$ (17 mg/L), H_3BO_3 (11 mg/L), Na-silicate (2 mg/L), NaF (1.2 mg/L), $(NH_4)NO_3$ (0.8 mg/L), Na_2HPO_4 (4 mg/L); pH 7.6) at 28 °C with shaking (160 rpm). When necessary, kanamycin sulfate (60 μg/mL) was added after autoclaving.

Feeding experiments, sampling and GC–MS analyses: Feeding experiments with [$^2H_6$]DMSP and DMTeP, sampling by CLSA or SPME (Supelco Analytical, Bellefonte, USA; 75 μm carboxen/polydimethylsiloxane) and GC–MS analyses were carried out as described previously [24]. For the feeding experiments with ^{34}S-labeled thiosulfate or sulfate, sodium sulfate deficient half-strength marine broth agar medium was amended after autoclavation with 2.9 mmol/l $Na_2{}^{34}SSO_3$ (50% ^{34}S-enrichment) or 5.7 mmol/l $NaH{}^{34}SO_4$ (25% ^{34}S-enrichment). For the feeding experiments with [*methyl*-$^2H_3$]methionine, selenate, and selenite, half-strength marine broth agar medium was supplemented after autoclaving with 1 mmol/l of [*methyl*-$^2H_3$]methionine, Na_2SeO_3, and Na_2SeO_4, respectively.

Construction of *P. gallaeciensis* strain CZ01: Primers used in this study are listed in Supporting Information File 1, Table S2. For the gene disruption of *dmdA* a 3.6 kb chromosomal fragment containing the gene was amplified with the primers Cl1f and Cl1r. The amplified product was ligated into the *Eco*RV site of pBluescript KS(+). The kanamycin resistance gene (amplified from pBBR1MCS-2 using the primers nptII-f and nptII-r) was cloned into the *Eco*RV site of the previously obtained plasmid that already carried the *dmdA* gene region. *P. gallaeciensis* DSM 17395 was transformed by electroporation with this plasmid, leading to the strain CZ01 (*dmdA*::*kan*), which was ratified by PCR.

General synthetic methods: Chemicals were purchased from Acros Organics (Geel, Belgium) or Sigma-Aldrich Chemie GmbH (Steinheim, Germany), and used without further purification. $^{34}S_8$ (99.93% enriched) was purchased from Campro Scientific GmbH (Berlin, Germany). Infrared spectra were recorded on a Bruker Tensor 27 ATR spectrometer.

$Na_2{}^{34}SSO_3{\cdot}5H_2O$: Elemental $^{34}S_8$ (0.800 g, 23.5 mmol, 1.0 equiv) was added to a solution of Na_2SO_3 (2.97 g, 23.6 mmol, 1.0 equiv) in water (40 mL) and stirred under reflux until the sulfur was consumed (48 h). Filtration and concentration in vacuo gave $Na_2{}^{34}SSO_3{\cdot}5H_2O$ (5.90 g, 23.6 mmol, quant.) as a colorless solid. IR (ATR): ν = 1133 (s), 1008 (s), 674 (s), 539 (w) cm^{-1}.

$NaH{}^{34}SO_4$: To an aqueous HCl solution (6 m, 400 mL) was added a saturated $KMnO_4$ solution (400 mL), and the emerging Cl_2 was condensed in a second flask at −40 °C. By slow warming to room temperature the evolving Cl_2 was funneled

through a solution of $Na_2{}^{34}SSO_3{\cdot}5H_2O$ (3.11 g, 12.4 mmol, 1.0 equiv) in water (50 mL). Filtration and concentration in vacuo gave $NaH^{34}SO_4$ (1.25 g, 10.3 mmol, 83%, 50% ^{34}S-enchrichment) as a colorless solid. IR (ATR): ν = 1160 (s), 1011 (m), 904 (m), 607 (m), 576 (m), 494 (w) cm^{-1}.

Supporting Information

Supporting Information File 1

Tables with strains, primers and the full results of the headspace analyses.
[http://www.beilstein-journals.org/bjoc/content/supplementary/1860-5397-9-108-S1.pdf]

Acknowledgements

Funding of the Deutsche Forschungsgemeinschaft by the Transregional Collaborative Research Center *Roseobacter* (Transregio TRR 51), by an Emmy Noether Fellowship (to J. S. D.) and the Fonds der Chemischen Industrie by a Chemiefonds Scholarship (for N. L. B.) is gratefully acknowledged. We thank Victoria Michael for construction of the 262 kb plasmid deletion mutant of *P. gallaeciensis*, Andrew Johnston for *R. pomeroyi* DSS-3 and the *R. pomeroyi dmdA* and *dddQ* mutants, and Stefan Schulz for support of our group.

References

1. Buchan, A.; González, J. M.; Moran, M. A. *Appl. Environ. Microbiol.* **2005,** *71,* 5665–5677. doi:10.1128/AEM.71.10.5665-5677.2005
2. Newton, R. J.; Griffin, L. E.; Bowles, K. M.; Meile, C.; Gifford, S.; Givens, C. E.; Howard, E. C.; King, E.; Oakley, C. A.; Reisch, C. R.; Rinta-Kanto, J. M.; Sharma, S.; Sun, S.; Varaljay, V.; Vila-Costa, M.; Westrich, J. R.; Moran, M. A. *ISME J.* **2010,** *4,* 784–798. doi:10.1038/ismej.2009.150
3. Thiel, V.; Brinkhoff, T.; Dickschat, J. S.; Wickel, S.; Grunenberg, J.; Wagner-Döbler, I.; Simon, M.; Schulz, S. *Org. Biomol. Chem.* **2010,** *8,* 234–246. doi:10.1039/b909133e
4. Hahnke, S.; Brock, N. L.; Zell, C.; Simon, M.; Dickschat, J. S.; Brinkhoff, T. *Syst. Appl. Microbiol.* **2013,** *36,* 39–48. doi:10.1016/j.syapm.2012.09.004
5. Trust, T. J. *Antimicrob. Agents Chemother.* **1975,** *7,* 500–506. doi:10.1128/AAC.7.5.500
6. Trust, T. J.; Bartlett, K. H. *Antimicrob. Agents Chemother.* **1975,** *8,* 381–383. doi:10.1128/AAC.8.3.381
7. Liang, L. Investigation of Secondary Metabolites of North Sea Bacteria: Fermentation, Isolation, Structure Elucidation and Bioactivity. Ph.D. Thesis, University of Göttingen, Göttingen, Germany, 2003.
8. Berger, M.; Brock, N. L.; Liesegang, H.; Dogs, M.; Preuth, I.; Simon, M.; Dickschat, J. S.; Brinkhoff, T. *Appl. Environ. Microbiol.* **2012,** *78,* 3539–3551. doi:10.1128/AEM.07657-11
9. Seyedsayamdost, M. R.; Case, R. J.; Kolter, R.; Clardy, J. *Nat. Chem.* **2011,** *3,* 331–335. doi:10.1038/nchem.1002
10. Seyedsayamdost, M. R.; Carr, G.; Kolter, R.; Clardy, J. *J. Am. Chem. Soc.* **2011,** *133,* 18343–18349. doi:10.1021/ja207172s
11. Curson, A. R. J.; Todd, J. D.; Sullivan, M. J.; Johnston, A. W. B. *Nat. Rev. Microbiol.* **2011,** *9,* 849–859. doi:10.1038/nrmicro2653
12. Yoch, D. C. *Appl. Environ. Microbiol.* **2002,** *68,* 5804–5815. doi:10.1128/AEM.68.12.5804-5815.2002
13. Wingenter, O. W.; Haase, K. B.; Strutton, P.; Friederich, G.; Meinardi, S.; Blake, D. R.; Rowland, F. S. *Proc. Natl. Acad. Sci. U. S. A.* **2004,** *101,* 8537–8541. doi:10.1073/pnas.0402744101
14. Howard, E. C.; Henriksen, J. R.; Buchan, A.; Reisch, C. R.; Bürgmann, H.; Welsh, R.; Ye, W.; González, J. M.; Mace, K.; Joye, S. B.; Kiene, R. P.; Whitman, W. B.; Moran, M. A. *Science* **2006,** *314,* 649–652. doi:10.1126/science.1130657
15. Reisch, C. R.; Moran, M. A.; Whitman, W. B. *J. Bacteriol.* **2008,** *190,* 8018–8024. doi:10.1128/JB.00770-08
16. Reisch, C. R.; Stoudemayer, M. J.; Varaljay, V. A.; Amster, I. J.; Moran, M. A.; Whitman, W. B. *Nature* **2011,** *473,* 208–211. doi:10.1038/nature10078
17. Thole, S.; Kalhoefer, D.; Voget, S.; Berger, M.; Engelhardt, T.; Liesegang, H.; Wollherr, A.; Kjelleberg, S.; Daniel, R.; Simon, M.; Thomas, T.; Brinkhoff, T. *ISME J.* **2012,** *6,* 2229–2244. doi:10.1038/ismej.2012.62
18. Mittenhuber, G.; Sonomoto, K.; Egert, M.; Friedrich, C. G. *J. Bacteriol.* **1991,** *173,* 7340–7344.
19. Wodara, C.; Kostka, S.; Egert, M.; Kelly, D. P.; Friedrich, C. G. *J. Bacteriol.* **1994,** *176,* 6188–6191.
20. Wodara, C.; Bardischewsky, F.; Friedrich, C. G. *J. Bacteriol.* **1997,** *179,* 5014–5023.
21. Friedrich, C. G.; Quentmeier, A.; Bardischewsky, F.; Rother, D.; Kraft, R.; Kostka, S.; Prinz, H. *J. Bacteriol.* **2000,** *182,* 4677–4687. doi:10.1128/JB.182.17.4677-4687.2000
22. Rother, D.; Henrich, H.-J.; Quentmeier, A.; Bardischewsky, F.; Friedrich, C. G. *J. Bacteriol.* **2001,** *183,* 4499–4508. doi:10.1128/JB.183.15.4499-4508.2001
23. Quentmeier, A.; Friedrich, C. G. *FEBS Lett.* **2001,** *503,* 168–172. doi:10.1016/S0014-5793(01)02727-2
24. Schröder, I.; Rech, S.; Krafft, T.; Macy, J. M. *J. Biol. Chem.* **1997,** *272,* 23765–23768. doi:10.1074/jbc.272.38.23765
25. Dickschat, J. S.; Zell, C.; Brock, N. L. *ChemBioChem* **2010,** *11,* 417–425. doi:10.1002/cbic.200900668
26. Ansede, J. H.; Pellechia, P. J.; Yoch, D. C. *Environ. Sci. Technol.* **1999,** *33,* 2064–2069. doi:10.1021/es9812296
27. Petersen, J.; Brinkmann, H.; Berger, M.; Brinkhoff, T.; Päuker, O.; Pradella, S. *Mol. Biol. Evol.* **2011,** *28,* 1229–1240. doi:10.1093/molbev/msq310
28. Kameoka, H.; Higuchi, M. *Nippon Nogei Kagaku Kaishi* **1976,** *50,* 185–186. doi:10.1271/nogeikagaku1924.50.4_185
29. Chen, C. C.; Ho, C. T. *J. Agric. Food Chem.* **1986,** *34,* 830–833. doi:10.1021/jf00071a016
30. Morita, K.; Kobayashi, S. *Tetrahedron Lett.* **1966,** *7,* 573–577. doi:10.1016/S0040-4039(01)99667-4
31. González, J. M.; Covert, J. S.; Whitman, W. B.; Henriksen, J. R.; Mayer, F.; Scharf, B.; Schmitt, R.; Buchan, A.; Fuhrman, J. A.; Kiene, R. P.; Moran, M. A. *Int. J. Syst. Evol. Microbiol.* **2003,** *53,* 1261–1269. doi:10.1099/ijs.0.02491-0
32. Shiba, T. *Syst. Appl. Microbiol.* **1991,** *14,* 140–145. doi:10.1016/S0723-2020(11)80292-4
33. Wagner-Döbler, I.; Rheims, H.; Felske, A.; El-Ghezal, A.; Flade-Schröder, D.; Laatsch, H.; Lang, S.; Pukall, R.; Tindall, B. J. *Int. J. Syst. Evol. Microbiol.* **2004,** *54,* 1177–1184. doi:10.1099/ijs.0.02850-0

34. Biebl, H.; Allgaier, M.; Tindall, B. J.; Koblizek, M.; Lünsdorf, H.; Pukall, R.; Wagner-Döbler, I. *Int. J. Syst. Evol. Microbiol.* **2005,** *55,* 1089–1096. doi:10.1099/ijs.0.63511-0
35. Biebl, H.; Pukall, R.; Lünsdorf, H.; Schulz, S.; Allgaier, M.; Tindal, B. J.; Wagner-Döbler, I. *Int. J. Syst. Evol. Microbiol.* **2007,** *57,* 1095–1107. doi:10.1099/ijs.0.64821-0
36. Biebl, H.; Tindall, B. J.; Pukall, R.; Lünsdorf, H.; Allgaier, M.; Wagner-Döbler, I. *Int. J. Syst. Evol. Microbiol.* **2006,** *56,* 821–826. doi:10.1099/ijs.0.63958-0
37. Biebl, H.; Allgaier, M.; Lünsdorf, H.; Pukall, R.; Tindall, B. J.; Wagner-Döbler, I. *Int. J. Syst. Evol. Microbiol.* **2005,** *55,* 2377–2383. doi:10.1099/ijs.0.63832-0

License and Terms

This is an Open Access article under the terms of the Creative Commons Attribution License (http://creativecommons.org/licenses/by/2.0), which permits unrestricted use, distribution, and reproduction in any medium, provided the original work is properly cited.

The license is subject to the *Beilstein Journal of Organic Chemistry* terms and conditions: (http://www.beilstein-journals.org/bjoc)

The definitive version of this article is the electronic one which can be found at: doi:10.3762/bjoc.9.108

Beilstein Journal of Organic Chemistry

Design and synthesis of tag-free photoprobes for the identification of the molecular target for CCG-1423, a novel inhibitor of the Rho/MKL1/SRF signaling pathway

Jessica L. Bell[1], Andrew J. Haak[2], Susan M. Wade[2], Yihan Sun[3], Richard R. Neubig[2] and Scott D. Larsen[*1]

Letter

Open Access

Address:
[1]Vahlteich Medicinal Chemistry Core, Department of Medicinal Chemistry, College of Pharmacy, University of Michigan, Ann Arbor, MI 48109, USA, [2]Department of Pharmacology, University of Michigan Medical School, University of Michigan, Ann Arbor, MI 48109, USA and [3]College of Pharmacy, University of Michigan, Ann Arbor, MI 48109, USA

Email:
Scott D. Larsen[*] - sdlarsen@umich.edu

* Corresponding author

Keywords:
CCG-1423; click ligation; photoaffinity labeling; Rho pathway inhibitor; tag-free photoprobe; target identification

Beilstein J. Org. Chem. **2013,** *9,* 966–973.
doi:10.3762/bjoc.9.111

Received: 13 February 2013
Accepted: 26 April 2013
Published: 21 May 2013

This article is part of the Thematic Series "Synthetic probes for the study of biological function".

Guest Editor: J. Aubé

© 2013 Bell et al; licensee Beilstein-Institut.
License and terms: see end of document.

Abstract

CCG-1423 and related analogues represent a new class of inhibitors of Rho/MKL1/SRF-mediated gene transcription, a pathway that has been implicated in both cancer and fibrosis. The molecular target for these compounds is unknown. To facilitate its identification, a series of tag-free photoaffinity probes was designed and synthesized, each one containing a photoactivatable group and an acetylenic end group for subsequent attachment to a fluorescent tag using click chemistry. All were confirmed to maintain biological activity in a cell-based assay for inhibition of SRE-Luc expression. The functional activity of the most potent probe **24** was further confirmed in an assay for PC-3 cell migration. Photolysis of **24** in intact PC-3 cells followed by cell lysis, click ligation of a fluorescent dye, and gel electrophoresis revealed specific labeling of a single 24 kDa band that could be blocked with an active competitor. Future work will focus on identifying the labeled protein(s).

Findings

Serum-induced signaling through Rho leads to gene-transcriptional effects, which are mediated by serum response factor (SRF), a MADS box transcription factor that binds to the serum response element (SRE) in the promoters of various immediate-early and muscle-specific genes. These signals involve release from cytosolic actin of the transcriptional coactivator MKL1, first identified in megakaryocytic leukemia (also known as myocardin-related transcription factor MRTF-A). Upon acti-

vation, MKL1 translocates to the nucleus where it binds to SRF to collaborate in the activation of the transcription of a number of genes including c-fos and SRF itself [1-4]. This pathway has been implicated in cancer metastasis [5] and, more recently, in fibrosis [6,7], making it an intriguing drug target.

We recently reported a series of compounds that inhibit gene expression mediated by this Rho/MKL1/SRF signaling pathway [8]. The lead CCG-1423 (**1**, Figure 1) was identified in a cell-based high-throughput screen as an inhibitor of expression of a luciferase reporter gene driven by the serum response element promoter (SRE-Luc) [9]. Analysis of the mechanism of **1** showed that it acts at or downstream of MKL1 but upstream of SRF. Recent observations from our lab and others [10] have shown that **1** blocks MKL1 nuclear localization. The specific molecular target leading to inhibition of MKL1 function by **1**, however, is not known.

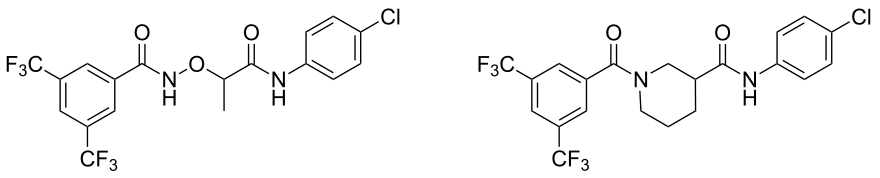
Identification of the macromolecular target(s) of **1** would allow us to employ rational and structure-based drug design to create more potent and selective therapeutics for the treatment of RhoA-related disorders. Early efforts at optimization in our laboratory led to nipecotic (bis)amide analogue **2** (CCG-100602, Figure 1), which was less potent (IC_{50} 9.8 μM versus 1.5 μM), but maintained similar maximal efficacy to that of **1** with significantly less cytotoxicity [8]. We therefore selected **2** as a template for the design of affinity probes.

The successful isolation/identification of molecular targets for low-affinity ligands and/or low-abundance targets requires photolabeling [11]. This permits extensive isolation and purification without premature dissociation from the target. Based on the structure–activity relationship (SAR) of **2**, we hypothesized that we could integrate photoactivatable functional groups without loss of activity. A variety of such groups that differ in their reactivities and chemoselectivities are available [12,13].

Photolabeling of cellular targets is typically done after cell lysis. However, if the molecular target for **2** is a multiprotein complex, membrane-bound, or integral to the nucleus, the process of cell lysis could compromise its integrity to such an extent that it would no longer retain its affinity for **2**. There are in fact reports of target ID studies that were only successful when performed using intact cells [14-16]. We considered this an ideal approach in light of our current hypothesis regarding the mechanism of action of **1** (redistribution of MKL primarily into the cytosol), which may require an intact actin cytoskeleton or nucleus. We thus elected to design photoaffinity probes that were tag-free, i.e., lacking either a biotin or fluorescent tag [17]. There are a number of distinct advantages to this approach: (1) the probes would retain low molecular weights and polar surface areas, and therefore good cell permeability, (2) minimal structural change would maximize the likelihood of maintaining affinity for the target; and (3) affinity for the target could be confirmed in cell-based phenotypic assays prior to any photolabeling studies. Tag-free photoprobes have also been reported to result in much less nonspecific binding relative to corresponding biotinylated photoprobes [18].

The design of our tag-free photoprobes followed the model pioneered by the Cravatt group in performing activity-based protein profiling (ABPP) [19,20]. This entails the incorporation of a ligand for recognition by the target, a reactive functionality for covalently bonding to the target, and either an azide or acetylene moiety as a latent linker for subsequent ligation of a tag for isolation and/or visualization (e.g., biotin or fluorophore) via click chemistry. This technology has been highly successful in profiling enzyme activity in living cells and even in whole organisms [21]. In ABPP, covalent linkage by the reactive functionality is usually dependent upon a particular enzymatic reaction, but photoactivatable groups (PGs) have also been used when this is not possible [22].

We envisioned adapting this technology to intracellular target identification as depicted in Figure 2. Whole cells would be incubated with a photoprobe (A) after confirmation of its biological activity. Following exposure to UV light, the cells would be lysed, releasing the labeled proteins bound covalently to the probe (B). Click chemistry would then be applied to covalently attach a biotin or fluorescent tag for visualization and/or isolation (C). Any isolated proteins would be digested and identified by high-resolution mass-spectral analysis.



1 (CCG-1423) **2** (CCG-100602)

Figure 1: Structures of lead Rho/MKL1/SRF inhibitor **1** and conformationally restricted analogue **2**.

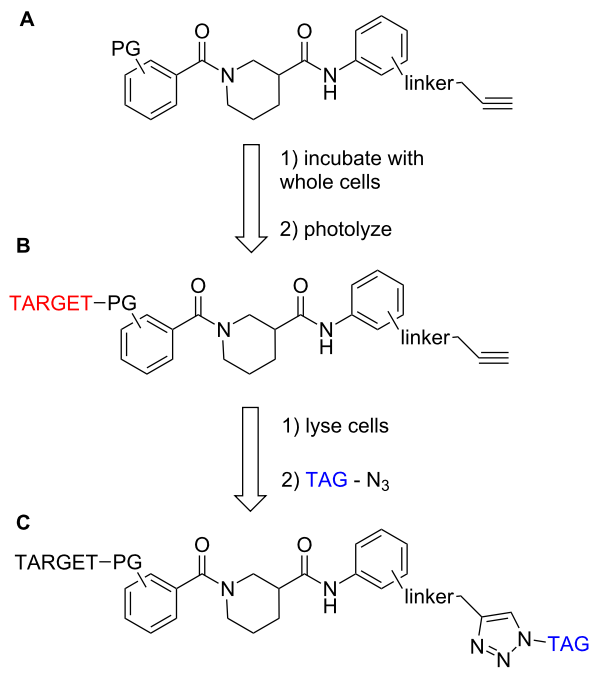
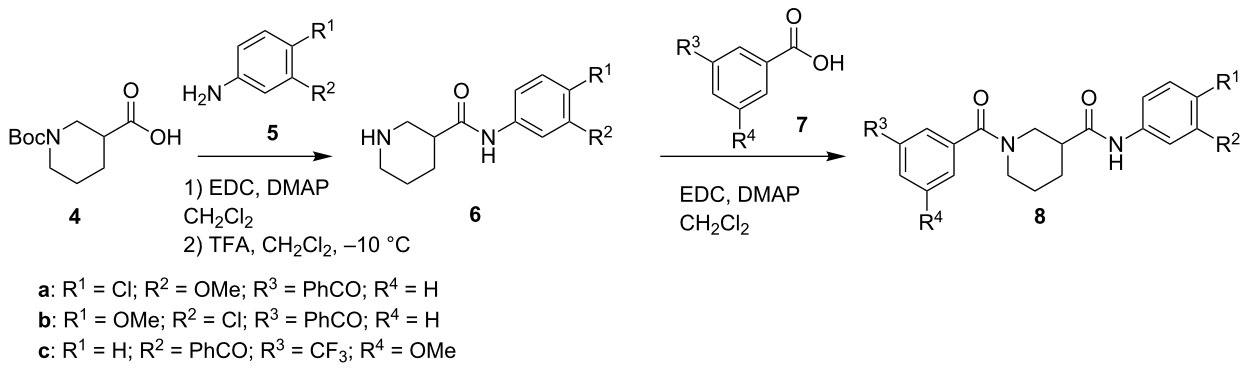


Figure 2: Strategy for tag-free photolabeling in whole cells (PG = photoactivatable group, TAG = fluorescent group or biotin).

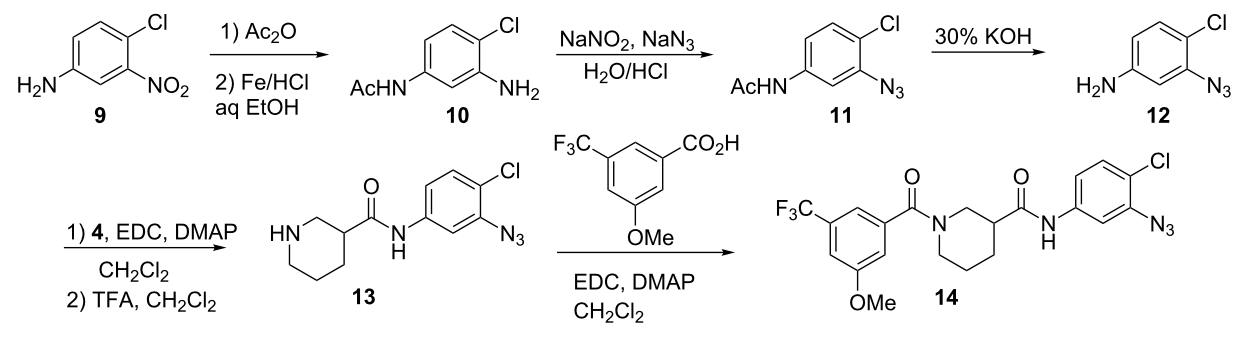
We selected benzophenone and azide as the PGs for incorporation into **2** based on synthetic ease and their complementary photoreactivities (benzophenone inserts into C–H bonds, azide into heteroatom–H bonds) [12]. Furthermore, we had previously established that benzophenone is tolerated on the benzamide ring with retention of the biological activity (**3**, Table 1) [23]. In addition to a PG, we needed a suitable linking functionality for attachment of a clickable acetylene group. Preliminary work (data not shown) established that an ether (versus amide) linker was superior with regard to maintenance of biological activity. A small set of model compounds was thus prepared to evaluate the impact of ether linker and PG placement on biological activity (see below in Table 1).

Scheme 1 depicts the general synthesis of model benzophenone-probes **8**. Boc-protected nipecotic acid (**4**) was reacted with substituted anilines **5** under standard EDC-mediated amidation conditions, followed by TFA-catalyzed deprotection to afford amides **6**. A subsequent second amidation with benzoic acids **7** afforded final bis(amide) analogues **8**.

We also synthesized a model azide (Scheme 2). Synthesis began with the acetylation of 4-chloro-3-nitroaniline (**9**) followed by reduction of the nitro group using iron and hydrochloric acid to



Scheme 1: General synthesis of model benzophenone probes.



Scheme 2: Synthesis of aryl azide model probe **14**.

generate aniline **10**. The azido group was introduced by diazotization/azidation to provide **11**. Deacetylation with potassium hydroxide revealed aniline **12**, which was then coupled with **4** and deprotected to give amine **13**. Final amidation with 3-methoxy-5-trifluoromethylbenzoic acid provided model probe **14**.

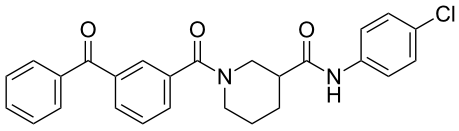
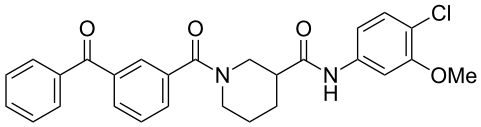
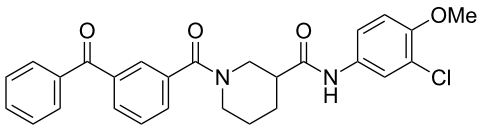
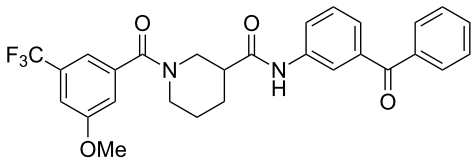
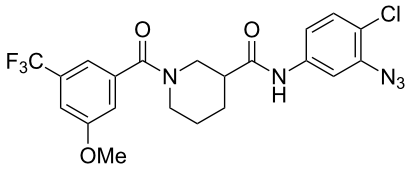
Table 1 presents biological activity data for all of the new model probes. These include: potency at inhibiting the Rho/MKL1/SRF-driven expression of a luciferase reporter gene (IC_{50} SRE.L) and a measure of maximal efficacy, as indicated by percent inhibition of SRE.L at the maximum dose tested (100 μM) [8,9]. We have noted in our previous work that both of these parameters are important for predicting activity in inhibiting cell migration [8]. As shown in Table 1, all of the model probes retained good activity relative to the lead compound **2** with little to no cytotoxicity. Based on these results we decided to install acetylenes in our final probes through ether linkages at the positions of the methoxy groups of the most active models **8a**, **8c** and **14**.

Preparation of the photoaffinity probe **19** is shown in Scheme 3. Aniline **15** was Boc-protected [24], and then alkylated using propargyl bromide to produce ether **16**. Following deprotection, aniline **17** was coupled with Boc-protected nipecotic acid (**4**), giving amide **18** after deprotection. Final coupling with 3-benzoylbenzoic acid afforded the final probe **19**.

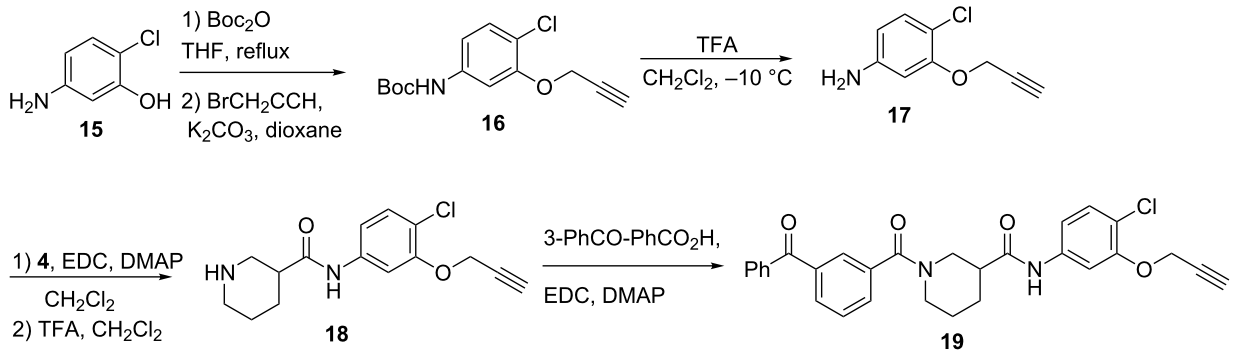
Synthesis of a photoprobe based on the most active model **8c** is shown in Scheme 4. Acid **20** was esterified prior to alkylation with propargyl bromide, affording ester **22**. Saponification, followed by amidation with the previously prepared piperidine **6c**, provided the final probe **24**.

Finally, two azide photoprobes were prepared. The first one, **25** (Scheme 5), based on model **14**, was synthesized in a straightforward manner by simply amidating acid **23** with previously prepared azide-containing piperdine **13** (Scheme 2). The second probe, **28**, reversing the placement of the azide and acetylene, was prepared from aniline **26**. Introduction of the azide was accomplished via diazotization/azidation, followed by standard

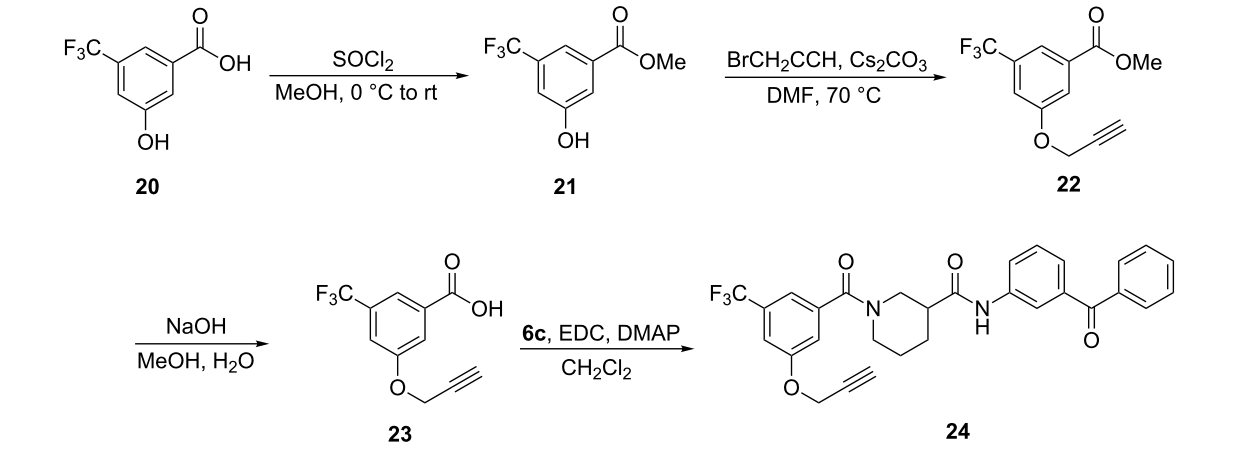
Table 1: Effects of model photoprobes on transcription and cytotoxicity in PC-3 cells[a].

compound	structure	IC_{50} SRE.L (μM)[b]	% inhibition SRE.L (100 μM)[b]	% inhibition WST-1 (100 μM)[c]
3		9.9	75	0
8a		8.3	84	0
8b		11	64	0
8c		5.3	60	0
14		7.0	77	13

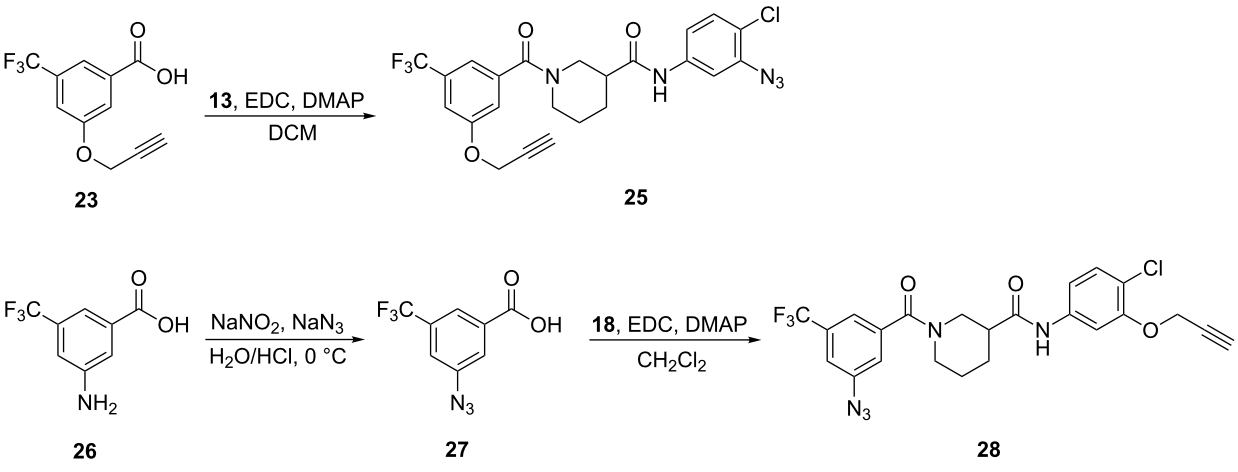
[a]For detailed assay descriptions, see Evelyn et al. [8,9]; [b]Inhibition of Rho-pathway selective serum response element-luciferase reporter gene expression; [c]Inhibition of mitochondrial metabolism of WST-1.



Scheme 3: Synthesis of benzophenone photoaffinity probe **19**.



Scheme 4: Synthesis of benzophenone photoaffinity probe **24**.



Scheme 5: Synthesis of aryl azide photoaffinity probes.

amide coupling of **27** and **18** to afford final aryl azide photoprobe **28**.

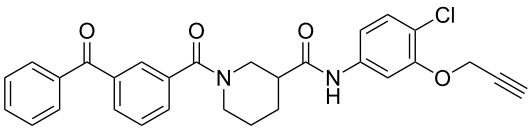
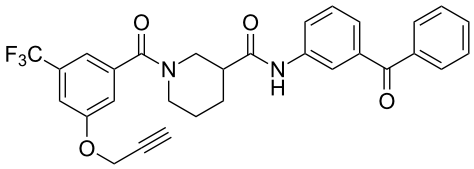
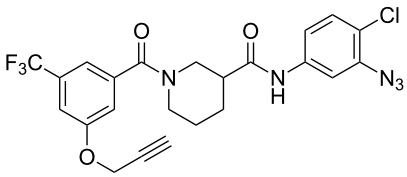
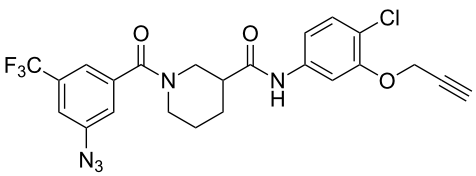
Table 2 summaries the biological data for the four final candidate photoprobes. Fortuitously, all of the probes remained active in our assay, although the benzophenone analogues **19** and **24** were more potent than the azide probes **25** and **28**. Based on its superior potency, we selected benzophenone **24** (IC_{50} = 2.7 μM) for further studies.

Prior to photolabeling, we wanted to confirm retention of functional activity in a PC-3 prostate cancer cell model of migration. Cells (5.0×10^5) were plated in DMEM containing 10% FBS and grown to confluence in a 12-well plate. After 24 h, a scratch was made using a 200 μL pipette tip. Medium was replaced with DMEM containing 0.5% FBS and varying concentrations of **24** or 0.1% DMSO control. Images of the wound were taken at the beginning of the experiment by using a bright-field inverted microscope (Leica DM IRB) at 2.5× magnification. After 24 h the cells were fixed (10% formalin) and stained (0.5% crystal violet) to obtain high-contrast images. Area quantification of the wound was determined computationally using the ImageJ® software (NIH). The results are summarized in Figure 3. Probe **24** was clearly able to inhibit PC-3 cell migration into the scratch wound with an IC_{50} (4.7 μM) comparable to its potency at inhibiting SRE.L (2.7 μM).

Preliminary photolabeling studies with **24** were undertaken in PC-3 prostate cancer cells. Intact cells were treated with 0.3 μM **24** for 30 min. To facilitate the identification of specifically labeled proteins, a parallel competition experiment was also performed by treating cells with 0.3 μM **24** and a large excess (10 μM) of **29** (Figure 4), i.e., an analogue of **2** with slightly greater potency (IC_{50} = 6.4 μM) that was identified in later SAR studies [23]. UV irradiation was applied for 30 min at room temperature by using the long-wavelength setting of a hand-held illuminator (366 nm, UVL-56 lamp, UltraViolet Products, San Gabriel CA). Cells were then lysed and subsequently fluorescently tagged by using an Invitrogen™ Click-iT® Reaction Buffer Kit to attach azido-Cy5.5 dye for visualization.

Electrophoresis of the tagged lysates was performed, using either 20 or 10 μg of protein, and is visualized in Figure 5. Lane 1 contains 0.3 μM of compound **24** alone, and lane 2 includes a much higher concentration of the competitor **29**. Lane 3 contains 0.3 μM of compound **24** alone without UV treatment. Although there is obviously a high degree of nonspecific

Table 2: Effects of tag-free photoprobes on transcription and cytotoxicity in PC-3 cells[a].

compound	structure	IC_{50} SRE.L (μM)	% inhibition SRE.L (100 μM)	% inhibition WST-1 (100 μM)
19		6.6	57	0
24		2.7	60	0
25		11	75	4
28		17	54	2

[a]See Table 1 for assay descriptions.

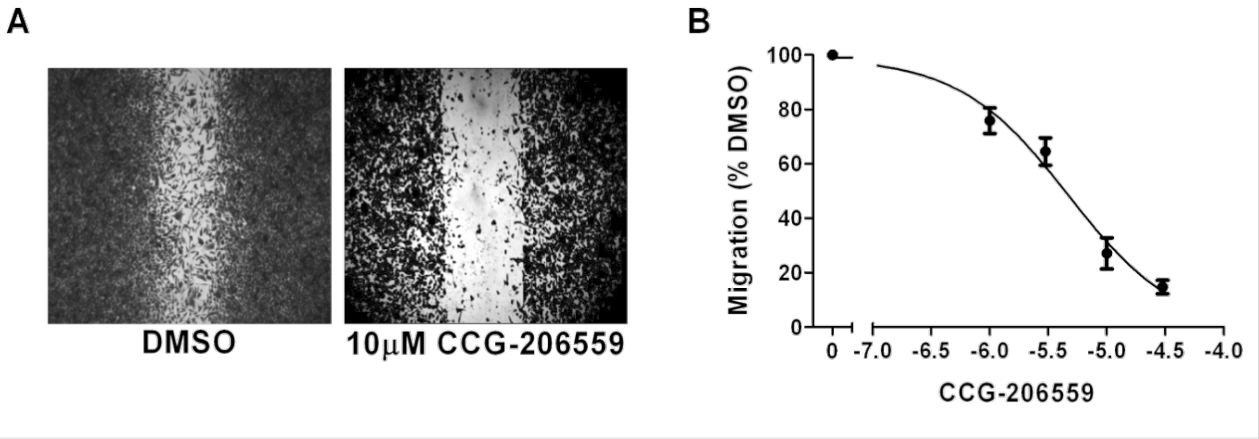
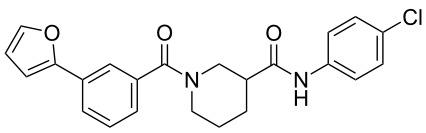


Figure 3: Photoprobe **24** (CCG-206559) retains biological activity to block prostate cancer migration. **A.** Cellular migration determined by wound assay. PC-3 prostate cancer cells were grown to confluence in 12-well plates and a scratch was made with a 200 µL pipette. Images were taken at the beginning of the experiment and after 24 h in DMEM containing 0.5% FBS and the indicated concentration of **24** or 0.1% DMSO. After 24 h the cells were stained with crystal violet to produce high-contrast images. Shown are examples of 10 µM **24** and DMSO after 24 h, from experiments with similar initial wound areas as determined by using image analysis software. **B.** Quantification of wound assay migration. The change in migration over 24 h was determined by the difference between the area of the wound after 24 h and the initial area of the wound. The percent inhibition was plotted by normalizing the compound-treated cells to the DMSO control. Results are expressed as the mean (±SEM) of triplicate experiments. A nonlinear least-squares regression curve was fit for CCG-206559 inhibition of migration, IC_{50} = 4.7 µM.



29

Figure 4: Structure of the competitor used in the photolabeling experiment.

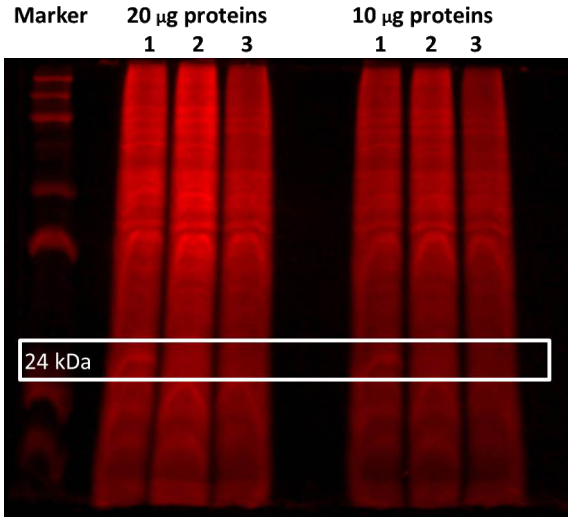


Figure 5: SDS-PAGE gel of photolabeling experiment in whole PC-3 cells. Lane 1 contains 0.3 µM **24** after 30 min UV treatment; lane 2 contains 0.3 µM **24** and 10 µM **29** after 30 min UV treatment; and lane 3 contains 0.3 µM **24** without UV treatment.

binding under these conditions, a single band appears at approximately 24 kDa (as indicated by the white box) that was competed off by **29** and does not appear without UV treatment, suggesting that it is a specific binding protein that has been successfully photolabeled.

Although the level of fluorescent labeling in the non-UV-irradiated control lanes 3 is clearly diminished relative to lanes 1 and 2, it is nevertheless much higher than expected. Unfortunately, we do not yet have a satisfactory explanation for this. Future experiments will include using an even lower concentration of photoprobe (which is reported to minimize nonspecific binding [11]) and rigorous exclusion of light during processing of the cell lysates.

In conclusion, we have designed and synthesized tag-free benzophenone and aryl azide photoaffinity probes that retain the biological activity of the lead Rho/MKL1/SRF transcription inhibitor **2** in whole cells. Significantly, a preliminary photolabeling study with the most potent photoprobe **24** in whole prostate cancer cells was successful at detecting specific binding to one or more proteins at 24 kDa. Future work will focus on identifying the labeled protein(s). We first plan to repeat the photolabeling study with **24** and tag the labeled proteins by clicking with azido-biotin, thereby enabling isolations with streptavidin. Following purification, the 24 kDa region of the lanes (± competitor **29**) will be trypsin-digested and analyzed for differences by high resolution LC/MS/MS. If this is not successful, future work will entail using probe **24** and competitor **29** in SILAC experiments [25].

Supporting Information

Supporting Information File 1

Full experimental synthetic procedures and spectral data are provided for compounds **4, 6a, 6b, 8a, 8b, 8c, 13, 14, 16–19, 21–25** and **28**.
[http://www.beilstein-journals.org/bjoc/content/supplementary/1860-5397-9-111-S1.pdf]

References

1. Miralles, F.; Posern, G.; Zaromytidou, A.-I.; Treisman, R. *Cell* **2003,** *113,* 329–342. doi:10.1016/S0092-8674(03)00278-2
2. Parmacek, M. S. *Circ. Res.* **2007,** *100,* 633–644. doi:10.1161/01.RES.0000259563.61091.e8
3. Pipes, G. C. T.; Creemers, E. E.; Olson, E. N. *Genes Dev.* **2006,** *20,* 1545–1556. doi:10.1101/gad.1428006
4. Cen, B.; Selvaraj, A.; Prywes, R. *J. Cell. Biochem.* **2004,** *93,* 74–82. doi:10.1002/jcb.20199
5. Medjkane, S.; Perez-Sanchez, C.; Gaggioli, C.; Sahai, E.; Treisman, R. *Nat. Cell Biol.* **2009,** *11,* 257–268. doi:10.1038/ncb1833
6. Small, E. M.; Thatcher, J. E.; Sutherland, L. B.; Kinoshita, H.; Gerard, R. D.; Richardson, J. A.; DiMaio, J. M.; Sadek, H.; Kuwahara, K.; Olson, E. N. *Circ. Res.* **2010,** *107,* 294–304. doi:10.1161/CIRCRESAHA.110.223172
7. Luchsinger, L. L.; Patenaude, C. A.; Smith, B. D.; Layne, M. D. *J. Biol. Chem.* **2011,** *286,* 44116–44125. doi:10.1074/jbc.M111.276931
8. Evelyn, C. R.; Bell, J. L.; Ryu, J. G.; Wade, S. M.; Kocab, A.; Harzdorf, N. L.; Showalter, H. D. H.; Neubig, R. R.; Larsen, S. D. *Bioorg. Med. Chem. Lett.* **2010,** *20,* 665–672. doi:10.1016/j.bmcl.2009.11.056
9. Evelyn, C. R.; Wade, S. M.; Wang, Q.; Wu, M.; Iñiguez-Lluhi, J. A.; Merajver, S. D.; Neubig, R. R. *Mol. Cancer Ther.* **2007,** *6,* 2249–2260. doi:10.1158/1535-7163.MCT-06-0782
10. Jin, W.; Goldfine, A. B.; Boes, T.; Henry, R. R.; Ciaraldi, T. P.; Kim, E.-Y.; Emecan, M.; Fitzpatrick, C.; Sen, A.; Shah, A.; Mun, E.; Vokes, V.; Schroeder, J.; Tatro, E.; Jimenez-Chillaron, J.; Patti, M.-E. *J. Clin. Invest.* **2011,** *121,* 918–929. doi:10.1172/JCI41940
11. Leslie, B. J.; Hergenrother, P. J. *Chem. Soc. Rev.* **2008,** *37,* 1347–1360. doi:10.1039/b702942j
12. Fleming, S. A. *Tetrahedron* **1995,** *51,* 12479–12520. doi:10.1016/0040-4020(95)00598-3
13. Dormán, G.; Prestwich, G. D. *Trends Biotechnol.* **2000,** *18,* 64–77. doi:10.1016/S0167-7799(99)01402-X
14. Evans, M. J.; Saghatelian, A.; Sorensen, E. J.; Cravatt, B. F. *Nat. Biotechnol.* **2005,** *23,* 1303–1307. doi:10.1038/nbt1149
15. Speers, A. E.; Cravatt, B. F. *Chem. Biol.* **2004,** *11,* 535–546. doi:10.1016/j.chembiol.2004.03.012
16. Colca, J. R.; McDonald, W. G.; Waldon, D. J.; Thomasco, L. M.; Gadwood, R. C.; Lund, E. T.; Cavey, G. S.; Mathews, W. R.; Adams, L. D.; Cecil, E. T.; Pearson, J. D.; Bock, J. H.; Mott, J. E.; Shinabarger, D. L.; Xiong, L.; Mankin, A. S. *J. Biol. Chem.* **2003,** *278,* 21972–21979. doi:10.1074/jbc.M302109200
17. Lapinsky, D. J. *Bioorg. Med. Chem.* **2012,** *20,* 6237–6247. doi:10.1016/j.bmc.2012.09.010
18. Qiu, W.-W.; Xu, J.; Li, J.-Y.; Li, J.; Nan, F.-J. *ChemBioChem* **2007,** *8,* 1351–1358. doi:10.1002/cbic.200700148
19. Speers, A. E.; Adam, G. C.; Cravatt, B. F. *J. Am. Chem. Soc.* **2003,** *125,* 4686–4687. doi:10.1021/ja034490h
20. Salisbury, C. M.; Cravatt, B. F. *J. Am. Chem. Soc.* **2008,** *130,* 2184–2194. doi:10.1021/ja074138u
21. Salisbury, C. M.; Cravatt, B. F. *QSAR Comb. Sci.* **2007,** *26,* 1229–1238. doi:10.1002/qsar.200740090
22. Li, X.; Hu, Y. *Curr. Med. Chem.* **2010,** *17,* 3030–3044. doi:10.2174/092986710791959747
23. Bell, J. L.; Haak, A. J.; Kirchhoff, P. D.; Neubig, R. R.; Larsen, S. D. *Bioorg. Med. Chem. Lett.*, in press.
24. Dhanak, D.; Knight, S. D. Sulfonamide derivative urotensin-II receptor antagonists, preparation, pharmaceutical compositions, and therapeutic use. WO Patent WO2001045694A1, June 28, 2001.
25. Ong, S.-E.; Schenone, M.; Margolin, A. A.; Li, X.; Do, K.; Doud, M. K.; Mani, D. R.; Kuai, L.; Wang, X.; Wood, J. L.; Tolliday, N. J.; Koehler, A. N.; Marcaurelle, L. A.; Golub, T. R.; Gould, R. J.; Schreiber, S. L.; Carr, S. A. *Proc. Natl. Acad. Sci. U. S. A.* **2009,** *106,* 4617–4622. doi:10.1073/pnas.0900191106

License and Terms

This is an Open Access article under the terms of the Creative Commons Attribution License (http://creativecommons.org/licenses/by/2.0), which permits unrestricted use, distribution, and reproduction in any medium, provided the original work is properly cited.

The license is subject to the *Beilstein Journal of Organic Chemistry* terms and conditions: (http://www.beilstein-journals.org/bjoc)

The definitive version of this article is the electronic one which can be found at:
doi:10.3762/bjoc.9.111

Beilstein Journal of Organic Chemistry

Methylidynetrisphosphonates: Promising C_1 building block for the design of phosphate mimetics

Vadim D. Romanenko and Valery P. Kukhar*

Review

Open Access

Address:
Institute of Bioorganic Chemistry and Petrochemistry, National Academy of Sciences, 02660 Kyiv, Ukraine. Fax: 38 044 5732552; Tel: 38 044 5732525

Email:
Valery P. Kukhar* - kukhar@bpci.kiev.ua

* Corresponding author

Keywords:
biomimetic synthesis; C_1 building blocks; phosphorylation; polyphosphonates; synthetic methods

Beilstein J. Org. Chem. **2013,** *9,* 991–1001.
doi:10.3762/bjoc.9.114

Received: 04 February 2013
Accepted: 26 April 2013
Published: 24 May 2013

This article is part of the Thematic Series "Synthetic probes for the study of biological function".

Guest Editor: J. Aubé

© 2013 Romanenko and Kukhar; licensee Beilstein-Institut.
License and terms: see end of document.

Abstract

Methylidynetrisphosphonates are representatives of geminal polyphosphonates bearing three phosphonate (PO_3H_2) groups at the bridged carbon atom. Like well-known methylenebisphosphonates (BPs), they are characterized by a P–C–P backbone structure and are chemically stable mimetics of the endogenous metabolites, i.e., inorganic pyrophosphates (PP_i). Because of its analogy to PP_i and an ability to chelate metal ions, the 1,1,1-trisphosphonate structure is of great potential as a C_1 building block for the design of phosphate mimetics. The purpose of this review is to present a concise summary of the state of the art in trisphosphonate chemistry with particular emphasis on the synthesis, structure, reactions, and potential medicinal applications of these compounds.

Introduction

Methylidynetrisphosphonic acid, $HC(PO_3H_2)_3$, or more commonly methylidynetrisphosphonates, $XC(PO_3R_2)_3$, also called methanetrisphosphonates, are representatives of geminal polyphosphonates among which methylenebisphosphonates, $H_2C(PO_3R_2)_2$, are well-known as metabolically stable analogues of the naturally occurring inorganic pyrophosphate (PP_i) [1-3]. Bisphosphonates are widely used drugs for the treatment and prevention of excessive osteoclast-mediated bone resorption associated with osteoporosis, Paget's disease, and tumour-induced osteolysis [4-6]. In the wide area of polyphosphonate chemistry, *gem*-trisphosphonates represent a new area of study and many of the important developments in their chemistry are based on their specific properties. The presence of three phosphonate (PO_3R_2) substituents at the bridged carbon atom causes pronounced physical and chemical effects and imparts unique electronic characteristics to 1,1,1-trisphosphonylated compounds. Most importantly, the replacement of the hydrogen atom attached to the bridge carbon in methylenebisphosphonates by a third ionisable phosphonate moiety results in *supercharged isosteric systems* relative to pyrophosphoric acid [7]. It was also demonstrated that steric effects play a significant role in trisphosphonate chemistry and allow efficient control of regio- and stereochemistry for addition reactions. Moreover, examples of the reactivity of functionalized methyli-

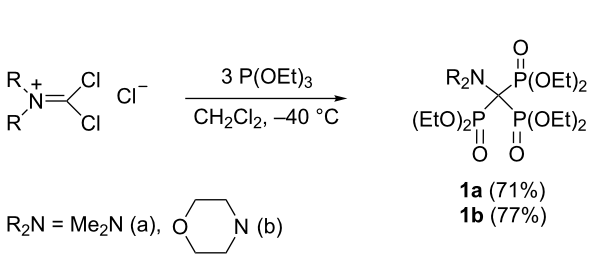
dynetrisphosphonates $XC(PO_3R_2)_3$ shown in this review indicate that the nature of the substituent X at the central carbon atom is the key to the optimization of their acidic and coordination properties thus providing excellent possibilities for the design of effective phosphate mimetics. Especially successful so far seem to be approaches for the synthesis of trisphosphonate-modified nucleotides and nucleosides, which represent a promising class of potential drugs [8].

Review

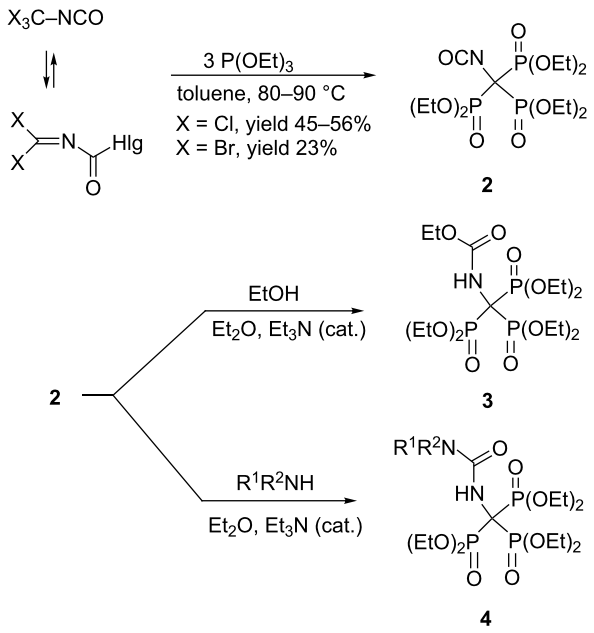
Preparation of methylidynetrisphosphonates

Synthesis via a Michaelis–Arbuzov reaction

Phosphonate esters are often prepared through Michaelis–Arbuzov reaction of a trialkyl phosphite with an alkyl halide [9]. However, contrary to the early patent claims, trisphosphonate esters cannot be derived from simple trihalomethyl derivatives [10-12]. Indeed, chloroform and bromoform do not react with triethyl phosphite even under harsh conditions [11]. In addition, no reaction occurred between benzotrichloride ($PhCCl_3$) and triethyl phosphite at a temperature below 150 °C. The CuCl-catalyzed reaction of $PhCCl_3$ and $(EtO)_3P$ at 120–140 °C produced 1,2-diphenyl-1,1,2,2-tetrachloroethane [13]. The early work reported that the trisphosphonate $PhC(PO_3Et_2)_3$ was formed from triethyl phosphite and dibenzoyl peroxide when reagents were boiled under reflux in chloroform, but proof of the trisphosphonate structure was not given [14]. It was later suggested that the product of this reaction is most likely a phosphate-phosphonate, $PhC(PO_3Et_2)_2OPO_3Et_2$ [15]. Birum postulated the preparation of the trisphosphonate $(Et_2O_3P)_3CSPO_3Et_2$ from Cl_3CSCl and $P(OEt)_3$, but once again, no definitive proof of trisphosphonate structure was provided [16,17]. The first authentic synthesis of 1,1,1-trisphosphonate derivatives **1a**,**b** was described by Kukhar, Pasternak and Kirsanov by allowing the addition of triethyl phosphite to dichloromethylene dialkylammonium chloride to proceed in dichloromethane at −40 °C (Scheme 1) [18]. Other researchers have confirmed this finding [19,20]. Trichloromethylisocyanate [21] and tribromomethylisocyanate [22] react similarly with 3 equivalents of triethyl phosphite forming isocyanate **2,** which was characterized by its IR and NMR spectra and also by its reaction products **3** and **4** (Scheme 2). Trisphosphonate **2** is also formed by the reaction of $[(EtO)_2P(O)]_2C(Cl)NCO$ as well as $(EtO)_2P(O)CCl_2NCO$ with 1 or 2 equiv of $(EtO)_3P$, correspondingly [21].

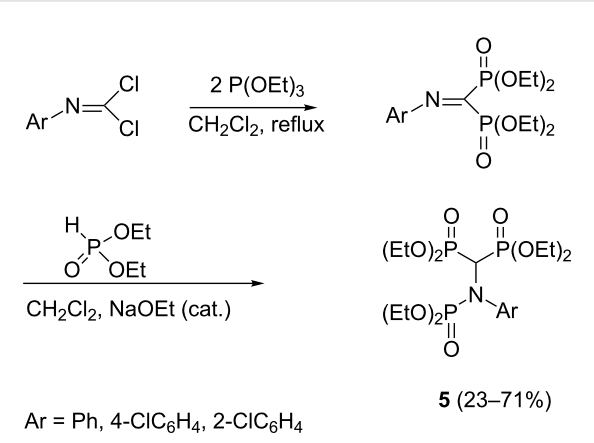


Scheme 1: Synthesis of hexaethyl dialkylaminomethylidynetrisphosphonates **1** from dichloromethylene dialkylammonium chlorides.



Scheme 2: Synthesis and some transformations of trisphosphonate **2**.

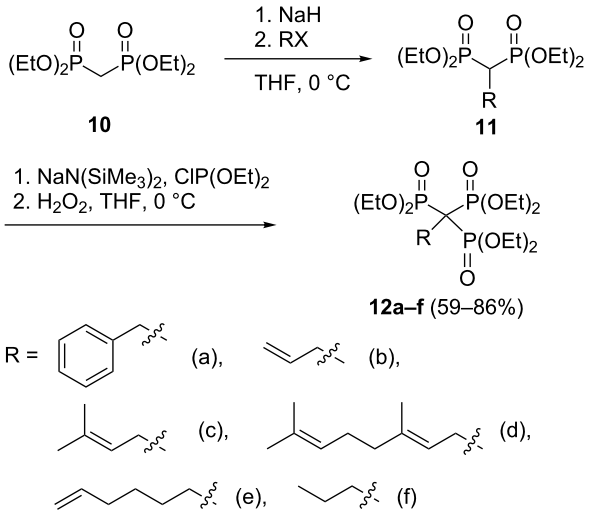
An unsuccessful attempt to synthesize trisphosphonates from isocyanide dichlorides was made by the combination of Arbuzov reaction and dialkyl phosphite addition. The reaction sequence leads to *N*-phosphorylated bisphosphonates **5** instead of the desired trisphosphonates (Scheme 3) [23,24].



Scheme 3: Attempt to synthesize trisphosphonates by the combination of Arbuzov reaction and dialkyl phosphite addition.

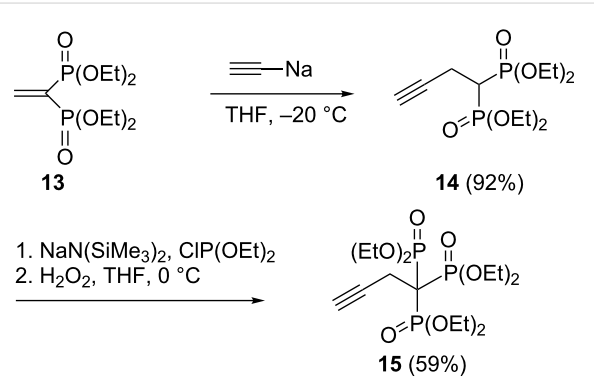
Synthesis via anionic methylenebisphosphonates

The anionic bisphosphonate $[CH(PO_3Et_2)_2]^-$ proved unreactive with diethyl chlorophosphate, $ClP(O)(OEt_2)_2$, but phosphinylation of the bisphosphonate anion with diethyl chlorophosphite, $ClP(OEt)_2$, followed by in situ oxidation with atmospheric oxygen of the presumed phosphinate intermediate to the trisphosphonate **6** was successful (Scheme 4) [25]. An improved version of this method includes oxidation of the phosphinate intermediate with hydrogen peroxide in tetrahydrofuran [26]. Mixed ethyl/isopropyl trisphosphonate ester **9** has been prepared by treatment of the bisphosphonate **7** with diethyl chlorophosphite and sodium hexamethyldisilazane, and subsequent oxidation of the phosphinate intermediate **8** with iodine in pyridine–THF–H_2O (Scheme 5) [7,27]. It was noted that the intermediate **8** was unstable during either acidic or basic workup and readily decomposed to the starting bisphosphonate **7**. However, oxidation of **8** gave stable trisphosphonate ester **9** in 72% yield.



Scheme 6: Synthesis of alkylidyne-1,1,1-trisphosphonate esters **12**.

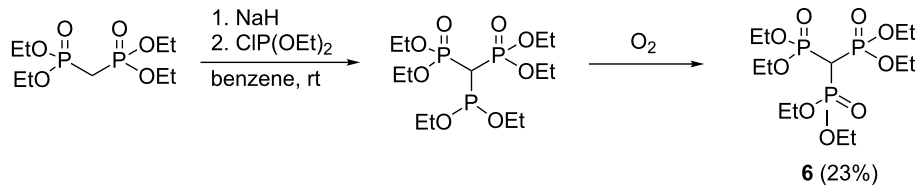
For the synthesis of alkylidyne-1,1,1-trisphosphonate esters **12a**–**f** a three-step protocol including synthesis of alkylidene-1,1-bisphosphonates **11** from tetraethyl methylenebisphosphonate (**10**), phosphinylation and oxidation has been developed (Scheme 6) [26]. Propargyl-substituted trisphosphonate **15** was prepared by conjugate addition of sodium acetylide to ethenylidenebisphosphonate **13** and the subsequent phosphinylation and oxidation (Scheme 7). This compound has been used in an elegant construction ("click" chemistry) of triazole derivatives (see Scheme 17) [26,28].



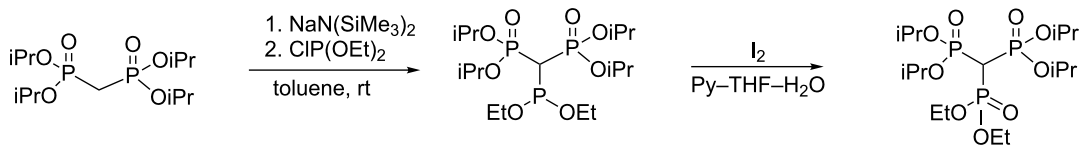
Scheme 7: Two-step one-pot synthesis of propargyl-substituted trisphosphonate **15**.

Synthesis via 7,7-bisphosphonoquinone methides

A unique route to trisphosphonate **18** via addition of diethyl phosphite to 7,7-bisphosphonyl-3,5-di-*tert*-butylquinone

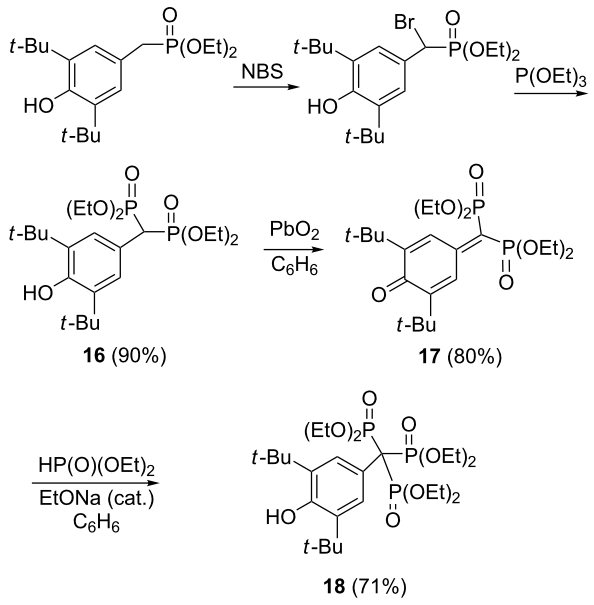


Scheme 4: Synthesis of hexaethylmethylidynetrisphosphonate **6** via phosphinylation of tetraethyl methylenebisphosphonate anion.

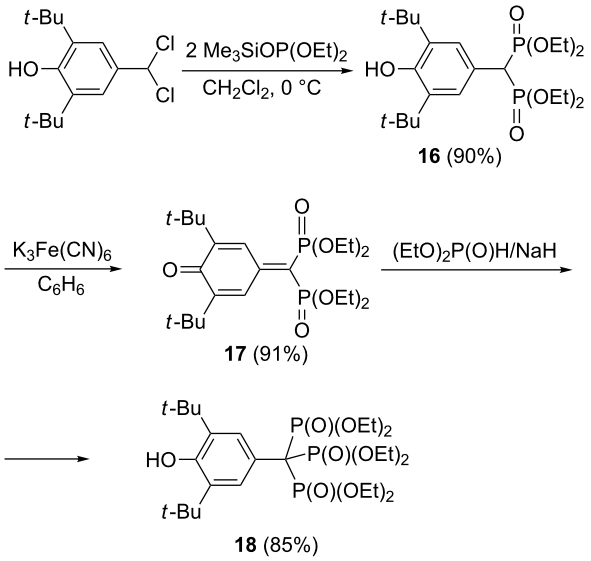


Scheme 5: Synthetic approach to methylidynetrisphosphonate ester **9**.

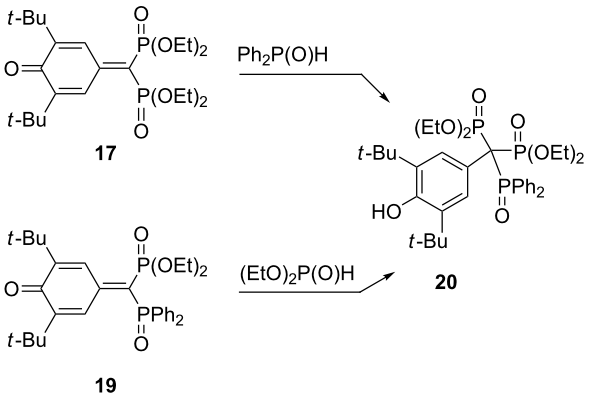
methide **17** derived by oxidation of bisphosphonate **16** was developed by Gross and co-workers (Scheme 8) [29]. More recent reports of this type of reaction are from laboratories of Russian researchers [30,31]. They showed that bisphosphonate **16** can be prepared in good yield by the Arbuzov reaction of trimethylsilyl esters of trivalent phosphorus acids with the easily accessible 2,6-di-*tert*-butyl-4-(dichloromethyl)phenol. In the next step, the bisphosphonate **16** was oxidized with $K_3Fe(CN)_6$ into quinone methide **17** in 91% yield. Further addition of diethyl phosphite in the presence of sodium hydride gives the triphosphonate **18** (Scheme 9). Note that bisphosphonate **16** is also available by the reaction 4-hydroxy-3,5-di-*tert*-butylbenzaldehyde with triethyl phosphite in the presence of malonic ester (yield 53%) [32].



Scheme 8: Synthetic route to trisphosphonate **18** via 7,7-bisphosphonyl-3,5-di-*tert*-butylquinone methide **17**.



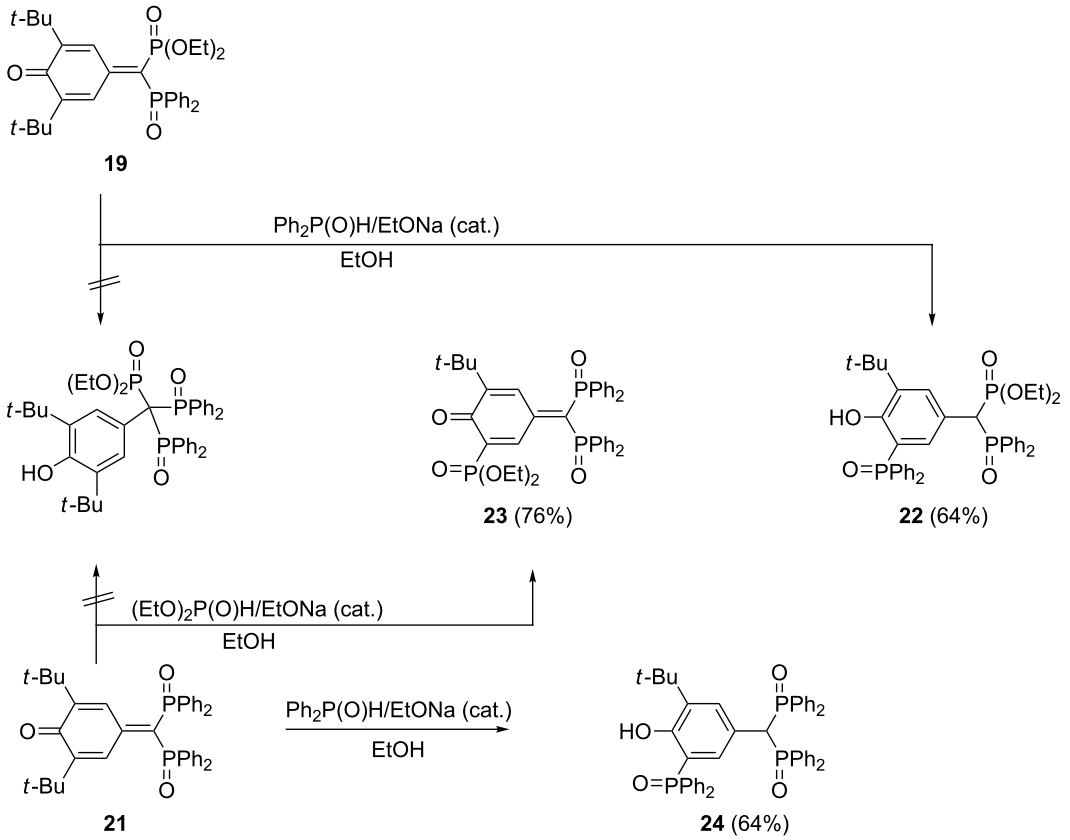
Scheme 9: Synthesis of trisphosphonate **18** starting from 2,6-di-*tert*-butyl-4-(dichloromethyl)phenol.



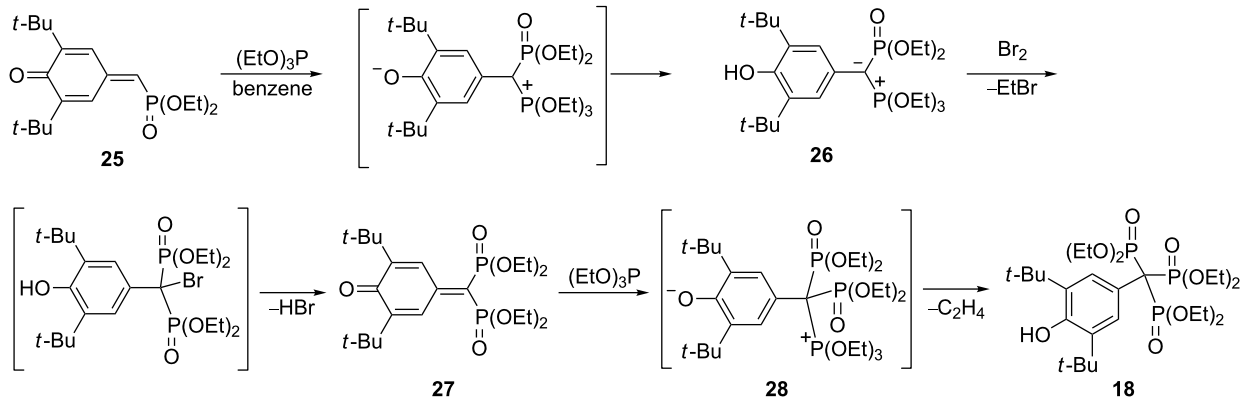
Scheme 10: Synthesis of triphosphorus derivatives **20** via quinone methides **17** and **19**.

This reaction mode takes place also for the interactions of quinone methide **17** with diphenylphosphinite and quinone methide **19** with diethyl phosphite (Scheme 10) [33]. However, when the same researchers tried to obtain triphosphorus derivatives with one phosphono and two phosphinoxido groups using quinone methides **19** and **21** as starting materials, phosphonylation of the aromatic nucleus via splitting off a *tert*-butyl group as isobutene and formation of bisphosphonates **22** and **23** was observed. The same happened when quinone methide **21** was treated with diphenylphosphinite (Scheme 11). The primary step of this reaction, which proceeds under mild alkaline conditions, is presumably a direct attack of the diphenylphosphinyl anion in 3-position, followed by the splitting off of isobutene [33,34].

Variations on the Arbuzov reaction have also been tested in the preparation of trisphosphonate **18**. Thus, a phosphonylation in three steps could be performed on monophosphonylated quinone methide **25**. The starting compound was first phosphonylated with triethyl phosphite to give the phosphonium betain **26**. This compound was subsequently transformed into the corresponding 7,7-bisphosphonoquinone methide **27** by treatment with bromine. Heating of **27** under reflux in triethyl phosphite resulted in the trisphosphonate **18** in a yield of 40%. The phosphonium betain **28**, which was expected from the reaction of **27** and triethyl phosphite was unstable and could not be isolated (Scheme 12) [35]. It should be noted that compound **18** can be easily oxidized to the corresponding stable phenoxyl radical with PbO_2 in toluene [36].



Scheme 11: Unexpected phosphonylation of the aromatic nucleus in reactions of quinone methides **19** and **21**.

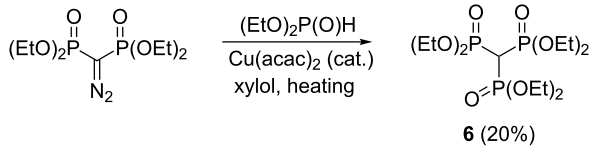


Scheme 12: Multistep synthesis of trisphosphonate **18** starting from quinone methide **25**.

Synthesis from diazomethylenebisphosphonates

The feasibility of synthesizing trisphosphonate esters under mild conditions via metal-carbenoid-mediated P–H insertion reactions was demonstrated by Gross et al. [25]. In particular, the reaction between tetraethyl diazomethylenebisphosphonate and diethyl phosphite in the presence of copper(II) bis(acetylacetonate) provides trisphosphonate ester **6** (Scheme 13). The yield is poor (20%) but the product can be isolated in the pure state and the method is presumably general (cf. [37]). The starting tetraalkyl diazomethylenebisphosphonates are prepared

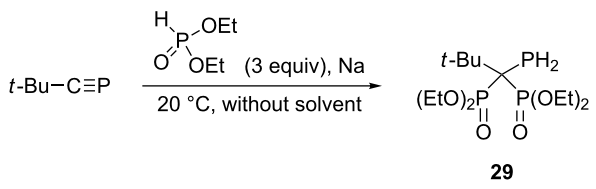
by the reaction of tosyl azide [38,39] or 2-naphthalenesulfonyl azide [40] with the corresponding methylenebisphosphonate precursors in the presence of a base.



Scheme 13: Synthesis of hexaethyl methylidynetrisphosphonate (**6**) via metal-carbenoid-mediated P–H insertion reaction.

Various methods

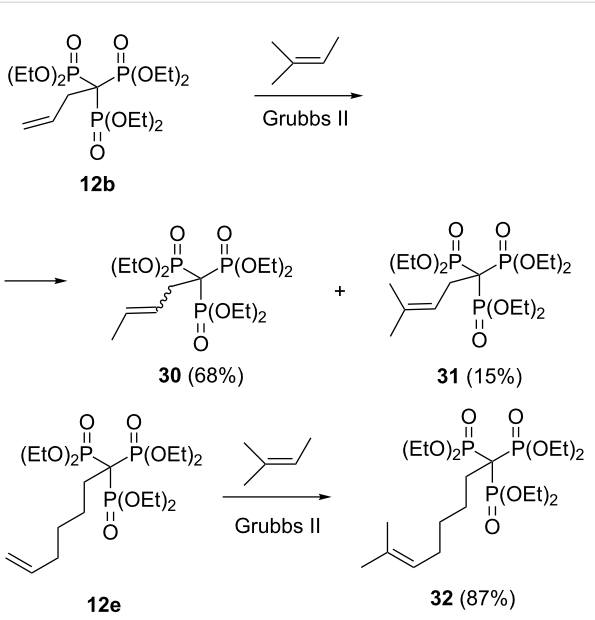
Quite interestingly, at room temperatures diethyl phosphite reacts with *tert*-butylphosphaethyne in the presence of sodium metal to form 1,1-bis(diethoxyphosphoryl)-2,2-dimethylpropylphosphine (**29**) (Scheme 14) [41]. The proof of structure **29** was given but no details were provided on the reaction course.



Scheme 14: Reaction between *tert*-butylphosphaethyne and diethyl phosphite in the presence of sodium metal.

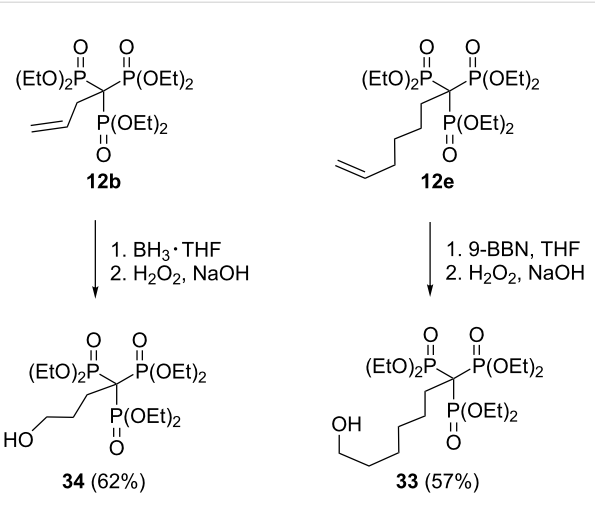
Reactions of methylidynetrisphosphonate esters

The $C(PO_3R_2)_3$ group is chemically resistant to attack by bases and oxidizing/reducing agents. Upon treatment of hexaethyl methylidynetrisphosphonate (**6**) with NaH in THF, formation of the sodium salt was suggested by a downfield shift in the ^{31}P NMR spectrum (from 14 to 32 ppm). However, no further alkylation reaction could be observed with benzyl bromide and allyl bromide, presumably because of high stabilization and strong steric shielding of the carbanionic center [26]. In fact, the importance of steric factors in the reactivity of trisphosphonate esters manifested in many reactions of α-alkyl-substituted trisphosphonates. Thus, attempted cross metathesis of allyl derivative **12b** with 2-methyl-2-butene and the Grubbs second-generation catalyst afforded the unexpected *cis* and *trans*-1,2-disubstituted olefins **30** as the major product and only a small amount of the expected trisubstituted olefin **31**. However, under similar conditions sterically less congested analogue **12e** smoothly undergoes cross metathesis to give the desired trisubstituted olefin **32** in high yield (Scheme 15) [26].

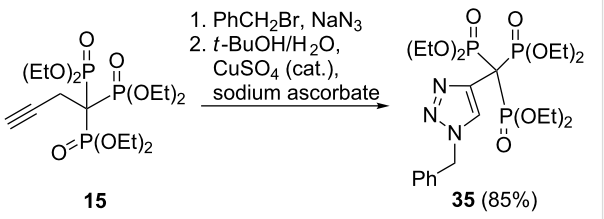


Scheme 15: Cross metathesis of trisphosphonates **12** with 2-methyl-2-butene and the Grubbs second-generation catalyst.

In a similar sense, reduction of the trisphosphonate **12e** with 9-borabicyclo[3.3.1]nonane (9-BBN) followed by standard oxidative workup afforded the primary alcohol **33** in reasonable yield, but the 1-allyl-substituted trisphosphonate **12b** did not undergo hydroboration with 9-BBN. However, treatment of **12b** with borane in THF resulted in conversion to the primary alcohol **34** in good yield (Scheme 16) [26]. A further example of the reactivity of trisphosphonates is provided by a click reaction of 3-butyn-1-ylidynetrisphosphonate **15** with benzyl azide, which results in novel triazole compound **35** bearing the trisphosphonate function (Scheme 17) [26].



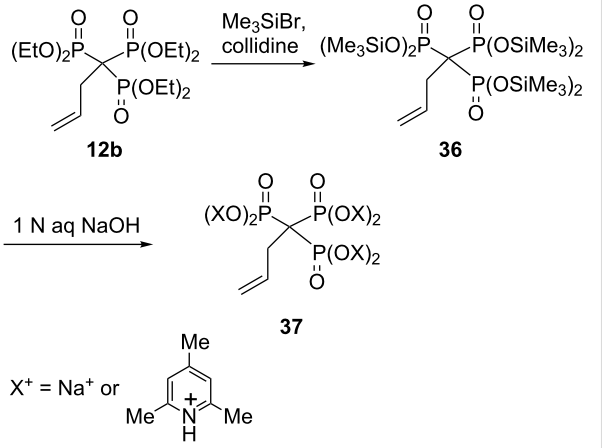
Scheme 16: Hydroboration–oxidation of trisphosphonates **12b**,**e**.



Scheme 17: Reaction of 3-butyn-1-ylidenetrisphosphonate **15** with benzyl azide.

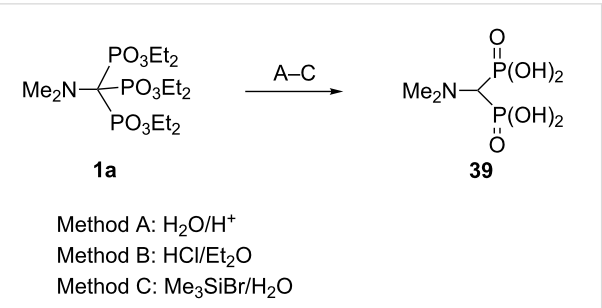
In contrast to methylenebisphosphonate esters, methylidynetrisphosphonate esters have a tendency to undergo dephosphonylation when subjected to acid hydrolysis. Thus, although the bisphosphonate $PhCH_2CH(PO_3Et_2)_2$ smoothly undergoes hydrolysis to the corresponding bisphosphonic acid by treatment with HCl under reflux, benzyltrisphosphonate $PhCH_2C(PO_3Et_2)_3$ undergoes dephosphonylation under similar conditions [25,26]. Synthesis of free trisphosphonic acids could be carried out by transsilylation of the corresponding hexaalkyl trisphosphonates with Me_3SiBr in the presence of a base followed by hydrolysis or alcoholysis [42]. This methodology has been particularly successful for preparing the parent methylidynetriphosphonic acid and its salts. Thus, heating **9** with Me_3SiBr in dichloromethane followed by solvolysis in the presence tri-*n*-butylamine gave methylidynetrisphosphonic acid as its tris(tributylammonium) salt. This product was converted into its trisodium salt by precipitation from a methanol solution using a NaI solution in acetone [7]. The method has been also applied to the preparation of the trisphosphonate salts **37**. Treatment of trisphosphonic acid ester **12b** with Me_3SiBr and collidine resulted in the formation of the silyl ester **36**, which was converted into a mixed sodium and collidinium salt **37** by the addition of 1 N aqueous NaOH (Scheme 18) [26].

Similarly, a sodium salt of an acid-labile trisphosphonic acid **38** could be prepared with minimal P–C scission by carbonate-buffered hydrolysis of in situ formed silyl ester (Scheme 19) [43].

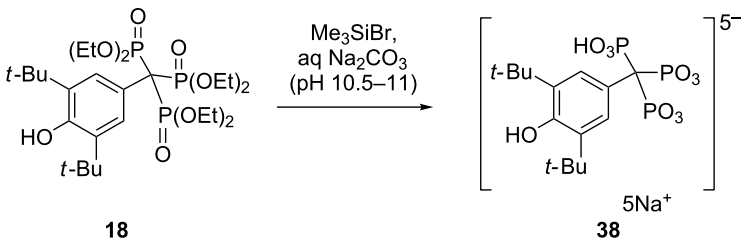


Scheme 18: The use of the transsilylation reaction for the synthesis of trisphosphonate salts **37**.

Amino-substituted trisphosphonate esters $Alk_2N–C(PO_3Et_2)_3$ are even less resistant to acid dephosphonylation than the parent trisphosphonate esters, $HC(PO_3R_2)_3$, or their α-carbo-substituted derivatives. In particular, in the case of aminotrisphosphonate ester **1a** all standard synthetic routes to phosphonic acids (A–C) via acidic hydrolysis of phosphonate esters lead to the elimination of one phosphonyl group and the formation of bisphosphonic acid **39**. Even with Me_3SiBr/H_2O, transsilylation and solvolysis under mild conditions afforded only the dephosphonylated product (Scheme 20) [43].

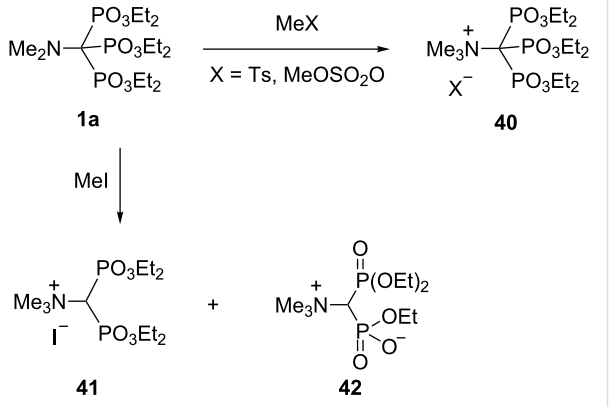


Scheme 20: Acidic hydrolysis of trisphosphonate ester **1a**.



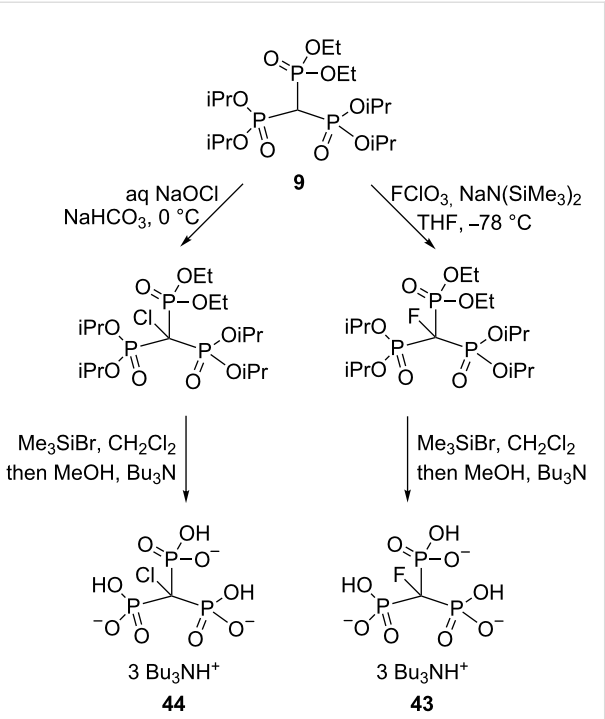
Scheme 19: Synthesis of the sodium salt of the acid-labile trisphosphonic acid **38**.

The result of the methylation of trisphosphonate **1a** depends on the reagent: treatment of **1a** with methyl *p*-toluenesulfonate or dimethyl sulfate leads to the expected quarternary ammonium salts **40**, while with iodomethane one phosphoryl group is split off, and a mixture of bisphosphonates **41** and **42** is formed (Scheme 21) [20].



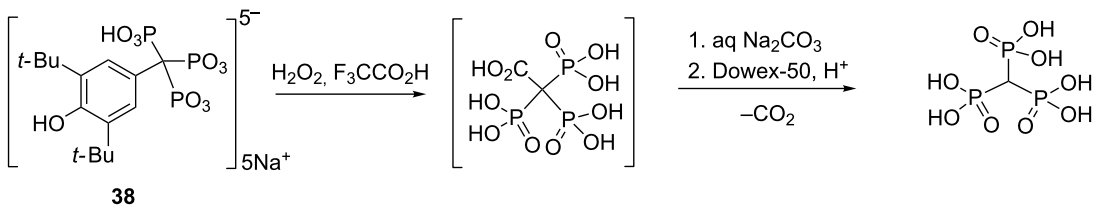
Scheme 21: Methylation of trisphosphonate **1a**.

In a fascinating series of publications, Blackburn and co-workers have realized the synthesis of "supercharged" mimics of pyrophosphoric acid capable of introducing additional anionic charge relative to simple methylenebisphosphonates when built into ATP and Ap$_n$A analogues [7,8,27,44]. They demonstrated that methylidynetrisphosphonic acid and especially its halogenated derivatives are key structure blocks in the synthesis of the nucleotide analogues with enhanced affinity for receptors and better charge correlation with transition states for selected kinases. Two synthetically useful approaches to the parent trisphosphonic acid $HC(PO_3H_2)_3$ have been developed. One of the procedures is based on the treatment of trisphosphonate salt **38** with a mixture of hydrogen peroxide in trifluoroacetic acid (Scheme 22). An alternative and more efficient synthesis of methylidynetrisphosphonic acid uses a transsilylation of hexaalkyl trisphosphonate **9** followed by hydrolysis [27]. Synthesis of halomethylidynetrisphosphonic acids **43** and **44** is shown in Scheme 23 [7].

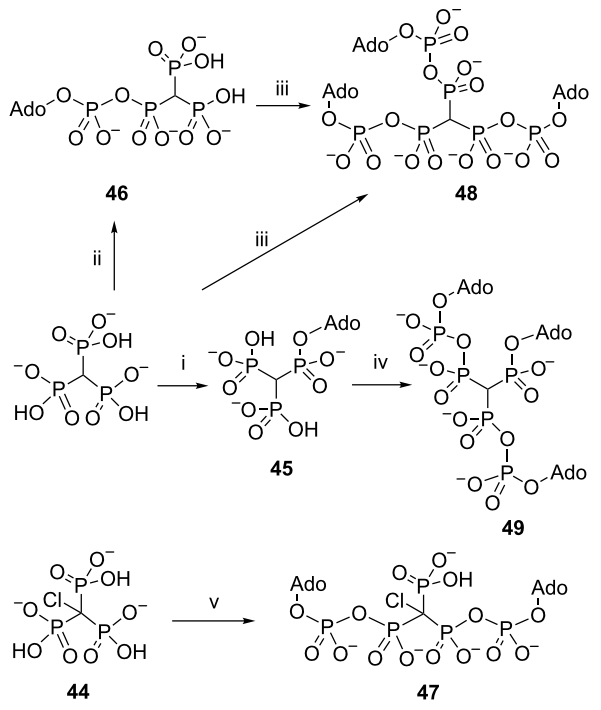


Scheme 23: Synthesis of halomethylidynetrisphosphonate salts **43** and **44** by modified Gross's procedure.

The tris(tributylammonium) salt of methylidynetrisphosphonic acid was transformed into an ADP analogue **45** and into an analogue of ATP **46** using the method of Poulter and the phosphoromorpholidate procedure of Khorana and Moffatt, respectively. Diadenosine tetraphosphate analogue **47** was obtained upon treatment of chloromethylidynetrisphosphonic acid **44** with excess AMP morpholidate. The incorporation of the third adenylate moiety was found to be extremely slow; however, the use of tetrazole as catalyst allowed the preparation of P^1,P^2,P^3-tris(5'-adenylyl)methylidynetrisphosphonate **48** and the tripodal P^1-5'-adenosyl P^2,P^3-bis(5'-adenylyl)methylidynetrisphosphonate **49** in good yields. Compounds **48** and **49** provide the first examples of species in which three adenylate moieties are linked together by a methylidynetrisphosphonate core (Scheme 24) [8].



Scheme 22: Synthesis of the free methylidynetrisphosphonic acid via trisphosphonate salt **38**.



Scheme 24: Synthesis of trisphosphonate modified nucleotides. Reagents: i, 5'-*O*-tosyl adenosine, MeCN; ii, AMP–morpholidate (0.8 equiv), tetrazole, pyridine; iii, AMP–morpholidate (5 equiv), tetrazole, pyridine; iv, excess AMP–morpholidate, pyridine; v, AMP–morpholidate (2.2 equiv), tetrazole, pyridine. All counterions are tri-*n*-butylammonium. Ado = 5'-adenosyl.

Structure features, spectroscopic and acid properties

Methylidynetrisphosphonic acid as tris(cyclohexylamine) salt, $HC(PO_3H_2)_3{\cdot}3C_6H_{11}NH_2$, is a stable, easy to handle colorless solid (mp 210–211 °C; ^{31}P NMR (H_2O) δ 12.8 ppm; ^{1}H NMR (D_2O) δ 2.73 (C<u>H</u>), J_{PCH} = 22.3 Hz; ^{13}C NMR (D_2O) δ 45.16 (<u>C</u>H), J_{PC} = 102.2 Hz) [25]. Methylidynetrisphosphonic acid hexaethyl ester, $HC(PO_3Et_2)_3$, is a light yellow oil (bp 135–138 °C/0.01 mmHg; ^{31}P NMR ($CHCl_3$) δ 14.4 ppm; ^{1}H NMR ($CDCl_3$) δ 3.23 (C<u>H</u>), J_{PCH} = 24.2 Hz; ^{13}C NMR ($CDCl_3$) δ 40.34 (<u>C</u>H), J_{PC} = 121.9 Hz) [24-26]. As expected, trisphosphonate ester $HC(PO_3Et_2)_3$ is a strong carbon acid (titration with NaOH gave a pK_a of ~6.5) [26].

Under the conception of Blackburn, methylidynetrisphosphonic acid, $HC(PO_3H_2)_3$, can be viewed as a "supercharged" mimic of pyrophosphoric acid (PP_i) since the introduction of a third ionizable phosphonate (PO_3H_2) group into methylenebisphosphonic acid delivers additional charge at physiological pH. Thus, the parent methylidynetrisphosphonic acid and its fluoro- and chloro-substituted derivatives have at least one more negative charge than pyrophosphate at pH 7 (Table 1) [7,27].

X-ray structure analysis of trisphosphonic salt $[FC(PO_3H)_3]^{3-}$ $3Na^+$ supported its isosteric character relative to pyrophosphate. In particular, the P–C–P geometry (both the P–C bond distance and the P–C–P angle) is close to the geometry in the methylenebisphosphonate salts while the phosphorus–phosphorus distance is close to that observed for methylenebisphosphonates and pyrophosphate salts (Figure 1) [7].

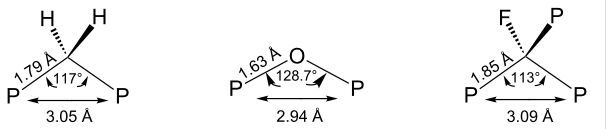


Figure 1: Bond angles and bond distances in pyrophosphate, methylene-1,1-bisphosphonate and fluoromethylidynetrisphosphonate.

Structural features of the trisphosphonate **18** were studied by NMR spectroscopy and by single-crystal X-ray diffraction. Only one ^{31}P NMR signal is observable for three equivalent phosphonate moieties in $CHCl_3$. In contrast, the ^{31}P solid-state NMR spectrum of **18** revealed three separable signals. The nonequivalence of the signals was attributed to hydrogen bonds and supported by crystallographic analysis. The molecules **18** bonded via hydrogen bonds form chains [45].

Table 1: Ionisation constants for polyphosphonic acids determined in the range 3.5 < pH < 10.5 at 37 °C and 0.152 M NaCl [7].

Polyphosphonic acid	pK_a3	pK_a4	pK_a5	Net charge at pH 7.0
$O(PO_3H_2)_2$	6.6	9.4	–	2.72
$HO_2CCH(PO_3H_2)_2$	–[a]	7.24	10.11	3.35
$HO_3SCH(PO_3H_2)_2$	–[a]	6.61	10.57	3.71
$HC(PO_3H_2)_3$	–[a]	6.46	9.90	3.77
$ClC(PO_3H_2)_3$	–[a]	5.92	9.08	3.92
$FC(PO_3H_2)_3$	–[a]	5.77	8.86	3.95

[a]The strongly acidic dissociation constants were off-scale for measurements by titration.

Short overview of biomedical application

Methylidynetrisphosphonate, $HC(PO_3H_3)_3^{3-}\cdot 3Bu_3NH^+$, and its fluoro (**43**) and chloro (**44**) derivatives do not detectably inhibit human-tumor-suppressor protein Fhit, but are strong inhibitors of the lupine enzyme. By contrast, the adenylated polyphosphonates AdoPPCCl(P)PPAdo (**47**) and $(AdoPP)_3CH$ (**48**) strongly and competitively inhibit Fhit while they are less effective as inhibitors of the lupine enzyme. Since the detection of levels of Fhit protein is an important problem relating to cancers, Fhit-selective inhibitors such as **47** and **48** can be valuable as Fhit diagnostics [8].

β,γ-Chlorophosphonomethylene–ATP, AdoPPCCl(P)P, is a weak antagonist at $P2X_{2/3}$ receptors (IC_{50} about 10 μM) [46].

The antioxidant activity of the compound $ArC(PO_3Et_2)_3$ (Ar = 2,6-*t*-Bu_2-4-MeC_6H_2) was studied in a model oxidation of oleic acid and with biological objects (liver homogenates of Wistar rats) [36].

Among polyphosphonic acids with a geminal arrangement of phosphonic groups efficient complexones and regulators of calcium exchange in humans were found [47-49]. Some data on the use of the methylidynetrisphosphonic acid and its derivatives as complexones were also published. The trisphosphonic acids $HC(PO_3H_2)_3$ and $ClC(PO_3H_2)_3$ are better chelating agents in the detergent compositions than methylenebisphosphonic acid and its alkali-metal salts and also sequester more calcium and magnesium ions, for example, than does $H_2C(PO_3H_2)_2$ [50,51]. The complexation behavior of the polydentate ligand $Me_2NC(PO_3Et_2)_3$ toward Co^{2+} ion has shown that the trisphosphonate molecule is coordinated in solution by its three donor (P=O, Me_2N) functions [52]. Evidently, further detailed structure studies of the individual complexes and the complex-forming driving factors are desired in order to understand trisphosphonate coordination abilities.

Conclusion

There has been a considerable interest in the preparation and use of the geminal trisphosphonates, $XC(PO_3R_2)_3$, because of the widespread biomedical application of methylenebisphosphonates as mimetics of biologically important pyrophosphate. Much of the trisphosphonate reactivity profile follows intuition based on the bisphosphonate analogy. However, despite the structural similarity to bisphosphonates, methylidynetrisphosphonic acid and its derivatives differ in their geometry, coordination properties and reactivity pathways. A particularly interesting characteristic of trisphosphonates is the possibility of constructing systems based on Blackburn's conception of supercharged nucleotide analogues in which an additional negative charge is provided without elongation of the polyphosphate chain. But there are still a lot of other aspects of their chemistry that remain to be investigated. From a synthetic point of view, since the introduction of a heteroatom substituent at the bridged carbon atom permits both modulation of pK_a values and hydrogen bonding, there is a need for profound study of α-functionalized trisphosphonate systems. Such compounds can be promising building blocks for the synthesis of false substrates or enzyme inhibitors involved in phosphate-based processes. In particular, some heterocyclic compounds functionalized by trisphosphonate substituents merit in-depth biological study. A further practical potential for trisphosphonate compounds is the development of new phosphorus-containing dendrimers and related species. Considerable interest is also associated with the use of trisphosphonic acids as ligands for calcium ligation and as potential bone affinity agents. Finally, there is no doubt that organometallic and coordination chemistry will benefit from future innovative application of these compounds.

Acknowledgements

Financial support from the National Academy of Sciences of Ukraine (grant 1/1-2012) is gratefully acknowledged.

References

1. Güven, A. Functions Containing at Least One Group 15 Element (and No Halogen or Chalcogen). In *Comprehensive Organic Functional Group Transformations II;* Katritzky, A. R.; Taylor, R. J. K., Eds.; Elsevier: Amsterdam, 2005; Vol. 6, pp 161–202. doi:10.1016/B0-08-044655-8/00126-4
2. Savignac, P.; Iorga, B. *Modern Phosphonate Chemistry;* CRP Press: Boca Raton, 2003. doi:10.1201/9780203503676
3. Fleisch, H. *Bisphosphonates in Bone Disease: From the Laboratory to the Patient;* Academic Press: London, 2000.
4. Ebetino, F. H.; Hogan, A.-M. L.; Sun, S.; Tsoumpra, M. K.; Duan, X.; Triffitt, J. T.; Kwaasi, A. A.; Dunford, J. E.; Barnett, B. L.; Oppermann, U.; Lundy, M. W.; Boyde, A.; Kashemirov, B. A.; McKenna, C. E.; Russell, R. G. G. *Bone* **2011,** *49,* 20–33. doi:10.1016/j.bone.2011.03.774
5. Zhang, S.; Gangal, G.; Uludağ, H. *Chem. Soc. Rev.* **2007,** *36,* 507–531. doi:10.1039/b512310k
6. Graham, R.; Russell, G. *Phosphorus, Sulfur Silicon Relat. Elem.* **1999,** *144,* 793–820. doi:10.1080/10426509908546364
7. Liu, X.; Adams, H.; Blackburn, G. M. *Chem. Commun.* **1998,** 2619–2620. doi:10.1039/a807162d
8. Liu, X.; Brenner, C.; Guranowski, A.; Starzynska, E.; Blackburn, G. M. *Angew. Chem.* **1999,** *111,* 1324–1327. doi:10.1002/(SICI)1521-3757(19990503)111:9<1324::AID-ANGE1324>3.0.CO;2-5
Angew. Chem., Int. Ed. **1999,** *38,* 1244–1247. doi:10.1002/(SICI)1521-3773(19990503)38:9<1244::AID-ANIE1244>3.0.CO;2-0
9. Engel, R. *Synthesis of Carbon-Phosphorus Bonds;* CRC Press: Boca Raton, 2003.
10. Curry, J. D.; Nicholson, D. A.; Quimby, O. T. *Top. Phosphorus Chem.* **1972,** *7,* 37–102.
11. Bhattacharya, A. K.; Thyagarajan, G. *Chem. Rev.* **1981,** *81,* 415–430. doi:10.1021/cr00044a004

12. Kirchner, B.; Reiher, M. *J. Am. Chem. Soc.* **2005,** *127,* 8748–8756. doi:10.1021/ja050614+
13. Kukhar, V. P.; Sagina, E. I. *Zh. Obshch. Khim.* **1976,** *46,* 2686–2689.
14. Burn, A. J.; Cadogan, J. I. G.; Bunyan, P. J. *J. Chem. Soc.* **1963,** 1527–1533. doi:10.1039/jr9630001527
15. Pudovik, A. N.; Gurianova, I. V.; Perevezentseva, S. P. *Zh. Obshch. Khim.* **1967,** *37,* 1090–1094.
16. Birum, G. H. Alkyl Phosphite Esters of Perchloromethylmercaptan and Insecticidal Compositions Comprising the Same. U.S. Patent 2,818,364, Dec 31, 1957.
17. Birum, G. H. Organic Phosphorus Compounds. U.S. Patent 2,857,415, Oct 21, 1958.
18. Kukhar, V. P.; Pasternak, V. I.; Kirsanov, A. V. *Zh. Obshch. Khim.* **1972,** *42,* 1169–1170.
19. Schindler, N.; Ploeger, W.; Haeusler, G. Dialkylaminomethan-triphosphonsaeureester. Eur. Pat. 2,237,879, Feb 14, 1974. *Chem. Abstr.* **1974,** *80,* 121096.
20. Gross, H.; Costisella, B. *J. Prakt. Chem.* **1986,** *328,* 231–236. doi:10.1002/prac.19863280212
21. Shokol, V. A.; Kozhushko, B. N.; Kirsanov, A. V. *J. Gen. Chem. USSR* **1973,** *43,* 547–553.
22. Silina, E. B.; Kozhyshko, B. N.; Shokol, B. A. *J. Gen. Chem. USSR* **1989,** *59,* 571–586.
23. Gross, H.; Costisella, B.; Brennecke, L.; Engelhardt, G. *J. Prakt. Chem.* **1972,** *314,* 969–974. doi:10.1002/prac.19723140538
24. Gross, H.; Costisella, B. *J. Prakt. Chem.* **1972,** *314,* 87–92. doi:10.1002/prac.19723140112
25. Gross, H.; Costisella, B.; Keitel, I.; Ozegowski, S. *Phosphorus, Sulfur Silicon Relat. Elem.* **1993,** *83,* 203–207. doi:10.1080/10426509308034363
26. Smits, J. P.; Wiemer, D. F. *J. Org. Chem.* **2011,** *76,* 8807–8813. doi:10.1021/jo201523w
27. Liu, X.; Zhang, X.-R.; Blackburn, G. M. *Phosphorus, Sulfur Silicon Relat. Elem.* **1999,** *144,* 541–544. doi:10.1080/10426509908546301
28. Skarpos, H.; Osipov, S. N.; Vorob'eva, D. V.; Odinets, I. L.; Lork, E.; Röschenthaler, G.-V. *Org. Biomol. Chem.* **2007,** *5,* 2361–2367. doi:10.1039/b705510b
29. Gross, H.; Ozegowski, S.; Costisella, B. *Phosphorus, Sulfur Silicon Relat. Elem.* **1990,** *47,* 7–13. doi:10.1080/10426509008046839
30. Prishchenko, A. A.; Livantsov, M. V.; Novikova, O. P.; Livantsova, L. I.; Milaeva, E. R. *Heteroat. Chem.* **2008,** *19,* 490–494. doi:10.1002/hc.20458
31. Prishchenko, A. A.; Livantsov, M. V.; Novikova, O. P.; Livantsova, L. I.; Shpakovskii, D. B.; Milaeva, E. R. *Russ. J. Gen. Chem.* **2006,** *76,* 1753–1756. doi:10.1134/S1070363206110132
32. Ismagilov, R. K.; Moskva, V. V.; Kopilova, L. Y. *Zh. Obshch. Khim.* **1989,** *59,* 1686–1687.
33. Gross, H.; Keitel, I.; Costisella, B. *Phosphorus, Sulfur Silicon Relat. Elem.* **1991,** *62,* 35–45. doi:10.1080/10426509108034456
34. Gross, H.; Keitel, I.; Costisella, B. *Phosphorus, Sulfur Silicon Relat. Elem.* **1993,** *75,* 83–86. doi:10.1080/10426509308037370
35. Gross, H.; Keitel, I.; Costisella, B. *Phosphorus, Sulfur Silicon Relat. Elem.* **1992,** *70,* 331–337. doi:10.1080/10426509208049182
36. Tyurin, V. Yu.; Gracheva, Yu. A.; Milaeva, E. R.; Prishchenko, A. A.; Livantsov, M. V.; Novikova, O. P.; Livantsova, L. I.; Maryashkin, A. V.; Bubnov, M. P.; Kozhanov, K. A.; Cherkasov, V. K. *Russ. Chem. Bull.* **2007,** *56,* 774–780. doi:10.1007/s11172-007-0116-y
37. Lecerclé, D.; Gabillet, S.; Gomis, J.-M.; Taran, F. *Tetrahedron Lett.* **2008,** *49,* 2083–2087. doi:10.1016/j.tetlet.2008.01.127
38. Mass, G.; Regitz, M. *Chem. Ber.* **1976,** *109,* 2039–2063. doi:10.1002/cber.19761090611
39. Regitz, M.; Anschütz, W.; Liedhegener, A. *Chem. Ber.* **1968,** *101,* 3734–3743. doi:10.1002/cber.19681011113
40. Khare, A. B.; McKenna, C. E. *Synthesis* **1991,** 405–406. doi:10.1055/s-1991-26478
41. Patsanovskiy, I. I.; Galkin, V. I.; Popova, E. V.; Ishmaeva, E. A.; Aminova, R. M.; Muller, K.; Shmutzler, R. *Zh. Obshch. Khim.* **1996,** *66,* 522.
42. Romanenko, V. D.; Shevchuk, M. V.; Kukhar, V. P. *Curr. Org. Chem.* **2011,** *15,* 2774–2801. doi:10.2174/138527211796378505
43. Gross, H.; Keitel, I.; Costisella, B.; McKenna, C. E. *Phosphorus, Sulfur Silicon Relat. Elem.* **1991,** *61,* 177–181. doi:10.1080/10426509108036796
44. Liu, X.; Zhang, X.-R.; Blackburn, G. M. *Chem. Commun.* **1997,** 87–88. doi:10.1039/a605828k
45. Ramm, M.; Costisella, B.; Gross, H. *Acta Crystallogr., Sect. C: Cryst. Struct. Commun.* **1995,** *C51,* 274–277. doi:10.1107/S0108270194009376
46. Spelta, V.; Mekhalfia, A.; Rejman, D.; Thompson, M.; Blackburn, G. M.; North, R. A. *Br. J. Pharmacol.* **2003,** *140,* 1027–1034. doi:10.1038/sj.bjp.0705531
47. Matczak-Jon, E.; Kurzak, B.; Kafarski, P.; Woźna, A. *J. Inorg. Biochem.* **2006,** *100,* 1155–1166. doi:10.1016/j.jinorgbio.2006.01.005
48. Matveev, S. V.; Bel'skii, F. I.; Matveeva, A. G.; Gukasova, A. Yu.; Polikarpov, Yu. M.; Kabachnik, M. I. *Russ. Chem. Bull.* **1998,** *47,* 1736–1740. doi:10.1007/BF02495696
49. Bollinger, J. E.; Roundhill, D. M. *Inorg. Chem.* **1994,** *33,* 6421–6424. doi:10.1021/ic00104a066
50. Budnick, E. G. Chelation. U.S. Patent 4,116,990, Sept 26, 1978.
51. Budnick, E. G. Chelation. U.S. Patent 4,579,720, April 1, 1986.
52. Sinyavskaya, E. I.; Konstantinovskaya, M. A.; Yatsimirskii, K. B.; Kuhar, V. P.; Sagina, E. I. *Russ. J. Inorg. Chem.* **1981,** *26,* 971–975.

License and Terms

This is an Open Access article under the terms of the Creative Commons Attribution License (http://creativecommons.org/licenses/by/2.0), which permits unrestricted use, distribution, and reproduction in any medium, provided the original work is properly cited.

The license is subject to the *Beilstein Journal of Organic Chemistry* terms and conditions: (http://www.beilstein-journals.org/bjoc)

The definitive version of this article is the electronic one which can be found at: doi:10.3762/bjoc.9.114

Beilstein Journal of Organic Chemistry

Use of 3-[^{18}F]fluoropropanesulfonyl chloride as a prosthetic agent for the radiolabelling of amines: Investigation of precursor molecules, labelling conditions and enzymatic stability of the corresponding sulfonamides

Reik Löser[*1,2], Steffen Fischer[3], Achim Hiller[3], Martin Köckerling[4], Uta Funke[3], Aurélie Maisonial[3], Peter Brust[3] and Jörg Steinbach[1,2,3]

Full Research Paper

Open Access

Address:
[1]Institute of Radiopharmaceutical Cancer Research (formerly Institute of Radiopharmacy), Helmholtz-Zentrum Dresden-Rossendorf (HZDR), Bautzner Landstraße 400, 01328 Dresden, Germany, [2]Department of Chemistry and Food Chemistry, Technical University of Dresden, Bergstraße 66c, 01062 Dresden, Germany, [3]Institute of Radiopharmaceutical Cancer Research, HZDR Research Site Leipzig, Permoserstraße 15, 04318 Leipzig, Germany and [4]Institute of Chemistry, University of Rostock, Inorganic Solid-State Chemistry Group, Albert-Einstein-Straße 3a, 18059 Rostock, Germany

Email:
Reik Löser[*] - r.loeser@hzdr.de

* Corresponding author

Keywords:
fluorine-18; hydrolytic metabolism; prosthetic groups; radiochemistry; sulfonamides

Beilstein J. Org. Chem. **2013,** *9,* 1002–1011.
doi:10.3762/bjoc.9.115

Received: 05 February 2013
Accepted: 26 April 2013
Published: 27 May 2013

This article is part of the Thematic Series "Synthetic probes for the study of biological function".

Guest Editor: J. Aubé

© 2013 Löser et al; licensee Beilstein-Institut.
License and terms: see end of document.

Abstract

3-[^{18}F]Fluoropropanesulfonyl chloride, a recently proposed prosthetic agent for fluorine-18 labelling, was prepared in a two-step radiosynthesis via 3-[^{18}F]fluoropropyl thiocyanate as an intermediate. Two benzenesulfonate-based radiolabelling precursors were prepared by various routes. Comparing the reactivities of 3-thiocyanatopropyl nosylate and the corresponding tosylate towards [^{18}F]fluoride the former proved to be superior accounting for labelling yields of up to 85%. Conditions for a reliable transformation of 3-[^{18}F]fluoropropyl thiocyanate to the corresponding sulfonyl chloride with the potential for automation have been identified. The reaction of 3-[^{18}F]fluoropropanesulfonyl chloride with eight different aliphatic and aromatic amines was investigated and the identity of the resulting ^{18}F-labelled sulfonamides was confirmed chromatographically by comparison with their nonradioactive counterparts. Even for weakly nucleophilic amines such as 4-nitroaniline the desired radiolabelled sulfonamides were accessible in satisfactory yields owing to systematic variation of the reaction conditions. With respect to the application of the ^{18}F-fluoropropan-sulfonyl group to the labelling of compounds relevant as imaging agents for positron emission tomography (PET), the stability of

N-(4-fluorophenyl)-3-fluoropropanesulfonamide against degradation catalysed by carboxylesterase was investigated and compared to that of the analogous fluoroacetamide.

Introduction

The importance of molecular imaging, i.e., the characterisation and measurement of biological processes in living organisms at the molecular level using remote imaging detectors, for both research and diagnostic purposes has considerably increased over the recent years. The success of this interdisciplinary field depends substantially on the development of molecular probes equipped with appropriate reporter groups [1].

Among the different imaging modalities, positron emission tomography (PET) stands out with regards to sensitivity and quantitative image evaluation. PET is based on the application of molecules labelled with a positron-emitting radionuclide, which are termed radiotracers. Although such radionuclides are known for many elements, fluorine-18 can be considered as the most suitable one for PET due to its intermediate half-life of 109.8 min, its high content of β^+-conversion (97%) and its rather low positron energy maximum of 640 keV [2].

From a chemical point of view, the introduction of fluorine-18 into molecules that are able to address biomolecular targets in vivo, requires a carefully developed methodology as the carbon–fluorine bond is rather difficult to tie [3,4]. Furthermore, as fluorine appears less frequently in biologically active compounds, molecules that show the potential to interact with certain imaging targets have to be modified with fluorine. For this purpose, generic groups that allow both derivatisation with fluorine as well as convenient introduction of radiofluorine are often used. These groups are referred to as prosthetic groups in preparative radiochemistry. For labelling with fluorine-18, a variety of prosthetic groups were suggested and developed [5,6]. Their careful individual selection is critical for radiotracer development as they often exert great influence on target binding and/or stability in vivo. This is particularly valid when PET imaging probes based on small molecules are considered.

Labelling based on the formation of carboxylic amides is an approach that allows convenient introduction of fluorine-18 (Figure 1) [7,8], which applies especially to [^{18}F]fluoroacetamides [9-15]. In several cases, [^{18}F]fluoroacetamides were proven to be metabolically unstable due to hydrolytic cleavage [15-17]. As an alternative to acyl-based prosthetic groups the 3-[^{18}F]fluoropropanesulfonyl group introduced by Li et al. attracted our interest [18]. Labelling with radiofluorine by sulfonamide formation seems to be intriguing not only because of the inertness against the metabolic cleavage of the label but also because of the polarity it can confer to the resulting tracer molecule. This can be an advantage especially for radiotracers based on small molecules [19]. Therefore, we planned to establish and to optimise the preparation of 3-[^{18}F]fluoropropanesulfonyl chloride in our labs and to study its reaction with a panel of aliphatic and aromatic amines of varying reactivity. Particular attention was paid to the synthesis of precursor molecules suitable for radiofluorination and nonradioactive reference compounds, as the information published in [18] is rather preliminary in this regard. Furthermore, we aimed to extend ^{18}F-fluoropropanesulfonylation to the labelling of aromatic amines. Additionally, the metabolic stability of 3-fluoropropanesulfonamides was proven and comparatively assessed to that of analo-

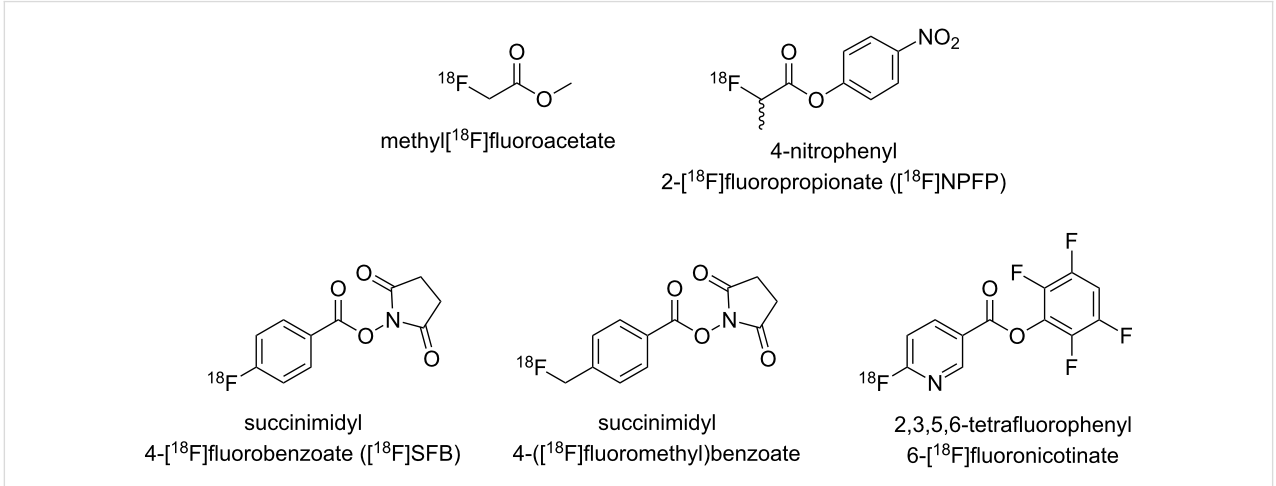


Figure 1: Selection of prosthetic agents for ^{18}F-labelling via acylation.

gous fluoroacetamides by degradation experiments with carboxylesterase from pig liver. Preliminary results of this study have been published previously as a conference abstract [20].

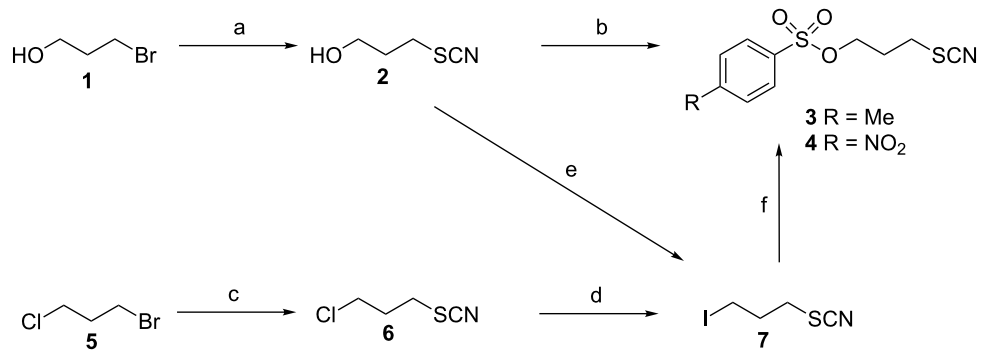
Results and Discussion

Synthesis of precursors and nonradioactive reference compounds

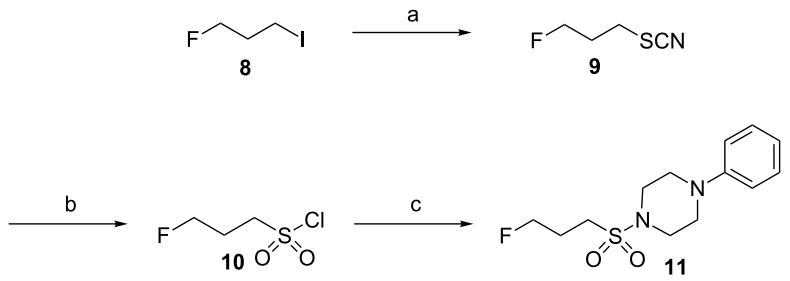
The preparation of ^{18}F-labelled sulfonyl chlorides is challenging as the chlorine atom in these electrophilic agents can be exchanged by reaction with fluoride even in the presence of water to form the corresponding sulfonyl fluorides [21]. Hence, the sulfonyl chloride has to be generated by interconversion of a different, less reactive sulfur-containing functional group after radiofluorination. Sulfonyl chlorides can be generated by oxidation with aqueous chlorine from a variety of organosulfur species such as thiols, sulfides, disulfides, thioesters, isothiouronium salts, xanthates and thiocyanates [22]. The latter class of organic sulfur compounds seems to be most advantageous, as organic thiocyanates are easily accessible, sufficiently stable to oxidation, and nonhygroscopic. Li et al. [18] decided to use a propyl spacer between the fluorine-18 atom and the thiocyanate moiety as radiofluorination by nucleophilic substitution proceeds easier at aliphatic than at aromatic electrophilic centres. In addition, the propyl spacer accounts for a balance between the limited size of the prosthetic unit on the one hand and the limited volatility of the radiofluorinated intermediates on the other. Thus, the general approach presented in [18] to generate ^{18}F-labelled sulfonyl chlorides seems to be well-conceived and was therefore adopted for our purposes.

Initially, the route described by Li et al. [18] was followed to synthesise the tosylate precursor **3** (Scheme 1). As the tosylation of the alcohol **2** proceeded in low yields and led to side products that were difficult to remove and impaired the reaction with [^{18}F]fluoride, an alternative procedure to afford **3** was envisaged. Esters of sulfonic acids can be also prepared by nucleophilic displacement of carbon-bound halogens with sulfonates, which works best with alkyl iodides and silver salts of sulfonic acids [23]. Therefore, the required 3-iodopropyl thiocyanate (**7**) was synthesised by subjecting the corresponding chloro-derivative **6** to the conditions of a Finkelstein reaction. Unexpectedly, this led to a mixture containing 1,3-diiodopropane and 1,3-dithiocyanatopropane beside **7**, as revealed by ^{1}H NMR analysis. From this mixture, the desired product **7** was isolated by distillation in a yield of 24%. Reduction of the amount of sodium iodide from 5 to 1.1 equivalents did not result in a more favourable product distribution. The course of this reaction becomes clear in the light of the pseudohalide concept: the thiocyanate functionality acts as a leaving group towards attack by iodide forming 1,3-diiodopropane. The thereby-released thiocyanate anion reacts with concomitantly formed **7** to give 1,3-dithiocyanatopropane. The reversibility of the iodide/thiocyanate displacement has been reported previously [24] and alkyl thiocyanates can be quantitatively transformed under controlled conditions into the corresponding iodides [25]. The preparation of compound **7** can be also achieved by the transformation of alcohol **2** in an Appel-type reaction, circumventing the problems encountered during the Finkelstein reaction. Conversion of **7** with silver tosylate proceeded smoothly leading to the desired tosylate **3**. In analogy, the nosylate **4** was obtained by reaction of the iodide **7** with silver nosylate, which was prepared according to a published procedure [26]. Alternatively, **4** was obtained by converting alcohol **2** with nosyl chloride. This procedure resulted in lower yields but can be considered as more efficient, as it is shorter by one step.

The synthesis of the ^{19}F-based reference compounds started with the conversion of commercially available 1-fluoro-3-iodopropane (**8**) with potassium thiocyanate, analogous to the preparation of **2** (Scheme 2). The key step was the transformation of the thiocyano group of **9** to the chlorosulfonyl group



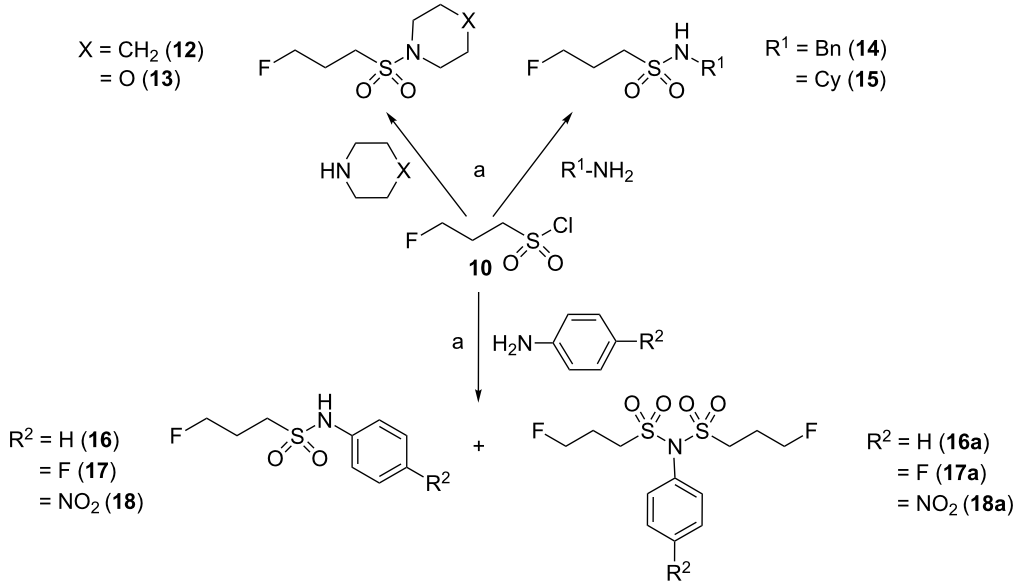
Scheme 1: Synthesis of radiofluorination precursors **3** and **4**. Reagents and conditions: (a) KSCN, CH_3OH, reflux; (b) TsCl, DIPEA, pyridine, CH_2Cl_2, rt (for **3**) or NsCl, $K(CH_3)_3SiO$, THF, rt (for **4**); (c) KSCN, CH_3OH, reflux; (d) NaI, acetone, reflux; (e) Ph_3P, I_2, imidazole, THF, rt; (f) silver tosylate (for **3**) or silver nosylate (for **4**), CH_3CN, rt.



Scheme 2: Synthesis of 3-fluoropropanesulfonamide **11** via intermediary 3-fluoropropanesulfonyl chloride (**10**). Reagents and conditions: (a) KSCN, CH_3OH, reflux; (b) Cl_2, H_2O/AcOH, rt; (c) *N*-phenylpiperazine, triethylamine (TEA), CH_2Cl_2, reflux.

leading to 3-fluoropropanesulfonyl chloride (**10**). This functional group interconversion using aqueous chlorine has been known for a long time [27] but has received little attention in synthetic organic chemistry. Following this approach, Millington et al. were able to obtain the sulfonylating agent **10** by saturating an aqueous suspension of thiocyanate **9** with chlorine gas [28]. In our hands, superior results were achieved when this transformation was carried out in a mixture of chlorine-saturated water and acetic acid as cosolvent for **9**. The desired intermediate was purified by vacuum distillation or transformed as crude product to the final 3-fluoropropanesulfonamides, as shown for compound **11**. Alternatively, **10** was obtained commercially. The reaction of **10** with aliphatic amines proceeded quantitatively and smoothly to the sulfonamides **12**–**15** (Scheme 3). In contrast, its reaction with aniline derivatives required a longer time and led to the formation of side products that were identified as the corresponding *N*,*N*-bissulfonylanilines **16a**–**18a**. The double sulfonylation of aromatic amines under strongly basic conditions was described earlier [29]. This side reaction was most pronounced for the reaction of **10** with 4-nitroaniline, which resulted in the formation of **18a** as the main product. Therefore, **10** was reacted with 4-nitroaniline in the presence of pyridine at room temperature resulting in the incomplete conversion to the mono-sulfonylated product **18**. This compound was obtained in the form of crystals suitable for X-ray diffraction analysis.

The molecular structure of **18** is shown in Figure 2A, confirming unambiguously its identity as *N*-(4-nitrophenyl)-3-fluoropropane-1-sulfonamide. Crystal data and structure refinement parameters are collected in Table 1. The length of the S–N bond in compound **18** is with 1.639(1) Å close to the average



Scheme 3: Synthesis of 3-fluoropropanesulfonamides **12**–**18**. Reagents and conditions: (a) triethylamine (TEA), CH_2Cl_2, reflux (for **12**–**17**) or pyridine, CH_2Cl_2, rt (for **18**).

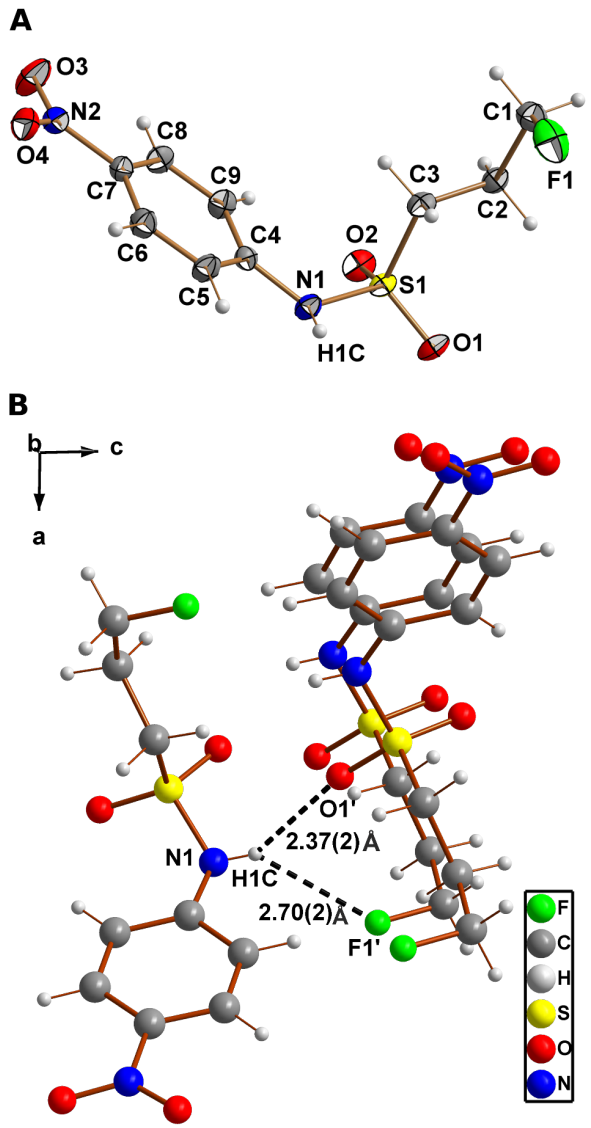


Figure 2: (**A**) View of the molecular structure of sulfonamide **18** with atom labelling scheme. Displacement ellipsoids are drawn at the 50% probability level. (**B**) View of the arrangement of molecules in crystals of sulfonamide **18** showing hydrogen-bond contacts of the amide H-atom H1C.

Table 1: Crystal data and structure-refinement parameters for compound **18**.

Crystal data	
Formula	$C_9H_{11}FN_2O_4S$
Formula weight	262.26 g·mol^{-1}
Temperature	173(2) K
Wavelength	0.71073 Å
Crystal system	monoclinic
Space group	$P2_1/n$
Unit cell dimensions	a = 10.7639(7) Å
	b = 5.2066(4) Å
	c = 19.532(1) Å
	β = 91.748(4)°
Volume	1094.1(1) Å^3
Z	4
Density (calcd.)	1.592 g·cm^{-3}
Absorption coefficient	0.316 mm^{-1}
F(000)	544
Crystal size	0.26 × 0.14 × 0.05 mm^3
Meas. Range, $2\theta_{max}$	59.02
Refinement	
Refinement method	Full-matrix least-squares on F^2
Data/restraints/param.	3047 / 0 / 159
Goodness-of-fit on F^2	1.030
Final R indices	R_1 = 0.0402
[$I > 2\sigma(I)$]	wR_2 = 0.0952
R indices (all data)	R_1 = 0.0613
	wR_2 = 0.1031
Largest diff. peak/hole	0.386/−0.328 e·Å^{-3}

value of 1.63(2) Å observed for sulfonamides [30]. Whereas the nitrogen atom of carboxylic amides is typically trigonal planar, that of sulfonamides tends to be pyramidalised [31,32]. This phenomenon can be also observed for the molecular structure of **18** in the crystal. This is indicated by the fact that the sum of the three valence angles around the sulfonamide nitrogen (C4–N1–S1, C4–N1–H1C, and S1–N1–H1C) is equal to 348(4)°, which is significantly less than 360° for trigonal planar geometry. Further evidence for pyramidalisation is provided by the out-of-plane angle for S1 (sulfonamide sulfur atom) with respect to the plane defined by the atoms N1, C4 and H1C, which is 34(2)° compared to zero for the trigonal planar shape.

The orientation of the N1 lone electron pair is antiperiplanar to the S1–C3 bond. Such conformational preferences have been also observed for other sulfonamides and give rise to an optimal n_N-$\sigma^*_{S,C}$ interaction [31]. Further notable features are the interactions between the molecules in the crystal involving the sulfonamide nitrogen. Together with the hydrogen attached to this atom (H1C) it acts as a two-fold hydrogen-bond donor towards the sulfonyl oxygen (O1) of a neighbouring molecule with an O···H distance of 2.37(2) Å (N1···O1': 3.015(2) Å) and an N–H···O angle of 142(2)° (Figure 2B). The second contact of the NH-group involves the fluorine atom (F1) of another neighbouring molecule with an F···H distance of 2.70(2) Å (N1···F1': 3.291(2) Å) and an N–H···F angle of 135(2)°, which can be interpreted as weak hydrogen bond. Although covalently bound fluorine is commonly considered as a poor hydrogen-bond acceptor [33,34], it tends to participate in multipolar contacts including hydrogen bonds [35], as observed herein. To our knowledge, all sulfonamides shown in Scheme 2 and Scheme 3 have not been described so far.

Radiochemistry

The sulfonate precursor molecules **3** and **4** were subjected to nucleophilic substitution with [^{18}F]fluoride. The reaction parameters (amount of precursor substance, solvent, volume, temperature, time) were carefully optimised. The following conditions were found to be optimal for the formation of radiolabelled thiocyanate [^{18}F]**9**: 2.5 to 3.0 mg of **3** or **4** in 0.3–0.5 mL of acetonitrile, 82 °C, 15 min. Thermal heating was advantageous compared to microwave irradiation (up to 50 W for 7 min, 75 °C (CH_3CN), 100 °C (DMF)). Higher labelling yields were achieved when the nosyl precursor **4** was used instead of tosylate **3** (75–85% (n = 12) versus 45–55% (n = 9), respectively; Figure 3). Notably, employing DMF as solvent resulted in significantly lower yields.

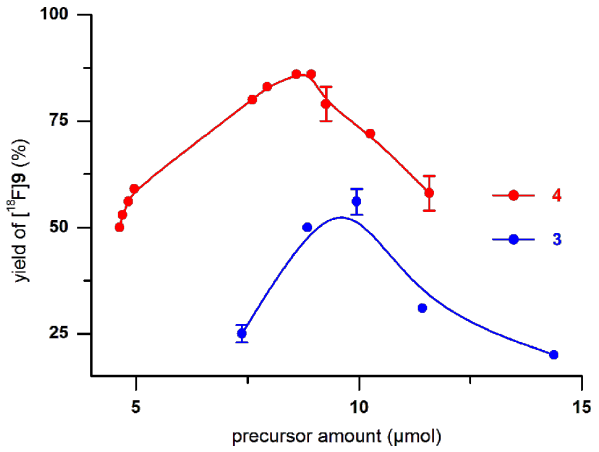


Figure 3: Dependence of the labelling yields of [^{18}F]**9** on the precursor amount. Reactions of tosylate **3** and nosylate precursor **4** with [^{18}F]F-Kryptofix$_{222}$-carbonate complex were carried out in 500 µL of acetonitrile at 82 °C for 15 min.

The crude reaction mixture containing [^{18}F]**9** was of sufficient radiochemical purity to be subjected to the next step. Alternatively, it can be isolated by distillation at atmospheric pressure in the argon stream at 80 °C and frozen out in a cooling trap at −60 °C within 10 min and a recovery of 92% (Figure 4). To transform the ^{18}F-labelled thiocyanate [^{18}F]**9** into the corresponding sulfonyl chloride [^{18}F]**10**, [^{18}F]**9** was adsorbed by a C_{18}-SPE-cartridge and repetitively treated with a saturated solution of chlorine in water (prepared immediately before use). In this way 3-[^{18}F]fluoropropanesulfonyl chloride ([^{18}F]**10**) was obtained in radiochemical purities of 90–95% and overall decay-corrected radiochemical yields of 40–45%, within 70 min of synthesis time. Attempts to obtain [^{18}F]**10** by using chlorine generated in situ from calcium hypochlorite (in 2 M HCl) were less efficient. After careful removal of excessive chlorine from the cartridge in the argon stream, we could isolate [^{18}F]**10** by elution with dichloromethane, and the remaining water was

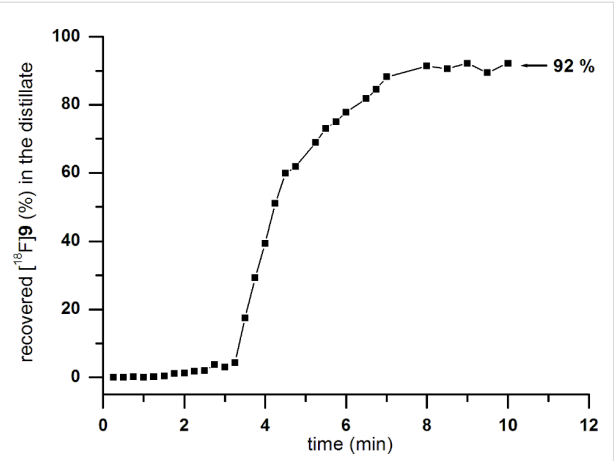
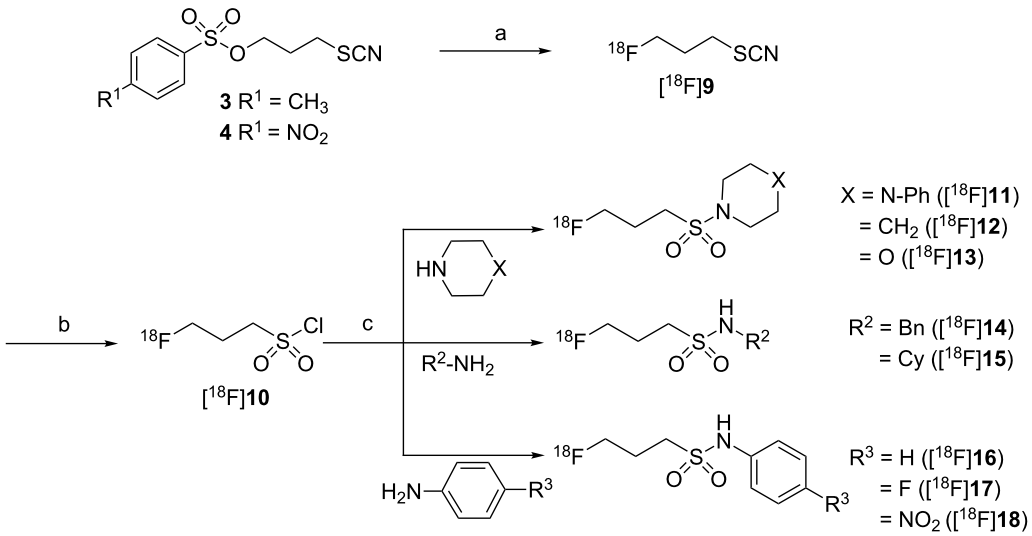


Figure 4: Time course of the distillation of 3-[^{18}F]fluoropropyl thiocyanate ([^{18}F]**9**) in the argon stream. For calculation of the distillation yield only the fraction of [^{18}F]**9** in the crude mixture is considered.

removed by passing the resulting solution through a Na_2SO_4-filled cartridge.

3-[^{18}F]Fluoropropanesulfonyl chloride ([^{18}F]**10**) was reacted with different primary and secondary aliphatic as well as primary aromatic amines (Scheme 4) at room temperature. The use of dichloromethane as solvent was superior compared to mixtures of acetonitrile and water. The reactions were carried out in the absence of any additive or with stoichiometric amounts of triethylamine (TEA) or 4-dimethylaminopyridine (DMAP) as auxiliary bases (Table 2). The radiochemical yields of the ^{18}F-labelled sulfonamides [^{18}F]**11**–[^{18}F]**15** derived from aliphatic amines did not improve or even become attenuated upon addition of TEA or DMAP. Obviously, the aliphatic amines are sufficiently nucleophilic to undergo sulfonylation readily within short reaction times of 2–3 min. In contrast, the presence of these agents proved to be beneficial for the reaction of [^{18}F]**10** with aniline and 4-fluoroaniline (Table 2 and Figure 5A) and the well known acylation catalyst DMAP was somewhat advantageous over TEA. Nevertheless, the radiochemical yields for the formation of the 4-nitroaniline-derived sulfonamide [^{18}F]**18** were below 10%, even in the presence of TEA and DMAP. This can be attributed to the poor nucleophilicity of the amino group of 4-nitroaniline which is by far lower than that of aniline and 4-fluoroaniline. The difference in the nucleophilicity of these three aromatic amines is reflected by the pK_a values of their corresponding ammonium ions decreasing from 4.65 over 4.58 to 1.02 for 4-fluoroaniline, aniline, and 4-nitroaniline, respectively [36]. To achieve satisfactory conversion of the ^{18}F-labelled sulfonyl chloride [^{18}F]**10** with 4-nitroaniline, potassium trimethylsilanolate was tested as auxiliary base. This reagent has good solubility in organic solvents and was suggested by Laganis and Chenard as equivalent for the O^{2-} ion



Scheme 4: Radiosynthesis of 3-[^{18}F]fluoropropanesulfonamides [^{18}F]**11**–[^{18}F]**18**. Reagents and conditions: (a) [^{18}F]F$^-$, Kryptofix$_{222}$, K_2CO_3, CH_3CN, 82 °C; (b) Cl_2/H_2O, C_{18}-modified silica gel; (c) auxiliary base as specified in Table 2, CH_2Cl_2, rt.

Table 2: Reaction of [^{18}F]**10** with various aliphatic and aromatic amines ($n \geq 2$). RCYs were determined by radio-TLC and refer to the fraction of the product related to the total ^{18}F-activity.

^{18}F-labelled sulfonamide	amine	RCY (%)					
		no auxiliary base	TEA	DMAP	KOSiMe$_3$ 1:2[a]	KOSiMe$_3$ 1:4[a]	KOSiMe$_3$ 1:20[a]
[^{18}F]**11**	phenylpiperazine	88–89	87	72–81	—	—	—
[^{18}F]**12**	piperidine	82–84	82	70–83	—	—	—
[^{18}F]**13**	morpholine	77–84	76–82	77–82	—	—	—
[^{18}F]**14**	benzylamine	86	74	71	—	—	—
[^{18}F]**15**	cyclohexylamine	85	7	71	—	—	—
[^{18}F]**16**	aniline	7	50	58	—	12–20	—
[^{18}F]**17**	4-fluoroaniline	4–8	56	65	25	30–35	—
[^{18}F]**18**	4-nitroaniline	<1	3	4–6	10–16	25–30	44–45

[a]Ratio of potassium trimethylsilanolate to amine.

and is typically used to convert carboxylic esters to the corresponding potassium carboxylates under mild anhydrous conditions [37]. Its successful use for the acceleration of *O*-sulfonylations was recently described by Musachio et al. [38]. Conversion of [^{18}F]**10** with 4-nitroaniline in the presence of potassium trimethylsilanolate led to the formation of the desired ^{18}F-labelled sulfonamide [^{18}F]**18** in radiochemical yields as high as 45%. Interestingly, a ratio of potassium trimethylsilanolate to 4-nitroaniline of 1:20 was considerably more efficient than ratios of 1:4 and 1:2 (Table 2 and Figure 5B). In this way, we could even accomplish the labelling of weakly nucleophilic amines such as 4-nitroaniline. The reason for the beneficial effect of potassium trimethylsilanolate on the sulfonylation reaction could be a partial deprotonation of the 4-nitroaniline as the basicity of siloxides is comparable to that of alkoxides [39]. A pK_a value of 21 has been reported for the amino group in 4-nitroaniline [40].

Stability against enzymatic degradation

Many compounds that are able to address biomolecular targets of interest for molecular imaging contain amino-substituted aromatic and heteroaromatic moieties. For the convenient radiolabelling of these molecules with fluorine-18 an ^{18}F-fluoroacetylation seems to be convenient from a chemical point of

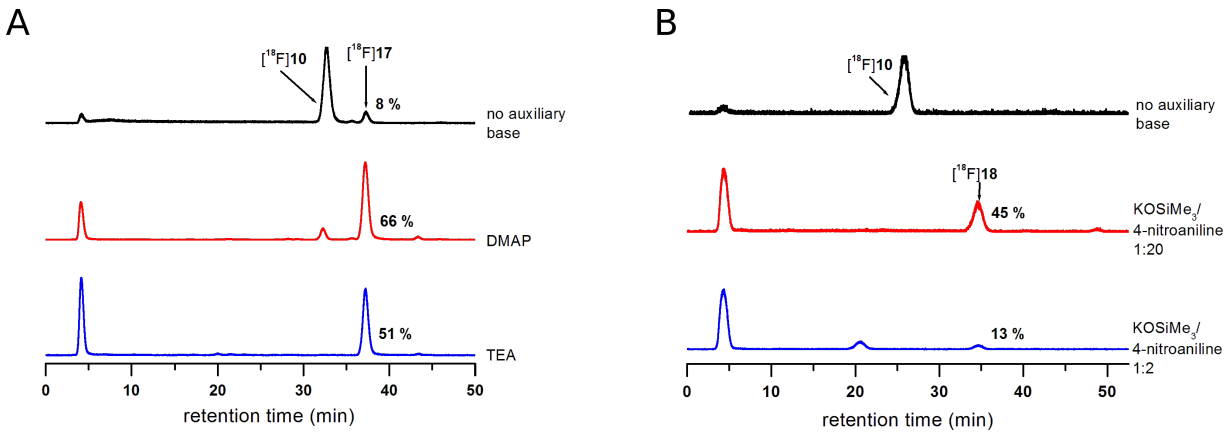


Figure 5: Radio-HPLC chromatograms for the reaction of [^{18}F]**10** with (A) 4-fluoroaniline in the absence and presence of 4-*N*,*N*-dimethylaminopyridine (DMAP) and triethylamine (TEA) and (B) 4-nitroaniline in the absence and presence of potassium trimethylsilanolate in varying amounts relative to the nucleophile. The ordinates (counts of ^{18}F-activity in arbitrary units) are omitted for clarity.

view. However, ^{18}F-labelled aromatic fluoroacetamides turned out to be unstable in vivo undergoing *N*-defluoroacetylation [41]. Nothing has been stated regarding the enzymes catalysing this metabolic transformation but the involvement of carboxylesterase (EC 3.1.1.1) is probable even though the participation of other hydrolases cannot be excluded [42,43]. Carboxylesterase belongs to the large class of α/β serine hydrolases, is located in the lumen of the endoplasmic reticulum of cells in many tissues, and is highly expressed in liver cells [44]. Beside its esterase activity the enzyme shows also amidase activity towards amides with various acyl chains and plays a prominent role in the hydrolytic metabolism of many drug molecules including radiopharmaceuticals [45,46]. Notably, the amidase activity of carboxylesterase is restricted to amides derived from aromatic amines [47]. This catalytic activity is crucial for the bioactivation of the acetanilide class of analgesic agents represented by paracetamol as the most important member [48]. Metabolic instability was also observed for aliphatic ^{18}F-labelled fluoroacetamides [13,49]. Their fate seems to be different from their aromatic counterparts in the way that they undergo defluorination at the α-methylene group rather than hydrolytic cleavage of the amide bond [13].

The metabolic hydrolysis of sulfonamide bonds has not been reported so far. Thus, this type of chemical function can be considered as metabolically inert [42]. To support this and to assess the metabolic stability of 3-fluoropropanesulfonamides in comparison to their fluoroacetamide analogues, *N*-(4-fluorophenyl)-3-fluoropropane-1-sulfonamide (**17**) and *N*-(4-fluorophenyl)-fluoroacetamide (**19**, see Supporting Information File 1) were exposed to pig-liver esterase (PLE), the porcine homologue of carboxylesterase, in buffered aqueous solution. Fluoroacetamide **19** was prepared by reacting 4-fluoroaniline with fluoroacetyl chloride. The activity of the enzyme preparation was verified using the chromogenic standard substrate 4-nitrophenyl butyrate in a spectrophotometric assay. The concentrations of **17** and **19** were monitored by RP-HPLC.

As expected, sulfonamide **17** proved to be stable against degradation by carboxylesterase (Figure 6). Under the same conditions, fluoroacetamide **19** underwent degradation with a pseudo-first-order rate constant of 0.012 min^{-1} corresponding to a half-life of 58 min at an enzyme concentration of

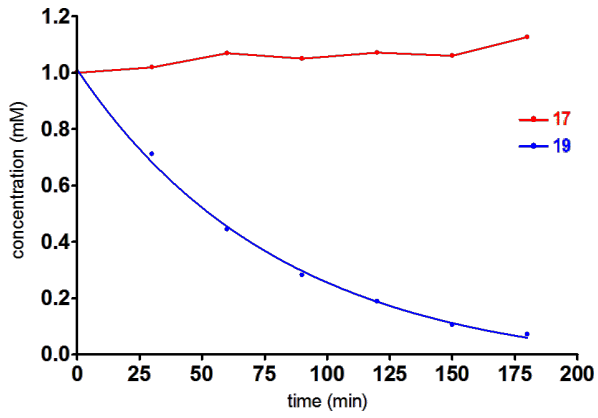


Figure 6: Time course of the carboxylesterase-catalysed degradation of 3-fluoropropansulfonamide **17** (red) and fluoroacetamide **19** (blue). The pseudo first-order rate constant for the decay of **19** was (0.012 ± 0.001) min^{-1} corresponding to a half-life of 57.8 min. Data points represent average values from two measurements originating from two independent experiments with SEM values less than 10% of the mean values.

1.4 mg/mL. This result demonstrates that the degradation of aromatic fluoroacetamides in vivo can be mediated by carboxylesterase. However, other hydrolases such as arylacetamide deacetylase might be involved in this process [43] and the nonhydrolytic disintegration of the fluoroacetyl moiety catalysed by other enzymes should be considered as well.

Conclusion

The radiosynthesis of 3-[^{18}F]fluoropropanesulfonyl chloride ([^{18}F]**10**) has been optimised with regard to the preparation of the labelling precursor as well as the conditions for its efficient radiofluorination and subsequent transformation to the radiolabelled sulfonyl chloride.

A variety of primary and secondary aliphatic as well as aromatic amines were studied with respect to their reaction with [^{18}F]**10** and the identity of the resulting sulfonamides was confirmed with the aid of the corresponding nonradioactive reference compounds. For one of these, *N*-(4-nitrophenyl)-3-fluoropropane-1-sulfonamide (**18**), the single-crystal X-ray structure was determined. The formation of ^{18}F-labelled sulfonamides derived from aliphatic amines did not require the addition of auxiliary bases, whereas the radiochemical yields for aromatic sulfonamides were generally low without their addition. By trying different auxiliary bases it was possible to convert even electron-deficient aromatic amines, such as 4-nitroaniline, to the corresponding ^{18}F-labelled sulfonamides in satisfactory yields.

The carboxylesterase-catalysed hydrolysis of an aromatic fluoroacetamide was demonstrated for the first time, implicating a radiopharmacological advantage for the 3-[^{18}F]fluoropropanesulfonamides over the corresponding [^{18}F]fluoroacetamides for their use in PET imaging.

Supporting Information

Supporting Information File 1

Experimental procedures, characterisation data of synthesised compounds and supplementary graphical material.
[http://www.beilstein-journals.org/bjoc/content/supplementary/1860-5397-9-115-S1.pdf]

Acknowledgements

We would like to thank Dr. Claudia Birkemeyer (University of Leipzig) for HRMS measurements. The dedicated technical assistance of Tina Spalholz, Peggy Wecke and Karin Landrock is gratefully acknowledged. R.L. acknowledges financial support by the Fonds der Chemischen Industrie.

References

1. Meade, T. J.; Aime, S. *Acc. Chem. Res.* **2009,** *42,* 821. doi:10.1021/ar900166c
2. Serdons, K.; Verbruggen, A.; Bormans, G. M. *Methods* **2009,** *48,* 104–111. doi:10.1016/j.ymeth.2009.03.010
3. Cai, L.; Lu, S.; Pike, V. W. *Eur. J. Org. Chem.* **2008,** 2853–2873. doi:10.1002/ejoc.200800114
4. Kilbourn, M. R. *Fluorine-18 labeling of radiopharmaceuticals;* National Academy Press: Washington D. C., 1990.
5. Kuhnast, B.; Dolle, F. *Curr. Radiopharm.* **2010,** *3,* 174–201. doi:10.2174/1874471011003030174
6. Wängler, C.; Schirrmacher, R.; Bartenstein, P.; Wängler, B. *Curr. Med. Chem.* **2010,** *17,* 1092–1116. doi:10.2174/092986710790820615
7. Olberg, D. E.; Hjelstuen, O. K. *Curr. Top. Med. Chem.* **2010,** *10,* 1669–1679. doi:10.2174/156802610793176747
8. Wester, H. J.; Schottelius, M. Fluorine-18 labeling of peptides and proteins. In *PET Chemistry: The driving force in molecular imaging;* Schubiger, P. A.; Lehmann, L.; Friebe, M., Eds.; Springer: Berlin, Germany, 2007; pp 79–111.
9. Müller-Platz, C. M.; Kloster, G.; Legler, G.; Stöcklin, G. *J. Labelled Compd. Radiopharm.* **1982,** *19,* 1645–1646.
10. Block, D.; Coenen, H. H.; Stöcklin, G. *J. Labelled Compd. Radiopharm.* **1988,** *25,* 185–200. doi:10.1002/jlcr.2580250210
11. Tada, M.; Iwata, R.; Sugiyama, H.; Sato, K.; Fukuda, H.; Kubota, K.; Kubota, R.; Fujiwara, T.; Takahashi, H.; Wakui, A.; Ido, T. *J. Labelled Compd. Radiopharm.* **1994,** *34,* 741–746. doi:10.1002/jlcr.2580340807
12. Mukhopadhyay, U.; Tong, W. P.; Gelovani, J. G.; Alauddin, M. M. *J. Labelled Compd. Radiopharm.* **2006,** *49,* 997–1006. doi:10.1002/jlcr.1122
13. Sorger, D.; Scheunemann, M.; Großmann, U.; Fischer, S.; Vercouille, J.; Hiller, A.; Wenzel, B.; Roghani, A.; Schliebs, R.; Brust, P.; Sabri, O.; Steinbach, J. *Nucl. Med. Biol.* **2008,** *35,* 185–195. doi:10.1016/j.nucmedbio.2007.10.004
14. Fischer, S.; Hiller, A.; Scheunemann, M.; Deuther-Conrad, W.; Hoepping, A.; Diekers, M.; Wegner, F.; Brust, P.; Steinbach, J. *J. Labelled Compd. Radiopharm.* **2008,** *51,* 123–131. doi:10.1002/jlcr.1473
15. Briard, E.; Pike, V. W. *J. Labelled Compd. Radiopharm.* **2004,** *47,* 217–232. doi:10.1002/jlcr.816
16. Hoepping, A.; Scheunemann, M.; Fischer, S.; Deuther-Conrad, W.; Hiller, A.; Wegner, F.; Diekers, M.; Steinbach, J.; Brust, P. *Nucl. Med. Biol.* **2007,** *34,* 559–570. doi:10.1016/j.nucmedbio.2007.03.011
17. Madan, A.; Fisher, A.; Jin, L.; Chapman, D.; Bozigian, H. P. *Xenobiotica* **2007,** *37,* 736–752. doi:10.1080/00498250701433054
18. Li, Z.; Lang, L.; Ma, Y.; Kiesewetter, D. O. *J. Labelled Compd. Radiopharm.* **2008,** *51,* 23–27. doi:10.1002/jlcr.1466
19. Fagerholm, U. *Drug Discovery Today* **2007,** *12,* 1076–1082. doi:10.1016/j.drudis.2007.10.005
20. Löser, R.; Hiller, A.; Fischer, S.; Funke, U.; Maisonial, A.; Brust, P.; Steinbach, J. *J. Labelled Compd. Radiopharm.* **2011,** *54,* S477.
21. Davies, W.; Dick, J. H. *J. Chem. Soc.* **1931,** 2104–2109.
22. Quaedvlieg, M. Herstellung und Umwandlung von aliphatischen Sulfonsäuren und ihren Derivaten. In *Schwefel-, Selen-, Tellur-Verbindungen,* 4th ed.; Müller, E.; Bayer, O.; Meerwein, H.; Ziegler, K., Eds.; *Houben-Weyl Methoden der Organischen Chemie*, Vol. IX; Georg Thieme Verlag: Stuttgart, Germany, 1955; pp 347–405.

23. Muth, F. Herstellung und Umwandlung aromatischer Sulfonsäureester. In *Schwefel-, Selen-, Tellur-Verbindungen,* 4th ed.; Müller, E.; Bayer, O.; Meerwein, H.; Ziegler, K., Eds.; *Houben-Weyl Methoden der Organischen Chemie*, Vol. IX; Georg Thieme Verlag: Stuttgart, Germany, 1955; pp 663–683.
24. Grung, K. E.; Rømming, C.; Songstad, J. *Acta Chem. Scand.* **1989,** *43,* 518–526. doi:10.3891/acta.chem.scand.43-0518
25. Ohtani, N.; Murakawa, S.; Watanabe, K.; Tsuchimoto, D.; Sato, D. *J. Chem. Soc., Perkin Trans. 2* **2000,** 1851–1856. doi:10.1039/b003491f
26. Junling, L.; Yongxian, W.; Haibin, T.; Wei, Z.; Xiuli, Z.; Yingwu, L.; Duanzhi, Y. *J. Radioanal. Nucl. Chem.* **2002,** *254,* 415–419.
27. Johnson, T. B.; Douglass, I. B. *J. Am. Chem. Soc.* **1939,** *61,* 2548–2550. doi:10.1021/ja01878a085
28. Millington, J. E.; Brown, G. M.; Pattison, F. L. M. *J. Am. Chem. Soc.* **1956,** *78,* 3846–3847. doi:10.1021/ja01596a079
29. Muth, F. Funktionelle N-Derivate der Arylsulfonsäuren. In *Schwefel-, Selen-, Tellur-Verbindungen,* 4th ed.; Müller, E.; Bayer, O.; Meerwein, H.; Ziegler, K., Eds.; *Houben-Weyl Methoden der Organischen Chemie*, Vol. IX; Georg Thieme Verlag: Stuttgart, Germany, 1955; pp 605–657.
30. Lyapkalo, I. M.; Reissig, H.-U.; Schäfer, A.; Wagner, A. *Helv. Chim. Acta* **2002,** *85,* 4206–4215. doi:10.1002/hlca.200290006
31. Ohwada, T.; Okamoto, I.; Shudo, K.; Yamaguchi, K. *Tetrahedron Lett.* **1998,** *39,* 7877–7880. doi:10.1016/S0040-4039(98)01746-8
32. Ohwada, T. *Yakugaku Zasshi* **2001,** *121,* 65–77. doi:10.1248/yakushi.121.65
33. Howard, J. A. K.; Hoy, V. J.; O'Hagan, D.; Smith, G. T. *Tetrahedron* **1996,** *52,* 12613–12622. doi:10.1016/0040-4020(96)00749-1
34. Dunitz, J. D.; Taylor, R. *Chem.–Eur. J.* **1997,** *3,* 89–98. doi:10.1002/chem.19970030115
35. Müller, K.; Faeh, C.; Diederich, F. *Science* **2007,** *317,* 1881–1886. doi:10.1126/science.1131943
36. Gross, K. C.; Seybold, P. G.; Peralta-Inga, Z.; Murray, J. S.; Politzer, P. *J. Org. Chem.* **2001,** *66,* 6919–6925. doi:10.1021/jo010234g
37. Laganis, E. D.; Chenard, B. L. *Tetrahedron Lett.* **1984,** *25,* 5831–5834. doi:10.1016/S0040-4039(01)81697-X
38. Musachio, J. L.; Shah, J.; Pike, V. W. *J. Labelled Compd. Radiopharm.* **2005,** *48,* 735–747. doi:10.1002/jlcr.991
39. Lickiss, P. D. *Adv. Inorg. Chem.* **1995,** *42,* 147–262. doi:10.1016/S0898-8838(08)60053-7
40. Bordwell, F. G.; Algrim, D. J. *J. Am. Chem. Soc.* **1988,** *110,* 2964–2968. doi:10.1021/ja00217a045
41. Briard, E.; Zoghbi, S. S.; Siméon, F. G.; Imaizumi, M.; Gourley, J. P.; Shetty, H. U.; Lu, S.; Fujita, M.; Innis, R. B.; Pike, V. W. *J. Med. Chem.* **2009,** *52,* 688–699. doi:10.1021/jm8011855
42. Testa, B.; Mayer, J. M. *Hydrolysis in Drug and Prodrug Metabolism. Chemistry, Biochemistry and Enzymology;* Verlag Helvetica Chimica Acta: Zürich, Switzerland, 2003. doi:10.1002/9783906390444
43. Fukami, T.; Yokoi, T. *Drug Metab. Pharmacokinet.* **2012,** *27,* 466–477. doi:10.2133/dmpk.DMPK-12-RV-042
44. Hosokawa, M. *Molecules* **2008,** *13,* 412–431. doi:10.3390/molecules13020412
45. Nics, L.; Haeusler, D.; Wadsak, W.; Wagner, K.-H.; Dudczak, R.; Kletter, K.; Mitterhauser, M. *Nucl. Med. Biol.* **2011,** *38,* 13–17. doi:10.1016/j.nucmedbio.2010.07.004
46. Testa, B.; Krämer, S. D. *Chem. Biodiversity* **2007,** *4,* 2031–2122. doi:10.1002/cbdv.200790169
47. Franz, W.; Krisch, K. *Hoppe-Seyler's Z. Physiol. Chem.* **1968,** *349,* 575–587. doi:10.1515/bchm2.1968.349.1.575
48. Testa, B.; Krämer, S. D. *Chem. Biodiversity* **2009,** *6,* 591–684. doi:10.1002/cbdv.200900022
49. Rogers, G. A.; Stone-Elander, S.; Ingvar, M.; Eriksson, L.; Parsons, S. M.; Widén, L. *Nucl. Med. Biol.* **1994,** *21,* 219–230. doi:10.1016/0969-8051(94)90012-4

License and Terms

This is an Open Access article under the terms of the Creative Commons Attribution License (http://creativecommons.org/licenses/by/2.0), which permits unrestricted use, distribution, and reproduction in any medium, provided the original work is properly cited.

The license is subject to the *Beilstein Journal of Organic Chemistry* terms and conditions: (http://www.beilstein-journals.org/bjoc)

The definitive version of this article is the electronic one which can be found at: doi:10.3762/bjoc.9.115

Beilstein Journal of Organic Chemistry

Amyloid-β probes: Review of structure–activity and brain-kinetics relationships

Todd J. Eckroat[1,2], Abdelrahman S. Mayhoub[2,§] and Sylvie Garneau-Tsodikova[*1,¶]

Review

Open Access

Address:
[1]Department of Pharmaceutical Sciences, University of Kentucky, 789 South Limestone Street, Lexington, KY, 40536-0596, United States and [2]Life Sciences Institute and Department of Medicinal Chemistry, University of Michigan, 210 Washtenaw Ave, Ann Arbor, MI, 48109-2216, United States

Email:
Sylvie Garneau-Tsodikova[*] - sylviegtsodikova@uky.edu

* Corresponding author
§ On leave from Faculty of Pharmacy, Al-Azhar University, Cairo, 11884, Egypt
¶ Phone: 859-218-1686

Keywords:
Alzheimer's disease; in vivo detection; near-infrared fluorescence probes; PET/SPECT imaging; radioactive probes

Beilstein J. Org. Chem. **2013,** *9,* 1012–1044.
doi:10.3762/bjoc.9.116

Received: 26 January 2013
Accepted: 30 April 2013
Published: 28 May 2013

This article is part of the Thematic Series "Synthetic probes for the study of biological function".

Guest Editor: J. Aubé

© 2013 Eckroat et al; licensee Beilstein-Institut.
License and terms: see end of document.

Abstract

The number of people suffering from Alzheimer's disease (AD) is expected to increase dramatically in the coming years, placing a huge burden on society. Current treatments for AD leave much to be desired, and numerous research efforts around the globe are focused on developing improved therapeutics. In addition, current diagnostic tools for AD rely largely on subjective cognitive assessment rather than on identification of pathophysiological changes associated with disease onset and progression. These facts have led to numerous efforts to develop chemical probes to detect pathophysiological hallmarks of AD, such as amyloid-β plaques, for diagnosis and monitoring of therapeutic efficacy. This review provides a survey of chemical probes developed to date for AD with emphasis on synthetic methodologies and structure–activity relationships with regards to affinity for target and brain kinetics. Several probes discussed herein show particularly promising results and will be of immense value moving forward in the fight against AD.

Introduction

Alzheimer's disease (AD) is a progressive neurodegenerative disorder of the central nervous system currently affecting ~5.4 million Americans, a number that could increase to 11–16 million by the year 2050. In the United States, AD represents the 6th leading cause of death. Between 2000 and 2008, the number of deaths caused by AD increased by 66%, a dramatic rise, especially when compared to other causes of death, such as heart disease, stroke, prostate and breast cancer,

and HIV, which decreased by 3–29% during that time period [1]. As these numbers indicate, AD represents a significant and increasing burden on our population, and efforts towards the development of new and improved diagnostics and therapeutics for this devastating disease are important research endeavors.

Several pathological hallmarks of AD have been identified, and they include decreased cholinergic neurons and acetylcholine (ACh) levels, plaques caused by aggregation of the protein fragment amyloid-β (Aβ), tangles associated with irregular phosphorylation of tau protein, inflammation and increased oxidative stress from reactive oxygen species (ROS), as well as dyshomeostasis and miscompartmentalization of metal ions such as Cu, Fe, and Zn. Observations of these hallmarks have led to several hypotheses in attempts to explain the underlying cause of the disease, which is likely multifactorial. However, the exact cause of AD still remains unknown.

Postmortem histopathological examination of Aβ plaques is currently the only way to firmly confirm AD [2]. In view of the limited accessibility to living brain and other central nervous system (CNS) tissues, AD is currently diagnosed through memory tests and/or based on the patients' history [2]. Obviously these kinds of diagnostic tools lack absolute sensitivity and accuracy, especially in the early stages of the disease. Therefore, as Aβ plaques precede the onset of dementia and cognitive decline in AD patients, their detection by nuclear imaging techniques such as positron emission tomography (PET) or single-photon emission computed tomography (SPECT) represents the presymptomatic diagnostic tool of choice for AD [3-5].

The presence of different binding sites in Aβ aggregates led medicinal chemists to investigate and develop a variety of chemical scaffolds as Aβ-imaging tracers [6-9]. To provide a high readable signal-to-background ratio, the ideal Aβ-imaging probes should have certain brain kinetics: a rapid initial brain uptake and a fast washout. Early efforts towards developing Aβ stains focused on dyes such as congo red (**1**), chrysamine G (**2**), pinacyanol (**3**), and thioflavin-T (**4**) (Figure 1A). However, the bulky and ionic natures of these dyes prevented them from crossing the blood brain barrier (BBB), and consequently, no in vivo benefits were obtained from these initial investigations [10,11]. During the past decade, efforts directed at developing probes that display uptake and retention that differ in healthy and AD-affected brains resulted in a variety of radiolabeled molecular probes for in vivo PET/SPECT imaging. The scaffolds from which these newer radiolabeled probes are derived include chalcone (**5**) and its conformationally restricted analogues flavone (**6**) and aurone (**7**); stilbene (**8**) and its analogues diphenyl-1,2,4-oxadiazole (**9**) and diphenyl-1,3,4-oxadiazole (**10**); and thioflavin-T analogues such as benzothiazole (**11**), benzoxazole (**12**), benzofuran (**13**), imidazopyridine (**14**), and benzimidazole (**15**); as well as quinoline (**16**) and naphthalene (**17**) derivatives (Figure 1B). In this review, we provide an overview of these AD radiolabeled early-diagnostic probes according to their scaffolds, with a special emphasis on their synthesis as well as their structure–activity and brain-kinetics relationships. We also provide a brief summary of the latest developments related to the detection of Aβ plaques by near-infrared fluorescence (NIRF) imaging.

Review

Radiolabels used in PET/SPECT molecular probes

Even though they decay rapidly, [^{11}C] ($t_{1/2}$ = 20 min) and [^{18}F] ($t_{1/2}$ = 110 min) are the most commonly used radiolabels in PET/SPECT molecular probes for in vivo imaging of Aβ plaques [4]. With a half-life ($t_{1/2}$) of 6.01 h compatible with the localization and residence time necessary for imaging, technetium-99m [^{99m}Tc] is also a radionuclide of choice that is easily produced by a ^{99}Mo/^{99m}Tc generator [12]. Iodine isotopes such as [^{125}I] are also employed, although much less frequently [13]. The general synthetic methods utilized to introduce radiolabels into PET probes are outlined in Scheme 1. These general strategies will be abbreviated as **Gs A–D** in all subsequent schemes in this review.

Chalcone and its conformationally restricted analogues

Chalcone derivatives

Chalcones and indolochalcones, such as **18a–l**, **19a**,**b**, **20a**,**b**, and **21**, have been widely reported as Aβ-imaging tracers (Scheme 2A). Structure–activity-relationship (SAR) studies on fluorinated chalcones **18a–l** have shown that, in general, chalcones with tertiary amines in their structures demonstrate good affinity for Aβ plaques in in vitro models (K_i = 20–50 nM) (Table 1) [14]. Dimethylation of the amino group seems to be crucial for Aβ binding, since analogues with free amino groups or monomethyl amino groups revealed lower affinity [14]. On the other hand, pegylation is not that essential for plaque binding as tertiary amine analogues with different degrees of pegylation (n = 0–3) all showed similar affinity. In biodistribution experiments using normal mice, the [^{18}F]-labeled chalcone **19a** showed high brain uptake rate and good clearance, whereas the [^{11}C]-labeled chalcone **19b** revealed reasonable brain uptake rate, but very fast clearance [14]. The [^{18}F]-labeled and [^{11}C]-labeled chalcones **19a** and **19b** were synthesized using similar methods, and a representative synthesis of **19a** is shown (Scheme 2B). Aldol condensation between the appropriate acetophenone **22** and benzaldehyde **23** afforded the chalcone backbone, which was subsequently pegylated to give **24** and

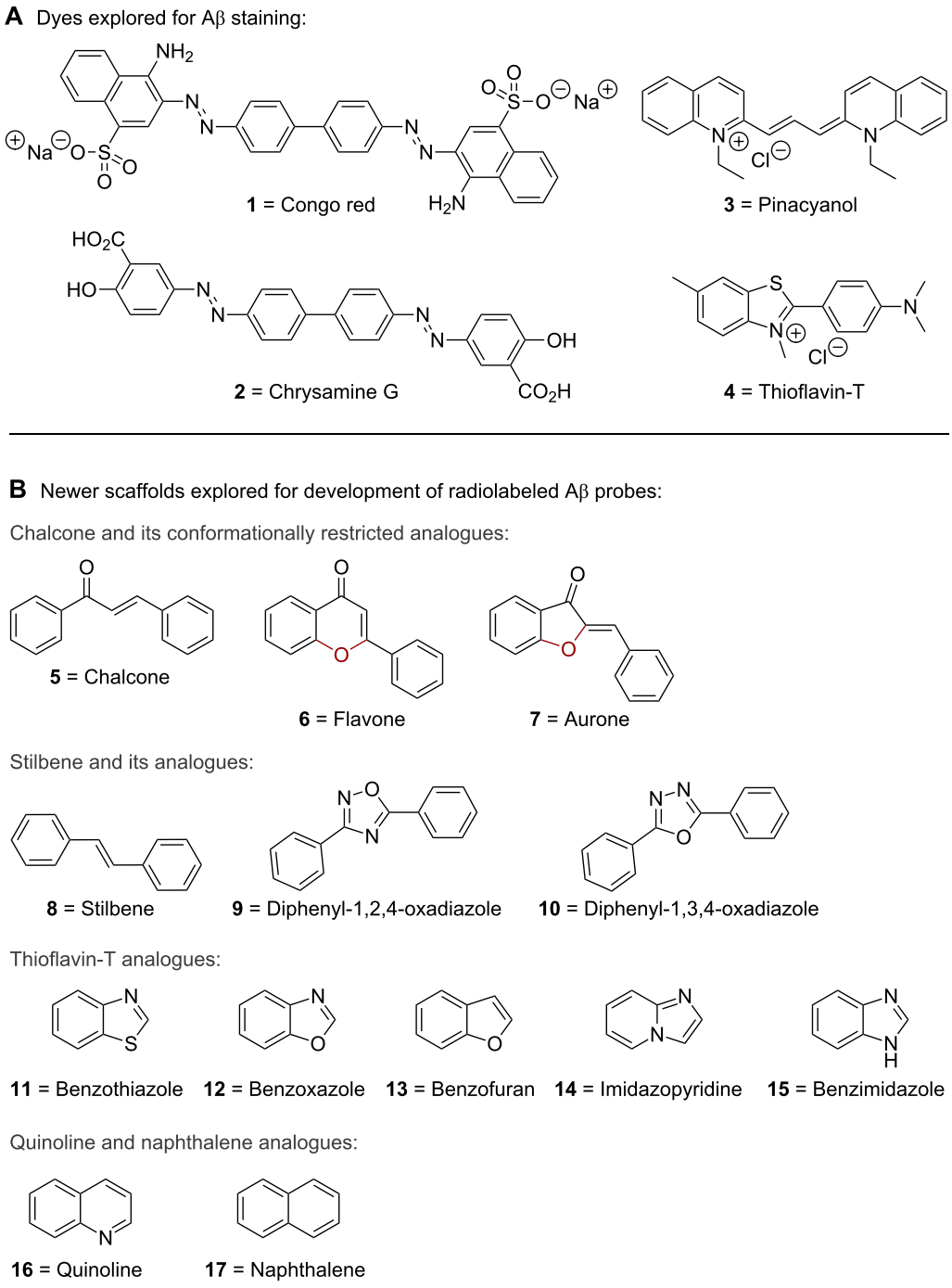
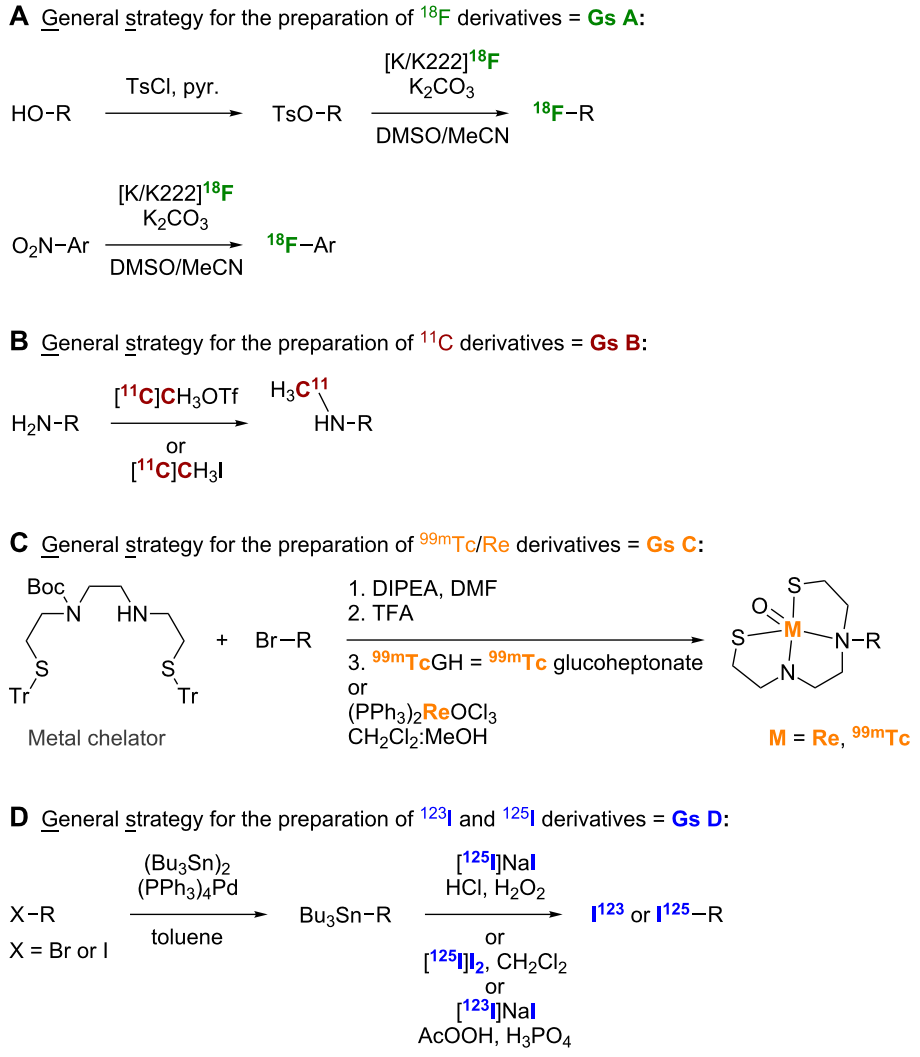


Figure 1: Structures of **A**. dyes originally used to stain Aβ and **B**. newer scaffolds explored for the development of radiolabeled Aβ probes.

radiolabeled to give **19a**. Compound **19b** was generated by using *p*-nitrobenzaldehyde instead of the corresponding dimethylamine **23** used in the preparation of **19a** [14]. The resultant nitrochalcone was then reduced by $SnCl_2$ in EtOH to yield the free amine, which was monomethylated by controlled addition of an equimolar amount of MeI. The final [^{11}C]-labeled compound **19b** was produced by reacting [^{11}C]CH_3OTf with the secondary amine precursor.

[Re]- and [^{99m}Tc]-labeled chalcone analogues **20a** and **20b** were also studied (Scheme 2A) [12]. The [Re]-labeled analogue **20a** displayed higher affinity for Aβ plaque than did the corres-



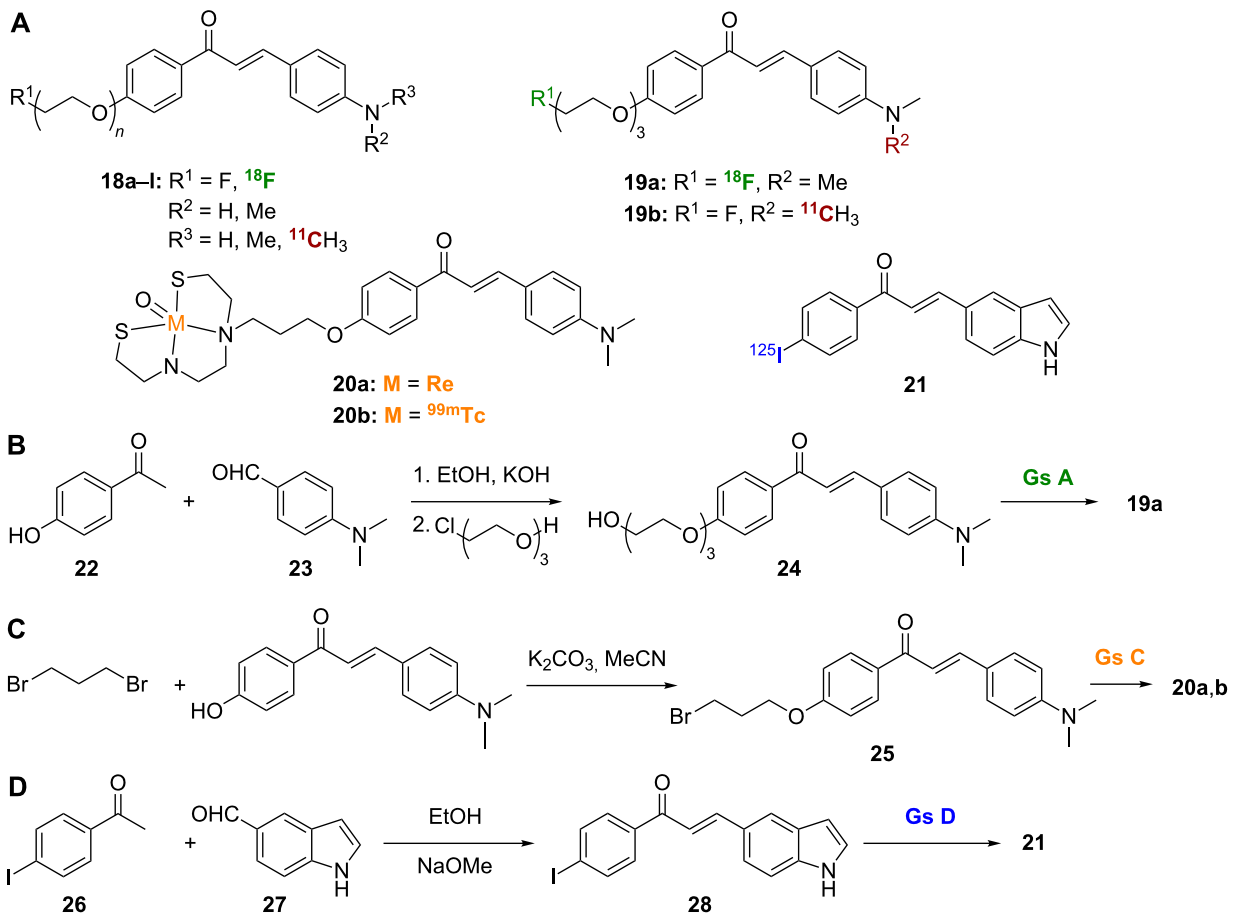
Scheme 1: General synthetic strategies (**Gs**) used to introduce **A**. ^{18}F, **B**. ^{11}C, **C**. ^{99m}Tc/Re, and **D**. ^{123}I and ^{125}I radiolabels into PET probes. Note: **Gs A**–**D** will be used in all subsequent schemes to describe these general synthetic strategies.

ponding [^{99m}Tc]-derived compound **20b**. However, **20b** showed better brain pharmacokinetics than **20a**, as indicated by its high brain-uptake rate (1.48% ID/g) and rapid wash out from the CNS (0.17% ID/g at 60 min). Compounds **20a** and **20b** were synthesized by reacting a Boc-protected metal chelator (Scheme 1C) with 4-*O*-(bromopropyl)hydroxychalcone **25** (Scheme 2C). After removal of the Boc protecting group, the final [Re]- and [^{99m}Tc]-labeled chalcones **20a** and **20b** were obtained by treatment with $(PPh_3)_2ReOCl_3$ and ^{99m}TcGH, respectively [12].

Finally, the radioiodinated indolochalcone **21**, among a series of other derivatives, was prepared through condensation of 4-iodoacetophenone (**26**) and indole-5-carboxaldehyde (**27**) to give **28**, which was radiolabeled to give the target compound (Scheme 2D) [15]. The indolochalcone **21** showed good binding affinity for $A\beta_{1\text{-}42}$ aggregates with a K_i < 10 nM. Replacement of the iodo substituent with a chloro, bromo, methoxy, or dimethylamino substituent all gave similar results, but replacement with a fluoro, hydroxy, amino, or methylamino substituent all reduced affinity to varying degrees. Autoradiography in sections of brain tissue from an AD animal model showed that **21** specifically labeled Aβ plaques, but its efficacy was hampered by low in vivo uptake into the brain (0.41% ID/g at 2 min) [15].

Conformationally restricted chalcones: flavones and aurones

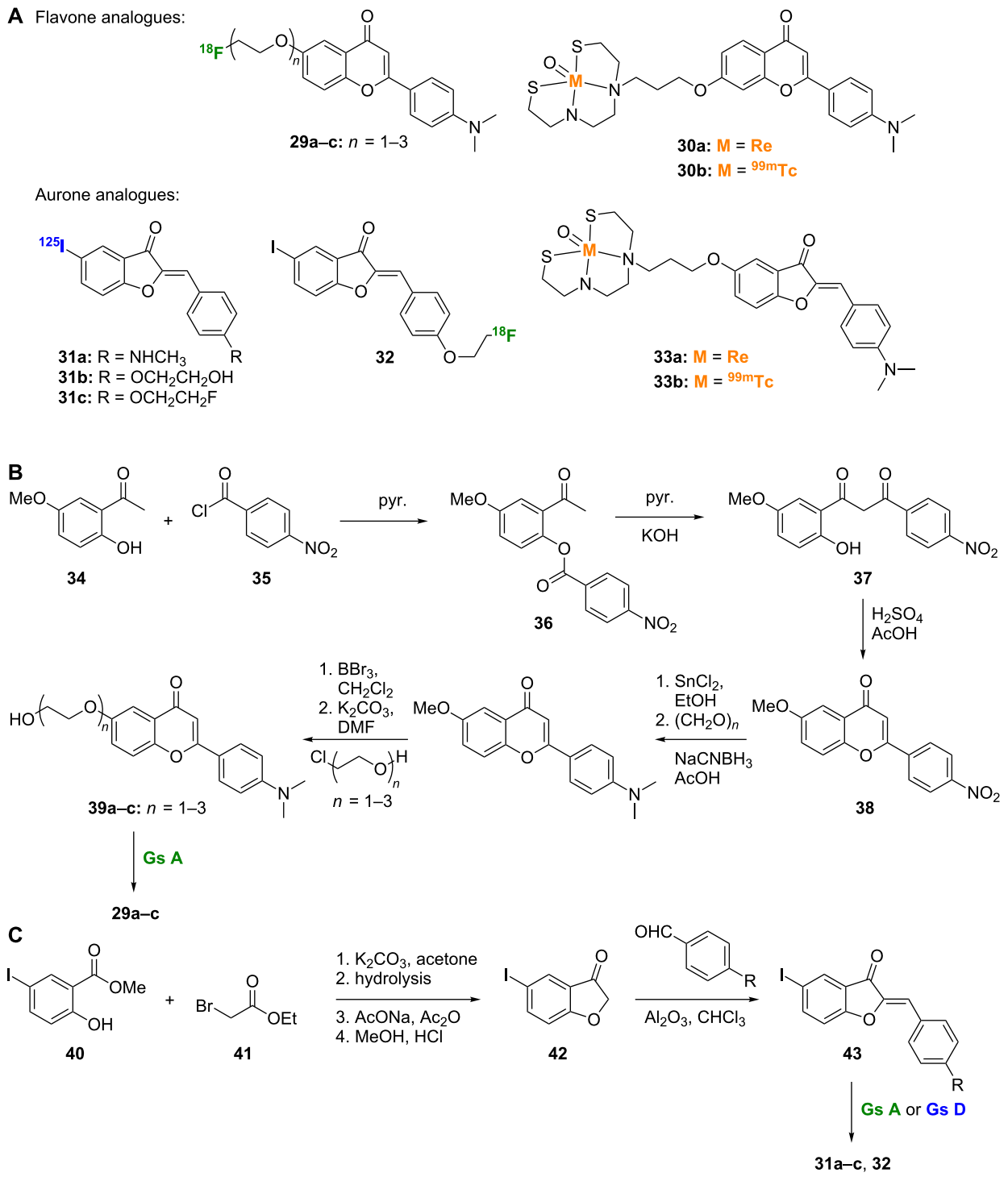
Flavones and aurones, such as **29a**–**c**, **30a**,**b**, **31a**–**c**, **32**, and **33a**,**b** (Scheme 3A), can be classified as conformationally restricted chalcone derivatives as their basic structures result from insertion of an oxygen atom between the double bond and



Scheme 2: A. Structures of radiolabeled chalcone analogues discussed. **B**.–**D**. Synthetic schemes for the preparation of radiolabeled chalcones **19a** and **20a**,**b**, and indolochalcone **21**.

Table 1: Inhibition constants and biodistribution of radioactivity of fluorinated chalcone derivatives **18a**–**l** and **19a**,**b** (values are from [14]).

Compound	*n*	R^1	R^2	R^3	$A\beta_{1-42}$ K_i (nM)	%ID/g at 2 min	%ID/g at 30 min
18a	1	F	Me	Me	45.7 ± 7.1	—	—
[^{11}C]**18a**	1	F	Me	^{11}CH$_3$	—	6.01 ± 0.61	2.26 ± 0.41
18b	2	F	Me	Me	20.0 ± 2.5	—	—
[^{11}C]**18b**	2	F	Me	^{11}CH$_3$	—	4.73 ± 0.47	1.00 ± 0.19
18c	3	F	Me	Me	38.9 ± 4.2	—	—
19a	3	^{18}F	Me	Me	—	3.48 ± 0.47	1.07 ± 0.17
19b	3	F	Me	^{11}CH$_3$	—	4.31 ± 0.33	0.35 ± 0.03
18d	1	F	H	H	678.9 ± 21.7	—	—
18e	2	F	H	H	1048.0 ± 114.3	—	—
18f	3	F	H	H	790.0 ± 132.1	—	—
18g	1	F	H	Me	197.1 ± 58.8	—	—
18h	2	F	H	Me	216.4 ± 13.8	—	—
18i	3	F	H	Me	470.9 ± 100.4	—	—
18j	0	F	Me	Me	49.8 ± 6.2	—	—
[^{11}C]**18j**	0	F	Me	^{11}CH$_3$	—	3.68 ± 0.35	1.04 ± 0.20
18k	0	F	H	H	663.0 ± 88.3	—	—
18l	0	F	H	Me	234.2 ± 44.0	—	—



Scheme 3: A. Structures of the radiolabeled flavone and aurone analogues discussed. **B**. Synthetic scheme for the preparation of [^{18}F]-labeled flavone derivatives. **C**. Synthetic scheme for the preparation of the aurone scaffold and its [^{18}F]- and [^{125}I]-labeled analogues.

the phenyl ring attached to the carbonyl group of the chalcone scaffold (Figure 1B, with oxygen atoms depicted in red). The affinity of flavonoids towards Aβ aggregates was first established by using fluorescence staining in brain sections of Tg2576 transgenic mice [10]. The absence of spots in wild-type mouse brain sections indicated the specificity of flavonoids towards Aβ aggregates in AD mouse models. The [^{18}F]-labeled pegylated flavones **29a–c** showed high affinity towards Aβ

aggregates with K_i values ranging between 5.3 nM for **29a** and 19.3 nM for **29c** (Scheme 3A) [16]. SAR studies suggest that, as with chalcones, the tertiary amine in these flavones was important for binding and tracing Aβ aggregates in mouse models, as they consistently outperformed secondary and primary amine analogues [16]. Also as with chalcones, the degree of pegylation had only minor effects on binding properties. Compounds **29a**–**c** showed uptake rates indicative of high to sufficient levels for brain imaging (2.89–4.17% ID/g at 2 min) and moderate clearance rates [16]. The flavone backbone of **29a**–**c** was built by acylating 2-hydroxy-5-methoxyacetophenone (**34**) with 4-nitrobenzoyl chloride (**35**) and subjecting the resulting 2-acyloxyacetophenone (**36**) to Baker–Venkataraman rearrangement [17] to afford the 1,3-diarylpropane-1,3-dione **37**, which was dehydrated with sulfuric acid to give **38**. Subsequent nitro reduction, reductive methylation, methyl ether cleavage, and pegylation gave the nonlabeled precursors **39a**–**c**. The [^{18}F]-label was introduced by using the standard [K/K222]^{18}F in DMSO and acetonitrile reaction conditions (Scheme 3B) [16]. The [Re]- and [^{99m}Tc]-labeled flavone complexes **30a** and **30b** were also prepared by using the procedure described for the synthesis of the [Re]- and [^{99m}Tc]-labeled chalcones **20a** and **20b** (Scheme 2). The [^{99m}Tc]-labeled flavone complex **30a** displayed high Aβ plaque affinity but limited brain uptake [18].

Aurone derivatives have been investigated for their Aβ plaque binding affinity [19]. The [^{125}I]-labeled methylamine aurone **31a** presented great binding affinity to Aβ aggregates (K_i = 1.2 nM), better than all reported flavones to date. It also showed rapid brain uptake rate (3.17% ID/g at 2 min) and rapid clearance (0.24% ID/g at 60 min) [19]. The effect of the tertiary amine in this aurone scaffold was less pronounced than that seen with chalcones or flavones. The dimethylamine analogue of **31a** had approximately six times weaker binding affinity, while the free amine analogue showed only two times weaker affinity. To further enhance the Aβ plaque traceability of **31a**, its methylamine moiety was replaced with ethylene oxide to provide compound **31b**, which exhibited a K_i value of 1.05 nM in an in vitro binding assay [13]. The brain kinetics of **31b** (brain uptake = 4.51% ID/g at 2 min and washout = 0.09% ID/g at 60 min) were found to be slightly better than those of **31a** [13]. Addition of 2 or 3 ethylene oxide units or replacement with a hydroxy or methoxy group did not significantly improve the plaque binding affinity and modestly affected the brain kinetics. Replacement of the terminal hydroxy group of **31b** with a fluorine atom negatively affected the brain uptake property of compound **31c** (2.34% ID/g at 2 min) when compared to **31b** [20]. However, it did not affect the washout character of the compound. These results were confirmed by preparation and analysis of the [^{18}F]-labeled compound **32** [20]. In general, the aurone derivatives **31a**–**c** and **32** were built from the reaction of methyl 5-iodosalicilate (**40**) with ethyl bromoacetate (**41**) followed by ester hydrolysis and cyclization to afford 5-iodo-3-coumaranone (**42**), which, after condensation with the proper benzaldehydes, gave the aurone scaffold **43**, which could be radiolabeled (Scheme 3C). As for the chalcone and flavone derivatives, [Re]- and [^{99m}Tc]-labeled aurone complexes **33a** and **33b** were also prepared [18]. The high affinity for Aβ aggregates observed with the [^{99m}Tc]-labeled aurone **33b** was hampered by its weak brain penetration, which made it unsuitable for in vivo application [18].

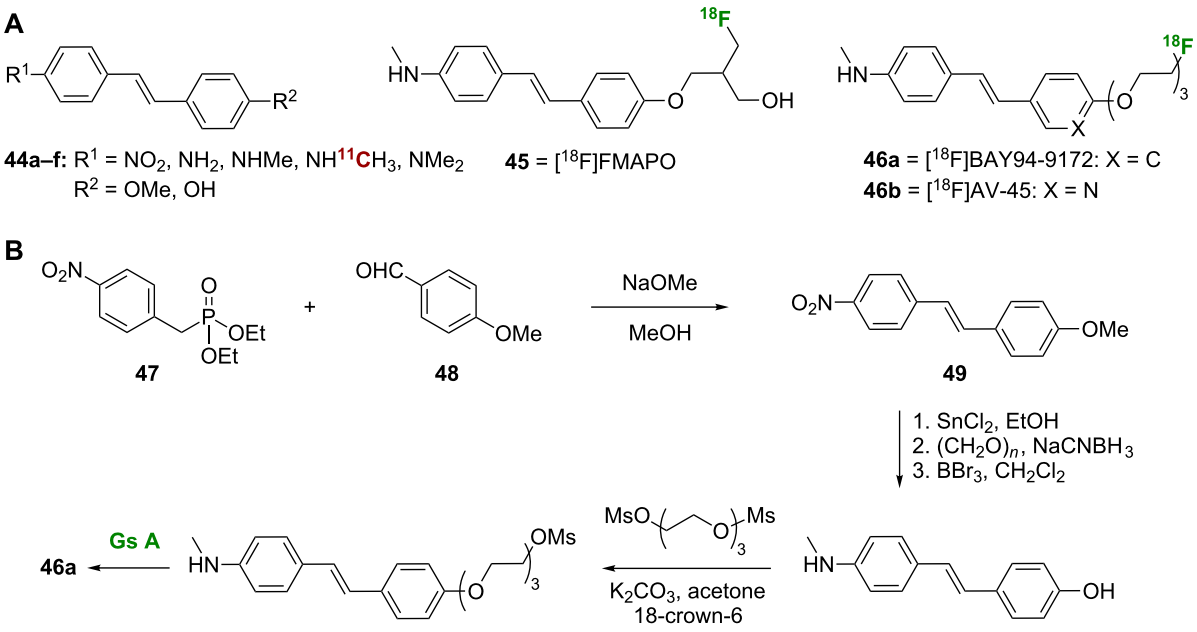
Stilbene and its analogues

Stilbene derivatives

The SARs of stilbene analogues, such as **44a**–**f**, **45**, and **46a**,**b** (Scheme 4A), as Aβ plaque tracers have been thoroughly investigated. In general, it was found that an electron-donating group at each end of the stilbene derivative is essential for Aβ plaque binding affinity [21]. Analysis of stilbenes **44a–f** shows that a monomethylated or dimethylated amine at one end of the stilbene core leads to strong binding affinity for $A\beta_{1\text{-}40}$ aggregates, while a free amine or nitro group reduces affinity. The opposite end of the stilbene core can be substituted with a hydroxy or methoxy substituent with little effect on binding affinity (Table 2). Derivative **44d**, which showed good affinity towards Aβ aggregates in vitro (K_i = 6.0 ± 1.5 nM), has been radiolabeled to give *N*-[^{11}C]methylamino-4'-hydroxystilbene ([^{11}C]**44d**), and this compound shows excellent labeling of Aβ plaques in TgCRDN8 mouse brain sections by in vitro autoradiography [22].

Table 2: Inhibition constants and biodistribution of radioactivity of stilbene derivatives **44a–f** and [^{11}C]**44d** (values are from [22]).

Compound	R^1	R^2	$A\beta_{1\text{-}40}$ K_i (nM)	%ID/g at 2 min	%ID/g at 60 min
44a	NO_2	OMe	151 ± 30	—	—
44b	NH_2	OMe	36 ± 5	—	—
44c	NHMe	OMe	1.2 ± 0.5	—	—
44d	NHMe	OH	6.0 ± 1.5	—	—
[^{11}C]**44d**	NH**^{11}C**H_3	OH	—	1.15 ± 0.08	0.30 ± 0.03
44e	NMe_2	OMe	1.3 ± 0.4	—	—
44f	NMe_2	OH	2.2 ± 0.6	—	—



Scheme 4: A. Structures of the radiolabeled stilbene analogues discussed. **B**. Synthetic scheme for the preparation of [^{18}F]BAY94-9172 (**46a**).

[^{18}F]-Labeled stilbene derivatives have enhanced brain kinetics rendering them appropriate for clinical use [23-25]. In order to control the lipophilicity and keep the partition coefficient (log *P*) value between 1 and 3, which reduces brain nonspecific binding and improves signal-to-noise ratio, additional hydroxy or ethylene oxide unit(s) were added [21]. An early fluorinated stilbene was [^{18}F]FMAPO (**45**), which demonstrated high binding affinity for Aβ aggregates (K_i = 5.0 ± 1.2 nM) in assays using human AD brain homogenates [26]. Even though addition of the fluoroalkyl side chain moiety had little effect on the binding affinity and the clearance rate, it improved brain kinetics significantly (from 1.15% ID/g at 2 min for [^{11}C]**44d** [22] to 9.75% ID/g at 2 min for **45** [26]). Florbetaben ([^{18}F]BAY94-9172, **46a**), another member of the stilbene class, showed strong binding affinity for human AD brain homogenates (K_i = 6.7 ± 0.3 nM) and promising pharmacokinetics [21], and this compound has progressed to clinical trials. Compound **46a** was tested clinically on 15 AD patients and a similar number of healthy elderly volunteers [4]. Interestingly, all AD patients showed widespread neocortical binding of **46a**, which was quantified by using the standardized uptake value ratio (SUVR) technique [4]. This observation was further supported by another study using a wider sample population where AD patients demonstrated significantly higher SUVRs when compared to healthy patients or patients with other neural diseases such as Parkinson's disease, mild cognitive impairment, frontotemporal lobar degeneration, dementia with Lewy bodies, and vascular dementia [27]. More recent phase 2/3 clinical trials collectively showed that compound **46a** displays a high degree of sensitivity and selectivity in discriminating between patients with probable AD and age-matched healthy controls [28].

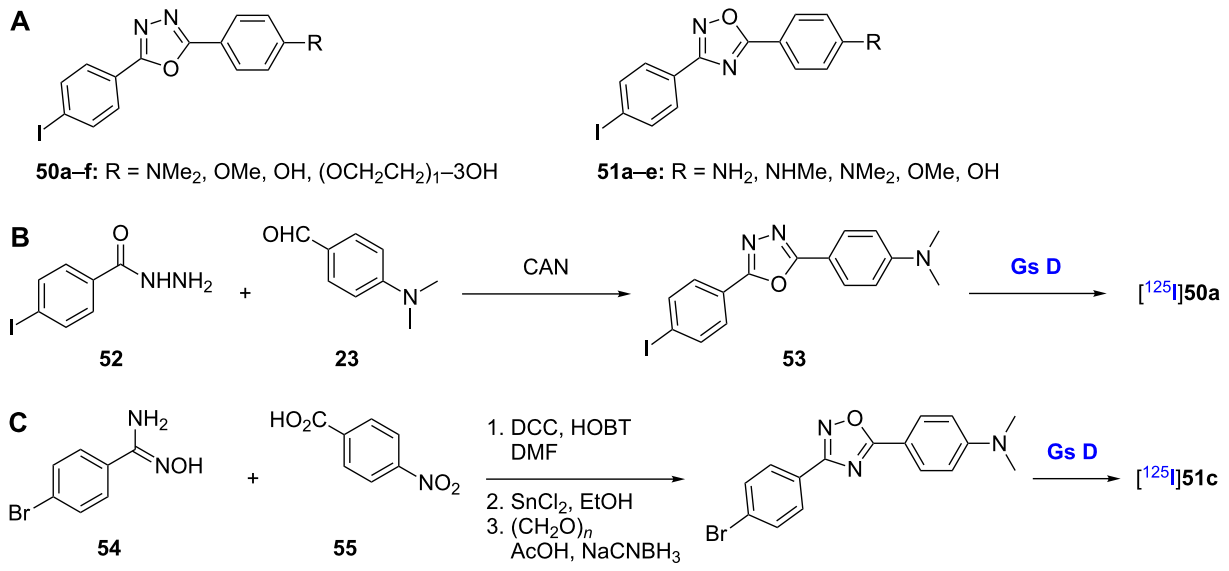
A pyridine analogue of **46a**, florbetapir ([^{18}F]AV-45, **46b**) was also prepared using a tosylate precursor with Sumitomo modules for radiosynthesis [23,29]. Compound **46b** displayed strong affinity for Aβ peptides in AD brain homogenates (K_i = 2.87 ± 0.17 nM), excellent pharmacokinetics [30], and an acceptable safety profile that paved the way to its clinical application in brain imaging [31]. A number of **46b**/PET studies have been conducted [23,32-39]. Using **46b** as an imaging probe, PET indicated that the drug accumulates explicitly in Aβ-deposition-rich cortical regions in AD patients with minimal accumulation observed in healthy volunteers [40].

In general, the stilbene nucleus was built using the Wadsworth–Emmons reaction, and a representative synthesis of stilbene **46a** is shown (Scheme 4B). Initial Wadsworth–Emmons reaction between diethyl (4-nitrobenzyl)phosphonate (**47**) and 4-methoxybenzaldehyde (**48**) constructed the stilbene core **49**. The target compound **46** was formed from a straightforward sequence of nitro reduction, reductive methylation, methyl ether cleavage, pegylation and radiolabeling. Several synthetic procedures have been described for the preparation of **46a** and its precursors in an effort to optimize yield [21,41,42]. The best reported yield and purity was obtained by mixing the mesylate precursor with the fluorinating agent in a modified PET-MF-2V-IT-1 synthesizer and by

purifying using plus C18 Sep-Pak cartridges [41]. In the preparation of [^{11}C]**44d**, the [^{11}C]-methylation of 4-amino-4'-hydroxystilbene was carried out using the "LOOP" method, in which trapping and reaction of [^{11}C]CH_3OTf with the appropriate stilbene analogue takes place inside an HPLC sample loop [43].

Diphenyl-1,2,4- and diphenyl-1,3,4-oxadiazoles

The replacement of the stilbene ethylene linker with different heterocycles is a common strategy in medicinal chemistry used to improve the pharmacokinetics and/or pharmacodynamics of stilbenes (Scheme 5A) [44-46]. In the case of Aβ probes, a series of 2,5-diphenyl-1,3,4-oxadiazoles **50a**–**f** and 3,5-diphenyl-1,2,4-oxadiazoles **51a**–**e** have been studied in this respect (Table 3 and Table 4). Among the 2,5-diphenyl-1,3,4-oxadiazoles, the dimethylamine analogue **50a** (K_i = 20.1 ± 2.5 nM) and methoxy analogue **50b** (K_i = 46.1 ± 12.6 nM) showed the best affinities towards Aβ aggregates, and radiolabeling has been performed for both of these compounds. In biodistribution studies, the dimethylamine analogue [^{125}I]**50a** showed good brain uptake and washout rates. Although methoxy analogue [^{125}I]**50b** showed poorer brain uptake, its washout rate was increased compared to its dimethylamine counterpart [47]. Interestingly, changing the heteroatom order in the central ring from 1,3,4 (**50a**–**f**) to 1,2,4 (**51a**–**e**) has great effects on both the physical characteristics and pharmacokinetics of the compounds. The 3,5-diphenyl-1,2,4-oxadiazole analogue **51c** was more lipophilic than its 1,3,4 counterpart **50a** (log P = 3.22 for **51c** and 2.43 for **50a**) [47]. In general, even though 3,5-diphenyl-1,2,4-oxadiazoles **51a**–**e** show excellent affinity for Aβ aggregates in in vitro binding experiments (K_i = 4.3–47.1 nM), they show poorer brain uptake rates (1.07–2.06% ID/g at 2 min) and slower washout rates (3.29–2.01% ID/g at 60 min) than their 1,3,4 counterparts [48].



Scheme 5: A. Structures of the diphenyl-1,3,4- and diphenyl-1,2,4-oxadiazoles discussed. **B**.,**C**. Synthetic schemes for the preparation of [^{125}I]**50a** and [^{125}I]**51c**, respectively.

Table 3: Inhibition constants and biodistribution of radioactivity of the 2,5-diphenyl-1,3,4-oxadiazole derivatives **50a**–**f** (values are from [47]).

Compound	R	$Aβ_{1-42}$ K_i (nM)	%ID/g at 10 min	%ID/g at 60 min
50a	NMe_2	20.1 ± 2.5	—	—
[^{125}I]**50a**	NMe_2	—	5.93 ± 0.76	1.78 ± 0.41
50b	OMe	46.1 ± 12.6	—	—
[^{125}I]**50b**	OMe	—	2.74 ± 0.37	0.36 ± 0.13
50c	OH	229.6 ± 47.3	—	—
50d	OCH_2CH_2OH	282.2 ± 61.4	—	—
50e	$(OCH_2CH_2)_2OH$	348.6 ± 51.7	—	—
50f	$(OCH_2CH_2)_3OH$	257.7 ± 34.8	—	—

Table 4: Inhibition constants and biodistribution of radioactivity of 3,5-diphenyl-1,2,4-oxadiazole derivatives **51a–e** (values are from [48]).

Compound	R	$A\beta_{1-42}$ K_i (nM)	%ID/g at 2 min	%ID/g at 60 min
51a	NH_2	14.2 ± 1.4	—	—
[^{125}I]**51a**	NH_2	—	1.61 ± 0.23	3.29 ± 0.58
51b	NHMe	14.3 ± 3.6	—	—
[^{125}I]**51b**	NHMe	—	1.44 ± 0.12	2.70 ± 0.33
51c	NMe_2	15.4 ± 1.4	—	—
[^{125}I]**51c**	NMe_2	—	1.07 ± 0.23	2.32 ± 0.64
51d	OMe	4.3 ± 2.1	—	—
[^{125}I]**51d**	OMe	—	2.06 ± 0.45	2.01 ± 0.33
51e	OH	47.1 ± 4.1	—	—

These findings, together with the close structural similarities between compounds **50a–f** and **51a–e**, highlight the importance of lipophilicity as a factor in controlling brain kinetics [47].

Representative syntheses of radioiodinated oxadiazoles **50a** and **51c** are shown (Scheme 5B and C). The 1,3,4-oxadiazole core of [^{125}I]**50a** was obtained from the reaction between 4-iodobenzhydrazide (**52**) and 4-dimethylaminobenzaldehyde (**23**) in the presence of ceric ammonium nitrate (CAN) followed by subsequent radioiodination of compound **53** (Scheme 5B) [47]. The 1,2,4-oxadiazole core of [^{125}I]**51c** was obtained by DCC/HOBt-mediated condensation of 4-bromobenzamidoxime (**54**) and *p*-nitrobenzoic acid (**55**). Subsequent nitro reduction, reductive methylation, and radioiodination gave [^{125}I]**51c** (Scheme 5C) [48].

Thioflavin-T analogues

Benzothiazoles

Of all the amyloid imaging classes, the benzothiazoles, such as **56a–w**, **57**, **58a**,**b**, and **59–65** (Figure 2), may well be one of the most prolific and well-studied. The amyloid imaging dye thioflavin-T (**4**, Figure 1) served as the inspiration for this class of radiotracers in which the ionic charge was removed to increase lipophilicity and to enhance in vivo BBB

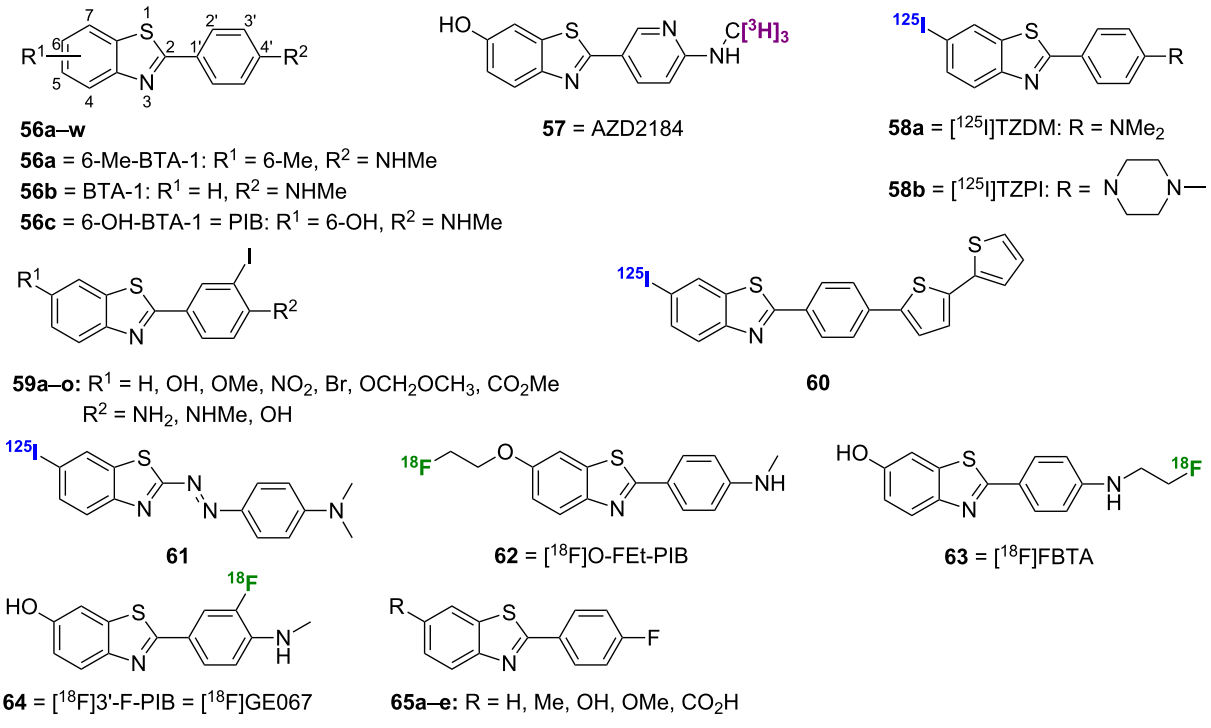


Figure 2: Structures of the radiolabeled benzothiazole analogues discussed.

permeability. Overall, this class of compounds shows high affinity for Aβ aggregates with promising in vivo pharmacokinetics.

One of the earliest radiolabeled benzothiazoles, [^{11}C]6-Me-BTA-1 ([^{11}C]**56a**; note: BTA = 2-(4'-methylaminophenyl)benzothiazole, Figure 2), was prepared by methylation of 4-(6-methyl-2-benzothiazolyl)aniline using [^{11}C]methyl iodide [49]. Compared to **4**, **56a** showed greatly increased lipophilicity and improved binding affinity for $A\beta_{1\text{-}40}$ (K_i = 890 nM for **4** and K_i = 20.2 for **56a**). In postmortem AD brain sections, [^{11}C]**56a** was able to stain both Aβ plaques and neurofibrillary tangles (NFTs), while pharmacokinetic studies in normal mice showed high brain uptake (7.61% ID/g at 2 min) and good washout (2.76% ID/g at 30 min). Additional modification of this scaffold by removal of the 6-Me group gave [^{11}C]BTA-1 ([^{11}C]**56b**) [50]. Compound **56b** was prepared by coupling of *p*-nitrobenzoyl chloride (**35**) and 2-aminothiophenol (**66**) followed by nitro reduction to **67** and methylation using [^{11}C]methyl iodide (Scheme 6A). While showing a near equal binding affinity for Aβ, the decreased lipophilicity of [^{11}C]**56b** to the ideal level led to improved pharmacokinetics over [^{11}C]**56a** as evidenced by improved uptake and washout rates in normal mice (12.9% ID/g at 2 min and 1.7% ID/g at 30 min). Compound [^{11}C]**56b** showed in vivo specificity for Aβ in the brains of PS1/APP transgenic mice, and it was subsequently shown to bind specifically to amyloid deposits in human AD brain homogenates [51].

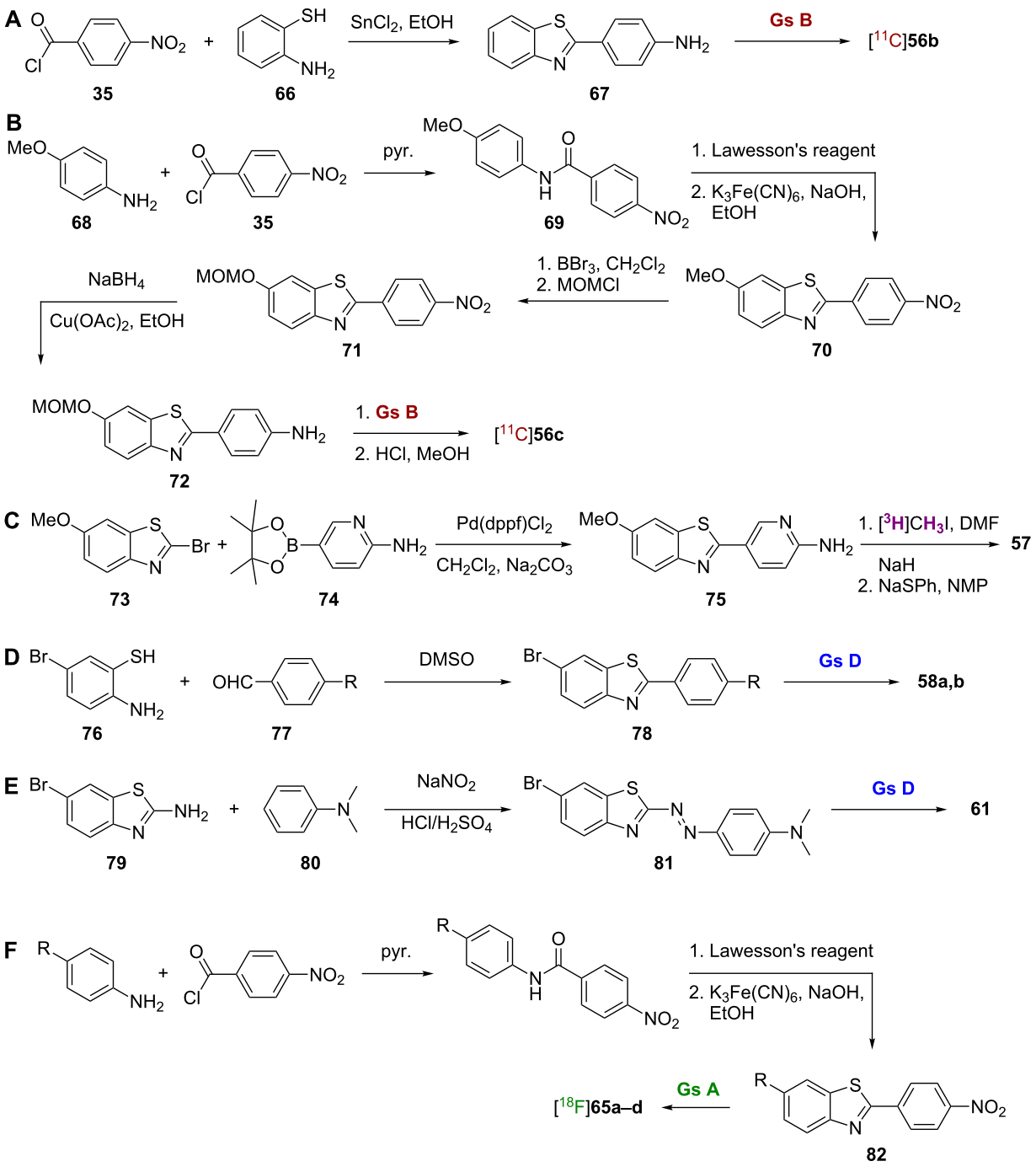
The addition of a hydroxy group at the 6-position of [^{11}C]**56b** gave [^{11}C]6-OH-BTA-1 ([^{11}C]**56c**) [52]. Compound [^{11}C]**56c** was synthesized by first coupling *p*-anisidine (**68**) with *p*-nitrobenzoyl chloride (**35**) to give the amide **69**, which was subsequently converted to the thioamide by using Lawesson's reagent and cyclized to form the benzothiazole core **70** (Scheme 6B). Demethylation with BBr_3 and protection of the resulting hydroxy moiety as the methoxymethyl (MOM) ether gave **71**. Reduction of the nitro group to **72**, methylation using [^{11}C]methyl iodide, and cleavage of the MOM ether gave [^{11}C]**56c**. Compound **56c** showed high affinity for $A\beta_{1\text{-}40}$ (K_i = 4.3 nM) (Table 5). This synthesis has since been refined to improve radiochemical yields and eliminate the need for a protecting group by use of [^{11}C]CH_3OTf as the methylating agent [53].

The 6-OH group of **56c** made it less lipophilic than both **56a** and **56b** and likely contributed to its moderate brain entry (0.21% ID-kg/g at 2 min) but good clearance (0.018% ID-kg/g at 30 min) in normal mice. Interesting SAR findings on this scaffold from comparison of **56c**–**t** (Table 5) included that the more lipophilic secondary and tertiary amines at the 4'-position were more potent (K_i) than primary amines. Also, in general, substitution at the 6-position seemed to have only a small effect in terms of K_i as 6-OH, -OCH_3, -CN, and -Br gave similar results. However, substitution at the 6-position had a larger effect on pharmacokinetics in the brain, as 6-OH clearly gave the best results [52]. As one of the most successful radiolabeled Aβ imaging probes to date, [^{11}C]**56c** has subsequently been named Pittsburgh Compound B (PIB).

Additional studies of [^{11}C]**56c** in humans have been promising and suggest that PET imaging with this compound can provide quantitative information on amyloid deposits in living patients. In postmortem tissue, [^{11}C]**56c** exhibited specific binding to the amyloid-laden frontal cortex of the AD brain, but little binding to the frontal cortex of the cognitively normal age-matched control brain. Compound [^{11}C]**56c** also displayed a rapid entry and clearance in the brain of healthy controls, but a marked retention in AD patients in areas of the brain known to contain large amyloid deposits [54]. Additional data suggested that [^{11}C]**56c** was suitable for early detection of pathological changes in AD patients before a significant loss of cognitive function is apparent [55].

The impact of changing the position of the hydroxy group of **56c** was investigated by synthesizing the 4-OH, 5-OH, and 7-OH analogues **56u**–**w** using methods similar to those described above [56]. The K_i values for these analogues in human AD brain homogenates were between 11–19 nM, indicating slightly reduced affinity compared to **56c** (K_i = 2.8 nM) (Table 6). However, each radiolabled analogue was able to stain plaques in sections from transgenic AD mouse brain and human AD brain. The 5-OH analogue [^{11}C]**56v** showed the best pharmacokinetic profile in normal mice with high brain uptake and a washout rate, that was 8 times faster than that of [^{11}C]**56c**. Interestingly, it was noted that the 4-OH analogue **56u** could form an intramolecular hydrogen bond (i.e. an extra pseudo ring), which could act to increase the lipophilicity of the compound and lead to nonspecific binding and residual background activity in the brain.

A [^{3}H]-labeled analogue of **56c**, AZD2184 (**57**), was also synthesized to give a higher signal-to-background ratio by virtue of its decreased lipophilicity [57]. This compound was prepared through palladium catalyzed Suzuki coupling of the starting halide **73** and boronic acid **74** followed by *N*-methylation of **75** with [^{3}H]methyl iodide and *O*-demethylation with sodium thiophenoxide (Scheme 6C). Compound **57** showed high affinity for $A\beta_{1\text{-}40}$ fibrils in vitro (K_d = 8.4 nM) and lower background binding levels than **56c**. While **57** was able to label amyloid deposits in APP/PS1 mice, its brain penetration was not as high as that of [^{11}C]**56c**.



Scheme 6: A.–F. Synthetic schemes for the preparation of [^{11}C]**56b**, [^{11}C]**56c**, **57**, **58a,b**, **61**, and [^{18}F]**65a–d**.

Besides [^{11}C], other radiolabels have been investigated for benzothiazole imaging agents. Two of the earliest [^{125}I]-labeled imaging agents reported were [^{125}I]TZDM (**58a**) and [^{125}I]TZPI (**58b**) [58]. The synthesis of these agents was achieved in two steps by condensation of 5-bromo-2-aminobenzenethiol (**76**) and the appropriate benzaldehyde **77** followed by radiolabeling of **78** (Scheme 6D). Both **58a** and **58b** showed high affinity for $A\beta_{1\text{-}40}$ and $A\beta_{1\text{-}42}$ aggregates with K_d values ≤0.15 nM in all cases. However, pharmacokinetics for these agents were less than ideal as both showed long retention in the brains of normal mice, which is indicative of nonspecific binding.

Table 5: Inhibition constants and biodistribution of radioactivity of 6-substituted 2-arylbenzothiazole derivatives **56c–t** (values are from [52]).

Compound	R^1	R^2	$A\beta_{1-40}$ K_i (nM)	(%ID-kg)/g at 2 min	(%ID-kg)/g at 30 min
56c	6-OH	NHMe	4.3	—	—
[^{11}C]**56c**	6-OH	NH^{11}CH$_3$	—	0.21	0.018
56d	6-OH	NH_2	46	—	—
56e	6-OH	NMe_2	4.4	—	—
[^{11}C]**56e**	6-OH	NMe^{11}CH$_3$	—	0.32	0.10
56f	6-H	NHMe	11	—	—
[^{11}C]**56f**	6-H	NH^{11}CH$_3$	—	0.43	0.057
56g	6-H	NH_2	37	—	—
56h	6-H	NMe_2	4.0	—	—
[^{11}C]**56h**	6-H	NMe^{11}CH$_3$	—	0.19	0.078
56i	6-Me	NHMe	10	—	—
[^{11}C]**56i**	6-Me	NH^{11}CH$_3$	—	0.22	0.083
56j	6-Me	NH_2	9.5	—	—
56k	6-Me	NMe_2	64	—	—
[^{11}C]**56k**	6-Me	NMe^{11}CH$_3$	—	0.078	0.15
56l	6-OMe	NHMe	4.9	—	—
[^{11}C]**56l**	6-OMe	NH^{11}CH$_3$	—	0.33	0.10
56m	6-OMe	NH_2	7.0	—	—
[^{11}C]**56m**	6-O^{11}CH$_3$	NH_2	—	0.32	0.084
56n	6-OMe	NMe_2	1.9	—	—
[^{11}C]**56n**	6-OMe	NMe^{11}CH$_3$	—	0.16	0.14
56o	6-CN	NHMe	8.6	—	—
[^{11}C]**56o**	6-CN	NH^{11}CH$_3$	—	0.32	0.063
56p	6-CN	NH_2	64	—	—
56q	6-CN	NMe_2	11	—	—
[^{11}C]**56q**	6-CN	NMe^{11}CH$_3$	—	0.24	0.097
56r	6-Br	NHMe	1.7	—	—
[^{11}C]**56r**	6-Br	NH^{11}CH$_3$	—	0.12	0.12
56s	6-Br	NH_2	7.2	—	—
56t	6-Br	NMe_2	2.9	—	—
[^{11}C]**56t**	6-Br	NMe^{11}CH$_3$	—	0.054	0.11

Table 6: Inhibition constants and biodistribution of radioactivity of hydroxy-substituted 2-arylbenzothiazole derivatives **56c**,**u–w** (values are from [56]).

Compound	R^1	R^2	human AD brain homogenates K_i (nM)	%ID/g at 2 min	%ID/g at 60 min
56c	6-OH	NHMe	2.8 ± 0.5	—	—
[^{11}C]**56c**	6-OH	NH^{11}CH$_3$	—	3.6 ± 1.4	0.6 ± 0.2
56u	4-OH	NHMe	18.8 ± 3.8	—	—
[^{11}C]**56u**	4-OH	NH^{11}CH$_3$	—	3.8 ± 0.9	0.3 ± 0.3
56v	5-OH	NHMe	11.5 ± 3	—	—
[^{11}C]**56v**	5-OH	NH^{11}CH$_3$	—	4.3 ± 0.45	0.09 ± 0.02
56w	7-OH	NHMe	11.2 ± 5	—	—
[^{11}C]**56w**	7-OH	NH^{11}CH$_3$	—	2.6 ± 0.76	0.16 ± 0.03

A series of iodinated benzothiazoles **59a–o** was synthesized using methods similar to those described above and SAR studies were performed (Table 7) [59]. Among the interesting findings was that the introduction of 3'-iodo increased lipophilicity and binding to $A\beta_{1-40}$ when R^2 = NHMe. However, the opposite effect on binding was observed when

R^2 = OH. Among the [^{125}I]-labeled derivatives, more polar compounds exhibited better clearance and less nonspecific binding in the brains of normal mice, a typical result for brain imaging probes. One of the most promising compounds identified in this study was [^{125}I]**59d**.

The [^{125}I]-labeled benzothiazole bithiophene **60** was synthesized by condensation of 5-bromo-2-aminobenzenethiol and 2,2'-bithiophene-5-carbaldehyde followed by installation of the radiolabel. In in vitro binding experiments, **60** displayed high affinity for both $A\beta_{1\text{-}40}$ and $A\beta_{1\text{-}42}$ aggregates with K_i values of 0.25 nM and 0.31 nM, respectively. In addition, it was used to clearly visualize Aβ plaques in AD brain sections and showed favorable pharmacokinetics in the brain with high uptake (3.42% ID/g at 2 min) and fast washout (0.53% ID/g at 60 min).

The [^{125}I]-labeled phenyldiazenyl benzothiazole **61** was prepared via a diazo coupling reaction between **79** and **80** to give **81** followed by installation of the radiolabel (Scheme 6E) [60]. Interestingly, in in vitro binding experiments, **61** displayed higher affinity for tau aggregates (K_i = 0.48 nM) than for Aβ aggregates (K_i = 8.24 nM). Although it was used to clearly visualize NFTs in AD brain sections, further modifications will be necessary to improve the pharmacokinetics of this compound in the brain, as it showed particularly slow washout rate (2.89% ID/g at 60 min).

Three [^{18}F]-labeled analogues of **56c**, [^{18}F]O-FEt-PIB (**62**), [^{18}F]FBTA (**63**), and [^{18}F]3'-F-PIB ([^{18}F]GE067, **64**) were also prepared. Compound **62** was synthesized by using the hydroxy group of **56c** to displace the tosylate of [^{18}F]fluoroethyltosylate. Compound **62** had a K_i value of 0.17 nM for AD brain homogenate and was able to stain Aβ plaques in postmortem AD brain [61]. Although its biodistribution was not as good as that of **56c**, **62** still showed promise in an in vivo study using a rat model of AD [62]. Moving the [^{18}F]fluoroethoxy substituent of **62** from the 6-position to the 3'-position resulted in a low binding affinity for Aβ and an inability to stain plaques in postmortem AD brain [63]. In compound **63**, the [^{11}C]methylamino group of [^{11}C]**56c** was replaced by a [^{18}F]fluoroethylamino group, and, while this compound showed better binding affinity than **56c**, its brain pharmacokinetics were not as good [64]. Compound **64** also showed promising results in whole-body biodistribution and radiation dosimetry studies [65].

A series of fluorinated benzothiazoles **65a**–**e** was synthesized by direct substitution of the nitro group of a key synthetic intermediate **82** (prepared using synthetic steps already describe for [^{11}C]**56c**) by an [^{18}F] atom (Scheme 6F) [66,67]. Compounds **65a**,**b**,**d** (R = H, Me, and OMe) all showed high binding affinity for AD brain homogenates with K_i values below 10 nM, which is comparable to that of **56c** in the same assay, while **65c** (R = OH) showed slightly reduced affinity (Table 8). In addition to showing a promising ability to stain Aβ plaques in vivo, [^{18}F]**65a**,**b** showed high brain uptake and rapid washout in normal mice. In fact, each of these compounds displayed better pharmacokinetics than [^{11}C]**56c** in the same assay.

Table 7: Inhibition constants and biodistribution of radioactivity of iodinated 2-arylbenzothiazole derivatives **59a–o** (values are from [59]).

Compound	R^1	R^2	$A\beta_{1\text{-}40}$ K_i (nM)	%ID/g at 2 min	%ID/g at 30 min
59a	H	NH_2	8.32	—	—
[^{125}I]**59a**	H	NH_2	—	9.08	3.4
59b	H	NHMe	4.94	—	—
[^{125}I]**59b**	H	NHMe	—	4.40	2.68
59c	H	OH	19.1	—	—
59d	OH	NH_2	11.1	—	—
[^{125}I]**59d**	OH	NH_2	—	5.64	0.36
59e	OH	NHMe	3.22	—	—
[^{125}I]**59e**	OH	NHMe	—	7.76	2.66
59f	OH	OH	71.2	—	—
59g	OMe	NH_2	4.4	—	—
59h	OMe	NHMe	1.93	—	—
59i	OMe	OH	15.8	—	—
59j	NO_2	NH_2	4.6	—	—
59k	NO_2	NHMe	1	—	—
59l	Br	NH_2	0.67	—	—
59m	Br	NHMe	1.6	—	—
59n	OCH_2OCH_3	NH_2	15.1	—	—
59o	CO_2Me	NH_2	3.34	—	—

Table 8: Inhibition constants and biodistribution of radioactivity of fluorinated 2-arylbenzothiazole derivatives **65a–e** (values are from [66,67]).

Compound	R	human AD brain homogenates K_i (nM)	%ID/g at 2 min	%ID/g at 30 min
65a	H	9.0 ± 2.0	—	—
[^{18}F]**65a**	H	—	3.20 ± 0.38	0.21 ± 0.03
65b	Me	5.7 ± 1.8	—	—
[^{18}F]**65b**	Me	—	5.33 ± 0.74	0.27 ± 0.06
65c	OH	22.5 ± 4.5	—	—
[^{18}F]**65c**	OH	—	4.70 ± 0.48	0.57 ± 0.36
65d	OMe	2.2 ± 0.5	—	—
[^{18}F]**65d**	OMe	—	5.10 ± 0.40	0.43 ± 0.12
65e	CO_2H	>4000	—	—

Benzothiazole probes such as **83a**,**b** and **84a**,**b** labeled with [Re] and [^{99m}Tc] were also synthesized (Scheme 7A) [68,69]. [Re] and [^{99m}Tc]MAMA-BTA (**83a** and **83b**; MAMA = monoamine-monoamide bisthiol-BTA) were prepared by first linking 2-(4-nitrophenyl)-6-hydroxybenzothiazole (**85**) via 1,5-dibromopentane (**86**) to monoamine-monoamide bisthiol protected with *p*-methoxy benzyl (MAMA-PMB, **87**) to give **88** (Scheme 7B) [68]. Nitro reduction of **88** followed by thioether deprotection gave MAMA-BTA (**89**), which was labeled through reaction with the [Re] (used for in vitro studies) or [^{99m}Tc] precursors to give the desired **83a**,**b**. [Re] and [^{99m}Tc]BAT-BTA (**84a** and **84b**; note: BAT = bis(aminoethanethiol)) were prepared by addition of ethyl bromoacetate (**41**) to the unprotected amine of the *S*,*S*'-bis-trityl-*N*-Boc-1,2-ethylenedicysteamine chelating agent (**90**) followed by saponification that gave the free acid intermediate **91**, which was coupled with 2-(4-aminophenyl)-1,3-benzothiazole (**92**) (prepared from 2-aminothiophenol (**66**) and 4-aminobenzoic acid (**93**)) by using EDCI·HCl and HOBt (Scheme 7C) [69]. Deprotection followed by reaction with the [Re] or [^{99m}Tc] precursors gave **84a** and **84b**. While both **83a** and **84a** showed promise as in vitro Aβ labeling agents, the [^{99m}Tc] analogues **83b** and **84b** exhibited problems in pharmacokinetic studies in vivo. Compound **83b** showed sufficient initial uptake (1.34% ID/g at 2 min), but delayed washout (0.65% ID/g at 60 min) in normal mice, while **84b** was unable to cross the BBB to a sufficient degree.

Benzoxazoles

Replacement of the sulfur of the benzothiazole backbone by oxygen affords the benzoxazole backbone. Compounds **94**, **95a**–**n**, and **96–99** (Figure 3) have also been successfully employed for radioimaging of Aβ plaques. The isosteric replacement of the sulfur of [^{125}I]TZDM (**58a**) with an oxygen was designed to decrease molecular weight and increase lipophilicity and afforded [^{125}I]IBOX (**94**) [70]. Compound **94** was prepared via boric acid catalyzed condensation of 5-nitro-2-aminophenol (**100**) and 4-dimethylaminobenzoic acid (**101**) to give the nitro intermediate **102**, which was reduced through catalytic hydrogenation to the amine (Scheme 8A).

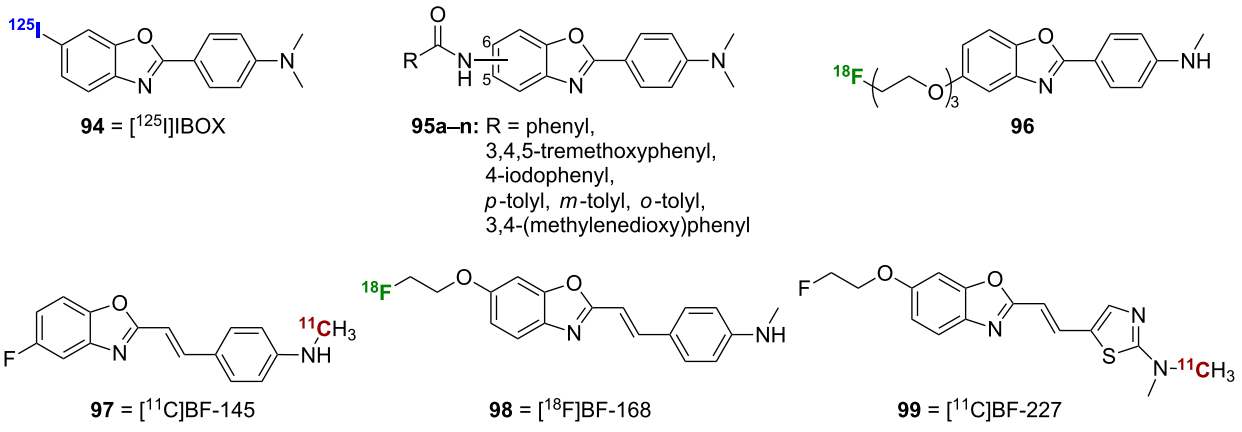
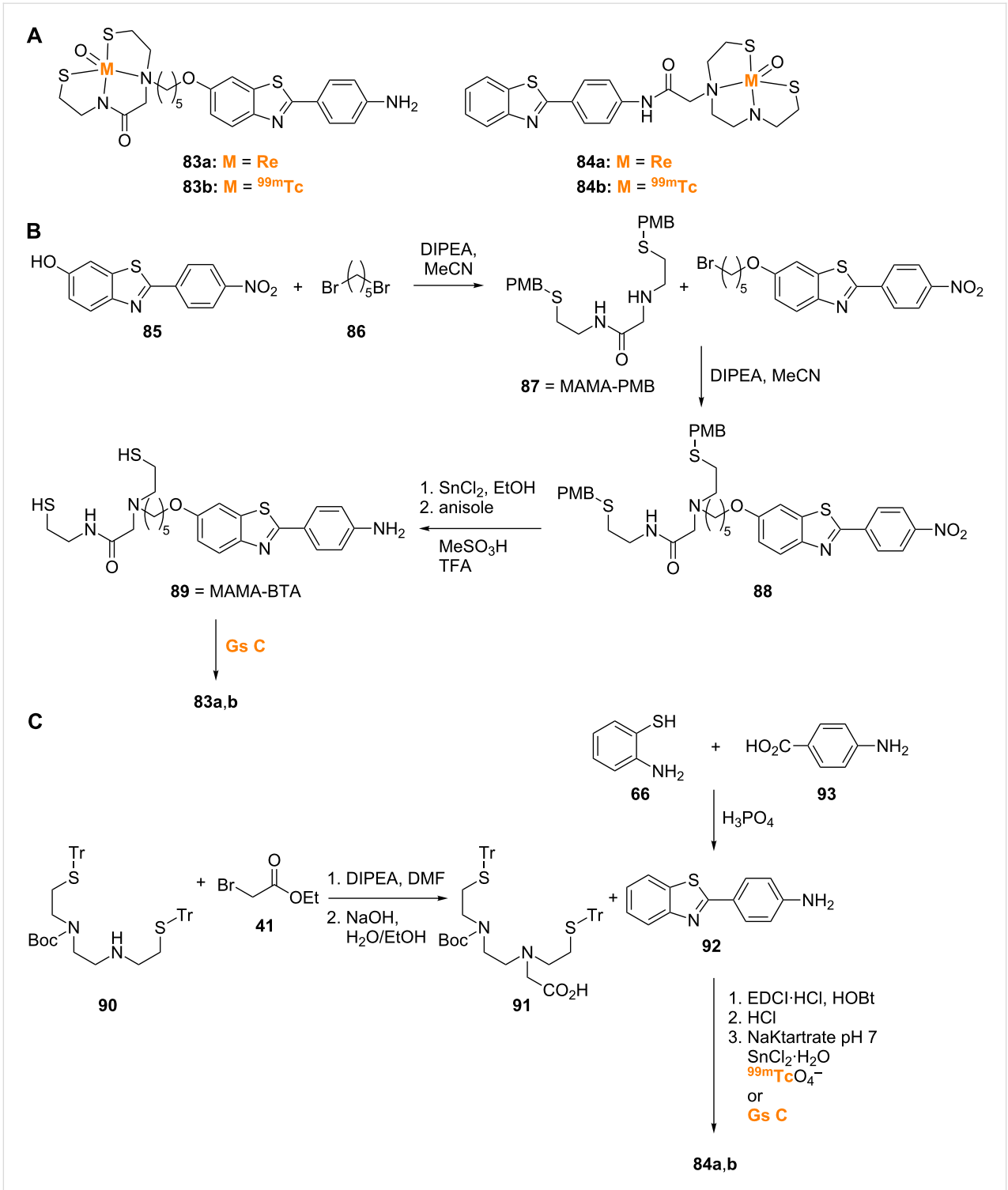
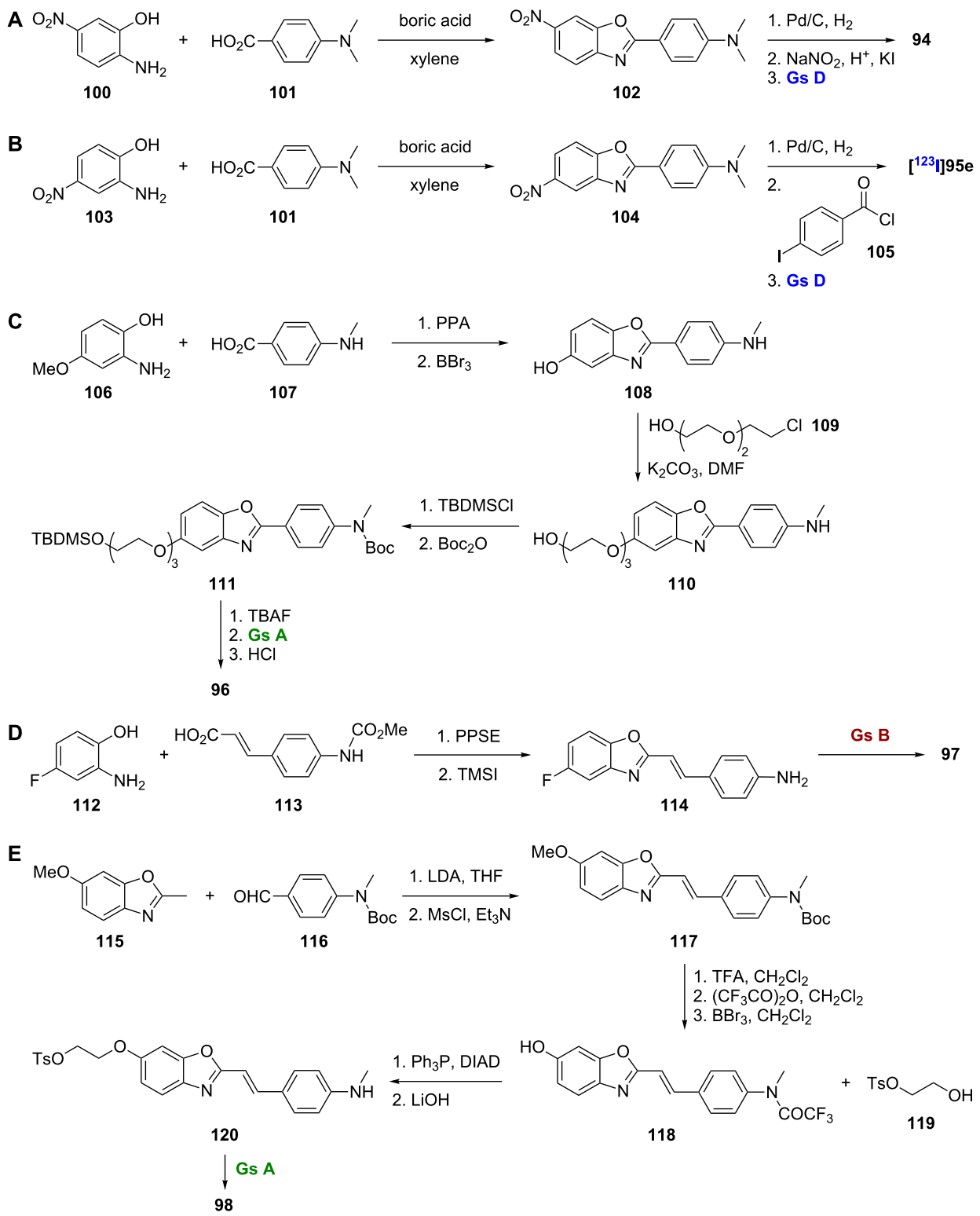


Figure 3: Structures of the radiolabeled benzoxazole analogues discussed.



Scheme 7: A. Structures of the [Re]- and [^{99m}Tc]-labeled benzothiazole analogues discussed. **B**.,**C**. Synthetic schemes for the preparation of **83a**,**b** and **84a**,**b**.

Subsequent conversion to the diazonium ion and displacement with iodide ion gave IBOX, which was radiolabeled to give **94**. Compound **94** showed similar affinity for $A\beta_{1\text{-}40}$ aggregates when compared to **58a**, and it was able to label Aβ plaques in postmortem AD brain sections. Importantly, **94** showed superior peak brain uptake (2.08% ID/g at 30 min) and faster brain washout than **58a** in normal mice.



Scheme 8: A.–E. Synthetic schemes for the preparation of **94**, [^{123}I]**95e**, **96**–**98**.

Expanding on this 2-arylbenzoxazole scaffold, a series of benzamide-substituted 2-arylbenzoxazoles **95a**–**n** was synthesized [71]. A representative synthesis of [^{123}I]**95e** is shown (Scheme 8B). Boric acid catalyzed condensation of 4-nitro-2-aminophenol (**103**) and 4-dimethylaminobenzoic acid (**101**) gave the nitro intermediate **104**. Catalytic hydrogenation as

above gave the amine intermediate, and subsequent reaction with 4-iodobenzoyl chloride (**105**) and installation of the radiolabel gave the target compound. SAR analysis of the compounds indicates that the benzamide moiety is favored at position 5 rather than 6 of the benzoxazole core in terms of binding affinity for Aβ plaques in vitro (Table 9). The best compound was **95e**, which had a K_i value of 9.3 nM, but [^{123}I]**95e** was unable to cross the BBB in vivo. This disappointing result could be appointed to the excessively high lipophilicity of the compound.

Table 9: Inhibition constants of benzamide-substituted 2-arylbenzoxazole derivatives **95a–n** (values are from [71]).

Compound	R	K_i (nM)
95a	5-phenyl	12.0
95b	6-phenyl	26.0
95c	5-(3,4,5-trimethoxyphenyl)	109
95d	6-(3,4,5-trimethoxyphenyl)	628
95e	5-(4-iodophenyl)	9.3
95f	6-(4-iodophenyl)	60.1
95g	5-(*p*-tolyl)	13.2
95h	6-(*p*-tolyl)	86.0
95i	5-(*m*-tolyl)	13.4
95j	6-(*m*-tolyl)	31.5
95k	5-(*o*-tolyl)	18.9
95l	6-(*o*-tolyl)	112
95m	5-(3,4-(methylenedioxy)phenyl)	17.2
95n	6-(3,4-(methylenedioxy)phenyl)	19.7

To improve the pharmacokinetic profile of **94**, the [^{18}F]-labeled analogue **96** was designed as an imaging probe [72]. Compound **96**, which contains an [^{18}F] end-capped polyethylene glycol chain at position 5 of the benzoxazole core in place of the [^{125}I] of **94** at position 6 to reduce lipophilicity, was prepared by polyphosphoric acid catalyzed condensation of 2-amino-4-methoxyphenol (**106**) and 4-monomethylaminobenzoic acid (**107**) to give the benzoxazole core, which was *O*-demethylated to give **108** (Scheme 8C). Subsequent coupling with 2-[2-(2-chloroethoxy)ethoxy]ethanol (**109**) gave **110**. TBDMS protection of the alcohol and Boc protection of the amine gave **111**. Finally, TBAF cleavage, installation of the radiolabel, and acid cleavage gave **96**. Compound **96** showed good affinity for $A\beta_{1\text{-}42}$ (K_i = 9.3 nM). This compound also showed promising pharmacokinetics in normal mice, with greatly improved uptake and washout rates compared to **94**, and it successfully labeled Aβ plaques in vitro. In addition, it showed increased retention in vivo in transgenic AD mice compared to wild-type. A *N*,*N*-dimethyl derivative was also synthesized, and, while it too showed good affinity for $A\beta_{1\text{-}42}$, its increased lipophilicity compared to the monomethyl compound gave slightly worse pharmacokinetic properties.

The [^{11}C]-labeled styrylbenzoxazole [^{11}C]BF-145 (**97**) and the related [^{18}F]-labeled styrylbenzoxazole [^{18}F]BF-168 (**98**) were prepared and studied for Aβ imaging [73-75]. The simple two-step synthesis of **97** used polyphosphoric acid trimethylsilyl ester (PPSE) catalyzed condensation of 4-fluoro-2-aminophenol (**112**) with a cinnamic acid **113** to give the benzoxazole core followed by conversion to the primary amine **114** and radiolabeling (Scheme 8D). The synthesis of **98** was more complex and began with a reaction between 2-methyl-6-methoxybenzoxazole (**115**) and 4-((*N*-Boc-*N*-methyl)amino)benzaldehyde (**116**) followed by a dehydration reaction to give **117** (Scheme 8E). Subsequent removal of the Boc group followed by installation of a trifluoroacetamide and *O*-demethylation gave the intermediate **118** used in a Mitsunobu reaction with 2-hydroxyethyl tosylate (**119**). Amine deprotection to **120** and installation of the [^{18}F] label gave the target compound **98**.

Both **97** and **98** showed good affinity for $A\beta_{1\text{-}42}$ aggregates (K_i = 4.5 nM and 6.4 nM, respectively). Interestingly, while **98** was able to selectively stain senile plaques (SPs) and NFTs in AD brain sections, **97** was only able to stain SPs. In addition, **97** and **98** showed substantial brain uptake and fast washout (4.4% and 3.9% ID/g at 2 min and 1.6% and 1.6% ID/g at 30 min, respectively) with promising in vivo imaging results in transgenic mice.

Building on the promising results of **97** and **98**, an optimized derivative, [^{11}C]BF-227 (**99**), was studied for Aβ imaging. The key difference in **99** is the replacement of a phenyl ring with a thiazole ring. Compound **99** demonstrated good affinity for synthetic $A\beta_{1\text{-}42}$ aggregates (K_i = 4.3 nM), rapid uptake (7.9% ID/g at 2 min) and clearance (0.64% ID/g at 60 min) in normal mice, the ability to selectively stain Aβ plaques in AD brain sections, and promising results in a clinical PET study in AD patients [76]. Additional studies suggest that **99** has the possibility to be useful for early detection of AD and also for predicting progression from mild cognitive impairment to AD [77,78]. Interestingly, **99** has also shown promise for diseases other than AD. It has been suggested that **99** may provide a means of diagnosis and disease monitoring in transmissible spongiform encephalopathies [79] and may be useful for monitoring α-synuclein deposits in conditions such as multiple system atrophy and Parkinson's disease [80]. A version of **99** labeled with [^{18}F] rather than [^{11}C] has also been proposed for use in Parkinson's disease [81].

Benzofurans

Replacement of the nitrogen of the benzoxazole backbone with carbon affords the benzofuran backbone of compounds **121**–**126** (Figure 4), which has also been successfully employed for radioimaging of Aβ plaques. The [^{11}C]-labeled benzofuran **121** was prepared via Wittig reaction between the triphenylphosphonium salt of 2-hydroxy-5-methoxybenzyl alcohol (**127**) and 4-nitrobenzoyl chloride (**35**) to give **128** followed by nitro reduction and *O*-demethylation to give **129** and radiolabeling (Scheme 9A). Using AD brain gray matter homogenates, compound **121** showed good binding affinity for Aβ plaques (K_i = 0.7 nM) and was able to stain both SPs and NFTs in vitro. In normal mice, this compound showed rapid uptake (4.8% ID/g at 2 min) and fast washout (0.2% ID/g at 60 min). In vivo plaque labeling in APP transgenic mice was also successful [82].

Using similar chemistry as described above, a series of iodinated 2-arylbenzofurans **122a**–**e** was prepared and studied [83]. A representative synthesis of [^{125}I]**122a**, which uses a similar Wittig as in the synthesis of **121**, is shown in Scheme 9A. It was found that the iodo substituent could be varied between the 5- and 6-positions, and the *N*,*N*-dimethylamino substituent could be changed to a secondary methylamino or hydroxy moiety with little effect on binding affinity for synthetic A$\beta_{1\text{-}40}$, as all compounds had a $K_i \leq 8$ nM (Table 10). While the [^{125}I]-labeled benzofurans in this series showed good brain uptake in normal mice, their washout was rather slow indicating nonspecific binding in vivo.

Several [^{18}F]-labeled benzofurans have been employed with success for Aβ imaging. [^{18}F]FPYBF-1 (**123a**), which has a *N*,*N*-dimethyl-2-aminopyridine group attached to the benzofuran core, was synthesized via Suzuki coupling between 5-methoxybenzofuran-2-boronic acid (**130**) and 2-amino-5-iodopyridine (**131**) to give **132**, which was followed by reductive amination and *O*-demethylation to give **133** (Scheme 9B). Finally, reaction with 2-[2-(2-chloroethoxy)ethoxy]ethanol

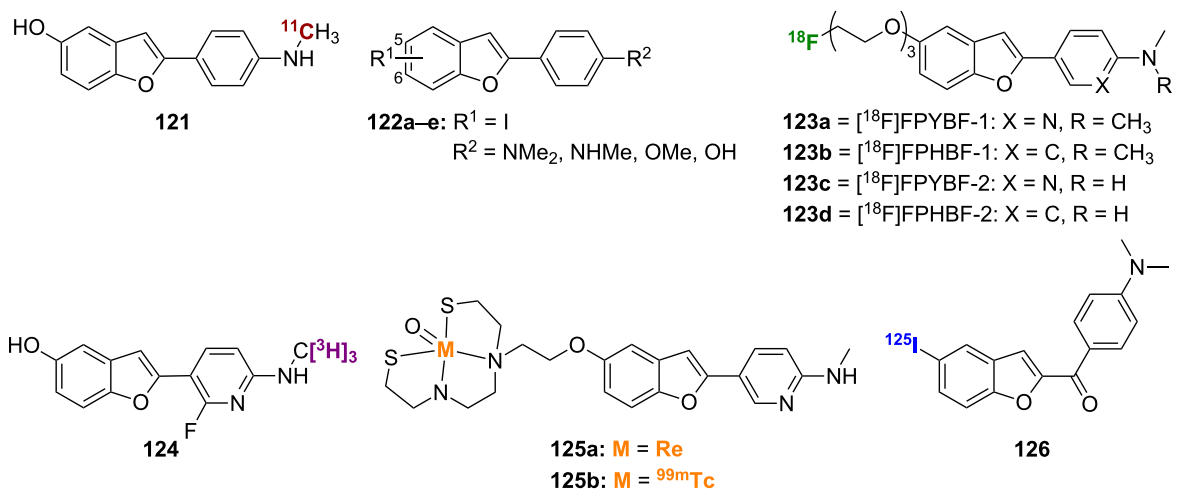
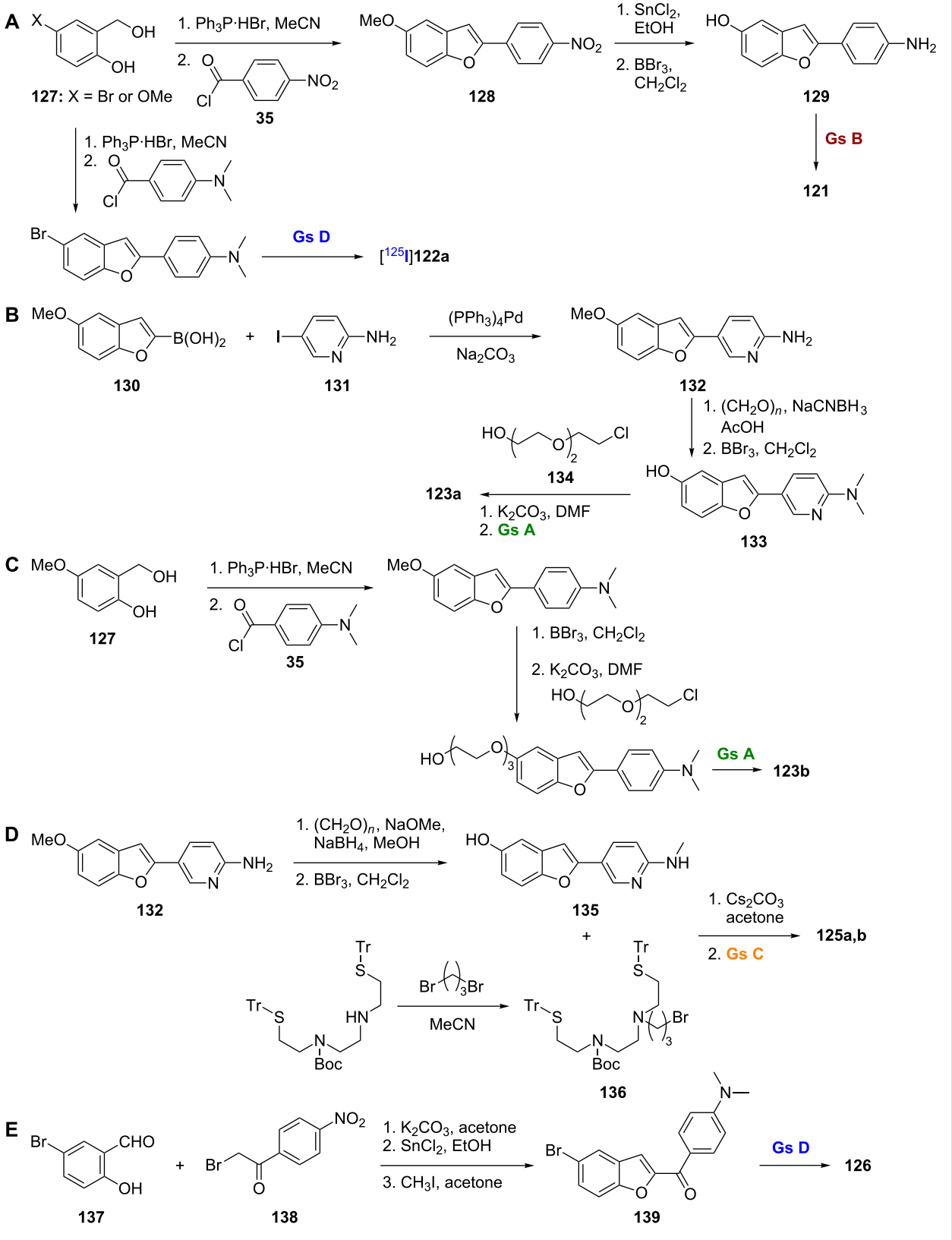


Figure 4: Structures of the radiolabeled benzofuran analogues discussed.

Table 10: Inhibition constants and biodistribution of the radioactivity of iodinated 2-arylbenzofuran derivatives **122a**–**e** (values are from [83]).

Compound	R^1	R^2	A$\beta_{1\text{-}40}$ K_i (nM)	%ID at 2 min	%ID at 60 min
122a	5-iodo	NMe_2	7.7 ± 1.2	—	—
[^{125}I]**122a**	5-iodo	NMe_2	—	0.51 ± 0.05	1.08 ± 0.15
122b	5-iodo	NHMe	1.1 ± 0.2	—	—
[^{125}I]**122b**	5-iodo	NHMe	—	0.78 ± 0.06	1.20 ± 0.34
122c	5-iodo	OMe	4.2 ± 0.8	—	—
122d	5-iodo	OH	6.5 ± 0.2	—	—
[^{125}I]**122d**	5-iodo	OH	—	1.40 ± 0.04	1.51 ± 0.20
122e	6-iodo	NMe_2	0.4 ± 0.1	—	—
[^{125}I]**122e**	6-iodo	NMe_2	—	0.48 ± 0.07	1.00 ± 0.22



Scheme 9: A.–E. Synthetic schemes for the preparation of **121**, [^{125}I]**122a**, **123a**,**b**, **125a**,**b**, and **126**.

(**134**) followed by radiolabeling gave **123a**. This compound showed high affinity for $A\beta_{1\text{-}42}$ aggregates (K_i = 0.9 nM), the ability to label plaques in postmortem AD brains, and suitable pharmacokinetic properties in normal mice (5.16% ID/g at 2 min and 2.44% ID/g at 60 min). In addition, it showed good in vivo binding to plaques in transgenic mice [84]. A closely related compound, [^{18}F]FPHBF-1 (**123b**), which has a *N,N*-dimethylaniline group in place of the *N,N*-dimethylaminopyridine group, was prepared using a Wittig reaction between the triphenylphosphonium salt of 2-hydroxy-5-methoxybenzyl alcohol (**127**) and 4-dimethylaminobenzoyl chloride (**35**), followed by *O*-demethylation and installation of the [^{18}F]-labeled linker (Scheme 9C). Like **123a**, compound **123b** showed good affinity for Aβ aggregates in vitro and in vivo. However, its slow washout from the brain, which can be attributed to its increased lipophilicity compared to **123a**, indicated that additional refinements will be needed [85].

Derivatives of **123a** and **123b** were also prepared [86]. These compounds, [^{18}F]FPYBF-2 (**123c**) and [^{18}F]FPHBF-2 (**123d**), have a secondary methylamino group in place of the dimethylamino group. Introduction of the secondary amine served to reduce lipophilicity. In addition, as the secondary amines are less rapidly metabolized than the tertiary amines, they may help improve the stability of these compounds in vivo. The synthesis of these derivatives used methodology similar to that already described for **123a** and **123b**. One key difference, however, was the need for orthogonal TBS and Boc protection/deprotection to prevent the secondary amine from reacting with the MsCl used to introduce the radiolabel. Both **123c** and **123d** showed good affinity for $A\beta_{1\text{-}42}$ aggregates (K_i = 2.41 nM and 3.85 nM, respectively) as well as the ability to label plaques in transgenic mice. Also, both **123c** and **123d** showed high uptake and rapid washout with improved pharmacokinetic properties when compared to **123a** and **123b**.

The [^{3}H]-labeled AZD4694 (**124**) also showed promise for Aβ imaging [87]. With good affinity for β-amyloid fibrils in vitro (K_d = 2.3 nM), this compound was able to label plaques in human AD brain sections with little nonspecific binding. In addition, the good pharmacokinetic profile of **124** warrants further investigation in vivo.

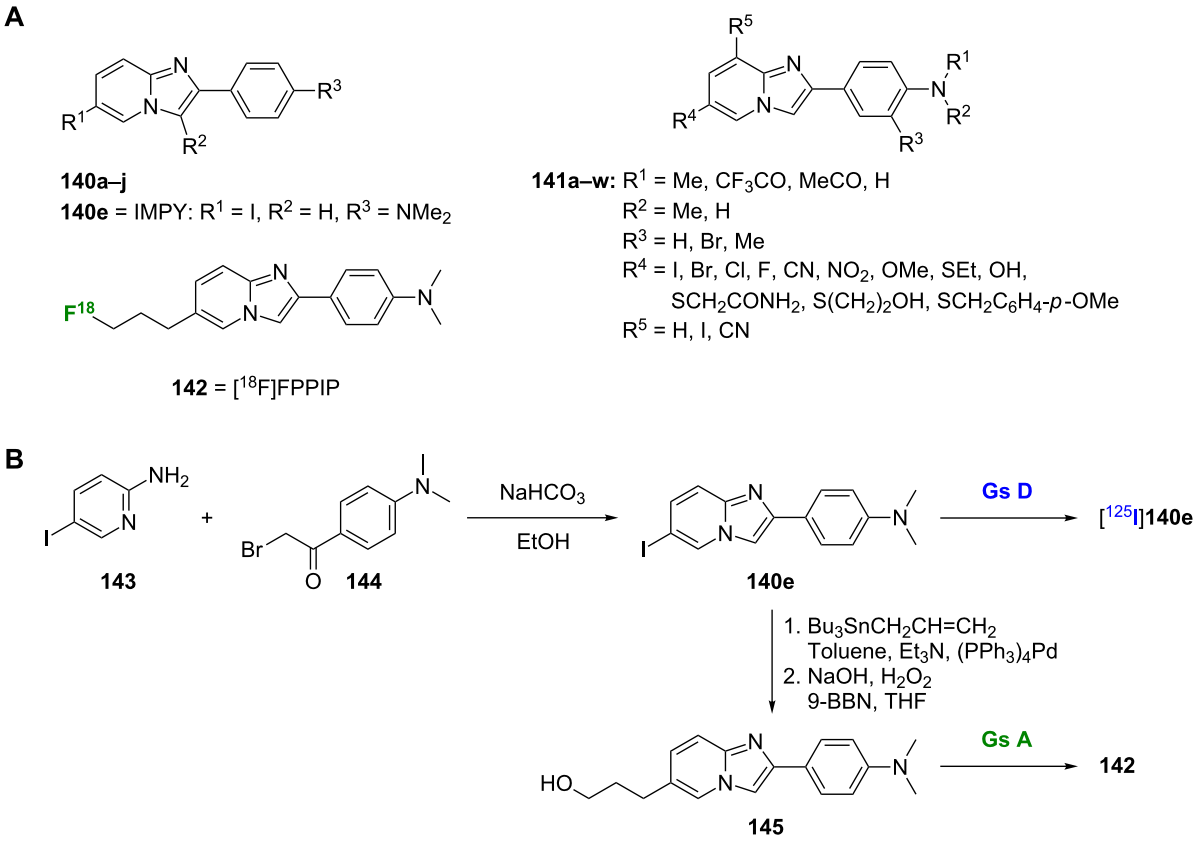
[Re] and [^{99m}Tc]-labeled benzofurans, BAT-Bp-2 (**125a**,**b**), were synthesized from **132** by reductive monoamination and *O*-demethylation to give **135** (Scheme 9D) [88]. Subsequent reaction with the protected chelation ligand TRT-Boc-BAT-Br (**136**) and labeling through reaction with the rhenium (used for in vitro studies) and technetium precursors gave compounds **125a** and **125b**, respectively. Compound **125b** showed decent affinity for $A\beta_{1\text{-}42}$ aggregates (K_i = 32.8 nM) in vitro, although, by comparison to other benzofuran probes of similar structure, it was clear that introduction of the BAT chelator decreased binding affinity. In contrast to other [^{99m}Tc]-labeled Aβ probes, **125b** showed decent brain uptake and washout rates in normal mice (1.80% ID/g at 2 min and 0.79% ID/g at 60 min). In addition, it was able to label Aβ plaques in vivo in transgenic mice, a first for a [^{99m}Tc]-labeled Aβ probe.

The [^{125}I]-labeled probe **126** contains the benzofuran core, but could also be classified as a chalcone, specifically a chalcone in which the conformation around the double bond is fixed [89]. Compound **126** was synthesized by using a Rap–Stoermer condensation between the bromo-substituted salicylaldehyde (**137**) and α-brominated 4-nitroacetophenone (**138**) to form the benzofuran core (Scheme 9E). Nitro reduction followed by methylation gave **139**, and radiolabeling gave **126**. This compound showed good affinity for $A\beta_{1\text{-}42}$ aggregates (K_i = 6.6 nM). Secondary methylamino and primary amino derivatives showed decreased binding affinity and poorer labeling of plaques in brain sections from transgenic mice. While the pharmacokinetics of this compound in normal mice were promising (3.53% ID/g at 2 min and 0.87% ID/g at 60 min), they were not as good as those previously reported for [^{125}I]-labeled *N,N*-dimethylamino chalcones and aurones.

Imidazopyridines

The imidazopyridine core has also been used in developing novel Aβ imaging agents such as **140**–**142** (Scheme 10A). Initial SAR studies were based on derivatives **140a–j**. One of the most successful imidazopyridines studied to date has been [^{125}I]IMPY ([^{125}I]**140e**). Representative of this scaffold, the synthesis of [^{125}I]**140e** used a fusion reaction between 2-amino-5-iodopyridine (**143**) and an α-bromoacetophenone **144** to form **140e**, which was then radiolabeled (Scheme 10B) [90]. This preparation has since been improved by Kung et al. who, through the use of a reverse-phase C4 minicolumn with stepwise washing and elution, have simplified the purification process by eliminating the need for HPLC purification [91]. While **140e** showed good affinity for $A\beta_{1\text{-}40}$ aggregates (K_i = 15.0 nM), SAR analysis demonstrated that, in general, other modifications to the scaffold were not well tolerated and reduced the binding affinity (Table 11). An exception was the replacement of the 6-iodo substituent with a bromine, as **140f** showed similar affinity to the parent compound [90].

In addition to its good binding affinity for Aβ, [^{125}I]**140e** showed other promising properties for use as an imaging probe. For example, it selectively labeled plaques in postmortem AD brain sections and showed plaque labeling with low background activity in a transgenic mouse model. The pharmacokinetics of [^{125}I]**140e** were also promising. It showed high uptake



Scheme 10: A. Structures of the radiolabeled imidazopyridine analogues discussed. **B**. Synthetic scheme for the preparation of [^{125}I]**140e** and **142**.

Table 11: Inhibition constants and biodistribution of radioactivity of 2-arylimidazopyridine derivatives **140a–j** (values are from [90]).

Compound	R^1	R^2	R^3	$A\beta_{1\text{-}40}$ K_i (nM)	%ID at 2 min	%ID at 60 min
140a	H	H	NHMe	>1000	—	—
140b	H	H	NMe_2	>2000	—	—
140c	Me	H	NHMe	>2000	—	—
140d	Me	H	NMe_2	242 ± 20	—	—
140e	I	H	NMe_2	15 ± 5	—	—
[^{125}I]**140e**	^{125}I	H	NMe_2	—	2.88 ± 0.25	0.21 ± 0.03
140f	Br	H	NMe_2	10.3 ± 1.2	—	—
140g	Me	H	Br	638 ± 30	—	—
140h	NMe_2	H	Br	339 ± 40	—	—
140i	H	I	NMe_2	>2000	—	—
140j	I	I	NMe_2	>2000	—	—

(2.9% ID/g at 2 min) and fast washout (0.2% ID/g at 60 min) in normal mice. These kinetic properties represented improvements over both **58a** and **94** [92]. Safety, biodistribution, and dosimetry studies of [^{123}I]IMPY, the [^{123}I]-labeled counterpart of **140e**, have indicated it may be a safe radiotracer with appropriate pharmacokinetics for use in AD patients [93].

More in depth SAR studies of the imidazopyridine scaffold have been conducted by synthesizing the series of analogues **141a**–**w** [94]. The effect of different substituents on binding affinity (K_i) for human Aβ plaques was examined (Table 12). In general, it was found that the *N*,*N*-dimethylamino analogues (R^1 = R^2 = Me) had higher binding affinity for human Aβ

Table 12: Inhibition constants of 2-arylimidazopyridine derivatives **141a–w** (values are from [94]).

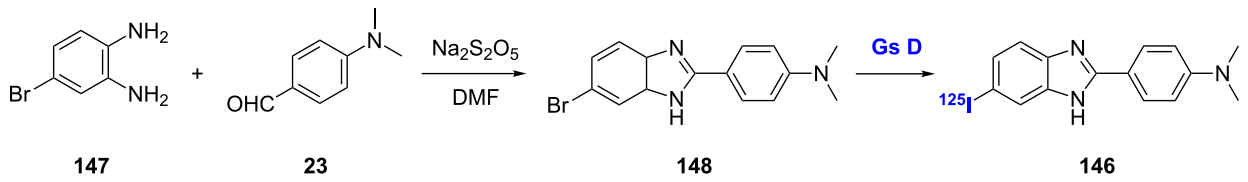
Compound	R^1	R^2	R^3	R^4	R^5	human AD brain homogenates K_i (nM)
140e	Me	Me	H	I	H	8.9 ± 0.7
141a	Me	Me	H	Br	H	5.9 ± 0.4
141b	Me	Me	H	Cl	H	24.2 ± 5.6
141c	Me	Me	H	F	H	13.0 ± 1.6
141d	Me	Me	H	CN	H	8.2 ± 1.0
141e	Me	Me	H	NO_2	H	7.6 ± 0.7
141f	Me	Me	H	OMe	H	38.5 ± 5.0
141g	Me	Me	H	SEt	H	8.3 ± 0.5
141h	Me	Me	H	Br	I	183 ± 61
141i	Me	Me	H	Br	CN	>180
141j	Me	Me	H	OH	H	177 ± 31
141k	CF_3CO	Me	Br	Br	H	>1000
141l	CF_3CO	H	Me	Br	H	>1000
141m	MeCO	Me	Me	Br	H	>1000
141n	H	Me	Br	Br	H	7.4 ± 0.6
141o	H	H	Me	Br	H	658 ± 47
141p	H	Me	Me	Br	H	>1000
141q	H	Me	H	SCH_2CONH_2	H	1840 ± 497
141r	H	Me	H	$S(CH_2)_2OH$	H	645 ± 75
141s	Me	Me	H	SCH_2CONH_2	H	391 ± 76
141t	Me	Me	H	$SCH_2C_6H_4$-*p*-OMe	H	8.3 ± 1.8
141u	Me	Me	H	$S(CH_2)_2OH$	H	88 ± 6
141v	H	Me	Me	SCH_2CONH_2	H	>1000
141w	H	Me	Me	$S(CH_2)_2OH$	H	>1000

plaques than did the secondary methylamino analogues (R^1 = H, R^2 = Me). Little tolerance for substitution at both R^3 and R^5 was seen, as the most potent compounds almost always had a hydrogen atom at these positions. One exception was observed with the secondary methylamino analogue when R^3 = Br, as **141n** showed high affinity. For R^4 it was seen that polarizable or electron-withdrawing substituents showed higher affinity than strongly electron-donating substituents. In addition, it was observed that bulky, hydrophobic thioether substituents (such as $R^4 = SCH_2C_6H_4$-*p*-OMe) were well tolerated at this position. This finding was of particular interest as it provided a possible means of generating new PET ligands via [^{11}C]- or [^{18}F]-labeling through *S*-alkylation.

The [^{18}F]-labeled imidazopyridine, [^{18}F]FPPIP (**142**), was prepared starting from **140e**. A palladium-catalyzed coupling with tributyl(vinyl)tin to give an alkene intermediate was followed by hydroboration-oxidation to give the hydroxypropyl intermediate **145**, which was radiolabeled to give **142** (Scheme 10B). This compound showed good binding affinity for Aβ (K_i = 48.3 nM) in using human AD cortical tissues, as well as specific labeling of Aβ plaques in postmortem AD brain. This, coupled with favorable pharmacokinetics observed in a normal rhesus monkey, made **142** a promising compound [95]. However, another [^{18}F]-labeled imidazopyridine, [^{18}F]FPM-IMPY, has shown less promising results. This compound, in which one of the *N*-methyl groups of IMPY was replaced with a [^{18}F]fluoropropyl moiety, showed lower binding affinity than IMPY and poor pharmacokinetics [96].

Benzimidazoles

The benzimidazole scaffold is highly similar to the imidazopyridine scaffold, but the benzimidazole ring has reduced lipophilicity when compared to imidazopyridines. This has the potential to reduce nonspecific binding and enhance signal-to-noise ratio. The [^{125}I]-labeled benzimidazole analogue of **140e**, compound **146**, was prepared through cyclization of 4-bromobenzene-1,2-diamine (**147**) and *p*-dimethylaminobenzaldehyde (**23**) to give **148** followed by installation of the radiolabel (Scheme 11) [97]. Compound **146** showed good binding affinity for $A\beta_{1\text{-}42}$ aggregates (K_i = 9.8 nM), as well as high uptake and rapid clearance in normal mice (4.14% ID/g at 2 min and 0.15% ID/g at 60 min). In vitro labeling of Aβ plaques in AD brain sections showed a strong



147 23 148 146

Scheme 11: Synthetic scheme for the preparation of the benzimidazole **146**.

signal with low background, and in vivo plaque labeling in transgenic mice was also successful. However, this scaffold is lacking in detailed SAR analysis compared to the imidazopyridine scaffold.

Quinoline and naphthalene analogues

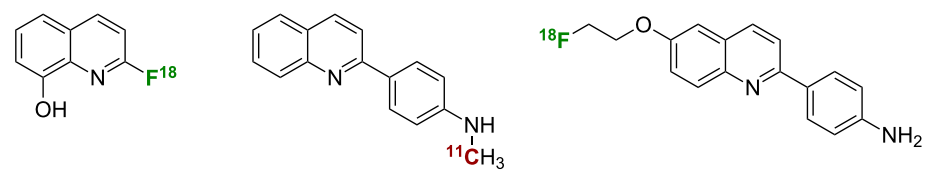
Quinolines

Investigation of the quinoline scaffold for imaging in AD has yielded some interesting results, despite there only being a few examples in the literature. The [^{18}F]-labeled 2-fluoroquinolin-8-ol [^{18}F]CABS13 (**149**) has recently been reported (Figure 5) [98]. The straightforward synthesis of this compound began with benzyl protection of 2-chloroquinolin-8-ol followed by installation of the [^{18}F]-label and Pd-catalyzed hydrogenolysis to give the target compound. Compound **149** potently bound to Aβ-Zn aggregates (K_d = 1.5 nM) and showed rapid uptake and washout in normal mice (10% ID/g at 2 min and 1.1% ID/g at 30 min). Also, delayed washout of **149** was observed in APP/Ps1 transgenic mice, which was indicative of non-specific binding to Aβ plaques. However, two other quinoline probes, [^{11}C]BF-158 (**150**) and [^{18}F]THK523 (**151**), had high affinity for tau pathology as opposed to Aβ. Compound **150** showed good uptake and washout in normal mice (11.3% ID/g at 2 min and 2.1% ID/g at 60 min), and was able to label NFTs in post-mortem AD brain section while only faintly staining plaques [99]. Compound **151** showed high affinity (K_d = 1.7 nM) and selectivity for recombinant tau fibrils in vitro, and, with favorable pharmacokinetics, it was able to highlight tau pathology in vivo in transgenic mice [100].

Naphthalenes

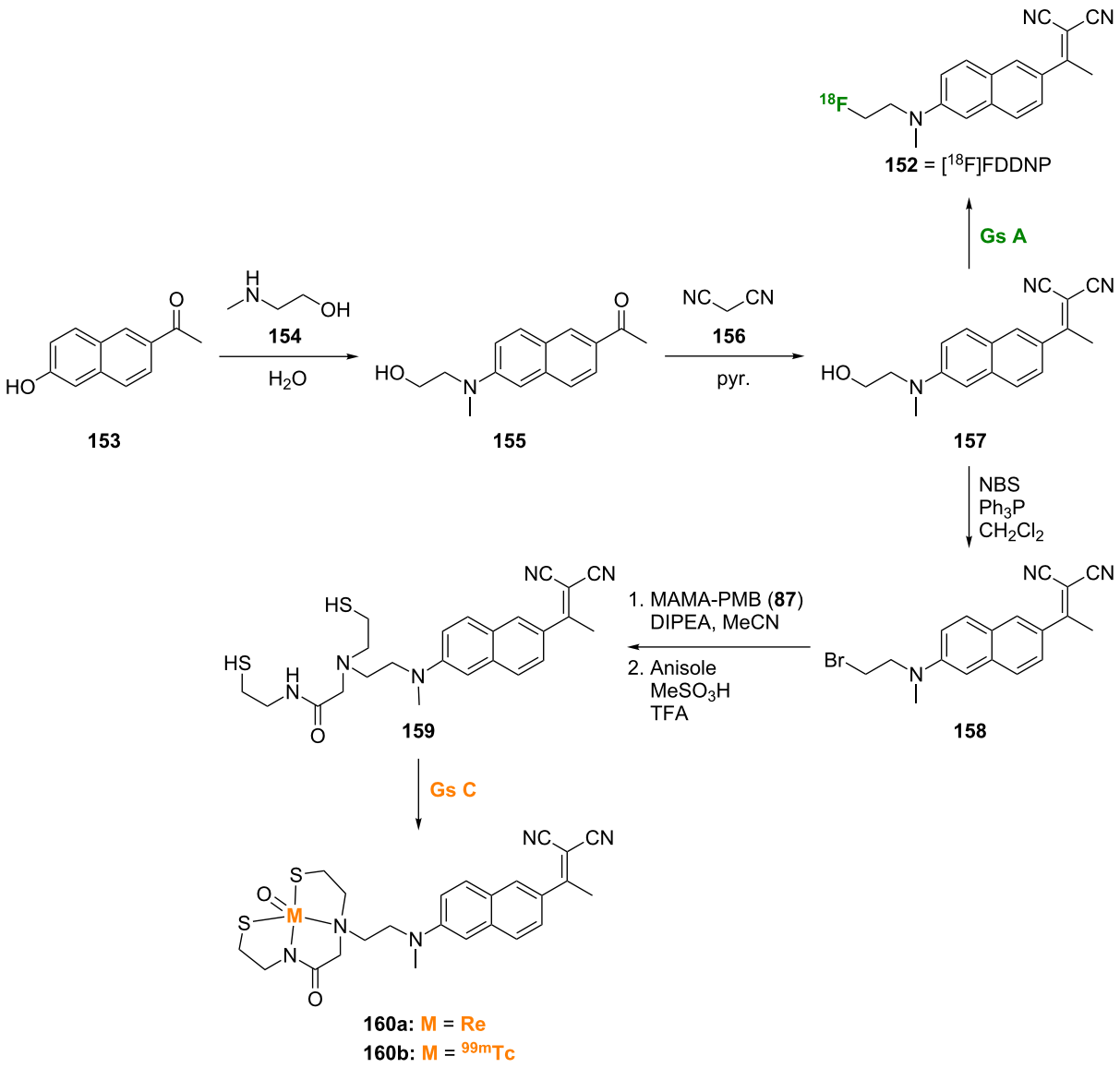
Replacement of the cyclic nitrogen in the quinoline scaffold described in the previous section affords the naphthalene scaffold. This scaffold has shown promising results for Aβ imaging, particularly [^{18}F]FDDNP (**152**), although this scaffold is also represented by only a few examples in the literature. Compound **152** was prepared starting from 1-(6-hydroxy-2-naphthyl)-1-ethanone (**153**) via a Bucherer reaction with 2-(methylamino)ethanol (**154**) followed by Knoevenagel reaction of **155** with malononitrile (**156**) and [^{18}F] labeling of **157** (Scheme 12) [101,102]. Compound **152** bound to synthetic A$\beta_{1\text{-}40}$ fibrils with high affinity (K_d = 0.12 nM) and crossed the BBB [103]. In addition, PET imaging studies using **152** demonstrated the ability of this compound to determine the localization and load of both SPs and NFTs in living AD patients [104], as well as the ability to differentiate between patients with no cognitive impairment, mild cognitive impairment, and AD [105].

[Re]- and [^{99m}Tc]-labeled derivatives of **152** have also been prepared by bromination of **157** with NBS to give **158** followed by conjugation with MAMA-PMB (**87**) and deprotection with acid to give **159**. Reaction with the technetium or rhenium precursors gave the target derivatives **160a**,**b** (Scheme 12) [106]. In vitro binding studies with the [Re]-labeled compound **160a** showed a 14-fold decrease in binding affinity for A$\beta_{1\text{-}42}$ aggregates compared to **152**. In addition, the [^{99m}Tc]-labeled compound **160b** showed very low brain uptake in normal mice indicating the need for additional refinements of this compound.



149 = [^{18}F]CABS13 **150** = [^{11}C]BF-158 **151** = [^{18}F]THK523

Figure 5: Structures of the quinolines discussed.

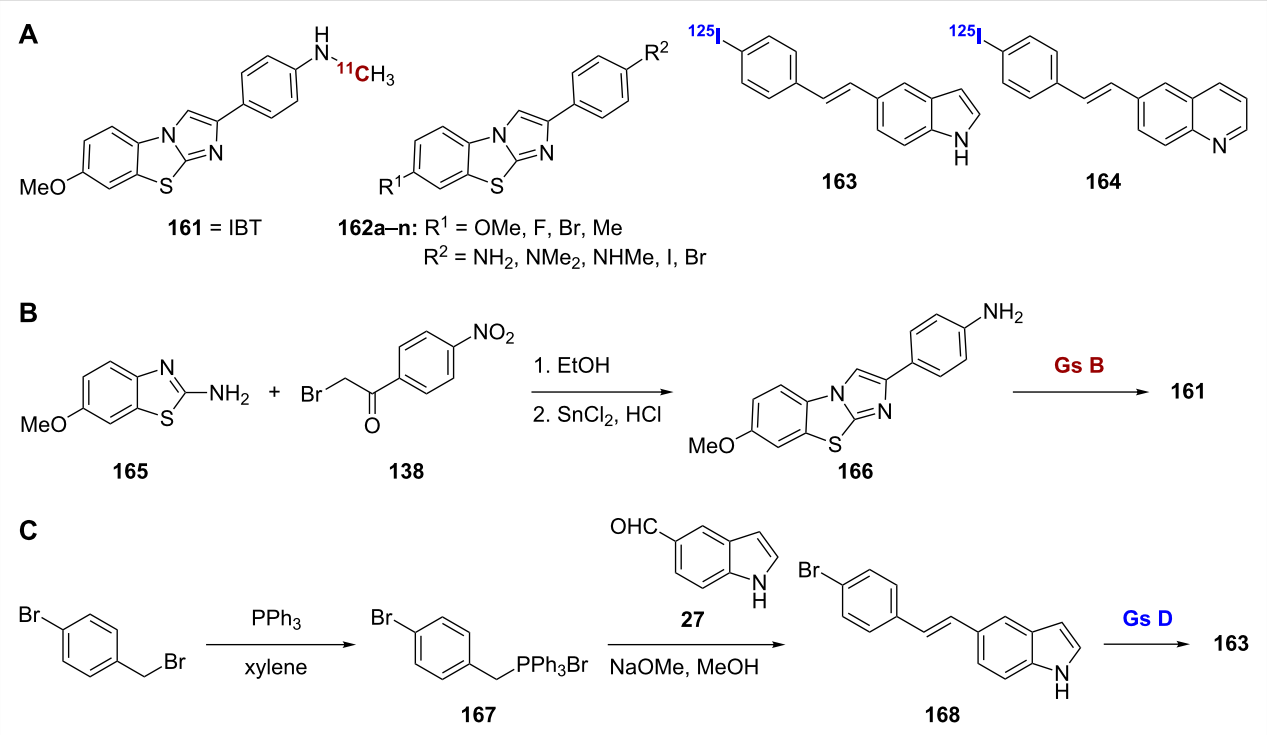


Scheme 12: Synthetic scheme for the preparation of the naphthalene analogues **152** and **160a**,**b**.

Combination of known scaffolds

With the success of the benzothiazole and imidazopyridine scaffolds for Aβ imaging, it was logical to suspect that combination of the two scaffolds into a single molecule could also provide a good imaging agent. Examples of this combination scaffold can be seen in compounds **161**–**164** (Scheme 13A). IBT (**161**) was prepared by direct coupling of 6-methoxybenzo[*d*]thiazol-2-amine (**165**) and the nitro substituted α-bromoacetophenone **138** to give **166** followed by installation of the radiolabel (Scheme 13B) [107]. Compound **161** showed good affinity for both $Aβ_{1-40}$ and $Aβ_{1-42}$ (K_i = 3.5 nM and 5.8 nM, respectively) and was comparable to compound **56c** in the same assay. The pharmacokinetics of this compound were also similar to those of [^{11}C]**56c**. In vivo specific plaque labeling by compound **161** was confirmed through studies in APP/Ps1 transgenic mice. Derivatives of this combination scaffold **162a**–**n** were also investigated (Table 13) [108]. Of note was derivative **162i** in which the secondary methylamino group of **161** has been replaced with iodine. This derivative showed high affinity for $Aβ_{1-40}$ (K_d = 10.9 nM), and the iodo substituent could readily be radiolabeled. However, the high lipophilicity of this compound may lead to nonspecific plaque labeling in vivo.

The [^{125}I]-labeled styrylindole **163** and styrylquinoline **164** scaffolds synthesized by Yang et al. can be thought of as stilbene combination scaffolds [109]. The synthesis of the [^{125}I]-labeled styrylindole **163** used a Wittig reaction between the triphenyl phosphonium ylide **167** and 1*H*-indole-5-carbalde-



Scheme 13: A. Structures of the radiolabeled analogues resulting from the combination of various scaffolds. **B**.,**C**. Synthetic schemes for the preparation of **161** and **163**.

Table 13: Inhibition constants of 2-arylimidazobenzothiazole derivatives **162a–n** (values are from [108]).

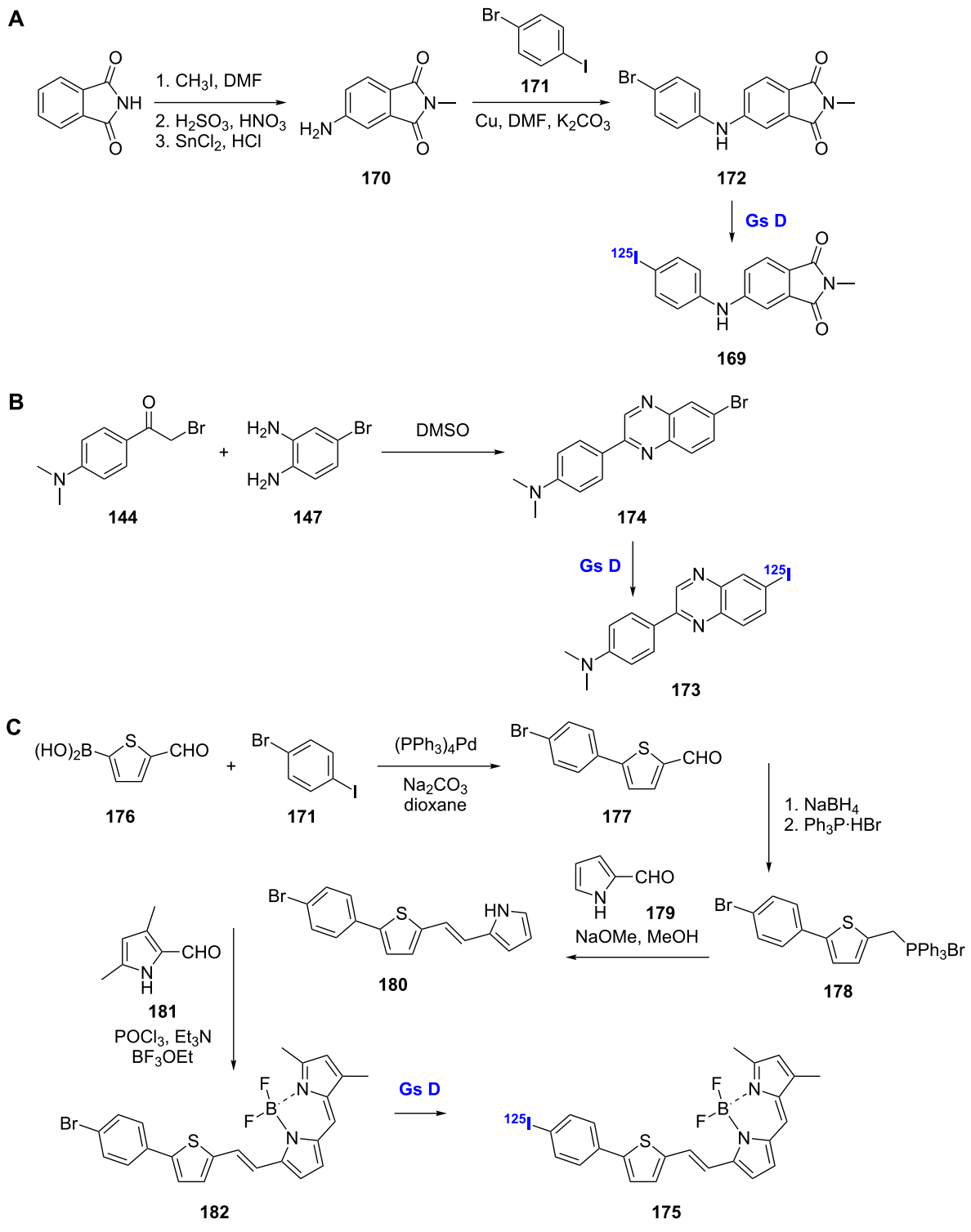
Compound	R^1	R^2	$A\beta_{1-40}$ K_i (nM)
162a	OMe	NH_2	29.8 ± 2.1
162b	OMe	NMe_2	58.6 ± 4.7
162c	F	NH_2	133 ± 21
162d	F	NHMe	38.1 ± 2.6
162e	F	NMe_2	42.9 ± 5.7
162f	Br	NH_2	28.8 ± 1.2
162g	Br	NHMe	34.5 ± 3.5
162h	Br	NMe_2	43.4 ± 5.7
162i	OMe	I	10.9 ± 0.18
162j	F	I	41.9 ± 5.2
162k	Br	I	21.1 ± 0.9
162l	Me	I	17.7 ± 1.9
162m	OMe	Br	9.40 ± 0.07
162n	Me	Br	26.0 ± 0.9

hyde (**27**) to give **168** followed by radiolabeling (Scheme 13C). The [^{125}I]-labeled styrylquinoline **164** was prepared by using an identical synthesis with substitution of the indole by quinoline-6-carbaldehyde. Both **163** and **164** showed good affinity for $A\beta_{1-40}$ aggregates (K_i = 4.1 nM and 8.6 nM, respectively). Compound **163** was able to stain Aβ plaques in in vitro brain sections from APP/Ps1 transgenic mice and showed high uptake and rapid clearance in normal mice (4.27% ID/g at 2 min and 0.28% ID/g at 60 min). However, compound **164** showed relatively low brain uptake and slow washout by comparison.

Others

Several other less common scaffolds have been evaluated as Aβ-imaging agents. The [^{125}I]-labeled *N*-methyl-4-anilinophthalimide derivative **169** was prepared and evaluated as a potential probe for Aβ plaques (Scheme 14A) [110]. This compound was generated via a Cu powder-catalyzed coupling reaction between *N*-methyl-4-aminophthalimide (**170**) and 1-bromo-4-iodobenzene (**171**) to give **172**, which was then radiolabeled. Compound **169** showed high binding affinity to AD brain homogenates (K_d = 0.21 nM) as well as excellent brain uptake (5.16% ID/g at 2 min) and fast washout (0.59% ID/g at 60 min). SAR studies with other *N*-methyl-4-anilinophthalimide derivatives demonstrated that a hydrophobic substituent at the 4-position of the aniline ring is important for the binding affinity of this family of compounds.

The [^{125}I]-labeled quinoxaline derivative **173** was also synthesized and evaluated for in vivo imaging of Aβ plaques (Scheme 14B) [111]. The quinoxaline backbone of this compound was prepared from the reaction of α-bromoacetophenone **144** and 4-bromobenzene-1,2-diamine (**147**) in DMSO in a one-



Scheme 14: A.–C. Synthetic schemes for the preparation of radiolabeled probes with unique scaffolds.

pot tandem oxide condensation procedure. This reaction gave the desired 2-aryl-6-substituted quinoxaline **174** as the major product and the isomeric 2-aryl-7-substituted quinoxaline (not shown) as a minor product. The radioiodinated probe was prepared from **174**. Compound **173** showed excellent affinity for $A\beta_{1\text{-}42}$ aggregates in vitro (K_i = 4.1 nM). In addition to being able to specifically label plaques in brain sections from AD patients, **173** readily crossed the BBB showing high uptake

into the brain (6.03% ID/g at 2 min). However, with moderate washout (1.12% ID/g at 120 min), additional refinements will be needed to improve the pharmacokinetics of these molecules.

The boron [^{125}I]-labeled dipyrro-methane (BODIPY) analogue **175** was prepared to serve as a dual functional SPECT/fluorescence probe for imaging Aβ (Scheme 14C) [112]. Compound **175** was synthesized through Suzuki coupling of the starting boronic acid **176** with 1-bromo-4-iodobenzene (**171**). Aldehyde reduction of **177** followed by reaction with triphenylphosphine gave the Wittig reagent **178** for reaction with 2-formylpyrrole (**179**). The Wittig product **180** was condensed with 3,5-dimethylpyrrole-2-carboxaldehyde (**181**) to form the BODIPY backbone **182**. Subsequent installation of the radiolabel gave **175**. Although **175** showed decent affinity for $A\beta_{1\text{-}42}$ aggregates (K_i = 108 nM) and the ability to label plaques in brain sections from transgenic mice, its in vivo use was limited by extremely low brain uptake, which could be attributed to rapid trapping of the compound in the liver.

Fluorescence probes

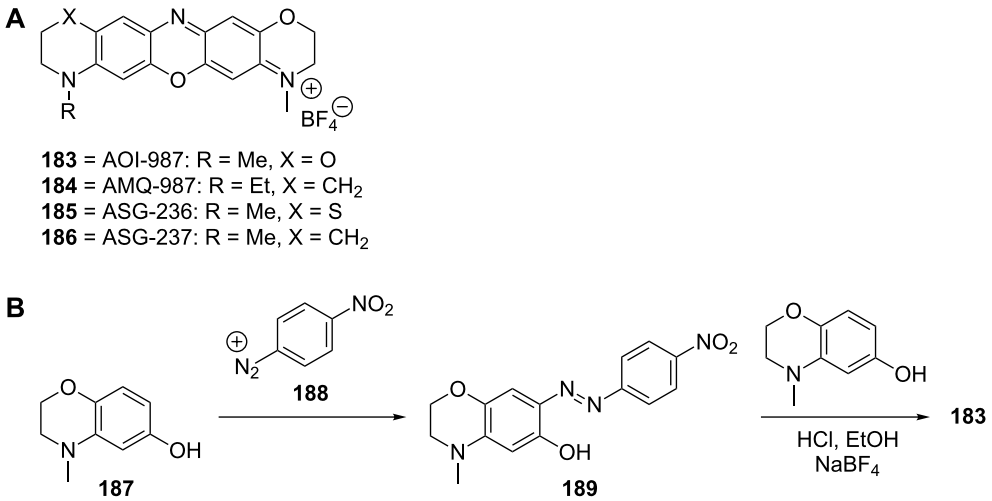
Although PET is currently the most promising approach for Aβ plaque detection, this technique has two main limitations: (i) the short half-life of positron-emitting nuclei ($t_{1/2}$ = 20 min for [^{11}C] and 110 min for [^{18}F]) and (ii) the narrow availability of this technology that requires a local cyclotron for generating short-lived positron-emitting radionuclides and a synthetic unit to produce radiolabeled agents [113]. Other imaging technologies have been investigated to overcome these problems. Different fluorescence techniques have been reported [114-116]; however, the near-infrared fluorescence (NIRF) imaging technique is the only one that has an in vivo application. Since normal biological tissues reveal limited photon absorbance in the near-infrared region, NIRF seems to be the second most promising Aβ deposits tracer tool [117]. In the following sections, we will briefly cover the different scaffolds that have been explored as NIRF ligands using in vivo models.

Oxazines

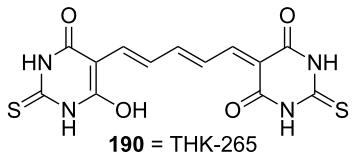
The oxazine dyes **183**–**186** were investigated as Aβ aggregate target-specific probes in the NIRF imaging technique (Scheme 15A) [113]. The preparation of **183** was accomplished through reaction of 4-methyl-3,4-dihydro-2*H*-benzo[*b*][1,4]oxazin-6-ol (**187**) with *p*-nitrobenzenediazonium ion (**188**) to give the key azo intermediate **189**, which afforded the desired oxazine dye **183** upon further reaction with 4-methyl-3,4-dihydro-2*H*-benzo[*b*][1,4]oxazin-6-ol (**187**) (Scheme 15B). Compound **183** proved to give a higher fluorescence intensity than other derivatives such as **184**–**186** [113]. Using APP23 transgenic mice and compound **183**, Aβ plaques could be traced quantitatively [113].

Thiobarbitals

The thiopental dimer THK-265 (**190**) (maximal emission wavelength >650 nm) was discovered as a good NIRF imaging ligand by screening a large pool of dye candidates (Figure 6) [117]. Compound **190** displayed high binding affinity towards Aβ aggregates (K_d = 97 nM) [117]. Its usefulness in AD diagnosis was confirmed in an animal model as it provided good discrimination between amyloid deposits in the brain and other normal tissues [117]. Compound **190** was also used in a quantitative correlation of different Aβ aggregation levels with NIRF signals [118].



Scheme 15: A. Structures of the oxazine-derived fluorescence probes discussed. **B**. Synthetic scheme for the preparation of the oxazine analogue **183**.



190 = THK-265

Figure 6: Structure of THK-265 (**190**).

Quinoxalines

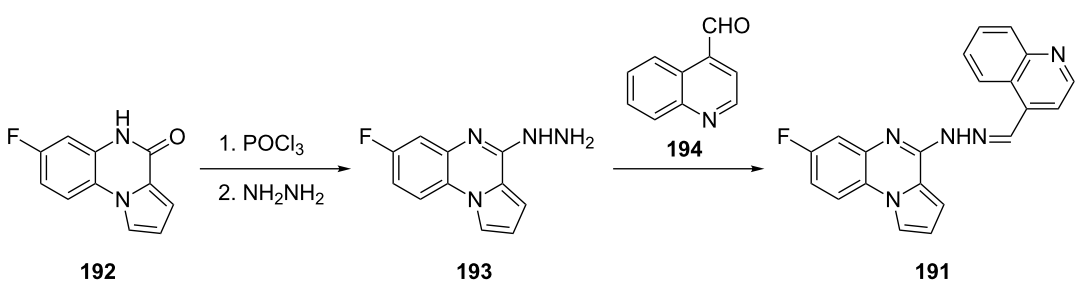
The use of the radiolabeled quinoxalines for imaging Aβ was discussed in the section "Others" of this review. A quinoxaline derivative, compound **191**, was also synthesized and explored for fluorescence imaging (Scheme 16) [119]. The synthesis of **191** began with conversion of the starting lactam **192** to the corresponding chloride by using phosphorus oxychloride followed by reaction with hydrazine. Condensation of the resulting hydrazino-derivative **193** with quinoline-4-carboxaldehyde (**194**) gave **191**. Although **191** has not been tested in vivo yet, this compound warrants further investigation as it has shown the ability to selectively stain amyloid structures in brain sections of transgenic mice, as well as the ability to cross the BBB. In addition, the 7-fluoro substituent of compound **191** could potentially be radiolabeled for in vivo application.

Conclusion

In summary, this review covered the main scaffolds used for radioimaging of Aβ plaques, one of the major pathological hallmarks of AD. Highlighted were important synthetic steps for scaffold formation and introduction of radiolabels, SAR findings where appropriate, and binding affinities and brain kinetics of each scaffold. The synthesis of each scaffold presented was fairly straightforward using well-established reactions, and synthetic complexity will likely not impede future development of Aβ chemical probes.

Most of the scaffolds present compounds with good binding affinity for Aβ in vitro. SARs tended to vary between scaffolds so it is impossible, without extensive computational work, to declare certain functionalities necessary for this class of chemical probes. However, the dimethylamine structural feature appears in a number of the compounds with high binding affinity, and it is likely that this functionality is important for Aβ interaction. Representative examples of this can be seen in examining SAR trends for chalcones **18a–l**, benzothiazoles **56c–t**, or imidazopyridines **141a–w** among others. With regards to pharmacokinetics in vivo, results varied between scaffolds and radiolabels. In general, [^{99m}Tc]-labeled compounds showed poor pharmacokinetic profiles with only **125b** being able to label plaques in animal studies. A balance in lipophilicity appeared to be particularly important in terms of pharmacokinetics, as imaging probes need to be lipophilic enough to easily penetrate the BBB, but not too lipophilic to avoid nonspecific binding in the brain.

Many of the molecules described in this review showed very promising results for the in vivo imaging of Aβ plaques in humans. For example, stilbenes **46a** and **46b**, benzothiazole [^{11}C]**56c**, and naphthalene **152** have been studied in clinical trials with favorable results. The half-life of the radiolabel and overall lipophilicity will continue to be two of the biggest factors for the clinical success of these probes. Future development and testing of these molecules will be of critical importance as the development of Aβ imaging probes will provide an effective means of monitoring new treatments for AD. While not the focus of this review, it should be noted that the current treatments for AD only treat cognitive symptoms and have little to no effect on slowing or reversing the progression of the disease. Current research efforts aimed at developing molecules that target Aβ plaques, specifically inhibition of plaque formation and disaggregation of already formed plaques, could lead to new therapeutics capable of reversing the progression of AD. Probes such as those described herein will play an important role in evaluating the effectiveness of such drugs. Additionally, the development of Aβ imaging probes will likely lead to better and earlier diagnosis of AD, which in turn will allow future treatments to be more effective.



Scheme 16: Synthetic scheme for the preparation of quinoxaline analogue **191**.

Acknowledgements

Our work on AD is supported by an Alzheimer's Art Quilt Initiative (AAQI) grant (S.G.-T.). We would like to acknowledge the work on the development of probes for AD of those that are not cited in this review due to the scope of the manuscript.

References

1. Thies, W.; Bleiler, L. *Alzheimers Dement.* **2011,** *7,* 208. doi:10.1016/j.jalz.2011.02.004
2. Ono, M.; Saji, H. *J. Pharmacol. Sci.* **2012,** *118,* 338. doi:10.1254/jphs.11R08FM
3. Klohs, J.; Rudin, M. *Neuroscientist* **2011,** *17,* 539. doi:10.1177/1073858410383433
4. Rowe, C. C.; Ackerman, U.; Browne, W.; Mulligan, R.; Pike, K. L.; O'Keefe, G.; Tochon-Danguy, H.; Chan, G.; Berlangieri, S. U.; Jones, G.; Dickinson-Rowe, K. L.; Kung, H. P.; Zhang, W.; Kung, M. P.; Skovronsky, D.; Dyrks, T.; Holl, G.; Krause, S.; Friebe, M.; Lehman, L.; Lindemann, S.; Dinkelborg, L. M.; Masters, C. L.; Villemagne, V. L. *Lancet Neurol.* **2008,** *7,* 129. doi:10.1016/S1474-4422(08)70001-2
5. Pike, K. E.; Savage, G.; Villemagne, V. L.; Ng, S.; Moss, S. A.; Maruff, P.; Mathis, C. A.; Klunk, W. E.; Masters, C. L.; Rowe, C. C. *Brain* **2007,** *130,* 2837. doi:10.1093/brain/awm238
6. Lockhart, A.; Ye, L.; Judd, D. B.; Merritt, A. T.; Lowe, P. N.; Morgenstern, J. L.; Hong, G.; Gee, A. D.; Brown, J. *J. Biol. Chem.* **2005,** *280,* 7677. doi:10.1074/jbc.M412056200
7. Thompson, P. W.; Ye, L.; Morgenstern, J. L.; Sue, L.; Beach, T. G.; Judd, D. J.; Shipley, N. J.; Libri, V.; Lockhart, A. *J. Neurochem.* **2009,** *109,* 623. doi:10.1111/j.1471-4159.2009.05996.x
8. Ye, L.; Morgenstern, J. L.; Lamb, J. R.; Lockhart, A. *Biochem. Biophys. Res. Commun.* **2006,** *347,* 669. doi:10.1016/j.bbrc.2006.06.126
9. Ye, L.; Morgenstern, J. L.; Gee, A. D.; Hong, G.; Brown, J.; Lockhart, A. *J. Biol. Chem.* **2005,** *280,* 23599. doi:10.1074/jbc.M501285200
10. Shan, L. In *Molecular Imaging and Contrast Agent Database (MICAD)* Bethesda (MD), 2004.
11. Sabaté, R.; Estelrich, J. *Biopolymers* **2003,** *72,* 455. doi:10.1002/bip.10485
12. Ono, M.; Ikeoka, R.; Watanabe, H.; Kimura, H.; Fuchigami, T.; Haratake, M.; Saji, H.; Nakayama, M. *ACS Chem. Neurosci.* **2010,** *1,* 598. doi:10.1021/cn100042d
13. Maya, Y.; Ono, M.; Watanabe, H.; Haratake, M.; Saji, H.; Nakayama, M. *Bioconjugate Chem.* **2009,** *20,* 95. doi:10.1021/bc8003292
14. Ono, M.; Watanabe, R.; Kawashima, H.; Cheng, Y.; Kimura, H.; Watanabe, H.; Haratake, M.; Saji, H.; Nakayama, M. *J. Med. Chem.* **2009,** *52,* 6394. doi:10.1021/jm901057p
15. Cui, M.; Ono, M.; Kimura, H.; Liu, B. L.; Saji, H. *Bioorg. Med. Chem. Lett.* **2011,** *21,* 980. doi:10.1016/j.bmcl.2010.12.045
16. Ono, M.; Watanabe, R.; Kawashima, H.; Kawai, T.; Watanabe, H.; Haratake, M.; Saji, H.; Nakayama, M. *Bioorg. Med. Chem.* **2009,** *17,* 2069. doi:10.1016/j.bmc.2009.01.025
17. Ares, J. J.; Outt, P. E.; Randall, J. L.; Murray, P. D.; Weisshaar, P. S.; O'Brien, L. M.; Ems, B. L.; Kakodkar, S. V.; Kelm, G. R.; Kershaw, W. C.; Werchowski, K. M.; Parkinson, A. *J. Med. Chem.* **1995,** *38,* 4937. doi:10.1021/jm00025a011
18. Ono, M.; Ikeoka, R.; Watanabe, H.; Kimura, H.; Fuchigami, T.; Haratake, M.; Saji, H.; Nakayama, M. *Bioorg. Med. Chem. Lett.* **2010,** *20,* 5743. doi:10.1016/j.bmcl.2010.08.004
19. Ono, M.; Maya, Y.; Haratake, M.; Ito, K.; Mori, H.; Nakayama, M. *Biochem. Biophys. Res. Commun.* **2007,** *361,* 116. doi:10.1016/j.bbrc.2007.06.162
20. Watanabe, H.; Ono, M.; Kimura, H.; Kagawa, S.; Nishii, R.; Fuchigami, T.; Haratake, M.; Nakayama, M.; Saji, H. *Bioorg. Med. Chem. Lett.* **2011,** *21,* 6519. doi:10.1016/j.bmcl.2011.08.063
21. Zhang, W.; Oya, S.; Kung, M.-P.; Hou, C.; Maier, D. L.; Kung, H. F. *Nucl. Med. Biol.* **2005,** *32,* 799. doi:10.1016/j.nucmedbio.2005.06.001
22. Ono, M.; Wilson, A.; Nobrega, J.; Westaway, D.; Verhoeff, P.; Zhuang, Z.-P.; Kung, M.-P.; Kung, H. F. *Nucl. Med. Biol.* **2003,** *30,* 565. doi:10.1016/S0969-8051(03)00049-0
23. Camus, V.; Payoux, P.; Barré, L.; Desgranges, B.; Voisin, T.; Tauber, C.; La Joie, R.; Tafani, M.; Hommet, C.; Chételat, G.; Mondon, K.; de La Sayette, V.; Cottier, J. P.; Beaufils, E.; Ribeiro, M. J.; Gissot, V.; Vierron, E.; Vercouillie, J.; Vellas, B.; Eustache, F.; Guilloteau, D. *Eur. J. Nucl. Med. Mol. Imaging* **2012,** *39,* 621. doi:10.1007/s00259-011-2021-8
24. O'Keefe, G. J.; Saunder, T. H.; Ng, S.; Ackerman, U.; Tochon-Danguy, H. J.; Chan, J. G.; Gong, S.; Dyrks, T.; Lindemann, S.; Holl, G.; Dinkelborg, L.; Villemagne, V.; Rowe, C. C. *J. Nucl. Med.* **2009,** *50,* 309. doi:10.2967/jnumed.108.055756
25. Barthel, H.; Luthardt, J.; Becker, G.; Patt, M.; Hammerstein, E.; Hartwig, K.; Eggers, B.; Sattler, B.; Schildan, A.; Hesse, S.; Meyer, P. M.; Wolf, H.; Zimmermann, T.; Reischl, J.; Rohde, B.; Gertz, H.-J.; Reininger, C.; Sabri, O. *Eur. J. Nucl. Med. Mol. Imaging* **2011,** *38,* 1702. doi:10.1007/s00259-011-1821-1
26. Zhang, W.; Oya, S.; Kung, M.-P.; Hou, C.; Maier, D. L.; Kung, H. F. *J. Med. Chem.* **2005,** *48,* 5980. doi:10.1021/jm050166g
27. Villemagne, V. L.; Ong, K.; Mulligan, R. S.; Holl, G.; Pejoska, S.; Jones, G.; O'Keefe, G.; Ackerman, U.; Tochon-Danguy, H.; Chan, J. G.; Reininger, C. B.; Fels, L.; Putz, B.; Rohde, B.; Masters, C. L.; Rowe, C. C. *J. Nucl. Med.* **2011,** *52,* 1210. doi:10.2967/jnumed.111.089730
28. Barthel, H.; Sabri, O. *J. Alzheimer's Dis.* **2011,** *26* (Suppl. 3), 117.
29. Yao, C.-H.; Lin, K.-J.; Weng, C.-C.; Hsiao, I.-T.; Ting, Y.-S.; Yen, T.-C.; Jan, T.-R.; Skovronsky, D.; Kung, M.-P.; Wey, S.-P. *Appl. Radiat. Isot.* **2010,** *68,* 2293. doi:10.1016/j.apradiso.2010.07.001
30. Choi, S. R.; Golding, G.; Zhuang, Z.; Zhang, W.; Lim, N.; Hefti, F.; Benedum, T. E.; Kilbourn, M. R.; Skovronsky, D.; Kung, H. F. *J. Nucl. Med.* **2009,** *50,* 1887. doi:10.2967/jnumed.109.065284
31. Lin, K.-J.; Hsu, W.-C.; Hsiao, I.-T.; Wey, S.-P.; Jin, L.-W.; Skovronsky, D.; Wai, Y.-Y.; Chang, H.-P.; Lo, C.-W.; Yao, C. H.; Yen, T.-C.; Kung, M.-P. *Nucl. Med. Biol.* **2010,** *37,* 497. doi:10.1016/j.nucmedbio.2010.02.003
32. Sperling, R. A.; Johnson, K. A.; Doraiswamy, P. M.; Reiman, E. M.; Fleisher, A. S.; Sabbagh, M. N.; Sadowsky, C. H.; Carpenter, A.; Davis, M. D.; Lu, M.; Flitter, M.; Joshi, A. D.; Clark, C. M.; Grundman, M.; Mintun, M. A.; Skovronsky, D. M.; Pontecorvo, M. J. *Neurobiol. Aging* **2013,** *34,* 822. doi:10.1016/j.neurobiolaging.2012.06.014
33. Tateno, A.; Okubo, Y. *Nippon Rinsho* **2011,** *69* (Suppl. 8), 561.

34. Kung, M.-P.; Weng, C.-C.; Lin, K.-J.; Hsiao, I.-T.; Yen, T.-C.; Wey, S.-P. *Chang Gung Med. J.* **2012,** *35,* 211.
35. Hsiao, I.-T.; Huang, C.-C.; Hsieh, C.-J.; Hsu, W.-C.; Wey, S.-P.; Yen, T.-C.; Kung, M.-P.; Lin, K.-J. *Eur. J. Nucl. Med. Mol. Imaging* **2012,** *39,* 1513. doi:10.1007/s00259-012-2137-5
36. Ballinger, J. R. *Eur. J. Nucl. Med. Mol. Imaging* **2012,** *39,* 1512. doi:10.1007/s00259-012-2136-6
37. Huang, K.-L.; Lin, K.-J.; Ho, M.-Y.; Chang, Y.-J.; Chang, C.-H.; Wey, S.-P.; Hsieh, C.-J.; Yen, T.-C.; Hsiao, I.-T.; Lee, T.-H. *J. Neurol. Sci.* **2012,** *319,* 124. doi:10.1016/j.jns.2012.04.014
38. Poisnel, G.; Dhilly, M.; Moustié, O.; Delamare, J.; Abbas, A.; Guilloteau, D.; Barré, L. *Neurobiol. Aging* **2012,** *33,* 2561. doi:10.1016/j.neurobiolaging.2011.12.024
39. Hsiao, I.-T.; Huang, C.-C.; Hsieh, C.-J.; Hsu, W.-C.; Wey, S.-P.; Yen, T.-C.; Kung, M.-P.; Lin, K.-J. *Eur. J. Nucl. Med. Mol. Imaging* **2012,** *39,* 613. doi:10.1007/s00259-011-2051-2
40. Wong, D. F.; Rosenberg, P. B.; Zhou, Y.; Kumar, A.; Raymont, V.; Ravert, H. T.; Dannals, R. F.; Nandi, A.; Brašić, J. R.; Ye, W.; Hilton, J.; Lyketsos, C.; Kung, H. F.; Joshi, A. D.; Skovronsky, D. M.; Pontecorvo, M. J. *J. Nucl. Med.* **2010,** *51,* 913. doi:10.2967/jnumed.109.069088
41. Wang, H.; Shi, H.; Yu, H.; Jiang, S.; Tang, G. *Nucl. Med. Biol.* **2011,** *38,* 121. doi:10.1016/j.nucmedbio.2010.06.009
42. Huynh, T. H. V.; Mantel, M. L.; Mikkelsen, K.; Lindhardt, A. T.; Nielsen, N. C.; Otzen, D.; Skrydstrup, T. *Org. Lett.* **2009,** *11,* 999. doi:10.1021/ol8029593
43. Wilson, A. A.; Garcia, A.; Jin, L.; Houle, S. *Nucl. Med. Biol.* **2000,** *27,* 529. doi:10.1016/S0969-8051(00)00132-3
44. Mayhoub, A. S.; Marler, L.; Kondratyuk, T. P.; Park, E.-J.; Pezzuto, J. M.; Cushman, M. *Bioorg. Med. Chem.* **2012,** *20,* 2427. doi:10.1016/j.bmc.2012.01.047
45. Mayhoub, A. S.; Marler, L.; Kondratyuk, T. P.; Park, E.-J.; Pezzuto, J. M.; Cushman, M. *Bioorg. Med. Chem.* **2012,** *20,* 510. doi:10.1016/j.bmc.2011.09.031
46. Mayhoub, A. S.; Kiselev, E.; Cushman, M. *Tetrahedron Lett.* **2011,** *52,* 4941. doi:10.1016/j.tetlet.2011.07.068
47. Watanabe, H.; Ono, M.; Ikeoka, R.; Haratake, M.; Saji, H.; Nakayama, M. *Bioorg. Med. Chem.* **2009,** *17,* 6402. doi:10.1016/j.bmc.2009.07.020
48. Ono, M.; Haratake, M.; Saji, H.; Nakayama, M. *Bioorg. Med. Chem.* **2008,** *16,* 6867. doi:10.1016/j.bmc.2008.05.054
49. Klunk, W. E.; Wang, Y.; Huang, G.-F.; Debnath, M. L.; Holt, D. P.; Mathis, C. A. *Life Sci.* **2001,** *69,* 1471. doi:10.1016/S0024-3205(01)01232-2
50. Mathis, C. A.; Bacskai, B. J.; Kajdasz, S. T.; McLellan, M. E.; Frosch, M. P.; Hyman, B. T.; Holt, D. P.; Wang, Y.; Huang, G.-F.; Debnath, M. L.; Klunk, W. E. *Bioorg. Med. Chem. Lett.* **2002,** *12,* 295. doi:10.1016/S0960-894X(01)00734-X
51. Klunk, W. E.; Wang, Y.; Huang, G. F.; Debnath, M. L.; Holt, D. P.; Shao, L.; Hamilton, R. L.; Ikonomovic, M. D.; DeKosky, S. T.; Mathis, C. A. *J. Neurosci.* **2003,** *23,* 2086.
52. Mathis, C. A.; Wang, Y.; Holt, D. P.; Huang, G.-F.; Debnath, M. L.; Klunk, W. E. *J. Med. Chem.* **2003,** *46,* 2740. doi:10.1021/jm030026b
53. Solbach, C.; Uebele, M.; Reischl, G.; Machulla, H.-J. *Appl. Radiat. Isot.* **2005,** *62,* 591. doi:10.1016/j.apradiso.2004.09.003
54. Klunk, W. E.; Engler, H.; Nordberg, A.; Wang, Y.; Blomqvist, G.; Holt, D. P.; Bergström, M.; Savitcheva, I.; Huang, G.-F.; Estrada, S.; Ausén, B.; Debnath, M. L.; Barletta, J.; Price, J. C.; Sandell, J.; Lopresti, B. J.; Wall, A.; Koivisto, P.; Antoni, G.; Mathis, C. A.; Långström, B. *Ann. Neurol.* **2004,** *55,* 306. doi:10.1002/ana.20009
55. Svedberg, M. M.; Hall, H.; Hellström-Lindahl, E.; Estrada, S.; Guan, Z.; Nordberg, A.; Långström, B. *Neurochem. Int.* **2009,** *54,* 347. doi:10.1016/j.neuint.2008.12.016
56. Serdons, K.; Verduyckt, T.; Vanderghinste, D.; Borghgraef, P.; Cleynhens, J.; Van Leuven, F.; Kung, H.; Bormans, G.; Verbruggen, A. *Eur. J. Med. Chem.* **2009,** *44,* 1415. doi:10.1016/j.ejmech.2008.09.038
57. Johnson, A. E.; Jeppsson, F.; Sandell, J.; Wensbo, D.; Neelissen, J. A. M.; Juréus, A.; Ström, P.; Norman, H.; Farde, L.; Svensson, S. P. S. *J. Neurochem.* **2009,** *108,* 1177. doi:10.1111/j.1471-4159.2008.05861.x
58. Zhuang, Z.-P.; Kung, M.-P.; Hou, C.; Skovronsky, D. M.; Gur, T. L.; Plössl, K.; Trojanowski, J. Q.; Lee, V. M.-Y.; Kung, H. F. *J. Med. Chem.* **2001,** *44,* 1905. doi:10.1021/jm010045q
59. Wang, Y.; Mathis, C. A.; Huang, G.-F.; Debnath, M. L.; Holt, D. P.; Shao, L.; Klunk, W. E. *J. Mol. Neurosci.* **2003,** *20,* 255. doi:10.1385/JMN:20:3:255
60. Matsumura, K.; Ono, M.; Hayashi, S.; Kimura, H.; Okamoto, Y.; Ihara, M.; Takahashi, R.; Mori, H.; Saji, H. *MedChemComm* **2011,** *2,* 596. doi:10.1039/c1md00034a
61. Zheng, M.-Q.; Yin, D.-Z.; Qia, J.-P.; Zhang, L.; Wang, Y.-X. *J. Fluorine Chem.* **2008,** *129,* 210. doi:10.1016/j.jfluchem.2007.11.005
62. Zheng, M.-Q.; Yin, D.-Z.; Zhang, L.; Lei, B.; Cheng, D.-F.; Cai, H.-C.; Han, Y.-J.; Wu, M.-X.; Zhang, H.; Wang, J. *Acta Pharmacol. Sin.* **2008,** *29,* 548. doi:10.1111/j.1745-7254.2008.00785.x
63. Neumaier, B.; Deisenhofer, S.; Sommer, C.; Solbach, C.; Reske, S. N.; Mottaghy, F. *Appl. Radiat. Isot.* **2010,** *68,* 1066. doi:10.1016/j.apradiso.2009.12.044
64. Berndt, U.; Stanetty, C.; Wanek, T.; Kuntner, C.; Stanek, J.; Berger, M.; Bauer, M.; Henriksen, G.; Wester, H.-J.; Kvaternik, H.; Angelberger, P.; Noe, C. *J. Labelled Compd. Radiopharm.* **2008,** *51,* 137. doi:10.1002/jlcr.1476
65. Koole, M.; Lewis, D. M.; Buckley, C.; Nelissen, N.; Vandenbulcke, M.; Brooks, D. J.; Vandenberghe, R.; Van Laere, K. *J. Nucl. Med.* **2009,** *50,* 818. doi:10.2967/jnumed.108.060756
66. Serdons, K.; Verduyckt, T.; Vanderghinste, D.; Cleynhens, J.; Borghgraef, P.; Vermaelen, P.; Terwinghe, C.; Van Leuven, F.; Van Laere, K.; Kung, H.; Bormans, G.; Verbruggen, A. *Bioorg. Med. Chem. Lett.* **2009,** *19,* 602. doi:10.1016/j.bmcl.2008.12.069
67. Serdons, K.; Terwinghe, C.; Vermaelen, P.; Van Laere, K.; Kung, H.; Mortelmans, L.; Bormans, G.; Verbruggen, A. *J. Med. Chem.* **2009,** *52,* 1428. doi:10.1021/jm8013376
68. Chen, X.; Yu, P.; Zhang, L.; Liu, B. *Bioorg. Med. Chem. Lett.* **2008,** *18,* 1442. doi:10.1016/j.bmcl.2007.12.071
69. Serdons, K.; Verduyckt, T.; Cleynhens, J.; Terwinghe, C.; Mortelmans, L.; Bormans, G.; Verbruggen, A. *Bioorg. Med. Chem. Lett.* **2007,** *17,* 6086. doi:10.1016/j.bmcl.2007.09.055
70. Zhuang, Z.-P.; Kung, M.-P.; Hou, C.; Plössl, K.; Skovronsky, D.; Gur, T. L.; Trojanowski, J. Q.; Lee, V. M.-Y.; Kung, H. F. *Nucl. Med. Biol.* **2001,** *28,* 887. doi:10.1016/S0969-8051(01)00264-5
71. Hausner, S. H.; Alagille, D.; Koren, A. O.; Amici, L.; Staley, J. K.; Cosgrove, K. P.; Baldwin, R. M.; Tamagnan, G. D. *Bioorg. Med. Chem. Lett.* **2009,** *19,* 543. doi:10.1016/j.bmcl.2008.05.033
72. Cui, M.; Ono, M.; Kimura, H.; Ueda, M.; Nakamoto, Y.; Togashi, K.; Okamoto, Y.; Ihara, M.; Takahashi, R.; Liu, B.; Saji, H. *J. Med. Chem.* **2012,** *55,* 9136. doi:10.1021/jm300251n

73. Okamura, N.; Suemoto, T.; Shiomitsu, T.; Suzuki, M.; Shimadzu, H.; Akatsu, H.; Yamamoto, T.; Arai, H.; Sasaki, H.; Yanai, K.; Staufenbiel, M.; Kudo, Y.; Sawada, T. *J. Mol. Neurosci.* **2004,** *24,* 247. doi:10.1385/JMN:24:2:247
74. Okamura, N.; Suemoto, T.; Shimadzu, H.; Suzuki, M.; Shiomitsu, T.; Akatsu, H.; Yamamoto, T.; Staufenbiel, M.; Yanai, K.; Arai, H.; Sasaki, H.; Kudo, Y.; Sawada, T. *J. Neurosci.* **2004,** *24,* 2535. doi:10.1523/JNEUROSCI.4456-03.2004
75. Shimadzu, H.; Suemoto, T.; Suzuki, M.; Shiomitsu, T.; Okamura, N.; Kudo, Y.; Sawada, T. *J. Labelled Compd. Radiopharm.* **2004,** *47,* 181. doi:10.1002/jlcr.811
76. Kudo, Y.; Okamura, N.; Furumoto, S.; Tashiro, M.; Furukawa, K.; Maruyama, M.; Itoh, M.; Iwata, R.; Yanai, K.; Arai, H. *J. Nucl. Med.* **2007,** *48,* 553. doi:10.2967/jnumed.106.037556
77. Furukawa, K.; Okamura, N.; Tashiro, M.; Waragai, M.; Furumoto, S.; Iwata, R.; Yanai, K.; Kudo, Y.; Arai, H. *J. Neurol.* **2010,** *257,* 721. doi:10.1007/s00415-009-5396-8
78. Shao, H.; Okamura, N.; Sugi, K.; Furumoto, S.; Furukawa, K.; Tashiro, M.; Iwata, R.; Matsuda, H.; Kudo, Y.; Arai, H.; Fukuda, H.; Yanai, K. *Dementia Geriatr. Cognit. Disord.* **2010,** *30,* 101. doi:10.1159/000318754
79. Okamura, N.; Shiga, Y.; Furumoto, S.; Tashiro, M.; Tsuboi, Y.; Furukawa, K.; Yanai, K.; Iwata, R.; Arai, H.; Kudo, Y.; Itoyama, Y.; Doh-ura, K. *Eur. J. Nucl. Med. Mol. Imaging* **2010,** *37,* 934. doi:10.1007/s00259-009-1314-7
80. Kikuchi, A.; Takeda, A.; Okamura, N.; Tashiro, M.; Hasegawa, T.; Furumoto, S.; Kobayashi, M.; Sugeno, N.; Baba, T.; Miki, Y.; Mori, F.; Wakabayashi, K.; Funaki, Y.; Iwata, R.; Takahashi, S.; Fukuda, H.; Arai, H.; Kudo, Y.; Yanai, K.; Itoyama, Y. *Brain* **2010,** *133,* 1772. doi:10.1093/brain/awq091
81. Fodero-Tavoletti, M. T.; Mulligan, R. S.; Okamura, N.; Furumoto, S.; Rowe, C. C.; Kudo, Y.; Masters, C. L.; Cappai, R.; Yanai, K.; Villemagne, V. L. *Eur. J. Pharmacol.* **2009,** *617,* 54. doi:10.1016/j.ejphar.2009.06.042
82. Ono, M.; Kawashima, H.; Nonaka, A.; Kawai, T.; Haratake, M.; Mori, H.; Kung, M.-P.; Kung, H. F.; Saji, H.; Nakayama, M. *J. Med. Chem.* **2006,** *49,* 2725. doi:10.1021/jm051176k
83. Ono, M.; Kung, M.-P.; Hou, C.; Kung, H. F. *Nucl. Med. Biol.* **2002,** *29,* 633. doi:10.1016/S0969-8051(02)00326-8
84. Cheng, Y.; Ono, M.; Kimura, H.; Kagawa, S.; Nishii, R.; Saji, H. *Bioorg. Med. Chem. Lett.* **2010,** *20,* 6141. doi:10.1016/j.bmcl.2010.08.016
85. Cheng, Y.; Ono, M.; Kimura, H.; Kagawa, S.; Nishii, R.; Kawashima, H.; Saji, H. *ACS Med. Chem. Lett.* **2010,** *1,* 321. doi:10.1021/ml100082x
86. Ono, M.; Cheng, Y.; Kimura, H.; Cui, M.; Kagawa, S.; Nishii, R.; Saji, H. *J. Med. Chem.* **2011,** *54,* 2971. doi:10.1021/jm200057u
87. Juréus, A.; Swahn, B.-M.; Sandell, J.; Jeppsson, F.; Johnson, A. E.; Johnström, P.; Neelissen, J. A. M.; Sunnemark, D.; Farde, L.; Svensson, S. P. S. *J. Neurochem.* **2010,** *114,* 784. doi:10.1111/j.1471-4159.2010.06812.x
88. Cheng, Y.; Ono, M.; Kimura, H.; Ueda, M.; Saji, H. *J. Med. Chem.* **2012,** *55,* 2279. doi:10.1021/jm201513c
89. Cui, M.; Ono, M.; Kimura, H.; Liu, B.; Saji, H. *Bioorg. Med. Chem.* **2011,** *19,* 4148. doi:10.1016/j.bmc.2011.04.049
90. Zhuang, Z.-P.; Kung, M.-P.; Wilson, A.; Lee, C.-W.; Plössl, K.; Hou, C.; Holtzman, D. M.; Kung, H. F. *J. Med. Chem.* **2003,** *46,* 237. doi:10.1021/jm020351j
91. Kung, M.-P.; Hou, C.; Zhuang, Z.-P.; Cross, A. J.; Maier, D. L.; Kung, H. F. *Eur. J. Nucl. Med. Mol. Imaging* **2004,** *31,* 1136. doi:10.1007/s00259-004-1487-z
92. Kung, M.-P.; Hou, C.; Zhuang, Z.-P.; Zhang, B.; Skovronsky, D.; Trojanowski, J. Q.; Lee, V. M.-Y.; Kung, H. F. *Brain Res.* **2002,** *956,* 202. doi:10.1016/S0006-8993(02)03436-4
93. Newberg, A. B.; Wintering, N. A.; Plössl, K.; Hochold, J.; Stabin, M. G.; Watson, M.; Skovronsky, D.; Clark, C. M.; Kung, M.-P.; Kung, H. F. *J. Nucl. Med.* **2006,** *47,* 748.
94. Cai, L.; Cuevas, J.; Temme, S.; Herman, M. M.; Dagostin, C.; Widdowson, D. A.; Innis, R. B.; Pike, V. W. *J. Med. Chem.* **2007,** *50,* 4746. doi:10.1021/jm0702231
95. Zeng, F.; Southerland, J. A.; Voll, R. J.; Votaw, J. R.; Williams, L.; Ciliax, B. J.; Levey, A. I.; Goodman, M. M. *Bioorg. Med. Chem. Lett.* **2006,** *16,* 3015. doi:10.1016/j.bmcl.2006.02.055
96. Cai, L.; Chin, F. T.; Pike, V. W.; Toyama, H.; Liow, J.-S.; Zoghbi, S. S.; Modell, K.; Briard, E.; Shetty, H. U.; Sinclair, K.; Donohue, S.; Tipre, D.; Kung, M.-P.; Dagostin, C.; Widdowson, D. A.; Green, M.; Gao, W.; Herman, M. M.; Ichise, M.; Innis, R. B. *J. Med. Chem.* **2004,** *47,* 2208. doi:10.1021/jm030477w
97. Cui, M.; Ono, M.; Kimura, H.; Kawashima, H.; Liu, B. L.; Saji, H. *Nucl. Med. Biol.* **2011,** *38,* 313. doi:10.1016/j.nucmedbio.2010.09.012
98. Vasdev, N.; Cao, P.; van Oosten, E. M.; Wilson, A. A.; Houle, S.; Hao, G.; Sun, X.; Slavine, N.; Ahasan, M.; Antich, P. P.; Bonte, F. J.; Kulkarni, P. *MedChemComm* **2012,** *3,* 1228. doi:10.1039/c2md20075a
99. Okamura, N.; Suemoto, T.; Furumoto, S.; Suzuki, M.; Shimadzu, H.; Akatsu, H.; Yamamoto, T.; Fujiwara, H.; Nemoto, M.; Maruyama, M.; Arai, H.; Yanai, K.; Sawada, T.; Kudo, Y. *J. Neurosci.* **2005,** *25,* 10857. doi:10.1523/JNEUROSCI.1738-05.2005
100. Fodero-Tavoletti, M. T.; Okamura, N.; Furumoto, S.; Mulligan, R. S.; Connor, A. R.; McLean, C. A.; Cao, D.; Rigopoulos, A.; Cartwright, G. A.; O'Keefe, G.; Gong, S.; Adlard, P. A.; Barnham, K. J.; Rowe, C. C.; Masters, C. L.; Kudo, Y.; Cappai, R.; Yanai, K.; Villemagne, V. L. *Brain* **2011,** *134,* 1089. doi:10.1093/brain/awr038
101. Agdeppa, E. D.; Kepe, V.; Petri, A.; Satyamurthy, N.; Liu, J.; Huang, S.-C.; Small, G. W.; Cole, G. M.; Barrio, J. R. *Neuroscience* **2003,** *117,* 723. doi:10.1016/S0306-4522(02)00907-7
102. Jacobson, A.; Petric, A.; Hogenkamp, D.; Sinur, A.; Barrio, J. R. *J. Am. Chem. Soc.* **1996,** *118,* 5572. doi:10.1021/ja9543356
103. Agdeppa, E. D.; Kepe, V.; Liu, J.; Flores-Torres, S.; Satyamurthy, N.; Petric, A.; Cole, G. M.; Small, G. W.; Huang, S. C.; Barrio, J. R. *J. Neurosci.* **2001,** *21,* RC189.
104. Shoghi-Jadid, K.; Small, G. W.; Agdeppa, E. D.; Kepe, V.; Ercoli, L. M.; Siddarth, P.; Read, S.; Satyamurthy, N.; Petric, A.; Huang, S.-C.; Barrio, J. R. *Am. J. Geriatr. Psychiatry* **2002,** *10,* 24.
105. Small, G. W.; Kepe, V.; Ercoli, L. M.; Siddarth, P.; Bookheimer, S. Y.; Miller, K. J.; Lavretsky, H.; Burggren, A. C.; Cole, G. M.; Vinters, H. V.; Thompson, P. M.; Huang, S.-C.; Satyamurthy, N.; Phelps, M. E.; Barrio, J. R. *N. Engl. J. Med.* **2006,** *355,* 2652. doi:10.1056/NEJMoa054625
106. Cui, M.; Tang, R.; Li, Z.; Ren, H.; Liu, B. *Bioorg. Med. Chem. Lett.* **2011,** *21,* 1064. doi:10.1016/j.bmcl.2010.11.096
107. Yousefi, B. H.; Manook, A.; Drzezga, A.; von Reutern, B.; Schwaiger, M.; Wester, H.-J.; Henriksen, G. *J. Med. Chem.* **2011,** *54,* 949. doi:10.1021/jm101129a
108. Alagille, D.; DaCosta, H.; Baldwin, R. M.; Tamagnan, G. D. *Bioorg. Med. Chem. Lett.* **2011,** *21,* 2966. doi:10.1016/j.bmcl.2011.03.052

109. Yang, Y.; Jia, H.-M.; Liu, B.-L. *Molecules* **2012,** *17,* 4252. doi:10.3390/molecules17044252
110. Duan, X.-H.; Qiao, J.-P.; Yang, Y.; Cui, M.-C.; Zhou, J.-N.; Liu, B.-L. *Bioorg. Med. Chem.* **2010,** *18,* 1337. doi:10.1016/j.bmc.2009.12.023
111. Cui, M.; Ono, M.; Kimura, H.; Liu, B.; Saji, H. *Bioorg. Med. Chem. Lett.* **2011,** *21,* 4193. doi:10.1016/j.bmcl.2011.05.079
112. Ono, M.; Ishikawa, M.; Kimura, H.; Hayashi, S.; Matsumura, K.; Watanabe, H.; Shimizu, Y.; Cheng, Y.; Cui, M.; Kawashima, H.; Saji, H. *Bioorg. Med. Chem. Lett.* **2010,** *20,* 3885. doi:10.1016/j.bmcl.2010.05.027
113. Hintersteiner, M.; Enz, A.; Frey, P.; Jaton, A.-L.; Kinzy, W.; Kneuer, R.; Neumann, U.; Rudin, M.; Staufenbiel, M.; Stoeckli, M.; Wiederhold, K.-H.; Gremlich, H.-U. *Nat. Biotechnol.* **2005,** *23,* 577. doi:10.1038/nbt1085
114. Hu, Y.; Su, B.; Kim, C.-S.; Hernandez, M.; Rostagno, A.; Ghiso, J.; Kim, J. R. *ChemBioChem* **2010,** *11,* 2409. doi:10.1002/cbic.201000435
115. Hu, Y.; Su, B.; Zheng, H.; Kim, J. R. *Mol. BioSyst.* **2012,** *8,* 2741. doi:10.1039/c2mb25148e
116. Marek, P.; Gupta, R.; Raleigh, D. P. *ChemBioChem* **2008,** *9,* 1372. doi:10.1002/cbic.200800052
117. Okamura, N.; Mori, M.; Furumoto, S.; Yoshikawa, T.; Harada, R.; Ito, S.; Fujikawa, Y.; Arai, H.; Yanai, K.; Kudo, Y. *J. Alzheimer's Dis.* **2011,** *23,* 37. doi:10.3233/JAD-2010-100270
118. Schmidt, A.; Pahnke, J. *J. Alzheimer's Dis.* **2012,** *30,* 651. doi:10.3233/JAD-2012-112168
119. Gemma, S.; Colombo, L.; Forloni, G.; Savini, L.; Fracasso, C.; Caccia, S.; Salmona, M.; Brindisi, M.; Joshi, B. P.; Tripaldi, P.; Giorgi, G.; Taglialatela-Scafati, O.; Novellino, E.; Fiorini, I.; Campiani, G.; Butini, S. *Org. Biomol. Chem.* **2011,** *9,* 5137. doi:10.1039/c1ob05288h

License and Terms

This is an Open Access article under the terms of the Creative Commons Attribution License (http://creativecommons.org/licenses/by/2.0), which permits unrestricted use, distribution, and reproduction in any medium, provided the original work is properly cited.

The license is subject to the *Beilstein Journal of Organic Chemistry* terms and conditions: (http://www.beilstein-journals.org/bjoc)

The definitive version of this article is the electronic one which can be found at: doi:10.3762/bjoc.9.116

Beilstein Journal of Organic Chemistry

ML212: A small-molecule probe for investigating fluconazole resistance mechanisms in *Candida albicans*

Willmen Youngsaye[1], Cathy L. Hartland[1], Barbara J. Morgan[1], Amal Ting[1], Partha P. Nag[1], Benjamin Vincent[2,3], Carrie A. Mosher[1], Joshua A. Bittker[1], Sivaraman Dandapani[1], Michelle Palmer[1], Luke Whitesell[2], Susan Lindquist[2,4], Stuart L. Schreiber[1,5] and Benito Munoz[*1]

Full Research Paper

Open Access

Address:
[1]Chemical Biology Platform and Probe Development Center, Broad Institute of MIT and Harvard, 7 Cambridge Center, Cambridge, MA 02142, USA, [2]Whitehead Institute for Biomedical Research, 9 Cambridge Center, Cambridge, MA 02142, USA, [3]Microbiology Graduate Program, Massachusetts Institute of Technology, 77 Massachusetts Avenue, Cambridge, MA 02139, USA, [4]Department of Biology and Howard Hughes Medical Institute, Massachusetts Institute of Technology, 77 Massachusetts Avenue, Cambridge, MA 02139, USA and [5]Howard Hughes Medical Institute, Broad Institute of Harvard and MIT, 7 Cambridge Center, Cambridge, MA 02142, USA

Email:
Benito Munoz[*] - bmunoz@broadinstitute.org

* Corresponding author

Keywords:
antifungal; *Candida albicans*; chemosensitizer; fluconazole; Molecular Libraries Probe Production Center Network (MLPCN)

Beilstein J. Org. Chem. **2013,** *9,* 1501–1507.
doi:10.3762/bjoc.9.171

Received: 12 March 2013
Accepted: 10 June 2013
Published: 26 July 2013

This article is part of the Thematic Series "Synthetic probes for the study of biological function".

Guest Editor: J. Aubé

© 2013 Youngsaye et al; licensee Beilstein-Institut.
License and terms: see end of document.

Abstract

The National Institutes of Health Molecular Libraries and Probe Production Centers Network (NIH-MLPCN) screened >300,000 compounds to evaluate their ability to restore fluconazole susceptibility in resistant *Candida albicans* isolates. Additional counter screens were incorporated to remove substances inherently toxic to either mammalian or fungal cells. A substituted indazole possessing the desired bioactivity profile was selected for further development, and initial investigation of structure–activity relationships led to the discovery of ML212.

Introduction

Discovery of antimicrobial agents possessing unique structural motifs or a novel mechanism of action is critical to counter and control the rising incidence of drug-resistant pathogens [1-6]. Chemosensitization of resistant organisms is a complementary approach that capitalizes upon the existing arsenal of antimicrobials to combat this medical dilemma [7-10]. By undermining

the resistance mechanisms of the target pathogen, it is possible to restore efficacy to previously ineffective drugs thereby prolonging their status as frontline treatments. This, in turn, affords critical lead-time towards the development of novel antimicrobial drugs.

The National Institutes of Health Molecular Libraries and Probe Production Centers Network (NIH-MLPCN) recently performed a high-throughput screening (HTS) campaign to search for potential chemosensitizers of the pathogenic fungus *Candida albicans* [11]. The *C. albicans* clinical isolates used in this study demonstrate a range of resistance to the widely prescribed triazole antimycotic fluconazole (Flc) [12], and the objective was to identify novel small molecules capable of surmounting this inherent resistance [13-16]. The screen was conducted by using a cell-based assay with integrated counter screens to remove compounds acting through previously established methods for overturning drug resistance in *C. albicans*. In addition, substances intrinsically toxic to either mammalian or fungal cells were eliminated.

Results and Discussion

Screening results

In order to identify nonfungitoxic chemosensitizers of *Candida albicans*, compounds from the NIH's Molecular Libraries Small Molecule Repository (MLSMR) [17] were evaluated in the screening cascade summarized in Figure 1. The *C. albicans* strains used in the primary screen and secondary assay 1

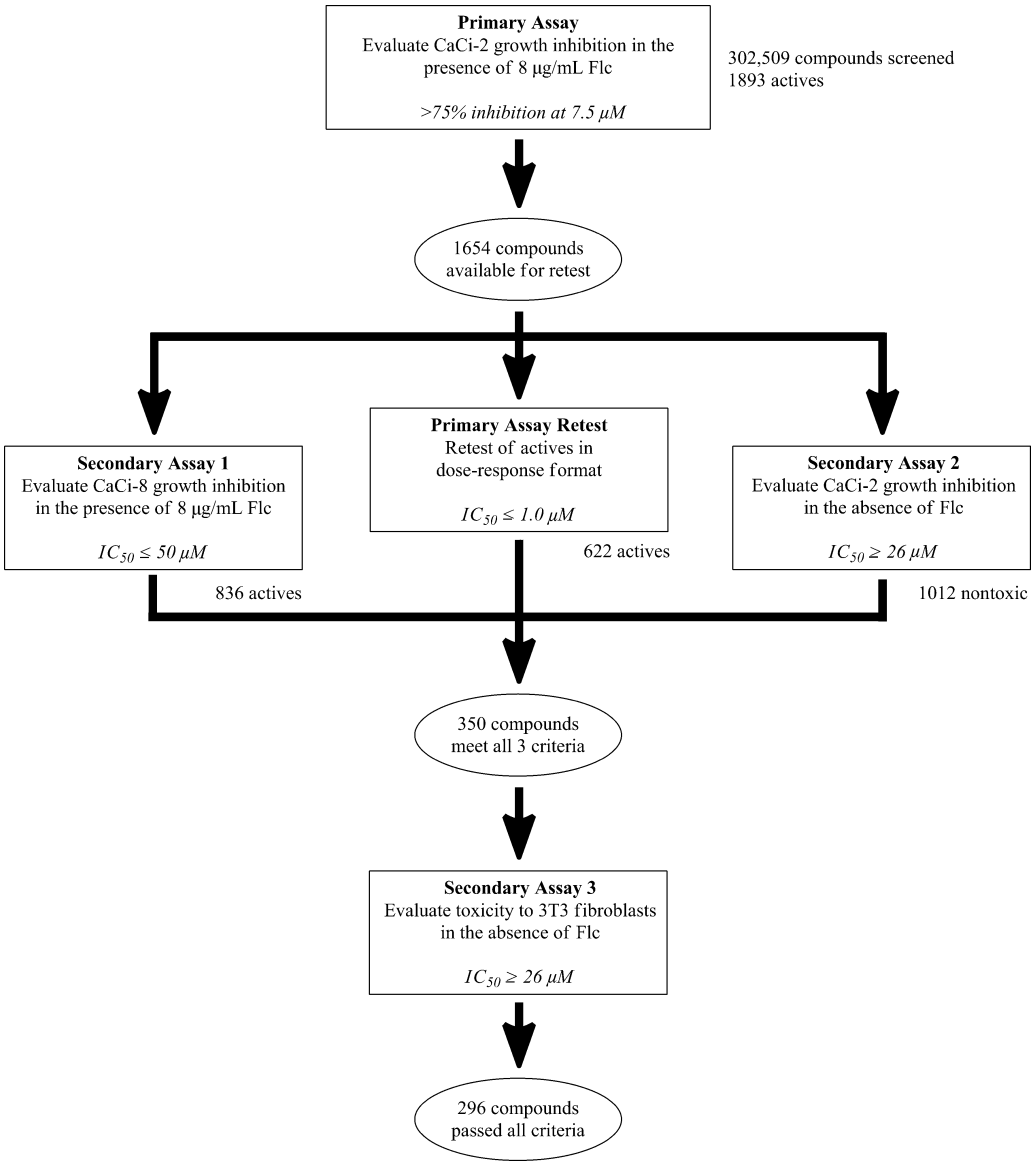


Figure 1: Assay pipeline for triaging hits. Individual assay cut-offs are given in italics.

(CaCi-2 and CaCi-8, respectively) are both clinical isolates that partially respond to fluconazole treatment [12]. The minimum inhibitory concentration (MIC) of fluconazole against CaCi-2 and CaCi-8 was reported to be 2 μg/mL and 8 μg/mL, respectively [12]. However in our hands, these strains continue to proliferate steadily (albeit at a reduced rate) when treated with fluconazole at or above the reported MIC. This behavior may contribute to the inability of fluconazole therapy to effectively clear the infection and allows for the further development of resistance [12].

A total of 302,509 compounds from the MLSMR were tested at 7.5 μM for their ability to inhibit completely the growth of CaCi-2 cells that are concurrently treated with 8 μg/mL fluconazole (Figure 1). With a minimum requirement of 75% inhibition, 1893 actives were recorded, corresponding to an overall hit rate of 0.6%. Of the active compounds, 1654 were available for retesting in a dose-response format. This subset was resubjected to the primary assay and was also tested concurrently in two secondary assays. Secondary assay 1 measured chemosensitization of the more resistant CaCi-8 strain. Secondary assay 2 eliminated anything with inherently antifungal activity. These three assays cooperatively removed almost 80% of the original hits, leaving 350 candidates. A final assay (secondary assay 3) was incorporated to discard any compound displaying toxicity to mammalian fibroblasts. The fibroblast toxicity assay removed another 54 compounds to leave a total of 296 hits.

From the 296 hits remaining, 29 were selected for revalidation from dry powders obtained from commercial vendors or resynthesis. Once their identity and purity was ascertained by LCMS and ^{1}H NMR analysis, these 29 candidates were tested once more in the entire assay tree outlined previously in Figure 1. Following this re-evaluation, methyl 3-phenyl-1*H*-indazole acetate (**1**, Figure 2) emerged as an attractive candidate for further development. A commercial sample of compound **1** shows good activity against CaCi-2 and CaCi-8 (IC_{50} = 0.8 and 2.3 μM, respectively) with no apparent effect on 3T3 fibroblasts (IC_{50} > 26 μM). Compound **1** also possesses good solubility in PBS (79 μM) and is synthetically tractable with several points of diversity readily accessible. Consequently, compound **1** and a collection of closely related analogues were prepared to enable investigation of possible structure–activity relationships (SAR) [18]. In addition to indazole **1**, two other structurally distinct scaffolds (**2** and **3**) were also selected for follow-up studies and those works are communicated elsewhere [19,20].

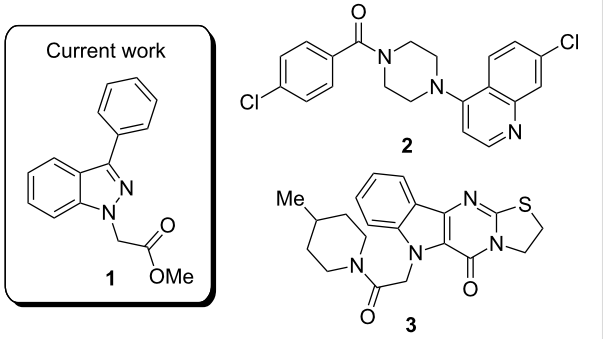
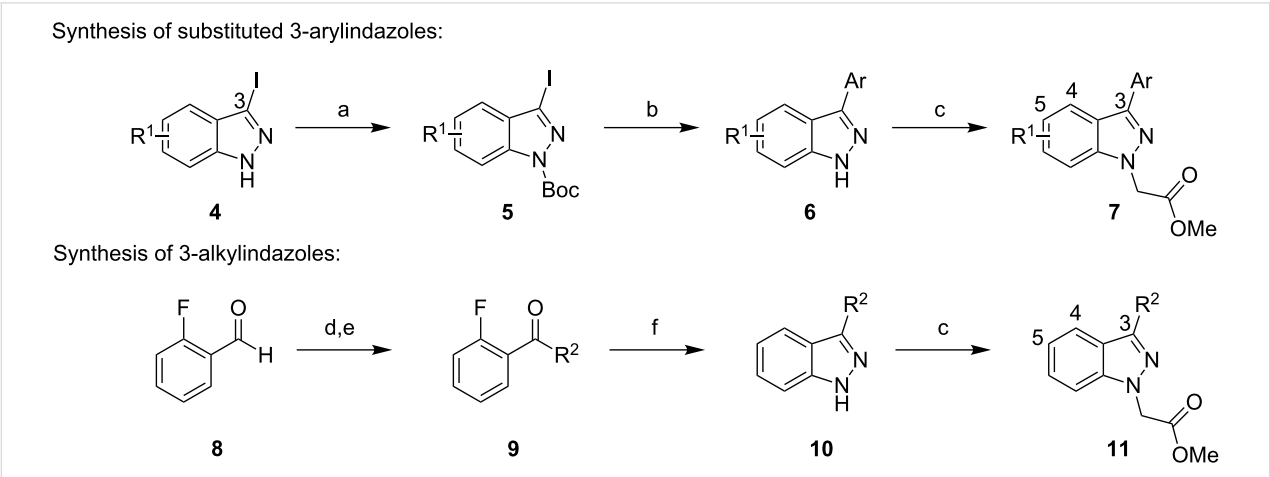


Figure 2: Hit compounds selected for further optimization.

Chemistry

Two different routes were adopted to access the various functionalized indazoles required to evaluate the SAR associated with hit compound **1** (Scheme 1). The robust Suzuki–Miyaura



Scheme 1: Preparation of substituted methyl 2-(1*H*-indazol-1-yl)acetates. Reagents and conditions: (a) Et_3N, Boc_2O, DMAP, tetrahydrofuran; (b) $ArB(OH)_2$, $Pd(PPh_3)_4$, aqueous Na_2CO_3, 1,4-dioxane, 120 °C; (c) methyl bromoacetate, K_2CO_3, acetone, 60 °C; (d) alkylmagnesium bromide, Et_2O, 0 °C; (e) Dess–Martin periodinane, CH_2Cl_2; (f) hydrazine hydrate, 175 °C.

reaction was selected for the preparation of analogues bearing substituents around the central indazole core. This approach also permitted rapid replacement of the phenyl ring at C3 with functionalized phenyl rings and alternative heterocycles. Preliminary attempts to couple substituted 3-iodoindazoles **4** failed to produce isolable amounts of the desired product directly. Subsequently, the indazoles were protected as their *tert*-butyl carbamates **5** prior to undergoing palladium-mediated Suzuki reactions with various boronic acid partners. Under the reaction conditions, the carbamate-protecting group was also cleaved to afford the desired 3-arylindazoles, albeit as the unprotected systems **6**. Alkylation with methyl bromoacetate and potassium carbonate in hot acetone completed the synthesis of compounds **7**.

In order to prepare 3-alkylindazoles, 2-fluorobenzaldehyde was first treated with alkylmagnesium bromides, and the resulting benzyl alcohols were immediately oxidized with Dess–Martin reagent. Alkyl phenyl ketones **9** and hydrazine hydrate were then reacted under microwave conditions to assemble the indazole ring **10**. The ester side chain of **11** was installed under the same conditions described above for the alkylation of 3-arylindazoles.

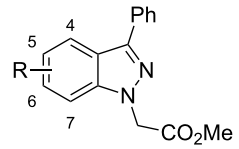
In vitro activity and SAR

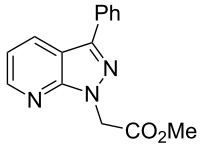
All of the compounds prepared above were evaluated for their ability to chemosensitize the *C. albicans* test strains CaCi-2 and CaCi-8 towards fluconazole. As described above, the fungi were simultaneously incubated with test compounds and fluconazole (8 μg/mL) for 48 hours to determine if any combinations could fully inhibit fungal growth. The DMSO/fluconazole combination served as an internal control.

Substitution of the indazole core generally leads to a potency reduction to varying degrees (Table 1). The 5- and 6-positions can accommodate smaller functionalities such as methyl or chloro groups (**11**, **15**, and **17**) and still retain modest efficacy. The inactivity of **14** compared to **17** suggests that the 6-position may occupy a slightly larger pocket. Electron-withdrawing substituents (**13**, **18**, and **19**) appear detrimental to activity regardless of their position, while the weak potency of the methoxy compounds (**12** and **16**) suggests that there may be a limit to how far the western region may be extended. Pyridylindazole **20**, wherein a nitrogen atom is inserted in the place of a carbon, displays no cellular activity. Based on these preliminary results, a more extensive SAR investigation of this region was postponed in order to explore other regions of the scaffold.

We proceeded to evaluate the SAR of the C3 substituent next (Table 2). Removal of the original benzene ring produces the inactive analogue **21**. Similarly, installing acyclic alkyl systems such as an ethyl (**22**) or *tert*-butyl group (**23**) does not yield active compounds. Proceeding to cycloalkanes, a SAR trend begins to emerge. With the smallest cycloalkane replacement, the cyclopropyl derivative **24** is inactive whereas the larger cyclohexane of **25** yields an active chemosensitizer (IC_{50} = 2.3 μM). When alternative heteroaromatic rings (**26**–**29**) were prepared, none of the examined systems possess any significant cellular activity.

Table 1: Activity of substituted indazole cores.[a]



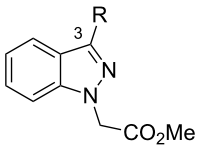
Cpd	R	CaCi-2 IC_{50} (μM)[b]	CaCi-8 IC_{50} (μM)[b]
1	H	2.2 ± 1.0	3.5 ± 1.9
11	5-Me	5.2 ± 2.2	8.2 ± 3.2
12	5-OMe	14.9 ± 5.7	22.1 ± 6.2
13	5-F	11.2 ± 7.2	inactive
14	5-Cl	inactive	inactive
15	6-Me	5.9 ± 3.1	inactive
16	6-OMe	9.5 ± 2.5	12.4 ± 0.5
17	6-Cl	4.0 ± 1.3	8.4 ± 0.5
18	6-CF_3	inactive	inactive
19	7-CF_3	inactive	inactive
20		inactive	inactive

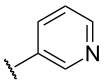
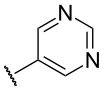
[a]CaCi-2 and CaCi-8 cells were incubated at 37 °C for 48 hours with test compound and 8 μg/mL (26 μM) fluconazole. [b]Average of at least three independent experiments, performed in duplicate. Inactive compounds displayed negligible activity at concentrations below 26 μM.

One possible explanation for the observed activity is that the binding pocket includes a small cleft that is best occupied by flat structures. Compounds **21**, **22**, and **24** are presumably too small to fit properly into this crevice, while the *tert*-butyl derivative **23** may simply be too large. However, the inactivity of the heteroaromatic counterparts **26**–**29** may imply that more than a steric constraint is operative within this putative groove; a possible electronic requirement for this substituent may exist as well.

Returning to the original phenyl ring, various substituents were introduced at different positions about the ring to probe for further electronic and steric effects associated with this region

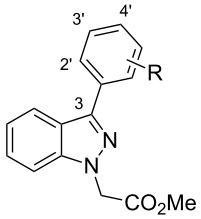
Table 2: Investigation of 3-substituted indazoles.[a]



Cpd	R	CaCi-2 IC_{50} (μM)[b]	CaCi-8 IC_{50} (μM)[b]
21	-H	inactive	inactive
22	-Et	inactive	inactive
23		inactive	inactive
24		inactive	inactive
25		2.3 ± 0.3	6.0 ± 1.7
26		inactive	inactive
27		inactive	21.1 ± 3.3
28		inactive	inactive
29		12.9 ± 1.7	inactive

[a]CaCi-2 and CaCi-8 cells were incubated at 37 °C for 48 hours with test compound and 8 μg/mL (26 μM) fluconazole. [b]Average of at least three independent experiments, performed in duplicate. Inactive compounds displayed negligible activity at concentrations below 26 μM.

Table 3: Substituent effects associated with the 3-phenyl ring.[a]



Cpd	R	CaCi-2 IC_{50} (μM)[b]	CaCi-8 IC_{50} (μM)[b]
1	H	2.2 ± 1.0	3.5 ± 1.9
30	4′-Me	4.8 ± 2.5	19.5 ± 14.2
31	4′-OMe	4.2 ± 1.7	14.1 ± 6.4
32	4′-F	8.3 ± 2.8	12.3 ± 3.9
33	4′-CF_3	inactive	inactive
34	4′-CN	inactive	20.5 ± 0.3
35	3′-Me	1.1 ± 0.6	1.9 ± 0.9
36	3′-OMe	0.7 ± 0.3	1.5 ± 0.6
37	3′-NMe_2	0.8 ± 0.1	2.0 ± 0.2
38	3′-F	1.7 ± 0.4	4.2 ± 4.1
39	2′-Me	5.3 ± 0.5	7.8 ± 2.6
40	2′-OMe	9.3 ± 3.6	11.4 ± 1.7
41	3′,5′-di-OMe	inactive	inactive

[a]CaCi-2 and CaCi-8 cells were incubated at 37 °C for 48 hours with test compound and 8 μg/mL (26 μM) fluconazole. [b]Average of at least three independent experiments, performed in duplicate. Inactive compounds displayed negligible activity at concentrations below 26 μM.

(Table 3). With regards to steric requirements, it appears that neither the *para*- (compounds **30**–**34**) nor *ortho*-positions (compounds **39** and **40**) are particularly amenable to functionalization. While bioactivity is still observed with these substances, they all appear to be only weakly active (IC_{50} = 2–8 μM). Conversely, the *meta*-substituted systems **35**–**38** prove to be the most conducive to potency. The methyl ether **36** is potent against CaCi-2 (IC_{50} = 0.7 μM) as is the *N*,*N*-dimethylamine variant (**37**, IC_{50} = 0.8 μM). The weakest compound of this series, 3-fluoro derivative **38**, still shows low micromolar activity (IC_{50} = 1.7 μM). The weak activity of **38** may be tied to the electronegativity of fluorine. This is best illustrated with compounds **32**–**34**. While the 4-fluoro analogue is a weak chemosensitizer of CaCi-2 and CaCi-8, introducing more electron-withdrawing substituents, such as trifluoromethyl (**33**) and cyano (**34**) groups, results in complete inactivity (IC_{50} > 26 μM). The activity of *p*-tolyl **30** and *p*-anisoyl **31** indicates that the inefficacy of **33** and **34** cannot be solely attributed to steric considerations. The inactivity of the 3,5-dimethoxyphenyl ring (**41**) suggests the indazole's C3 substituent may reside in an asymmetric pocket.

As the most potent chemosensitizer of both *C. albicans* CaCi-2 and CaCi-8 (IC_{50} = 0.7 and 1.5 μM, respectively) with good solubility (55 μM in PBS), compound **36** was nominated as MLPCN probe ML212. Exposure to human or murine plasma revealed significant chemical instability (<10% remaining after 5 h incubation), and this is attributed to the ester hydrolysis of the side chain. Follow-up studies investigating the SAR of the side chain and addressing this liability will be reported shortly. Additional profiling of ML212 determined that the probe is nontoxic to *C. albicans* in the absence of fluconazole (IC_{50} > 26 μM after 48 h incubation), neither does it show any toxicity towards murine 3T3 fibroblasts (IC_{50} > 26 μM). Hsp90-dependent and calcineurin-dependent signaling pathways have been previously implicated in maintaining fluconazole resistance in *C. albicans* [21], but ML212 does not inhibit these pathways in yeast-reporter assays (IC_{50} > 26 μM). Identification of ML212's molecular target is ongoing, as well as

efforts to determine the efficacy of ML212 against diverse mechanisms of fluconazole resistance, including biofilm formation, drug-target mutations, and efflux-pump amplification.

Conclusion

High-throughput screening of 300,000 compounds from the NIH's MLSMR collection identified several substances that potentiate the effect of fluconazole in fluconazole-resistant *Candida albicans* clinical isolates. Among the numerous hits, 3-phenylindazole **1** was selected for chemical optimization, resulting in the identification of 3-(3-anisoyl)indazole **36** as new small-molecule probe (ML212) to facilitate investigation of the various mechanisms used by *C. albicans* to withstand fluconazole. Elucidation of ML212's mechanism of action may afford new targets to exploit in the continuing efforts to develop novel antimycotics and combat increasingly prevalent drug-resistance. Samples of ML212 are available free of charge, on request.

Supporting Information

Detailed experimental protocols for cellular assays and for the preparation of representative compounds **25** and **36** are provided. Proton NMR spectra for all prepared compounds are also available.

Supporting Information File 1

Detailed assay protocols and compound synthesis.
[http://www.beilstein-journals.org/bjoc/content/supplementary/1860-5397-9-171-S1.pdf]

Supporting Information File 2

NMR spectra of reported compounds.
[http://www.beilstein-journals.org/bjoc/content/supplementary/1860-5397-9-171-S2.pdf]

Acknowledgements

This work was funded by the NIH's MLPCN program (1 U54 HG005032-1 awarded to S.L.S.). BV, LW, and SL are grateful for funding from the NIH (1 R03 MH086456-01). The authors are grateful to Dr. Spencer Redding (University of Texas Health Science Center San Antonio) for graciously providing samples of *C. albicans* CaCi-2 and CaCi-8.

References

1. Martínez, J. L. *Future Med. Chem.* **2012,** *4,* 347–359. doi:10.4155/fmc.12.2
2. Hawkey, P. M.; Jones, A. M. *J. Antimicrob. Chemother.* **2009,** *64* (Suppl. 1), i3–i10. doi:10.1093/jac/dkp256
3. Gould, I. M. *Int. J. Antimicrob. Agents* **2008,** *32* (Suppl. 1), S2–S9. doi:10.1016/j.ijantimicag.2008.06.016
4. Vandeputte, P.; Ferrari, S.; Coste, A. T. *Int. J. Microbiol.* **2012,** No. 713687. doi:10.1155/2012/713687
5. Pfaller, M. A.; Diekema, D. J. *Clin. Microbiol. Rev.* **2007,** *20,* 133–163. doi:10.1128/CMR.00029-06
6. Sanglard, D.; Odds, F. C. *Lancet Infect. Dis.* **2002,** *2,* 73–85. doi:10.1016/S1473-3099(02)00181-0
7. Lavigne, J.-P.; Brunel, J.-M.; Chevalier, J.; Pagès, J.-M. *J. Antimicrob. Chemother.* **2010,** *65,* 799–801. doi:10.1093/jac/dkq031
8. Gallo, S.; Chevalier, J.; Mahamoud, A.; Eyraud, A.; Pagès, J.-M.; Barbe, J. *Int. J. Antimicrob. Agents* **2003,** *22,* 270–273. doi:10.1016/S0924-8579(03)00215-2
9. Kim, J.; Campbell, B.; Mahoney, N.; Chan, K.; Molyneux, R.; May, G. *Biochem. Biophys. Res. Commun.* **2008,** *372,* 266–271. doi:10.1016/j.bbrc.2008.05.030
10. Cernicka, J.; Kozovska, Z.; Hnatova, M.; Valachovic, M.; Hapala, I.; Riedl, Z.; Hajós, G.; Subik, J. *Int. J. Antimicrob. Agents* **2007,** *29,* 170–178. doi:10.1016/j.ijantimicag.2006.08.037
11. The complete results of the HTS assay can be viewed online free of charge on PubChem. http://pubchem.ncbi.nlm.nih.gov/assay/assay.cgi?aid=1979.
12. Redding, S.; Smith, J.; Farinacci, G.; Rinaldi, M.; Fothergill, A.; Rhine-Chalberg, J.; Pfaller, M. *Clin. Infect. Dis.* **1994,** *18,* 240–242. doi:10.1093/clinids/18.2.240
13. DiGirolamo, J. A.; Li, X.-C.; Jacob, M. R.; Clark, A. M.; Ferreira, D. *J. Nat. Prod.* **2009,** *72,* 1524–1528. doi:10.1021/np900177m
14. Gamarra, S.; Rocha, E. M. F.; Zhang, Y.-Q.; Park, S.; Rao, R.; Perlin, D. S. *Antimicrob. Agents Chemother.* **2010,** *54,* 1753–1761. doi:10.1128/AAC.01728-09
15. Guo, X.-L.; Leng, P.; Yang, Y.; Yu, L.-G.; Lou, H.-X. *J. Appl. Microbiol.* **2008,** *104,* 831–838. doi:10.1111/j.1365-2672.2007.03617.x
16. Mai, A.; Rotili, D.; Massa, S.; Brosch, G.; Simonetti, G.; Passariello, C.; Palamara, A. T. *Bioorg. Med. Chem. Lett.* **2007,** *17,* 1221–1225. doi:10.1016/j.bmcl.2006.12.028
17. Additional information about the MLSMR can be found online at http://mli.nih.gov/mli/secondary-menu/mlscn/ml-small-molecule-repository/
18. The Present Communication details a portion of the work previously described in official Probe Report submitted to the NIH upon project completion. The official Probe Report has been made available online by the NIH, free of charge: Hartland, C. L.; Youngsaye, W.; Morgan, B.; Ting, A.; Nag, P.; Burhlage, S.; Johnston, S.; Bittker, J.; Vincent, B.; Whitesell, L.; Dandapani, S.; MacPherson, L.; Munoz, B.; Palmer, M.; Lindquist, S.; Schreiber, S. L. "Identification of small molecules that selectively inhibit fluconazole-resistant *Candida albicans* in the presence of fluconazole but not in its absence - Probe 2". In: *Probe Reports from the NIH Molecular Libraries Program* [Internet]. Bethesda (MD): National Center for Biotechnology Information (US); **2010**-. Available from: http://www.ncbi.nlm.nih.gov/books/NBK98920/
19. Youngsaye, W.; Vincent, B.; Hartland, C. L.; Morgan, B. J.; Buhrlage, S. J.; Johnston, S.; Bittker, J. A.; MacPherson, L.; Dandapani, S.; Palmer, M.; Whitesell, L.; Lindquist, S.; Schreiber, S. L.; Munoz, B. *Bioorg. Med. Chem. Lett.* **2011,** *21,* 5502–5505. doi:10.1016/j.bmcl.2011.06.105
20. Youngsaye, W.; Dockendorff, C.; Vincent, B.; Hartland, C. L.; Bittker, J. A.; Dandapani, S.; Palmer, M.; Whitesell, L.; Lindquist, S.; Schreiber, S. L.; Munoz, B. *Bioorg. Med. Chem. Lett.* **2012,** *22,* 3362–3365. doi:10.1016/j.bmcl.2012.02.035
21. Cowen, L. E.; Lindquist, S. *Science* **2005,** *309,* 2185–2189. doi:10.1126/science.1118370

License and Terms

This is an Open Access article under the terms of the Creative Commons Attribution License (http://creativecommons.org/licenses/by/2.0), which permits unrestricted use, distribution, and reproduction in any medium, provided the original work is properly cited.

The license is subject to the *Beilstein Journal of Organic Chemistry* terms and conditions: (http://www.beilstein-journals.org/bjoc)

The definitive version of this article is the electronic one which can be found at: doi:10.3762/bjoc.9.171